

PERSPECTIVES IN ENGINEERING, SCIENCE & TECHNOLOGY



Edited by

NG KHAI MUN

GOLNOOSH MANTEGHI

NORHAIZA NORDIN

PERSPECTIVES IN ENGINEERING, SCIENCE & TECHNOLOGY

Edited by
NG KHAI MUN
GOLNOOSH MANTEGHI
NORHAIZA NORDIN

Published by

IKRAM Education Sdn. Bhd.for
INFRASTRUCTURE UNIVERSITY KUALA LUMPUR
Ground Floor, Block 11, Unipark Suria,
Jalan Ikram-Uniten, 43000 Kajang,
Selangor Darul Ehsan.
Tel: (603)8926 6993
Fax: (603)8734 102

Printed by

Printing Unit
KUMPULAN IKRAM SDN. BHD.

© 2024 IKRAM Education Sdn Bhd
ISBN 978-629-98359-9-8
eISBN 978-629-99622-3-6



Cataloguing-in-Publication Data

Perustakaan Negara Malaysia

A catalogue record for this book is available
from the National Library of Malaysia

ISBN 978-629-98359-9-8

CONTENTS

<i>PREFACE</i>	i
CIVIL ENGINEERING AND CONSTRUCTION	
NUMERICAL INVESTIGATION OF THE NATURAL FREQUENCIES OF A PROFILED STEEL SHEET DRY BOARD (PSSDB) DISASTER RELIEF SHELTER FLOOR PANEL USING ANSYS	1
Norhaiza Nordin, Azzam Ali, Mohamed Emierul & Mohd Nasir Hussin	
EXPERIMENTAL STUDIES ON CONCRETE UTILISING RED MUD AS A PARTIAL REPLACEMENT FOR CEMENT WITH SUGAR CANE FIBRE	8
Abdullah Alkurshumi, Mohd Nizam Shakimon, Mohamad Ayob & Zulhazmee Bakri	
COMPRESSIVE STRENGTH AND WATER ABSORPTIONS OF CEMENTITIOUS GROUT CONTAINING TREATED PALM OIL FUEL ASH (POFA)	18
Mohamed Emierul, Megat Azmi, Mohd Nasir Hussin & Norhaiza Nordin	
ECCENTRICALLY BRACED FRAMES AS EARTHQUAKE RESISTANT SYSTEM AND SEISMIC ANALYSIS OF THE STEEL FRAMES	29
Mohd Nasir Hussin, Pema Tashi, Norhaiza Nordin & Mohamed Emierul	
DESCRIPTIVE STATISTICAL ANALYSIS OF WATER QUALITY DATA IN SELANGOR RIVER BASIN	39
Muhammad Nurasmadi Mohd Rifa'at, Nurazim Ibrahim, Norul Wahida Kamaruzaman, Naimah Yusoff, Sangeetha Valloo, Janagiammal & Jaya Malathy	
POME TREATMENT EFFICIENCY ENHANCEMENT IN CONTINUOUS FLOW STIRRED-TANK REACTOR BY POLYVINYL ALCOHOL GEL	55
Nik Nuraini Azhari, Chen Chee Xiang, Nadzifah Che Mat, Khairunisah Kamaruzaman, Nurazim Ibrahim & Syazana Syahirah Jamaluddin	
DECONTAMINATION OF Zn IONS FROM AQUEOUS SOLUTION USING PAPAYA SEED AS LOW-COST ADSORBENT	65
Khairunisah Kamaruzaman, Vinot A/L Arthimulam, Nik Nuraini Azhari, Nadzifah Che Mat & Syazana Syahirah Jamaluddin	
A STUDY ON THE EFFECT OF STYRENE-BUTADIENE RUBBER LATEX TO THE CONCRETE MECHANICAL PERFORMANCE	75
Nadzifah Che Mat, Eric Wong Fa Yao, Nik Nuraini Azhari & Khairunisah Kamaruzaman	
MANAGING HYDROGRAPHIC DATA BY USING GIS TECHNOLOGY IN MALAYSIA	86
Hanah Zakariah, Saleh Mohamed Mohamud Ibrahim, Haslina Mohamed & Mohd. Ashraf Mohd. Fateh	

GEOMETRIC DESIGN OF ROAD IN URBAN AREA USING AUTODESK INFRAWORKS	96
Ranjit Singh Dharam Singh & Yong Fatihah Daman Huri	
MECHANICAL, ELECTRICAL AND ELECTRONICS	
HUMIDITY CONTROL STORAGE CABINET FOR SEMICONDUCTORS MATERIALS	107
Anandan Subramaniam & Mohd Zamri Ibrahim	
DEVELOPMENT OF A BATTERY ENERGY STORAGE SYSTEM FOR PEAK SHAVING	116
N. Mohamed, N. A. Omar, I. Sulaiman & R. Noreldaim	
ANALYSIS ON VEHICLE PERFORMANCES BETWEEN SINGLE PLATE CONVENTIONAL AND AFTER MARKET CLUTCH	127
Muhammad Fathurrahman Daud, Ts. Engku Amirul Rashidin Engku Ariff & Muhammad Fahmi Md Isa	
DEVELOPMENT OF MONITORING SYSTEM USING RASPBERRY PI AND SENSORS WITH INSTANT NOTIFICATION	139
S.S. Mazlan, N. Mohamed, K. W. Hon & I. Sulaiman	
EMISSION CHARACTERISTICS AND FUEL CONSUMPTION OF SI ENGINE BY USING RON95, RON97 WITH DIFFERENT TYPES OF SPARK PLUG	151
Noorradiah Ismail, Masud Mohammed, Ida Rasyada Daud, Norhaslina Aziz, Ir Malek Idrus, & Fahmi Isa	
EXPERIMENTAL INVESTIGATION ON DAMPING PROPERTIES AND PERFORMANCE OF ADJUSTABLE SHOCK ABSORBER	167
Joel Wong Khai Sheng, Ng Khai Mun, Koh Chu Eyam & Abdullah Idris	
FIELD INVESTIGATION OF ELECTRIC VEHICLE DISCHARGE RATE AND ITS ECONOMIC ASPECT UNDER INFLUENCE OF DIFFERENT ON-THE-ROAD DRIVING CONDITIONS – A CASE STUDY IN CHINA	186
Su Jiajing, Ng Khai Mun, Noorradiah Ismail, Sai-Keong Chan & Tan Chee Fai	
LINEAR STATIC ANALYSIS AND PERFORMANCE OF LOWER SUSPENSION ARM USING FINITE ELEMENT METHOD	198
Muhammad Fahmi Md Isa, Araoye Ibrahim Oyeyemi, Ida Rasyada Daud & Norhaslina Abdul Aziz	
RUNNER SIZING ON CAVITY FILLING IN PLASTIC INJECTION MOULDING	208
Abdulrahman Adil Elhag Eltahir, Yap Ai Kin, Ida Rasyada Daud & Mohd Shahrudin Mohd Alias	

PERFORMANCE ANALYSIS OF DC-DC CONVERTERS FOR STAND-ALONE HYBRID ENERGY SYSTEM	219
N. Sulaiman, Y.K. Lim, L.C. Kuan & K. Thana Pakkiam	
MULTI BAND MICRO STRIP PATCH ANTENNA DESIGN FOR WLAN APPLICATIONS	239
K. Thana, Aiman, R.Sanjay, N. Ajlaa & N. Sulaiman	
MONITORING AND CONTROLLING FOR PRECISION HYDROPONICS	245
LC Kuan, K.W. Hon, N. Sulaiman & M. Ramesh	
OPTIMIZATION OF TURNING PROCESS PARAMETERS USING TAGUCHI METHOD	263
Mohd Shahrudin Mohd Alias, Abueid Ammar Ahmed Mahammed	
PULSE OXIMETER WITH ALARMING NOTIFICATION FEATURE	282
H. Norazam, N. A. Omar, H. K. Wye, S. Kumar, T. Pakkiam, I. Sulaiman	
TEMPERATURE COMPARISON ON THE EFFECTS OF AN AIR-COOLING SYSTEM INSTALLED ON TO A BRAKE ROTOR	294
Muhammad Fahmi Md Isa, Muhammad Eizlan Ezzat Abdul Shukor, Engku Amirul Rashidin Engku Ariff, Noorradayah Ismail	
UNIFIED GDI LIBRARY CREATION FOR THE STANDARD LOGIC CELL FOR SILTERRA 130nm PROCESS	301
Jebashini Ponnian, Ima Sulaiman & Darshini Sankaran	
INFORMATION TECHNOLOGY	
IoT BASED REAL TIME MONITORING SYSTEM USING BLYNK APPLICATION	309
Sangeetha Valloo, Janagiammal Ramasamy, Jaya Malathy Poloha Nadan, Christopher Mark Mark Anthony, Norul Wahida Kamaruzaman, Nurazim Ibrahim, Naimah Yusoff	
ZERO TRUST TAXONOMY FOR ACADEMIC DISHONESTY: A REVIEW PAPER	322
Tadiwa Elisha Nyamasvisva, Atiff Abdalla Mahmoud Arabi, Noradibah Binti Adnan & Valeriano Dasalla Jr	
SCIENCE	
ANTIMICROBIAL ACTIVITY OF GUM ARABIC (Acacia senegal & Acacia seyal) AGAINST PYOGENIC BACTERIA_PROBIOTIC PROVEN	344
Noura Karam M. Salih, Fazlen S. M. Khan, Ahmed A. Bagi	
ASSESSMENT OF BACTERIAL CONTAMINATION IN PUBLIC SWIMMING POOLS	365
Noura Karam M. Salih & Ibrahim M. Oumar	

IDENTIFICATION OF MARINE SPONGE USING DNA-BARCODING APPROACH	376
Aizat Mohd Razali, Samson Soon & Teffanie Arputheraj	
MEDICAL CANNABINOIDS AS PROMISING THERAPEUTICS IN MAINSTREAM MEDICINE	381
Samson Soon, Lenny Chong; Noor Inayah Ya'akub; Sai-Keong Chan; Chee Fai Tan; Khai Mun Ng.	
GLUCAGON-LIKE PEPTIDE-1 (GLP-1) EFFECTS ON TYPE 2 DIABETES MELLITUS (T2DM)-INDUCED 3T3-L1 ADIPOCYTES	391
Noor Mazuin Abu Bakar, Shatrah Othman & Kavitha Rajagopa	
GENE EXPRESSION PROFILE OF PSYCHROPHILIC YEAST GLACIOZYMA ANTARCTICA PI12 UNDER STATIONARY GROWTH PHASE	401
Tay Lih Jinq, Farah Diba Abu Bakar, Nor Muhammad Mahadi & Abdul Munir Abdul Mura	

PREFACE

Perspectives in Engineering, Science & Technology covers a wide range of critical issues related to science and technology. The contributions in this volume are the results of research by researchers from the faculty of Engineering, Science and Technology (FEST) at the Infrastructure University Kuala Lumpur (IUK).

The chapters in the book are divided into four main areas. Part One includes research work in the fields of Civil Engineering and Construction. Part Two covers topics in Mechanical Engineering, Electrical Engineering and Electronics. In Part Three, the chapters cover several topics in Information Technology. Finally, Part Four includes research work on Biotechnology and topics in general science.

The originality of most of the works in this book makes them a valuable addition to literature in the field of Engineering and Information Technology and Science in general. It is hoped that engineers, technologists, information scientists, biotechnologists, university students and researchers in general will immensely benefit from the contributions in this volume and include them as part of their own efforts to further explore and understand the various phenomena studied here.

Muhammad Rashaad Bakashmar
Director
Academic and Research Management Centre
Infrastructure University Kuala Lumpur (IUKL)

NUMERICAL INVESTIGATION OF THE NATURAL FREQUENCIES OF A PROFILED STEEL SHEET DRY BOARD (PSSDB) DISASTER RELIEF SHELTER FLOOR PANEL USING ANSYS

Norhaiza Nordin, Azzam Ali, Mohamed Emierul, Mohd Nasir Hussin
Infrastructure University Kuala Lumpur

1. INTRODUCTION

The number of natural disasters being reported each year has steadily increased in the recent decades. This increase in natural disasters is due to extreme weather events caused by climate change according to the United States Geological Survey (2020). Climate change has a severe impact on the intensity of hydro-meteorological disasters such as tsunamis, hurricanes, droughts, typhoons and floods. In addition to the thousands of lives claimed by these natural disasters, they leave thousands of people homeless or displaced and in need of evacuation and adequate shelters. It is therefore vital to have safe and reliable disaster relief shelters that can be quickly constructed to cater for such need. A potential application is the Profiled Steel Sheet Dry Board (PSSDB) system.

PSSDB system is a light weight composite load-bearing structural system consist of profiled steel sheet (PSS) and dry board (DB) attached together by self-drilling and self-tapping screws. The system can be used in the place of traditional floors, roofs and walls (Samir et al, 2017) Due to its light weight and slender members, it is important to determine that the PSSBD system as a disaster relief shelter floor will not vibrate excessively under service load.

When using any system for the purpose of construction, it is crucial to know the natural frequency which is the frequency at which a system oscillates when it is not subjected to any external force, as to avoid resonance which can result in a catastrophic failure of the structure (Gandomkar et al, 2013).

Even if the issue of vibration is not critical enough to lead to a structural failure, vibrations can cause discomfort to the users of a structure and give them the impression and feeling that the structure is unsafe and not structurally sound. Gandomkar F.A. (2013) states that slender structural floors could experience irritating vibration problems due to human walking load and therefore, vibration acceptability of such floors is an essential subject in addition to the usual strength c...riterion.

2. LITERATURE REVIEW

According to IFRC/RCS (2013), Disaster shelters are considered vital for personal safety, climate protection, security, and resistance to disease and ill health. Meeting the shelter needs of survivors after a disaster remains a major challenge for governments, non-governmental

organizations and humanitarian agencies. With its various benefits, the PSSDB system could aid in meeting this challenge.

The Profiled Steel Sheet Dry Board system was first developed as a replacement to traditional flooring and walling systems. PSSDB is comparatively light-weight and the construction procedure is simple, quick and can be constructed by unskilled labour (Wan Badaruzzaman & Wright 1998, Wright & Evans, 1994) It can be transported easily as the members can be neatly stacked up on top of each other and easily transported to remote areas. The system has been successfully utilised to construct two temporary school cabin classrooms in rural area in Malaysia (Nordin et al, 2009) These characteristics make it very potential to be used in the construction of Disaster Relief Shelters as well.

However, due to the its slender and light weight character, knowledge of its natural frequency is crucial from a design point of view, to maintain the acceptable vibration limit and to obtain forced response of the structure (Murray et al, 1997). This is also essential to predict the occurrence of resonance conditions in order to avoid a disaster.

Ehsan & Wan Badaruzzaman (2013), carried out investigations on the vibration performances of the PSSDB floor panel. The authors focused mainly on the fundamental frequency of PSSDB floor panels. Experimental tests were conducted in the laboratory to observe the effect of various board types, board thickness, and connectors spacing the fundamental frequencies of such floor panels. The results obtained from the study showed that for all panels tested, the fundamental frequency was more than 8 Hz and therefore the occupants of buildings with such floor panels will not experience discomfort due to vibrations. Increasing the amount of damping may help improve the vibration characteristics of the panels. The authors recommended 16-24 mm thick boards for PSSDB flooring systems, based on considerations made about workability and stress conditions. The authors also concluded that when the connectors are spaced closer to each other, the stiffness of the panel can be increased, thus giving higher fundamental frequency. Despite this, the authors refrained from recommending spacing less than 50 mm due to concerns about economy. Instead, they recommended the use of 100-200 spacing of connectors.

Gandomkar et al., (2013) used frequency response functions (FRFs), estimated experimentally, to determine the natural frequencies of three different PSSDB panels with different screw spacing. For this study, the authors developed Finite element models to predict the natural frequencies of the tested panels. They also studied the effect of screw spacing, profiled steel sheeting and dry board thicknesses and boundary conditions, on the fundamental natural frequency (FNF). From this study, the authors determined that the highest value of the FNF occurs for the maximum thickness of Peva 45 and the minimum thickness of plywood. They also observed that the lowest value of FNF occurs for the maximum thickness of plywood and minimum thickness of plywood.

Although numerous studies have been conducted on the PSSDB floor system, the experimental and numerical investigations conducted on the natural frequencies of PSSDB floor panels for a potential disaster relief shelter have not been done before and therefore will be

tackled by establishing a finite element model of the experiment by Gandomkar (2013), verify the results and use the model to conduct a parametric study.

3. METHODOLOGY

The Finite Element Modelling software employed for this study was ANSYS 2019 R2. The FE model of Gandomkar et al., (2013) consisted of Peva45 of 0.8 mm thickness as the profiled steel sheet and plywood of thickness 0.8 mm as the dry board with the length of 2400 mm and a width of 795 mm. The connections between the PSS and DB were modelled using springs which gave similar results to the DS-FH 432 self-drilling and self-tapping screws used in physical testing. The springs were placed at 100 mm spacing. The system was supported by a pin support at one end, and a roller support at the other end, both at the bottom flange of the PSS.

In the FEMs, the screws forming the connection between the PSS and DB were modelled as springs with a stiffness value of 610 N/mm. The values to be used for stiffness for the connections were taken directly from a study by Nordin et al 2009).

Murray et al (1997), stated that dynamic modulus of elasticity for steel can be adopted as 210 GPa, which is similar to its static value from BS 5950 Part 4:1994. Therefore, in this study, the dynamic modulus of elasticity for steel was chosen as 210 Gpa. The static modulus of elasticity of plywood was chosen as 7164 Mpa, with reference to the materials available in the local market. The density of Steel and plywood were chosen as 7850 kg/m³ and 600 kg/m³ respectively and were input in Ansys. An example of the screenshot from Ansys is shown in Figure 1 below:

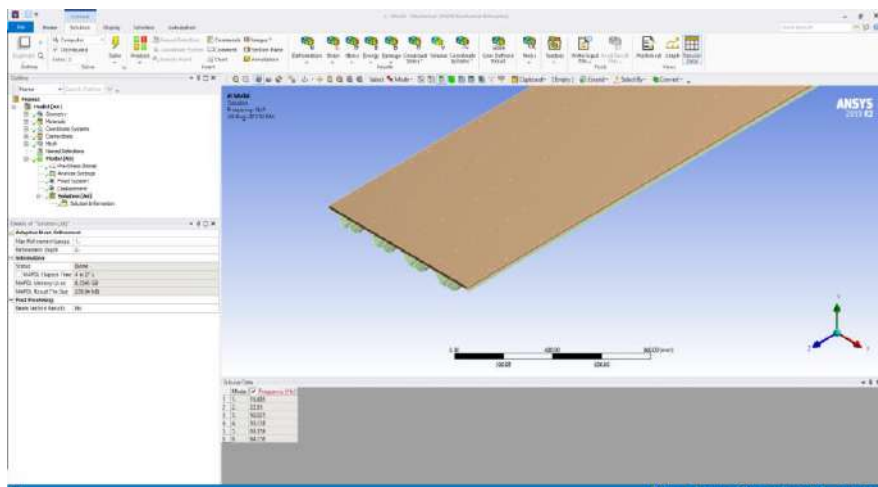


Figure 1: Screenshot from Ansys

4. ANALYSIS AND DISCUSSION

Results of the Verification Study

The result obtained from the Ansys output for the FE model of the experiment is shown in Figure 2 in the next page.

```

***** MODAL MASSES, KINETIC ENERGIES, AND TRANSLATIONAL EFFECTIVE MASSES SUMMARY *****

```

FREQUENCY	MODAL MASS	KENE		EFFECTIVE MASS					
				X-DIR	RATIO%	Y-DIR	RATIO%	Z-DIR	RATIO%
16.69	0.1788E-01	98.26		0.2664E-12	0.00	0.3076E-01	81.50	0.3271E-05	0.01
22.85	0.6161E-02	63.50		0.3229E-05	0.01	0.2309E-08	0.00	0.5144E-13	0.00
50.03	0.6021E-02	297.4		0.2527E-14	0.00	0.8386E-05	0.02	0.9045E-08	0.00
53.14	0.2778E-02	154.8		0.1661E-09	0.00	0.4709E-06	0.00	0.7563E-06	0.00
63.56	0.1122E-01	894.3		0.1440E-08	0.00	0.1007E-10	0.00	0.1407E-04	0.04
84.16	0.5373E-02	751.1		0.3963E-10	0.00	0.1544E-08	0.00	0.5838E-08	0.00

Figure 2: Ansys Solver Output of The Control FEM

The results are compared to the natural frequency form the experimental data as tabulated in Table 1 below:

Table 1: Comparing the Results of the FEM with Experimental Results

Mode No.	Experimental Natural Frequencies (Hz)	Natural Frequencies from FEM (Hz)	Percentage Difference (%)
1	18.8	16.685	11.25%
2	23.1	22.85	1.08%
3	46.9	50.025	6.66%
4	55.0	53.138	3.39%
5	64.4	63.559	1.31%
6	81.3	84.158	3.52%

It can be observed that the FEM that was constructed was able to produce very similar values to the values obtained from the physical experiment conducted by Gandomkar et al. (2013). The FEM was able to predict the natural frequencies of the real life PSSDB system with relative accuracy – within the range of 1%-11%. Therefore, the Finite Element Model can be utilized to obtain the Natural Frequencies of PSSDB systems for the parametric studies.

The small differences between the values of Natural Frequency obtained from the experimental tests and the FEM is likely since Finite element method is an approximate numerical method. Furthermore, the differences could also result from imperfections present in the dry board, profiled steel sheet and screws that were used in the practical tests. The FEM does not account for these imperfections.

Results of the Parametric Study

A sample result obtained from the Ansys output for the FE model of the parametric study is shown in Figure 3 in the next page.

```

***** MODAL MASSES, KINETIC ENERGIES, AND TRANSLATIONAL EFFECTIVE MASSES SUMMARY *****

```

FREQUENCY	MODAL MASS	KENE		X-DIR	RATIO%	EFFECTIVE MASS			RATIO%
						Y-DIR	Z-DIR	RATIO%	
15.89	0.1530E-01	76.24		0.6789E-11	0.00	0.2648E-01	81.56	0.2362E-05	0.01
21.21	0.5294E-02	47.00		0.2412E-05	0.01	0.1745E-07	0.00	0.1372E-11	0.00
46.64	0.5755E-02	247.1		0.9678E-10	0.00	0.6459E-05	0.02	0.1922E-07	0.00
47.55	0.2385E-02	106.5		0.3558E-09	0.00	0.1205E-06	0.00	0.3195E-06	0.00
60.59	0.8155E-02	591.0		0.3352E-07	0.00	0.7970E-08	0.00	0.1026E-04	0.03
76.24	0.4809E-02	551.9		0.5415E-10	0.00	0.9050E-08	0.00	0.6575E-08	0.00

Figure 3: Ansys Solver Output of Sample 1 (DB T= 16 Mm, PSS T= 0.6 Mm)

The complete result of all the parametric study is tabulated in Table 2 below:

Table 2 - Summary of the Parametric Study

Peva 45	Plywood					
	t = 16 mm		t = 18 mm		t = 20 mm	
	FNF (Hz)	PD (%)	FNF (Hz)	PD (%)	FNF (Hz)	PD (%)
t = 0.6 mm	15.891	4.76	15.504	7.08	15.189	8.97
t = 0.8 mm	17.085	2.40	Control sample	Control sample	16.35	2.01
t = 1.0 mm	18.047	8.16	17.646	5.76	17.303	3.70

PD = Percentage of difference compared with control sample

From Table 2 it can be observed that as the thickness of Plywood is increased while maintaining the same thickness of Peva45, the Fundamental Natural Frequency (FNF) of the PSSDB system decreases. For instance, while maintaining the thickness of Peva45 at 0.6 mm, when the thickness of the Plywood was increased from 16 mm to 18 mm, it was observed that the FNF of the system decreased by 2.44 %. Similarly, when the thickness of the Plywood was increased from 18 mm to 20 mm, it was observed that the FNF of the system decreased by 2.03 %. This pattern holds true for all the values obtained.

It can also be observed that when the thickness of Peva45 is increased while maintaining the same thickness for the Plywood, the FNF of the PSSDB system increases. For instance, while maintaining the thickness of plywood at 16 mm, when the thickness of the Peva45 was increased from 0.6 mm to 0.8 mm, it was observed that the FNF of the system increased by 6.99 %. Similarly, when the thickness of the Peva45 was increased from 0.8 mm to 1.0 mm, it was observed that the FNF of the system increased by 5.33 %. This pattern can be observed in all the obtained values. 10

From the above-described pattern, it can be seen that the mass and stiffness of Peva45 and plywood has a direct effect on the Fundamental Natural Frequency experienced by a

particular PSSDB system. The maximum FNF occurred for the maximum tested thickness of Peva45 and minimum tested thickness of plywood. The maximum FNF, 18.047 Hz was observed for the PSSDB system utilizing Peva45 of thickness 1.0 mm and Plywood thickness 16 mm. The minimum FNF occurred for the minimum tested thickness of Peva45 and maximum tested thickness of plywood. The minimum FNF, 15.189 Hz was observed for the PSSDB system utilizing Peva45 of thickness 0.6 mm and Plywood thickness 20 mm.

According to Middleton & Brownjohn, (2010), if the Fundamental Natural Frequencies of a panel is above 10 Hz, it falls in the category of High Fundamental Frequency (HFF) and the panel is considered as comfortable for the users. All the samples tested in this paper experienced a Fundamental Natural Frequency well above 10 Hz. Therefore, all the tested samples fall under the HFF category and are therefore comfortable to the users.

The thickness of the Peva45 and plywood can be varied to obtain an increase in the maximum FNF of 15.84%. In this case it is an increase from 15.189 Hz at the lowest end of FNF to an FNF of 18.047 Hz at the highest end. The observations made and conclusions arrived at in this chapter are quite similar to the observations made by Gandomkar et al., (2013).

5. CONCLUSION

The validity of the Finite Element Model was achieved by comparing its results with the experimental data. The Percentage Difference (PD) between the Experimental Natural Frequencies by Gandomkar et al., (2013) and the Natural Frequencies from the FEM. The maximum value obtained for the percentage difference was just 11.25%, which is within the acceptable limit. Therefore, the FEM was able to predict the natural frequencies of the experimental PSSDB floor system with good accuracy.

For the parametric study, variations in the thickness of both the Peva45 and Plywood was made to study the impact of these variations on the Fundamental Natural Frequencies of the PSSDB floor system. A total of 8 samples were tested for the parametric study. The results of the parametric study showed that the maximum FNF occurred for the maximum tested thickness of Peva45 and minimum tested thickness of plywood and that the minimum FNF occurred for the minimum tested thickness of Peva45 and maximum tested thickness of plywood. These observations are similar to the observations made by other researchers, namely Gandomkar et al., (2013), further proving the validity of the results obtained in this study.

REFERENCES

- Ansys Inc. 2020. Structural analysis for every application and experience level. *Ansys.com*. Retrieved January 23, 2020, from <https://www.ansys.com/products/structures>.
- Ehsan, A. and Wan Badaruzzaman W.H., 2013. Vibration performance of Profiled Steel Sheet Dry Board composite floor panel. *KSCE Journal of Civil Engineering*. 17(1), 133-138.
- Gandomkar F.A., 2013. Dynamic response of low frequency Profiled Steel Sheet Dry Board

- (PSSDB) floor system, *Latin American Journal of Solids and Structures*, 10, 1135-1154. 12
- Gandomkar F.A., Wan Badaruzzaman W.H., Osman S.A., and Ismail A. 2013. Experimental and numerical investigation of the natural frequencies of the composite profiled steel sheet dry board (PSSDB) system, *Journal of The South African Institution of Civil Engineering*, 55, 11–21.
- IFRC/RCS 2013. Post-disaster shelter: Ten designs, *International Federation of Red Cross and Red Crescent Societies*, Geneva.
- Middleton, C.J and Brownjohn, J.W.W., 2010. Response of high frequency floors: A literature review. *Engineering Structures*, 32(2): 337–352.
- Murray M. M., Allen D. E. and Ungar E. E., 1997. *Floor vibration due to human activity*, AISC: 11th Steel Design Guide Series, Chicago, US
- Nordin N., Wan Badaruzzaman W. H., and Awang H. 2009. Connector stiffness of ‘Peva-Cemboard’ screwed connection in Profiled Steel Sheet Dry Board (PSSDB) panel. *Proceedings*, 5th International Conference on Construction in the 21st Century (CITC-V), “Collaboration and Integration in Engineering Management and Technology”, Istanbul, Turkey, 1476–1482.
- Samir, M., Wan Badaruzzaman, W. H., and Baharom, S., and Hilo, S.J., 2017. Theoretical and finite element analysis of the two-way PSSDB floor system. *Journal of Constructional Steel Research*. 135, 10.1016/j.jcsr.2017.04.006.
- United States Geological Survey, 2020. How can climate change affect natural disasters? usgs.gov, Retrieved January 25, 2020, from https://www.usgs.gov/faqs/how-can-climate-change-affect-natural-disasters-1?qt-news_science_products=3#qt-news_science_products.
- Wan Badaruzzaman ,W.H. and Wright H.D., 1998. Lightweight Thin Walled Profiled Steel Sheeting Dryboard (PSSDB) Composite Floor System. *Thin-Walled Structures: Research and Development*, 355-365.
- Wright H.D. and Evans H.R. 1994. Profiled Steel Sheet Dry Board Construction. *New Steel Construction*, 2:6, 20.

EXPERIMENTAL STUDIES ON CONCRETE UTILISING RED MUD AS A PARTIAL REPLACEMENT FOR CEMENT WITH SUGAR CANE FIBRE

Abdullah Alkurshumi, Mohd Nizam Shakimon, Mohamad Ayob & Zulhazmee Bakri
Infrastructure University Kuala Lumpur

1. INTRODUCTION

Much research has been performed to improve concrete strength and make it a sustainable construction material. The previous research includes investigating waste's effect as a partial replacement in the concrete mix. One of the wastes is red mud. Red mud is a waste material generated by the Bayer process, commonly used worldwide to create bauxite alumina [1]. The Bayer process for alumina production from Bauxite ore is characterised by low energy efficiency. It produces significant amounts of dust-like, high-alkalinity bauxite residues known as red mud [2, 3]. Red mud is the most significant industrial waste generated during alumina production. With the rapid growth of aluminium output in recent years, the discharge amount of red mud has increased accordingly. About 120,000,000-ton red mud is discharged globally every year [9]. Because of red mud's complex physical-chemical properties, it is a very challenging task for the designers to find out the economical utilisation and safe disposal of red mud [21, 22]. Disposal of this waste was the first major problem encountered by the alumina industry after adopting the Bayer process [7]. Some notable incidents, back in August 2016, after a waste pond dam collapsed, two towns in the Henan Province of China were covered with red mud, releasing 2 million m³ of aluminium by-products. The toxic waste pond is situated in Dahegou Village, which about 300 individuals call home in Henan's Luoyang. The lining wall broke, and silt mixed with stones swept down the mountainside, drowning the village. The red mud has engulfed many farm and domestic animals despite no recorded deaths. Over 400 individuals have been evacuated. A similar incident occurred in Hungary on October 4 2010, in which a waste pond containing red mud collapsed in Ajka City, killing ten individuals, while 150 others suffered severe chemical burns. The toxic material also destroyed all life in the nearby river [1].

Furthermore, bauxite mining in Malaysia has caused pollution around Bukit Goh, Gebeng and the port of Kuantan. Some district areas, particularly Bukit Goh, have suffered for months due to significant air pollution caused by bauxite dust and residue generated by processing plants or leaked during transport to Kuantan Port. The roads and the rivers were affected by pollution due to heavy rain showers, and the bauxite residue flowed out to the sea. It was previously reported that local citizens were earlier alarmed by the colour of the ocean turning red [1].

The previous study on the possibility of using red mud as a partial replacement for cement shows that 5% is the optimum value before the concrete compressive and tensile strength decreases [20, 23, 24, 28]. However, adding 5% hydrated lime to the concrete mix increased the optimum percentage of red mud replacement to 15% [2, 16]. The concrete mix with a higher

percentage of red mud replacement reduces the cement but increases the concrete workability [2].

Bagasse fibre is another waste and can be used as a natural binder in the concrete mix to improve its tensile strength. Bagasse fibre is a by-product of the sugarcane industry whose role is sugar, rum or biofuel production [6, 8, 12, 14]. Previous research shows that increasing sugarcane bagasse fibre percentage in the concrete mix decreases its compressive strength, but the tensile strength increases [12]. Fibres are tiny pieces of reinforcing material that has specific properties and features. Fibres are a construction material for enhancing flexural and tensile strength and a binder that combines Portland cement with cement matrices. The idea of utilising fibres as reinforcement is not new. Asbestos fibres were used in concrete during the 1900s. However, asbestos use has been discouraged owing to health risk detection. Later in 1963, Romualdi and Botson released their article on Fibre-reinforced Concrete (FRC). Asbestos was substituted by new concrete materials such as steel, glass and synthetic fibres. Research on this technology is still in progress. Fibre Reinforced Concrete (FRC) is a preferable construction engineering headway [8].

In this study, the investigation is made on the concrete performance in compression strength and tensile strength with different percentages of the red mud partially replacing the cement and a constant percentage of sugarcane bagasse fibre as an additive in the concrete mix. Finally, the optimum percentage of red mud is proposed.

2. EXPERIMENTAL PROGRAMME

Seventy-two (72) concrete samples (Figure 1 and Figure 2) were prepared, comprising thirty-six (36) concrete samples for each compression and tensile test. A concrete mix design using grade C25 is used. Six (6) by weight percentages of 0%, 5%, 10%, 15%, 20%, and 25% were proposed to replace cement with red mud. A constant 2% sugarcane bagasse fibre measured by volume was added as a binder. Table 1 shows the details of the concrete samples.

Table 1: Concrete samples with different percentages of red mud.

Sample	Red mud %	Sugarcane %	No. Of Cubes	No. Of Cylinder
CS	0	0	6	6
S1	5	2	6	6
S2	10	2	6	6
S3	15	2	6	6
S4	20	2	6	6
S5	25	2	6	6



(a)



(b)

Figure 1: Concrete samples (a) Concrete cylinder (b) concrete cube

Material preparation for red mud

The Bayer process for the production of alumina from bauxite ore is characterised by low energy efficiency, and it results in the production of significant amounts of dust-like, high-alkalinity bauxite residues known as red mud. The red mud was dried and crushed, finally sieved to produce the uniform red mud powder that only passed through a 1.18mm sieve.

Material preparation for sugarcane bagasse fibre

The sugarcane bagasse fibre (Figure 2) was collected from the nearby hawkers. The volume of the sugarcane bagasse fibre was 2%, cut to 100mm -150mm in length, cleaned and treated in clean water for 24 hours to remove the impurities, and finally dried before adding into the concrete mix.



Figure 2: Sugarcane bagasse fibre

Slump test

The test setup is shown in Figure 3. The test procedures were according to BS EN 12350-1:2009. The steel slump cone was placed on a solid, impermeable, level base and filled with fresh concrete in three equal layers. Each concrete layer was tamped for 25 strokes, with the tamping rod should penetrate the underlying layer. The concrete was then levelled to the top

surface of the cone. Finally, the cone was lifted, leaving a heap of concrete settled or slumped. The upturned slump cone was placed next to the concrete to measure the collapse difference between the concrete and the cone.



Figure 3: Slump test setup and procedure.

The results of the slump test are shown in Table 2. The higher the percentage of red mud replacement, the higher the slump values, which means the workability increase. Hence, it can be deduced that the more red mud replaces the cement, the workability of fresh concrete increases. All concrete samples show slump values of more than 60mm. The standard or high-quality slump is where the slump is between 30 - 60 mm. Therefore, the concrete samples did not achieve the slump value specified. The possible factor was that the fine and coarse aggregates used in the concrete mix were uncovered outdoors, thus exposed to rain, which then affected the water-cement ratio of the wet concrete. The higher water content reduces the strength of the concrete. The type of concrete produced in this research is a true slump with a medium degree of workability.

Table 2: Concrete samples slump values.

No.	Types of Concrete	Slump Value (mm)	Degree of Workability
CS	Control sample	62	Medium
S1	Sample 1 (5% Red mud and 2% sugarcane fibre)	60	Medium
S2	Sample 2 (10% Red mud and 2% sugarcane fibre)	65	Medium
S3	Sample 3 (15% Red mud and 2% sugarcane fibre)	69	Medium

S4	Sample 4 (20% Red mud and 2% sugarcane fibre)	72	Medium
S5	Sample 5 (25% Red mud and 2% sugarcane fibre)	76	Medium

Compression test

The test setup is shown in Figure 4. The test procedures were according to BS EN 12390-3:2009. A total of 36 concrete cube samples of size 150 mm x 150 mm x 150 mm were prepared with the red mud percentage replacement of 0%, 5%, 10%, 15%, 20% and 25% by its weight and 2% of sugarcane bagasse fibre added to the concrete mix by the concrete volume. The concrete cube samples were cured in water for 7 and 28 days before the compression test. The compression strength of the concrete cube samples was calculated by:

$$\sigma_c = \frac{P}{A} \quad (1)$$

where σ_c is the compression strength, P is the applied compression load, and A is the cross-sectional area of the concrete cube sample.



Figure 4: Compression test setup and the instrumentation.

The observed damage of samples after the compression test is shown in Figure 5. The average value of the maximum compression strength was measured after the compression test. The highest compression strength is from concrete cube sample S2, which measures 26.6 N/mm² on day 7 and 32.8 N/mm² on day 28. The values are higher than the concrete cube sample without red mud and sugarcane bagasse fibre replacement. The average compression strength values on day 7 and day 28 are shown in Figure 6 and Figure 7. The concrete achieves strength maturity on day 28. It can be seen that only concrete cube sample S5 with 25% red mud

replacement shows average compression strength below the target value set in the concrete mix design. The average compression strength value shows an increment with the red mud replacement percentage of up to 10%, and a further increase in the replacement percentage shows the decline of the average compression strength.



Figure 5: The damaged concrete cube samples after the compression test.

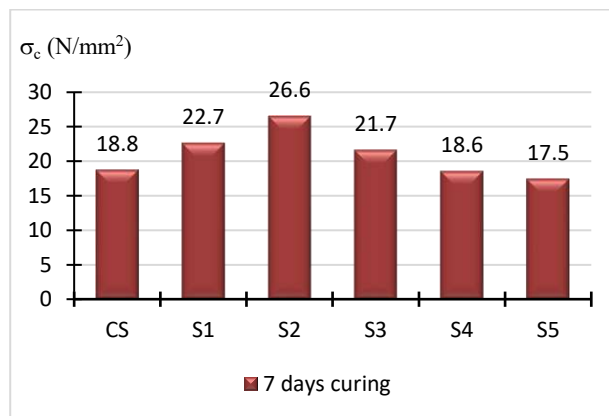


Figure 6: The average compression strength on day 7

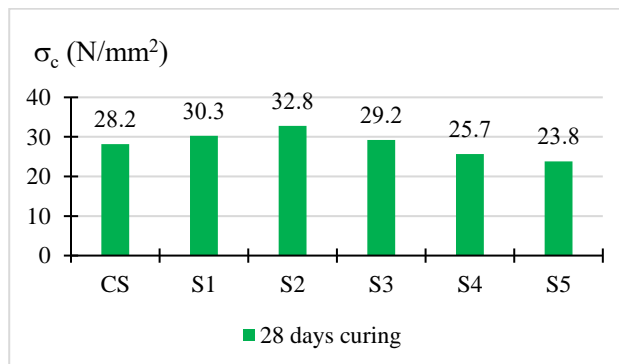


Figure 7: The average compression strength on day 28.

Tensile test

The test setup is shown in Figure 8. A total of 36 concrete cylinder samples 150 mm in diameter and 300 mm in length were prepared for the test with the red mud percentage replacement of 0%, 5%, 10%, 15%, 20% and 25% by its weight and 2% of sugarcane bagasse fibre added to the concrete mix by the concrete volume. The concrete cylinder samples were cured in water for 7 and 28 days before the tensile test. The test procedures were according to BS EN 12390-5:2009. The tensile strength of concrete cylinder samples was obtained by applying a compressive force along the length of the concrete cylinder samples. The concrete cylinder tensile strength was calculated by:

$$\sigma_t = \frac{2P}{\pi ld} \quad (2)$$

where σ_t is the split tensile strength of the concrete cylinder in N/mm^2 , P is the applied compression load, l is the length of the concrete cylinder, and d is the diameter of the concrete cylinder.

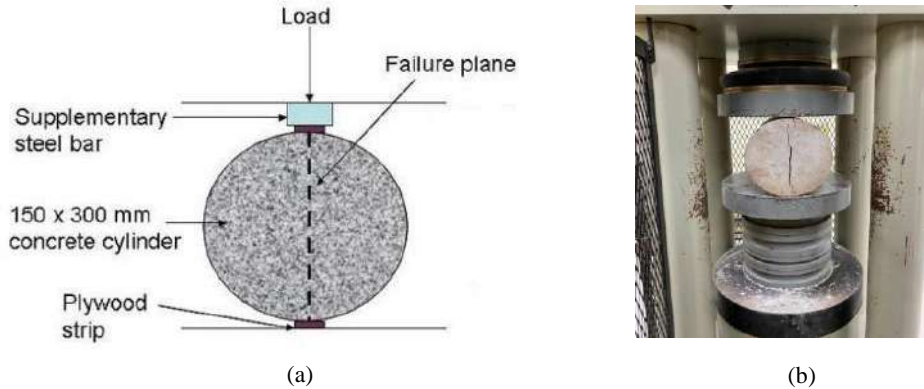


Figure 8: Test setup for split tensile test and instrumentation (a) schematic (b) experimental.

The observed damage of samples after the compression test is shown in Figure 9. The average value of the maximum tensile strength was measured after the split tensile test. The highest tensile strength is from concrete cube sample S2, which measures 7 N/mm^2 on day 7 and 9.8 N/mm^2 on day 28. The values are higher than the concrete cube sample without red mud and sugarcane bagasse fibre replacement. The average tensile strength values on day 7 and day 28 are shown in Figure 6 and Figure 7. The concrete achieves strength maturity on day 28. The average tensile strength value shows an increment with the red mud replacement percentage of up to 10%, and a further increase in the replacement percentage decreases the average tensile strength.



Figure 9: The damaged concrete cylinder after the split tensile test.

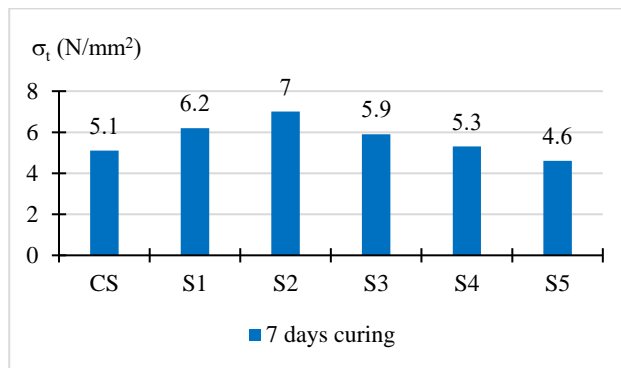


Figure 10: Average tensile strength on day 7.

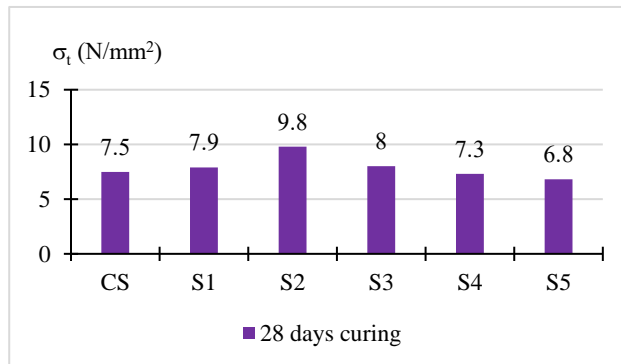


Figure 11: Average tensile strength on day 28

3. CONCLUSION

The main conclusions of this research are summarised below:

1. Experimental results from the slump test show that all concrete mix recorded slump below 60mm. The possibility factor was that the fine and coarse aggregates were not uncovered outdoors, thus, exposing them to rain and increasing the moisture content.
2. The concrete cube sample with 10% red mud replacement and a constant 2% sugarcane bagasse fibre as an additive recorded the highest average compression strength. However, a further increase above 10% in red mud replacement decreases the concrete cube samples' concrete strength.
3. The concrete cylinder sample with 10% red mud replacement and a constant 2% sugarcane bagasse fibre recorded the highest average tensile strength. However, further increases above 10% in red mud replacement decrease the tensile strength of the concrete cylinder.
4. The optimum percentage of red mud to replace cement is 10%.

REFERENCES

- [1] Abdullah, N. I. 2016. Bauxite mining's unhealthy effects on people, environment. Retrieved from <https://www.malaysiakini.com/letters/326807>.
- [2] Ashok, P., & Sureshkumar, M. P. 2014. Experimental studies on concrete utilising red mud as a partial replacement of cement with hydrated lime. *J. Mech. Civil Eng: London*.
- [3] Chandra, S. 1996. *Waste materials used in concrete manufacturing*. Elsevier: London.
- [4] D. Govindarajan and G. Jayalakshmi. 2014. *Microstructure studies of calcined sugarcane bagasse ash*, *Advances in Applied Science Research: New York*.
- [7] Deepika, K., Ananthakumar, S., & Mariadoss, R. 2007. *Experimental Investigation of Concrete by Red mud as Replacement of Cement and Using Strengthening Admixture*. *International Journal of Innovative Research in Science, Engineering and Technology: Brussels*.
- [8] *Fibre Reinforced Concrete - Types, Properties and Advantages*. 2017. Retrieved from <https://theconstructor.org/concrete/fibre-reinforced-concrete/150/>.
- [9] Gowsalya. R & Bhagyalakshmi. A. 2015. *Experimental Study on Partial Replacement of Cement by Red mud*. *IJERT International Journal of Engineering Research & Technology: Brussels*.
- [10] Khalid, F. S., Herman, H. S., & Azmi, N. B. 2017. *Properties of Sugarcane Fibre on the Strength of the Normal and Lightweight Concrete*. In *MATEC Web of Conferences: Les Ulis*.
- [11] M.S. Frías, E. Villar-Cocina and E. Valencia-Morales. 2017. *Characterisation of sugar cane straw waste as pozzolanic material for construction: Calcining temperature and kinetic parameters*, *Waste Management: Amsterdam*.
- [12] Mahin Sha O B, Remya C P, Salja P A & Shifal K S. 2016. *Red mud Concrete*. *IRJET International Research Journal of Engineering and Technology: Brussels*.
- [13] Metilda, D. L., Selvamony, C., Anandakumar, R., & Seenii, A. 2015. *Investigations on*

- optimum possibility of replacing cement partially by redmud in concrete. Scientific Research and Essays: Sapele.
- [14] P. Syam Sai & Chandana Sukesh. 2017. Strength Properties of Concrete by Using Red mud as A Replacement of Cement with Hydrated Lime. IJCIET International Journal of Civil Engineering and Technology: Brussels.
- [15] Patel, S., & Pal, B. K. 2015. Current status of an industrial waste: red mud an overview. Ijltemas: Delhi.
- [16] Portland Cement: A Brief History. 2014. Retrieved from <http://www.screedscientist.com/portland-cement-a-brief-history/>.
- [17] Rathod, R. R., Suryawanshi, N. T., & Memade, P. D. 2013. Evaluation of the properties of red mud concrete. IOSR Journal of Mechanical and Civil Engineering: New York.
- [18] Red mud – addressing the problem. 2016. Retrieved from <https://aluminiuminsider.com/red-mud-addressing-the-problem/>.
- [19] Sawant, A. B., Kumthekar, M. B., & Sawant, S. G. 2013. Utilisation of neutralised red mud (industrial waste) in concrete. Int. J. Inventive Eng. Sci.(IJIES): Madhya Pradesh.
- [20] Sawant, A. B., Kumthekar, M. B., Diwan, V. V., & Hiraskar, K. G. (2012). Experimental study on Partial replacement of cement by neutralised red mud in concrete. Int. J. Eng. Adv. Technol: Madhya Pradesh.
- [21] Sithar Pateliya & Chetan Solanki. 2017. Experimental studies on concrete utilising red mud as a partial replacement of cement. IJARIE International Journal of Advance Research and Innovative Ideas in Education: Gujarat.
- [22] Sonasath, M. (2014, October 21). Fibre Reinforced Concrete. Retrieved from <https://www.slideshare.net/mustafasonasath/fibre-reinforced-concrete-40540346>
- [23] Sunitha M.Pujar, D. K. B. P. 1INTRODUCTION. Retrieved from <https://www.ijser.org/paper/Effect-of-Replacement-of-Cement-by-Red-mud-on-the-Properties-of-Concrete.html>.
- [24] Tang, L. 2014. Study of the possibilities of using Red mud as an additive in concrete and grout mortar. Svensk Kärnbränslehantering AB Swedish Nuclear Fuel and Waste Management Co: Solna.

COMPRESSIVE STRENGTH AND WATER ABSORPTIONS OF CEMENTITIOUS GROUT CONTAINING TREATED PALM OIL FUEL ASH (POFA)

Mohamed Emierul, Megat Azmi, Mohd Nasir Hussin & Norhaiza Nordin
Infrastructure University Kuala Lumpur

1. INTRODUCTION

In Malaysia, the palm oil industry has been one of the most important contributors to the economy of the country. In 2015, the amount of palm oil production has peaked to a new level. As one of the biggest procedures of palm oil, Malaysia has been an active member of the council of Palm Oil Producing Countries (CPOC) (MPOB, 2015).



Figure 1: Fruit Bunche

POFA in raw state came from some collection of waste that being treat from palm trees. Figure 1 shows one of the waste that being collected from the tress that weren't in used. According to MPOB (2015), there were many concerns that are related to the impact of palm oil to the environment. One of them is sustainability. The article stated that the palm oil plantation which utilizes large quantities of fertilizers and pesticides is not sustainable. In this case, there are many attempts that have been tried to modify the waste in order to put them into use and to reduce their quantity. Besides that, the table also shows the expected 5 years average of the production. Form the calculation, by the end of 2020 Malaysia still contributes about 37.7 % of the world total palm oil production. Hence, there seems to be decreasing trend of the country's contribution towards world total palm oil production. This is due to the significant increase in production by Indonesia and others countries. Nonetheless, the annual production of palm oil by Malaysia is still on the increasing trend.

Through the rapid rises on the usage of palm oil in Malaysia. The amounts of POFA produced are uncontrollable. Day by days, the consumers are worried on how to manage the production of it. POFA in chapter has confirmed the present of pozzolanic substance which can

leads to the usage as a partial replacement on the mixture of grout. The demand of grout in other hand has increased in the construction industry. Since the cost of material producing it is high, an idea of replacing the cement with waste materials reduces the cost of producing grout materials was applied. Throughout the chapter, a full potential of POFA as the replacement will be tested in order to minimize the problems due to cost. A full examination on the properties of the grout with POFA alone could show the potential of the POFA to become one of the replacements of the cement. Grout act as a filler in many applications in the construction industry.

Earlier cahpter has shown that POFA has potential pozzolanic property to be used as concrete material (Tay, 1990). In addition, Megat Johari et al., (2012) reported that the reactivity and efficiency of the POFA as a pozzolanic material can be improved significantly by subjecting the POFA to series of treatment processes involving drying, seieving, grinding, heating and regrinding. The resulting POFA was able to be used at a replacement level of up to 60% in high strength concrete, yet comparable and better properties of concrete were continued. Mujah (2015) state that the purposes of ordinary Portland cement were categorized as a cementitious material. The available of ground POFA was used as pozzolan while river sand used as the fine aggregates. Differ from this chapter, the mixture of grout the usage of the sand has not been used. According to Tay & Show (1995) the chapter was made on the POFA as the replacement of the cement in a mixture. The chapter was on the changes of densities and water absorptions of the mixture when the ashes were added were insignificant. The results also reveal the improvement of workability of the mixture when the ashes being added. From Megat Johari et al., (2012) chapter on the chemical and physical composition of the POFA gives a clear view on the potential of POFA to become one of partial replacement of cement in a mixture. Besides that, the chapter sees that according to ASTM C 6128, POFA can be classified as a mineral admixtures Class F.

Based on the study of Tangchirapat et al., (2012), for strength, sulphate resistance and water permeability, the ground palm oil fuel ash characters have improved all the parameters due to high amount of recycled concrete aggregates. Farhan (2015), chapters on the application of grout through the post tension application. The range of up to 30% replacement gives a various potential results of the POFA. The aim of the chapter were completed when the strength of the desire were achieved. Through bigger size of surface of UPOFA helps on acting as a transport agent that fills the void that required in the post tension.

The physical properties and the chemical properties are the influence of the entire properties of the mixture. According Tangchirapat et al., (2007), the fineness of palm oil fuel ash influences the strength of the mixture. The chapter was based on the palm oil fuel ash as the supplementary cementations material to produce a high strength concrete. The chemical reaction between the materials is the properties that revile the potential of the material to become one of the cement replacements. If the materials possess the potential of pozzolanic reaction aspect, it could highly use in the mixture of grout. According to Hewlett (2006), the chapter on the chemical reaction of pozzolan materials were conclusive with the reaction of it improves the properties of the cement grout. From the strength to others, the reaction did increase the quality of the cement.

Curing process is one of the ways to increase the strength of the mixture. The development of pozzolanic material through the chemical reactions is much slower compare to the ordinary Portland cement reaction. POFA in other hand is one of the waste material that possess a pozzolanic characteristics. Similar to the OPC the reaction chain was based to the hydration process. By combining the OPC and the POFA, the reaction between the materials are prescribe in the chemical chain that gives the optimum standard that were requires.

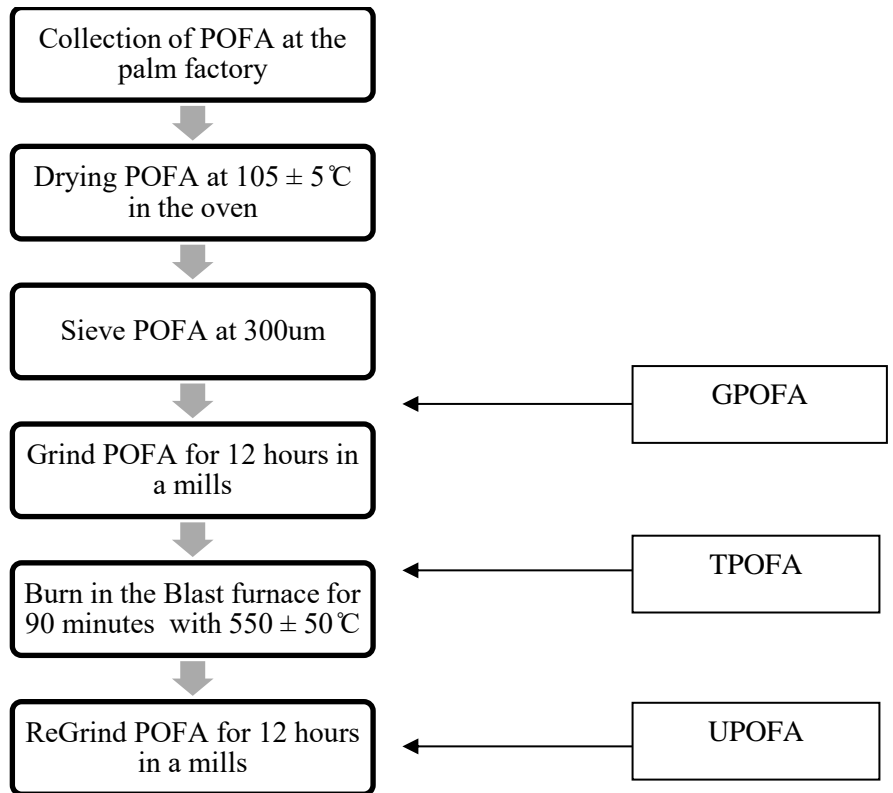
2. METHODOLOGY

In any production of grout, the most important material required is cement. The cement used is Ordinary Portland Cement (OPC). The specification of the cement was based on the standard that was set up by the ASTM.

Preparation of POFA

Palm oil fuel ash (POFA) is another important material used in this chapter as it was utilized as a supplementary cementitious material. The POFA was obtained from a palm oil mill located in Nibong Tebal. The collected POFA was first subjected to a treatment process to improve its reactivity and to obtain a uniform material.

In brief, the process involved drying of the POFA at $105 \pm 5^\circ\text{C}$ in an electric oven for 24 hours to remove moisture. The dried POFA was then subjected to a screening process where only materials passing 30 μm sieve was further treated. Subsequently, the sieved POFA was grind for 12 hours in a ball mill. Several trial mixes were done in order to determine the suitable water/binder ratio of the mixtures. According to Rosquoet et al., (2003) the suitable range is between 0.3-0.5. Through a series of flow cone tests to check the fluidity of the grout, a ratio of 0.4 was found to give promising results that satisfy flow requirements. Superplasticizer is an admixtures added in a grout mixture in order to increase the fluidity of the mixture. The content used is 2.0 % from the total binder content. The type superplastizer used is Glenium ACE 393. Throughout the treatments, few steps need to be done in order to achieve the final result of treated POFA (TPOFA).



The next step was burning the POFA at $550 \pm 50^\circ\text{C}$ in a gas furnace. The result as in the figure 3.3. This is to remove excess unburnt carbon. Lastly the POFA was again grind in a ball mill for 12 hours to obtain the ultrafine POFA and also to ensure the uniformity and consistency of the ultrafine POFA



Figure 2: Blast furnace burning for 90 minutes

The POFA then will be burn in the blast furnace for 90minutes with controlled temperature of 550 + 50°C. The results as in the Figure 2. At this stage, the burning process will remove the excessive unburned carbon in POFA. Then the POFA were regrinding in order to obtain ultrafine POFA and also to ensure the uniformity and consistency of the ultrafine POFA. The mixture starts with 4 batches. The OPC controlled (0% POFA replacement), OPC 20 (20% POFA replacement), OPC 40(40% POFA replacement) and OPC 60 (60% POFA replacement).

Mix Proportions

The exact amount and ration of every material need to be accurately calculated to achieve the standard. Below Table 1 shows the overall design mix proportions of the entire projects. The ratio was based on the calculation design of the materials.

Table 1 The Mix Proportions of Cement Grout

NO	Mix	0.0185 m ³ (kg)			
		OPC	POFA	WATER	SUPERPLASTICISER
1	Controlled	28	0	12.88	0.28
2	OPC with 20% POFA	22.4	5.6	12.88	0.28
3	OPC with 40% POFA	16.8	11.2	12.88	0.28
4	OPC with 60% POFA	11.2	16.8	12.88	0.28
TOTAL		78.4	34	51.52	1.12

Casting

For this chapter, the cubes of 50 mm × 50 mm were used in the testing of compressive strength. For the Porosity and Water Absorptions tests, the PVC pipes of 50 mm were used as a mould. The cubes of 100 mm × 100 mm were used for the permeability test of hybrid grout.

Curing

All the specimens were cured in the curing pond which fills with water for 7 days, 14 days and 28 days until the day of testing.

Testing Procedure

All the testing was done based on the standard that being used. The Testing were categories in two sections, which is the properties and also the application section.

Water Absorptions

The procedure of porosity was taken from RILEM CP 113 (1984). As soon as the mould being opened and cured. The specimen needs to be oven dried for 24 hours, in order to lose all the moisture in the specimen. All the specimens were inserted into the vacuum and leave it for 3 hours. The vacuum then was filled with water and let the entire specimen submerged for 3 hours. For the last steps of the procedure, the vacuum was turn off and leave the specimen to cool done in the vacuum.

Compressive Strength Test

This test was done according to the ASTM C109/C109M which standard is Standard Test Method for Compressive Strength of Hydraulic Cement Mortar using 50 mm by 50 mm specimens. The compression machine 3000 kN was used.

The compressive strength of the grout mixture can be written as Equation 3.1 below:

$$\text{Compressive Stregth, } f_m = \frac{F}{A} \quad (1)$$

Where,

F = Maximum Load (N)

A= Area of loaded surface (mm^2)

f_m = Compressive Strength (MPa)

3. RESULTS AND DISCUSSION

The effect of POFA was clearly stated in this chapter. The results obtained show the potential of the POFA to become of the cement replacement in grout.

Fresh grout test

There were two tests that required testing directly after the mixing of the grout completed.

Water Absorptions

Water absorptions properties are much related to the porosity test. This is because in porosity testing, the results came out on how much percentage that the gas can go through pore that exist through mixing of materials. This property is very important to know how much the grout could restrain water from entering. The water entering inside the grout could reduce the strength and ages of the grout itself. Figure 3 shows the results that obtain through the water absorptions testing.

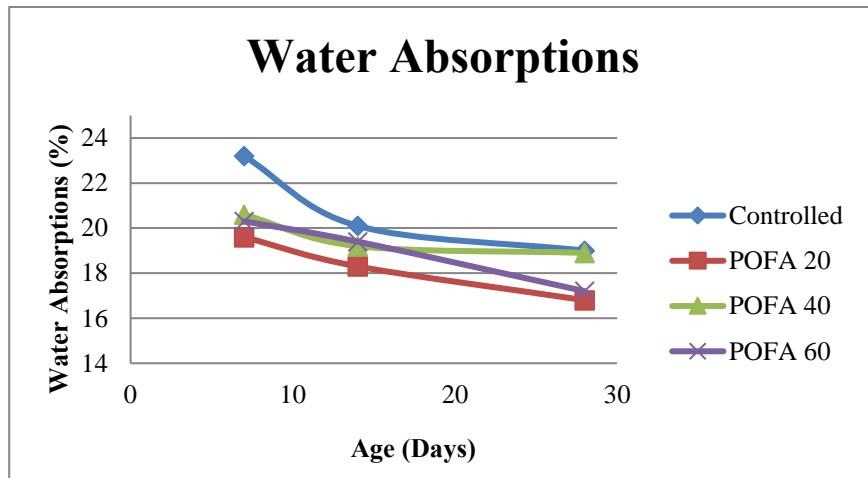


Figure 3: Graph of Water Absorptions of the Grout Mixtures

The declining graph trend gives promising results which the water absorption rate should be decreasing. Controlled mix start out to be a bit lower compare to POFA40 but through ages the controlled results seems to shown a highest rate of water absorptions. This is obviously due to size of surface area of the materials. The higher the surface area, the stronger the materials shall act as a bonding agent filling out to the voids. Hence decreases the rate of water absorptions. POFA 60 as expected turn out to be the most effective for the water absorptions due to its high surface area. With only 17.2% at the age of 28, the rate shows the lowest comparing to the other mixtures.

Compressive Test

For the application section, the starter bar that often used in the construction industry was evaluated. One of the tests that were run is the compressive test. The result recorded was tabulated in the table and the graphical at this section. Table 2 is a set of result recorded for the compressive strength of hybrid concrete at the age of 28days

Table 2: Compressive Strength results

Mix	Age	Average Compression Strength (N/mm^2)
Full Concrete	28 Days	41.3
Concrete/Controlled	28 Days	47.1
Concrete/POFA 20	28 Days	49.1
Concrete /POFA 40	28 Days	50
Concrete/POFA 60	28 Days	46.4

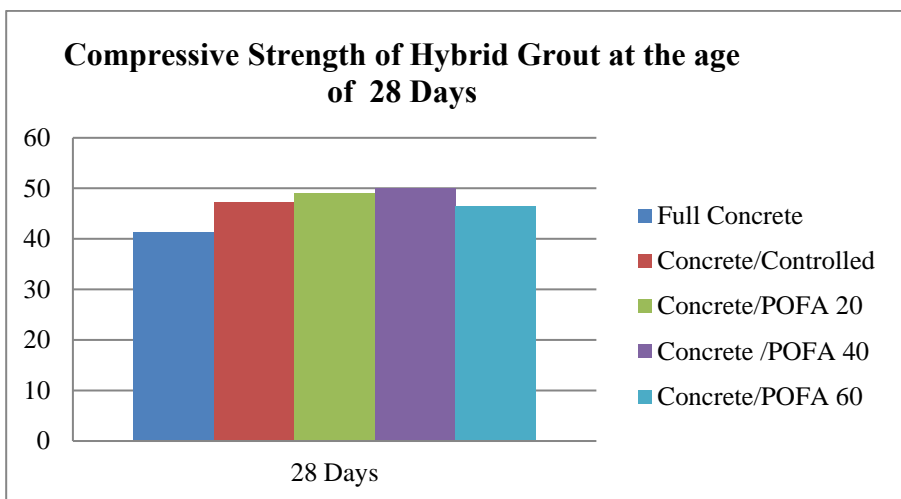


Figure 4: Graphical results of compressive strength of Hybrid Grout at the age of 28 days.

According to the graphical result in Figure 4.11, It shows that the compressive strength of hybrid grout with concrete. The aim of the test is to determine the actual application that could occur in the construction industry. Through this test, an actual strength of the hybrid grout can be known. The simple application of newly fresh grout that contains POFA inserted into cored parent concrete with reinforcement bar.

Influence of Fineness of Particles in the Grout Properties

The treated POFA possess the higher fineness compare to the OPC. The more increase of fineness, the higher the surface area. Thus, the contact between the particles increases due to the surface area. The interlock between the materials are fully utilized since the fineness of the materials increase. The increment affects most of the properties of the mixture. Through many applications that were done at the construction industry, the usage of POFA has highly exposed to its potential. According to Tangchirapat, C. (2007), chapters on the POFA potential in

concrete. The research states that the fineness of the POFA does influence the strength of the mixture.

4. CONCLUSION

The potential of POFA was tested by applying all the necessary steps and treatment to active the treated ultrafine POFA. The potential of POFA as a partial replacement to the cement were investigate up to 60% of replacement. The POFA were going through treatment that recommended in order achieving the fineness that could give advantages to the POFA in the mixture of grout. In strength, POFA inclusion mix shows a slow increment at the early age. The fineness of the POFA does give affect and shows at the longer ages of curing at 28 days.

REFERENCES

- Altwair, N., Johari, M.A. M. & hashim, S.S. (2014). Influence of treated palm oil fuel ash on compressive properties and chloride resistance of engineered cementitious composites. *Materials and Structures.*, 47, 667-682
- Asmawati, N. (2015) CPOPC *Satukan negara pengeluar kelapa sawit*, 5 December 2015, Available from :Berita Harian Online
- ASTM Standard (2007) *C109/C109M Standard Test method for Compressive Strength of Hydraulic Cement Mortar using 50mm Cube specimens*. West Conshohocken, PA: ASTM International.
- ASTM Standard (2003) C125-03, *Standard Terminology Relating to Concrete and Concrete Aggregates*. West Conshohocken, PA: ASTM International.
- ASTM Standard (1988) C618, *Standard Specification for Fly Ash and Raw or Calcined Natural Pozzolan Use as Mineral Admixture in Portland Cement Concrete*. West Conshohocken, PA: ASTM International.
- ASTM Standard (2009) C940 -98a, *Standards Test Method for Expansion and Bleeding of Freshly Mixed Grout*. West Conshohocken, PA: ASTM International.
- ASTM Standard (2003) C939-02, *Standard Test Method for Flow for Preplaced Aggregate Concrete (Flow Cone Method)*. West Conshohocken, PA: ASTM International.
- ASTM C 6128, *Standard Specification for Coal Fly Ash and Raw Calcined Natural Pozzolan for Use In Concrete*. West Conshohocken, PA: ASTM International.
- ASTM 900, *Standard Test Method for Pullout Strength of Hardened Concrete*. West Conshohocken, PA: ASTM International.
- Babatunde, A.S., Megat Johari, M.A., Zainal, A.A., & Mohammad, M. (2015). Impact of added water and superplasticizer on early compressive strength of selected mixtures of palm oil fuel ash based engineered geopolymer composites. *Construction and Building Materials*, 109, 198-206
- British Standards Institution. (1983). BS 1881-114: 1983 *Methods for Determination of Denisty of Hardened Concrete*. London: BSI
- British Standard Institution (2007). BS 445 *Grout for Prestressing Tendons. Test Methods*.

London: BSI

- Bruce, A. & Jeffery L. (1991). Designing grout mixes: tested, custom-designed grout mixes provide consistent quality.
- Cabrera , J.G. & Lynsdale C.J. (1988). A new gas permeameter for measuring the permeability of mortar and concrete. *Management Concrete Research*, 40, 77-82
- Concrete Network (2016). Post-Tensioned cable in beam images. Available:<
<http://www.concrtenetwork.com>
- FDOT (2002). *Grouting of Bridge Post-Tensioning Tendons. Training Manual*. Florida: State of Florida Department of Transportation
- Gagne R, Boisvert A, & pigeon M. (1996). Effect superplasticizer dosage on mechanical properties, permeability and freeze-thaw durability of high strength concrete with and without silica fume. *ACI MaterJournal*, 93: 111
- GrubeH., LawrenceC.D., (1984) Permeability of concrete to oxygen. In: Proceedings of the RILEM seminar on The Durability of Concrete Structures under Normal Outdoor Exposure. Hanover Institute fur baustoffkunde und Material Prufung. P68-79
- Harris, J. (2014). Ecological hardscape choices for today's landscape. *Stormwater Management*. Available:< <http://www.ecolandscaping.org/12/stormwater-management/ecological-hardscape-choices-for-todays-landscapes/>
- Malaysia Palm Oil Board (MPOB), M.P.O.B (2015) .Issues related to the impact of oil palm in the environment. Available :< <http://www.mpob.gov.my/en/palminfo> [May 2016]
- Megat Johari, M. A., Zeyad, A. M., Muhamad Bunnori, N. & Ariffin, K.S. (2012). Engineering and transport properties of high strength green concrete containing high volume of ultrafine palm oil fuel ash. *Construction and Building Materials*, 30, 281-288
- Mujah, D (2015), Compressive strength and chloride resistance of grout containing ground palm oil fuel ash. *Journal of Cleaner Production*, 112, 712-722
- Muller, U., Miccoli, L. & Fotana, P. (2015). Development of lime based grout for cracks repair in earthen constructions. *Construction and Building Materials*, 110, 323-332
- Rahman, M. E., Boon , A.L., Muntohar, A.S., Hashem Tanim, M.N., Pakrashi, V., (2014). Performance of masonry blocks incorporating palm oil fuel ash .*Journal Cleaner Production*, 78, 195-201.
- Rosquoet, F., Alexis, A., Khelidj, A. & Phelipot, A. (2003). Experimental study of cement grout: Rheological behavior and sedimentation. *Cement and Concrete Research*, 33, 713-722.
- RILEM CP113. (1984) Absorption of Water by Immersion Under Vacuum, *Material and Structures*, 12, 393-4
- Satyarno, I., Solehudin, A. P., Meyarto, C., Hadiyatmoko, D., Muhammad, P. & Afnan, R. (2014). Practical Method for Mix Design of Cement-based Grout. *Procedia Engineering*, 95, 356-365.
- Tangchirapat, W., & Jaturapitakkul, C. (2012). Strength, drying shrinkage, and water permeability of concrete incorporating ground palm oil fuel ash. *Cem Concrete Composite*, 32, 767-774
- Tangchirapat, W., Saeting, T., Jaturapitakkul, C., Kiattikomol, K. & Siripanichgorn, A. (2007). Use of waste ash from palm oil industry in concrete. *Waste Management*, 27, 81-88
- Tay, J. & Show, K. (1995). Use of ash derived from oil palm waste incineration as a cement replacement materials resources. *Conservation Recycle*, 13, 10
- VSL International Limited (2002). *Grouting of Post-Tensioning Tendons. 5 VSL Report Series*.

Switzerland: VSL International Ltd.

Ying, L. (2014) *Addressing palm oil concerns*, 8 september 2014, Available from :The Star Online

Yusuf, M.O., Megat Johari, M.A., Ahmad, Z.A., Maslehuddin, M., (2014) . Evolution of alkine activated ground blast furnace slag ultrafine palm oil fuel ash based concrete. *Material Des*, 55, 387-393

ECCENTRICALLY BRACED FRAMES AS EARTHQUAKE RESISTANT SYSTEM AND SEISMIC ANALYSIS OF THE STEEL FRAMES

Mohd Nasir Hussin Pema Tashi Norhaiza Nordin, Mohamed Emierul
Infrastructure University Kuala Lumpur

1. INTRODUCTION

Earthquake force has a critical effect on the construction industries around the seismic prone areas. The appropriate seismic design is necessary to save millions of lives as well as cost after the catastrophic past records of the earthquake. This study proposes the use of eccentrically braced frame as an efficient and ideal structural system to resist the earthquake forces. To test the validity of the proposed frame, the following objectives are set:

- Perform a linear static analysis on Staad Pro to determine and compare the story drift and nodal displacement of eccentrically braced frame with a steel frame without bracings and concentrically braced frame where all the three frames are subjected to seismic load.
- Perform a non-linear static analysis on Staad Pro to compare the strength and stiffness of eccentrically braced frame and concentrically braced frame under seismic effect.

Eccentrically braced frame is a structural system which combines the high energy dissipation capacity of the moment-resisting frame and the high stiffness of the concentrically braced frame. Eccentrically braced frame transfers the lateral loads such as seismic loads to another brace or to the column through shear and through bending in the beam link which can be seen in Figure 1. Hosseini & Amiri (2017) performed an analysis to compare the strength and resistance of the eccentrically braced frame and buckling-restrained braces in eccentric configuration by modelling a 5 story frames of same elevation and concluded that eccentrically braced frame is superior to the buckling-restrained braces against the progressive collapse.

Eccentrically braced frame absorbs the energy released during the earthquake by the link which undergoes a plastic deformation in the process while other frame members and the braces provide the resistance to the strain hardening of the link. Eccentrically braced frame is also a cost saving system because we can use the high strength steel for the members other than the link. Shen Li et al, (2017) did an experimental and analytical study on eccentrically braced frame combined with the high strength steel and found out that the link suffered inelastic rotation while other members retained its elasticity. They concluded that the eccentrically braced frame combines with high strength steel is a reliable system to resist lateral loads such as seismic loads. There are four widely used system of eccentrically braced frame which is shown in the Figure 1.

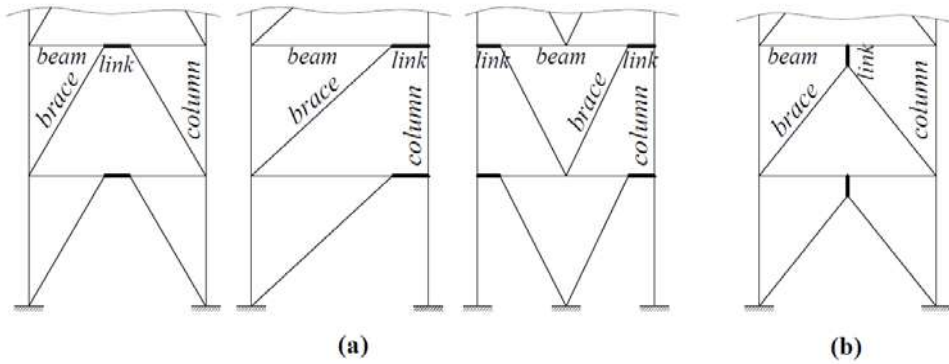


Figure 1: (a) Horizontal links: K frame; D frame; V frame; (b) Vertical links (Y frame)

Florea (2012) performed a combination of linear and non-linear FEM analysis under seismic effect on the four widely used system of eccentrically braced frame which are shown in the Figure 1. The linear analysis demonstrated that the K-frame has the lowest bending moment in the columns, static non-linear analysis showed that the Y-frame has the most unstable hysteretic behaviour and it is found that D-frame suffered the maximum displacement from the dynamic non-linear analysis. In general, eccentrically braced frame with short links demonstrated good energy dissipation capacity with respect to the seismic loads.

2. METHODOLOGY

Modelling of the Frames

Three structural frames are modelled on Staad Pro software in which Frame A is a normal steel bay frame, Frame B is an eccentrically braced frame and Frame C is a concentrically braced frame. All the three frames have same elevation and floor plan. The frames are of 6 stories of 3.5m story height. The frames are shown in the figures below:

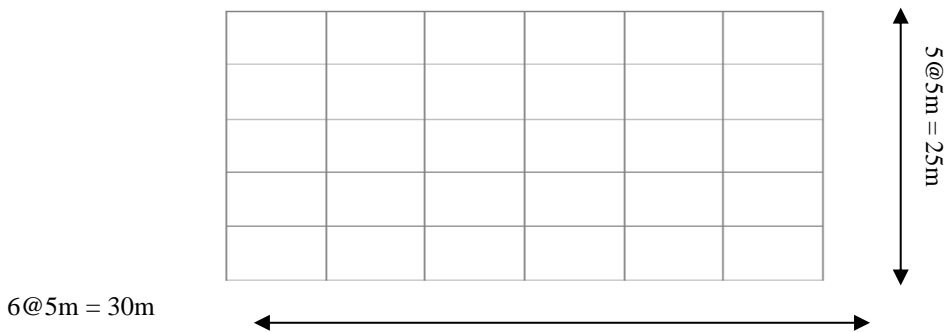


Figure 2: Floor plan of all the three frames

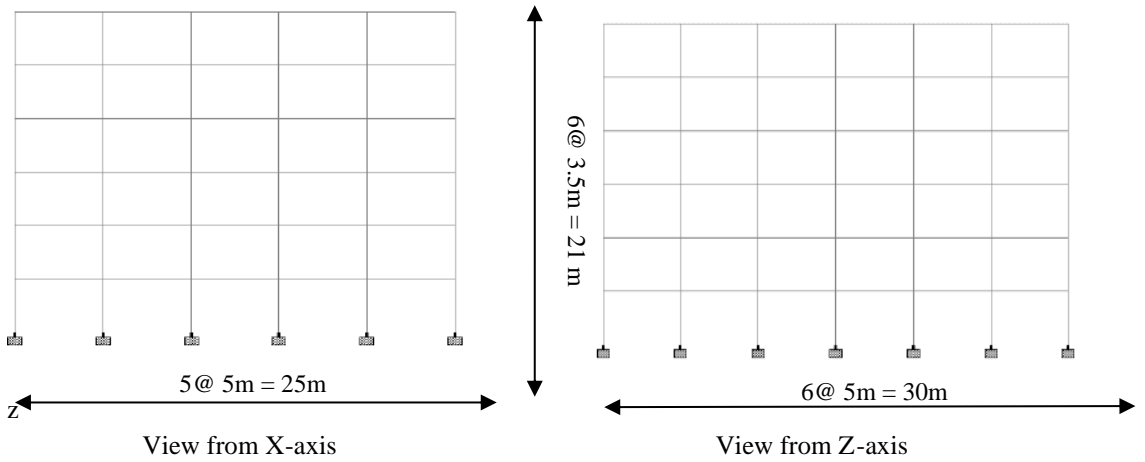


Figure 3: Elevation view of Frame A

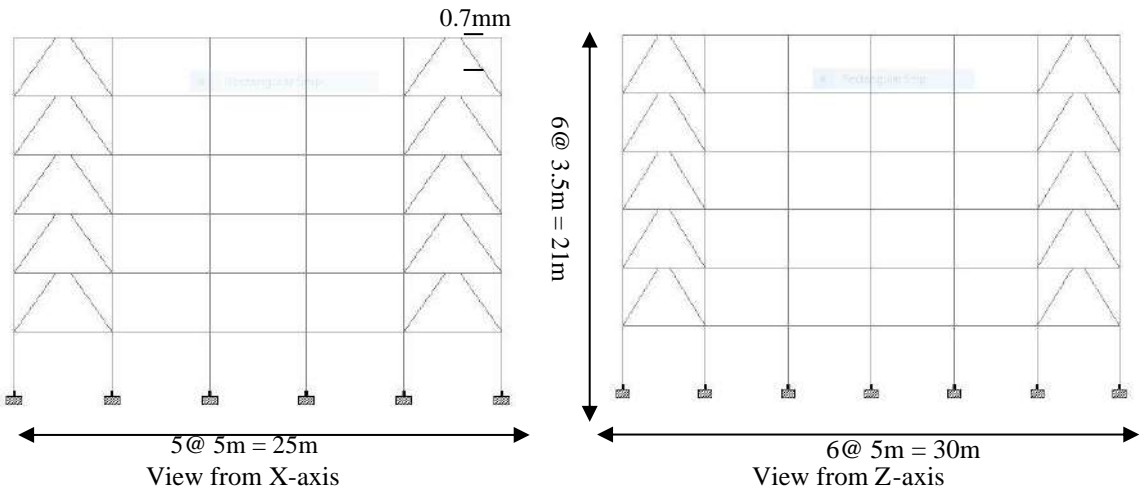


Figure 4: Elevation view of the Frame B (EBF)

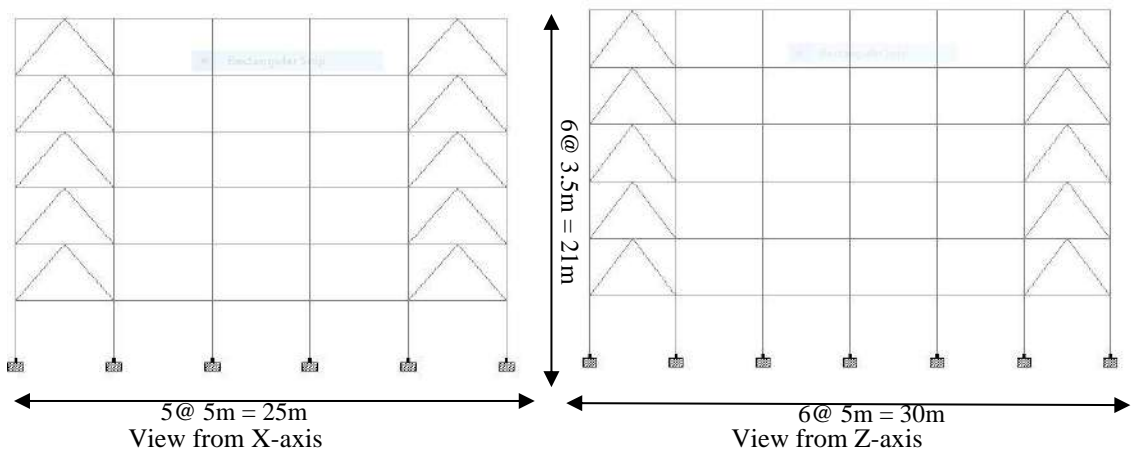


Figure 5: Elevation view of Frame C (CBF)

Design of the Frames

All the three frames are in Bhutan which is one of the seismic prone countries in the world. Since, Bhutan uses the Indian standard for all the construction works, the design of the three structural model frames are based on the Indian standard for general construction in steel IS 800: 2007 and Indian seismic design guideline IS1893 (Part 1): 2002.

Materials dimension

All the three frames are designed using the same material size as follow:

1. Beams: ISWB 400
2. Columns: ISMB 500
3. Bracings: ISMB 300
4. Link used in EBF: ISHB 450

Supports

All the supports for all the three frames are considered as fixed.

Loadings

Three different load types are considered in this software analysis:

1. Seismic load: Indian standard IS 1893 (Part 1): 2002 is used as the guideline. The zone considered is Zone V of zone factor 0.36 since Bhutan lies in Zone V of the earthquake zone division.
2. Dead load: For dead load, self-weight of the frame and the member load of the beams are considered. Self-weight is also generated automatically by the Staad Pro. 0.65kN/m is considered as the member load for the ISWB 400 beams.
3. Live load: For this study only the floor weight is considered as the live load. Floor load for all the frames is 4.375kN/m.

Load combinations

The load combinations for seismic design of steel frame from the IS 1893 (Part 1): 2002 are as follows:

1. 1.7 (DL + LL)
2. 1.7 (DL \pm EL)
3. 1.3 (DL + LL \pm EL)

3. ANALYSIS AND RESULTS

A combination of linear and non-linear analysis is done using the Staad Pro. Linear analysis is done for all the three frames (normal steel frame, eccentrically braced frame and concentrically braced frame). The purpose of the linear static analysis is to compare the displacements and the

story drifts of the three frames when it is subjected to the same seismic loads and the same load cases as mentioned above. In order to achieve the objective of the study, Pushover analysis is done using the Staad Pro. The Pushover analysis is non-linear static analyses where the specimens are pushed to different loads until the specimen reach its maximum capacity to deform or the capacity of the maximum displacement. The Pushover analysis is done for the Frame B (eccentrically braced frame) and Frame C (centrically braced frame) where both the frames are subjected to the same seismic loads.

Linear Analysis

Linear Analysis is a type of analysis where the relationship between the force applied and the resultant displacement is linear. Linear Analysis is applicable where the stress of the used materials lies in the linear elastic range. Linear analysis is comparatively shorter analysis and it is often used before performing the full non-linear analysis. The linear analysis results are interpreted below.

Story Drift Comparison

Table 1: Story Drifts for the Three Frames

FLOOR LEVELS	H (m)	LOAD	FRAME	AVG. DISP (cm)		DRIFT (cm)	
				X	Z	X	Z
1-2	3.50	EL-X	A	0.3131	0.0000	0.3131	0.0000
			B	0.2865	0.0000	0.2865	0.0000
			C	0.2857	0.0001	0.2857	0.0001
		EL-Z	A	0.0000	4.1741	0.0000	4.1741
			B	0.0000	4.1119	0.0000	4.1119
			C	0.0000	4.1273	0.0000	4.1273
2-3	7.00	EL-X	A	0.8157	0.0000	0.5026	0.0000
			B	0.6177	0.0000	0.3312	0.0000
			C	0.6347	0.0000	0.3491	0.0001
		EL-Z	A	0.0000	8.5393	0.0000	4.3652
			B	-0.0004	6.4161	0.0004	2.3042
			C	0.0001	6.4583	0.0001	2.3310
3-4	10.50	EL-X	A	1.3256	-0.0001	0.5099	0.0000
			B	0.9723	0.0001	0.3546	0.0001
			C	1.0036	0.0001	0.3689	0.0001
		EL-Z	A	-0.0001	12.7036	0.0001	4.1643
			B	-0.0007	8.2849	0.0003	1.8688
			C	0.0002	8.4756	0.0001	2.0173
4-5	14.00	EL-X	A	1.7852	-0.0001	0.4596	0.0000
			B	1.3017	0.0002	0.3295	0.0001
			C	1.3469	-0.0001	0.3433	0.0001
		EL-Z	A	-0.0002	16.4318	0.0001	3.7282

			B	-0.0009	9.9850	0.0003	1.7001
			C	0.0003	10.3141	0.0001	1.8385
5-6	17.50	EL-X	A	2.1493	-0.0001	0.3641	0.0000
			B	1.5734	0.0001	0.2717	0.0001
			C	1.6299	-0.0002	0.2831	0.0001
		EL-Z	A	-0.0002	19.3816	0.0000	2.9498
			B	0.0045	11.3840	0.0055	1.3990
			C	0.0003	11.8271	0.0001	1.5130
6-7	21.00	EL-X	A	2.3802	-0.0001	0.2309	0.0000
			B	1.7600	0.0003	0.1866	0.0002
			C	1.8228	-0.0002	0.1929	0.0000
		EL-Z	A	-0.0002	21.1163	0.0000	1.7346
			B	-0.0013	12.2761	0.0058	0.8921
			C	0.0004	12.7820	0.0000	0.9549

From the above table, we can say that Frame A without bracing has the highest story drift and the Frame B with the eccentrically bracings have the lowest story drift. The story drifts for concentrically braced Frame C are higher than Frame B but lower than the Frame A. It also shows that the story drift increases to its maximum until second floor and then the story drift starts to fall back from third floor reaching its lowest value at the sixth floor. The seismic load acting along the z-axis tends to result in greater story drift compared to that of the seismic load along the x-axis.

Nodal Displacements

Six nodes located at the same position in all three frames are selected to compare the nodal displacements due to the seismic loads on the three frames. The graphs below show the difference of the displacements at the six nodes in the three frames.

Figure 6: Graph showing Resultant Nodal Displacement Comparison for the Frames due to EL-X

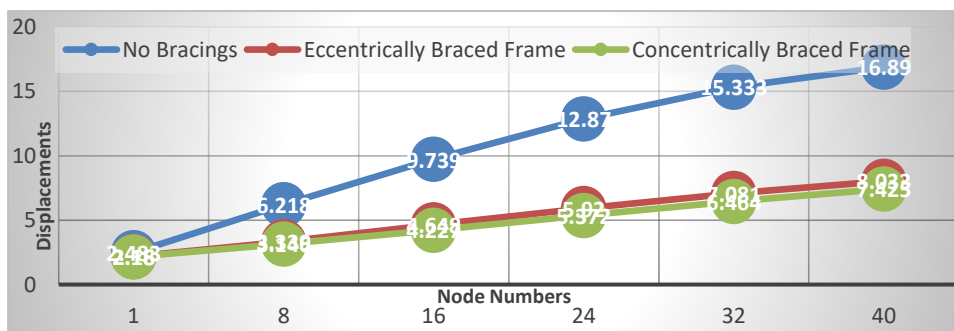


Figure 6 is a graphical representation of the nodal displacements due to the seismic load acting along the x-axis of the three frames for six nodes which I selected to make the

comparison. The graph shows that the displacements of the six nodes of the Frame B and Frame C is relatively lower to the nodal displacements of the no bracing Frame A. Concentrically braced Frame C is found to have the lowest nodal displacements.

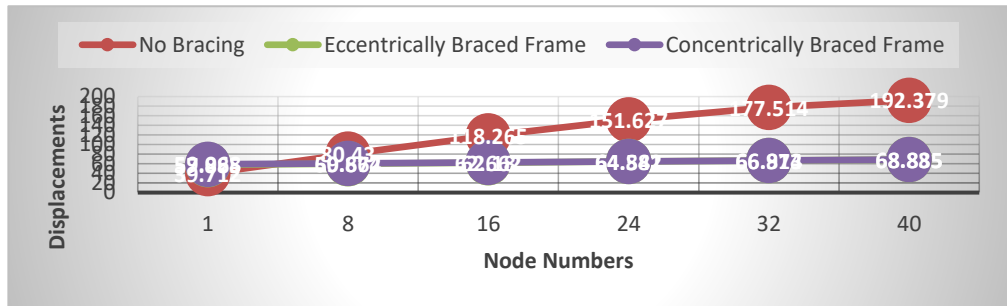


Figure 7: Graph showing Nodal Displacement Comparison for the Frames due EL-Z

Figure 7 is graphical representation of the nodal displacements due to the seismic load along the z-axis of the frames. The graph shows that the nodal displacement for eccentrically braced frame is the lowest. There is not much difference between the nodal displacements of the eccentrically braced frame and concentrically braced frame because of which the grey graph line for the eccentrically braced frame is submerged under the yellow graph line of the concentrically braced frame. But it is clear that the nodal displacements of the no bracing Frame A are relatively higher than the other two braced frames.

Non-Linear Analysis

Non-linear analysis is the type of analysis where the relationship between the force applied and the resultant displacement is non-linear. Pushover Analysis is done for the three frames as per FEMA 356: 2000. Pushover analysis is a static non-linear analysis, which uses incremental static analysis to determine the force-displacement relationship. The analysis involves applying horizontal loads thereby pushing the structure and plotting the applied shear force at each increment and the resultant lateral displacement. The goal of the pushover analysis is to compare the seismic performance of the proposed eccentrically braced frame with its well-regarded competitor concentrically braced frame and to determine the superiority of the braced frames over unbraced frame in resisting seismic loads.

Capacity Curve: Base Shear Vs Displacement

Frame A (Steel Frame without Bracings)

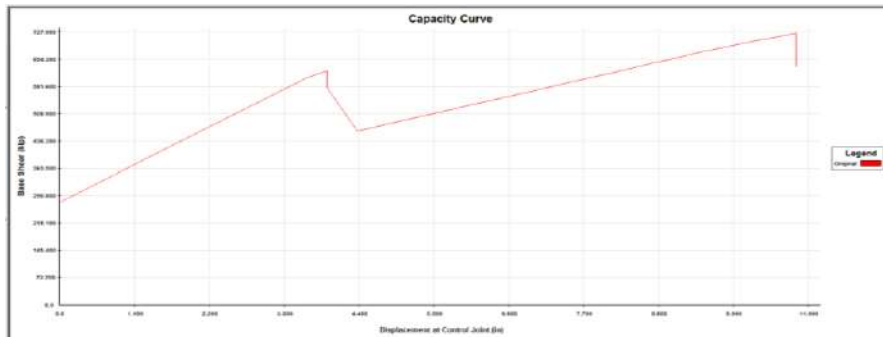


Figure 8: Capacity curve for Steel Frame without Bracings

The above capacity curve tells us that the steel frame without bracings can resist an ultimate seismic load of 720 kips which results in a displacement about 10.7 inches after which the frame collapses completely.

Frame B (Eccentrically Braced Frame)

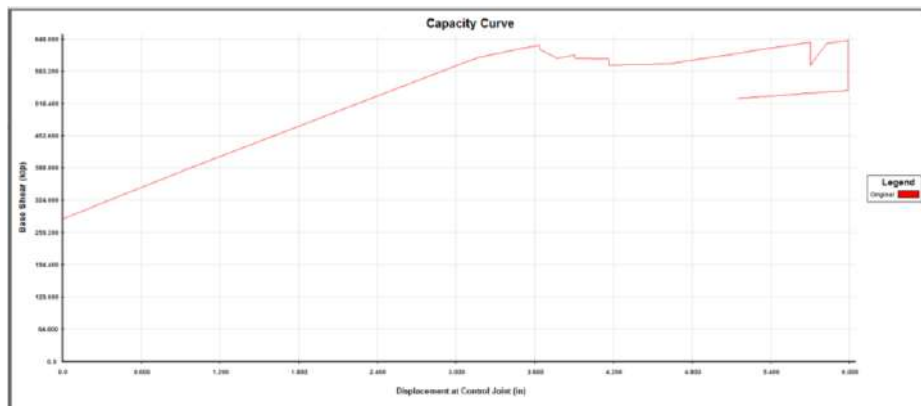


Figure 9: Capacity curve for Eccentrically Braced Frame

The capacity curve of the eccentrically braced frame shown in Figure 9 clearly shows that the frame will collapse at an approximate load of 848 kips at a displacement of approximately 6 inches.

Frame C (Concentrically Braced Frame)

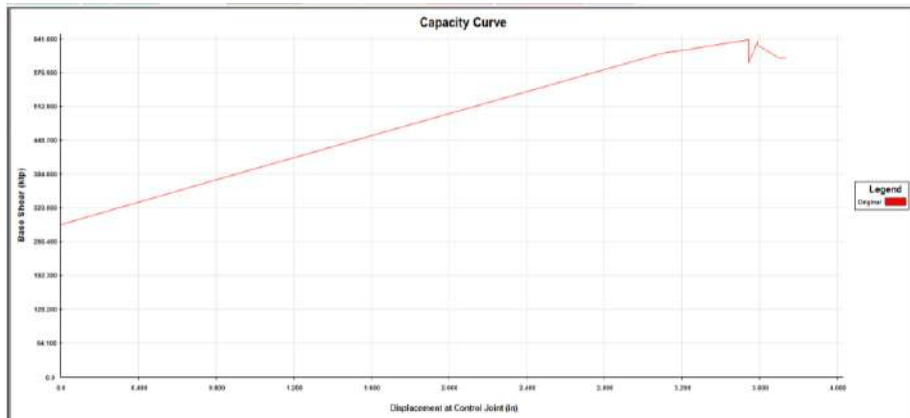


Figure 10: Capacity Curve for Concentrically Braced Frame

From the capacity curve, the frame will collapse at approximate shear of 830 kips with a lateral displacement of 3.70 inches. Eccentrically braced frames have a greater resistance against seismic load than the steel frame without bracings by a margin of 15%. Therefore, the braced frames are superior to the unbraced frames in resisting seismic loads. From the capacity curve of the frames that eccentrically braced frame can resist more seismic load compared to the concentrically braced frame. Eccentrically braced frame can endure a maximum load of 848 kips while the concentrically braced frame can resist a maximum shear of 830 kips. In another word, the eccentrically braced frame can resist a shear of 2.12% more compared to the concentrically braced frame. Therefore, among the braced frames, eccentrically braced frame is the superior choice for seismic resistance.

4. CONCLUSIONS

The earthquake loads contribute to the total collapse of the buildings. However, given a careful and huge consideration in the seismic design provides a strong resistant to the earthquake loads. The review of the literature and the analysis provides enough information to say that providing the building with eccentrically braced frame will increase the stiffness and seismic resistance of the building. The use of eccentrically braced frame not only improves the seismic resistance but also provide a good cost value. It can be concluded that eccentrically braced frame adds the advantage of the moment-resisting frame and the concentrically braced frame and reduces the disadvantages of the two frames. The principal conclusion drawn from the study is as follows:

1. Story drift of eccentrically braced frame < story drift of concentrically braced frame < story drift of the frame without bracings.
2. Concentrically braced frame has the least nodal displacement due to the seismic load along x-axis while the frame without bracings has the highest nodal displacement
3. Eccentrically braced frame has the least nodal displacement due to the seismic load along the z-axis of the frame while the frame without bracings has the highest nodal displacement.

4. The eccentrically braced frame possesses greater stiffness and seismic resistance compared to the steel frame without bracings by a factor of 15% and compared to the concentrically braced frame by a factor of 2.12%.

REFERENCES

- Salmasi, A. and Sheidaii, M. 2017. Assessment of eccentrically braced frames strength against progressive collapse. *International Journal of Steel Structures*, 17(2), pp.543-551.
- Duan, L. and Su, M. 2017. Seismic testing of high-strength steel eccentrically braced frames with a vertical link. *Proceedings of the Institution of Civil Engineers - Structures and Buildings*, 170(11), pp.874-882.
- Fakhraddini, A., Saffari, H. and Fadaee, M. 2018. A hybrid force/displacement seismic design method for steel eccentrically braced frames. *Asian Journal of Civil Engineering*, 19(1), pp.93-102.
- Kuşyılmaz, A. and Topkaya, C. 2013. Design overstrength of steel eccentrically braced frames. *International Journal of Steel Structures*, 13(3), pp.529-545.
- Li, S., Liu, Y. and Tian, J. 2018. Experimental and Analytical Study of Eccentrically Braced Frames Combined with High-Strength Steel. *International Journal of Steel Structures*, 18(2), pp.528-553.
- Faroughi, A., Moghadam, A. and Hosseini, M. 2017. Seismic progressive collapse of MRF–EBF dual steel systems. *Proceedings of the Institution of Civil Engineers - Structures and Buildings*, 170(1), pp.67-75.
- Hosseini, S. and Amiri, G. 2017. Successive collapse potential of eccentric braced frames in comparison with buckling-restrained braces in eccentric configurations. *International Journal of Steel Structures*, 17(2), pp.481-489.
- Akbari Hamed, A. and Mofid, M. 2017. Plastic design of eccentrically braced frames with shear panels. *Proceedings of the Institution of Civil Engineers - Structures and Buildings*, 170(1), pp.17-32.
- Mohammadrezapour, E. and Danesh, F. 2018. Experimental investigation of bolted link-to-column connections in eccentrically braced frames. *Journal of Constructional Steel Research*, 147, pp.236-246.

DESCRIPTIVE STATISTICAL ANALYSIS OF WATER QUALITY DATA IN SELANGOR RIVER BASIN

**Muhammad Nurasmadi Mohd Rifa'at, Nurazim Ibrahim, Norul Wahida Kamaruzaman,
Naimah Yusoff, Sangeetha Valloo, Janagiammal & Jaya Malathy**
Infrastructure University Kuala Lumpur

1. INTRODUCTION

Over the past decades, development of water resources has been the basis for the socio-economic growth in Malaysia. Population growth and urbanization, industrialization and the expansion of irrigated agriculture are imposing rapidly increasing demands and pressure on water resources, besides contributing to the rising water pollution thus causing the water supply situation in the country to change from one of relative abundance to one of scarcity. The way forward to a prosperous and sustainable future is to keep development to a level that is within the carrying capacity of the river basins while protecting and restoring the environment Ti and Façon (2002). The climate in Malaysia is governed by the yearly alternation of the northeast and southwest monsoons. The northeast monsoon brings heavy rains and extensive flooding to the east coast of Peninsular Malaysia, while the west coast receives relatively little rain during the southwest monsoon owing to the sheltering effect of the mountains in Sumatra. Based on the record from Huang et al. (2015), the average annual rainfall in Malaysia is 3,000 mm, with a total volume of about 990 billion m³/year. Besides annual rainfall, the water resources in Malaysia also includes surface artificial storage (lakes and dams) and groundwater storage (aquifers).

In terms of water supply in Malaysia, streams, and rivers with and without impounding reservoirs are the biggest contributors as compared to groundwater. According to Ti and Façon (2002), river flow regimes are irregular and to secure safe yield from surface water sources, storage facilities were constructed. As per Malaysia Water Industry Report by JKR in 1998 records, there are a total of 63 dams in Malaysia with a total storage capacity of 25 billion m³. The current total storage capacity has increased by now with the vast development and construction of new dams. Malaysia has 189 river basins, 89 being in Peninsular Malaysia, 78 in Sabah and 22 in Sarawak. According to Ti and Façon (2002), surface water resources are easily available with over 150 river systems in Malaysia, being the main reason of the lack of groundwater use in this country.

For the past decades, water quality has become an important concern as a direct consequence of accelerated economic development. The number of polluted rivers in Malaysia is increasing every year. The degradation rate of river water quality especially in the urbanized area is very alarming. Selangor is one of the urban areas in Malaysia that has been facing major river water pollution problems. According to LUAS (2014), Selangor River Basin which comprises of 10 sub-basins is the most important water resource in the state of Selangor that provides over 60% of the water used in Klang Valley. It has a catchment area of 2,200 km²

which is about 28% of the state area.

Based on Othman et al. (2018), heavy metals are also introduced into rivers and waterways through surface runoff and industrial effluent. Some of the heavy metals such as copper (Cu), zinc (Zn), iron (Fe), manganese (Mn), and nickel (Ni) are vital for aquatic biological systems to function optimally. However, excessive concentrations can be toxic to living organisms. Heavy metal contaminants such as chromium (Cr), nickel (Ni), copper (Cu), zinc (Zn), cadmium (Cd), and lead (Pb) are generally more persistent than organic contaminants (Lou et al., 2017). Metal nutritional requirements vary substantially among animals or plant species and differ with a range of element types (Adepoju & Adekoya, 2014). Both industrial and urbanization activities have greatly increased the heavy metal burden on the environment (Shikazono et al., 2012).

Due to rapid urbanization and industrialization, the water bodies of the Selangor River Basin have unfortunately been polluted with Ammonia-N (NH₃-N) and heavy metals namely Iron (Fe) and Manganese (Mn). These anthropogenic NH₃-N and metals pollutants can be transferred to consumers through drinking waters and food chain. The contamination of NH₃-N, Fe and Mn in Selangor tributaries is not new. The concentration of these elements has been exceeding the permissible limit for water quality permitted by the Ministry of Health (MOHE), Malaysia (Abu Hassan et al., 2011). High concentration of ammonia in river water is contributed by the sewage discharged and effluent from an industrial activity (Ahammed & Davra, 2010). The problem has been continued for more than a decade without any concrete solution and the increase of NH₃-N and Mn concentration in the river water is becoming more frequent in the recent years (Abu Hassan, et al., 2011). The high concentration of these pollutant affecting the water supply to the Selangor population. Several water treatment plants in Selangor were forced to shut down due to high concentration of NH₃-N in the raw water. From 1998 to 2010, the total number of shut down recorded was 24 times (Abu Hassan, et al., 2011).

3. METHODOLOGY

Descriptive statistics can be useful to provide basic information about variables in a dataset and to highlight potential relationships between variables. In this study, descriptive statistics are carried out to investigate the concentrations of NH₃-N, Iron and Manganese in the Selangor River basin. There are four (4) major types of descriptive statistics i.e., (i) measures of frequency, (ii) measures of central tendency, (iii) measures of dispersion or variation, and (iv) measures of position. The selected scholarly literatures on NH₃-N, Fe and Mn contamination in Selangor River is the population of the study whereas purposive or selective sampling of the study is set based on the scholarly literatures that were published with water sampling data from 2011 – 2021, scholarly literatures that use Selangor River as the study area and the scholarly literatures that involve study on the contamination of NH₃-N, Fe and/or Mn. The systematic review is carried out on the selected scholarly literatures to classify, analyze and synthesize the best available evidence to provide insightful and evidence-based answers (Boland and Dickson, 2017).

Table 3.1 presents the list of research papers that have been selected in this study. The guidelines and standards that is being referred to in this study is the National Water Quality Standards for Malaysia (NWQS) published by the Department of Environment (DOE), Malaysia. In this study, the regulated standard limit for drinking water quality of raw and treated water focusing on the specified inorganic pollutants (NH₃-N, Fe and Mn) can be referred to in Table 3.2. The increasing anthropogenic activities through the rising industrial development has been contributing to environmental degradation including the water and soil contaminants that involve organic and inorganic compound and impacting the stability of physical–chemical properties for soil and water in the urban lake as well as the implications on plants, animals, and human health.

Table 3.1: The selected scholarly literatures in this study

No	Title	Author
1	Variations of water quality in the monitoring network of a tropical river	Camara, M., et al. (2020)
2	Assessment of Pollution and Improvement Measure of Water Quality Parameters using Scenarios Modeling for Sungai Selangor Basin	Chowdhury et al. (2018)
3	Assessing Risk and Sources of Heavy Metals in a Tropical River Basin: A Case Study of the Selangor River, Malaysia	Othman, F., et al. (2018)
4	Integrated River Basin Management: incorporating the use of abandoned mining pool and implication on water quality status	Kusin, F. M., et al. (2016)
5	The distribution of heavy metals and nutrients along Selangor River and its adjacent mining ponds, Malaysia	Daniel and Kawasaki (2016)
6	Biomonitoring Agent for Heavy Metals Run Off from Acid Sulfate Soil of Aquaculture Industries in Selangor, Malaysia	Othman et al. (2014)
7	Problems of Ammonia and Manganese in Malaysian Drinking Water Treatments	Hasan et al. (2011)

Table 3.2: Standard limit on drinking water quality for NH₃-N, Fe and Mn

Parameters	Unit	Class				
		I	IIA/II B	III	IV	V
NH ₃ -N	mg/l	< 0.1	0.1 - 0.3	0.3 - 0.9	0.9 - 2.7	>2.7
Fe	mg/l	Natural Levels or Absent	1	1	1 (Leaf) 5 (Others)	Level above IV
Mn	mg/l		0.1	0.1	0.2	

Dissolved Oxygen (DO)

Cold water holds more oxygen than warm water and water holds less oxygen at higher altitudes as shown in Table 3.3. DO is measured either in milligrams per liter (mg/L) or "percent saturation." milligrams per liter is the amount of oxygen in a liter of water. Percent saturation is the amount of oxygen in a liter of water relative to the total amount of oxygen that the water can hold at that temperature. DO samples are collected using a special BOD bottle: a glass bottle with a "turtleneck" and a ground glass stopper. The bottle can be filled directly in the stream if the stream is wadable or boatable, or a sampler that is dropped from a bridge or boat into water deep enough can be used to submerge the sampler. Dissolved oxygen is measured primarily either by using some variation of the Winkler method or by using a meter and probe.

Table 3.3: Maximum Dissolved Oxygen Concentration with Temperatures

Temperature (°C)	DO (mg/l)	Temperature (°C)	DO (mg/l)	Temperature (°C)	DO (mg/l)
0	14.60	16	9.85	32	7.28
1	14.19	17	9.65	33	7.16
2	13.81	18	9.45	34	7.16
3	13.44	19	9.26	35	6.93
4	13.09	20	9.07	36	6.82
5	12.75	21	8.90	37	6.71

6	12.4 3	22	8.72	38	6.61
7	12.1 2	23	8.56	39	6.51
8	11.8 3	24	8.40	40	6.41
9	11.5 5	25	8.24	41	6.41
10	11.2 7	26	8.09	42	6.22
11	11.0 1	27	7.95	43	6.13
12	10.7 6	28	7.81	44	6.04
13	10.5 2	29	7.67	45	5.95
14	10.2 9	30	7.54		
15	10.0 7	31	7.41		

Biological Oxygen Demand (BOD)

BOD measurement requires taking two samples at each site. One is tested immediately for dissolved oxygen, and the second is incubated in the dark at 20 °C for 5 days and then tested for the amount of dissolved oxygen remaining. The difference in oxygen levels between the first test and the second test, in milligrams per liter (mg/L), is the amount of BOD.

Chemical Oxygen Demand (COD)

The COD test only takes a few hours to complete, giving it a major advantage over the 5-day BOD test. Wastewater treatment system personnel can use COD as an almost real-time operational adjustment parameter. COD can test wastewater that is too toxic for the BOD test. The COD test should be considered an independent measure of the organic matter in a wastewater sample rather than a substitute for the BOD test. The COD test uses a chemical (potassium dichromate in a 50% sulfuric acid solution) that “oxidizes” both organic (predominate) and inorganic substances in a wastewater sample, which results in a higher COD concentration than BOD concentration for the same wastewater sample since only organic compounds are consumed during BOD testing.

PH

The pH of river water is the measure of how acidic or basic the water is on a scale of 0 - 14. It is a measure of hydrogen ion concentration. Based in the NQWS, the pH of river water should fall between 6.5 and 8.5 (Class I) as well as between 6.0 and 9.0 (Class IIA & IIB) for Water

Supply I and Water Supply II (conventional treatment) respectively.

Total Suspended Solids (TSS)

The laboratory procedure of this test is by using Whatmann filter paper with pore size of 0.45 µm that is put in petri dish each and dried in the drying oven at the temperature of 105 °C for 1 h. After an hour, the petri dish was taken out and cooled for 30 min in the desiccator. Before performing filtration of the samples, the weighed filter paper was obtained. This was the initial weight of the filter paper (A). This filter paper then was used in filtration process. For the filtration process, the filter paper was inserted between the Buchner funnel and the suction flask. The water sample in the bottle was shaken and about 200 ml of sample was used in the filtration. After that, the filter paper was put back into petri dish and was dried in the drying oven at 105 °C and the final weight of the filter paper was recorded (B). Turbidity concentration of samples are measured by turbidity meter model 2100N using 25 mm round sample cell with sample volume of 30 mL. The turbidity meter is equipped with a stable halogen-filled tungsten filament lamp as required by EPA Method 180 and capable to read the turbidity from 0.001 to 4000 NTU. The reading precision is ± 1% of reading or ± 0.01 NTU, whichever is greater.

$$\text{TSS mg/L} = \frac{\text{average weight (in g) of B} - \text{average initial weight (in g) from A}}{1000} \text{mg/L}$$

Ammoniacal Nitrogen (NH₃-N)

The laboratory procedure to measure ammoniacal-nitrogen is by using HACH DR 2700 based on Nessler Method. 25 ml of sample and 25 ml of deionized water (blank) are transferred into glass cell each and then three drops of mineral stabilizer, three drops of polyvinyl alcohol and 1.0 ml of Nessler reagent were added to each transferred sample. The mixture was measured by using spectrometer at 425 nm. Deionized water is used as blank, and the reading was recorded for each sample.

Heavy Metals Contamination (Fe, Mn)

The concentration of dissolved metals was quantified using Inductively Coupled Plasma Optical Emission Spectroscopy (ICP- OES) model 715-ES by Varian, complimented with ICP Expert II software. ICP-OES operation was conducted according to the instruction from provider whereas US EPA method 200.7 and 200.5 were used as guidelines to prepare and analyze the sample.

3. RESULT AND DISCUSSION

In order to analyze the trend of river water quality index (WQI) and heavy metal pollution index (HPI) in Selangor River for the past 10 years from the selected scholarly literatures, it is necessary to fully understand the impacts of major activities in areas nearby to the river as it will affect the quality of water at the rivers downstream. Measurable information on the chemical, physical and biological parameters of water must be acquired to overview the water quality trend of the Selangor River. The data extracted in this study were collected from a total of 46 sampling locations of which (a) nine (9) locations under river water quality monitoring program by the DOE Malaysia from 2005 to 2015 (Camara et al., 2020), (b) 11 locations collected from October 2013 until September 2014 (Chowdhury et al., 2018; Othman et al., 2018), (c) 15 locations in Bestari Jaya (Rantau Panjang sub-basin) collected on June to August 2013 & 2014 and March to April 2015 (Kusin et al., 2016), and (d) 13 locations collected on February 2015 (Daniel & Kawasaki, 2016). Figure 4-1 shows the locations of the sampling points of the extracted 48 water samples data.

Data Synthesis on the Organic Pollutants Affecting Water Supply

Oxygen is a necessary element to all forms of life. Natural river purification processes require adequate oxygen levels to provide for aerobic life forms. However, when dissolved oxygen (DO) levels in water drop below 5.0 mg/L, aquatic life is put under stress. Although high DO level in the water supply is good as it improves the taste of drinking water, the risk of corrosion of water pipes also increases. This is why industries, especially boiler plant operators tend to use water with the least possible amount of DO by keeping the oxygen levels to 0.007 ppm (equivalent to mg/L) or less. The threshold of DO concentration by DOE Malaysia for very good quality water (Class I) is > 7 mg/L. Descriptive statistics according to the 2005 – 2015 data ($n = 66$) analysed by Camara et al. (2020), shows that the DO parameter has minimum concentration of 2.340 mg/L and maximum concentration of 9.820 mg/L with mean of 7.064 mg/L. Based on the result, DO indicated negative trends at four (4) sampling locations located in the middle of the basin and one (1) location in the downstream area. No trend was recorded at the Sungai Kerling branch sampling location whereas positive/upward trends were recorded at the other three (3) sampling locations.

On the other hand, BOD shows downward trends at all stations except at one location in the middle of the basin (no trend) whereas COD shows increasing trend at all stations except at three (3) sampling locations. These water quality trends detection and monitoring over long term is important for planning and management of freshwater resources and predicting the river water quality. Generally, for the 10 years period from 2005 until 2015, water quality of Selangor River is reported to have improved over time except at the most downstream location of Selangor River and at Kerling River branch. The water quality status expressed in terms of WQI indicates that the river water is generally of good quality (Class II) and can therefore be used directly for recreational activities with body contact, but conventional treatment is required for other uses such as domestic supply. In measuring the dispersion of the extracted data for the 48 water samples collected from 2005 until 2018 (reference made from scholarly articles published in 2016 until 2020), the range of the data is given by the smallest and the

largest reported DO, BOD and COD concentrations. Tables 4-1 until 4-3 shows the measures of dispersion and central tendency for the reported water sampling period of DO, BOD and COD concentrations, respectively.

Table 4-1: Measures of dispersion and central tendency of DO concentration

No	Sampling period	Reference	Number of data samples	Minimum (mg/L)	Maximum (mg/L)	Mean (mg/L)
1	2005 - 2015	(Camara et al., 2020)	9	5.2	8.1	7.1
2	2013 - 2014	(Chowdhury et al., 2018; Othman et al., 2018)	11	2.6	7.1	5.0
3	2013 - 2015	(Kusin et al., 2016)	15	3.5	6.6	5.3
4	2015	(Daniel & Kawasaki, 2016)	13	0.5	3.4	1.3
Summary of Data			48	0.5	8.1	4.5

Table 4-2: Measures of dispersion and central tendency of BOD concentration

No	Sampling period	Reference	Number of data samples	Minimum (mg/L)	Maximum (mg/L)	Mean (mg/L)
1	2005 - 2015	(Camara et al., 2020)	9	2.6	6.6	3.8
2	2013 - 2014	(Chowdhury et al., 2018; Othman et al., 2018)	11	0.9	13.0	4.9
3	2013 - 2015	(Kusin et al., 2016)	15	0.5	5.9	9.2
Summary of Data			35	0.5	13.0	3.1

Table 4-3: Measures of dispersion and central tendency of COD concentration

No	Sampling period	Reference	Numbers of data samples	Minimum (mg/L)	Maximum (mg/L)	Mean (mg/L)
1	2005 - 2015	(Camara et al.,	9	15.3	34.6	19.8

		2020)				
2	2013 - 2014	(Chowdhury et al., 2018; Othman et al., 2018)	11	18.3	50.8	30.7
3	2013 - 2015	(Kusin et al., 2016)	15	7.0	1216.0	95.9
Summary of Data			35	7.0	1216.0	55.8

Inorganic Pollutants Affecting Water Supply

Aside from ammoniacal nitrogen, inorganic pollutants comprise mainly of heavy metals, which are toxic or poisonous even at low concentrations. These inorganic pollutants and their organic forms have devastating negative health effects (Balakrishnan et al., 2020). Ammonia (NH₃) is a gaseous inorganic compound with a characteristic, pungent odour whereas ammoniacal nitrogen (NH₃-N) is a measure of the toxic level amount of all forms of ammonia as well as organic nitrogen such as proteins and DNA in a sample. Based on the 2005 – 2015 data (n = 66) analysed by Camara et al. (2020), the NH₃-N concentrations in mg/L for the nine (9) sampling locations are between 0.10 and up to 0.75. The data is in line with the poor DO concentrations (< 7 mg/L) at two (2) sampling locations (at the most downstream location of Selangor River and at Kerling River branch) whereby the concentration of NH₃-N at these two locations are quite high i.e., 0.31 mg/L and 0.75 mg/L, respectively. The maximum threshold level of NH₃-N for Selangor Rivers should be below 0.1 mg/L and between 0.1 to 0.3 mg/L to be classified as Class I and Class II respectively in accordance with the NWQS.

In a more recent study by Othman et al. (2018), environmental risk assessment was conducted by comparing the HPI within the 11 sampling locations. Among the 12 types of heavy metal concentrations being studied in water samples from the Selangor River, Iron (Fe) and Magnesium (Mg) had shown to have the highest minimum concentrations with the average concentrations values that had exceeded the limit if the NSDWQ and the standard proposed by the MOH. Other metals such as Ag, Cd, Co, Pb and Ni shows very minimum concentration values and were less than the standards. The maximum and mean value of Fe have exceeded both limits whereas the average concentration of Mn is below the MOH and NSWQS but the maximum value of Mn exceeded both limits (200 mg/L and 100 mg/L respectively). Suggestively high Fe concentration were observed at three (3) locations. Two (2) of the locations situated at Rawang sub-basin (an industrial area as well as former tin mining region) and the other one (1) location at the Air Hitam River (surrounded by peatland, palm oil plantation and factories).

Similarly, the maximum values of Mn concentrations (which have exceeded the limits) are also located the two (2) locations at Rawang sub-basin. High concentrations of metals are usually associated with acidic drainage, as the solubility of metals increases with decreasing of pH. In measuring the dispersion of the extracted data for the 35 water samples collected from 2005 until 2018 (reference made from scholarly articles published in 2016 until

2020), the range of the data is given by the smallest and the largest reported NH₃-N, Fe and Mn concentrations. Tables 4-4 until 4-6 shows the measures of dispersion and central tendency for the reported water sampling period of NH₃-N, Fe and Mn concentrations, respectively.

Environmental consequences at areas which were formerly used for tin mining are water reservoirs' pollution. This phenomenon can be observed not only in Malaysia but also at other countries whereby substantial impairment to water quality occurs at the abandoned mining sites. This indicates that land use of the Selangor River basin could have had negative influences on the metal concentrations of the river water. Selangor and Kuala Lumpur have been the most urbanized state and hence, the increase in heavy metal concentration in the river water are highly probably due to the continuous increase in the industrial activities and urban expansion along the riverbanks. Therefore, proper management of water resources should be further implemented by continuous monitoring of the standard guideline values of heavy metals.

Table 4-4: Dispersion and central tendency of NH₃-N concentration

No.	Sampling period	Reference	Numbers of data samples	Minimum (mg/L)	Maximum (mg/L)	Mean (mg/L)
1.	2005 - 2015	(Camara et al., 2020)	9	0.1	0.8	0.2
2.	2013 - 2014	(Chowdhury et al., 2018; Othman et al., 2018)	11	0.5	5.5	1.4
3.	2013 - 2015	(Kusin et al., 2016)	15	0.0	0.2	0.1
Summary of Data			35	0.0	5.5	0.5

Table 4-5: Measures of dispersion and central tendency of Fe concentration

No.	Sampling period	Reference	Numbers of data samples	Minimum (mg/L)	Maximum (mg/L)	Mean (mg/L)
1.	2013 - 2014	(Chowdhury et al., 2018; Othman et al., 2018)	11	947.45	3356.20	1733.76
2.	2013 - 2015	(Kusin et al., 2016)	15	0.01	11.27	1.42

3	2015	(Daniel & Kawasaki, 2016)	13	0.21	518.52	51.99
Summary of Data			28	0.01	3356.20	878.83

Table 4-6: Measures of dispersion and central tendency of Mn concentration

o	Samplin g period	Reference	Numbers of data samples	Minimum (mg/L)	Maximum (mg/L)	Mea n (mg/L)
1	2013 - 2014	(Chowdhury et al., 2018; Othman et al., 2018)	11	45.04	430.27	93.32
2	2013 - 2015	(Kusin et al., 2016)	15	0.04	0.74	0.29
Summary of Data			28	0.04	430.27	46.81

Data Visualization

Based on the extracted data, several graphical representations of information and data can be presented to better understand the trends, outliers, and patterns in the river water quality index (WQI) and heavy metal pollution index (HPI) in Selangor River for the past 10 years.

Dissolved Oxygen (DO)

Figure 4-2 shows the DO concentrations of all water samples that have been extracted from the scholarly literatures. Based on the threshold class limit of the DO parameters concentration in river water in accordance with DOE Malaysia, out of 48 sampling data, there are only 14.6 % of the data falls under Class 1 category, 33.3 % falls under Class II, and the rest of the water samples data needs extensive treatment (Class III) and are not suitable for water supply.

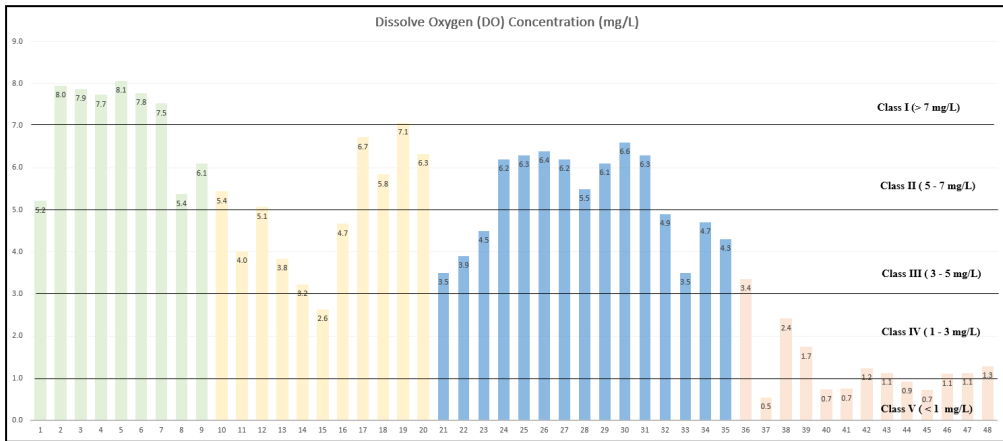


Figure 4-2: DO Concentrations of all water samples extracted (n=48)

Biological Oxygen Demand (BOD)

Figure 4-3 shows the BOD concentrations of all water samples that have been extracted from the scholarly literatures. Out of 35 sampling data that were tested for BOD, 28.6 % of the data falls under Class 1 category, 31.4 % falls under Class II, and the rest of the water samples data needs extensive treatment (Class III) and are not suitable for water supply.

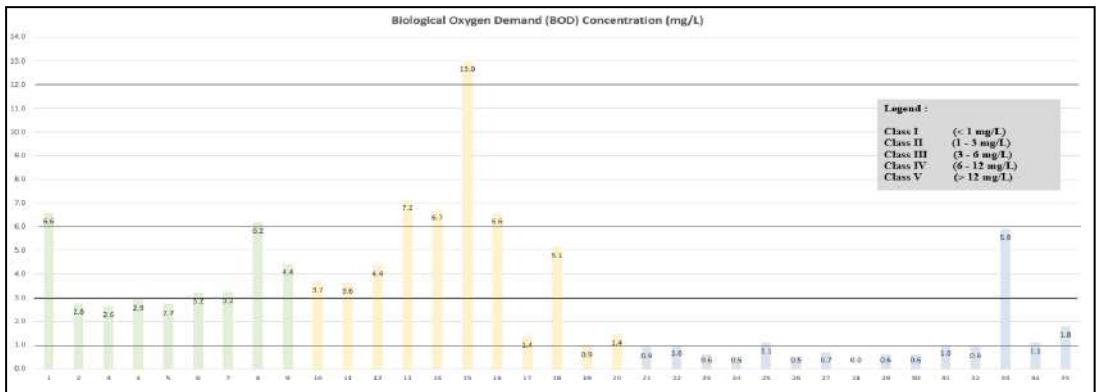


Figure 4-3: BOD Concentrations of all water samples extracted (n=35)

Chemical Oxygen Demand (COD)

Figure 4-4 shows the COD concentrations of all water samples that have been extracted from the scholarly literatures. Based on the threshold class limit of the COD parameters concentration in river water in accordance with DOE Malaysia, out of 35 sampling data that were tested for COD, 11.4 % of the data falls under Class 1 category, 60.0 % falls under Class II, and the rest of the water samples data needs extensive treatment (Class III) and are not suitable for water supply.

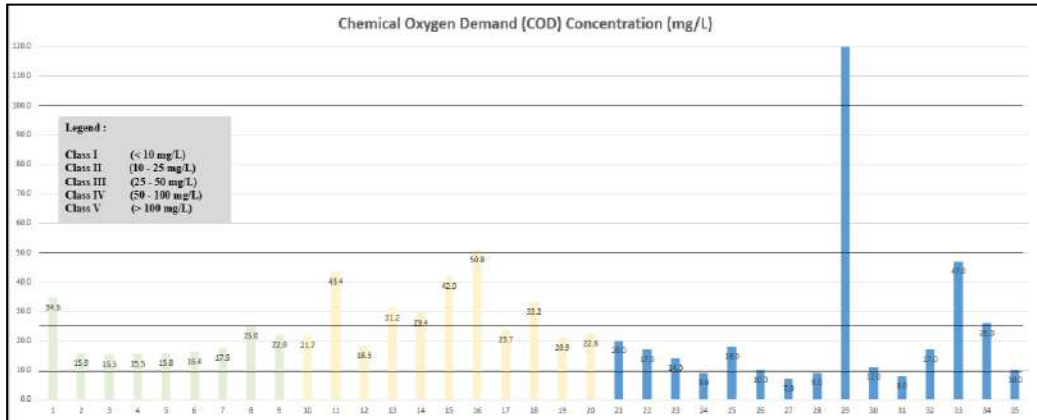


Figure 4-4: COD Concentrations of all water samples extracted

Ammoniacal Nitrogen (NH₃-N)

Figure 4-5 shows the NH₃-N concentrations of all water samples that have been extracted from the scholarly literatures. Based on the threshold class limit of the NH₃-N parameters concentration in river water in accordance with DOE Malaysia, out of 35 sampling data that were tested for NH₃-N, 22.9 % of the data falls under Class 1 & III category, 37.1 % falls under Class II, and the rest of the water samples data are not suitable for water supply.

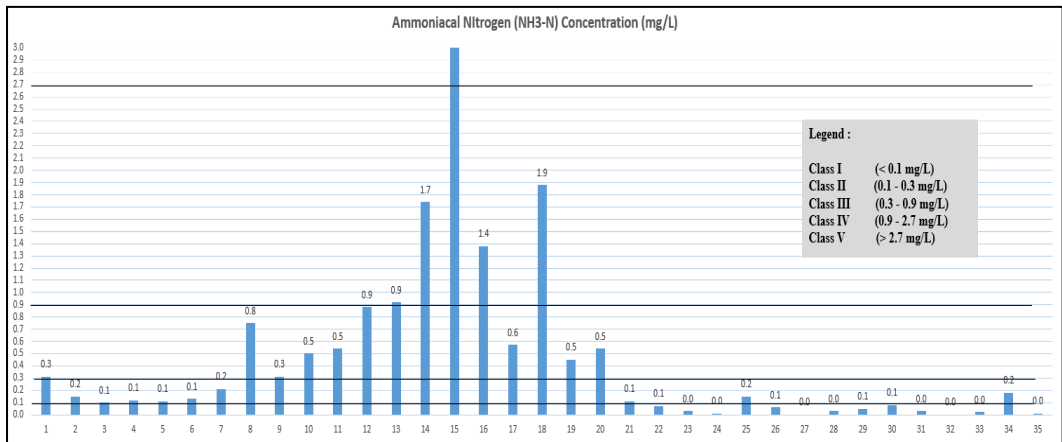


Figure 4-5: NH₃-N Concentrations of all water samples extracted

Heavy Metals Contamination (Fe, Mn)

According to MOH (2009) guidelines on the threshold limit of Fe and Mn concentration, the safe concentration of both Fe and Mn in untreated raw water are 1.0 mg/L and 0.2 mg/L respectively. On the other hand, for treated water, the safe concentration of both Fe and Mn should be below 0.3 mg/L and 0.1 mg/L respectively. Figure 4-6 shows the Fe and Mn concentrations of all water samples that have been extracted from the scholarly literatures.

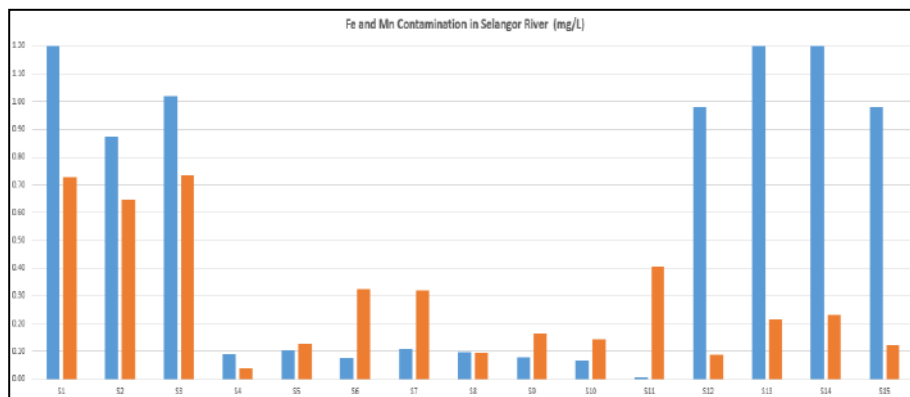


Figure 4-6: Fe and Mn contamination of all water samples extracted

5. CONCLUSION

The river water quality index (WQI) and heavy metal pollution index (HPI) for Selangor River basin have been analyzed. Hence, the second objective set in this study is also achieved. Over the years, water quality of Selangor River has been somewhat improved, as a result of water management efforts of local authorities (Camara et al., 2020). From this study, it can also be deduced that water quality patterns and trends can be investigated by various analytical techniques to reveal hidden information for better planning and management purposes. These techniques are also capable to illustrate temporal variation in water quality and indicate variables that cause variation in water quality.

REFERENCES

- Abou Zakhem, B., Hafez, R. Heavy metal pollution index for groundwater quality assessment in Damascus Oasis, Syria. *Environ Earth Sci* **73**, 6591–6600 (2015). Retrieved on 29/1/2020: <https://doi.org/10.1007/s12665-014-3882-5>.
- Abu Hasan.H, Sheikh Abdullah.S.R, Kamarudin.S.K, Tan Kofli.N, (2011) Problems of Ammonia and Manganese in Malaysian Drinking Water Treatment.
- Adepoju, M., & Adekoya, J. (2014). Heavy metal distribution and assessment in stream sediments of River Orle, Southwestern Nigeria. *Arabian Journal of Geosciences*, *7*(2), 743-756.

- Balakrishnan,. (2020), *Inorganic Pollutants in Water* (pp. ix-x). Elsevier. <https://doi.org/https://doi.org/10.1016/B978-0-12-818965-8.00026-3>
- Camara, M., Jamil, N., & Abdullah, F. (2020). Variations of water quality in the monitoring network of a tropical river. *Global Journal of Environmental Science and Management*, 6(1), 85-96.
- Chowdhury, M. S. U., Othman, F., Jaafar, W. Z. W., Mood, N. C., & Adham, M. I. (2018). Assessment of pollution and improvement measure of water quality parameters using scenarios modeling for Sungai Selangor Basin. *Sains Malaysiana*, 47(3), 457-469.
- Daniel, R., & Kawasaki, N. (2016). The distribution of heavy metals and nutrients along Selangor River and its adjacent mining ponds, Malaysia. *International Journal of Advances in Agricultural and Environmental Engineering*, 3(2), 241-244.
- Edet, A., & Offiong, O. (2002). Evaluation of water quality pollution indices for heavy metal contamination monitoring. A study case from Akpabuyo-Odukpani area, Lower Cross River Basin (southeastern Nigeria). *GeoJournal*, 57(4), 295-304.
- Garbarino, J., Hayes, H., & Roth, D. (1995). Contaminants in the Mississippi River US Geological survey circular, 1133. Virginia USA. In.
- Giri, S., Singh, G., Gupta, S., Jha, V., & Tripathi, R. (2010). An evaluation of metal contamination in surface and groundwater around a proposed uranium mining site, Jharkhand, India. *Mine Water and the Environment*, 29(3), 225-234.
- Hasan, H. A., Abdullah, S. R. S., Kamarudin, S. K., & Kofli, N. T. (2011). Problems of ammonia and manganese in Malaysian drinking water treatments. *World Appl Sci J*, 12(10), 1890- 1896.
- Huang, Y. F., Ang, S. Y., Lee, K. M., & Lee, T. S. (2015). Quality of water resources in Malaysia. *Research and Practices in Water Quality*, 3, 65-94.
- Juahir, H., Zain, S. M., Yusoff, M. K., Hanidza, T. I. T., Armi, A. S. M., Toriman, M. E., & Mokhtar, M. (2011). Spatial water quality assessment of Langat River Basin (Malaysia) using environmetric techniques. *Environmental Monitoring and Assessment*, 173(1), 625- 641. <https://doi.org/10.1007/s10661-010-1411-x>
- Kadhum, S. A., Ishak, M. Y., Zulkifli, S. Z., & Hashim, R. b. (2015). Evaluation of the status and distributions of heavy metal pollution in surface sediments of the Langat River Basin in Selangor Malaysia. *Marine Pollution Bulletin*, 101(1), 391-396. <https://doi.org/https://doi.org/10.1016/j.marpolbul.2015.10.012>
- Kusin, F. M., Muhammad, S. N., Zahar, M. S. M., & Madzin, Z. (2016). Integrated River Basin Management: incorporating the use of abandoned mining pool and implication on water quality status. *Desalination and Water Treatment*, 57(60), 29126-29136.
- Lou, S., Liu, S., Dai, C., Tao, A., Tan, B., Ma, G., Chalov, R. S., & Chalov, S. R. (2017). Heavy metal distribution and groundwater quality assessment for a coastal area on a Chinese Island. *Polish Journal of Environmental Studies*, 26(2).
- LUAS. (2014). Sumber Air Alternatif Negeri Selangor. In: Selangor Waters Management Authority (SWMA)/Lembaga Urus Air Selangor (LUAS).
- Mahato, M. K., Singh, P. K., & Tiwari, A. K. (2014). Evaluation of metals in mine water and assessment of heavy metal pollution index of East Bokaro Coalfield area, Jharkhand, India. *Int J Earth Sci Eng*, 7(04), 1611-1618.
- Mohamed, I., Othman, F., Ibrahim, A. I. N., Alaa-Eldin, M. E., & Yunus, R. M. (2014). Assessment of water quality parameters using multivariate analysis for Klang River

- basin, Malaysia. *Environmental Monitoring and Assessment*, 187(1), 4182. <https://doi.org/10.1007/s10661-014-4182-y>
- Mohan, S. V., Nithila, P., & Reddy, S. J. (1996). Estimation of heavy metals in drinking water and development of heavy metal pollution index. *Journal of Environmental Science & Health Part A*, 31(2), 283-289.
- Othman, F., Chowdhury, M. S. U., Wan Jaafar, W. Z., Faresh, E. M. M., & Shirazi, S. M. (2018). Assessing Risk and Sources of Heavy Metals in a Tropical River Basin: A Case Study of the Selangor River, Malaysia [journal article]. *Polish Journal of Environmental Studies*, 27(4), 1659-1671. <https://doi.org/10.15244/pjoes/76309>
- Othman, R., Hatta, F. A. M., & Shafiai, S. (2014). Biomonitoring Agent for Heavy Metals Run Off from Acid Sulfate Soil of Aquaculture Industries in Selangor, Malaysia. International Conference on Global Trends in Academic Research,.
- Prasad, B., & Bose, J. (2001). Evaluation of the heavy metal pollution index for surface and spring water near a limestone mining area of the lower Himalayas. *Environmental Geology*, 41(1), 183-188.
- Ravikumar, P., Mehmood, M. A., & Somashekar, R. (2013). Water quality index to determine the surface water quality of Sankey tank and Mallathahalli lake, Bangalore urban district, Karnataka, India. *Applied water science*, 3(1), 247-261.
- Razali, A., Ismail, S. N. S., Awang, S., Praveena, S. M., & Abidin, E. Z. (2018). Heavy Metals Contamination and Potential Health Risk in Highland River Watershed (Malaysia).
- Reza, R., & Singh, G. (2010). Heavy metal contamination and its indexing approach for river water. *International journal of environmental science & technology*, 7(4), 785-792.
- Shikazono, N., Tatewaki, K., Mohiuddin, K., Nakano, T., & Zakir, H. (2012). Sources, spatial variation, and speciation of heavy metals in sediments of the Tamagawa River in Central Japan. *Environmental geochemistry and health*, 34(1), 13-26.
- Singh, G., & Kamal, R. K. (2017). Heavy metal contamination and its indexing approach for groundwater of Goa mining region, India. *Applied water science*, 7(3), 1479-1485.
- Ti, L. H., & Façon, T. (2002). Malaysia's Water Vision: The Way Forward-The Malaysian Water Partnership in From Vision to Action: A Synthesis of National Water Visions in Southeast Asia. *The FAO-ESCAP Pilot Project on National Water Visions; Food and Agriculture Organization of the United Nations: Bangkok, Thailand*, 25-42.
- Tiwari, A. K., Singh, P. K., & Mahato, M. K. (2014). GIS-based evaluation of water quality index of ground water resources in West Bokaro Coalfield, India. *Current world environment*, 9(3), 84

POME TREATMENT EFFICIENCY ENHANCEMENT IN CONTINUOUS FLOW STIRRED-TANK REACTOR BY POLYVINYL ALCOHOL GEL

**Nik Nuraini Azhari, Chen Chee Xiang, Nadzifah Che Mat, Khairunisah
Kamaruzaman, Nurazim Ibrahim & Syazana Syahirah Jamaluddin**
Infrastructure University Kuala Lumpur

1. INTRODUCTION

Palm Oil Mill Effluent (POME) is an origin of pollution that worth attention since surface water contamination will be done when released into local rivers or lakes with absent of purification. POME is generated within the procedure of palm oil milling such as fresh oil palm fruit bunches sterilization, palm oil clarification and hydro-cyclone operations to produce fresh crude oil as effluent (Abdurahman et al., 2013; Zhen et al., 2021). By reduce the environmental impact cause by POME, various type of anaerobic digester was invented and applied to palm oil industry. Anaerobic treatment process generally governed by 3 essential step which is hydrolysis, acidogenesis, acetogenesis and methanogenesis to convert the high complex organic matter into elementary secondary products which is biogas. The main composition of the biogas produced is methane (CH₄) and carbon dioxide (CO₂) (Elvira et al., 2022; Era et al., 2022).

One of the anaerobic digester that been used widely in oil palm industry is continuous flow stirred-tank reactor (CSTR). The treatment efficiency of CSTR in POME required modification to achieve better effluent (Abdurahman et al., 2013). Polyvinyl Alcohol (PVA) Gel in this study come in and play a role on enhancing the treatment efficiency of CSTR. PVA Gel is made of polyvinyl alcohol and has high porosity and water content inside. By its excellent bacteria immobilization advantage, COD, SS, total nitrogen and ammonia are effectively decompose by the correspond bacteria. Treatment efficiency by using PVA gel can be enhanced up to 5 times compared to conventional activated sludge process thus excellent for capacity enhancement of purification facilities with significant footprint reduction (Kuraray Aqua Co., Ltd.,2017; Sitthakarn et al., 2022).

In this study, a conventional CSTR system and a prototype modified CSTR system will be introduced to degrade the high concentration of organic compounds in POME. The modified CSTR is a new prototype and not been applied in the palm oil industry. Therefore, investigation of the applicability of this modified CSTR system is desirable. Also, the utilise bio-carrier as known as PVA gel in this study was previously applied in the sewage treatment in others place around the world. However, this material is still a new approach for palm oil industry. Effluent quality from the modified CSTR will used to compare with effluent quality from conventional CSTR. Biogas production rate will be measured throughout the study in both reactors.

2. METHODOLOGY

Sampling of Deoiled POME and POME Sludge

To conduct this study, deoiled POME and POME sludge is required. These sample was collected from Palm Oil Mill Effluent Zero Discharge Green Technology Centre (POMTEC). POME sludge that used in microorganism cultivation process was sampled in sludge tank of the system (MPOB, 2016). Deoiled POME that used in experiment as feed was sampled at the clarifier after oil water separator process. Both POME sludge and deoiled POME was sampled with several plastic bottle with 5.5 litre capacity. Worker that responsible for the operation of plant was assisted in the sampling process with using a long stick that tied with a small bucket. The sample was placed into laboratory refrigerator at 4 °C to retard any reaction occur in the sample (APHA, 2005).

Set up of Continuous Flow Stirred-tank Reactor CSTR System

Two 1 litre reaction flask is used as the CSTR body. One reaction flask act as control while another one act as testing setup. The diameter of reactor is 9 cm and the height of reactor is 21 cm. The volume of the PVA gel placed is 20% of the content in reactor which is 140ml in testing setup. However, there is no any PVA gel in the control setup (Kuraray, 2017). Mixing is provided by magnetic stirrer to the system and the agitation speed is adjusted at 200 rpm (revolution per minute) to provide a homogeneous mixing within the POME sample. At the same time, temperature of reactor which is 35 °C is adjusted throughout the whole experiment period. The biogas produced is sampling with using gas bag which attached with the biogas outlet tightly. OLR that introduced into the system is constant, 3.01 g COD/L.d since the COD of POME is same and the flow rate of the system is constant which is 70 ml/day. The HRT implemented in this study is 3 and 5 days. Since 70 ml of deoiled POME will introduced into the reactor, 70 ml of processed POME will allow to overflow from the reaction flask. Therefore, the overflowed POME will test daily with pH to confirm the stability of the system. For every 3 and 5 days, the overflowed POME will test with the pre-set parameter.

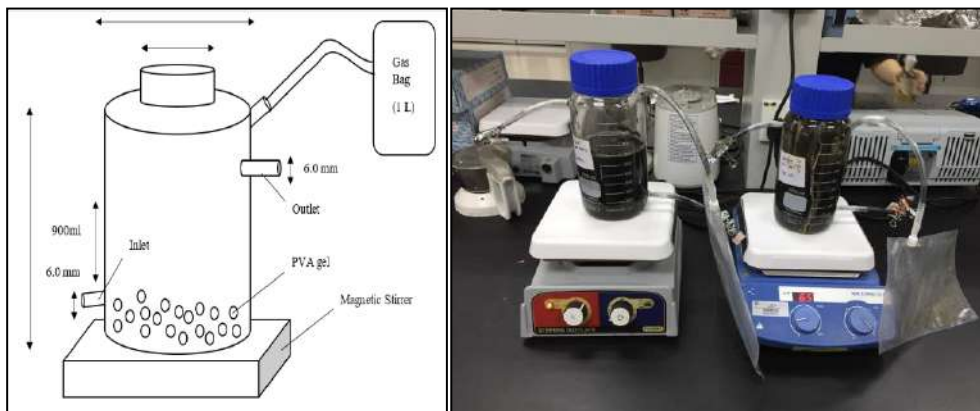


Figure 1: Detailed Experimental Set up

Cultivation of Anaerobic Bacterial Process

Anaerobic digestion generally required cultivation of anaerobic bacterial before the operation of digester. In this study, modified lab scale CSTR with PVA gel was implemented and CSTR required cultivation as others anaerobic digestion method. POME sludge was selected as cultivation method because the sludge contained abundance of anaerobic bacterial. Cultivation method was referred to Kuraray Limited Corporate since PVA gel was supplied by them. From Kuraray, the volume of PVA gel required is 20% of the total volume of liquid. Therefore, in this study, 140 ml of PVA gel was placed into 700 ml of deoiled POME. During cultivation period, PVA gel was placed into CSTR reactor, POME sludge was placed into the reactor and magnetic stirrer was activated with 200 rpm for better contact between sludge and bio-carrier and temperature was adjusted at 35 °C. 10% of the liquid volume of deoiled POME was feed into the reactor for every 6 days. This process will subsequently remove 10% of POME sludge from the reactor. This process was repeated until 100% of content was filled with deoiled POME and the total cultivation period is 60 days (Kuraray, 2017).

Experimental Process

COD is measured with USEPA Reactor Digestion Method, TSS is measured with using equipment such as AND GR-200 analytic balance, Memmert oven and Carbolite muffle furnace as stated in Standard Examination Method for Water and Wastewater. Ammonia nitrogen is measured with Hach Nessler method while total nitrogen is measured with Hach Persulfate Digestion Method, Method 10071. pH is measured with using SensION™ + PH3 Hach Method pH meter. Biogas is expected to release during the operation of anaerobic digestion regardless of PVA gel. Therefore, preparation of gas sampling bag to sample the biogas released is necessary. However, gas chromatograph is usually required to analyse the composition of biogas and it is not available in university lab. Therefore, a comparison will be done by comparing the volume of biogas supposed to be released based on the COD removed with using calculation formula and the actual biogas released.

Biogas Collection

The net weight of biogas was obtained by minus the weight of empty weight of gas bag by weight of full gas bag. After that, in order to convert the weight of biogas to volume of biogas, the general density of biogas is used and it is 1.15 kg/m³. After that, by using formula [volume of biogas produced / Volume of liquid in reactor)/ times], the biogas production rate will be obtained. The formula 3.1, 3.2 and 3.3 that used for biogas calculation is as below.

$$\text{Weight of full gas bag} - \text{weigh of empty gas bag} = \text{weight of biogas} \quad (1)$$

$$\text{Weight of biogas} / 1.15 \text{ kg/m}^3 = \text{Volume of biogas} \quad (2)$$

$$(\text{Volume of biogas produced} / \text{Volume of liquid in reactor}) / \text{times} \quad (3)$$

3. RESULT AND DISCUSSION

Before placing deoiled POME into reaction flask, deoiled POME was unfrozen to room temperature. Deoiled POME was taken out from refrigerator for 2 hours and place somewhere in laboratory before experiment started. Deoiled POME was tested with pre-set parameter which is COD, TSS, ammonia nitrogen, total nitrogen and pH before placed into CSTR reactor. Initial characteristic of POME is shown in Table 1.

Table 1: Initial Characteristic of POME

Parameter	Deoiled POME
pH	6.21
COD (mg/L)	43,000
TSS (mg/L)	24,000
TN (mg/L)	550
Ammonia Nitrogen (mg/L)	264
Weight of Gas Bag (g)	8.50

The Table 1 shown deoiled POME that used for this study consists of high concentration of COD and TSS, nearly neutral pH and high nitrogen content. However, the characteristic of deoiled POME is significantly different from characteristic of raw POME which used for previous research. This is because the deoiled process in POMTEC is advanced microbelt filter and rotary drum screening. This will significantly decrease the fiber and the oil and grease containing in POME. This was also proved that raw POME is containing more pollutant compared to deoiled POME in term of COD, TSS and nitrogen. Also, significant different of pH between raw POME and deoiled POME was observed by comparing the data from previous research and this study.

This experiment was repeated 3 times to maximise the accuracy of result. During experimental run, significant COD and TSS removal was observed in both conventional and modified CSTR. However, by comparing HRT of 3 days and 5 days, HRT of 5 days possessed treatment efficiency almost double the treatment efficiency recorded in HRT of 3 days. Also, not forget to mention that the system was remained stable throughout the first experimental period. Ammonia nitrogen was proved that not effectively removed throughout the experimental run while total nitrogen was effectively removed in HRT of 3 and 5 days. Biogas production rate was observed greater in modified CSTR compared to conventional CSTR regardless of HRT. Therefore, in overall, modified CSTR have better performance compared to conventional CSTR. The result shown in Table 2 is the average value from 3 repeated experiment.

Table 2: Experimental Result in both Control reactor and PVA reactor

Day	3		5	
OLR (g COD/l/d)	3.01			
Parameter	Conventional	Modified	Conventional	Modified
pH	8.24	8.37	7.86	7.61
COD (mg/L)	26,733	23,301	11,597	9,838
TSS (mg/L)	15,933	13,005	7,406	6,134
TN (mg/L)	340	330	270	240
Ammonia Nitrogen (mg/L)	261	262	260	260
Weight of Gas Produced (g)	14.15	15.75	24.61	26.90
Volume of gas produced (L)	12.3	13.7	21.4	23.4
Biogas Production Rate (l/d)	5.86	6.52	6.11	6.68
COD Removal (%)	38.83%	45.81%	73.03%	77.12%
TSS Removal (%)	33.61%	41.10%	69.14%	74.44%

During the run of experiment, system stability was achieved. This is the conclusion from measuring result of pH. There is no any peak value was observed from the result and the pH is all dropped under the optimal methanogenesis range as shown in Table 3 and Figure 1. pH in conventional CSTR is ranged from 6.44 to 8.24 and pH in modified CSTR is ranged from 6.42 to 8.37 which are all in normal and desired range, thus no any pH adjustment is required (Senturk et al, 2014).

Table 3: pH of Modified CSTR and Conventional CSTR.

Time (days)	pH	
	Conventional	Modified
0	6.44	6.42
2	7.89	7.91
3	8.24	8.37
4	8.13	8.22
5	7.86	7.61

The pH in this experiment run was shown consistent excepted for day 3 and 4 with higher pH recorded. However, the higher pH recorded is still within the optimal methanogenesis pH range, therefore no pH adjustment action was taken in this run. Although minimization of shock loading by introduce constant OLR to the system was done to maximum the system

stability, but the system shown peak pH in day 3 and 4. This proved that the introduction of feed into the system in day 3 and 4 was consisted of error such as higher loading was introduced or injection of oxygen.

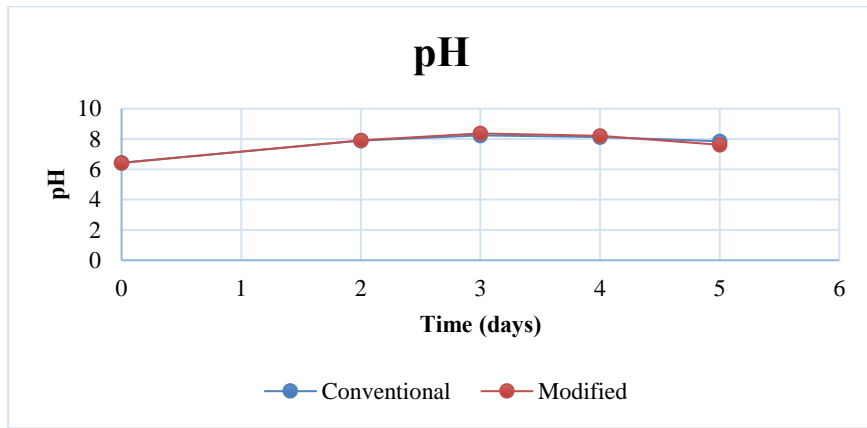


Figure 1: pH of Modified CSTR and Conventional CSTR.

Modified CSTR having better performance in term of COD removal efficiency compared to conventional CSTR as shown in Figure 2. In term of COD removal, 38.83% was achieved in conventional CSTR while 45.81% was achieved in modified CSTR with HRT of 3 days. Also, 73.03% of COD removal was achieved in conventional CSTR while 77.12% of COD removal was achieved in modified CSTR with HRT of 5 days. Although modified CSTR having only 4% COD removal better than conventional CSTR, but PVA gel enhancement in POME treatment still valid.

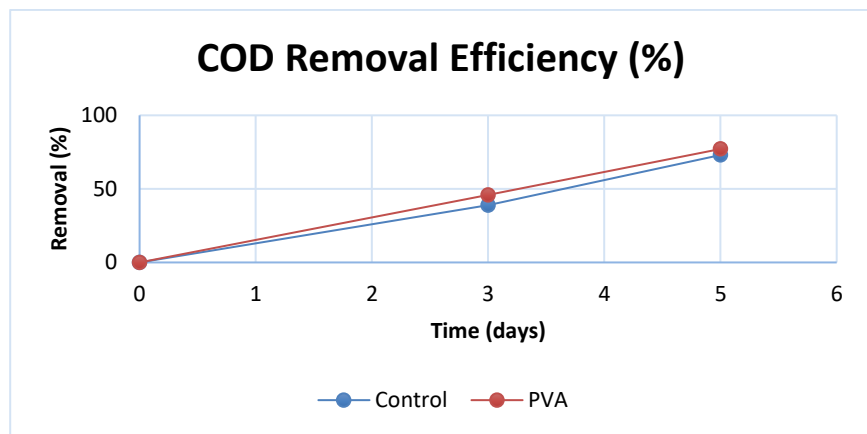


Figure 2: COD Removal Rate of Conventional and Modified CSTR.

From the result and graph, the removal pattern showed the system removal efficiency is almost directly proportional to the time. This may because the cultivation process was excellent

which causing the bacterial growth well on the surface of bio-carrier, in this case PVA gel. Also, the bacterial cultivation on conventional CSTR which act as control are well performed. This prove that the time used on cultivation which is 60 days is sufficient. On the others hand, POME sludge from POMTEC that used mainly for cultivation process is fresh and contained sufficient bacteria group for cultivation as the more the functional bacterial, the higher the consuming efficiency of organic matter.

In the other hand, TSS removal rate is somehow proportional to COD removal. Overall, conventional CSTR having lesser TSS removal compared to modified CSTR as shown in Figure 3. There are 33.61% of TSS removal was achieved in conventional CSTR while 41.10% of TSS removal was achieved in modified CSTR with HRT of 3 days. Also, 69.14% of TSS removal was achieved in conventional CSTR while 74.44% was achieved in modified CSTR with HRT of 5 days. By comparing both CSTR, modified CSTR having approximately 5% to 6% better treatment efficiency with HRT of 3 and 5 days, thus modified CSTR have greater performance compared to conventional CSTR.

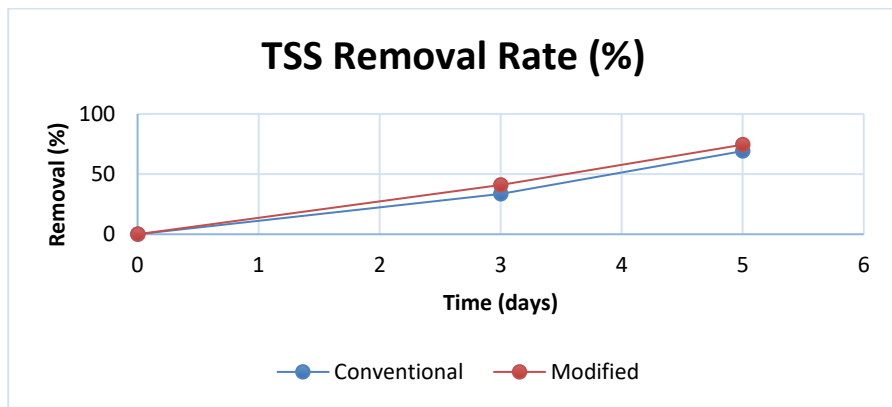


Figure 3: TSS Removal Rate of Conventional and Modified CSTR.

From the result and graph, the TSS removal pattern showed the system removal efficiency is almost directly proportional to the time. This may because the cultivation process was excellent which causing the bacterial growth well on the surface of bio-carrier, in this case PVA gel. Also, the bacterial cultivation on conventional CSTR which act as control are well performed. This prove that the time used on cultivation which is 60 days is sufficient. On the others hand, POME sludge that used mainly for cultivation process is fresh and contained sufficient functional bacteria group.

In term of ammonia nitrogen and total nitrogen, although both conventional and modified CSTR achieved significant TSS and COD removal with HRT of 5 days, but ammonia nitrogen was not significantly removed throughout the run as shown in Figure 4. Ammonia nitrogen in initial deoiled POME was 264 mg/L, after HRT of 3 days, 3 mg/L of ammonia nitrogen was removed in conventional CSTR while 2 mg/L of ammonia nitrogen was observed removed in modified CSTR. After HRT of 5 days, 1 mg/L of ammonia nitrogen was removed in

conventional CSTR while 2 mg/L of ammonia nitrogen was removed in modified CSTR. The overall ammonia nitrogen removal rate in both conventional CSTR and modified CSTR was 1.5 %.

However, there are significant removal of total nitrogen occurred in both CSTR. Approximately 210 mg/L or 38.1% of total nitrogen was removed in conventional CSTR and 220 mg/L or 40.0% of total nitrogen was removed in modified CSTR with HRT of 3 days. Also, 280 mg/L or 50.9% of total nitrogen was removed in conventional CSTR while 310 mg/L or 56.3% of total nitrogen was cut off in modified CSTR with HRT of 5 days. This proved that ammonia nitrogen is not effectively removed in both CSTR while others type of nitrogen such as nitrate, nitrite and inorganic nitrogen was effectively removed by bacterial in both systems.

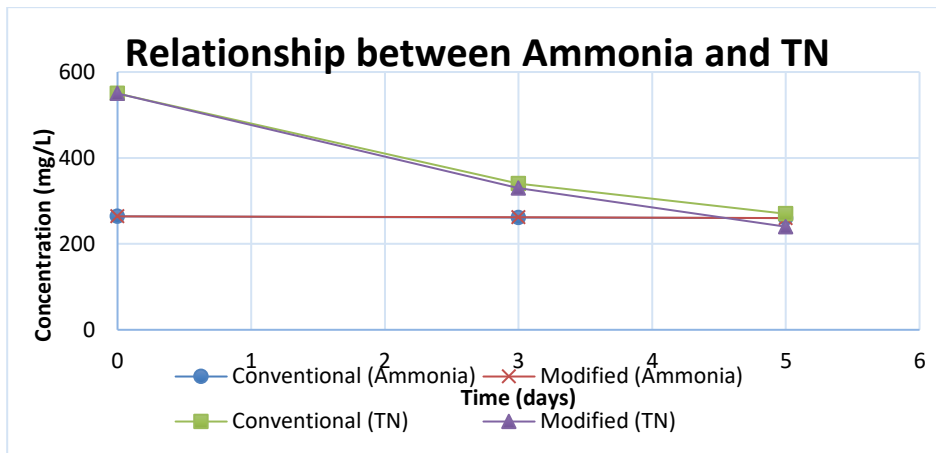


Figure 4: Relationship between Ammonia Nitrogen and Total Nitrogen in Conventional and Modified CSTR.

Total nitrogen in this run was removed effectively. However, ammonia nitrogen in this run was not well removed. This is mainly because ammonia removal bacterial required oxygen to perform nitrification process while anaerobic reactor was not supporting this process. However, some of the ammonia was still removed from the experiment. This may be because some of the oxygen was entered the system while injecting the feed. This is possible since oxygen may enter syringe while sucking the feed into it and eventually transfer the oxygen into the system. Although the volume of oxygen entered may be small enough for not paralysing the system, nitrification process still able to be functioned. Another possible way that oxygen able to enter the system is during the discharge process of feed that used for second experimental run despite the main plastic cap are not opened.

When focusing on total nitrogen effectively removed, the main reason may be nitrite effectively removed throughout the experiment period since denitrification are not required oxygen. However, it is still possible for others type of organic nitrogen removed from the system others from nitrite since the testing is not specific on any others nitrogen type. Also, total nitrogen level at days 5 was reached a point where near the level of ammonia nitrogen. The leftover total nitrogen may be consisting of mainly ammonia nitrogen.

In term of biogas production rate, conventional CSTR have weaker biogas production rate compared to modified CSTR as shown in Figure 5. Biogas production rate of 5.86 l/l.d was achieved in conventional CSTR while 6.52 l/l.d was recorded in modified CSTR with HRT of 3 days. Also, 6.11 l/l.d of biogas production rate was recorded in conventional CSTR while 6.68 l/l.d of biogas production rate was achieved in modified CSTR with HRT of 5 days.

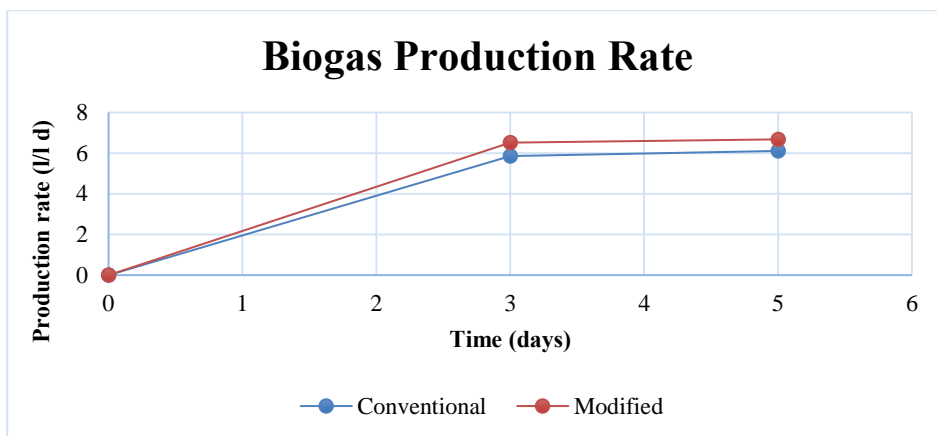


Figure 5: Biogas Production Rate of Conventional and Modified CSTR.

The result shown a strong biogas production rate at the initial stage of experiment while a weaker biogas production rate in the later stage of experiment. Since organic matter consumed by bacterial are converted into biogas, the early stage of experiment has a stronger conversion rate compared to later stage of experiment. However, result of biogas production in this study are based on estimation only, the result is calculated based on the weight of biogas captured as mentioned in previous section.

4. CONCLUSION

Based on the result, CSTR incorporated with PVA gel is effectively removing COD and SS in POME. However, modified CSTR have slightly higher removal efficiency compared to conventional CSTR. Biogas production rate in modified CSTR is slightly higher than conventional CSTR. Removal efficiency of ammonia nitrogen is insignificant in both reactors. However, total nitrogen is effectively reduced in both reactors. Both reactors are stable throughout the experiment from the result of pH testing, no paralysis of system observed.

REFERENCES

- Abdurahman, N.H., Rosli, Y.M., and Azhari, N.H. (2013). The performance evaluation of anaerobic methods for Palm Oil Mill Effluent (POME) Treatment: A Review. *International Perspectives on Water Quality Management and Pollutant Control*, 87-106.
- Director General of MPOB, Dr. Mohd. Basri Wahid, 19 January 2006, overview of the Malaysia oil palm industry 2005, http://econ.mpob.gov.my/economy/su_review2005.htm (30 July 2017).
- Elvira, E.Z., Svetlana, S.B., & Ayrat, M.Z. (2022). Impact of granular activated carbon on anaerobic process and microbial community structure during mesophilic and thermophilic anaerobic digestion of chicken manure. *Journal of Sustainability*, 14, 447.
- Era, R.F., Joni, P., Nurdiah, R., Tyas, P.R., Zulaicha, D.H., Novio, V., & Samuel, P. (2022). Development of Bio-CSTR design for Bio-H₂ from POME as renewable fuel. *Journal of Novel Carbon Resources Sciences & Green Asia Strategy*, Vol.09, Issue 02, pp491-499.
- APHA, Standard methods for the examination of water and wastewater, 21sted. (2005), Washington, DC, New York: American Public Health Association.
- Kuraray Aqua Co., Ltd., PVA Gel Bioreactor, <http://www.kurarayaqua.co.jp/en/product/pvgel.html> (access on 17 July 2017).
- Malaysia Palm Oil Board, Economics & Industry Development Division, Oil Palm Planted Area By States As At December 2016, http://bepi.mpob.gov.my/images/area/2016/Area_summary (access on 30 July 2017).
- Senturk, E., Ince, M., Engin, G.O., (2014). The effect of shock loading on the performance of a thermophilic anaerobic contact reactor at constant organic loading rate. *Journal of Environmental Health Science & Engineering*, Volume 12, 1-6.
- Sitthakarn, S., Masahi, H., & Takashi, Y. (2022). Accelerating anaerobic propionate degradation and studying microbial community using modified polyvinyl alcohol beads during anaerobic digestion. *Journal of Bioresource Technology Reports*, 17.
- Zhen, K.L., Yi, J.C., Zheng, T.H., Yew, H.Y., Ming, C.T., Ameer, I.T.A.A., Chong, S., Pau, L.S., & Chew, C.L. (2021). Biogas production enhancement by co-digestion of empty fruit bunch (EFB) with palm oil mill effluent (POME): Performance and kinetic evaluation. *Journal of Renewable Energy*.

DECONTAMINATION OF Zn IONS FROM AQUEOUS SOLUTION USING PAPAYA SEED AS LOW-COST ADSORBENT

**Khairunisah Kamaruzaman, Vinot A/L Arthimulam, Nik Nuraini Azhari,
Nadzifah Che Mat & Syazana Syahirah Jamaluddin**
Infrastructure University Kuala Lumpur

1. INTRODUCTION

Nowadays, heavy metals become the main concern of our authority since it will increase the toxicity level of water intake. Heavy metals accumulate in water quality resulting by discharge of wastewater from industrial, agricultural runoff and urban. The characteristics of heavy metal are not easily degraded by the natural environment. It will accumulate in aquatic biota and become organic complexes and create harmful effects on human health (Cuadrado et al., 2019). Therefore, levels and amount of contamination by heavy metal need to be traced to prevent the possible risks (Karahana et al., 2018).

Zinc, copper, lead and calcium are heavy metals that are highly detected in water intake. These heavy metals are required for the human body in small quantities but excessive exposure to these chemicals cause toxicity to the human body. Hypercalcemia, a condition of high level of calcium in the human body. It will weaken the bones, cause kidney stones and failure in heart and brain function. Neurotoxicity, liver toxicity, and lung cancer results in high exposure to copper. Harmful effects on the human body caused by high exposure of zinc and lead may cause elevated blood levels, mortality and fatal death (Agwaramgbo et al., 2021).

Others, it is reported that these normal discharges of zinc add up to 5.9 million metric tons each and every year. These unsafe metals may achieve more noteworthy wellbeing dangers. Hence in wastewater treatment innovation, various procedures have been passed down for the extraction of these dangerous metals from solution. In any manner or capacity ever, these customary strategies are for the most part costly and do spring up with potential disadvantages, for example, arrangement of metal creating waste and imperfect metal disposal (Li et al., 2008). Hence there is surely a demand for strategies that are economic, inexpensive, eco-friendly so as to expel overwhelming metals from an answer. In the late decade, disclosures have been made by using agricultural waste materials as bio-adsorbents to take out substantial metals, particularly zinc particles.

Inorganic coagulants which are chemical based create harmful effects on water quality and human health. Hence, bio-adsorbents being introduced to replace usage of this inorganic coagulant. Several studies have been conducted in usage of these bio-adsorbents. Bio-adsorbents such as sunflower (Marathe 2019), banana peel (Akpomie et al., 2020), durian peel (Adunphatcharaphon et al., 2020), pineapple peel (Abd Ghapar et al., 2020) and papaya peel (Mittal et al., 2021) have proven in successful removal water contaminants.

Instead of usage of fruit peel, fruit seed as well is able to reduce the water contaminants. One of the seeds that can be applied in water treatment is papaya seed. Papaya seed widely being disposed of as solid waste. In order to control the disposal of this papaya seed, it can be upgraded as bio-adsorbent since its ability to treat water. Papaya seeds contain 40% of water, antioxidants, protein and carbohydrates (Nurowidah et al., 2019). Seeds are a standout amongst the most essential assets for plant breeding and they are the conventional engendering medium to build up business papaya estates, in spite of the fact that this society can likewise be propagated by vegetative strategies. Papaya seeds carry on all the more likewise to standard seeds, whose feasibility is reached out by at the same time decrease in water substance and temperature amid capacity. This conduct has profitable preserves for protecting germ plasmas for extended time frames.

Papaya seeds act as adsorbents in wastewater treatment to remove the heavy metals, microorganism and dyes. The Absorption process by papaya seed is able to replace the high-cost adsorbents as low-cost alternatives. The papaya seed biomass can be modified to alter its surface functional group to improve the adsorption efficiency (Khee et al.,2022).

Decontamination of wastewater free from heavy metals such as zinc can be achieved by these research objectives. The objectives of this study are (1) to determine the effect of pH, contact time and effect of initial concentration of Zn ions, effect of mixing rate and effect of particle size on the adsorption of Zn ions on the papaya seed and (2) to study the efficiency of papaya seed as adsorbent of Zn ion from aqueous solution using the biosorption equilibrium isotherms

2. MATERIALS AND METHODS

The preparation of the Papaya seed powders is the first step of this experiment as it required (7+1) days of drying, grinding, and sieving. Papaya seed powder after grinding as shown in Figure 1. Preparation of zinc (Zn) stock solution needs the usage of Zinc Sulphate (ZnSO₄). Both the adsorbent and adsorbate are mixed using the jar test to allow the adsorption process by adjustment of a few parameters like pH of the solution, initial Zinc ion concentration, particle size of the adsorbent, and contact and mixing time. Langmuir and Freundlich isotherm models are used to interpolate the experimental data into graphical form to study the adsorption process and its effectiveness.



Figure 1: Papaya seed powder

Preparation of Adsorbent

The papaya seeds as shown in Figure 2 were collected freshly at several fruit shops situated in De Centrum City and Taman Sepakat Indah, Kajang. These seeds then were flushed altogether to evacuate all debasements and soil on the seeds. Washed seeds were dried under the daylight for 7 days and ensured the seeds turned dim. Further drying was finished by applying the warmth of a microwave at 105°C for 24 hours as shown in Figure 3. The dried papaya seed had been crushed into fine powder form using a mixer. An airtight compartment was utilized to store and seal the ground powder to guarantee no contact of air.



Figure 2: Papaya seed



Figure 3: Drying of papaya seed

Preparation of Adsorbate

Zinc (Zn) stock solution has been prepared at a concentration of 500 mg/l by the dilution of exactly 0.6175g of $ZnSO_4$ with 500ml of distilled water in a 500ml volumetric flask.

Batch Experiments

Batch experiments will be led by blending 1.5g papaya seed powder with 300ml of Zn solution in 500ml beaker by utilizing the jar tester at desired initial Zn concentration, contact time, mixing time and pH of solution. The blending rate is at 100 rpm for 2 hours until it achieves stability. At that point, the mixing will be stopped and the powder will be expelled from the solution using filter paper. The filtrate was later inspected to quantify the centralization of Zinc (Zn) particles utilizing a spectrophotometer. All testing will be done under the same standard using APHA standard (APHA 2017).

pH Adjustment

pH range 2 to 8 were adjusted. The test was done by blending 1.5 g of papaya seed powder into 300 ml of Zinc stock solution at concentration of 10 mg/L in a 500 ml beaker. Later the samples were blended at a blending rate of 100 rpm with 2 hours of contact time. The blending rate must be kept consistent until the experiment achieves a stable state. The pH of the solution required improvement by including suitable expansion of 1.0 N of Hydrochloric acid (HCl) or 1.0 N of Sodium hydroxide (NaOH) to the 10 mg/L Zinc Solution.

Initial Zinc Concentration and Contact Time

By investigating simultaneously both these effects of scopes upon the rate of adsorption of papaya seed powder and Zinc. Next, proceed to the study by blending 1.5 g papaya seed powder with 300ml of 5 mg/L Zn solution utilizing a 500 ml measuring glass. Later proceeding by the progression above must repeat at various concentration of Zn solution, for example, (5 mg/L, 10 mg/L, 20 mg/L and 30 mg/L) and jar test blending the samples at 100rpm over different eras, for example, 5, 10, 20, 30, 45, 60 minutes.

Mixing Rate

The testing of Mixing rate upon the rate of adsorption of papaya seed powder and Zn particles is comprehensive of 1.5 g of papaya seed powder to 300 ml of 5 mg/L Zn solution in a 500 ml beaker and continue with blending utilizing jar test equipment after a few time periods of 5, 10, 20, 30, 45, 60 minutes as shown in Figure 4. The mixing rate must be controlled at 50, 100, and 150 rpm (Jeyaletchumy, 2016).



Figure 4: Mixing using jar test

Biosorption Equilibrium Isotherms

The impact of papaya seed powder on the adsorption of Zn particles is considered in this project. Langmuir and Freundlich were the two isotherm models being utilized here as a part of request to insert the graphical study of the adsorption stabilization.

Particle Size of Adsorbent

The investigation of the molecule size of adsorbent upon the rate of adsorption of papaya seed powder and Zn particles is by including 1.5 g of papaya seed powder to 300 ml of 5 mg/L Zn solution in a 500 ml measuring glass. This must be blended by utilizing jar test equipment over a mixing rate of 100 rpm for 60 minutes. The above procedure will be repeated for 5, 10, 20, 30, 45 and 60 minutes furthermore by controlling the molecule size of the papaya seed powder by < 0.600 mm and > 0.600 mm. Later using sieve analysis analyze the size of the adsorbent particle.

3. RESULT AND DISCUSSION

Effects on pH

The outcome of pH of the zinc (Zn) solution upon the adsorption proficiency was studied by modifying the pH of the solution around the range of pH 2 to pH 8 as shown in Figure 5. Effectiveness on adsorption rates rely on suitable pH value (Xueyu et al., 2022). The adsorption rate increases starting from pH 2 to pH 8. This was due to the high concentration of H^+ ions. Hydrogen particles have a tendency to clash with metal particles for adsorption of the adsorbent. The highest Zn removal was found to be on pH 8.0 by 82%. More alkaline range suits on removal of Zn in this solution. The concentration of hydrogen particles would be partial. At pH more than 6.5, the metal particle hydrolyses and precipitates as the hydroxides would diminish the adsorption rate. Highest adsorption activity occurs in high pH due to cationic charges attracted to the negative surfaces through the electrostatic reaction in between

adsorbent and adsorbate (Aragaw et al., 2022).

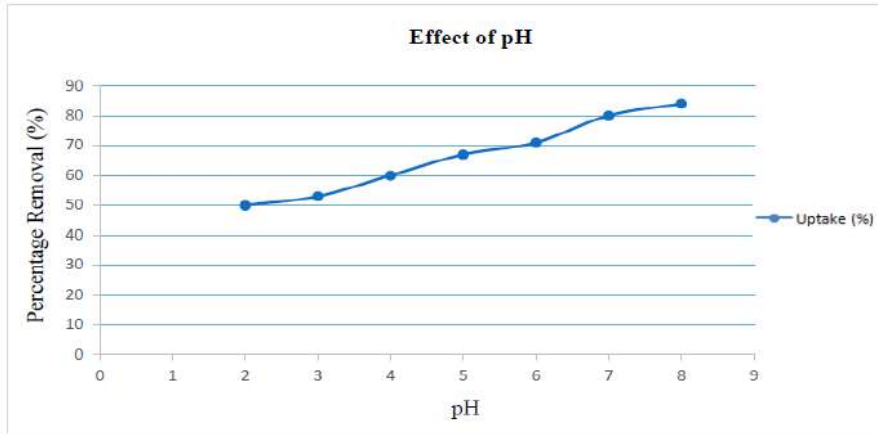


Figure 5: Effect of pH of Zn solution on the uptake of Zn ions by papaya seed

Effects of Contact time and initial Concentration of Zn particles

As per the initial concentration the sample was tested at 5 mg/L, 10 mg/L, 20 mg/L and 30 mg/L respectively as shown in Figure 6. The rate of adsorption has drastically increased during the first few minutes in regard to concentration of the solution. The presence of a bigger surface area of the adsorbent was the reason behind this phenomenon (Lock, 2015). Initial removal will be rapid with inflating concentration of metal ions and tend to slow down with higher concentration. This was due to the rapid saturation of adsorption areas. Highest metal removal was observed by 76% as the initial concentration was 5 mg/L. While the minimum metal uptake was observed when the initial pH concentration was 30 mg/L by 46.5%.

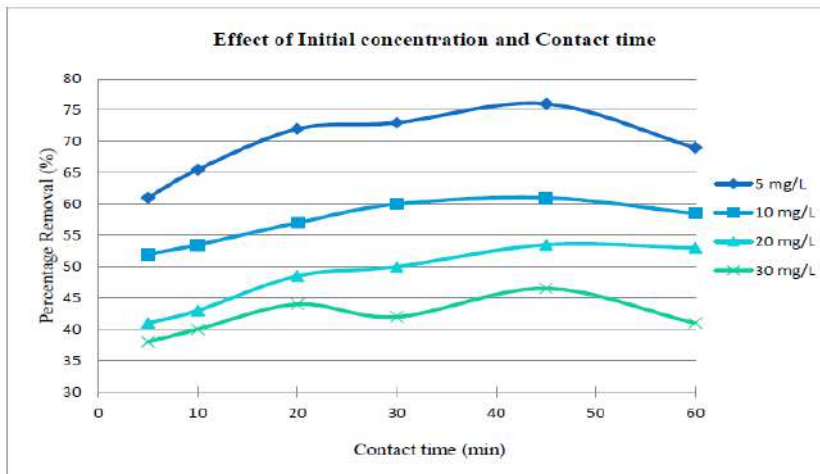


Figure 6: Effect of Initial Concentration of Zn Solution and Contact Time on the Uptake of Zn Ions by Papaya Seed

Effect of Mixing Rate

Figure 7 shows the effect of mixing rate using the papaya seed. Longest mixing time shows the highest removal efficiency which at 60 minutes on 50 rpm, the result reaches until more than 70% removal. The particle contact of adsorbate and adsorbent can bind wells in slow mixing. It was the combination of both stirring speed and time taken to stir the sample. The adsorption capacity was affected by the mixing speed and mixing time. As the speed of the stirring increases, the adsorption capacity decreases in terms of boundary layer thickness.

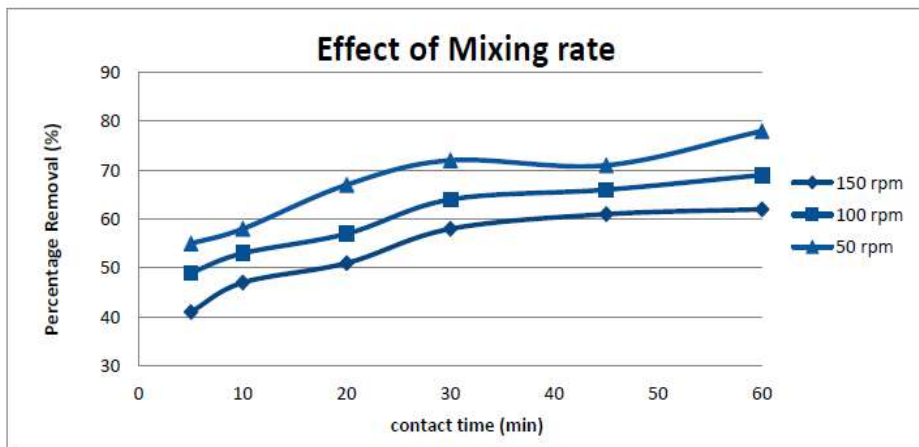


Figure 7: Effect of Mixing Rate on the Uptake of Zn Particles by the Papaya Seed

Effect of Particle Size of Adsorbent

Molecule size of adsorbent impacts the adsorption limit as shown in Figure 8. The expansion in the territory per unit weight of the adsorbent limitedly affects the metal adsorption rate. According to study, the rate of metal evacuation was relied upon to increment with the decrease of molecule size. This was because of the way that littler particles have bigger surface area. It tended to deliver shorter time to achieve harmony and it did so.

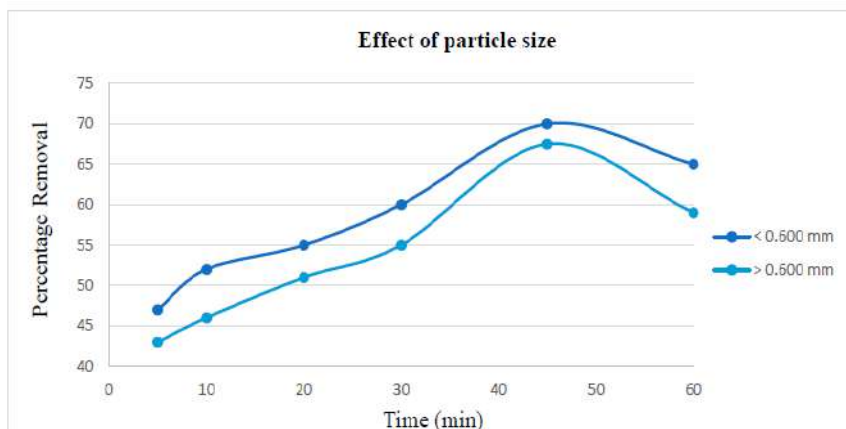


Figure 8: Effect of Molecule Size of Adsorbent on the Uptake of Zn Particles by Papaya Seed

Biosorption Equilibrium Isotherms

Freundlich Isotherm Model

Figure 9 shows the graph of $\log q_e$ vs $\log C_e$. The Freundlich isotherm model that describes the adsorption relationship between Zinc ions and the papaya seed was studied in this plot. The graph yields a correlation coefficient of 0.9795. This indicates that the coefficient which was close to identification and testifies that the data obtained can adjust well with the Freundlich isotherm model.

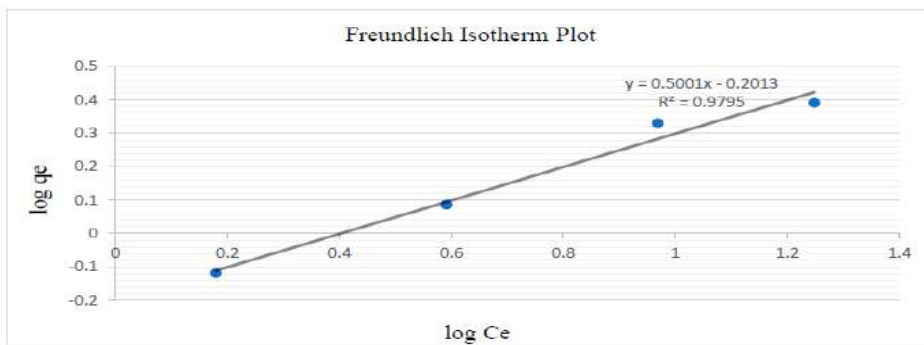


Figure 9: Freundlich Isotherm Plot for the Adsorption of Zinc Ions onto Papaya Seed

Langmuir Isotherm Model

Figure 10 shows the graph of $\log q_e$ vs $\log C_e$. Langmuir isotherm model that describes the adsorption relationship between Zn ions and the papaya seed was studied in the plot. The graph gives out a correlation coefficient of 0.9815. This indicates that the coefficient which was close to unity testifies that the data obtained can also adjust well with the Langmuir isotherm model. According to the Langmuir Equation, the maximum adsorption capacity for Zinc ions was 3.103 mg/g. The adsorption data obtained by plotting isotherm graphs proves that they can conform well to both Freundlich and Langmuir isotherm models. However, as the correlation coefficient plotted using Langmuir isotherm model (0.9815) seems to be much closer towards unity, this particular model is believed to fit best for the result obtained.

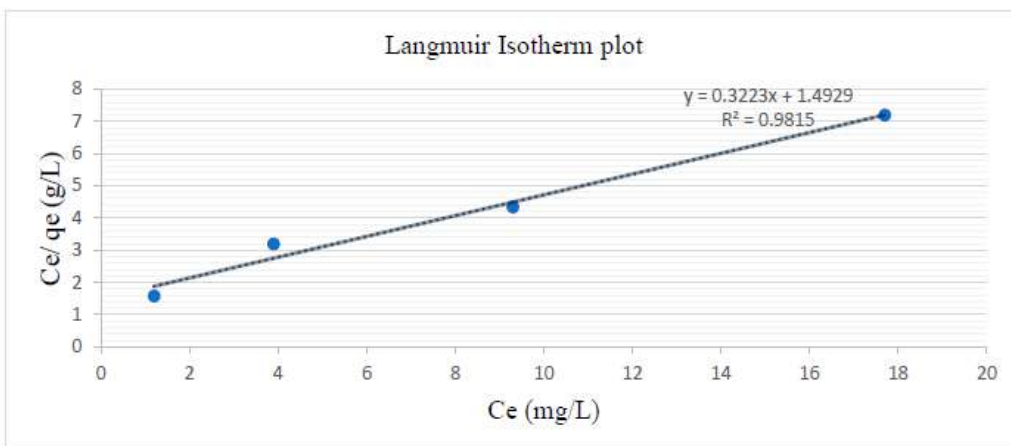


Figure 10: Langmuir Isotherm Plot for the Adsorption of Zinc Ions onto Papaya Seed

4. CONCLUSION

This study demonstrated that the removal of zinc particles from solution is highly influenced by the 4 major factors which are pH of solution, contact time and initial metal particle concentration, mixing rate and the molecule size of adsorbent. Equilibrium is achieved at the 45th minute of batch mixing process and pH 6 is observed to be the optimum pH for adsorption. The equilibrium information balanced well with the Langmuir isotherm model by yielding a correlation coefficient of 0.9815. This shows a mono layer pattern is trailed by the adsorption mechanism of the Zn particle onto papaya seed. The maximum adsorption limit determined using the Langmuir isotherm model is 3.103 mg/g.

REFERENCES

- Abd Ghapar, N. F., Samah, R. A., & Abd Rahman, S. (2020, December). Pineapple Peel Waste Adsorbent for Adsorption of Fe (III). In IOP Conference Series: *Materials Science and Engineering* (Vol. 991, No. 1, p. 012093). IOP Publishing.
- Adunphatcharaphon, S., Petchkongkaew, A., Greco, D., D'Ascanio, V., Visessanguan, W., & Avantaggiato, G. (2020). The effectiveness of durian peel as a multi-mycotoxin adsorbent. *Toxins*, 12(2), 108.
- Agwaramgbo, L., Doyle, J., Harrison, C., & Williams, H. (2021). Comparative Evaluation of Calcium, Magnesium, Copper and Zinc Removal by Wood Ash, Sodium Carbonate and Sodium Hydrogen Phosphate. *Journal of Environmental Protection*, 12(7), 454-461.
- Akpomie, K. G., & Conradie, J. (2020). Banana peel as a biosorbent for the decontamination of water pollutants. A review. *Environmental Chemistry Letters*, 18(4), 1085-1112.
- APHA, 2017 APHA Standard Methods for the Examination of Water and Wastewater (23rd ed.), American Public Health Association, American Water Works Association, Water

- Environment Federation, Washington, DC (2017)
- Aragaw, T. A., & Alene, A. N. (2022). A comparative study of acidic, basic, and reactive dyes adsorption from aqueous solution onto kaolin adsorbent: Effect of operating parameters, isotherms, kinetics, and thermodynamics. *Emerging Contaminants*, 8, 59-74.
- Cuadrado, W., Custodio, M., Espinoza, C., Vicuña, C., & Uribe, M. (2019). Capacity of absorption and removal of heavy metals from *Scirpus californicus* and its potential use in the remediation of polluted aquatic environments. *Open Journal of Marine Science*, 9(02), 74.
- Jeyaletchmy. (2016). Efficiency of durian leaves as adsorbent of Fe (II) ion from aqueous solution. KARAHAN, G., TAŞKIN, H., BİNGÖLDAĞ, N.,
- Kapdan, E., & Yilmaz, Y. Z. (2018). Environmental impact assessment of natural radioactivity and heavy metals in drinking water around Akkuyu Nuclear Power Plant in Mersin Province. *Turkish Journal of Chemistry*, 42(3), 735-747.
- Khee, Y. L., Kiew, P. L., & Chung, Y. T. (2022). Vaporizing papaya seed waste for wastewater treatment: a review. *International Journal of Environmental Science and Technology*, 1-20.
- Lock, L. S. (2015). Utilization of Durian leaves as low cost adsorbent for the removal of Zn(II) ions from aqueous solution.
- Marathe, S. (2019) Potential of Sunflower to Extract Heavy Metals from Leachate. *International Journal of Geosciences*, 10, 1115-1127
- Mittal, J., Ahmad, R., Mariyam, A., Gupta, V. K., & Mittal, A. (2021). Expeditious and enhanced sequestration of heavy metal ions from aqueous environment by papaya peel carbon: a green and low-cost adsorbent. *Desalin. Water Treat.*, 210, 365-376.
- Nurowidah, A. (2019, April). The potency of *Carica papaya* L. seeds powder as anti-obesity 'coffee' drinks. In IOP conference series: materials science and engineering (Vol. 515 No. 1, p. 012098). IOP Publishing.
- Wei Li, Libo Zhang, Jinhui Peng, Ning Li, Shimin Zhang, Shenghui Guo (2008), Tobacco stems as a low-cost adsorbent for the removal of Pb (II) from wastewater: Equilibrium and kinetic studies, *Industrial Crops and Products*, 28(3), 294-302.
- Xueyu Wang, Heng Zhang, Yaoyao Wei, Lei Bao, Shasha Liu, Shideng Yuan, Shiling Yuan (2022). Effect of pH on caffeine removal from aqueous media by graphene/graphene oxide adsorption, *Colloids and Surfaces A: Physicochemical and Engineering Aspects*, 644

A STUDY ON THE EFFECT OF STYRENE-BUTADIENE RUBBER LATEX TO THE CONCRETE MECHANICAL PERFORMANCE

Nadzifah Che Mat, *Eric Wong Fa Yao*, Nik Nuraini Azhari & Khairunisah Kamaruzaman

Infrastructure University Kuala Lumpur

1. INTRODUCTION

Ordinary concrete is a composite material made from cement (fluid form) bonded with aggregates (fine and coarse) that will harden over time. This composite material is used for many years in construction. It is expected to effectively perform well in its purpose throughout its designed life span. By 200 BC, Romans successfully implemented the use of concrete in their majority of development. In an article reported by Laticrete International, INC (5 November 2007), England was the first commercial use of latex in Portland cement in the early 1902's. Natural rubber latex, imported from Malaysia, was introduced as an admixture to fortify the portland cement mortars to repair the sea walls. Regular concrete deteriorates from exposure to water, sun, drying, and salt. Additionally, steel reinforcements are also damaged by salt corrosion.

Latex modified concrete (LMC) is a modified concrete that uses latex emulsion to replace a mixing water portion to improve the properties of concrete such as durability, compressive strength, tensile strength, flexural strength, workability, chemical resistance. Based on researchers' studies, the latex-modified concrete (LMC) is excellent as a rehabilitation method for building such as parking building structures and bridge overlays. It also has been regarded as a material for the top layer of rooftop concrete. There are several types of latex used to modify concrete which are polyvinyl acetate, natural rubber, acrylic and styrene-butadiene Etc. Previous researchers' studies have shown latex is excellent at improving microstructure of concrete. Since the durability and hydration process of concrete depends on the microstructure. (Soni & Joshi, 2014; Prasad et al., 2010).

Styrene-butadiene rubber (SBR) latex is a type of polymer composed of water, butadiene and styrene which can be bonded quickly with other materials. SBR is well known as the material of making tires; in the construction industry, SBR used to replace water as a binder to improve compressive, flexural and tensile strength. The appearance of SBR is a thick white liquid with 52.7 per cent water content. In this study, the effect of modifying concrete with SBR latex on compressive strength and workability has been investigated. The strength development of LMC was studied at 7 and 28 days age and compared to ordinary portland concrete (OPC).

2. LITERATURE REVIEW

The engineers and scientists carried out the research and investigated the LMC with good quality to fulfil the requirements for several conditions. LMC was developed at the start of the twentieth century. The first method to be used on latex was the use of natural rubber latex and cement as an overlay in the method. After a year, based on Lefebure (1920), the new concept of a polymer latex-modified method was introduced as well as the latex-modified mortar (LMM) and concrete was developed using natural rubber latexes with the blending process. In the early 1900s, studies on latex in the world embraced the concept and produced different kinds of latex-modified mortars and concrete tempering with NR latexes. The use of latex in engineering, particularly in building, was rapidly developed when discovered in the 1940s, the innovations for LMC systems with synthetic latexes such as polychloroprene rubber and polyacrylic ester latexes were authorized and granted. Furthermore, mortar and concrete modified with polyvinyl acetate have been successfully developed for practical uses.

Properties of Latex Modified Concrete

Durability

Based on research by M. M. Reda et al. (1997), the durability of Styrene-Butadiene(SB) latex modified concrete(LMC) was proved to be outstanding compared to the conventional concrete. The significant difference between LMC and conventional concrete is the microstructure shown by the Scanning Electron Microscope(SEM) investigation. The microstructure of LMC is denser, smaller irregular pores, and has a more excellent bond between the cement matrix and aggregate.

Water Tightness

Based on research by M. M. Reda et al. (1997), the water-tightness of the SBLMC is excellent, which is measured by absorption test, sorptivity test, and water penetration tests. From the tests, LMC proved to have more excellent resistance to absorption, sorptivity, and water penetration compared to OPC, which the tests observed at all test ages.

Compressive Strength

Based on research by Ismail et al. (2012), the Natural Rubber(NR) latex modified concrete (LMC) strength increase was 86.2% higher than the OPC within 84 days.

Application of Latex Modified Concrete

Based on research by Kuhlmann (1985), the LMC is suitable for the repair and rehabilitation of bridges based on the latex properties. From the analysis, SBR provides enough protection for bridges exposed to saltwater and also improves the bond, flexural and tensile strength of concrete. However, it is difficult to control the cracks of LMC due to the construction conditions of bridge deck pavement in which significant water evaporation occurs, and as a result, plastic shrinkage cracks and drying shrinkage cracks often occurs (Yun et al. 2002; Choi et al. 2016).

3. METHODOLOGY

Article Selections

The selection of the article was referred to as the objective of the current study. First, the selection of properties of SBR latex must be similar. The tests in the article at least have the compressive strength test. Other tests in the article used for comparison is slump tests, flexural strength test and water absorption test. The addition of admixture in the article also uses to study the behaviour of the LMC. The number of articles is selected is 7 article. Other than that, the articles must be published in the last 5 year to ensure the result is new and can be used in the future

Analysis Method

The narrative analysis method was applied for the analysis of data obtained from the researcher. The reason for using the narrative analysis method is to have a better understanding of the behaviour of the LMC at the view of the researcher. The experiences and explanation from the researchers are one of the best ways to aid in the study of the properties of LMC.

Selected Cases

The selected cases are Joshi(2014), Sohu(2020), Qadri(2020), Varghese(2017), Palson(2017), Moodi(2018), Kadhim(2016).

4. RESULTS AND DISCUSSION

Slump Test Analysis

According to Palson (2017), the LMC has a plasticising effect and ball bearing action in the SBR latex particle due to the increase of concrete workability which maintained between 50mm (5% SBR) to 75mm (15% SBR).

Based on Qadri (2020), results showed the workability of LMC increased with the addition of SBR. The 5% SBR sample has 44mm of slump value compared to 23mm of OPC. On further addition, 20% of SBR had a maximum slump of 136mm following a similar trend. The result signifies that the SBR can reduce friction between the particles and perform concrete flow better at a constant water ratio. The results summarised in Figure 1 are similar to previous researchers' study, including Palson (2017) and Joshi (2014).

According to Sohu (2020), the highest value of slump is 40mm (0% SBR), and the lowest is 27mm (20% SBR). The result was observed with reducing slump value due to the less water available. SBR required some water to coat the surface to achieve lower friction properties and affect concrete workability, as shown in Figure 1.

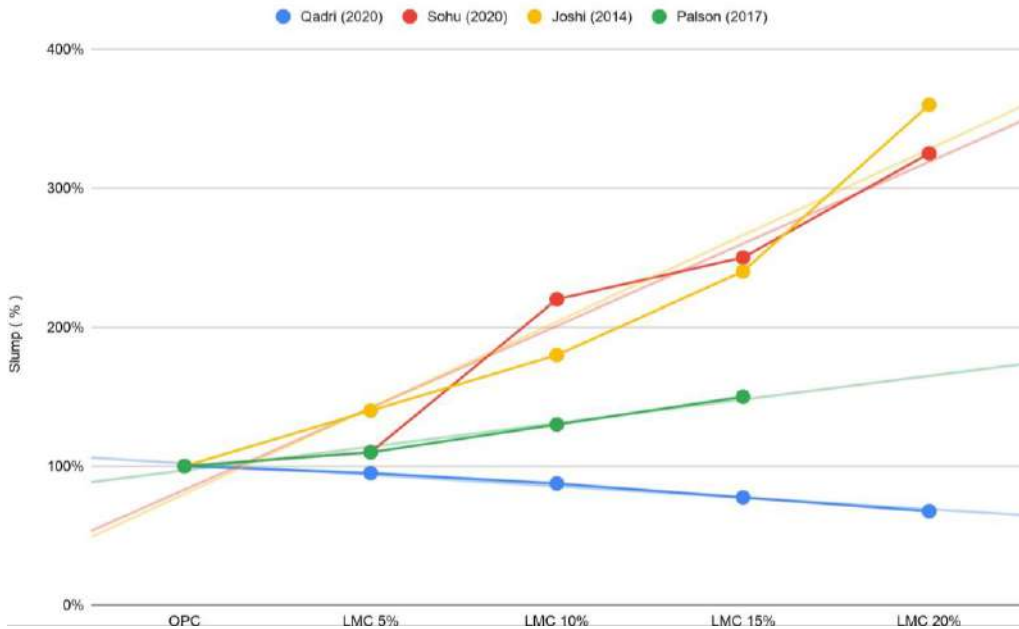


Figure 1: Slump Test Comparison.

From the researchers' results, SBR has physical properties that decrease the particle's friction, resulting in more excellent concrete workability at fresh state. The water ratio will also affect the workability, as the case from Sohu (2020), the water-cement ratio is 0.59 higher than other researchers, but the mix proportion of Sohu (2020) has a higher mix ratio 1:2.85:3.51. The resulting water is insufficient due to the lower cement-aggregate ratio. In some cases, higher slump value will result in segregation, and the concrete's mechanical properties will be affected.

Compressive Strength Test Analysis

According to Joshi (2014), the compressive strength test results decrease with the addition of SBR at an early age. However, the strength increases at 28 days with the addition of SBR. Table 2 shows that LMC with 15% of SBR is the optimum ratio for the compressive strength with a 17% increase compared to OPC.

Based on Sohu (2020), the compressive strength increase with the adds of SBR at both 14 days and 28 days. Figure 2 shows that compressive strength increase as SBR increase is up to 15%, then the strength starts declining. The highest strength measured is 3260 psi (14 days), and 3715 psi (28days) which is LMC 15% and the lowest strength obtained is 2745 psi (14 days) and 3175 psi (28 days) which is LMC with 20% SBR. As a result, the optimum SBR percentage is 15% for highest LMC compressive strength.

According to Qadri (2020), 5% LMC has a compressive strength of 24.5MPa with an increase of 22.8% compared to OPC. However, the strength starts to decrease from 23.2 MPa (10%) to 19.2 MPa (20%). Inordinate use of SBR would make the concrete lower strength compare to smaller partial replacements. The increasing percentage of SBR in the mix will push

its presence and reduce hydration, affecting the bonding strength outcome, having lower bonding strength.

Figure 2 shows that the optimum percentage is 5% for the highest compressive strength, similar to Varghese (2017).

Based on Palson (2017), the concrete’s compressive strength in general, a weakening pattern accompanied by the increase in SBR. The strength at 28days decreased by 8.72% (5% SBR), 14.61% (10% SBR) and 22.87% (15% SBR). The strength reduction at 90 days is 8.4% (5% SBR), 12.80% (10% SBR) and 20.77% (15% SBR). The decrease in the compressive strength of LMC is attributed to the presence of rubber material as a soft partition of cement gel particles and rise in air contents of latex modified concrete.

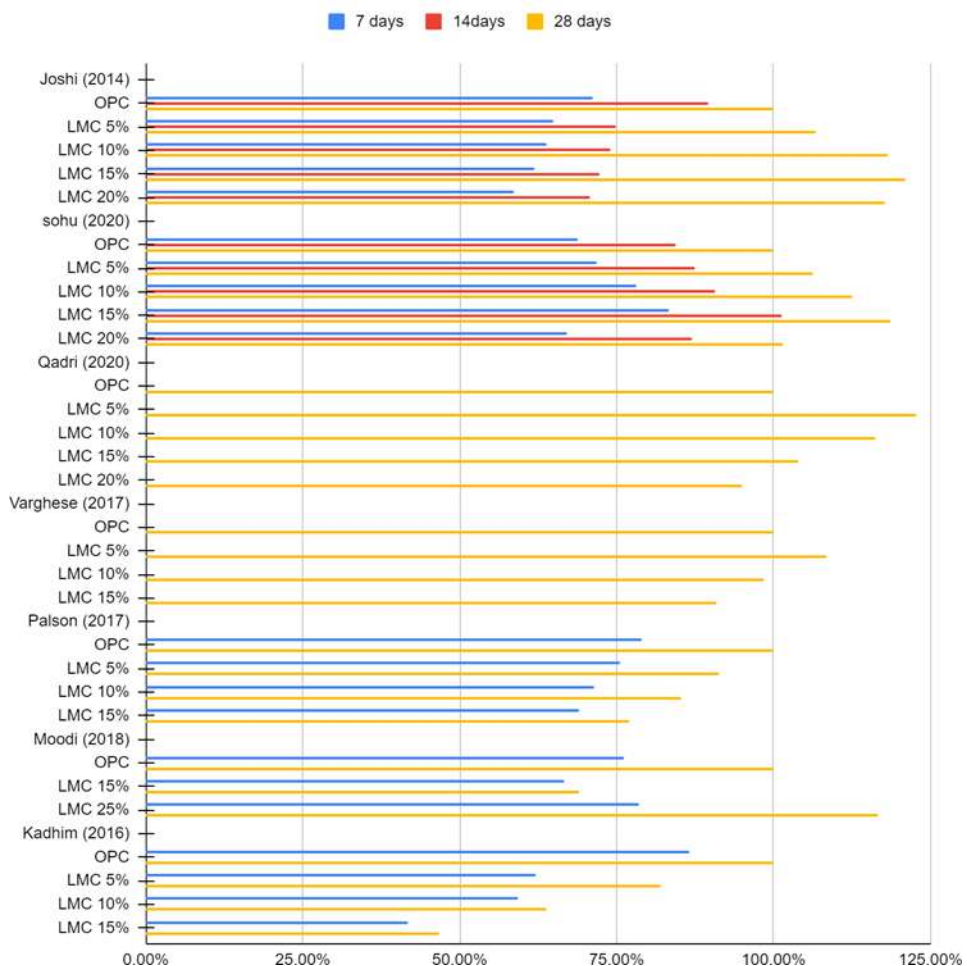


Figure 2: Compressive Strength Test.

According to Moodi (2018), SBR 25%’s strength was 29% higher than OPC after 90 days. Other than that, SBR 15% had a lower compressive strength than OPC at various age.

Figure 2 show that for the highest compressive strength, 25% is the optimum percentage of SBR.

Based on Kadhim (2016), the LMC's compressive strength is lower than the High-Performance Concrete (HPC) in all test periods and the percentage decrease with an increase in the latex cement ratio. This property may be due to SBR leads to form a polymer network which interpenetrates the cement, or the porosity of SBR reduces by the partial filling of the pores with the particles.

From the results, the optimum percentage of SBR has two option which is 15% supported by Joshi (2014) and Sohu (2020) and 5% supported by Varghese (2017) and Qadri (2020). From the observation, the properties of SBR will highly affect the performance of LMC. For high strength concrete, SBR shows no benefit to its compressive strength. However, determining the optimum % of SBR still needs to take other performance into accounts, such as flexural strength, tensile strength, water penetration, ETC.

Flexural Strength Test Analysis

According to Joshi (2014), the same case as observed in compressive strength, the flexural strength at seven days shows the decreasing trend in which the highest strength is OPC and the lowest value is LMC with 20% SBR. However, The flexural strength improvement at 28days is significant compared to the Compressive Strength of LMC. Figure 3 shows that the optimum percentage is 15% SBR for maximum strength increase.

According to Qadri (2020), the OPC had a 1.84 MPa flexural strength. With 5% SBR the flexural strength gains to 2.52MPa. A further increase is 2.73 MPa (10% SBR), 2.95 Mpa (15% SBR). When 20% of SBR is added to the mix, the observation shows the strength slightly decrease to 2.74 MPa. The SBR gluing effect enhance in resist bending stresses with an increase flexural strength result but when adding 20% SBR, the strength value decrease in result show the superiority of the polymer in the sample, which decreases the flexural potential of the prism studied. Figure 3 shows that the optimum percentage is 15% SBR which is the highest value of flexural strength. There are similar studies from Varghese (2017) and Palson (2017) have identical flexural increase trend which the highest value is 15%SBR.

Based on Moodi (2018), the performance of LMC is better than ordinary concrete at various ages. In all age range, SBR 25% showed higher strength compare to SBR 15% and OPC especially at 90 days SBR 25% has a huge leap with a 117% higher than OPC compare to SBR 15% only 25% higher. Figure 3 shows that the optimum percentage is 25% SBR which is the highest value of flexural strength.

According to Kadhim (2016), as a result, flexural strength is greater than OPC and this number rise with an increase in the percentage of SBR at all ages except 15 per cent of SBR is smaller than OPC.

From the results, the optimum percentage is 15% SBR with the studies supported by Varghese (2017), Palson (2017), Qadri (2020), and Joshi (2014). The study range of these four

researchers is between 5% SBR to 20% SBR. The decrease and increase of strength are suspected of performing the polymer film's surface that maintains internal pressure to continue its cement hydration. Other than this, SBR needs time to create the SBR structure and the formulation of the cement matrix. This polymer film develops with age, which is why an improvement in compressive and flexural strength is identified with SBR latex addition at 28 days of age. Even so, the creation of SBR structure and cement hydration is in the process of forming at an early age. As a result, the SBR latex addition has a negative strength effect.

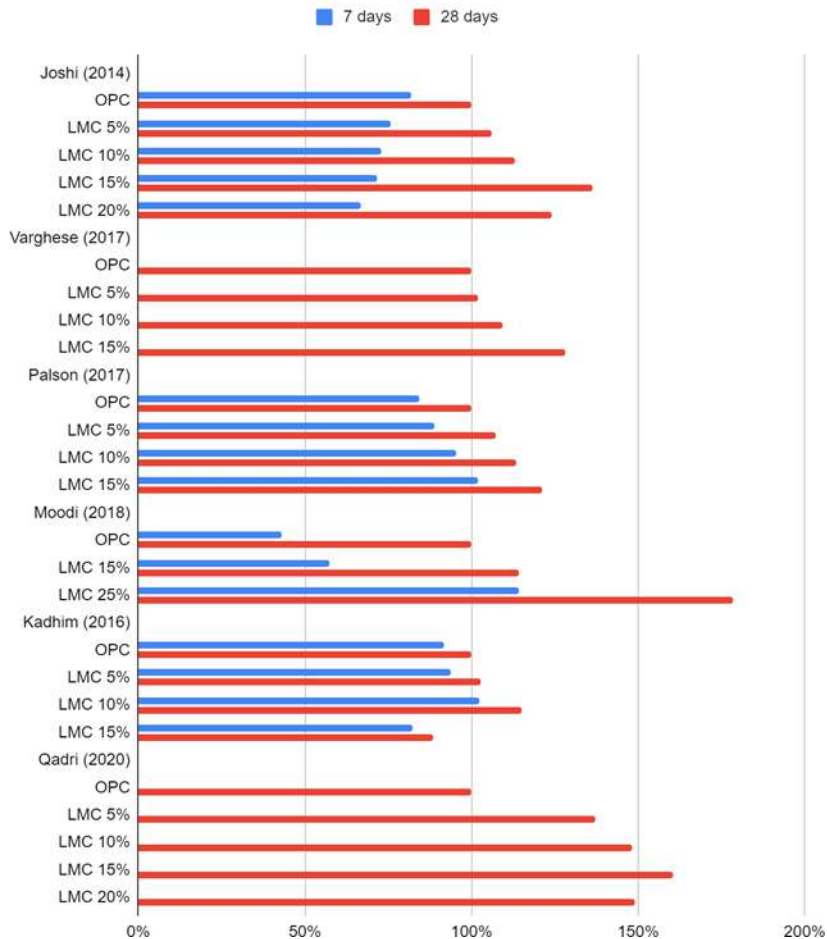


Figure 3: Flexural Strength Test.

Water Absorption Test Analysis

According to Qadri (2020), the OPC had 4.1% water absorption after 28 days. The increase in the SBR value lowered the penetration of water. In comparison to 5% SBR, the absorption of water was 3.7%, which also decreased to 10% SBR by 3.1%. In comparison, the amount of 15% SBR declined to 2.8%. The minimum value of 2.6% of additional SBR was observed at 20%. The findings demonstrate that the inclusion of SBR increases the concrete's water tightness as

the SBR picks up the concrete's valves. The formation of SBR in these voids prevents water ingress by reducing the concrete's total porosity. Figure 4 shows that the addition of SBR percentage the better performance for water absorption resistance. Therefore, the optimum percentage of SBR is 20%.

Based on Kadhim (2016), the dry density of OPC and LMC increase gently with the increase of SBR % at 7 days and 28 days but the water absorption and porosity decrease. The LMC's density is greater compare to OPC but the absorption and porosity of LMC are lower compared to OPC.

From the results, the improvement of the water tightness is due to the following reason. These properties based on two causes :

1. The increase of SBR % cause reduces in porosity which also decreases the water absorption.
2. During periods between 7 days to 28 days, the cement shrinkage process makes the porosity and voids reduce.

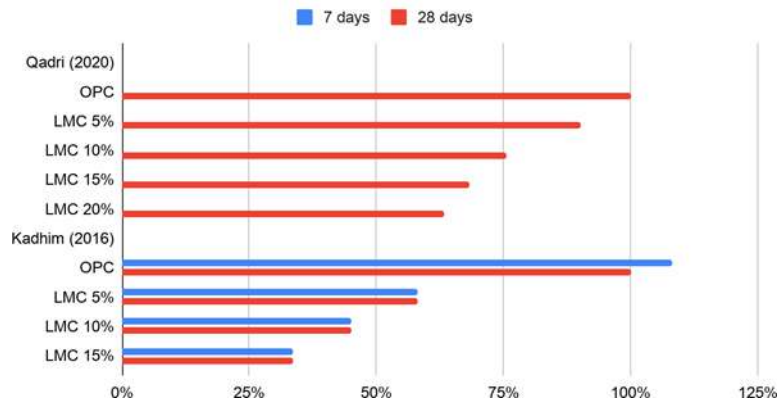


Figure 4: Water Absorption Test

5. CONCLUSION

According to the physical properties of LMC, the early compressive strength of LMC is weaker than OPC. However, the compressive strength of LMC at/after 28 days has great improvement which at range 21% to 29% increase compared to OPC. Other than that, there is a case, the compressive strength is lower than OPC at all age range. According to the researcher, the reason for the low compressive strength is due to lack of water which causes the ability of the SBR unable to enchant the performance of LMC. From studied cases, there are various cases able to support the improvement of compressive strength at/after 28days, LMC has higher strength due to the SBR providing better bonding strength to the concrete to support the additional forces.

Flexural strength has the same trend as compressive strength, the early flexural strength of LMC is also weaker than OPC. However, the strength improvement at 28 days is huge compare to the improvement of compressive strength. The improvement range is between 21% to 117% from various cases. There is no exception, which all cases have strength improvement compare to OPC. Therefore, all the studied cases are able to support the improvement of flexural strength at 28 days. The increase of flexural strength is also due to the strong bonding strength provided by SBR. From the observation, at early age the LMC is still in the formation process which causes the negative strength effect. Therefore, the LMC required time to become stronger where the LMC is stronger at 28 days.

Water tightness from various cases has a similar and stable trend, as the addition of SBR% the better the water tightness. The water absorption reduction is at 2.6% which OPC is 4.1%, the lower the water absorption the better the water tightness. There is a case, where the LMC is mixed with 1% of superplasticizer based on the weight of concrete. With the help of superplasticizer, water absorption reduction is huge compared to LMC which is 0.9%. From the studies, the SBR hv the ability to fill void and increase the water tightness of the concrete.

From the cases studied, the higher the percentage of SBR the better the performance. However, when 20% of SBR is added, the performance starts to decrease compared to the maximum performance at 15% of SBR. Therefore, the optimum percentage is 15% of SBR to achieve the best performance.

REFERENCES

- Andayani, S. W., Suratman, R., Imran, I., & Mardiyati. (2018, May). Copolymer natural latex in concrete: Dynamic evaluation through energy dissipation of polymer modified concrete. In AIP Conference Proceedings (Vol. 1958, No. 1, p. 020012). AIP Publishing LLC.
- Yun, K. K., Lee, J. H., & Hong, C. W. (2002). Properties of Latex modified concrete with rapid-setting cement using antifoamer. *Journal of the Korea Society of Civil Engineer*, 22(5-A), 114
- Atiyah, A. A., Farid, S. B., & Kadhim, A. S. (2016). High Performance Concrete Improvement by Styrene-Butadiene Rubber Addition. *Engineering and Technology Journal*, 34(12), 2296-2309.
- Çolak, A. (2001). Characteristics of acrylic latex-modified and partially epoxy-impregnated gypsum. *Cement and Concrete Research*, 31(11), 1539-1547.
- Çolak, A. (2005). Properties of plain and latex modified Portland cement pastes and concretes with and without superplasticizer. *Cement and Concrete Research*, 35(8), 1510-1521.
- Diab, A. M., Elyamany, H. E., & Ali, A. H. (2013). Experimental investigation of the effect of latex solid/water ratio on latex modified co-matrix mechanical properties. *Alexandria Engineering Journal*, 52(1), 83-98.
- Diab, A. M., Elyamany, H. E., & Ali, A. H. (2014). The participation ratios of cement matrix and latex network in latex cement co-matrix strength. *Alexandria Engineering Journal*, 53(2), 309-317.
- Doğan, M., & Bideci, A. (2016). Effect of Styrene Butadiene Copolymer (SBR) admixture on

- high strength concrete. *Construction and Building Materials*, 112, 378-385.
- EN, B. (2000). 12390-1.(2000). British standard for testing hardened concrete–Part 1: Shape, dimensions and other requirements for specimens and moulds.
- EN, B. (2009). 12350-2: 2009. Testing fresh concrete. Slump-test. British Standards Institution.
- EN, B. (2019). 12390-3: 2019. Testing Hardened Concrete. Compressive Strength of Test Specimens; British Standard Institute: London, UK.
- EN, B. 12390-5: 2019 Testing hardened concrete. Flexural strength of test specimens.
- Harish, G. R., & Zai, S. A. K. (2010). Behavior Of SBR-Latex Modified Polypropylene Fibre Reinforced Railway Sleepers Under Static Loading. In 35th Conference on our world in concrete & structures (pp. 25-27).
- Hoang, N. D., & Pham, A. D. (2016). Estimating Concrete Workability Based on Slump Test with Least Squares Support Vector Regression. *Journal of construction engineering*, 2016.
- Ismail, M. O. H. A. M. M. A. D., Muhammad, B. A. L. A., Yatim, J. M., Noruzman, A. H., & Soon, Y. W. (2011). Behavior of concrete with polymer additive at fresh and hardened states. *Procedia engineering*, 14, 2230-2237.
- Ismail, M., Muhammad, B., Yussuf, A. A., Majid, Z., & Ismail, M. E. (2011). Mechanical capabilities and fire endurance of natural rubber latex modified concrete. *Canadian Journal of Civil Engineering*, 38(6), 661-668.
- Khan, A. N., Bheel, N. D., Ahmed, M., Abbasi, R. A., & Sohu, S. (2020). Use of styrene butadiene rubber (SBR) polymer in cement concrete. *Indian Journal of Science and Technology*, 13(5), 606-616.
- Kim, D. G., Lee, D. U., Yang, E. I., & Cha, H. (2016). Durability of latex-modified concrete carried by ready-mix truck for concrete rooftops. *Magazine of Concrete Research*, 68(6), 318-324.
- Kim, D. H., & Park, C. G. (2013). Strength, permeability, and durability of hybrid fiber-reinforced concrete containing styrene butadiene latex. *Journal of Applied Polymer Science*, 129(3), 1499-1505.
- Kuhlmann, L. A. (1985). Latex modified concrete for the repair and rehabilitation of bridges. *International Journal of Cement Composites and Lightweight Concrete*, 7(4), 241-247.
- Moodi, F., Kashi, A., Ramezani-pour, A. A., & Pourebrahimi, M. (2018). Investigation on mechanical and durability properties of polymer and latex-modified concretes. *Construction and Building Materials*, 191, 145-154.
- Muhammad, B., & Ismail, M. (2012). Performance of natural rubber latex modified concrete in acidic and sulfated environments. *Construction and Building Materials*, 31, 129-134.
- Palson, P., & Vidivelli, B. (2017). Mechanical properties of latex modified concrete with silica fume. *International Journal of Civil Engineering and Technology*, 8(9), 701-710.
- Polymer Concrete (Epoxy, Polyester, Latex) Market - Global Forecast to 2022 - ResearchAndMarkets.com. (2018, February 12). Retrieved September 07, 2020, from [https://www.businesswire.com/news/home/20180212005792/en/Polymer-Concrete-Epoxy-Polyester-Latex-Market-](https://www.businesswire.com/news/home/20180212005792/en/Polymer-Concrete-Epoxy-Polyester-Latex-Market)
- Prasad, B. K., Gupta, U., & Choubey, U. B. (2010). Behaviour of latex-modified concrete under cyclic loading. *Proceedings of the Institution of Civil Engineers-Construction Materials*, 163(1), 27-34.
- Qadri, M. A., Hameed, H., & Bhutta, O. (2020). Fresh and Hardened Properties of Styrene

- Butadiene Rubber (SBR) Modified Concrete. *European Journal of Engineering and Technology Research*, 5(4), 457-461.
- Rajkumar, D., & Vidivelli, B. (2010). Performances of SBR latex modified ferrocement for repairing reinforced concrete beams. *Australian Journal of Basic and Applied Sciences*, 4(3), 520-531.
- Shaker, F. A., El-Dieb, A. S., & Reda, M. M. (1997). Durability of styrene-butadiene latex modified concrete. *Cement and concrete Research*, 27(5), 711-720.
- Siddiqi, Z. A., Hameed, R., Saleem, M., Khan, Q. S., & Qazi, J. A. (2013). Determination of Compressive Strength And Water Absorption of Styrene Butadiene Rubber (SBR) Latex Modified Concrete. *Pakistan journal of science*, 65(1), 124.
- Soni, K., & Joshi, Y. P. (2014). Performance analysis of styrene butadiene rubber-latex on cement concrete mixes. *Journal of Engineering Research and Applications*, 3(1), 838-44.
- Sprinkel, M. M. (1984). Overview of Latex Modified Concrete Overlays (No. VHTRC 85-R1). Virginia Transportation Research Council.
- Sprinkel, M. M. (1999). Very-early-strength latex-modified concrete overlay. *Transportation research record*, 1668(1), 18-23.
- STANDARD, B. (1983). BS 1881-122: Testing concrete. Method for determination of water absorption.
- The Aberdeen, G. (1984). Latex-modified concrete and mortar for repair. Retrieved August 08, 2020, from https://www.concreteconstruction.net/_view-object?id=00000153-8b9c-dbf3-a177-9fbd049b0000
- Varghese, A. S. S. A Study on Properties of SBR Latex Modified Polypropylene Fibre Reinforced Concrete.

MANAGING HYDROGRAPHIC DATA BY USING GIS TECHNOLOGY IN MALAYSIA

**Hanah Zakariah, Saleh Mohamed Mohamud Ibrahim, Haslina Mohamed & Mohd. Ashraf
Mohd. Fateh**

1. INTRODUCTION

The science of hydrographic surveying identifies the positions of points and objects on the globe's surface, as well as the depths of the water. When they discovered a means to measure depths in the 1920s, hydrographic technology revolutionized. Many instruments have been created to improve the surveying standards. Surveyors can do better and simpler data acquisition of observation in surveying by using sophisticated instruments, while also improving the accuracy of their observations.

The processing of large volumes of data collected by these new depth-measuring technologies has become a serious difficulty to all survey vessels. They now have computer systems on board that process the data online and, in some situations, produce digital charts. Data visualization has become an important duty for surveyors to refine their work while still in the field, as well as result in the form of electronic charts for navigators and other users. Different types of equipment will necessitate different methods in conducting hydrographic surveys, whether it is the traditional method or the GIS-based method.

Furthermore, collecting maritime data has become prohibitively expensive, it would appear reasonable that a growing demand for efficient and precise data management systems to store, handle, and distribute exceedingly large data sets is emerging. The proposed solution for the above problem revolves around the use of new technologies. This new technology ought to revolve around GIS technologies.

As hydrographers seek to collect real time data, GIS will help them to gather larger volumes at a high speed. It will also help them to process the said data and visualize results quickly. Finally, with GIS, large volumes of information will be stored and they can refer to the system that is able to come up with images, manage, conduct analysis, and map all kinds of information required. This offers a foundation for mapping and analysis that is utilized in science and particular industries like hydrology. Geographic Information System assists its end users to decipher common patterns, liaisons between variables, and geographic contexts.

As hydrographers seek to collect real time data, GIS will help them to gather larger volumes at the highest of speeds. It will also help them to process said data and visualize results quickly. With GIS, large volumes of information will be stored. By and large, GIS will solve the above-mentioned problem by bringing forth speed into the picture.

2. LITERATURE REVIEW

GIS has become widely used in a range of engineering applications in a relatively short period of time. GIS is rapidly being utilized in modelling applications, where geographic data can be easily accessible, processed, and shown, as it was originally envisioned and used as a geographic mapper with an integrated spatial database. Large institutions, such as federal, state, and local government agencies, have been the primary users of GIS, with mapping and management of spatial data being the most common applications (Wade T, 2016).

The Army Corps of Engineers has developed a floodplain management connection between HEC- 2, a widely used floodplain determination tool, and GRASS, a software designed to cope with raster data (Walker et al., 2017). The integration software reads tabular HEC-2 output and translates it to GRASS format. (Talbot et al, 2017) created a GIS program that uses water elevations as input to determine floodplains.

Their method is meant to be generic, accepting stage numbers from any model that can calculate water levels in a stream channel. Stage values can be obtained from HEC-1 and HEC-2, according to the authors. The application requires the intersection of two TINs, one representing the terrain and the other reflecting the water heights in the channel, in order to determine the floodplain's banks. The authors claim that the generated floodplain is reasonable locally and representative of the entire floodplain.

Beavers (2018) created ARC/HEC2, a collection of AMLS (Arc/Info Macro Language) and C programmed that extract terrain data from contour coverages, incorporate user- supplied data (such as hardness indices or the location of left and right overbanks), and format the results into HEC-2 readable data. Following the completion of HEC-2, ARC/HEC2 may retrieve the HEC-2 output and create an Arc/Info floodplain coverage. This method allows the generated floodplain to be saved in a coverage format that can be easily accessible by users who want to combine floodplain data with other Arc/Info coverages.

To give correct cross-section profiles to HEC-2, ARC/HEC2 involves the creation of a terrain surface. Contour lines, survey data, or other techniques of producing terrain relief are used to produce these terrain surfaces in the form of TINs or grids in Arc/Info. For accurate floodplain calculations, the precision of the surface depiction is critical (Wilson, 2018).

A geographic information system (GIS) is a database that extends an object relational database to store geographic data, create maps, and perform spatial analytic functions. Geodatabases built on Oracle 8, SQL Server, Informix, DB2, and Sybase are currently supported by ArcGIS. Some of the functions that GIS software adds to an object-relational database management system are the capacity to store the geometric shapes of features directly in a database column, which GIS software adds to an object-relational database management system and the framework for defining data map layers and drawing methods. Moreover, a platform that allows for the construction of both simple and complex maps. Many of the most common map-making tasks have been simplified and establishing and storing topologic connections between elements such as network connectivity and integrated polygon topology. Also, two-dimensional

spatial index for retrieving geographic features quickly and a set of operators that can be used to determine geographic relationships, such as proximity, adjacency, overlay, and spatial comparison together with a wide range of spatial query techniques, including network tracing and polygon overlay analysis (Wilson, 2018).

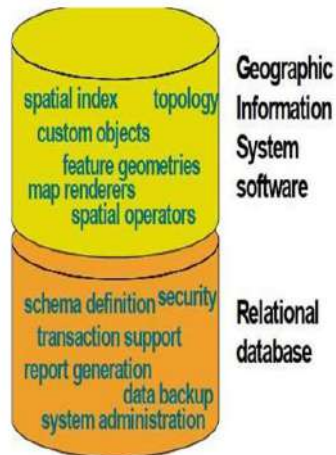


Figure 1: GIS Software VS Relational Database



Figure 2 : Typical GIS Laboratory with Components: (1)Scanner; (2)Digitizing Table; (3)AutoCAD/ArchiCAD Personal Computer; (4)Tape Driver; (5)Workstation; (6)Colour Printer; (7)PCARC/INFO Personal Computer; (8)Typical Drainage Map. (De Mesnard, 2017)

3. METHODOLOGY

The analysis in this study is based on a research study that looked at QGIS software and gvSIG software using GIS technology and a questionnaire. A total of 10 linked papers can be found using Google Scholar, a popular search engine. Moreover, the selected study must be done using GIS technology and conducted on hydrographic survey.

Table 1: Selection of Studies

No.	Title	Author
1.	Hydrographic Survey Using Real Time Kinematic Method For River Deepening	Schut
2.	Hydrographic Data Management Using GIS Technologies	Achiellos
3.	Hydrographic Survey and Data Management Using GIS	De Mesnard
4.	An Approach to Hydrographic Data Management Using Customized GIS and Geodatabases	Chen
5.	A Novel Method on Hydrographic Survey Technology Selection Based on The Decision Tree Supervised Learning	Ivana
6.	A Study on The Assessment Of Bathymetric Changes Via Gis	Ayhan Ceylan
7.	QGIS Software Review	Ashish Kr.Jangid
8.	Introduction To Basic GIS And Spatial Analysis Using QGIS	Mustafa Kamal
9.	GvSIG: A GIS Desktop Solution For an Open SDI	Alvaro Anguix
10.	Evaluating Open-Source GIS For Libraries	Francis P. Donnelly

In its entirety, the table above gives a snippet of some of the peer-reviewed sources that will comprise the core and seminal literature of the study. Note that the sources are no more than 10 years old for the purposes of relevance. From Google Scholar, the search criteria revolved around key words such as Geographical Information Systems, gvSIG, QGIS, hydrology, hydrology software, Malaysia. Overall, the mandatory words that had to be included in the search of suitable journals are Geographical Information Systems.

The questionnaire of this study consisted of three parts. The first part includes demographic information of the respondents. Questions asked were about the respondent's total years of experience (both in local and international projects), and position. The second section of the questionnaire consisted of 8 questions that are to compare between QGIS software and gvSIG software in terms of capacity, efficiency and level of usage difficulties. The respondents will be asked to rate the statements based on a 5-point of Likert scale of 1 = totally disagree, 2 = disagree, 3 = neutral/do not know, 4 = agree, and 5 = totally agree. The last section contained 7 questions to promote the use of Geographic Information System (GIS) technology in order to provide effective and efficient data management for processed hydrographic data.

The role of each question of the survey was measured based on the agreement of the respondents on the given statement. Similarly, the agreement level was measured using a 5-point Likert scale (1 = totally disagree to 5 = totally agree). Going through the information that the questionnaire provided, the study will feed off the answers that the literature review will provide. The expected result from the questionnaire and the systematic review is that

Geographical Information Systems software is a reliable approach in prospecting water bodies owing to the volumes of data that can be keyed in and processed within a short time period. From the review of literature study made in the second chapter, the expectation is that there will be a commonality in the way different authors seek information.

4. RESULT AND DISCUSSION

The result is primarily divided into two sections. The first section comprises findings from a systematic literature review the systematic review of literature feeds from 16 peer reviewed sources that demonstrate the usefulness of gvSIG, QGIS, and GIS technologies at large the second section findings are based on the responses of 25 professional hydrographers who were asked questions on GIS and to compare gvSIG and QGIS.

Systematic review

Naidu (2015) affirms that Geographic Information Systems (GISs) have become a useful and relevant tool in hydrology and hydrologists in the management and scientific study of water resources. Changes in climate and a lot of demand on water catchment areas need a highly knowledgeable disposition of arguably one of humanity's most important resources. As is known to many hydrologists, water is constantly moving.

Given that the occurrence of water varies temporarily and spatially all through the hydrologic cycle, its research by means of GIS is arguably practical. Before the advent of gvSIG and QGIS, GIS systems were mostly static in their geospatial representation of hydrologic features. Today, gvSIG and QGIS have brought forth a lot of dynamics, closing the gap between historical information and current hydrologic reality. The study by Senanayake et al. (2016) recommends the GIS approach to delineate possible artificial recharge sites. Its affirmations are backed up by data on how hydrographers utilized GIS technology to delineate possible artificial recharge sites in the Ambalontota region within Hambantota.

Using a weighted linear combination approach, the hydrographers involved integrated influential thematic layers like lineament, rainfall, drainage, slope, land cover, soil characteristics, and geomorphology. The study's outcomes demonstrated high to medium groundwater recharge potential in about 50 percent of the Ambalantota region.

Data analysis and findings

The information gathered from responses analysed in this section will discuss how much people with a GIS background think that GIS technology will be a great tool to manage and analyse hydrographic data in Malaysia.

These are some main questions which the research will answer; (1) is GIS being effective and efficient in hydrographic data management? (2) why is GIS the right tool to manage hydrographic data in Malaysia? (3) which software is good in terms of capacity,

efficiency, and level of usage difficulty, QGIS software or gvSIG software? The first two questions were closed and required the respondents to answer yes or no.

All the participants agreed to the idea that GIS was the best-suited tool to deal with hydrographic information. In addition, 98% of the participants marked yes for GIS's ability to handle hydrographic data in Malaysia. This is demonstrated in Table 2.

Table 2: Respondents answer to GIS Effectiveness in Processing Data

Need for GIS technology to provide effective and efficient data management for process hydrographic data in Malaysia:	Frequency Analysis		Percentage
	1 = yes	2 = no	
Is GIS the right tool to deal with hydrographic data?	100	0	100
Has GIS been able to handle hydrographic data in Malaysia before?	23	2	98

From table 2, it is clear to see that on both questions, at least 98% of the respondents agreed that GIS technologies were effective in the prospecting of hydrographic data. Given that all the respondents had knowledge and experience with GIS in Malaysia, it is plausible to affirm the potency of mass adoption of GIS technologies in Malaysia.

Table 3: Respondents answer to GIS Effectiveness in Providing Data Management

No	All the questions in the rows below are seeking to affirm that GIS technology is capable of providing effective and efficient data management for processed hydrographic data in Malaysia:	Frequency Analysis					Average Index
		1	2	3	4	5	
1.	The depth and bottom configuration of water bodies in Malaysia is mostly measured using GIS technologies during hydrographic surveys.	0	0	3	19	3	4.00
2.	GIS is effective and efficient with intelligent data objects and methods in hydrographic data management.	0	0	4	15	6	4.08
3.	The most important aspect influencing the implementation of hydrographic data management is the cost.	0	0	6	11	8	4.08
4.	Using GIS to manage hydrographic data in Malaysia helps reduce operating costs and time.	0	0	6	10	9	4.12

5.	GIS-based hydrographic models are more effective for building storm drainage systems in Malaysia.	1	0	5	14	5	3.88
6.	GIS is effective in positioning and orienting hydrographic data.	1	0	2	17	5	4.00

In Table 3, the Likert Scale with the options given: 1 = strongly disagree, 2 = disagree, 3 = neutral, 4 = agree, 5 = strongly agree. For every question that got an average index of 4 in the row that is far right, there is a connotation that most of the respondents, which are the hydrographers, agreed with whatever leading question that the researcher presented. For example, the question in the first row has an average index of 4.0.

This means that most respondents agreed with the postulations of the statement i.e., newly discovered water bodies' depth and bottom configuration in Malaysia should be measured using GIS technologies during a hydrographic survey. Overall, the respondents agreed to the following leading points:

1. The depth and bottom configuration of water bodies in Malaysia should be measured using GIS technologies during hydrographic surveys.
2. GIS is effective and efficient with intelligent data objects and methods in hydrographic data management.
3. The most important aspect influencing the implementation of hydrographic data management is the cost.
4. Using GIS to manage hydrographic data in Malaysia helps reduce operating costs and time.
5. GIS-based hydrographic models are more effective for building storm drainage systems in Malaysia.
6. GIS is effective in positioning and orienting hydrographic data.

Comparison of QGIS and gvSIG software in terms of capacity, efficiency and level of usage.

From Table 4, it is evident that participants think that both software are equal as indexes in range of 3. All the same, more participants responded that QGIS is more friendly, providing more vector data formats, and has better remote monitoring, management, and raster processing, widely innovative and inventive And gvSIG is good in layouts creation, navigation and editing of vectors.

Despite the fact that most of the answers were inclined to QGIS, the Likert scale average range of >3 but <4 is a sure fire way of affirming the neutrality of the respondent's feelings towards which GIS software was more effective than the other. As a whole, it is best to conclude that neither gvSIG nor QGIS were more effective than the other.

Table 3: Respondents answer to the Comparison between QGIS and gvSIG

No	QGIS software and GVSIG software in term of capacity, efficiency and level of usage difficulty:	Frequency Analysis					Average Index
		1	2	3	4	5	
1.	QGIS is more user friendly than GVSIG.	2	1	11	9	2	3.32
2.	QGIS provides more vector data formats while exporting data than GVSIG.	0	5	7	11	2	3.40
3.	GVSIG allows you to browse and navigate with GPS better than in QGIS.	0	1	7	15	2	3.72
4.	QGIS is a better remote Monitoring and Management software than GVSIG.	0	6	7	10	2	3.32
5.	QGIS is widely innovative and inventive.	1	1	9	9	5	3.64
6.	Raster data processing is better in QGIS than GVSIG.	1	2	7	12	3	3.56
7.	For editing of vector data, the use of GVSIG software is appropriate than QGIS	0	3	9	8	5	3.60

From the above table demonstrating Likert scale results, it is possible to see that none of the average indices presents a value of 3.0. Additionally, it is also clear that none of the average indices reads 4.0. All the indices range between 3.0 and 4.0. The weightage of the answers therefore oscillates between 3 and 4.

On the Likert scale, the number 3 scale is a sign of neutrality. The correct inference of the results shows that neither gvSIG nor QGIS surpass the other when it comes to efficiency and user friendliness. There is more correlation in the commonalities and little correlation in the differences between gvSIG and QGIS software. This is a sure-fire way of saying that both technologies have the capacity to gather information, process it, and store it for future use by hydrographers.

5. CONCLUSION

The entirety of this chapter will give invaluable insights on the findings that this study has been able to amass. Findings on the usefulness of GIS technologies and their capacity to prospect hydrographic information will be mentioned. In addition to that, the study's conclusions on the capacity of gvSIG and QGIS will be highlighted. Geographic Information Systems (GIS) is a vital apparatus in hydrographic data management.

Nowadays, GIS stages have gotten to be progressively energetic, narrowing the crevice between authentic information and current hydrologic reality. According to questionnaires survey and literature study GIS is the perfect tool to manage, process and analyse hydrographic data. By this we can make predictions to solve real world problems. We can identify water ways, oceanic data and changes, quality of water, use of water, hydro management in agriculture and

catchment areas etc.

GIS effectively validates hydrographic data and GIS is effective and efficient with intelligent data objects and methods in hydrographic data management. GIS based hydrographical models are especially valuable apparatuses for examining the numerous common-sense issues that emerge amid the arranging, plan, operation, and administration of water asset frameworks in Malaysia. Managing hydrographic data in Malaysia by using GIS technologies, that makes the data accessible to clients and Population.

According to questionnaires, both QGIS and GVSIG software are user friendly, have great efficiency and level of usage in terms of difficulty. But when we come to literature study, we see QGIS has wider use than GVGIS. QGIS has a better ability to handle data. By considering both survey and literature study, several recommendations could improve the practice and use of GIS software.

The Malaysian Government should consider moving towards the use of GIS in hydrographic data management which would reduce time complexity and cost. These would offer better systems for management of hydrographic data and also for the depth measuring and bottom configuration of water bodies in hydrographic application of GIS. This ensures efficiency and lower costs hence the Malaysian Government should consider the use of GIS. The GIS-based hydrographic model is also effective for building storm drainage systems for use on highways, hilly areas and some of the Malaysian cities.

The gvGIS software is adapted to browse, navigate and optimize data with GPS better compared to QGIS. Nevertheless, QGIS is better in remote monitoring and management of software than gvGIS and more widely used.

REFERENCES

- Achiellos. (2018), *Hydrographic Data Management using GIS Technologies*. O'Reilly Media, Sebastopol, CA. Vol. 7 No. 14.
- Ayhan CEYLAN. (2016), *A Study On The Assessment Of Bathymetric Changes Via GIS*. International Journal of Geographical Information Science, forthcoming. Vol. 9 No. 42.
- Borgman et al. (2014), *Why was MapWindow GIS developed ?*, MapWindow GIS, Vol. 7 No. 18, p. 29.
- Chen. (2018). *An Approach To Hydrographic Data Management Using Customized GIS And Geodatabases*, National Center for Digital Government, MA. Vol. 3 No. 16.
- Casella. (2020). *The case for open source*, Technology & Learning, Vol. 27 No. 7, pp.16-21.
- De Mesnard. (2017), "*Hydrographic Survey and Data Management using GIS*", Journal of Web Librarianship, Vol. 1 No. 3, pp. 111-22. Vol. 12 No. 6.
- Erodgan. (2019), *Spatial Data Collections and Services*, SPEC Kit, 291, Association of Research Libraries, Office of Leadership and Management Services, Washington, DC.
- Fotheringham. (2019), *Open-Source Server Applications*, Library Technology Reports, Vol. 43 No. 3, pp. 48-53.

- Grant C. (2016), *GIS and the academic library: a survey of libraries offering GIS services in two consortia*, Issues in Science Technology Librarianship, Vol. 48 No. 1.
- Ivana. (2021), *A Novel Method on Hydrographic Survey Technology Selection Based on the Decision Tree Supervised Learning*, Pragmatic Bookshelf, Raleigh, NC. Vol. 7 No. 14.
- Kejuruteraan, J. (2021). *Database Development for Water Quality Index using Geographical Information System*. <https://www.ukm.my/jkukm/wp-content/uploads/2021/3302/06.pdf>
- Khalid, K., Ali, M. F., Abd Rahman, N. F., Mispan, M. R., Haron, S. H., Abd Rasid, M. Z., ... & Kamaruddin, H. (2016). *Application of the SWAT hydrologic model in Malaysia: recent research. The challenges of agro-environmental research in Monsoon Asia*, 237-246.
- Lata, L. (2020). *Catchment Delineation for Vjosa River WEAP Model, using QGIS Software*. Ana Sayfa »DergiPark
<https://dergipark.org.tr/en/download/article-file/1447446>
- Longley P. (2018), *The future of FLOSS in libraries*, in Gordon, R.S. (Ed.), *Information Tomorrow: Reflections on Technology and the Future of Public and Academic Libraries*, Information Today, Medford, NJ, pp. 19-32.
- Lister. (2014), *An online tool for selecting colour schemes for maps*, Cartographic Journal, Vol. 40 No. 1, pp. 27-37. ColorBrewer.org
- Naidu, D. S. (2015). *Use of GIS in Hydrological Investigations*. Pdf). International Journal of Interdisciplinary Advanced Research Trends. Ii
- Schut . (2016), *Hydrographic Survey Using Real Time Kinematic Method For River Deepening*, Refractions Research White Papers, Vol. 2 No. 12.
- Senanayake, I. P., Dissanayake, D. M. D. O. K., Mayadunna, B. B., & Weerasekera, W. L. (2016). *An approach to delineate groundwater recharge potential sites in Ambalantota, Sri Lanka using GIS techniques*. Geoscience Frontiers, 7(1), 115-124.
- Talbot et al. (2017), *Follow-up survey of GIS at smaller academic libraries*, Issues in Science & Technology Librarianship, Vol. 43 No. 1.
- Tufto, J. and Cavallini, P. (2005), *Should wildlife biologists use free software?*, Wildlife Biology, Vol. 11 No. 1, pp. 67-76.
- Wade T. (2016), *Administering an open-source wireless network*, Information Technology & Libraries, Vol. 27 No. 3, pp. 44-54.
- Walker et al. (2017), *Comparison of Geographic Information System Software (ArcGIS 9.0 and GRASS 6.0): implementation and case study*. Vol. 121 No. 19.
- Weber S. (2018), *Open Source: Technology and Policy*, Cambridge University Press, New York, NY. Vol. 9 No. 7.
- Wilson.(2015), *gvSIG: Open Source Solutions In Geospatial Technologies*, GIS Planet Conference, Vol. 27 No. 3.

GEOMETRIC DESIGN OF ROAD IN URBAN AREA USING AUTODESK INFRAWORKS

Ranjit Singh Dharam Singh & Yong Fatihah Daman Huri
Infrastructure University Kuala Lumpur

1. INTRODUCTION

In Malaysia, urban areas are defined as areas which population is greater than 1000. Buildings and houses in these areas are assembled closely with each other and business activity is prevalent (Public Work Department of Malaysia, 2015). Meanwhile, Weeks (2010) defined urban area as a place with higher concentration of people whose day-to-day activities are organized around non-agricultural activities and are now home to almost one in two human beings, and almost two out of every three people will be urban dwellers by the middle of the 21st century. When talking about road in urban area, it is expected to be congested due to high population density and many assume it comprises only the highways. However, urban road actually includes other types of road such as expressway, arterial, collector and local street (Public Work Department of Malaysia, 2015).

Public Work Department of Malaysia (2015) assigned six design standards for urban road in Malaysia which are U1, U2, U3, U4, U5 and U6. The design standards are categorized based on traveling speed and access control. Each road in urban area falls under different category set by the speed and access control. Therefore, in order for the engineers to start estimating the design speed, they must first categorize the desired road into the suitable category. Design speed is a speed chosen to set up a specific minimum geometric design element on a specific section of the road (Public Work Department Malaysia, 2015). The design speed for urban road is from 20 km/h to 100 km/h.

The geometrical design of the road consists of horizontal alignment and vertical alignment. Horizontal alignment is the road path, geometrically defined as a series of straight lines and curves. The types of curves are circular curves, spiral curves, composite curves and reversed curves (Taylor, 2013; Raji et al., 2017). Horizontal alignment is done with respect to the terrain and the area's condition and primarily includes the design of tangents and curves (Easa & Mehmood, 2007). In urban area, horizontal alignment may highly be influenced by the existing buildings in the packed metropolitan city. In order to develop the safest alignment, a design speed must be established based upon the guidelines given in each region or country. Specific values for a minimum radius (based on speed limit), curve length, and sight distance rely on the curve design (Uren & Price, 2018; Manoj et al., 2019; Mojtaba et al., 2015). The minimum radius of the curve for urban road is from 15 m to 435 m and the minimum length of spiral curve is from 25 m to 48 m.

The vertical alignment significantly contributes to the safety, aesthetics, operations, and cost of a road. Broad, gentle vertical curves provide the drivers with greater viewing distances

and a more attractive appearance. The topography of an area plays an important role in design of vertical curves. Straight sections (grades) link by vertical curves made up vertical alignment of a road. So, selection of suitable grades for the tangent sections and the appropriate length of vertical curves play important parts in the vertical alignment design (Garber & Hoel, 2015). There are two types of vertical curve which are crest and sag vertical curves. The desirable maximum grade for urban road is from 3% to 9%.

The cross section elements are divided into principal elements and marginal elements (Garber & Hoel, 2015). The principal elements are pavement, shoulders and medians while the latter element consists of barriers and gutters. The view obtained in a segment between the right-of-way lines cut perpendicular to the travel path along the road is what defines the cross section of a roadway.

The most critical features of a road regarding to the safety and comfort of driving are lane widths and the condition of the pavement surface (Public Work Department Malaysia, 2015). Travel lane width, which must be adequate to accommodate the design vehicle, allows for imprecise steering manoeuvres and provides adjacent lanes with clearance for opposing traffic. The lane width for urban road is from 3.00 m to 3.65 m.

A shoulder is the continuous portion of the roadway with the purpose of stopped vehicle accommodation, emergency use, and even lateral pavement support (Public Work Department, 2015; Garber & Hoel, 2015). Even in wet weather, the shoulder should be sturdy enough to withstand the weight of a fully loaded truck. To provide working space around a stopped vehicle, the shoulder width should be sufficient (Mathew & Rao, 2007). Shoulders can be used for pedestrian and bicycle traffic on certain roadways, where no separate paths for these functions are given (Hall et al., 1995). The usable shoulder width for urban road is from 1.50 m to 3.00 m.

A median is the portion of a divided highway in opposite directions that divides the lanes. The median functions are to provide the desired freedom from opposite traffic interference, to provide out-of-control vehicles with a recovery area, to provide for speed adjustments and storage of right-turning and U-turning vehicles, and to provide for potential lanes (Public Work Department Malaysia, 2015). The desirable median width for urban road is from 2.0 m to 9.0 m.

Roads in urban areas are marked by busy pedestrian activities and regular stopping of vehicles due to short spacing of intersections and congested built-up areas. For urban roads, lower design speeds are generally adopted and various cross sectional elements are implemented to take into account the dynamics of traffic and adjacent land use (Public Work Department of Malaysia, 2015). So, in order to design the perfect urban road, several geometric design criteria must be satisfied such as vertical and horizontal alignment, cross sections of the road, truck climbing lanes, bicycle paths and parking facilities (Garber & Hoel, 2015).

Designing the road to be up to recent standards falls on the shoulder of the engineers. These roads must be designed accordingly with the standards set by the authority or in Malaysia

usually by following the standards set by the Public Work Department of Malaysia (2015). Roads designed by following the guidelines will provide comfort and safety for the users.

In this study an urban area shall be selected to design an urban road following the geometric design guidelines set by the Public Work Department of Malaysia (2015). The objectives of this study are as follows:-

- i. To identify the road design criteria in urban area.
- ii. To design an urban road in the selected area.
- iii. To analyse the horizontal and vertical alignment and cross section elements from the design for its suitability and safety.

2. METHODOLOGY

In this study an urban area at Semenyih Town is selected to design an urban road. Therefore, a new entrance road into Semenyih Town will be proposed and its alignment is expected to be approximately 424 m. The proposed alignment is depicted in Figure 1.



Figure 1: Proposed Alignment for a New Entrance to Semenyih Town

This study will design a new route to solve the congestion problem in Semenyih during peak hour by using the Autodesk InfraWorks software. The new route will be designed by obtaining data such as design speed, topography details and obstruction along the route. Then, alignments and safety features will be added to the design for safety and comfort of users.

The road is designed on a satellite image and topography data of the area of the proposed road. Basically, the procedure of route design consists of determining the design criteria, designing the horizontal alignment, designing the vertical alignment and estimating the earthworks volume.

Satellite Image and Topography Data

After an area has been selected, the satellite image and topography data of the area will be collected. The reason behind this is to guide researcher in designing the horizontal and vertical alignment of the new road. These alignments are important to ensure the safety of road users. The satellite image and topography data will be obtained from Google Earth and Autodesk InfraWorks.

Design Criteria

Design criteria is a set of requirements to start the road design. Most of the criteria are obtained from guidelines by Public Work Department of Malaysia (2015). To obtain these criteria, the road to be designed must first categorized. In this study a major collector road of design standard U4 will be designed by using the Autodesk InfraWorks software.

The design criteria for the U4 urban road are as below:-

- i. The design speed is 60 km/h.
- ii. The area type is 2.
- iii. The maximum superelevation rate is 6%.
- iv. The minimum radius of the curve is 135 m.
- v. The maximum desirable grade is 6%.
- vi. The minimum k value for the crest curve is 17.
- vii. The minimum k value for the sag curve is 18.
- viii. The lane width is 3.50 m.
- ix. The shoulder width is 3.00 m.
- x. The median width is 2.50 m.
- xi. The marginal strip width is 0.25 m.
- xii. The minimum reserve width is 40 m.
- xiii. The landscape corridor is 2.75m.
- xiv. The drain reserve is 1.50m.
- xv. The service reserve is 3.00m.

Design using Autodesk InfraWorks

Autodesk InfraWorks is software developed by Autodesk for designing civil infrastructure works (Kuok et al., 2021). In this study the software will be used to design a new road in the selected area. The first step in designing the road is to generate a 3D model of the area. The model will provide both top view and topographical data of the area so vertical and horizontal alignment can be proposed. The road will be designed according to the design criteria. The road will be aligned to adhere to the surrounding area.

Analysing the Results of the Road Design

In this step the results of the road design include the cut and fill volume required for the construction of the new road. By using the software the volume of cut and fill for the soil will be calculated along the proposed road alignment. Next, the horizontal and vertical alignment of the design will be analysed in terms of safety and suitability.

The flowchart of the road design using Autodesk InfraWorks is depicted in Figure 2.

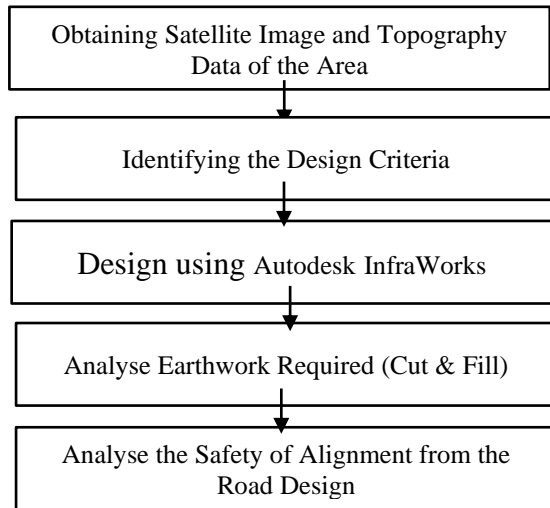


Figure 2: Flow Chart of Route Design using Autodesk InfraWorks

3. RESULTS

The proposed alignment of the road stretches approximately 424 metres connecting from an existing road in Taman Semenyih Sentral to Jalan Broga Junction (Figure 3). The road would also cross Semenyih River and a local road situated right beside the river.



Figure 3: Proposed Alignment of the Road

The road is designed based on the design criteria for urban road design standard of U4 according to the guidelines by Public Work Department Malaysia (2015). The horizontal alignment is designed with the curve radius and spiral curve length assigned its own specific radius and length. There are four horizontal curves in the designed horizontal alignment as shown in Figure 4. The curves are planned to avoid certain buildings and to align the proposed

road to the existing junction. The radius and length of these curves are depicted in Table 1.

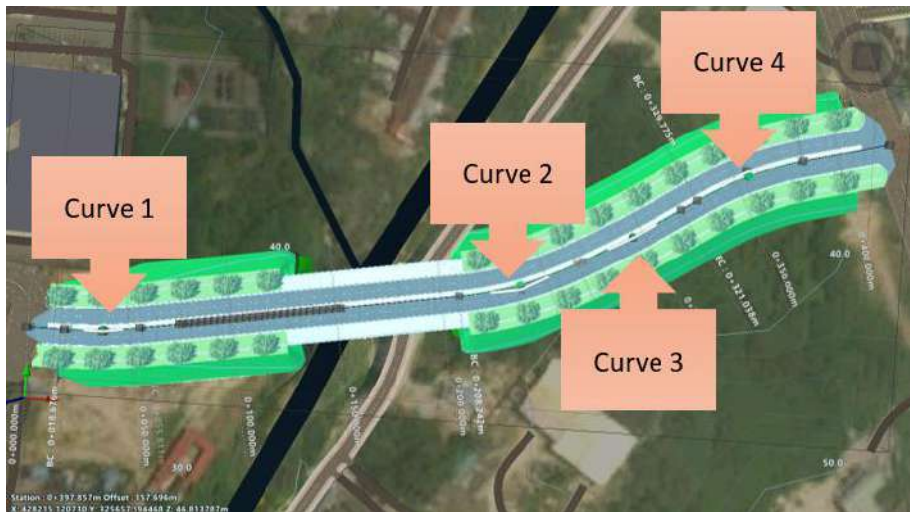


Figure 4: Horizontal Curves on the Proposed Alignment

Table 1: The Radius and Length of the Horizontal Curves

Curve	Radius (m)	Length (m)
Curve 1	246.00	37.14
Curve 2	170.00	57.56
Curve 3	607.52	52.32
Curve 4	156.00	53.29

From the results obtained, the proposed curves radius ranges between 156.00 m to 607.52 m and the minimum radius required is 135.00 m. The proposed curve radius meets the requirement by Public Work Department Malaysia (2015) and therefore the design of the horizontal curves for the alignment is acceptable.

Autodesk InfraWorks allows users to create a 3D model of the area in order to generate a profile along the horizontal alignment. Vertical alignment is then designed on the profile with the start of the alignment is proposed at an elevation of 36.68 m. In order to cross the river and an existing local road, the proposed vertical alignment reached its maximum elevation of 43.00 m. Then, approximately 30.00 m from the end of the bridge, the elevation of the road would be decreased to 42.50 m in order to connect to the existing Broga Junction which elevation is at 42.49 m.

In this design, there are six vertical curves consisting of five sag vertical curves and one crest vertical curve (Figure 5). In the profile view, we can determine the types of curves by observing the tangent lines. If the point of vertical tangent (PVT), located above the curve, it will be classified as crest vertical curve and vice versa (Garber & Hoel, 2015).

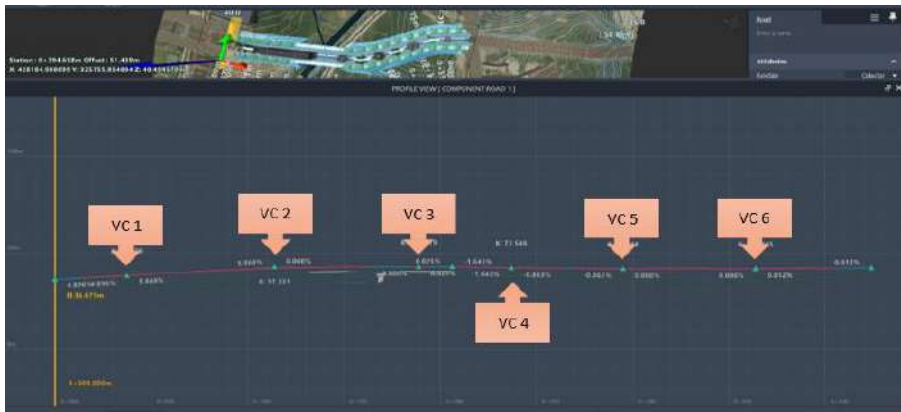


Figure 5: Vertical Curves on the Vertical Alignment

The vertical alignment is designed to provide an adequate clearance for the bridge. Due to the road alignment being proposed to cross a river and an existing road, a recommendation of 5.3 m of clearance of the bridge is to be followed (Arshad, 2001). For the design, the clearance for the bridge is set to be approximately 5.5 m from the surface of the existing road. Table 2 shows that the design vertical curves length (L) is larger than the minimum length (L_{min}) required. This proved that the length of vertical curve in the design is acceptable and thus can be used in vertical alignment design.

Table 2: Comparison of Design Length of Curve and Minimum Length

Vertical Curve	Length, L (m)	K values	A (%)	Minimum Length, L_{min} (m)	Remarks
VC 1	49.41	18	-0.972	17.50	$L > L_{min}$; OK
VC 2	101.70	17	5.868	99.76	$L > L_{min}$; OK
VC3	10.00	18	-0.025	0.45	$L > L_{min}$; OK
VC4	57.41	18	-0.780	14.04	$L > L_{min}$; OK
VC5	52.75	18	-0.863	15.53	$L > L_{min}$; OK
VC6	84.86	18	-0.812	14.62	$L > L_{min}$; OK

Cross section of roads in Malaysia depends heavily on the road design standard the engineer chose and the design criteria set by Public Work Department Malaysia (2015). Design standard U4 is the chosen urban road standard for this particular alignment as shown in Figure 6.

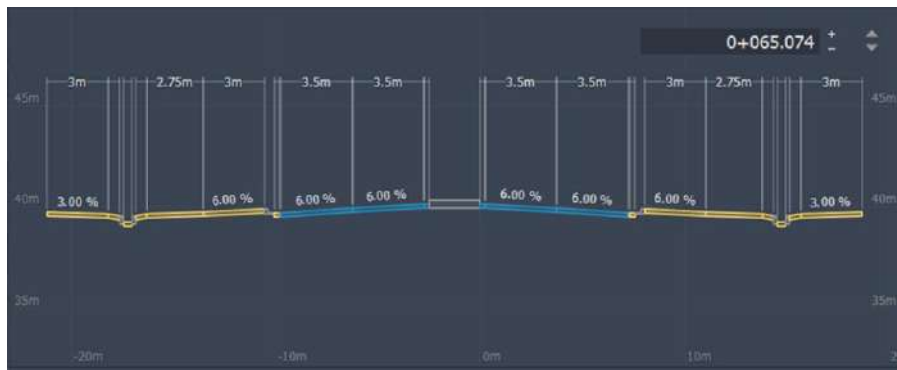


Figure 6: Cross Section of Road Design on Ground

The pavement to be used for this road is asphaltic concrete. Asphalt concrete is a high-temperature mixture of coarse aggregate, fine aggregate, and filler with a binder, with the composition inspected and regulated by technical specifications. This type of pavement will also be used for marginal strip since it is still considered as part of the carriageway.

Road shoulders are a portion of road that provides lateral support to the pavement as well as spaces for stopping vehicles, and sidewalk. The design will use shoulder length of 3.00 m right beside the carriageway and separated by kerb to prevent vehicles from leaving their lane and will be covered with turfing and sloped to 6% in order to provide adequate water draining from the surface of the shoulder. The design is in line with guidelines by Public Work Department Malaysia (2015) and by AASHTO as mentioned by Hall et al. (1995) and thus the design can be accepted.

In between the 4-lane carriageway, a median of 2.50 m wide will be placed. A median is an element that needs to be integrated in the assemblies of the road design. Its main purpose is to give the required freedom from opposing traffic interference (Public Work Department Malaysia, 2015). Based on the guidelines, the median width is recommended to be set at 2.50 m to 5.50 m which are the range of median width required for standard U4 road and the final assemblies and cross section can be seen in Figure 7.



Figure 7: 3D Rendering of the Road Cross Section

In this alignment as well, a bridge is included to be able to cross a river and existing road. In this alignment as well, a bridge is included to be able to cross a river and existing road. The bridge is designed to have the same lane number and width as the alignment on the ground level. However, the cross section of the bridge will be slightly different from the ground road (Figure 6 & 7) due to the absence of landscape corridor and service reserve. To provide the lateral support for the bridge, a shoulder of 3.00 m was provided and it doubles as sidewalk as recommended by Public Work Department Malaysia (2015). At the side of the bridge, a kerb and guardrails were added as safety measures. Details of the cross section and 3D rendering are shown in Figure 8 and Figure 9.

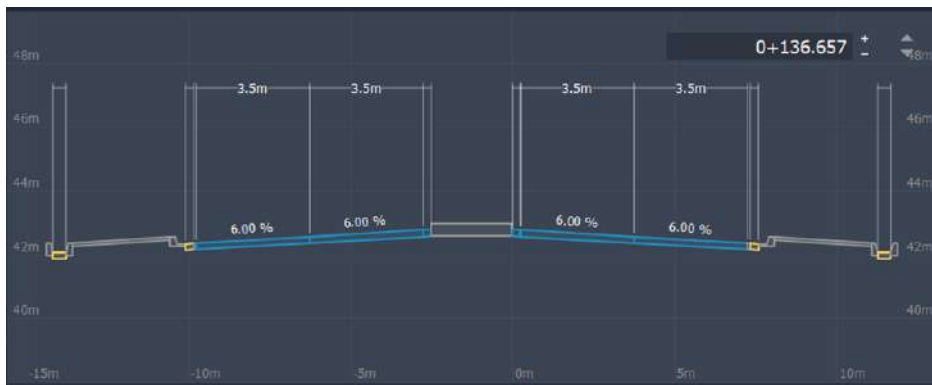


Figure 8: Cross Section of Road on Bridge



Figure 9: 3D Rendering of the Road Cross Section on the Bridge

One of the great features of Autodesk InfraWorks is it allows for earthwork calculation for any alignment of road or any other project. The calculation depends on the contour data of the location and the road alignment. Report generated by InfraWorks can be used by engineers to evaluate the volume of earthwork required during the project. Figure 10, Figure 11 and Figure 12 depict the fill area in green colour.



Figure 10: Fill Area on the Right Side of the Road



Figure 11: Fill Area on the Left Side of the Road



Figure 12: Plan View of the Fill Area along the Road

4. CONCLUSION

In conclusion, when designing a road, it is crucial to choose suitable design criteria to ensure high safety standard. As shown in this study, engineers in Malaysia should always abide by the standards set in the Public Work Department of Malaysia (2015) guidelines. These standards are made to ensure the safety and comfort of the users as well as the people in the vicinity such as

the local residents. Using InfraWorks to design the road alignment had helped in achieving the desired design standard. It had also allowed an easier process to design the horizontal and vertical alignments. The model builder which uses recent satellite images and contour details had allowed the alignments for this design to consider the surrounding area more easily and accurately. Furthermore, the 3D rendering of the model allowed engineers to have a better visualisation on what is needed in their project and can assist in presentation to clients.

It is recommended that a traffic study may need to be conducted for the selected area. Traffic data will assist engineers in understanding the demand of the location. From this traffic study, the engineers then can choose the right criteria and materials to be used for the road.

REFERENCES

- Arshad, A.A.B. (2001). *Bridge Design to JKR Specification*. Civil & Structural Engineering Technical Division, The Institution of Engineers, Malaysia.
- Easa, S.M., & Mehmood, A. (2007). *Establishing highway horizontal alignment to maximize design consistency*. Canadian Journal of Civil Engineering, 34(9), 1159–1168.
- Garber, N.J. and Hoel, L.A. (2015). *Traffic & Highway Engineering*. Cengage Learning. Connecticut. 5th Ed.
- Hall, L.E., Powers, R.D., Turner, D.S., Brilon, W.R. & Hall, J.W. (1995). *Overview of cross section design elements*. International Symposium on Highway Geometric Design Practices (p. 12).
- Kuok, K.K., Tan, K.W.K., Chan, C.P., Chin, M.Y., Rahman, M.R. & Bakri, M.K. (2021). *Application of Building Information Modelling (BIM) Technology in Drainage System using Autodesk InfraWorks 360 software*. Proceedings of the 5th International Conference on Water Resources (ICWR), Springer, 1st Ed.
- Mathew, T.V. & Rao, K.V.K. (2007). *Cross sectional elements*. Introduction to Transportation Engineering, 1–9.
- Mojtaba, A. & Armin B.Z. (2015). *Evaluation of Horizontal Curve Superelevation Using Road Surface Profiler*. **International Journal of Pavement Research and Technology**, 8(3), 185-191
- Public Work Department Malaysia (2015). *A Guide on Geometric Design of Roads. 86(Pindaan)*. Kuala Lumpur
- Raji, S., Zava, A., Jirgba, K. & Osunkunle, A. (2017). *Geometric Design of a Highway Using Autocad Civil 3d*. Journal of Multidisciplinary Engineering Science and Technology (JMEST), Vol. 4 Issue 6, 7415-7421.
- Taylor, G.J. (2015). *Roadway Horizontal Alignment Design*. Continuing Education and Development, Inc., New York.
- Uren, J. & Price, W.F. (2018). *Surveying for Engineers*, Bloomsbury Publishing, 5th edition.
- Weeks, J.R. (2010). *Defining Urban Areas*. Remote Sensing of Urban and Suburban Areas, Springer Dordrecht, 1st Ed., 33-45.

HUMIDITY CONTROL STORAGE CABINET FOR SEMICONDUCTORS MATERIALS

Anandan Subramaniam & Mohd Zamri Ibrahim
Infrastructure University Kuala Lumpur

1. INTRODUCTION

The Peltier effects originated by French watchmaker and part time physicist Jean Charles Athanase Peltier in 1834 [1]. Peltier found that the application of a current at an interface between two dissimilar materials' results in the absorption or release of heat [1]. The relationship between the amount of current and heat absorbed or released at the junction of two dissimilar semiconductors is given by the Peltier coefficient [2]. It can produce heating and cooling effects. [1]

Peltier cooler consists of blocks of a semiconductor like bismuth telluride that are alternately doped N-type and P-type [3]. The blocks are electrically connected by strips of metal like copper and bismuth. When the current pass through the device it causes the result of the different energy levels of materials, particularly N and P type materials [3]. As electrons move from P-type material to N-type material, electrons jump to a higher energy state absorbing energy, in this case heat, from the surrounding area [4]. The reverse is also true. As electrons move from N-type material to P-type material, electrons fall to a lower energy state releasing energy to the surrounding area. [4]

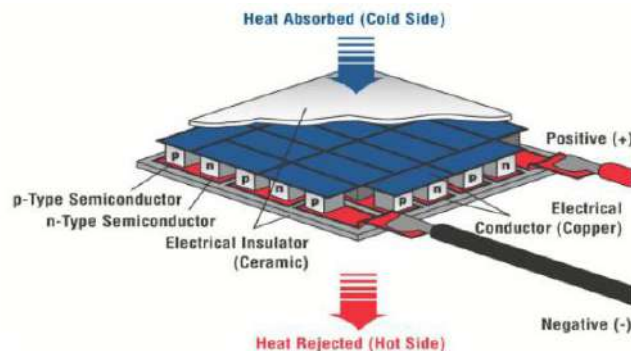


Figure 1: A Cutaway of Thermoelectric Module [3]

2. THE WORKING PRINCIPLES

The moist air enters the dehumidifier pass through the front fan. It's being pulled into the dehumidifier by the fan and touches the cold side heat sink. Here is where the dehumidification occurs. Just like warm air condenses onto the cold condenser coils of a compressor-based dehumidifier, the moist air that enters the thermoelectric dehumidifier condenses onto its cold side heat sink. As the hot air become cold, it will reach the dew point and start to saturation. The

air will lose its moisture content by condensation. The cold side heat sink has a smooth finish with an angled finned design to allow for the condensate to easily drip down into the condensate collection reservoir below it.

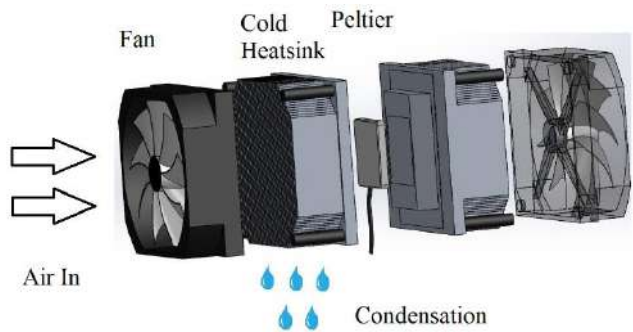


Figure 2: Working principles of Peltier Dehumidifier

3. FLOW CHART

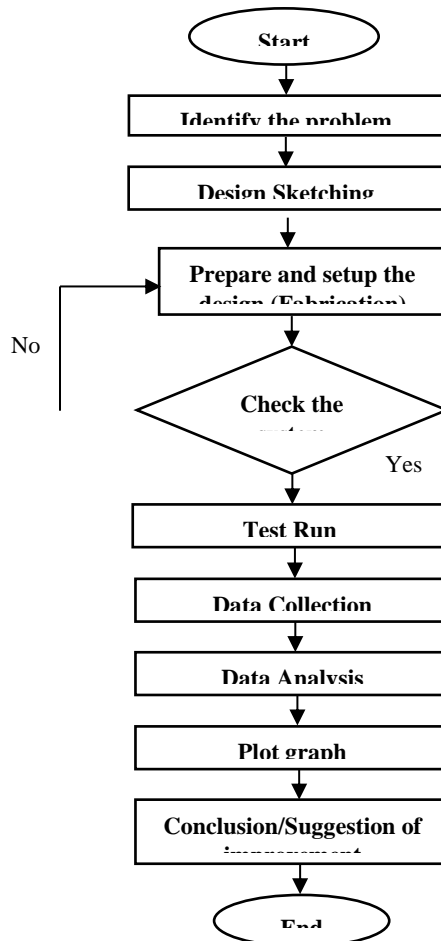


Figure 3: Flow chart used for this study.

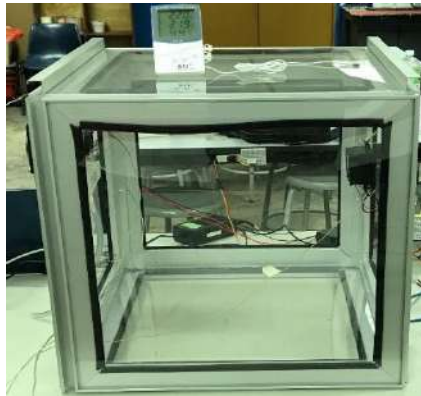


Figure 4: The picture of dehumidifier storage

4. STRUCTURE DESIGN

As shown in Figure 3, a test rig model consists with an aluminum structure and acrylic sheet is build up in this experiment. The size of the whole cabinet is 500 mm x 500 mm x 500 mm, with acrylic sheet with thickness of 3 mm. Blind rivet is used to fixed the structure aluminum bar and silicone as adhesive to close the gap as to ensure no leaking in this experiment. The Peltier dehumidifier placed on the left and the humidity sensor placed at center of cabinet.

Arduino software is used as a microcontroller where the input from humidity sensor is stored to the SD card module. A relay is used to turn ON/OFF the dehumidifier when the humidity level reaches the desired level. A 12V DC power supply is used in this experiment. The dehumidifier is connected to relay. The relay is set as it will shut off the dehumidifier once it reaches 42 % of humidity level.

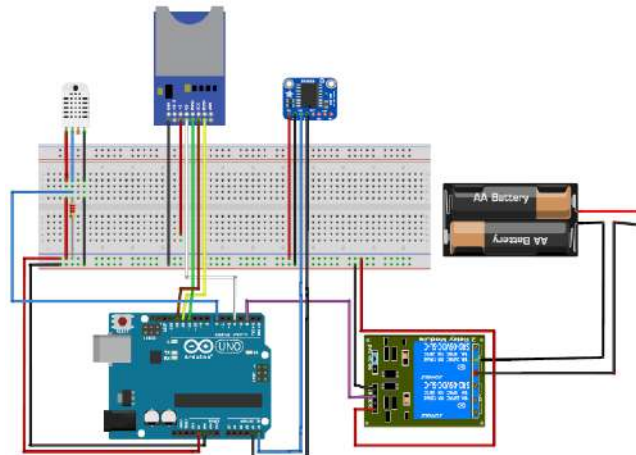


Figure 5: The schematic drawing of the connection.

5. RESULT AND DISCUSSION

The experiment was conducted in outdoor condition and indoor room (24°C). Once it's the humidity level is reduced to around 42% the front door purposely open for 10 seconds causing the humidity level rise back.

a. Result with Humidity Controller at Outdoor

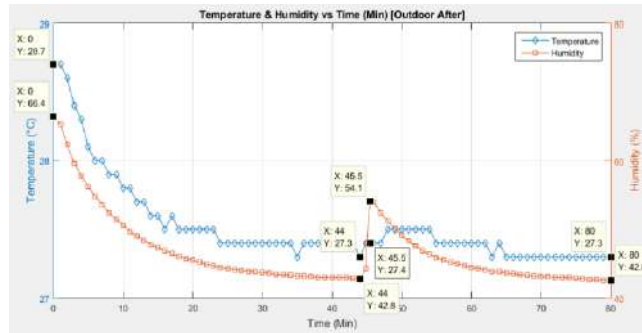


Figure 6: Temperature and humidity value after the experiment at outdoor condition.

Analysis

Table 1: Temperature and Humidity inside storage initial and after at outdoors.

	Initial	After
Temperature (°C)	28.7	27.3
Humidity, ϕ (%)	66.4	42.8
Humidity ratio, ω (kg H ₂ O/kg dry air)	0.01638	0.00956

$$\text{Volume} = 0.5\text{m} \times 0.5\text{m} \times 0.5\text{m} = 0.125\text{m}^3$$

$$\text{Pressure, } P = 100 \text{ kpa}$$

$$\text{Gas constant (Air), } R_a = 0.2870 \text{ kJ/kg. K}$$

Table 2: Analysis of water removed inside storage at outdoors.

Initial	After
$T_{\text{sat}} = 3.96 \text{ kpa}$	$T_{\text{sat}} = 3.57 \text{ kpa}$
$P_v = \phi P_{\text{sat}}$	$P_v = \phi P_{\text{sat}}$
$P_v = 0.664(3.96) = 2.63 \text{ kpa}$	$P_v = 0.428(3.57) = 1.53 \text{ kpa}$
$P_a = 100 - 2.63 = 97.37 \text{ kpa}$	$P_a = 100 - 1.53 = 98.47 \text{ kpa}$
$Ma = \frac{PaVa}{RaT}$	$Ma = \frac{PaVa}{RaT}$
$Ma = \frac{97.37(0.125)}{0.287(301.7)}$	$Ma = \frac{98.47(0.125)}{0.287(300.3)}$
$Ma = 0.1406 \text{ kg}$	$Ma = 0.1428 \text{ kg}$

$M_w = \omega Ma$ M_w $= (0.01638)(0.1406)$ $M_w = 0.0023 \text{ kg}$	$M_w = \omega Ma$ M_w $= (0.00956)(0.1429)$ $M_w = 0.00137 \text{ kg}$
----------------------------------------------------------------------------------	-----------------------------------------------------------------------------------

Mass of water removed = 0.0023 kg - 0.00137 kg = **0.93 gram**

b. Result with Dehumidifier Only at Indoor

The air conditioner is set to 24°C and the experiment took place after the temperature becomes stable.

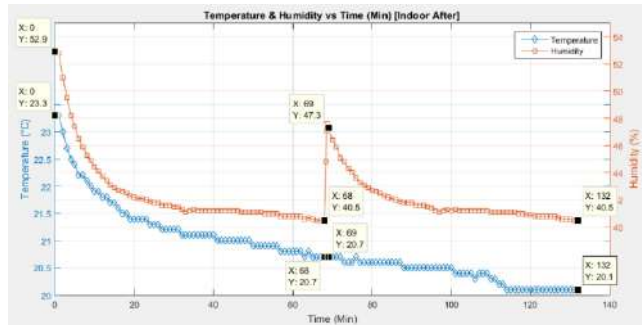


Figure 7: Temperature and humidity value after the experiment at indoor condition without relay.

Analysis water removed

Table 3: Temperature and Humidity inside storage initial and after at indoor 24 °C without relay.

	Initial	After
Temperature (°C)	23.3	20.7
Humidity, ϕ (%)	52.9	40.5
Humidity ratio, ω (kg H ₂ O/kg dry air)	0.00943	0.00613

Table 4: Analysis of water removed inside storage at outdoor 24°C without relay.

Initial	After
$T_{sat} = 2.86 \text{ kpa}$	$T_{sat} = 2.44 \text{ kpa}$
$P_v = \phi P_{sat}$	$P_v = \phi P_{sat}$
$P_v = 0.529(2.86) = 1.51 \text{ kpa}$	$P_v = 0.405(4.08) = 0.99 \text{ kpa}$
$P_a = 100 - 1.51 = 98.49 \text{ kpa}$	$P_a = 100 - 0.99 = 99.01 \text{ kpa}$
$Ma = \frac{PaVa}{RaT}$	$Ma = \frac{PaVa}{RaT}$
$Ma = \frac{98.49(0.125)}{0.287(296.3)}$	$Ma = \frac{99.01(0.125)}{0.287(293.7)}$
$Ma = 0.1447 \text{ kg}$	

M_w $= (0.00943)(0.1447)$ $M_w = 0.00137 \text{ kg}$	$M_a = 0.1468 \text{ kg}$ M_w $= (0.00613)(0.1468)$ $M_w = 0.0009 \text{ kg}$
--------------------------------------------------------------	----------------------------------------------------------------------------------------------

Mass of water removed = 0.00137 kg - 0.0009 kg = **0.47 gram**

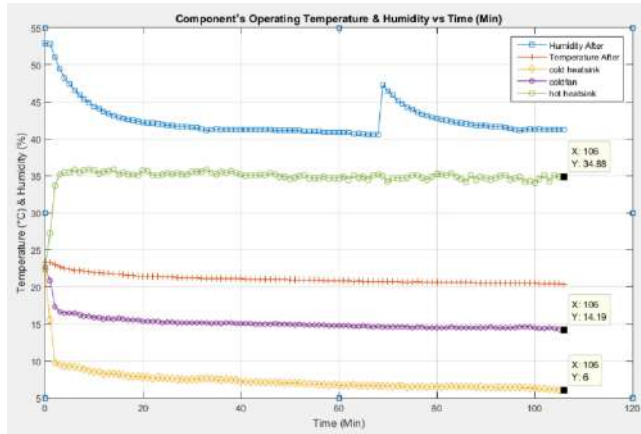


Figure 8: Component's temperature and humidity value after the experiment at indoor condition.

Table 5: Component's Temperature at indoor condition.

Component	Temperature (°C)
Cold Heatsink	6
Cold Fan	14.19
Hot Heatsink	34.88

c. Result with Dehumidifier Controller at Indoor

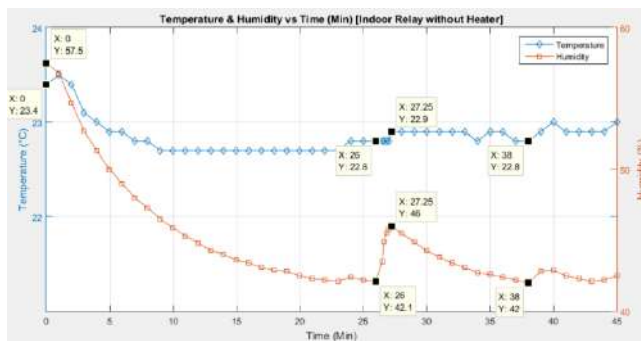


Figure 9: Temperature and humidity value after the experiment at indoor condition with relay and without heater.

We can see that the dehumidifier if off when the humidity reached to 42%.

Analysis water removed

Table 6: Temperature and Humidity inside storage initial and after at indoor 24°C with relay without heater.

	Initial	After
Temperature (°C)	23.4	22.8
Humidity, ϕ (%)	57.5	42.1
Humidity ratio, ω (kg H ₂ O/kg dry air)	0.01033	0.00726

Table 7: Analysis of water removed inside storage at outdoor 24°C with relay without heater.

Initial	After
$T_{sat} = 2.88$ kpa	$T_{sat} = 2.78$ kpa
$P_v = \phi P_{sat}$	$P_v = \phi P_{sat}$
$P_v = 0.575(2.88) = 1.66$ kpa	$P_v = 0.421(2.78) = 1.17$ kpa
$P_a = 100 - 1.66 = 98.34$ kpa	$P_a = 100 - 1.17 = 98.83$ kpa
$Ma = \frac{PaVa}{RaT}$	$Ma = \frac{PaVa}{RaT}$
$Ma = \frac{98.34(0.125)}{0.287(296.4)}$	$Ma = \frac{98.83(0.125)}{0.287(295.8)}$
$Ma = 0.1445$ kg	$Ma = 0.1455$ kg
$Mw = (0.01033)(0.1445)$	$Mw = (0.00726)(0.1455)$
$Mw = 0.00149$ kg	$Mw = 0.00106$ kg

Mass of water removed = 0.00149 kg - 0.00106 kg = **0.43 gram**

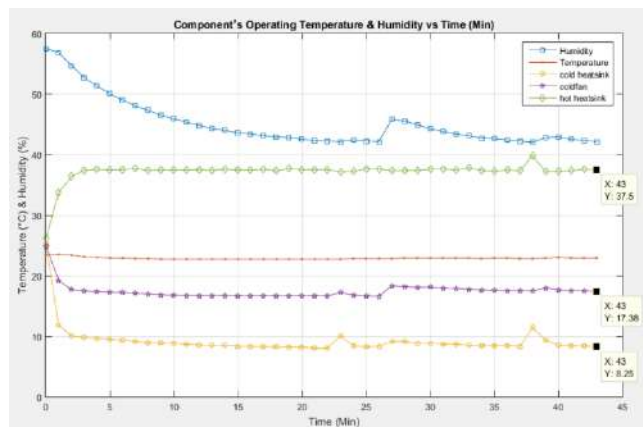


Figure 10: Component’s temperature and humidity value after the experiment at indoor condition with relay and without heater.

Table 8: Component’s Temperature at indoor condition with relay without heater.

Component	Temperature (°C)
Cold Heatsink	8.25
Cold Fan	17.38
Hot Heatsink	37.50



Figure 11: The picture of Cold Heatsink being condensed.

5. CONCLUSION

Thermoelectric peltier has a promising potential in the situations where both lower power and the smaller space are required. The present work was performed to develop an alternative to the current nitrogen-purged cabinet. From the experimental results discussed above, the peltier dehumidifier can reduce up to 40% and it a reasonable design to build a dehumidifier for small space dehumidification with advantages such as simple and efficient.

The SD card module was connected Arduino microcontroller where it also can store both temperature and humidity level inside the storage according to date and time. The data will be stored in micro SD memory card. The data will be saved as text file, and it can be extracted to Microsoft Excel. The data can keep for the future reference.

6. RECOMMENDATIONS

The study and experiments conducted helps in better understanding of the performance and effectiveness of the peltier dehumidifier and humidity control storage. Further studies and investigation should be performed to have the deeper understanding of the performance of the storage. Based on the results and analysis, the recommendations are as follows:

1. Use big heat sink and fan for the cold side.

Since the actual heat sink is in small size so it can cause the dehumidification process to take some time. The big heat sink has the ability to fasten the condensation process because the moist air can be condensed more when it is in linked with big surface area. Big fan also will provide higher flow rate of dry air to the compartment [5].

2. No gape.

The storage that used in this experiment has some spaces that allows the outer air enters in the compartment. This is one of the cause the relay on back faster when it is off when humidity level less than 42%. So, when designing the storage should make sure about the air tight.

3. Use transistor to regulate the voltage.

The current microcontroller using relay to control the dehumidifier where in will on and off it. But it seems in only off for a while only. By using the transistor, it will regulate the voltage like reducing the input voltage to maintain the humidity level.

REFERENCES

- [1] Ajitkumar N. Nikam¹, Dr. Jitendra A, “A Review on use of Peltier Effects”, International Journal of Science, Spirituality, Business and Technology (IJSSBT), Vol. 2, No. 2, May 2014
- [2] Ashok Kumar Yadav , Shatrughan Singh , & Gaurav Gupta, “Solar Air-Conditioning: Design for a Compressor-Less System using Peltier Effects”, International Journal of Advance Research and Innovation, Volume 2, Issue 2 (2014)
- [3] Prof. N. B. Totala, Prof. V. P. Desai, Rahul K. N. Singh, Debarshi Gangopadhyay, Mohd. Salman Mohd. Yaqub, Nikhil Sharad Jane, “Study and Fabrication of Thermoelectric Air Cooling and Heating System”, International Journal of Engineering Inventions (August 2014)
- [4] Swapnil S. Khode, Abhilash Arsod , Kushal Turankar, Krunal Waghmare, “ Fabrication and Result Obtained Of Portable Thermoelectric Air cooler System”, International Journal of Engineering and Technical Research (IJETR)
- [5] Mr. Nilesh Yadav, Dr. Nirvesh Mehta, Jaspalsinh Dabhi, “Review on Design and Theoretical of Thermoelectric”, International Journal of Engineering and Technical Research (IJETR)

DEVELOPMENT OF A BATTERY ENERGY STORAGE SYSTEM FOR PEAK SHAVING

N. Mohamed, N. A. Omar, I. Sulaiman & R. Noreldaim
Infrastructure University Kuala Lumpur, Malaysia

1. INTRODUCTION

Electrical power consumption in a big city is very huge. As the population increased and more buildings are developed, there is a need to use more electrical energy for the buildings and users' appliances. From many researches carried out by (J.M. Whitney, I.M. Daniel and R. Byron, 2018), (Y.M. Tarnopolskii, L.A. Carlsson and R.L. Crane, 2016), (D.F. Adams and S.L. Phonix, 2017), it showed that the consumer loads activities never end. This leads to the results of varying power consumptions curve over the time. This power consumptions curve over the time period is called load curve. The load curve consists of peak power and low power. The peak power is where the consumers use the most energy from the grid. The low power is where the consumers use the minimum energy from the grid. Because the power generator and resource is limited, the electricity provider often encourages people use alternative energy to reduce the burden of the grid power. The alternative energies are those energies obtained in nature and never end in usage. Such energies are wind and solar which massively available in Malaysia. When the power consumption is very high in a particular of time, this force the generators in the power plant supply more energy to the loads. Continue do like that will causes the generators reduce its life span and reduce the its service time. Thus, there should be alternative way to help the generators maintain good health condition.

The best alternative way to maintain life span of the generator is to help it reduces the amount of power supplies to the load. This can be done using switching method and control method. The control and switching methods often work together. The control method uses some kind of technologies to detect large power supplied from the generator and then trigger the relay to switch the power generated from the generator to the backup power. The switching must be fast enough so that the electrical loads continue receive the power without 'feel' on sudden breakdown and transient.

When the electrical loads get the power from the backup power, the main power from the generator will no longer used. Hence, this help to reduce the burden of the generator. In this project, as mentioned in the abstract, there are four main components involve to demonstrate the basic peak shaving. These components are SONOFF energy meter, microcontroller, Apps and battery.

2. LITERATURE REVIEW

Power system network is a complex power network that deliver electrical energy to many electrical loads attached on it. The variation of electrical loads will cause variations of power needed from the source or from the sending end. Therefore, the power generation site has to ensure power is enough used by the electrical loads. The electrical loads often classified as inductive loads, resistive loads, capacitive loads, inductive -resistive loads and capacitive-resistive loads or resistive-capacitive-inductive loads. The electrical loads can be anything. The electrical loads usually come from the electrical consumers.

The loads are classified according to the power needed. Normally those electrical loads consume high current will have high power. The electrical loads like air conditioner, water heater, induction motors and high power lamp are all consume high current. The manufacturer of electrical appliances often places the total amount of power consumed template at the back of the appliances. This is important to give information to the user about the energy consumed by the load.

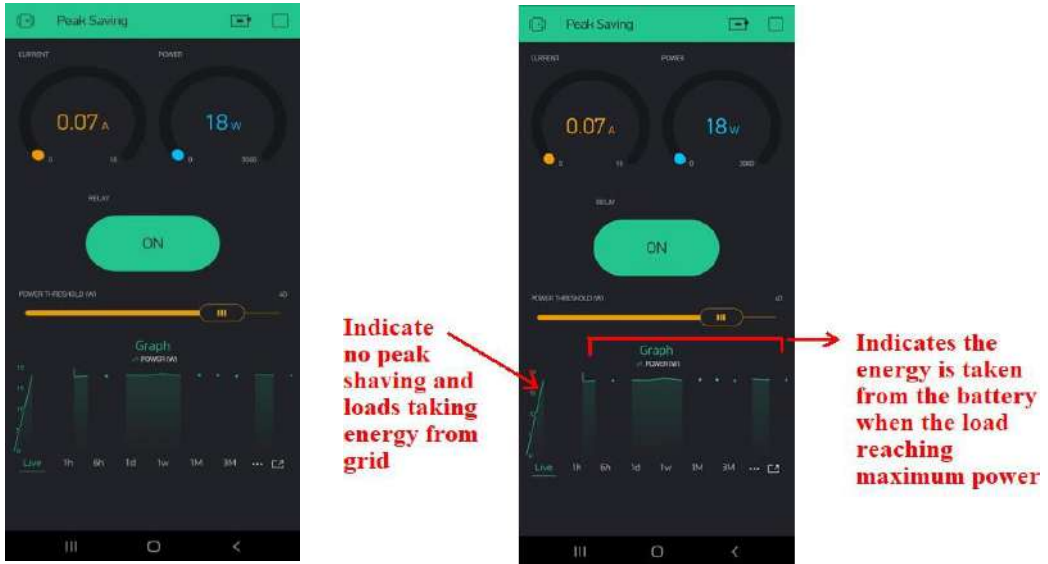
Some electrical loads have less resistance but more reactance. Such load like induction motor has higher inductive reactance than the resistance. In this case, the load has very low power factor. In order to start up the load, a compensated capacitive reactance is added into the load so that capacitive and inductive reactance are cancelled out and leaving only the resistance in the load. By doing this, the power factor is improved and the load start to work. When all the electrical loads connected into the grid network, they will either consume electrical energy or death in the network. Death in the network means, they connected but not active or not turn ON.

The total amount of energy or power consumed basically depends on the time operating the loads (turn ON the loads). Power shaving often targets on the peak power consumption over a period of time. To save the power or energy used, the power network designer should plan a system to switch the power from grid to some other renewable energy network so that this new network can continue supplies energy to the loads. The supplies of energy from new network must be transparent to the load. This means that, the loads will not feel sudden disconnection and re-connect to the new network. Also, the new network must ensure the voltage, current, frequency and phase are same with the grid after connect to the loads. When the switching switches the power from the grid to the new network, the grid power is no longer used by the load. Hence, this save the energy usage from the grid (H.T. Hahn and R.Y. Kim, 2016).

There is another approaches in peak shaving system which is, the grid still supply power to the loads but less because additional power is added during the peak power consumption to help the grid reduce the burden (H. Weisshaus, O. Ishai, G. Menges and A. Pora, 2016). This technique is the one most often encouraged by engineers and researchers. This is because the second power add in does not require so high. As long as there is a power added from outside, the grid will reduce amount of power needed to support the peak power.

4. RESULTS

Figure 2 shows the power plot versus the time when loads are connected. The loads are the light bulb. Different power consumption of light bulbs are added to the system so that the graph can show the power consumption versus the time. Note that when the load power reaching maximum which is 100 W, the system will switch to battery mode. Under this condition, total power used from grid will drop and the remaining power is supported by the battery.



(a) Peak shaving captured during the operating of automatic switching

(b) Explanation on peak shaving system

Figure 2: The Apps indicate the power consumption versus time with and without peakshaving

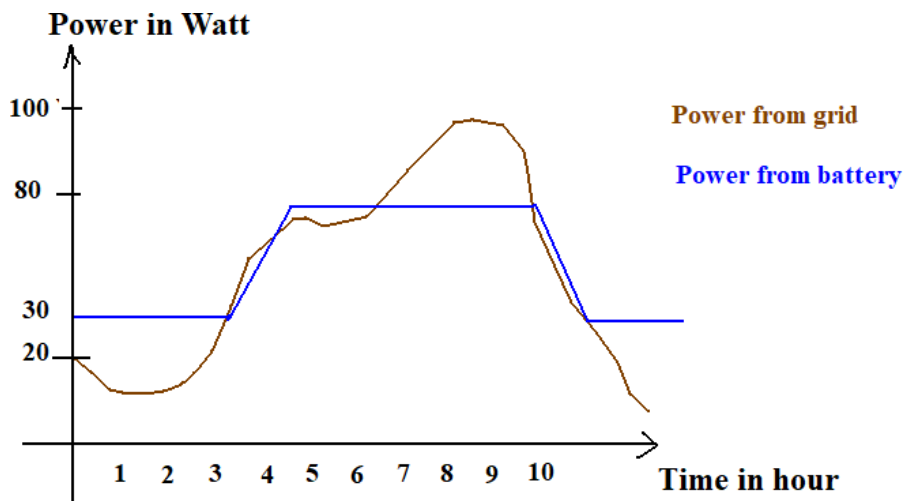


Figure 3: The results of observation on variation of loads added into the system

Figure 3 shows the results of power consumption with and without battery mode. The results were taken in 10 hours on various light bulbs. Notice that when power reaching 100 W, the battery supports the power and hence making the peak only 80 W. This has 20 W saving. During the peak shaving time, the battery does its work to supply electrical energy to the load.

Table 1, 2, 3, 4 and 5 shows the battery charging results, the apps power reading from Figure 2, the current consumptions recorded on day time and night time, the actual power reading from the TNB meter compared with the power shown in the apps and discharge of energy from the battery when connected to inverter.

Table 1: Battery charging results

Time	Charging voltage (V)
8 am - 9 am	8.67
9 am - 10 am	9.23
10 am - 11 am	9.88
11 am - 12 pm	10.25
12 pm - 1 pm	10.86
1 pm - 2 pm	11.33
2 pm - 3 pm	11.67
3 pm - 4 pm	12.01
4 pm - 5 pm	12.01

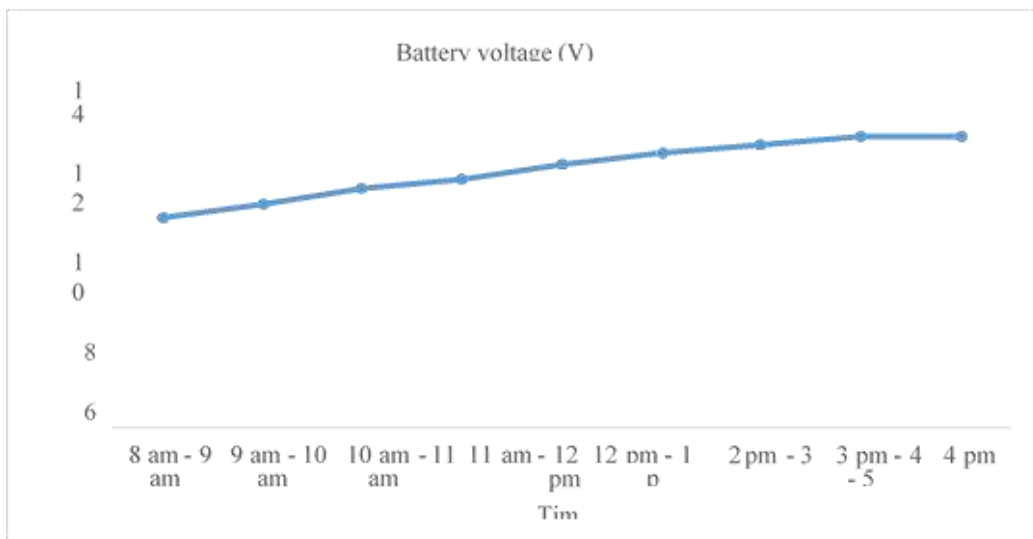


Figure 4: The plot of 12 V battery charging voltage

Table 2: The power reading for a day activities

Time	Power in (W)
8 am - 9 am	130
9 am - 10 am	130
10 am - 11 am	145
11 am - 12 pm	200
12 pm - 1 pm	250
1 pm - 2 pm	145
2 pm - 3 pm	130
3 pm - 4 pm	150
4 pm - 5 pm	145
5 pm - 6 pm	165
6 pm - 7 pm	155
7 pm - 8 pm	100
8 pm - 9 pm	100

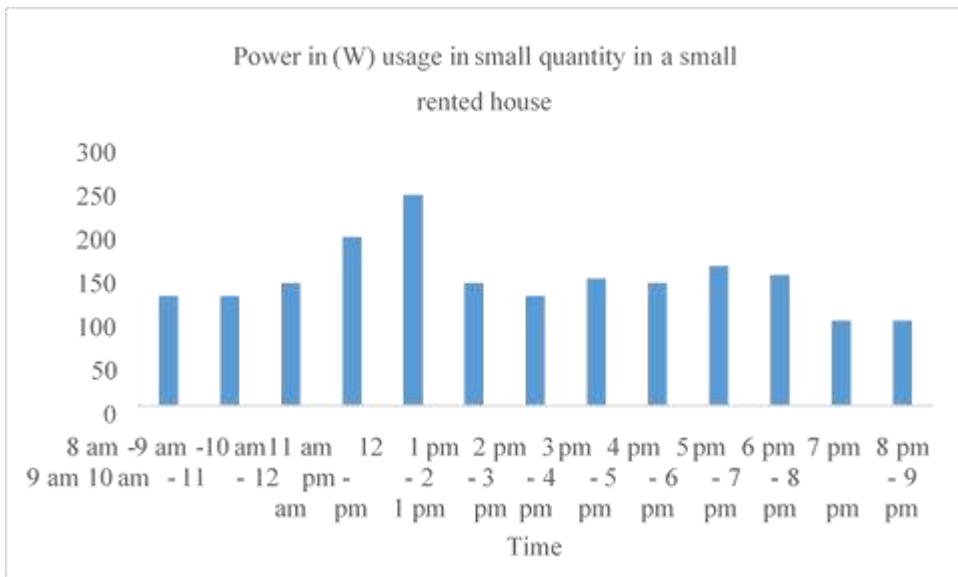


Figure 5: Total power recorded for a day using a small quantity of electricity

Table 3: The actual power consumption from meter compared with the Apps

Time	Power read by Apps (W)	Power Read by Energy Meter (W)
8 am - 9 am	130	133.4
9 am - 10 am	130	133.2
10 am - 11 am	145	140.4
11 am - 12 pm	200	201.5
12 pm - 1 pm	250	255
1 pm - 2 pm	145	140
2 pm - 3 pm	130	140
3 pm - 4 pm	150	155
4 pm - 5 pm	145	140.3
5 pm - 6 pm	165	160.3
6 pm - 7 pm	155	158.3
7 pm - 8 pm	100	104.5
8 pm - 9 pm	100	103.3

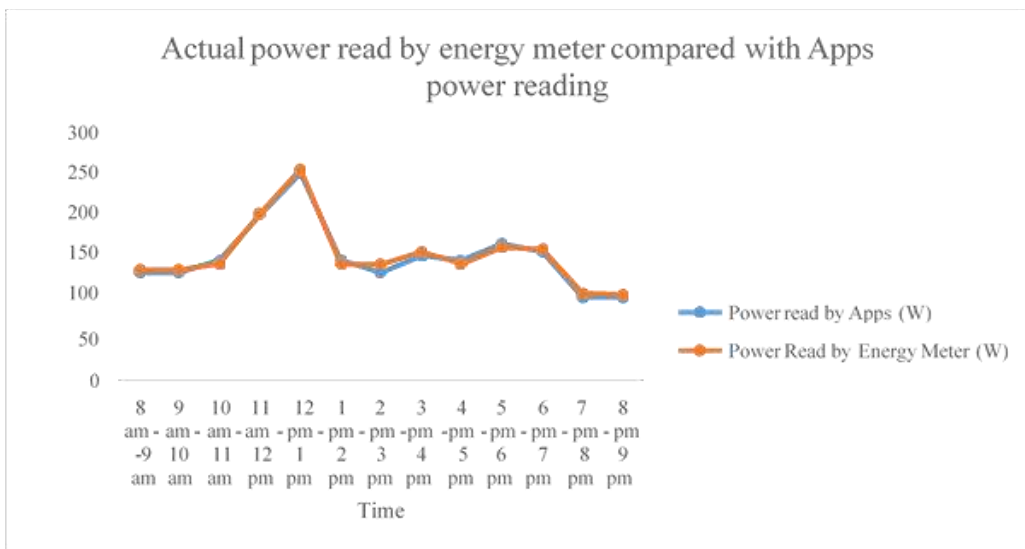


Figure 6: Actual power reading by energy meter compared with Apps power reading

Table 4: The current consumption for the day in small activities

Time	Current in (A)
8 am - 9 am	1.5
9 am - 10 am	2.3
10 am - 11 am	3.3
11 am - 12 pm	2.1
12 pm - 1 pm	1.5
1 pm - 2 pm	1
2 pm - 3 pm	1.5
3 pm - 4 pm	2.3
4 pm - 5 pm	2.5
5 pm - 6 pm	2.2
6 pm - 7 pm	2
7 pm - 8 pm	1.3
8 pm - 9 pm	1.6

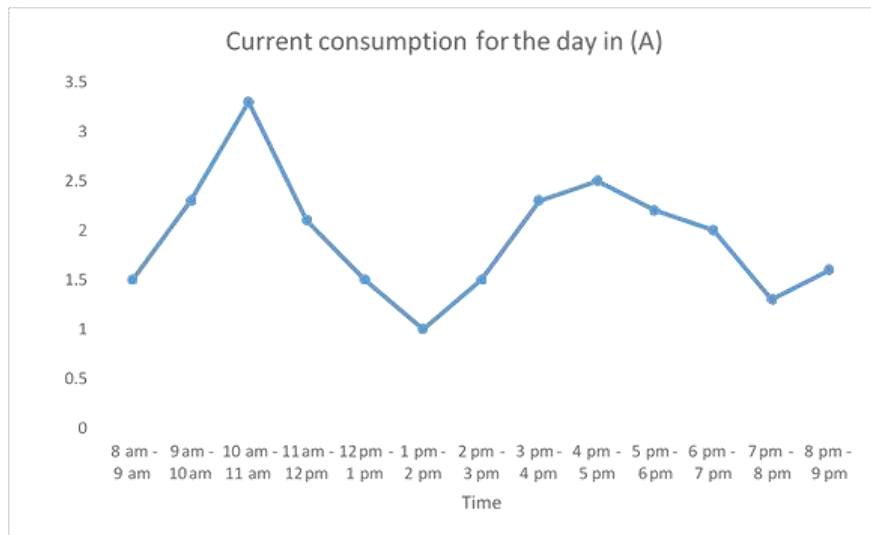


Figure 7: The current consumption on the day

Table 5: The battery voltage discharged when connected to power inverter

Time	Voltage
8 am - 9 am	12
9 am - 10 am	12
10 am - 11 am	11.3
11 am - 12 pm	10.87
12 pm - 1 pm	10.55
1 pm - 2 pm	10.1
2 pm - 3 pm	9.98
3 pm - 4 pm	9.5
4 pm - 5 pm	9.1
5 pm - 6 pm	8.8
6 pm - 7 pm	8.8
7 pm - 8 pm	8.6
8 pm - 9 pm	8.3

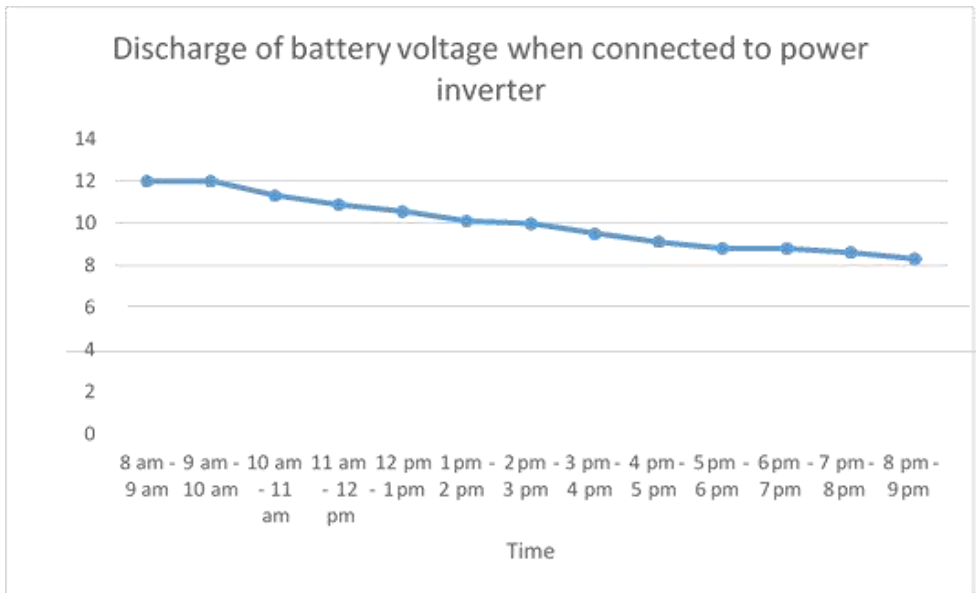


Figure 8: Discharge of battery voltage

Figure 4 shows the graph of battery voltage being charged by the circuit. As seen in the graph, initial voltage of the battery is 8.67 V. This voltage increased to 12.01 V after 5 hours of charging. The circuit is able to charge the battery as long as the battery is rechargeable battery and the power supply is keeping supplying from the grid.

Figure 5 shows the power consumption recorded for the day where a small activities happen in a house. Assuming no air conditioner used and just normal use of table fan, electric kettle and light, the energy seems varies from day time and night time. The day time using much

energy compared to the night time. This is because in day time, activities are going on whereas in night time most of the lights are turned OFF for rest.

In order to verify the power reading is correct and valid, a comparison with real energy reading was carried out. Figure 6 shows the energy meter reading compared with the apps power reading. As can be seen in the graph and table, the power consumption almost closed to each other. There is a small difference and this could be because of meter round the reading.

Figure 7 shows the amount of current consumed at the day and Figure 8 shows the battery voltage discharged. When the power consumption is varied, the current also varies. The current increased when more power needed by the loads. The current reduced when the electrical loads are shutdown. The current consumption is high at day time and low at night time. The current consumption will reduce when the peak shave is happened. This put the grid current power supply turned off and all the current is from the power inverter.

When the power used by the inverter, this will cause the voltage of the battery reduced. As seen in Figure 8, the voltage reduced proportional to the loads connected at the output of the inverter. The higher the power consumption of the load, the more the voltage discharged. The overall performance of the peak shaving is summarized as shown in Table 6.

Table 6: Performance of peak shaving on power and current

Without peak shaving		With peak saving	
When SONOFF is idle		When SONOFF is working	
Power (W)	Current (A)	Power (W)	Current (A)
50	1.2	100	1.3
60	1.5	120	1.4
70	1.3	104	1.2
30	0.5	150	1.6
80	2.3	200	1.8
55	1.6	250	2.3

The SON OFF does nothing when it is in idle condition. When SON OFF perform switching where the usage of electricity is switched to power inverter, the current get reduced whereas the load is keep running. This is how the energy being saved.

5. CONCLUSION

From the project, it is seen the power consumption of the loads being saved when the power reaching 100 W. Hence objective 3 is achieved. The total energy saved is 20 W from 4 to 10 hours. The saving time is 6 hours. It is also seen that the microcontroller does its job to perform the switching when detects the loads power reaching maximum. This shows the objective 1 is achieved.

The Apps used to show the power consumption is Blynk. The Apps needs to connect to the WiFi and links the data from the prototype. The Apps show the power and current measurement. The Apps does not show the voltage measurement because the voltage is fixed at 230 V. Since the entire Apps developed can shows the power and current as well as the graph, thisproved that objective 2 is achieved. A more power can be shown if high load power is used. But because of safety issues, lowcurrent loads are used for demonstration on peak shaving.

REFERENCES

- J.M. Whitney, I.M. Daniel and R. Byron. (2018). "The Characteristics of Load Curve", *IEEE Trans on Electrical Energy*, Vol. 12, Issue 10, pp. 4 - 10.
- Y.M. Tarnopolskii, L.A. Carlsson and R.L. Crane. (2016). "The Peak Power Analysis for Complex Load Curve", *IEEE Trans on Electrical Power*, Vol. 10, Issue 8, pp. 3 - 15.
- D.F. Adams and S.L. Phonix.(2017). "Understanding the Load Curve", *International Journal on Electrical Power Engineering*, Vol. 3, Issue 9, pp. 10 -20.
- H.T. Hahn and R.Y. Kim. (2016). "Power Switching Design for 100 MW Loads", *International Journal on Engineering and Technology*, Vol. 26, Issue 32, pp. 30 - 48.
- H. Weisshaus, O. Ishai, G. Menges and A. Pora. (2016). "Peak Power Shaving Strategy", *IEEE Trans on Electrical Power*, Vol. 45, pp. 67 - 88.

ANALYSIS ON VEHICLE PERFORMANCES BETWEEN SINGLE PLATE CONVENTIONAL AND AFTER MARKET CLUTCH

Muhammad Fathurrahman Daud, Ts. Engku Amirul Rashidin Engku Ariff & Muhammad Fahmi Md Isa

Infrastructure University of Kuala Lumpur

ABSTRACT

A clutch is one of the most important parts in a vehicle drive system. It is a mechanical device that located between the engine and transmission. Its main function is to transmit, engage and disengage power, torque and speed from the engine to the transmission input shaft. It is made up of flywheel, clutch housing, clutch plate and linkage that is necessary to operate the clutch. Gradually engagement of the clutch overtime will increase the clutch slippage thus reduce vehicle performance. In this project, the differences of performances between the vehicles that installed with a conventional clutch and an aftermarket clutch had been analysed due to compare the overall output results. Most of the conventional clutch have a certain limit to transmit the engine power and torque. Therefore, by installing the aftermarket clutch, the limit to transmit the engine torque is usually can be increased. Clutch design and material are the keys in increasing vehicle performances. Both types of clutches which were installed into the same vehicle by replacement were tested on a chassis dynamometer to compare the performances such as torque and horsepower. As the obtained results from the vehicle horsepower and torque curves, the power output of vehicle with aftermarket clutch had produced 184 PS at 8000 rpm, which considered to have 4 PS higher of power output compare to the vehicle with conventional clutch at high engine speed. Moreover, in the output torque curve, it can be seemed that both vehicles had produced a same level of performance during the low engine speed but start to increase about 5 Nm at 5200 rpm.

1. INTRODUCTION AND PROBLEM STATEMENT

The clutch is a mechanical device, which is used to connect or disconnect the source of power from the remaining parts of the power transmission system at the will of the operator. Currently, there are several types of clutches are being used in the motor industry based on certain characteristics. Some of them named as Friction clutch, Hydraulic clutch, Centrifugal clutch, Semi-centrifugal clutch, Cone clutch, Diaphragm clutch, Electromagnetic clutch, Dog and spline clutch, Vacuum clutch and Freewheel unit clutch. Furthermore, single plate clutch is one of the common type of clutches used in most modern light vehicles and main function is to transmit directly power and torque from the engine to the transmission input shaft. As the name stated, it has only one clutch plate and consists of a clutch plate, friction plate, pressure plate, flywheel, bearings, clutch spring, and nut-bolts arrangement.

Moreover, high performance vehicles such as race cars, drag racers, circle track cars, etc., require rapid gear changes in order to make the car competitive with other racers, and

hopefully to achieve a slight advantage to increase the efficiency and speed of the vehicle during a race. Most high-performance vehicles have either three or four-speed manual transmissions. Thus, if time can be saved during the changing or shifting of gears, even a fraction of a second, such saved time can be multiplied considerably over the racing time period to change appreciably the efficiency and results achieved by the racing vehicle.

Nevertheless, different specification of engine will produce a different range of brake horsepower. Therefore, clutch plate selection is really important as the main component that is function to transfer the output power, speed and torque from engine to the wheels. A full-face lining clutch, the friction material is placed fully on the clutch plate. Thus, the rate of clutch and power transmission is affected by the temperature of the friction surface. Hence, providing an air gap between two segments in the face helps in heat dissipation and lower down the friction lining temperature. As the result, it increases integrity and improves the ability of the clutch in power transmission.

Nowadays some performance enthusiast like to change the clutch system by modifying the clutch plate and pressure plate. Improper configuration of these components definitely affects the vehicle performances. Other than that, trial and error on different clutch plate and pressure plate are time consuming and costly. However, most motorsport racers use an aftermarket clutch that have much higher torque potential and less spinning mass than the conventional clutch. In this study, a measurement of output horsepower, speed and torque will be presented based on the two types of single clutch plate and the results would be analysed and compared in order to determine which type can produce higher performances.

2. LITERATURE REVIEW

The clutch a component which interfaces two or more rotating shafts. In a manual transmission vehicle, the clutch controls the connection between the shaft coming from the engine and the shafts which turn the wheels. High performance clutches ordinarily include heavier springs and distinctive plate materials. Employing a heavier spring will result in a clutch with more clamping pressure, meaning more torque can be transmitted without the clutch slipping. Different materials will result in different characteristics for a clutch. Organic compounds are more common for production vehicles, as these permit for smooth engagement and long life, but they do not fundamentally work well at high temperatures. Whereas Kevlar, carbon and ceramic material being able to function at higher temperatures. Regularly, high performance clutches will utilize “puck” design with gaps between the clutch plate pieces. With less friction surface the pressure on the clutch plate will be higher, and some materials will give more grip at certain pressure. As stated in Trupti Chavan 2015, the gaps in the clutch plate helps in heat dissipation which increased the power transmission ability and efficiency.

There are four main types of clutch lining material available in the automotive industry, with combinations of any two able to be bonded and/or bolted on either side of the clutch plate. Note that for each type of lining, aluminium or steel backings can be indicated. This decreases the probability of high rpm clutch explosion, whereas the aluminium type backings have the

advantage to reduce mass when compared to steel. The thickness of the clutch lining is additionally critical. Thick linings offer longer benefit life and smoother operation but are not as appropriate for race or competition applications. As mentioned in Patil, Kedar Kishor, et al. 2020, the simulation was carried out using ANSYS software for different materials. By giving the same pressure intensity of 0.5 N/mm^2 for different materials, heat flux, total deformation, stress, strain and first six modal frequencies for different materials has been observed. By comparing the results, ceramic has less deformation and less modular frequencies than all other. This data helps the analysts to choose proper material to reduce wear and increase the performance of the clutch.

In term of main operation, a clutch is characterized as a system that is utilized to interface or disengage the engine from the transmission components. It is located between the motor and gearbox. When the engine is running and is in a static position, the clutch is always in the engaged position. The clutch withdraws when the driver depressed the clutch pedal. This system allows the clutch to disconnect during starting, changing gears, stopping and idling. This device is important to transfer power from the engine to the wheels. Commonly, there are three main function of a clutch which are to allow the engagement or disengagement of gear when the vehicle is stationary and the engine is running, transfer engine power to the gearbox and to the wheel and grant the engaging of gears when the vehicle is moving. In automotive sector, various types of clutch plate have been design based on the vehicle specifications such as single plate friction clutch, multiplate friction clutch (wet and dry), cone clutch, centrifugal clutch, diaphragm clutch, hydraulic clutch, electromagnetic clutch and etc.

There are several effects of clutch system towards vehicle output performances such as transmission of torque from engine to a gearbox. Engine torque is always wasted when the clutch is slightly engaged or slightly pressed. This can be done when the need to control power to the wheels or smoothly engage the engine. Ideally there should not be any slip between the engine and the transmission when the pedal is not depressed, i.e., the clutch should lock-up. As a worn-out clutch cannot lock up due to lack of friction, engine torque is wasted. With a high-performance clutch, the clutch is able to withstand high temperature as this will reduce the occurrence to have a clutch slip. Therefore, maximum engine torque can be transferred to the wheel. Also, vehicle acceleration is greatly increased because of the high friction material used. The lightweight parts allow an increased rate of revolutions and, therefore a bump in horsepower. The horsepower increase varies from driveline to driveline and we have seen it range from 5 to 30 horsepower in dyno testing (Brent Davis 2016).

3. METHODOLOGY

In this study, the parameter of conventional clutch and aftermarket clutch will be measured in order to calculate the activation force and torque capacity by using the equation that based on uniform wear theory. Besides, difference in performances such as output horsepower and torque between the conventional clutch and the aftermarket clutch will be completely measured and analysed from 2000 to 8000 rpm by using a Toyota Soluna as shown in Figure 1(a) as a testing vehicle that powered by the modification engine which is 2ZZ-GE engine (Figure 1(b)) from

Toyota Celica ZZT231. Engine specification is shown in Table 1.



Figure 1(a): Toyota Soluna and **1(b)** 2ZZ-GE Engine Overall View (www.toyota.co.jp)

Table 1: 2ZZ-GE Engine Specification (www.toyota.co.jp)

Engine code	2ZZ-GE
Layout	Four Stroke, inline-4 Cylinder
Fuel type	Petrol
Production	1999-2011
Displacement	1.8 L
Fuel system	Multi-Point Fuel injection
Power output	164 HP to 189 HP
Torque output	141 Nm to 230 Nm
Firing order	1-3-4-2

In vehicle testing, the conventional and aftermarket clutches will be considered as a used part. Therefore, the same equation of uniform wear theory will be used to calculate the activation

force and torque capacity. The equation of activation force for uniform pressure can be expressed as:

$$N = \pi P_a / 4 (D^2 - d^2)$$

Where,

N = Activation Force (kN)

P_a = Pressure Max (MPa)

D = Outer diameter of the clutch plate (m)

d = inner diameter of the clutch plate (m)

For torque capacity,

$$T = N\mu(D^3 - d^3) / 3(D^2 - d^2)$$

Where,

T = Torque capacity (Nm)

N = Activation force (kN)

D = Outer diameter of clutch plate (m)

d = Inner diameter of clutch plate (m)

The testing vehicle (Toyota Soluna) with conventional clutch will be tested first using the chassis dynamometer. The vehicle is placed on the chassis dynamometer according to the suitable vehicle length. The wheels must be placed on top of the roller for the front wheel. After the first test, the gearbox is removed and the conventional clutch is replaced with the aftermarket clutch for the second test. As shown in Figure 2, the vehicle is placed on the chassis dynamometer according to the suitable vehicle length. Then it is strapped down with the ratchet tie down on the front and rear of the vehicle.



Figure 2: Vehicle Strapped on Chassis Dynamometer

4. DISCUSSION

The overall findings were divided into three sections which are the calculation result of activation force and torque capacity that applied on the clutch friction plate, the result of vehicle horse power and vehicle output torque that were obtained with chassis dynamometer. Detail findings are as titles follow:

Calculation of Activation Force and Torque Capacity

Figure 3 and 4 are illustrated the method of measuring the parameter of inner diameter and contact surface area of conventional clutch. It is made from organic material, usually it's a mix of fiberglass and other materials (including brass in some cases) molded or woven into a friction pad. Table 2 is shown the properties of commonly used materials lining of friction surfaces.



Figure 3: Clutch Plate Inner Diameter (Conventional)



Figure 4: Clutch Plate Contact Surface Area (Conventional)

Table 2: Properties of Commonly Used Materials Lining of Friction Surfaces

Friction combinations		Wet-running				Dry-running		
		Sintered bronze/ steel	Sintered iron/ steel	Paper/ steel	Steel/ hardened steel/ hardened	Sintered bronze/ steel	Organic linings/ cast iron	Steel/ nitrided/ steel/ nitrided
Coefficient of friction	Dynamic coefficient of friction μ	0.05 to 0.1	0.07 to 0.1	0.1 to 0.12	0.05 to 0.08	0.15 to 0.3	0.3 to 0.4	0.3 to 0.4
	Static coefficient of friction μ_0	0.12 to 0.14	0.1 to 0.14	0.08 to 0.1	0.08 to 0.12	0.2 to 0.4	0.3 to 0.5	0.4 to 0.6
	Ratio μ_0 / μ	1.4 to 2	1.2 to 1.5	0.8 to 1	1.4 to 1.6	1.25 to 1.6	1.0 to 1.3	1.2 to 1.5
Technical data guideline values ¹⁾	Max. sliding speed v_R [m/s]	40	20	30	20	25	40	25
	Max. friction surface pressure p_R [N/mm ²]	4	4	2	0.5	2	1	0.5
	q_{AE} [J/mm ²] ²⁾	1 to 2	0.5 to 1	0.8 to 1.5	0.3 to 0.5	1 to 1.5	2 to 4	0.5 to 1
	\dot{q}_{Ao} [W/mm ²] ³⁾	1.5 to 2.5	0.7 to 1.2	1 to 2	0.4 to 0.8	1.5 to 2	3 to 6	1 to 2
	Area-related cooling flow \dot{V}_A [$\frac{mm^3}{mm^2 \cdot s}$]	0.1 to 2	0.1 to 1	0.1 to 2	0.1 to 0.5			
Lubricant	Unalloyed and slightly blended oils	X	X	X	X			
	Oils with additives	-	X	X	X			

Calculations:

The conventional clutch friction plate parameters:

- i. Outer diameter of friction surface (D) = 0.211 m
- ii. Inner diameter of friction surface (d) = 0.139 m
- iii. Maximum pressure = 1 MPa = 1000000 Pa
- iv. $\mu = 0.35$ (Table 2)

Activation force:

$$N = \pi P a d / 2 (D - d)$$

$$N = \pi(1000000)(0.139) / 2 (0.211 - 0.139)$$

$$N = 15720.53 \text{ N}$$

Torque capacity:

$$T = N \mu / 4 (D + d)$$

$$T = (15720.53)(0.35) / 4 (0.211 + 0.139)$$

$$T = 481.44 \text{ Nm}$$

Figure 5 and 6 show the method of measuring the parameter of inner diameter and contact surface area of aftermarket clutch. Made of ceramic clutch material, which is mostly a mix of silicon dioxide and various metals and additives, sintered or brazed onto the clutch disc. Table 3 shows the properties of different materials of aftermarket clutch.



Figure 5: Clutch Plate Inner Diameter (Aftermarket)



Figure 6: Clutch Plate Contact Surface Area (Aftermarket)

Table 3: Properties of Different Materials

Material	Friction Coefficient, f	Maximum Pressure, p_{max} [psi]
Cermet	0.32	150
Sintered metal (dry)	0.29-0.33	300-400
Sintered metal (wet)	0.06-0.08	500
Rigid molded asbestos (dry)	0.35-0.41	100
Rigid molded asbestos (wet)	0.06	300
Rigid molded asbestos pads	0.31-0.49	750
Rigid molded nonasbestos	0.33-0.63	100-150
Semirigid molded asbestos	0.37-0.41	100
Flexible molded asbestos	0.39-0.45	100
Wound asbestos yarn and wire	0.38	100
Wound asbestos yarn and wire	0.38	100
Woven cotton	0.47	100
Resilient paper (wet)	0.09-0.15	400

Calculations:

The aftermarket clutch friction plate parameters:

- i. Outer diameter of friction surface (D) = 0.208 m
- ii. Inner diameter of friction surface (d) = 0.138 m
- iii. Maximum pressure = 2.069 MPa = 2069000 Pa
- iv. $\mu = 0.4$ (Table 3)

Activation force:

$$N = \pi P a d / 2 (D - d)$$

$$N = \pi (2069000) (0.138) / 2 (0.208 - 0.138)$$

$$N = 31394.78 \text{ N}$$

Torque capacity:

$$T = N \mu / 4 (D + d)$$

$$T = (31394.78) (0.4) / 4 (0.208 + 0.138)$$

$$T = 1086.26 \text{ Nm}$$

Based on the calculation result, it shows that aftermarket clutch was produced higher activation force and torque capacity which are 31394.78 N and 1086.26 Nm compare to conventional clutch which had produced about 15720.53 N and 481.44 Nm of activation force and torque capacity.

Comparison of Vehicle Horsepower

As illustrated in Table 4 and Figure 7, the power output of vehicle which installed with aftermarket clutch had produced 184 PS at 8000 rpm which considered to have 4 PS more power compare to the vehicle with conventional clutch at high engine speed. In addition, it can be indicated that during the engine revs up from approximately 5100 to 5900 rpm, the vehicle with aftermarket clutch had performed a higher range of power output. This result would be the essential factor to prove that higher output torque definitely can give advantage on increasing the power output. However, at 6200 rpm the vehicle with conventional clutch had showed an earlier climbing of power output compare to the aftermarket clutch's vehicle. This may be happened because of the clutch slipping throughout the engagement between clutch plate and disc due to the human error. Besides, both power output curves during low engine speed had displayed a quite similar shape.

Table 4: Comparison of Vehicle Power Data from Chassis Dynamometer

Engine Speed (rpm)	Conventional Clutch Power (PS)	Aftermarket Clutch Power (PS)
2000	39	40
3000	60	60
4000	90	90
5000	113	113

6000	125	125
7000	172	172
8000	180	184

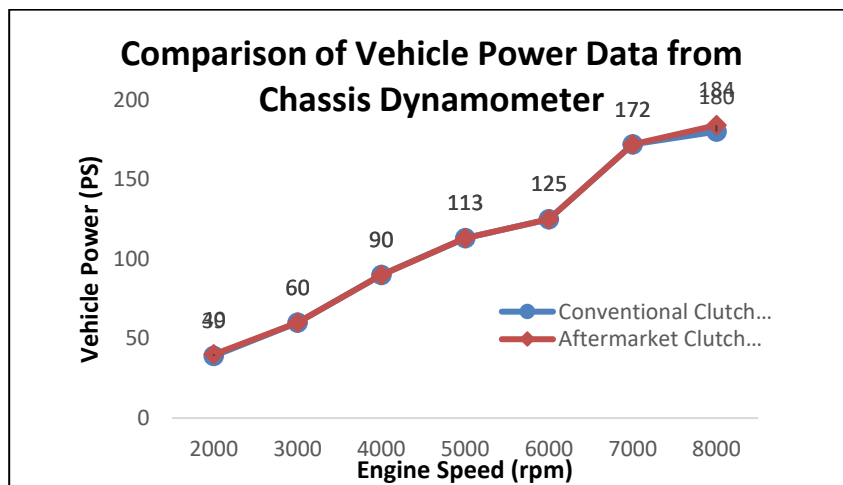


Figure 7: Comparison of Vehicle Power Data

Comparison of Vehicle Torque

As shown in Table 5 and Figure 8, it can be seen that both vehicles had produced a same level of performance during the low-speed range which start from 2000 until 5000 rpm. However, at the same range of engine speed of power output curve, the torque of aftermarket clutch's vehicle had started to increase at engine speed of 5200 rpm. Even though it is less than 5 Nm, it's still proving that with higher values of torque and engine speed, a vehicle would develop an optimum level of power output. Besides that, as shown in the torque curve, from 3200 rpm to 4400 rpm it is clearly can be noticed that vehicle with conventional clutch was slipping and caused the unsmooth of torque transfer process compare to the aftermarket clutch. In conclusion, these have proven that by installing an aftermarket clutch, vehicle performance can be increased.

Table 5: Comparison of Torque Data from Chassis Dynamometer

Engine Speed (rpm)	Conventional Clutch Torque (Nm)	Aftermarket Clutch Torque (Nm)
2000	134	139
3000	145	145
4000	157	157
5000	160	160
6000	143	145
7000	172	172
8000	159	164

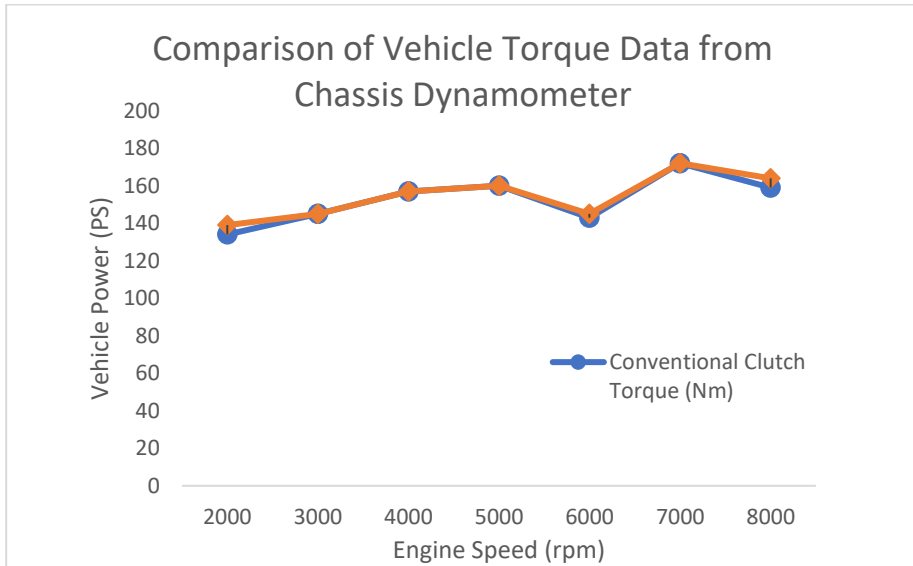


Figure 8: Comparison of Vehicle Torque

5. CONCLUSION

In clutch system, clutch plate plays a very important role in transferring engine torque to the transmission. With friction material property and the design of the clutch plate is very crucial in increasing vehicle performance. Not only that, wear rate of the clutch plate is also increased. In this project, a standard quality aftermarket clutch was installed in one of the vehicles. Therefore, only a few of improvements can be seen based on the overall results. The improvements in performance will greatly benefit if the vehicle is driven in the race track.

Additionally, due to the materials and design of the clutch plate, it can withstand high temperature and abusive use without losing friction. As for drag use, the clutch plate must be able to grab well during a launch. With high quality aftermarket clutch, surely there would be greater improvements in many performances. Unfortunately, high quality aftermarket clutch is much more expensive. Some of the recommendations that can be added on the future study in order to furthermore improve the analysis are to change the conventional flywheel to a lighter flywheel as this modification will improve the clutch performance and to change or modify the clutch housing diaphragm spring due to produce higher clutch clamping force.

REFERENCES

- Trupti Chavan. Comparative Analysis of Performance of Full Face and Staggered Geometry Friction Lining in Automated Single Plate Clutch. Retrieved from <http://www.ierjournal.org/pupload/mitpgcon/MD1-05.pdf>
- Patil, K. K., Randive, V., Mulla, S., Parit, R., Mane, S., & Kadam, S. (2020). Design and analysis of single plate clutch by mathematical modelling and simulation. *International Journal*, 8(3), 248-252.
- Sharma, N., Bhoi, A., & Mahato, N. (2020). Design and structural assessment of single clutch plate with variant of materials. 8, 3779. <https://www.ijert.org/papers/IJCRT2005501.pdf>
- Davis, B. (2016, March 18). SPEC Clutch Helps Put It Down and Increase Your Power. *LSX Magazine*. <https://www.lsxmag.com/news/spec-clutch-helps-to-put-it-down-and-up-your-power/>
- Stone, R., & Ball, J. K. (2004). *Automotive engineering fundamentals*. SAE International.

DEVELOPMENT OF MONITORING SYSTEM USING RASPBERRY PI AND SENSORS WITH INSTANT NOTIFICATION

S.S. Mazlan, N. Mohamed., K. W. Hon & I. Sulaiman
Infrastructure University Kuala Lumpur, Malaysia

1. INTRODUCTION

Internet of Things (IoT) creates a new platform for information sharing, productivity, and modern living [1]. IoT has facilitated modernity and ease in human lifestyle. Over the past few years, people have become more dependent on IoT to fulfil tasks like work, school, research, and daily chores. Consequently, this advancement has the ability to broaden the fundamental functions of a surveillance system [5].

Any organization needs a surveillance system, used to protect people and their possessions from various risks including theft and burglary. The demand for a sophisticated surveillance system that interfaces with the Internet to enable continuous monitoring of activities from anywhere, at any time, has grown as a result of Malaysia's rise in crime cases. According to the crime index, there were 52344 theft cases in 2020, which will make up nearly 80% of all instances [10]. Despite being widely used, closed-circuit television (CCTV) is still regarded as a passive monitoring system that requires constant and continuing human supervision, requires more time, is very expensive, and frequently produces corrupted files [14].

Researchers and academics were motivated to create a non-passive surveillance system because of the drawbacks of passive monitoring technologies described above [17]. The majority of researchers then utilized Wireless Sensor Networks (WSN) for monitoring, taking full advantage of its features and advantages [15],[4]. Due to the wireless connectivity, sensor nodes can be placed anywhere in a building, giving them the advantage of portability when being deployed [18].

The main objective is to build a system that can monitor belonging and property for security purpose, and this research is to design a surveillance system that integrate with open-source application programming interphase (API). The open-source API can provide a cost-effective surveillance system. It gives an instant problem solving and crime prevention as the surveillance system using medium of communication which are Telegram and Email. These implementations are to provide a complete and relevant evidence for forensic investigation in case any crime happens by having ten second video recording.

2. LITERATURE REVIEW

The Raspberry Pi 3 computer, a USB webcam, a Passive Infrared Sensor (PIR) sensor, a current sensor, and an ESP8266 Wi-Fi module make up the system's hardware in this study. The Python programming language, the Arduino Integrated Development Environment (IDE), and the Raspbian operating system are all used in these articles. This paper describes a security system that sends the user a telegraph message with an image attachment in the event of an intrusion. As opposed to a surveillance system, the system described in this work is more general because it uses the Message Queuing Telemetry Transport (MQTT) protocol to read the state of numerous sensors as well as monitoring.

[

As long as the user is connected to the same network as the surveillance system, the monitoring system proposed in the research proposal by researcher(s) [13] enables consumers to monitor their homes live through mobile application. Additionally, a motion sensor that detects an intruder nearby will send an email notification with a picture attachment as well as two notifications through SMS and email. This project makes use of the Raspberry Pi, the Pi camera, the PIR motion sensor, the Ultrasonic sensor, the buzzer, and the LED. The applications employed in this study include MQTT broker, Node-Rack, and ThingSpeak. The investigation by is one more study utilizing Node technology [2].

An ingenious motion detection method that enables the Raspberry Pi to send email notifications with image attachments when motion is detected is described in research by [20]. The study also covered how to send emails using Transmission Control Protocol on port 55 and SMTP on port 587. In the study, researcher employ the Raspberry Pi 3 model B, PIR sensor, Pi camera, and female to female wiring. The email configuration in this study uses the Raspbian and Windows operating systems. This research has its own mail server so that only designated recipients may read the email.

N. Patil, S. Ambatkar, and S. Kakde 2017, proposed a surveillance system with a motion detector that sends an email to the user when motion is detected. The article makes use of the Raspberry Pi, a camera module, and a motion sensor. The notification is sent as an email attachment. The email notification is sent using a Python script, as suggested discussed.

In the study, T. Gualotuña, E. Macías, Á. Suárez, E. C., and A. Rivadeneira 2018, explains on a video surveillance system service that sends email and telegram notifications with a video attachment. The approach, however, is unique; the paper employs a Raspberry Pi B+ as a video streaming server and storage device, as well as an Atmega 328 Arduino as a microcontroller and CPU. The Raspberry Pi used in this article has a speed of 1.5 GHz, which is significantly faster than the 20 MHz speed of the Arduino used in the research reported [7]. The use of Arduino has an effect on the system's performance in terms of speed which it slows down the system.

3. METHODOLOGY

The system is designed to monitor personal, property and belongings, send instant email notifications with video attachments of detected motion near surveillance systems, send instant Telegram notifications with video attachments when the system detects motion, and allow live monitoring where users can view live video after the Python code is executed. Furthermore, it is a low-cost and simple-to-implement surveillance system.

The hardware for this system comprises of a motion sensor, a camera module, and a Raspberry Pi 4 Model B computer with 8 Gigabyte (GB) of Random Access Memory (RAM) [11]. The camera is integrated into the Raspberry Pi through a specific camera connector. A General-Purpose Input/Output (GPIO) pin on the Raspberry Pi connects it to the motion sensor. The GPIO4 pin, 5V, and GND on the Raspberry Pi have all been used. The complete hardware installation for the surveillance system is shown in Figure. 1.

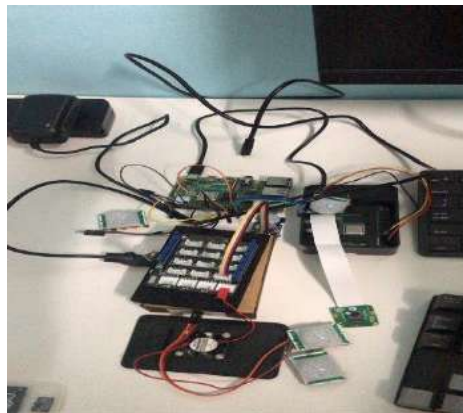


Figure 1: Complete Hardware Installation

As seen in Figure 2, a motion sensor and camera are attached to the Raspberry Pi. The Raspberry Pi's Python software must be launched in order to begin the camera's live feed of the residence, its contents, and its occupants. Any intruders will be caught by the property's motion sensor as they approach. Within 10 seconds, the camera module will start capturing the events. A Python script will send the 10 second video recording and transmit it to the user's email and Telegram. The camera module can carry on live streaming even after motion is no longer recognized detection based on the same script.

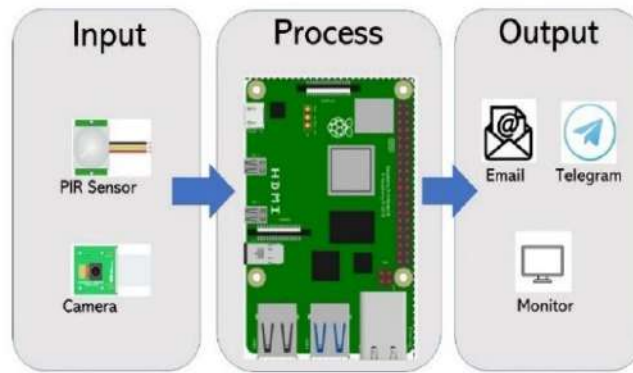


Figure 2: System Flow

In this investigation, a 32 GB storage memory is employed. Raspbian OS, the operating system for the Raspberry Pi, is installed using an SD card (Dow, 2018). The operating system affects how the camera module and motion sensor are set up, as well as how Telegram and email are integrated. All live recordings and ten seconds of video recordings will also be stored on the micro-SD card for forensic use.

In this study, application programming interface (API) is used. As an IoT standard, MQTT messaging protocol is used [12]. It serves as an exceptionally lightweight publish/subscribe message transport and is designed to connect faraway devices with little code footprint and little network bandwidth [9]. MQTT is used by many different industries, such as the automobile, manufacturing, telecommunications, oil and gas, etc. The MQTT API is most suited for this study due to a select few features. It is quick and effective, scales to many IoT devices, supports unstable networks regardless of speed, allows bi-directional communication, and last but not least, is security enabled.

There are three main types of client authentication methods accessible for any MQTT broker to verify the identity of MQTT clients, which is important for the security and optimization of the MQTT API protocol. Client ID, username and password, and client certificate are the available ways. Client ID, username, and password are the approaches that are used in this study.

The client id for sending Telegram notifications is hard coded in the script, whereas the username and password for sending email notifications are written and programmed by the researcher. The MQTT broker verifies the authentication credentials that a client sends it along with the CONNECT packet before accepting the MQTT session. In the CONNECT packet, which uses port 8883 for connection, the credentials are provided to the broker in clear text first and they are being encrypted at the transport layer with port 8883 mentioned above.

The surveillance system's API structural diagram is shown in Fig. 3. The user must first enable the connection by allowing the client's Telegram ID and email credentials to be hard coded in the Python code that runs on the IoT devices. The API will then start the MQTT

Service, execute the script code, and finish the IoT system.

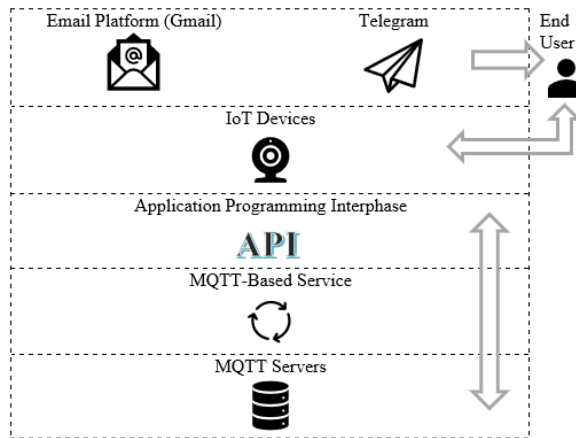


Figure 3: API Structural Diagram

Algorithms called Dynamic Programming Algorithms (DPA) are used. The Dynamic Programming Algorithm is made up of Python, PHP, and JavaScript. Primarily written in Python, the script combines Telegram and Email notifications with the required hardware, such as a motion sensor and camera module. Regardless of the communication medium used, the Python code may be trusted for hardware and software integration [6].

Additional software needs used in the development of the suggested system include Thonny IDE and Raspbian OS. The code was written using Visual Studio Code and Thonny. For the Python programming language, an Integrated Development Environment (IDE) called Thonny was developed for free. It has the ability to perform step-by-step analysis and has an integrated debugger that can be used to run in order to fix faults.

The notification alert is sent via the Email API as well as the Telegram API. An open-source, cloud-based, cross-platform instant messaging service is called Telegram. File sharing, VoIP, and a number of other capabilities are also available. In this project, a ten-second video attachment will be transmitted over Telegram as an immediate warning if a motion sensor detects any intruder movement. Email can be used to communicate with others, exchange messages, or alert a system. Google Mail, also known as Gmail, is used for this project.

Setup of the Raspberry Pi, the camera module V2 and motion sensor, Telegram, and email will be broken down into five critical steps. For live streaming and video capture, the Raspberry Pi 4's camera port was connected to the camera module V2. Ten seconds of video recording were set up using Python code. H.264 video recording is the industry standard, thus that is how the video will be saved by default. The Python code will convert it to MP4 because the majority of devices do not support this video format.

The system starts out with the capability to feed live video of the structure or property, and the motion is immediately activated. If the motion sensor notices motion, the live streaming

feature will stop and record the intruder for 10 seconds. Even if the sensor doesn't detect any motion, the video recording features will continue to function. The flowchart for video notifications is based on Figure 4.

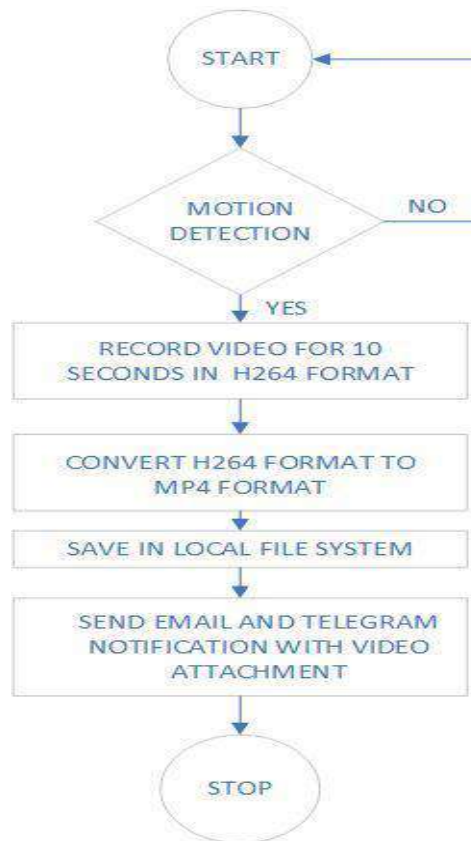


Figure 4: Flowchart of The Video Notification

Users can access the surveillance system using any device, including smartphones, tablets, laptops, and computers, thanks to Python coding. Not all users are allowed to sign into the web application, which increases security and assurance. Only the owner of the monitoring system is authorized to sign into the dashboard. The live streaming video flow chart is based on Figure 5.

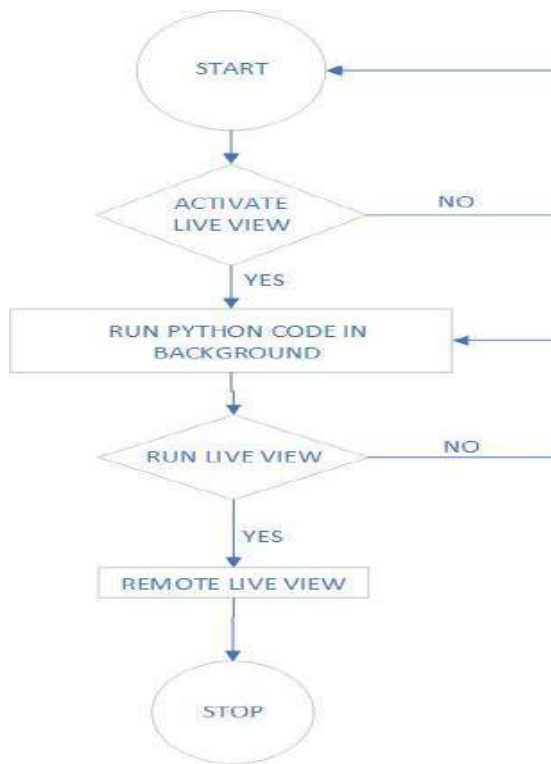


Figure. 5: Flowchart of The Video Notification

4. RESULT AND ANALYSIS

The camera module can first automatically save the file after ten seconds of video recording. The Camera Module's saved videos are displayed in Figure. 6. When a crime occurs, the videos are essential as a backup for forensic investigation. The films will be available to the authorities via local files as well as email and Telegram. By introducing a command in the Python code, these files were taken. "raspistill o nameOfFile.jpg" and "raspivid -o nameOfFile.h24" are the commands used [3]. These files will be stored in the memory automatically.

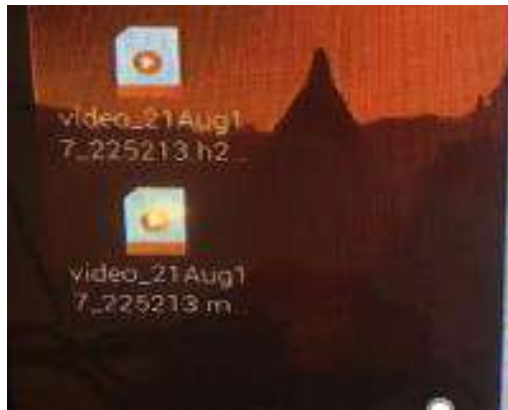


Figure 6: Saved Video

The Motion Sensor will then immediately send an email notification when it senses movement. Figure 7 displays the Telegram notification when a Raspberry Pi attached motion sensor detects movement. The Python code had previously been established to specify the sender and recipient of the message with video recording.

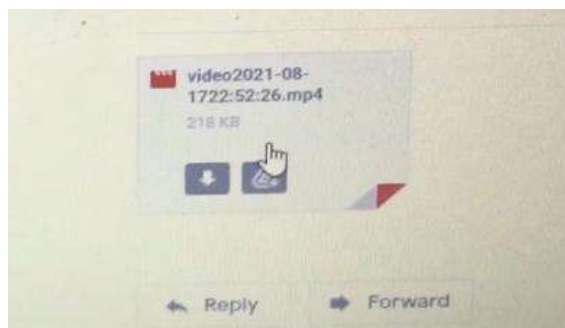


Figure 7: Saved Image and Video

Next, an immediate Telegram notice will be sent when the Motion Sensor detects movement. When a motion sensor coupled to a Raspberry Pi detects movement, Figure 8 displays the Telegram notification. With the help of the Telegram bot's user token, the recipient of the notification has already been set. The Python code's setting of the token.

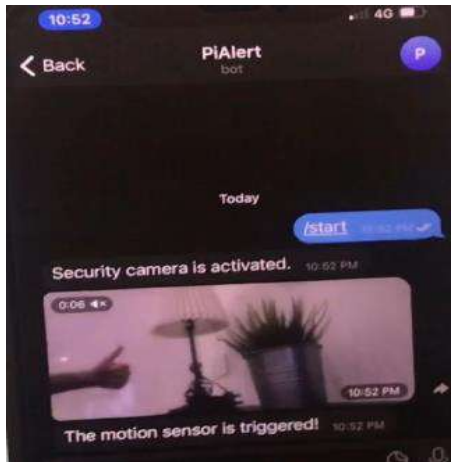


Figure 8: Saved Image and Video

The reliability and capability of the sensor were examined next. The motion sensor's responses to movement and light conditions are displayed in Table 1 and Table 2 below. The sensor is unable to detect subject movement at distances greater than 3 meters, based on the test that has been conducted within a range of 1 to 5 meters. Movement of the test subject can be detected in both light and dark environments in the presence of light. In conclusion, the motion sensor detection range and light condition restriction on subject movement is 1-3 meters apart. The flames can only be located within 1-2 meters, though.

Table 1: Sensors respond to Movement

Testing subject	Distance (Meter)				
	1.0	2.0	3.0	4.0	5.0
Human	✓	✓	✓	✗	✗
Cat	✓	✓	✓	✗	✗
Ball	✓	✓	✓	✗	✗
Fire	✓	✓	✗	✗	✗

Table 2: Sensors respond to Light Condition

Testing subject	Light Condition	
	Light	Dark
Human	✓	✓
Cat	✓	✓
Ball	✓	✓
Fire	✓	✓

Conclusions can be derived from the test results in Table 3. Specifically, the delay between sending and receiving a message alert is 2 seconds for repetitions 1-3 and 3 seconds for repetitions 4 and 5. Different video file sizes and the state of the internet network connection can have an impact on this disparity. The Raspberry Pi's sensor and camera continue to function even without internet access, but the video is preserved instead of being sent straight to message as an alarm. When the internet is back up and running, it will be transmitted.

Table 3: Testing Result of Notification

Testing	Time (hour: minute: second)		
	Sending	Received	Delay
1	10:18:20	10:18:22	2 second
2	10:18:30	10:18:32	2 second
3	10:19:12	10:19:14	2 second
4	10:19:40	10:19:42	3 second
5	10:20:02	10:20:04	3 second

5. DISCUSSION AND CONCLUSION

The Raspberry Pi starts a completely new era in terms of modern technologies. not just for its size, but also for what it is capable of. It can be used for nearly anything because of its portability [8]. The surveillance system project serves as an example of this. With the advancement over the prior research, this study has succeeded in achieving its four goals, which were described in detail in the introduction.

The goals were to monitor people, property, and belongings, to send instant email notifications with video attachments when nearby surveillance systems detect motion, to send instant Telegram notifications when motion is detected, and to build a microprocessor-based surveillance system that is cost-effective. When the system detects motion, the research has improved to deliver an instant Telegram and email message with a 10-second video file.

With this enhancement, the efficiency, adaptability, security, and quick response whenever a threat is detected by the monitoring system have all been maximized. The system's drawback is that it can be challenging for non-technical people to set up without a clear written manual, and it significantly relies on internet connectivity to send the warning, making it challenging for people who live in rural areas with limited internet access.

More GPIO pins in the Raspberry Pi can be utilized to this surveillance system to maximized its functionality and research applications. More features and applications can make daily tasks and activities easier for users. To sum up, this project can be expanded to completely employ the suggested system with cutting-edge technology like an AI recognition feature or other detection, making it a full security system.

REFERENCES

- [1] S. Ahmad et al., "Application of Raspberry Pi and PIR Sensor for Monitoring of Smart Surveillance System," *International Journal of Science and Research (IJSR)*, vol. 5, no. 2, pp. 736–737, Feb. 2016, doi: 10.21275/v5i2.nov161248.
- [2] P. V. Luu, J. Weed, S. Rodriguez, and S. Akhtar, "An AI-based web surveillance system using raspberry Pi," *Journal of Advances in Technology and Engineering Research*, vol. 5, no. 6, Dec. 2019, doi: 10.20474/jater-5.6.2.
- [3] D. Amos, D. Bader, J. Jablonski, and F. Heisler, *Python basics : a practical Introduction to Python 3*. Middletown, De: Real Python, 2021.
- [4] Y. V. Narkhed and S. G. Khadke, "Application of Raspberry Pi and PIR Sensor for Monitoring of Smart Surveillance System," *International Journal of Science and Research (IJSR)*, vol. 5, no. 2, pp. 736–737, Feb. 2016, doi: 10.21275/v5i2.nov161248.
- [5] C. Dow, *Internet of things programming projects : build modern IoT solutions with the Raspberry Pi 3 and Python*. Birmingham: Packt Pub, 2018.
- [6] N. Fatima, "IoT based Interactive Home Automation with SMS and Email Alert System," *International Journal for Research in Applied Science and Engineering Technology*, vol. 7, no. 10, pp. 569–574, Oct. 2019, doi: 10.22214/ijraset.2019.10085.
- [7] T. Gualotuña, E. Macías, Á. Suárez, E. C., and A. Rivadeneira, "Low Cost Efficient Delivering Video Surveillance Service to Moving Guard for Smart Home," *Sensors*, vol. 18, no. 3, p. 745, Mar. 2018, doi: 10.3390/s18030745.
- [8] Gareth Halfacree and E. Upton, *Raspberry Pi User Guide*. John Wiley & Sons, 2012.
- [9] R. Ramlee, E. L. C. Yong, S. K. Subramaniam, AsemKhmag, and A. S. Rahman, "Home Switching using IoT System via Telegram and Web User Interface," *International Journal of Recent Technology and Engineering*, vol. 8, no. 2S6, pp. 814–819, Sep. 2019, doi: 10.35940/ijrte.b1151.0782s619.
- [10] D. S. D. M. U. Mahidin, "Department of Statistics Malaysia Official Portal," www.dosm.gov.my, 2020. https://www.dosm.gov.my/v1_/
- [11] S. Mcmanus and M. Cook, *Raspberry Pi for dummies*. Hoboken, Nj: For Dummies, 2021.
- [12] MQTT, "MQTT - The Standard for IoT Messaging," mqtt.org, Jun. 13, 2022. <https://mqtt.org/>
- [13] S. Noorjannah Ibrahim, A. H. Hasan Basri, and A. Liza Asnawi, "Development of web-based surveillance system for Internet of Things (IoT) application," *Bulletin of Electrical Engineering and Informatics*, vol. 8, no. 3, pp. 1108–1116, Sep. 2019, doi: 10.11591/eei.v8i3.1520.
- [14] R. P. A., "IOT Based Surveillance System for CCTV," *International Journal for Research in Applied Science and Engineering Technology*, vol. 6, no. 3, pp. 959–963, Mar. 2018, doi: 10.22214/ijraset.2018.3153.
- [15] G. K. Pathak, "A Review of IOT based SMS & Email Enabled Smart Home Automation System," *International Journal for Research in Applied Science and Engineering Technology*, vol. V, no. XI, pp. 2872–2875, Nov. 2017, doi: 10.22214/ijraset.2017.11395.
- [16] N. Patil, S. Ambatkar, and S. Kakde, "IoT based smart surveillance security system using raspberry Pi," *2017 International Conference on Communication and Signal Processing (ICCSP)*, vol. 02, no. IV, pp. 0344–0348, Apr. 2017, doi: 10.1109/iccsp.2017.8286374.
- [17] R. Rani and S. Indora, "A Review IoT Based Camera Surveillance System," *International Journal of Computer Sciences and Engineering*, vol. 7, no. 6, pp. 793–800, Jun. 2019, doi: 10.26438/ijcse/v7i6.793800.

- [18] M. Z. Sasongko and S. Sucipto, "Desain Prototype IoT Menggunakan Bot Telegram Berbasis Text Recognition," *RESEARCH : Journal of Computer, Information System & Technology Management*, vol. 4, no. 1, p. 21, Apr. 2021, doi: 10.25273/research.v4i1.7420.
- [19] H. K. Sharma and M. Sharma, "Iot Based Home Security System with Wireless Sensors and Telegram Messenger," *SSRN Electronic Journal*, vol. 1, no. 1, pp. 584–588, 2019, doi: 10.2139/ssrn.3341106.
- [20] N. Widiyasono, A. Rahmatulloh, and H. Firmansah, "Automatic Email Alert on the Internet of Things-based Smart Motion Detection System," *Selected Papers from the 1st International Conference on Islam, Science and Technology, ICONISTECH-1 2019, 11-12 July 2019, Bandung, Indonesia*, vol. 1, no. 1, 2020, doi: 10.4108/eai.11-7-2019.2297829.

EMISSION CHARACTERISTICS AND FUEL CONSUMPTION OF SI ENGINE BY USING RON95, RON97 WITH DIFFERENT TYPES OF SPARK PLUG

Noorradiah Ismail , Masud Mohammed , Ida Rasyada Daud , Norhaslina Aziz , Ir Malek Idrus & Fahmi Isa⁶

Infrastructure University Kuala Lumpur

1. INTRODUCTION

Emissions have been shown to have a variety of negative effects on public health and the natural environment. Followed by the United State of America as a full model in 1968, conjointly in 1966, the primary emission check cycle was enacted within the State of CA to measure piping emissions in PPM (parts per million). The standards were increasingly tightened year by year, as mandated by the independent agency.

Hydrocarbons (HC) – A class of burned or partially burned fuel, hydrocarbons are toxins. Hydrocarbons are a major contributor to smog, which can be a major problem in urban areas. Prolonged exposure to hydrocarbons contributes to asthma, liver disease, lung disease, and cancer. Regulations governing hydrocarbons vary according to type of engine and jurisdiction; in some cases, “non-methane hydrocarbons” are regulated, while in other cases, “total hydrocarbons” are regulated.

High fuel consumption – Consequently, highway fuel consumption increases by approximately 1.3%. The average wind speed is also higher in the winter, which increases aerodynamic resistance and fuel consumption. U.S. EPA data show that fuel consumption can increase 7 to 35% because of poor road conditions. Carbon monoxide (CO) – A product of incomplete combustion, inhaled carbon monoxide reduces the blood’s ability to carry oxygen; overexposure (carbon monoxide poisoning) may be fatal.

2. LITERATURE REVIEW

Researcher Mohamad TI and How, (2014) conducted on a 1.6-L, four-cylinder Mitsubishi 4G92 engine with CR 11:1, the engine was run at a constant speed of between 1500 and 3500 rpm with an increment of 500 rpm under various part load conditions. RON95 produced a higher engine performance for all part load conditions within the speed range. An average 4.4% increase in brake torque, brake power and brake mean effective pressure was achieved compared to RON97. In terms of exhaust emissions, RON95 produced 7.7% lower Nox emissions, but higher CO₂ (7.9%), CO (36.9%) and HC (20.3%) emissions. However, RON97 was found to be advantageous with a lower BSFC of 2.3% for all load conditions.

On the exhaust emissions aspects, the formation of emissions from internal combustion engines mainly consist of Carbon Dioxide (CO₂), Carbon Monoxide (CO), Hydrocarbon (HC) and Nitrogen Oxides (NO_x). In fact, the CO and HC are the main pollutants by the internal combustion (IC) engine due to the incomplete combustion of hydrocarbon fuels during the combustion process. The level of emissions mainly depend on the octane number of gasoline and engine operating conditions such as ignition timing, load, speed and the air-fuel ratio.

Recently, another experimental study on a compression ratio (11:1) engine with RON 95, RON 97 and RON 102 has been studied by Rashid, Adnan, Mansor, Radzi, Wan Ghopa, Zambri, and Wan Mohd (2016). The engine was operated at a constant throttle position of 18% and with constant speed between 1000 rpm to 3500 rpm with 500 rpm increment. The results with RON 102 gasoline showed that the average torque of the engine increased by 13% and 6% compared to the RON 95 and RON 97, respectively. The highest output brake power produced by using RON 102 gasoline, followed by RON 97 and RON 95. The brake thermal efficiency for RON 97 and RON 102 gasoline improved at an average of 12% compared to RON 95 gasoline. RON 102 fuel produced the highest CO emission compared to RON 97 and RON 95 fuel at an average of 12.4% and 17% respectively. For the emission of NO_x, RON 102 fuel reduced an average of 34% and 40% compared to the RON 95 and RON 97 fuel respectively.

In this chapter, the experimental study was performed using three (3) fuel samples which included baseline gasoline RON 95, RON 97 and RON 100. As tabulated in Table 2 is the primary physicochemical properties of the fuels. The density analysis for all fuels were performed in an accredited laboratory and were tested according to the ASTM procedure D1217.

Level was measured with a SHATOX SX-200 portable octane meter. The result of octane level was tested according to ASTM D2699-86 method and it can be seen that the RON 100 fuel has a greater octane level than RON 97 and RON 95 fuels. In addition, the heating value for all fuels was cited by Ghanaati, Ali, Mohd Farid and Intan Z, (2017). Clearly, the heating value for RON 100 fuel was greater than that of RON 97 and followed by RON 95 fuel.

3. METHODOLOGY

The purpose of the experiment is to analyze the emission characteristics and fuel consumption by using different types of RON fuel grades and different types of spark plug devices. An Engine 4G13 will be used to carry out the whole experiment.. Bosch emission analyzer was used to analyze emission characteristics upon using RON 95 and RON 97 to measure the value of fuel consumption.



Figure 1: Proton Iswara 4G13 Engine System

In order to measure the level of fuel consumption in 180 seconds, the device stopwatch has been used to calculate time duration of engine run and measurement container to measure the volume of fuel consumed during the experiment. The connecting hose supply connected with the return pipe of the original fuel tank was removed and attached to the measurement container which serves as a custom fuel tank to fill up the petrol. The fuel level was left in the container after the experiment was recorded to calculate the fuel consumption level.

In order to check the composition of emission released by the exhaust gas, Bosch emission analyzer was used to measure as shown in Figure 2. The Emission analyzer provides the precise amount for each type of gas such as HC, CO, CO₂ , and O₂, besides that oil temperature has also been measured using the emission analyzer. The Emission analyzer contains two sensors to obtain information about the condition of engine and exhaust gas, which is the gas valve sensor and oil temperature sensor. The equipment was set the gas valve sensor at the very end of exhaust pipe and the oil temperature sensor inserted into the engine block through engine oil dipstick passageway.



Figure 2: Bosch Emission Analyzer

An approach that has been used to give the pressure in the engine increases, it required compromise the condition of the spark plugs, the fuel consumption and the composition of the

exhaust gas. To carry out the experiment, the selection of the engine speed parameter is determined by revolution per minute (RPM) which is a measurement of the frequency of rotation, specifically the number of rotations around a piston in one minute. The objective of the experiment being carried out to measure and identify the difference in emission release and fuel consumption when different types of spark plug are used. In order to get precise and solid results, the test was conducted 6 times for all the materials changed. The results obtained were categorized based on the three types of spark plug. The materials that are changed are shown in Table 1.

Table 1: Classification of procedure

Engine Used	4g13P SOHC 1.3 L
Types of spark plugs perform	Iridium, platinum, copper
Type of fuel use	RON95 & RON97
Parameter Setting	1500 rpm , 2000 rpm (moderate) , 3000 rpm (fast)
Data Output measurement	Level of emission gasses percentage when different spark plugs & fuel are used.



Figure 3: Fuel Measurement Collection



Figure 4: Exhaust Gas Analyzer Installed at the exhaust pipe.



Figure 5: Output Exhaust Gas Emission

4. RESULTS AND DISCUSSION

Data collection for the experiment was recorded in the form of table design to compare the differences of each type of spark plug which is located at Table 2 and Table 3. The collected data was used to make a comparison of the difference between each type of spark plug tested in this experiment. Data collected used to compare the fuel consumption composition of exhaust gas using RON 95 and RON 97.

Table 2 to Table 7 below shows all the fuel consumption readings which are continuously taken for a duration of 3 minutes based on three different types of spark plugs and different revolutions per minute (rpm). The table will show fuel consumption during 1500 rpm, 2000rpm & 3000rpm based on different fuel types.

Table 2: Fuel Consumption Measurement for Iridium Spark plug using Ron 95

No.	Time (minute)	Fuel consumption , grams (g)		
		1500 RPM	2000 RPM	3000 RPM
1.	3	47	145	368

Table 3: Fuel Consumption Measurement for Iridium Spark plug using Ron 97

No.	Time (minute)	Fuel consumption , grams (g)		
		1500 RPM	2000 RPM	3000 RPM
1.	3	51	139	368

Table 4: Fuel Consumption Measurement for Platinum Spark plug using Ron 95

No.	Time (minute)	Fuel consumption , grams (g)		
		1500 RPM	2000 RPM	3000 RPM
1.	3	47	192	408

Table 5: Fuel Consumption Measurement for Platinum Spark plug using Ron 97

No.	Time (minute)	Fuel consumption , grams (g)		
		1500 RPM	2000 RPM	3000 RPM
1.	3	51	145	408

Table 6: Fuel Consumption Measurement for Copper Spark plug using Ron 95

No.	Time (minute)	Fuel consumption , grams (g)		
		1500 RPM	2000 RPM	3000 RPM
1.	3	47	139	450

Table 7: Fuel Consumption Measurement for Iridium Spark plug using Ron 97

No.	Time (minute)	Fuel consumption , grams (g)		
		1500 RPM	2000 RPM	3000 RPM
1.	3	51	145	450

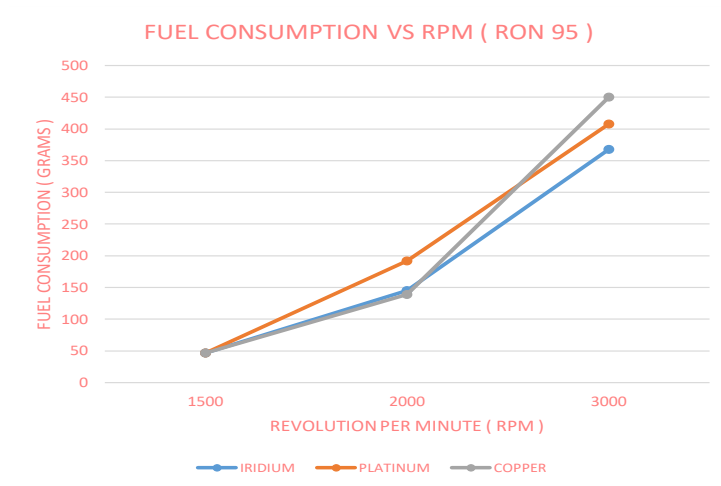


Figure 6: Fuel Consumption VS rpm using three different plugs and Ron 95

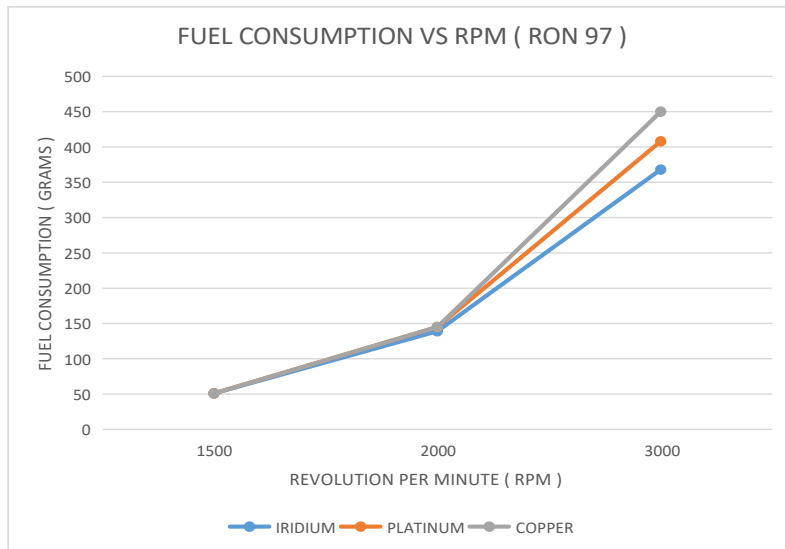


Figure 7: Fuel Consumption vs RPM using 3 different plugs and Ron 97

Experiment Results for Composition of Exhaust Gas

Table 8 to Table 9 below shows the obtained reading of Hydrocarbon (HC) and Carbon Monoxide (CO) based on three types of spark plugs used while the engine is running under various designated revolutions per minute (RPM). These tables will be able to show the amount of hydrocarbon (HC) and carbon monoxide (CO) during a designated speed of 1500 rpm, 2000 rpm and 3000 rpm. The average value for each reading is also shown.

Table 8: Hydrocarbon and Carbon Monoxide Measurement using Iridium plugs and Ron 95

No of times recorded	1500 RPM		2000 RPM		3000 RPM	
	CO (%)	HC (PPM)	CO (%)	HC (PPM)	CO (%)	HC (PPM)
1.	3.491	233	1.761	155	0.333	75
2.	3.757	234	2.145	156	0.390	75
3.	3.373	244	1.362	157	0.338	77
Average	3.450	237	1.756	156	0.354	76

Table 9: Hydrocarbon and carbon monoxide measurement using Iridium plugs and Ron 97

No of times recorded	1500 RPM		2000 RPM		3000 RPM	
	CO (%)	HC (PPM)	CO (%)	HC (PPM)	CO (%)	HC (PPM)

)))
1.	4.516	227	1.462	143	0.332	73
2.	3.532	232	1.700	156	0.332	73
3.	3.612	233	1.766	156	0.332	74
Average	3.88	230.7	1.643	151.7	0.332	73.3

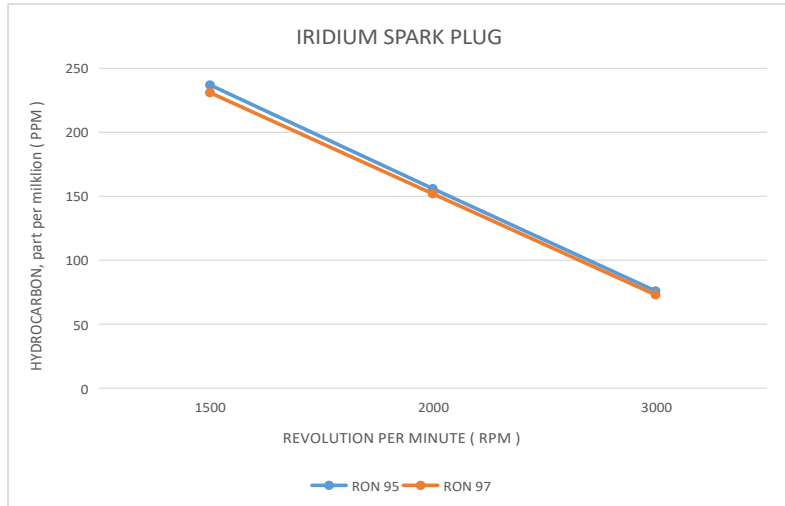


Figure 8: Hydrocarbon Emission at different level of speed using Iridium spark Plug

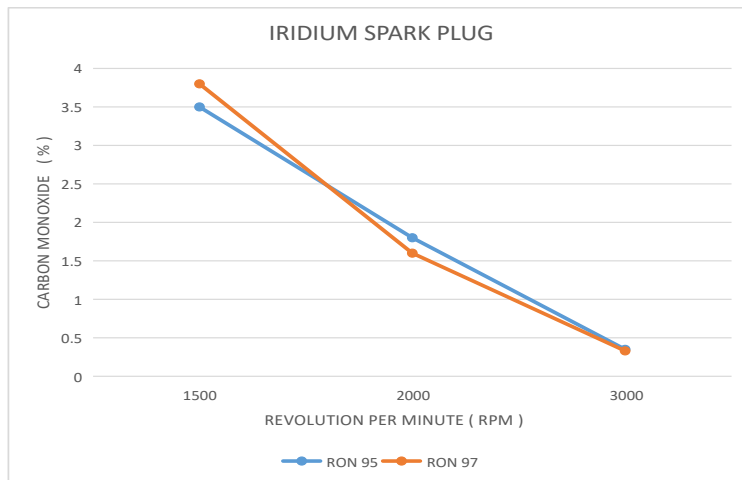


Figure 9: Carbon monoxide emission level at different engine speed using different fuel

Table 10: Hydrocarbon and carbon monoxide measurement using Platinum plugs and Ron 95

No of times recorded	1500 RPM		2000 RPM		3000 RPM	
	CO (%)	HC (PPM)	CO (%)	HC (PPM)	CO (%)	HC (PPM)
1.	3.152	245	2.072	175	0.485	98
2.	3.954	255	2.072	175	0.504	101

3.	4.045	256	2.298	175	0.537	106
Average	3.717	252	2.15	175	0.509	102

Table 11: Hydrocarbon and carbon monoxide measurement using Platinum plugs and Ron 97

No of times recorded	1500 RPM		2000 RPM		3000 RPM	
	CO (%)	HC (PPM)	CO (%)	HC (PPM)	CO (%)	HC (PPM)
1.	4.330	257	2.113	183	0.478	81
2.	4.217	266	2.112	184	0.381	90
3.	4.337	268	2.118	184	0.466	90
Average	4.30	263	2.114	184	0.442	87.6

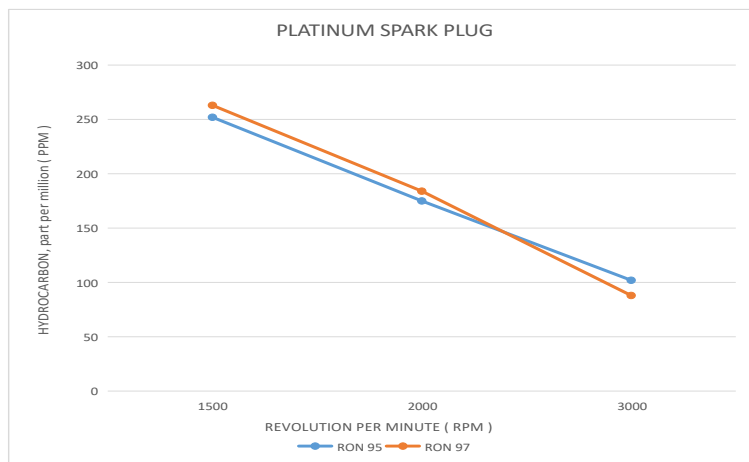


Figure 10: Hydrocarbon Emission at Different levels of Engine speed using Platinum spark plug.

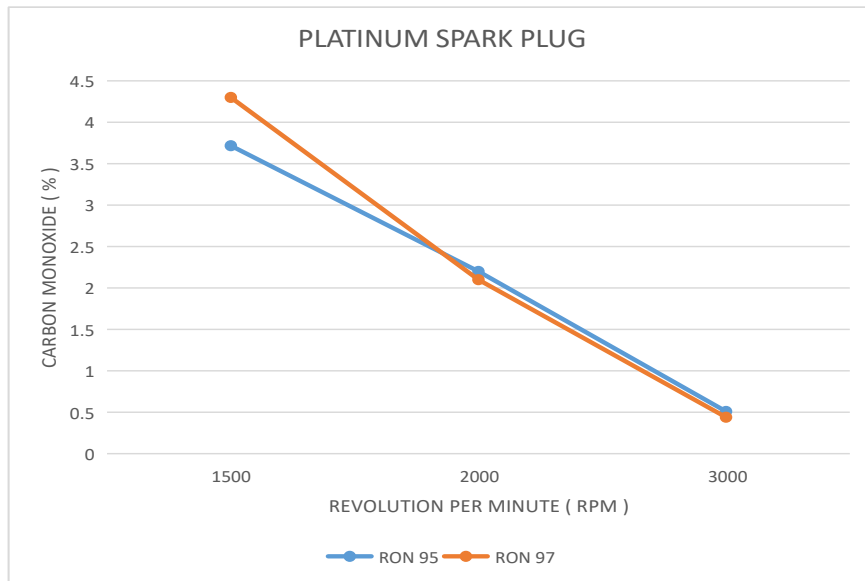


Figure 11: Carbon monoxide emission level at different speed using different fuel

Table 12: Hydrocarbon and Carbon monoxide measurement using Copper plugs and Ron 95

No of times recorded	1500 RPM		2000 RPM		3000 RPM	
	CO (%)	HC (PPM)	CO (%)	HC (PPM)	CO (%)	HC (PPM)
1.	3.200	219	1.693	190	0.375	131
2.	3.489	284	2.324	191	0.412	137
3.	3.143	217	2.684	194	0.449	151
Average	3.28	240	2.23	192	0.412	140

Table 13: Hydrocarbon and carbon monoxide measurements using Copper plugs and Ron 97

No of times recorded	1500 RPM		2000 RPM		3000 RPM	
	CO (%)	HC (PPM)	CO (%)	HC (PPM)	CO (%)	HC (PPM)
1.	3.137	217	2.013	182	0.405	109
2.	3.143	217	2.114	183	0.591	115
3.	3.203	217	2.256	189	0.353	116
Average	3.161	217	2.13	185	0.45	113

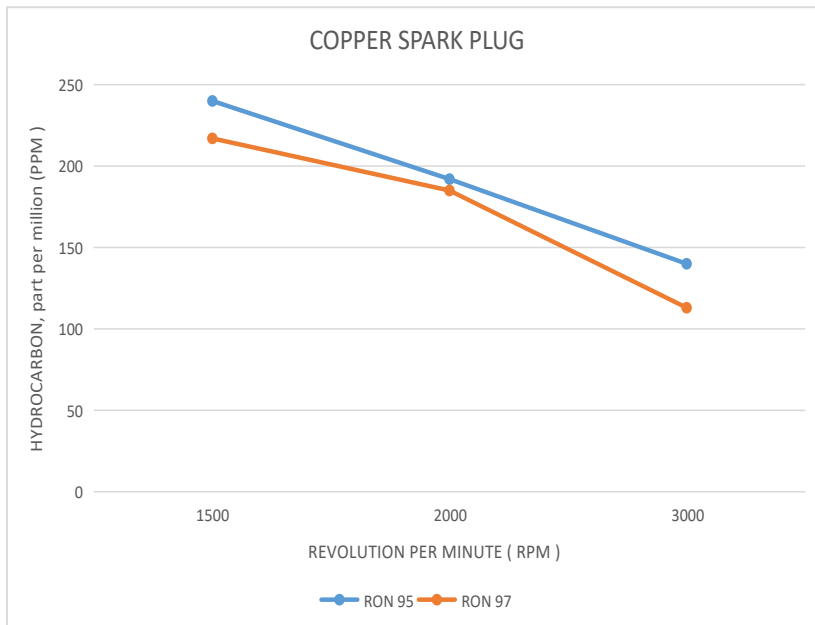


Figure 12: Hydrocarbon Emission at different levels of Engine speed using Copper spark plug.

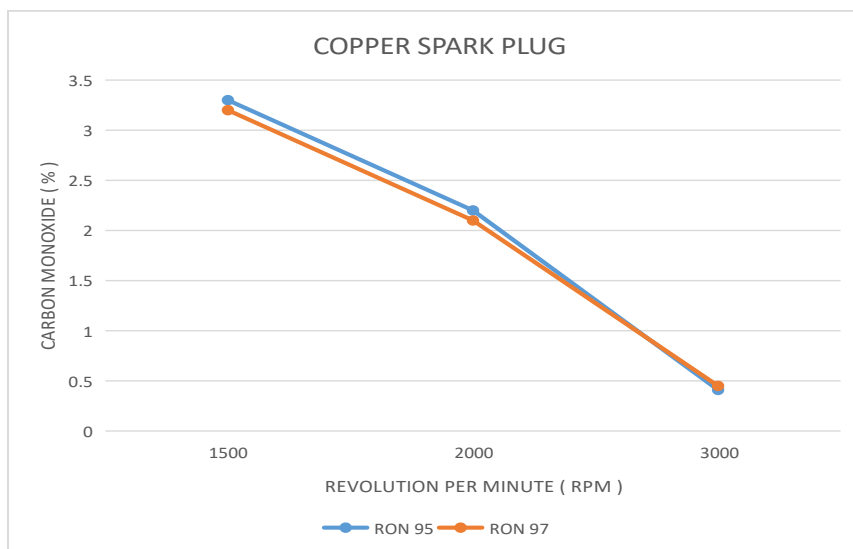


Figure 13: Carbon Monoxide emission level at different speeds using different fuel.

Overall Comparison between Three types of Spark Plug

Table 14 and Table 15 shows the percentage of harmful releases between different types of spark plug such as Iridium spark plug compared to Platinum and Copper Spark Plug using RON 95 and RON 97 as a fuel source. In this table, comparison between Spark plugs will be made in the term of level of harmful gasses such as CO & HC.

Table 14: Comparison Between Iridium Spark Plug, Platinum Spark Plug and Copper Spark Plug using RON 95

Engine speed (RPM)	Iridium Spark Plug			Platinum Spark Plug			Copper Spark Plug		
	FC (g)	HC (ppm)	CO (%)	FC (g)	HC (ppm)	CO (%)	FC (g)	HC (ppm)	CO (%)
1500 rpm	47 (0%)	237 (↓6.3%)	3.540 (↓5%)	47 (0%)	252 (↑5%)	3.717 (↑13.3%)	47 (0%)	240 (↑1.3%)	3.28 (↓7.9%)
2000 rpm	145 (↓32.4%)	156 (↓12.2%)	1.756 (↓22.4%)	192 (↑38.1%)	175 (↓9.7%)	2.15 (↓3.7%)	139 (↓4.3%)	192 (↑23%)	2.23 (↑27%)
3000 rpm	368 (↓10.9%)	76 (↓34.2%)	0.354 (↓43.7%)	408 (↓10.3%)	102 (↓37.3%)	0.509 (↑23.5%)	450 (↑22.3%)	140 (↑84.2%)	0.412 (↑16.4%)

 % Comparison Between Iridium & Platinum
 % Comparison Between Platinum & Copper
 % Comparison Between Copper & Iridium

Table 15: Comparison between Iridium Spark Plug, Platinum Spark Plug and Copper Spark Plug using Ron 97

Engine speed (RPM)	Iridium Spark Plug			Platinum Spark Plug			Copper Spark Plug		
	FC (g)	HC (ppm)	CO (%)	FC (g)	HC (ppm)	CO (%)	FC (g)	HC (ppm)	CO (%)
1500 rpm	51 (↑8.5%) (0%)	230.7 (↓2.7%) (↓14%)	3.88 (↑9.6%) (↓10.8%)	51 (↑8.5%) (0%)	263 (↑4.4%) (↑21.2%)	4.30 (↓15.7%) (↑36%)	51 (↑8.5%) (0%)	217 (↓10.6%) (↓6.3%)	3.161 (↓3.8%) (↓22.7%)
2000 rpm	139 (↓4.3%) (↓38.1%)	151.7 (↓2.8%) (↓21.3%)	1.643 (↓6.9%) (↓28.7%)	192 (0%) (↑32.4%)	184 (↑5.1%) (↓0.1%)	2.114 (↓1.7%) (↓0.01%)	145 (↑4.3%) (↑4.3%)	185 (↓3.8%) (↑22%)	2.13 (↓4.7%) (↑29.6%)
3000 rpm	368 (0%) (↓10.9%)	73.3 (↓3.7%) (↓19.5%)	0.332 (↓6.6%) (↓33.1%)	408 (0%) (↓10.3%)	87.6 (↓16.4%) (↓29%)	0.442 (↓15.2%) (↓1.9%)	450 (0%) (↑22.3%)	113 (↓23.9%) (↑54.2%)	0.45 (↑9.2%) (↑35.5%)

 % Comparison Between Ron 97 & Ron 95
 % Comparison Between Iridium & Platinum
 % Comparison Between Platinum & Copper
 % Comparison Between Copper & Iridium

The comparison between the subjects tested which are the emission release using Iridium, Platinum and Copper spark plugs was obtained as shown in figure 6 and figure 7. Although it's been proved in the form of percentage comparison between all 3 different types of

spark plug and also the comparison between Ron 95 and Ron 97 shown in Figure and Figure 8. Figure 9 shows the fuel consumption level of all three types of spark when the engine is ran for 3 minutes using Ron 95 appears to be the same but when the engine speed is increased to 2000 rpm, the amount of fuel consumption begins to change meanwhile platinum spark plug consumed 24.5% higher compared to Iridium spark plug and 27.6% higher compared to copper spark plug. Based on the data the fuel consumption of copper and iridium is compared, the copper consumed 4.13% lower than Iridium plugs. When the engine speed is raised to 3000 rpm, the fuel consumption level of platinum spark plug is 9.8% higher than iridium spark plug but it consumes 9.33% lower than copper spark plug. Therefore the iridium and the copper are tested, it is proven that the copper consumed 18.2% higher than iridium.

The hydrocarbon content when the engine speed at 1500 rpm using Ron 95 meanwhile using iridium spark plug is 5.9% lower when it is compared to platinum spark plug meanwhile platinum is 4.76% higher than copper spark plug. at an engine speed of 2000 rpm, the iridium spark plug proves for a 10.8% lower hydrocarbon emission compared to platinum spark plug while the latter proves approximately 8.85% lower hydrocarbon content compared to copper spark plug. at 3000 rpm, the hydrocarbon content of the iridium spark plug is 25.5% lower than the platinum spark plug. while platinum is 27.1% lower than copper and to confirm my prediction, the copper spark plug shows a percentage of 45.7% higher than iridium.

Carbon monoxide content, it came out with a result of a 4.76% decrease when iridium is compared to platinum spark plugs. When platinum plug is tested with copper spark plug, an increment of 11.8% is obtained meanwhile copper spark plug is 7.3% lower than iridium spark plug. When the engine speed is increased to 2000 rpm, the iridium plug carbon monoxide content is 18.3% lower than platinum spark plug while platinum also shows a drop of 3.58% when compared to copper spark plug. As of prediction, the copper spark plug is higher by 21.2% than the iridium spark plug when it is compared in terms of carbon monoxide content. When the engine speed is raised another 1000 rpm, the co content of the iridium spark plug is 30.4% compared to platinum plugs while platinum is 19.1% lower than the copper spark plug. However, copper spark plug shows a 14.1% rise when it is compared to iridium plugs.

Fuel consumption level of all three types of spark when the engine is run for 3 minutes using ron 97 appears to be the same but when the engine speed is increased to 2000 rpm, the amount of fuel consumption begins to change. platinum spark plug consumed 27.6% higher compared to iridium spark plug and 24.4% higher compared to copper spark plug. when the fuel consumption of copper and iridium is compared, the copper consumed 4.13% higher than iridium plugs. When the engine speed is raised to 3000 rpm, the fuel consumption level of the platinum spark plug is 9.8% higher than the iridium spark plug but it consumes 9.33% lower than the copper spark plug. When iridium and copper are tested, it is proven that the copper consumed 18.2% higher than iridium.

The hydrocarbon content when the engine is run at 1500 rpm using ron 97 meanwhile using iridium spark plug is 12.3% lower when it is compared to platinum spark plug meanwhile platinum is 17.5% higher than copper spark plug. at an engine speed of 2000 rpm, the iridium spark plug proves for a 17.6% lower hydrocarbon emission compared to platinum spark plug

while the latter proves a 0.5% lower hydrocarbon content compared to copper spark plug. at 3000 rpm, the hydrocarbon content of the iridium spark plug is 16.3% lower than the platinum spark plug. while platinum is 22.5% lower than copper and to confirm my prediction, the copper spark plug shows a percentage of 35% higher than iridium.

Carbon monoxide content, it came out with a result of a 9.76% decrease when iridium is compared to platinum spark plugs. When platinum plug is tested with copper spark plug, an increment of 26.5% is obtained meanwhile copper spark plug is 18.5% lower than iridium spark plug. When the engine speed is increased to 2000 rpm, the iridium plug carbon monoxide content is 22.2% lower than platinum spark plug while platinum also shows a slight drop of 0.5% when compared to copper spark plug. As of prediction, the copper spark plug is higher by 22.8% than the iridium spark plug when it is compared in terms of carbon monoxide content. When the engine speed is raised another 1000 rpm, the co content of the iridium spark plug is 24.8% compared to platinum plugs while platinum is only 1.7% lower than the copper spark plug. However, copper spark plug shows a 26.2% rise when it is compared to iridium plugs.

Comparison between ron 95 & ron 97, the fuel consumption when the engine is at 1500 rpm remains the same but when it is raised to 2000, the iridium (ron 97) shows a decrease of 4.13% compared to iridium (ron 95). The platinum spark plug for both ron 95 & ron 97 are both the same but the copper spark plug shows a 4.13% increment between copper (ron 97 & ron 95). at 3000 rpm, the fuel consumption level of all three spark plugs when used ron 95 and ron 97 are the same.

Based on the part per million of hydrocarbons when iridium spark plug is used with ron 97 shows a drop of 2.65% when compared to its ron 95 cousin. Platinum (ron 97) and copper (ron 97) both show an increment of 4.1% and a drop of 9.5% respectively. At 2000 rpm, the iridium spark plug using ron 97 proves a 2.75% lower compared to iridium ron 95 but the platinum plugs using the ron 97 show a rise of 4.8 % in hydrocarbon content. The copper plug shows a drop of 3.6% when ron 97 is used. At 3000 rpm, the hydrocarbon content of iridium, platinum and copper plugs shows a drop of 3.5 %, 14.1% and 19 % respectively compared to iron 95.

The composition of carbon monoxide when iridium spark plug is used with ron 97 shows a rise of 8.76% when compared to its ron 95 cousin. Platinum (ron 97) and copper (ron 97) both show a drop of 13.5% and a drop of 3.6% respectively. At 2000 rpm, the iridium spark plug using ron 97 proves a 6.4% lower compared to iridium ron 95 and the platinum plugs using the ron 97 also show a drop of 1.6 % in carbon monoxide content. The copper plug shows a drop of 4.48% when ron 97 is used. At 3000 rpm, the carbon monoxide content of iridium and platinum plugs shows a drop of 6.21 % and 13.1% respectively, meanwhile the copper used with ron 97 shows a rise of 8.4% compared to the ron 95.

Based on the result as above there is no major difference between the fuel consumption levels between all subjects tested. A drastic increase is observed which proves that the iridium spark plug is the best used when compared with platinum and copper spark plug. As we all know, hydrocarbon (HC) is the most deadly form of harmful emission release gas. It causes several major problems such as health and it interrupts the ozone deformation process which can

cause severe damage to mankind.

5. CONCLUSION

The aim of this experiment is to determine the effects of different types of spark plug when different types of fuels are used on engine exhaust gas (Emission) release and the fuel consumption level. From the experimental data retrieved, it is proven that the most effective in the terms of fuel efficiency and exhaust gas release (Emission) which is Carbon Monoxide and Hydrocarbon are Iridium spark plugs used with Ron 97 fuel.

Iridium spark plug used with Ron 97 provides a better and cleaner combustion in terms of Carbon Monoxide (CO) and Hydrocarbon (HC) emission and fuel consumption compared to the other two types of Spark plug when RON 95 & RON 97 is used respectively.

Platinum spark plug used with Ron 97 takes the second place and becomes the benchmark in comparison because of the cheaper price and it is sold in most of the stores unlike Iridium spark plug as it is only sold in the high end parts shop. Platinum spark plug achieved better results in the terms of fuel consumption and emission release when it is compared to Copper spark plug.

Results of the Copper spark plug used with Ron 95 shows that it has the worst effects in terms of both fuel consumption and emission release. Its harmful emission gas level proves to outrun both the Iridium and Platinum spark plug as it contains the maximum harmful gas level. This type of spark plug is most commonly found on the low budget category people's car.

REFERENCES

- Mohamad TI, How HG. Part-load performance and emissions of a spark ignition engine fueled with RON95 and RON97 gasoline: Technical viewpoint on Malaysia's fuel price debate. *Energy Conversion and Management*. 2014; 88:928-35.
- Sayin, Cenk, Ibrahim Kilicaslan, Mustafa Canakci, and Necati Ozsezen. "An experimental study of the effect of octane number higher than engine requirement on the engine performance and emissions." *Applied Thermal Engineering* 25, no. 8-9 (2005): 1315-1324.
- Mohamad, Taib Iskandar, and Heoy Geok How. "Part-load performance and emissions of a spark ignition engine fueled with RON95 and RON97 gasoline: Technical viewpoint on Malaysia's fuel price debate." *Energy Conversion and Management* 88 (2014): 928-935.
- Akihama, Kazuhiro, Masahiro Taki, Semon Takasu, Takanori Ueda, Yoshihiro Iwashita, John T. Farrell, and Walter Weissman. *Fuel octane and composition effects on efficiency and emissions in a high compression ratio SIDI engine*. No. 2004-01-1950. SAE Technical Paper, 2004.
- Rashid, Adnan Kadhim, Abu Mansor, Mohd Radzi, Wan Aizon Wan Ghopa, Zambri Harun, and Wan Mohd Faizal Wan Mahmood. "An experimental study of the performance and emissions of spark ignition gasoline engines." *International Journal of Automotive &*

Mechanical Engineering 13, no. 3 (2016).

- Ghanaati, Ali, Mohd Farid Muhamad Said, and Intan Z. Mat Darus. "Comparative analysis of different engine operating parameters for on-board fuel octane number classification." *Applied Thermal Engineering* 124 (2017): 327-336.
- Mustafa Atakan Akar² , Şafak Yıldızhan³ , Mustafa Özcanlı⁴ , Hasan Serin⁵ ,Effect of Spark Plug Alteration on Performance Using Hydrogen Enriched Gasoline in Si Engine Under Various Loads and Compression Ratios Oğuz Baş^{1*}, (July 2018).
- Pulkrabek W.W (2004) *Engineering Fundamentals Of Internal Combustion ;Engine*, Pearson Prentice Hall, New Jersey
- Klimstra J. The optimum combustion phasing angle—a convenient engine tuning criterion. SAE technical paper; 1985 [852090]
- Nishiyama A, Ikeda Y. Improvement of lean limit and fuel consumption using microwave plasma ignition technology. SAE technical paper; 2012 [2012-01- 1139].
- A. K. . Rashid, M. R. . Abu Mansor, W. A. . Wan Ghopa, Z. . Harun, and W. M. F. . Wan Mahmood, "An experimental study of the performance and emissions of spark ignition gasoline engine", *Int. J. Automot. Mech. Eng.*, vol. 13, no. 3, pp. 3540–3554, Dec. 2022.

EXPERIMENTAL INVESTIGATION ON DAMPING PROPERTIES AND PERFORMANCE OF ADJUSTABLE SHOCK ABSORBER

Joel Wong Khai Sheng, Ng Khai Mun, Koh Chu Eyam & Abdullah Idris
Infrastructure University Kuala Lumpur

1. INTRODUCTION

An automobile consists of many inter-functional and integrated systems, in which one of the main systems is known as the suspension system. Suspension system is meant to let the drivers and passengers experience comfort, stability and safety when driving a vehicle. The main purpose of vehicle suspension systems is to increase the comfort of drivers and passengers and ultimately road safety. In this chapter, the investigation has focused on the damper system. Damper or shock absorber is one of the components which are very important in a suspension system serving as the main factor that provides both driving safety and comfort for the vehicle.

From the observation by the authors in the current market, it has been noticed that there is no standard guideline yet in the actual practice to conduct the optimized absorber rebound setting as per driver needs. The setting typically depends on the experience of a professional tuner, and the feeling of the driver. There is no structured study on this aspect to provide a reference to the tuners to carry out the setting of the rebound damping. As there are many variables to be considered when tuning the rebound damping, it usually takes a long time to fine tune the rebound setting for the absorber due to the multiple on the road testing procedures and fine tuning that have resulted in the work being lengthy and inefficient. The present work is intended to investigate the characterisation of the different rebound damping settings of an adjustable shock absorber to provide a guiding reference to the tuners. HWL performance shock absorber was used as a testing sample. The shock absorber tester was used and the static drop test was conducted to determine the damping ratio of HWL performance shock absorber.

2. LITERATURE REVIEW

Automotive suspension system has been a focus to the researcher as it is to enhance the vehicle stability, handling properties and comfort to the drivers as well as the passengers. Since the passenger cars have been historically one of the primary methods of ground transportation (A. Belhocine, 2016), it is essential to have a very good vehicle suspension system that can reduce vibration of the chassis to a great extent without compromising vehicle handling quality. Suspension consists of the system of springs, shock absorbers and linkages that connects a vehicle to its wheels (Ayman, 2013). The main function of vehicle suspension systems is to support the vehicle body and provide riding comfort (Agharkakli, 2012). A shock absorber is the key element of the suspension system. It is used to reduce vertical oscillation of the vehicle during the unevenness of the road surface. Comfort and road-handling performance of a vehicle are mainly determined by the damping characteristics of the shock absorbers (Lauwerys, 2005).

Twin Tube Shock Absorber

A twin tube shock absorber has 2 chambers. Twin tube shock absorber refers to the inner tube with the outer tube of the piston mounted on the inner tube provided with valves that permit adjustability of compression damping separate from rebound damping. The piston slides in the inner tube mounted within the outer tube. The first chamber is formed within the inner tube and the second chamber is formed between the outer tube and the inner tube. Base valve is positioned between the first and second chambers to control the compression flow and rebound flow separately and independently. A gas chamber positioned within the inner tube assists the main compression spring in the inner and outer tubes which also acts as a part of a volume compensation system when the shock absorber is compressed and rebounded (Powers, 2005). HWL suspension Malaysia is mainly focusing on Twin Tube Shock Absorber. Figure 1 shows the twin tube shock absorber.

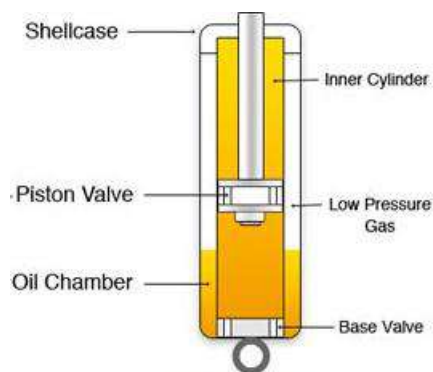


Figure 1: Twin Tube Shock Absorber (Johnny, 2016)

Monotube Shock Absorber

A monotube shock absorber is different from a twin tube shock absorber. It uses only 1 tube rather than 2 tubes like twin tube shock absorbers. It also includes a body tube that houses a working piston and a bypass tube that is attached to the external to the body tube, a control valve influences flow volume and rate of oil that passes through the bypass tube in a manner that correspondingly influences damping and other characteristics of the monotube shock absorber. Monotube shock absorber can include a floating piston separating a volume of gas from a volume of oil; the volumes of gas and oil may be entirely housed in the body of the tube (Fredrick J. Furrer, 2010). Figure 2 shows the monotube shock absorber.

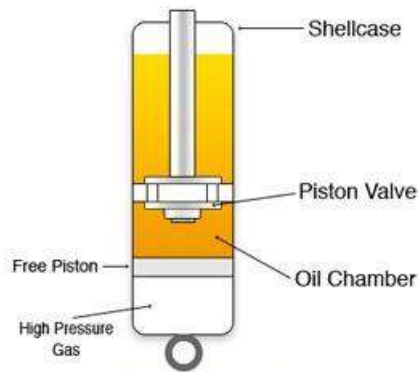


Figure 2: Monotube Shock Absorber (Johnny, 2016)

Dynamic Material Testing Machine HT-911

Figure 3 shows a dynamic material testing machine modelled HT-911. The restoring force and the relative displacement of the shock absorber can be measured by a load cell and a displacement transducer fixed at the end of the damper. The loading conditions on the test platform include sine wave and random displacement (Shaohua Li, 2012).



Figure 3: Dynamic Material Testing Machine HT-911 (Shaohua Li, 2012)

Field Test

Field tests are important to validate the testing data in any vehicle related experimental work. An acceleration transducer could be used for an experimental work related to shock absorber. Acceleration transducers are typically placed on the vehicle body and also the seat. When the vehicle runs on road, the shock absorber is acted on by random loads with many frequencies composed of the vehicle's natural frequencies and frequencies of road surface roughness. It is a critical question waiting to be solved that which loading condition should be used in absorber dynamic properties test and modelling with the aim of vehicle dynamics simulation (Shaohua Li, 2012). Figure 4 shows the vehicle in a field test and acceleration transducer location.



(a) The vehicle in the field test (b) Acceleration transducer on cab seat (c) Acceleration transducer on vehicle body

Figure 4: Vehicle in Field Test and Acceleration Transducer Location (Shaohua Li, 2012)

Quarter Vehicle Model

The quarter vehicle model means one-fourth of the vehicle mass. Figure 5 shows the quarter vehicle model. It is the basic model of a single degree of freedom system, represented by single mass, M , spring of stiffness, K and damper with viscous damping, C (Idris, 2019). Figure 6 shows the single degree of freedom diagram.

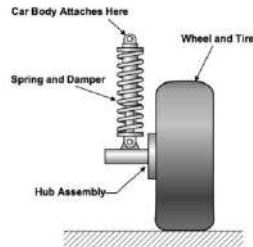


Figure 5: Quarter vehicle model (Idris, 2019)

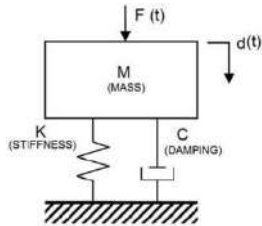


Figure 6: Single degree of freedom diagram (Idris, 2019)

Based on Figure 6, it shows that single degree of freedom diagram can be formulated as follows:

Spring force $F_k \propto$ deflection, X ; $F_k = K X$

Damping force \propto velocity \dot{X} ; $F_d = C \dot{X}$

Equation of motion $[\Sigma F = M \ddot{x}]$

$$(-)C \dot{X} - K X = M \ddot{x}$$

or

$$M \ddot{x} + C \dot{X} + K X = 0 \tag{1}$$

Solution to be in the form of:

$$X = A e^{St}$$

Thus giving,

$$\dot{X} = SA e^{St} \text{ and } \ddot{x} = S^2 A e^{St} \quad (2)$$

Substitute into equation (1)

$$M S^2 A e^{St} + C S A e^{St} + K A e^{St} = 0$$

Simplifying,

$$M S^2 + C S + K = 0 \quad (3)$$

Finding the roots for Equation (3)

$$S_1 = -\frac{c}{2M} + \sqrt{\left(\frac{c}{2M}\right)^2 - \frac{K}{M}} \quad ; \quad S_2 = -\frac{c}{2M} - \sqrt{\left(\frac{c}{2M}\right)^2 - \frac{K}{M}}$$

$$S_1 = (-) \xi \omega_n + \sqrt{(\xi \omega_n)^2 - \omega_n^2} \quad ; \quad S_2 = (-) \xi \omega_n - \sqrt{(\xi \omega_n)^2 - \omega_n^2}$$

$$S_1 = [(-) \xi + \sqrt{\xi^2 - 1}] \omega_n^2 \quad ; \quad S_2 = [(-) \xi - \sqrt{\xi^2 - 1}] \omega_n^2 \quad (4)$$

Substituting values for S_1 and S_2 into

$$X = A_1 e^{S_1 t} + A_2 e^{S_2 t} \quad (5)$$

Getting the general equation for free vibration with viscous damping as:

$$X = A_1 e^{[-\xi + \sqrt{\xi^2 - 1}] \omega_n t} + A_2 e^{[-\xi - \sqrt{\xi^2 - 1}] \omega_n t} \quad (6)$$

$$X = e^{-\xi \omega_n t} [A_1 e^{[i \sqrt{1 - \xi^2}] \omega_n t} + A_2 e^{[-i \sqrt{1 - \xi^2}] \omega_n t}] \quad (7)$$

Above equation can be written as:

$$X = x e^{-\xi \omega_n t} \sin \{ \omega_d t + \phi \} \quad (8)$$

Where ω_d is define as,

$$\omega_d = \omega_n + \sqrt{1 - \xi^2} \quad (9)$$

At time $t = t_0$, $X = X_0$ then substituting into equation (8)

$$X_0 = X e^{-\xi \omega_n t_0} \sin \sin \{ \omega_d t_0 + \phi \} \quad (10)$$

and after one complete oscillation (after one period), $t = t_0 + T_d$, $X = X_1$, then,

$$X_1 = X e^{-\xi\omega_n(t_0+T_d)} \sin \sin \{ \omega_d(t_0 + T_d)t_0 + \phi \} \quad (11)$$

Dividing equation (10) by equation (11),

$$\frac{X_0}{X_1} = \frac{X e^{-\xi\omega_n t_0} \sin \sin \{ \omega_d t_0 + \phi \}}{X e^{-\xi\omega_n(t_0+T_d)} \sin \sin \{ \omega_d(t_0 + T_d)t_0 + \phi \}}$$

$$\frac{X_0}{X_1} = e^{\xi\omega_n T_d} \quad (12)$$

Taking the natural log,

$$\ln \frac{x_0}{x_1} = \xi\omega_n T_d = \frac{\xi\omega_n X 2\pi}{\omega_n \sqrt{1-\xi^2}} \quad (13)$$

Logarithmic decrement, δ

$$\ln \frac{x_0}{x_1} = \frac{2\pi\xi}{\sqrt{1-\xi^2}} \quad (14)$$

Logarithmic Decrement

The logarithmic ratio of amplitudes after one oscillation is often called logarithmic decrement, δ . The equation for logarithmic decrement is (Idris, 2019):

$$\delta = \ln \frac{x_0}{x_1} = \frac{2\pi\xi}{\sqrt{1-\xi^2}} \quad (15)$$

If more than one oscillation are involved, then the equation needed to use is:

$$n\delta = \ln \frac{x_0}{x_n} = \frac{2n\pi\xi}{\sqrt{1-\xi^2}} \quad (16)$$

Response to Step Forced Vibration

According to Yang (2005) and Hanchey (2012) the forced vibration is given in few damping cases which are:

Case 1: Un-damped ratio ($\zeta = 0$)

Un-damped ratio basically the shock absorber has no resistance to hold the car from the spring and results in a very bouncy suspension.

Case 2: Under damped ratio ($0 \leq \zeta < 1$)

The under damped ratio shock absorber provides comfort and handling to the drivers. Most of the vehicle manufacturers will prefer using under damped shock absorbers. The ratio depends on the manufacturers. If the damping ratio is less than 0.5, for example, the suspension will be bouncy which provides comfort but not handling as well as not comfortable on long distance trips. If the damping ratio is 0.5 above and below 1, it provides better handling but less comfort. According to Idris (2019), the ideal damping ratio is 0.5 which provides a decent comfort and

handling to the vehicle.

Case 3: Critically damped ratio ($\zeta = 1$)

Critically damped ratio is the border between the overdamped and under damped cases.

Case 4: Over damped ratio ($\zeta > 1$)

An over damped ratio shock absorber will result in sluggish suspension where the shock absorber does not return to steady state quickly. It gives a very uncomfortable driving experience but provides good handling. This kind of setting is usually used on racing track cars.

3. METHODOLOGY

The methodology of the present work has included lab tests and outdoor field tests. This topic provides a detailed explanation of the methods throughout the project.

Mathematical Formulation

The logarithmic decrement (δ) equation is used to calculate the logarithmic ratio of amplitudes after one oscillation at the static drop test (Idris, 2019).

To remove the square root, square all the values. $\ln \frac{x_0}{x_n} = \frac{2\pi\xi}{\sqrt{1-\xi^2}}$

Simplified:

$$\left[\ln \left(\frac{x_0}{x_n} \right) \right]^2 = \frac{4\pi^2\xi^2}{1-\xi^2} \quad (17)$$

Assume:

$$\left[\ln \left(\frac{x_0}{x_n} \right) \right]^2 = A$$

$$A = \frac{4\pi^2\xi^2}{1-\xi^2}$$

$$A - A\xi^2 = 4\pi^2\xi^2$$

$$4\pi^2\xi^2 + A\xi^2 = A$$

$$\xi^2(4\pi^2 + A) = A$$

$$\xi^2 = \frac{A}{4\pi^2 + A}$$

$$\therefore \xi^2 = \frac{\left[\ln \left(\frac{x_0}{x_n} \right) \right]^2}{4\pi^2 + \left[\ln \left(\frac{x_0}{x_n} \right) \right]^2} \quad (18)$$

Where,

ξ = damping ratio

x_0 = the height of the starting point before the drop

x_n = the highest point at the first rebound

The input values of x_0 and x_n will be average from three sampling of experiment tests.

Experimental Setup and Testing

Shock absorber tester MST-10kN is used to test the capacities of rebound and compression forces of an absorber. The output data is measured as force (N) and velocity (m/s). In this project, the HWL performance shock absorber ST-1 series for Toyota Vios NCP93 was tested by using the shock absorber tester MST-10kN to get the result for Click No.0 (Soft) to Click No.15 (Hard), the adjustable range of mode. Rebound and compression were recorded as force (N) vs velocity (m/s). The collected data is used to identify the characteristics of the shock absorber from soft to hard and to observe the performance profile from soft to hard.

The lab test was conducted at HWL Suspension Malaysia HQ located at Sungai Buloh. Figure 7 shows the shock absorber tester MST-10kN. Figure 8 shows the sample result of the shock absorber tester on the monitoring display.

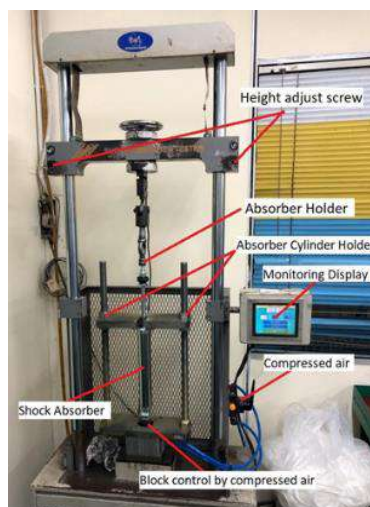


Figure 7: Shock absorber tester MST-10kN



Figure 8: Sample result of shock absorber tester on the monitoring display

Field test was carried out at Unipark Condominium car park. Graph paper was stuck on the wall with the laser pointer mounted on the test subject's fender pointing at the graph paper as the drop test begins from click No.0 to No.15. The progress profile was then recorded using a camera, model Fujifilm X-T1. The recorded video will be analysed in slow motion and to determine the damping ratio of the shock absorber from click No.0 to No.15. Static drop test is to collect and record the data to measure the test subject rebound after the 1st drop from soft to hard. The test subject was raised about 200mm and drop. The collected data was calculated using the logarithmic decrement, δ equation.

Figure 9 shows the set-up planning at an experimental site with a measuring tool. Figure 10 shows the actual set-up static drop test. Figure 11 presents a sample result of a static drop test. Figure 12 shows the data analysis from recorded data using video editor in frame and time.

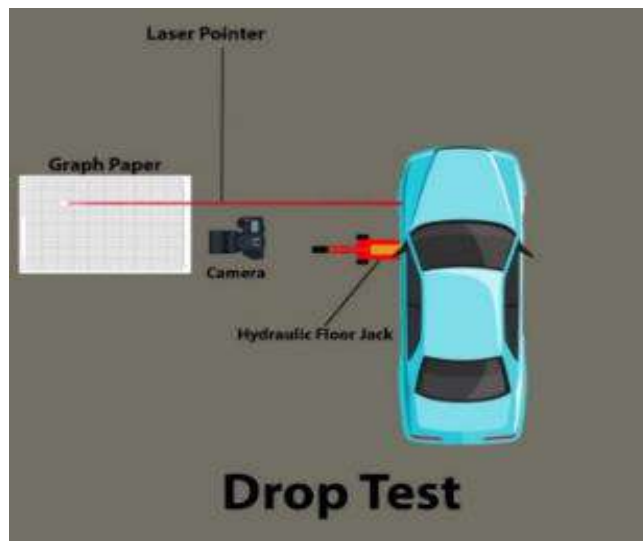


Figure 9: Set-up planning at experimental site with measuring tool



Figure 10: Actual set-up static drop test

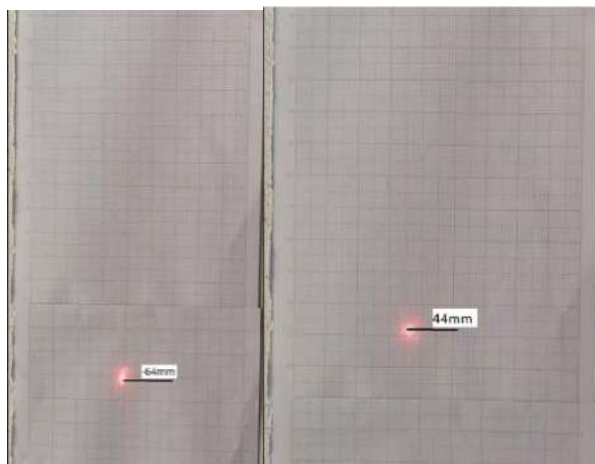


Figure 11: Sample result of static drop test

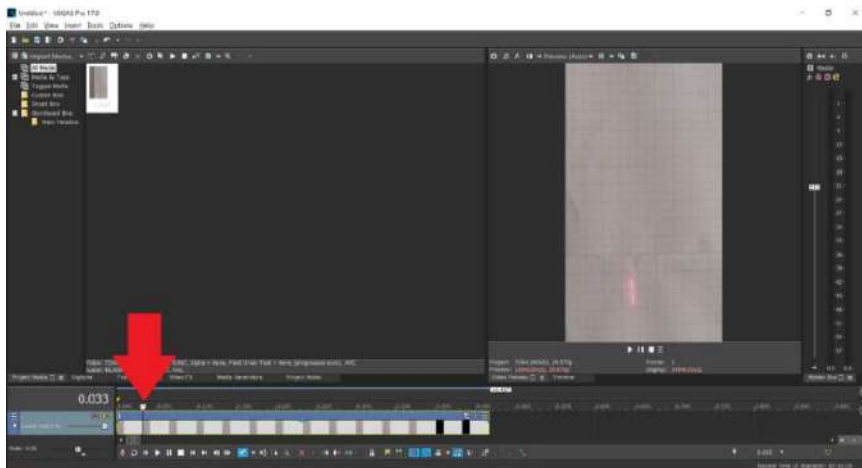


Figure 12: Data Analysis from Recorded Data using Video Editor in frame and time

6. RESULTS AND DISCUSSION

Laboratory Test using Shock Absorber Tester MST-10Kn

Figures in this section show the rebound force (N) of the shock absorber in different velocity (m/s). The dyno test was conducted 3 repeated times and got the average data. Figure 13 shows the average rebound data from Click 0 to Click 7. Figure 14 shows the average rebound data from Click 8 to Click 15.

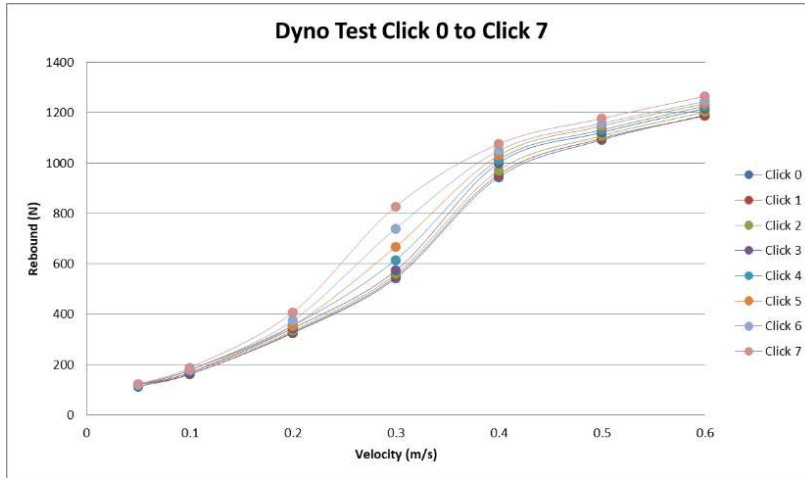


Figure 13: Average Rebound Data from Click 0 to Click 7

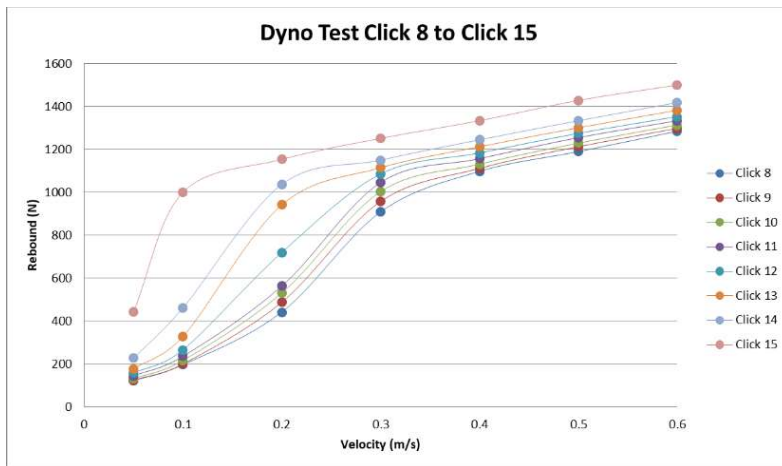


Figure 14: Average Rebound Data from Click 8 to Click 15

The damping rebound force of the shock absorber is tested by velocity (m/s). From Figures 13 and 14, both show that as the click is higher, the rebound force is increased. Adjustable shock absorber is made to adjust the soft and hard damping conditions by turning the damping adjuster to soft or hard. From Click 0 to Click 7 the profile pattern is almost similar. It clearly shows that Click 4 to Click 7 had bigger gap rebound force at velocity 0.3. The damping rebound forces at Clicks 8, 9, 10 and 11 are increasing steadily. Clicks 12, 13 and 14 at velocity

0.2 have increased a lot compared to Clicks 8 to 11. Click 15 has the highest rebound force as it is the maximum of the click. When the click is increased the resistance of fluid flow in the shock absorber increases. It will incur higher pressure and therefore higher rebound force. The harder the fluid flow the harder the shock absorber rod gets back to its original state after compress.

The data collected from the shock tester MST-10kN is based on rebound damping force (N) versus velocity (m/s) which can be used to find the damping coefficient of the shock absorber. Whereby, $F = cv$, c (damping coefficient) = $\frac{F (force)}{v (velocity)}$.

Figure 15 shows the regions of damping coefficient of the shock absorber Clicks 0 to 7. Figure 16 shows the regions of damping coefficient of the shock absorber Clicks 8 to 11. Figure 17 shows the regions of damping coefficient of the shock absorber Clicks 13 to 14. Figure 18 shows the regions of damping coefficient of the shock absorber Click 15.

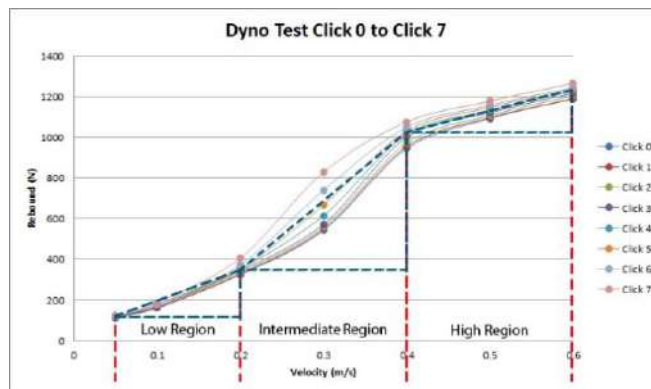


Figure 15: Regions of Damping Coefficient of the Shock Absorber Click 0 to Click 7

Low region:

$$c = \frac{F (force)}{v (velocity)} = \frac{235N}{0.15m/s}$$

$$c = 1566.67 \text{ Nm/s}$$

Intermediate region:

$$c = \frac{F (force)}{v (velocity)} = \frac{677N}{0.2m/s}$$

$$c = 3385 \text{ Nm/s}$$

High region:

$$c = \frac{F (force)}{v (velocity)} = \frac{206N}{0.2m/s}$$

$$c = 1030 \text{ Nm/s}$$

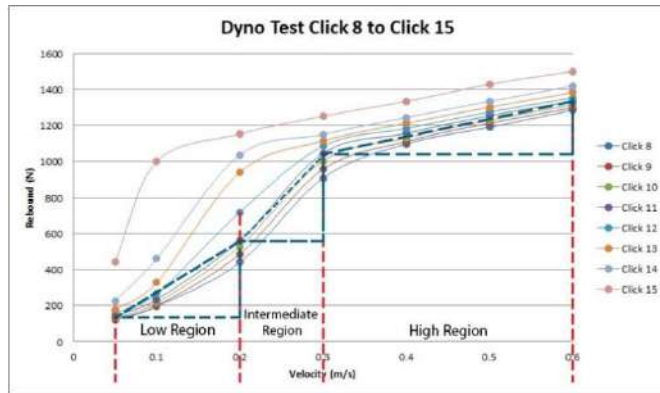


Figure 16: Regions of Damping Coefficient of the Shock Absorber Click 8 to Click 11

Low region:

$$C = \frac{F (force)}{v (velocity)} = \frac{418.66N}{0.15m/s}$$

$$c = 2791.07 Nm/s$$

Intermediate region:

$$C = \frac{F (force)}{v (velocity)} = \frac{483.67N}{0.1m/s}$$

$$c = 4836.7 Nm/s$$

High region:

$$C = \frac{F (force)}{v (velocity)} = \frac{288N}{0.3m/s}$$

$$c = 960 Nm/s$$

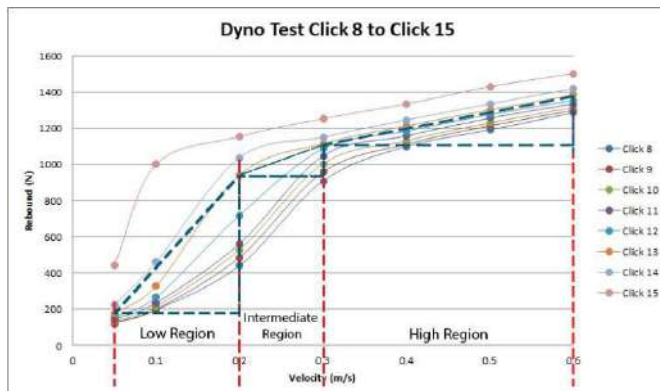


Figure 17: Regions of Damping Coefficient of the Shock Absorber Click 13 to Click 14.

Low region:

$$c = \frac{F(\text{force})}{v(\text{velocity})} = \frac{764.33N}{0.15m/s}$$

$$c = 5095.53 \text{ Nm/s}$$

Intermediate region:

$$c = \frac{F(\text{force})}{v(\text{velocity})} = \frac{173.34N}{0.1m/s}$$

$$c = 1733.4 \text{ Nm/s}$$

High region:

$$c = \frac{F(\text{force})}{v(\text{velocity})} = \frac{268.33N}{0.3m/s}$$

$$c = 894.43 \text{ Nm/s}$$

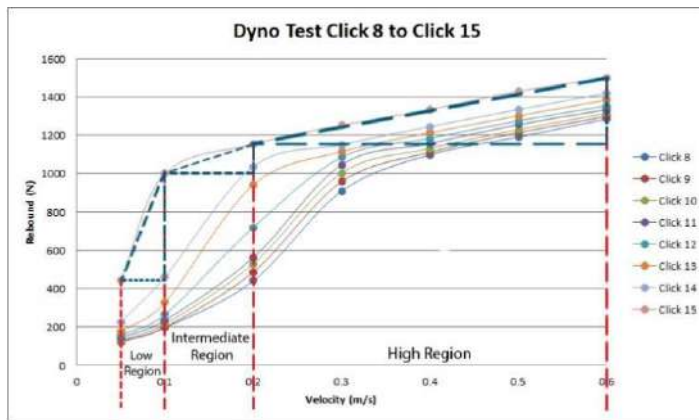


Figure 18: Regions of Damping Coefficient of the Shock Absorber Click 15.

Low region:

$$c = \frac{F(\text{force})}{v(\text{velocity})} = \frac{764.33N}{0.15m/s}$$

$$c = 5095.53 \text{ Nm/s}$$

Intermediate region:

$$c = \frac{F(\text{force})}{v(\text{velocity})} = \frac{173.34N}{0.1m/s}$$

$$c = 1733.4 \text{ Nm/s}$$

High region:

$$c = \frac{F(\text{force})}{v(\text{velocity})} = \frac{268.33N}{0.3m/s}$$

$$c = 894.43 \text{ Nm/s}$$

Damping coefficient is a property which indicates the piston rod of a shock absorber to rebound back or return to its initial state. If the shock absorber has a low damping coefficient, the piston rod rebound will be faster. High damping coefficient shock absorber on the other hand has a slow rebound. According to the data obtained from the shock absorber tester MST-10kN, the profile pattern from Clicks 0 to 7 and Clicks 8 to 12 are identical. Furthermore, Clicks 13, 14 and 15 are different from the rest. There are three regions in the graphs that are low, intermediate and high regions. The damping coefficient in Clicks 0 to 7 at low region is 1566.67 Nm/s. Intermediate region is 3385 Nm/s and the high region is 1030 Nm/s.

Damping coefficient in Clicks 8 to 12 at the low region is 2791.07 Nm/s. Intermediate region is 4836.7 Nm/s and high region is 960 Nm/s. Moreover, the damping coefficient in Clicks 13 to 14 at low region is 5095.53 Nm/s. Intermediate region is 1733.4 Nm/s, and high region is 894.43 Nm/s. Lastly, the damping coefficient in Click 15 at low region is 11173.4 Nm/s. Intermediate region is 1536.7 Nm/s, and high region is 866.65 Nm/s.

The profile pattern for twin tube and monotube shock absorber is different because of the piston design. Twin tube shock absorber piston usually get digressive profile pattern because the piston for twin tube shock absorber is designed with smaller hole and does not have straight hole for the fluid to flow through while monotube shock absorber piston is linear because it is designed with straight and larger hole for the fluid to flow through the piston in the shock absorber. Figure 19 shows the piston profile pattern.

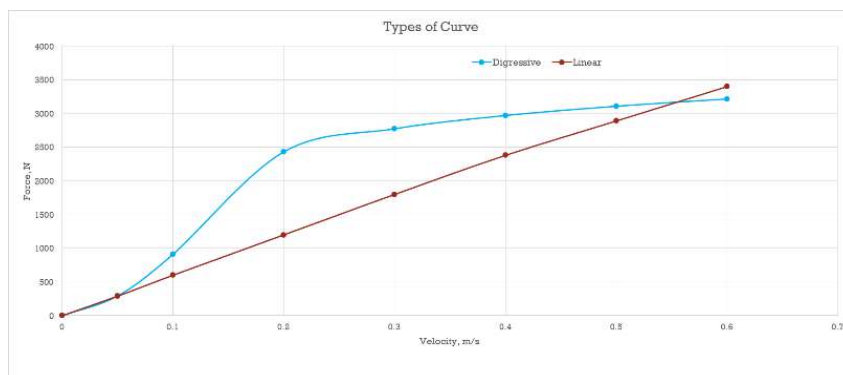


Figure 19: Piston Profile Pattern

Vehicle Static Drop Test

Figures in this section demonstrated the damping of the shock absorber in different stiffness from Click 0 (Softest) to Click 15 (Hardest). The Static drop test was conducted 3 repeated times. Figure 20 shows the average static drop test from Clicks 0 to 7. Figure 21 shows the average static drop test from Clicks 8 to 15.

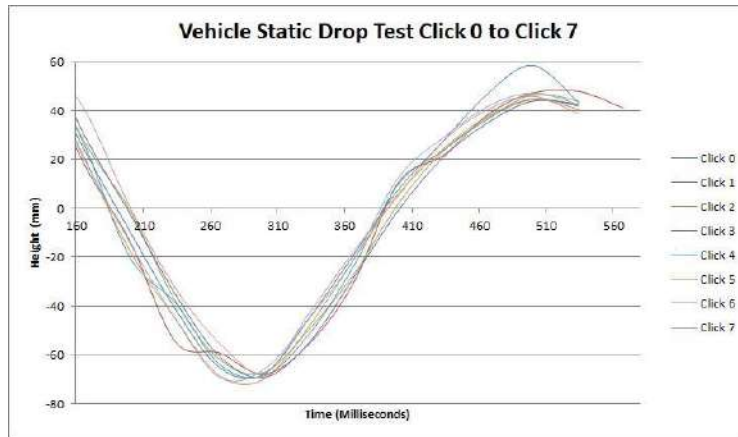


Figure 20: Average Static Drop Test from Click 0 to Click 7

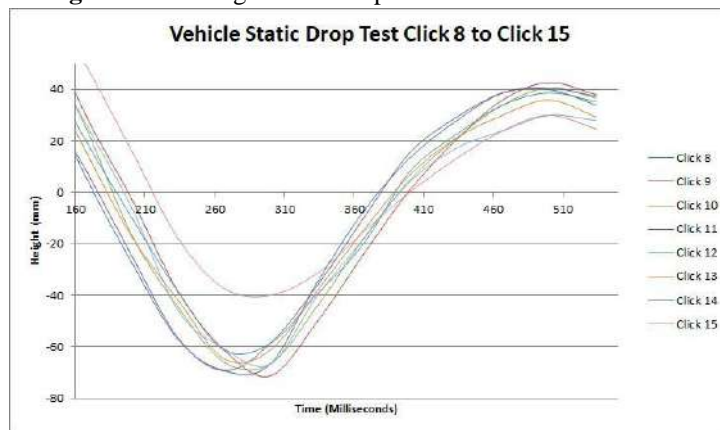


Figure 21: Average Static Drop Test from Click 8 to Click 15

In the static drop test, the laser pointer is pointing at 0mm on the graph paper when the vehicle is at its original state. The vehicle was then raised up by a hydraulic jack until the laser pointer was pointing at 200mm and dropped. Negative value means that the body of the car is compressing. The next positive value means that the car will rebound. From the line pattern of Click 0, it shows that the rebound is much higher than the rest due to less fluid flow restriction at click 0. As the click increases, the fluid flow restriction in the shock absorber will be increased. The line pattern of Click 1 at 234 to 267 milliseconds shows that it dropped from -54.7mm to -59.3. Click 2 to 7 have almost the same profile pattern and the gap differences are not big.

Next, by comparing Clicks 8 to 14, there are not much difference at the gap. It shows that as the click increases the height of the rebound decreases because of the fluid flow restriction. Click 15 shows there is a big gap compared to the others because the rebound force increases a lot at Click 15 compared to Click 14 which is shown at the laboratory test.

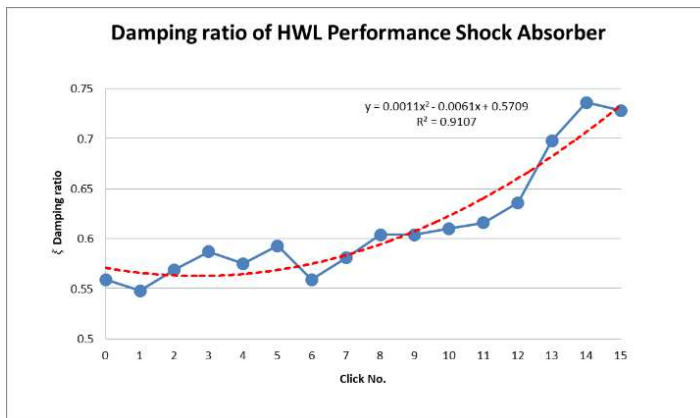
Calculation for Logarithmic Decrement, δ

Table 1 shows the computed damping ratio for the Clicks 1 to 15 using the Equation (18).

Table 1: Damping Ratio from Click No. 0 to 15

Click No.	x_0	x_n	ξ
0	200.0	47.3	0.559
1	200.0	48.7	0.548
2	200.0	46.0	0.569
3	200.0	44.0	0.587
4	200.0	45.3	0.575
5	200.0	43.3	0.593
6	200.0	47.3	0.559
7	200.0	44.7	0.581
8	200.0	42.0	0.604
9	200.0	42.0	0.604
10	200.0	41.3	0.610
11	200.0	40.7	0.616
12	200.0	38.7	0.636
13	200.0	32.7	0.698
14	200.0	29.3	0.736
15	200.0	30.0	0.728

Figure 22 shows the damping ratio profile of the HWL performance shock absorber on static drop tests. The pattern profile shows the average damping ratio on three repeated sampling tests. At Clicks 6 and 7, the damping ratio is lower than Clicks 3 and 5. The damping ratios of Clicks 9 to 12 are increasing steadily. From Clicks 12 to 13 and Click 14, there are big increases on the damping ratio. As the damping ratio is higher the higher the fluid flow restriction and slower the piston rod back to its initial state which means lesser bounce on the vehicle. By calculating the damping ratio of the static drop test without load, the HWL performance shock absorber is rated as under damped ratio as the output damping ratio is ($0 \leq \xi < 1$)

**Figure 22:** Damping ratio of HWL performance shock absorber

A correlation between the damping ratio ξ and number of different clicks can be developed which could be useful to predict its damping ratio. The equation of the correlation is $\xi = 0.0011x^2 + 0.0061x + 0.5709$ with $R^2 = 0.9107$. Table 2 tabulates the comparison of the laboratory test and the static drop test in the field.

Table 2: Comparing laboratory test and static drop test

	Velocity (m/s)					
	Low region	Intermediate region	High region	Laboratory test $\xi = \frac{c}{c_c}$	Static drop test ξ	Deviation %
Click 0 – 7 (Click 5)	0.05 – 0.2	0.2 – 0.4	0.4 – 0.6	0.794	0.593	25.32%
Click 8 – 12 (Click 11)	0.05 – 0.2	0.2 – 0.3	0.3 – 0.6	1.141	0.616	46.01%
Click 13 – 14 (Click 13)	0.05 – 0.2	0.2 – 0.3	0.3 – 0.6	1.026	0.728	40.93%
Click 15 (Click 15)	0.05 – 0.1	0.1 – 0.2	0.2 – 0.6	1.803	0.698	61.29%

7. CONCLUSION

The experimental investigation on damping properties and performance of an adjustable shock absorber has been demonstrated and analysed. The findings showed that there existed the difference of the rebound damping force as the click number increases from 0 (soft) to 15 (hard) on a HWL performance shock absorber. For click 0 (softest), the result was found to be at the average of 111.33N at 0.05m/s and average of 1190.00N at 0.6m/s. For click 15 (hardest), it was on the average of 441.33N at 0.05m/s and average of 1500.33N at 0.6m/s. From the static drop test, the damping ratio can be computed by using the formulation of logarithmic decrement, δ . The damping ratio of HWL performance shock absorber for Clicks 0 to 15 is more than 0.5 but less than 1 which is identified under the category of damped ratio. At click 0 (softest) the results are 43.3mm rebound after compress at 534 milliseconds from 200mm drop. At click 15 (hardest), it rebounds 24.7mm after compressing at 534 milliseconds from 200mm drop. It indicated that as the click increases, the rebound high is lesser in which the vehicle bounce is restricted due to the increasing of the damping ratio on the shock absorber. As a result, the HWL performance shock absorber has a higher rebound damping force compared to the normal shock absorber. The HWL performance shock absorber is tuned to have high rebound damping force to let the car be more stable during the drive on the highway as well as cornering, nevertheless it would sacrifice the comfort of the vehicle.

Shock absorbers play an important role in vehicle comfort and handling. A comfortable ride requires a soft shock absorber which can dissipate the shock energy from the road while a hard shock absorber gives a good handling to the vehicle. It is very important to determine the characteristics of a damping system which can achieve the driver's needs.

ACKNOWLEDGMENT

The authors would like to express gratitude to HWL Suspension Malaysia for sharing their testing facility at its Sungai Buloh HQ Plant throughout the completion of this research.

REFERENCES

- A. Agharkakli, G. S. (2012). Simulation and Analysis of Passive and Active Suspension System Using Quarter Car Model for Different Road Profile. *International Journal of Engineering Trends and Technology*, 3, 636.
- A. Belhocine, N. G. (2016). Effects of Young's modulus on disc brake squeal. *International Journal of Acoustics and Vibrations*, 21, 292.
- Ayman A. Aly, a. F. (2013). Suspension system model. *Vehicle suspension systems control*, 2(2), 46-47. Retrieved 2019
- C. Lauwerys, J. S. (2005). Robust linear control of an active suspension on a quarter car test-rig. *Control Engineering Practice*, 13(5), 577-586.
- Johnny. (2016, June 1). *ISC suspension*. Retrieved from <https://iscsuspension-na.com/monotube-vs-twin-tube-difference-better/>
- Idris, A. P. (2019). Logarithmic Decrement, Damping Coefficient, Critical Damping. *Viscous damped vibration*, 1-12. Malaysia: Assoc. Prof. Hj. Abdullah Idris.
- Shaohua Li, Y. L. (2012). Hydraulic Shock Absorber. *Dynamical Test and Modeling for Hydraulic Shock Absorber on Heavy Vehicle*, 4, 1904 - 19407.
- Fredrick J. Furrer, P. W. (2010). *United States Patent No. US 2010/0109277 A1*. Retrieved 2019
- Powers, P. H. (2005). *United States Patent No. US5996746A*. Retrieved 2019
- .

FIELD INVESTIGATION OF ELECTRIC VEHICLE DISCHARGE RATE AND ITS ECONOMIC ASPECT UNDER INFLUENCE OF DIFFERENT ON-THE-ROAD DRIVING CONDITIONS – A CASE STUDY IN CHINA

Su Jiajing, Ng Khai Mun, Noorradiah Ismail, Sai-Keong Chan & Tan Chee Fai
Infrastructure University Kuala Lumpur.

1. INTRODUCTION

To achieve the national agenda in environmental conservation and to combat the high energy price in the long term, countries around the world are vigorously developing EV technology to replace traditional fuel vehicles. Despite the great impact of COVID- 19, the sales of electric vehicles in 2020 were positive, benefiting from the focus of car companies on the technological development of new energy vehicles as well as the supportive policy from the governments. Figure 1 shows an encouraging trending of EV market share [1]. Due to the efforts of the government and car companies, more and more people are beginning to pay attention to owning an EV. As compared to traditional fuel vehicles, the usage of EV on the road is still in the earlier stage, and technically the energy of EV cannot be fully charged as quickly as gasoline. This kind of issue has caused energy companies and car companies to cooperate more strategically to build not only charging stations at gas stations, but also at the parking lot and common access area around the households to develop a feasible eco-system to support the EV development.

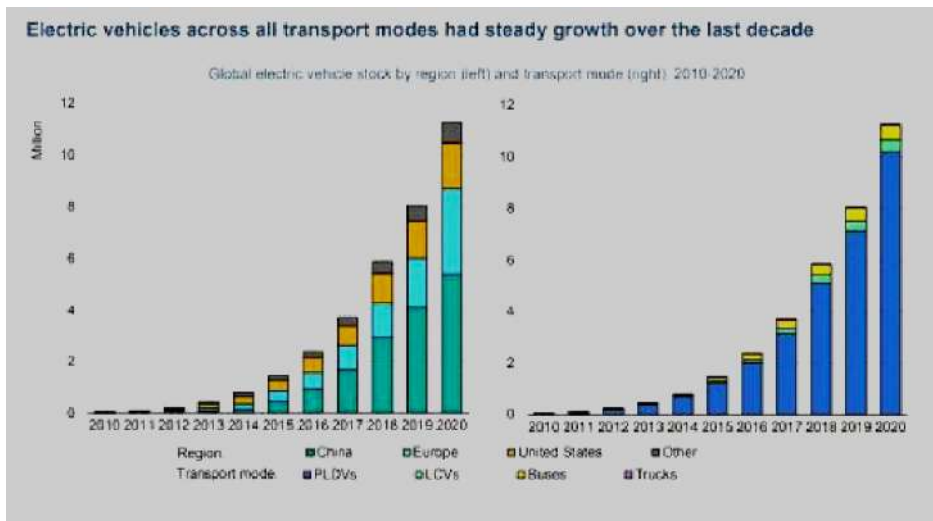


Figure 1: IEA analysis on EV market share [1]

According to literatures, the energy charge and discharge of the battery are related to many factors, including road factors (such as road gradient [2]), environmental factors (such as

ambient temperature [3]), vehicle factors (self-power loss [4]), and driving factors (such as driving behaviour and charging habits [5]). Among them, the road factor is a part that people tend to ignore when driving, however this factor has a great impact on the driving of the vehicle.

Limited by the battery performance of electric vehicles, the driving range of EV is not sufficiently competitive compared to internal combustion engine vehicles. Through the measurement methods prescribed by some countries, the results obtained may be subject to large variance, besides limited mileage information available to users. The New European Driving Cycle (NEDC), the legislative driving cycle in the EU countries for certifying vehicle fuel consumption and emission levels, tends to underestimate the consumption levels obtained under the real-world conditions [6,7]. Due to the actual road conditions with numerous random environmental factors and the NEDC test that is a bench test commonly, the results of the data are only for reference purposes. For example, the BYD Han EV long-endurance version has officially claimed that NEDC can reach an astonishing endurance of over 600 km, while BYD's engineers even have claimed it can run nearly 650 km in the actual test; nevertheless, the owner's actual test is only about 470 km. When dealing with the complex road conditions, such as traffic jams, uphill and downhill, high speed, etc., the cruising range might not be similar to the ones claimed in the lab tests. Besides, due to the slow charging rate and the short travelling mileage of EV, drivers feel anxious about the remaining energy in their EV. Therefore, accurate power prediction is the key to minimize the anxiety and help drivers make full sense and plan their road journey appropriately [8, 9].

The present work is intended to investigate the discharge rate of battery of an EV model under the different driving modes, such as traffic jam, high speed and uphill driving modes, with high and low battery status, as well as the influence of air conditioner. Besides, a comparison study of the battery discharge pattern and the economic aspect under the influences of different conditions have been conducted.

2. METHODOLOGY

This section explains the methodology of conducting the project. In the present work, the on the road experimental field test was conducted, in which Toyota C-HR EV has been employed as a testing model. The appearance of the vehicle is shown in Figures 2 and 3. This EV model is based on the improvement of the gasoline version, the appearance is only different from the front face, and there are many more electric-specific logos. Under the conditions of the NEDC, a constant speed of up to 400 km can be achieved on a single charge. This enables it to fully meet the daily transportation needs of most urban users. The battery capacity of Toyota C-HR EV is 54.3 kWh and the energy density is 131 Wh/kg, which can store more energy under the same volume. It provides an average power consumption of 13.1 kWh/100 km, and supports fast charge and slow charge modes with the time consumed at ranges of 50 min and 8h, respectively, for battery power level from 0 to 75%.



Figure 2: Toyota C-HR EV



Figure 3: Chassis structure and battery module of Toyota C-HR EV

Site Survey for Field Test

The test was carried out on the roads in Wuhan, China and its vicinity. The choice of test site should be verified to meet the required parameters of the road conditions, the convenience of charging, and ultimately the road safety.

For the road condition with traffic jams, the congested roads around Jiefang Avenue in Wuhan were chosen. Even the road sections come with 8 two-lane lanes and an overpass, it is still very congested. Figures 4 and 5 illustrate the traffic conditions on site. In terms of charging facility, since it is in the central city, the supporting facilities of charging piles are easily available around. There are about 40 stations located near the test road section, thus there are sufficient supplies for the high and low battery test conditions. Figure 6 shows the location points of the charging stations.



Figure 4: Traffic flow on Jiefang Avenue, Wuhan, China



Figure 5: Map of Jiefang Avenue and its road conditions



Figure 6: Location of the charging stations

For the road with uphill condition, the typical chosen test location is around the mountain. A round-trip road, at Mulan Mountain, with an average gradient of 8% and 14.2 km was chosen. Figure 7 shows the location.

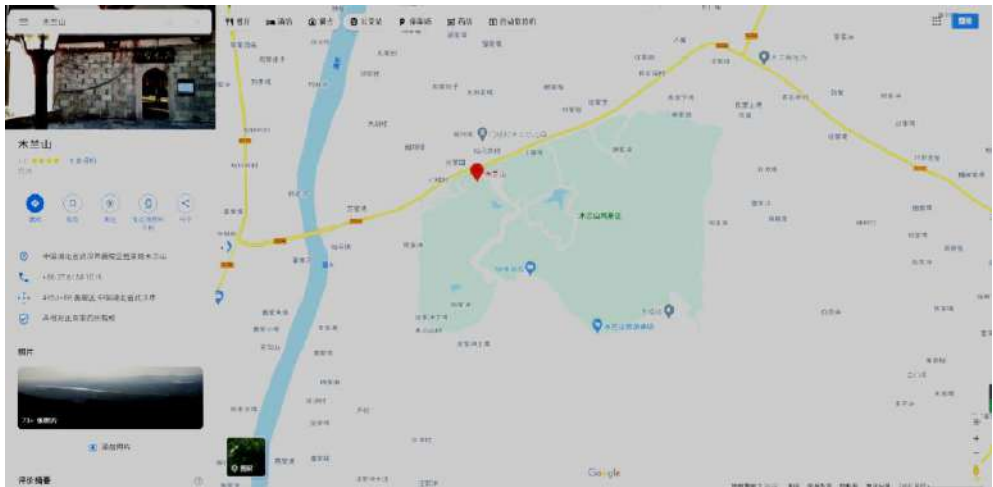


Figure 7: Location of Mulan Mountain

In contrast to the one in the city, as the mountain road in the model is in the suburb with low population density, there are not limited charging stations around. Thus, detailed journey planning is required to meet the charging need to avoid running out of power in the round trip. The location of the charging pile is shown in Figure 8.



Figure 8: Location of the charging stations around Mulan Mountain.

For the highway road condition, it is easily accessible in many town areas. The road speed limit is strictly 70-80 km/h, with an average speed of 73 km/h and a round trip road at 38.3 km. Figure 3.9 shows the location and condition of the highway road. According to the road speed limit regulations of the Traffic Management Bureau of Wuhan Public Security Bureau, the speed limit for highways cannot be over 80km/h, and the speed limit for mountain roads is 40 km/h.

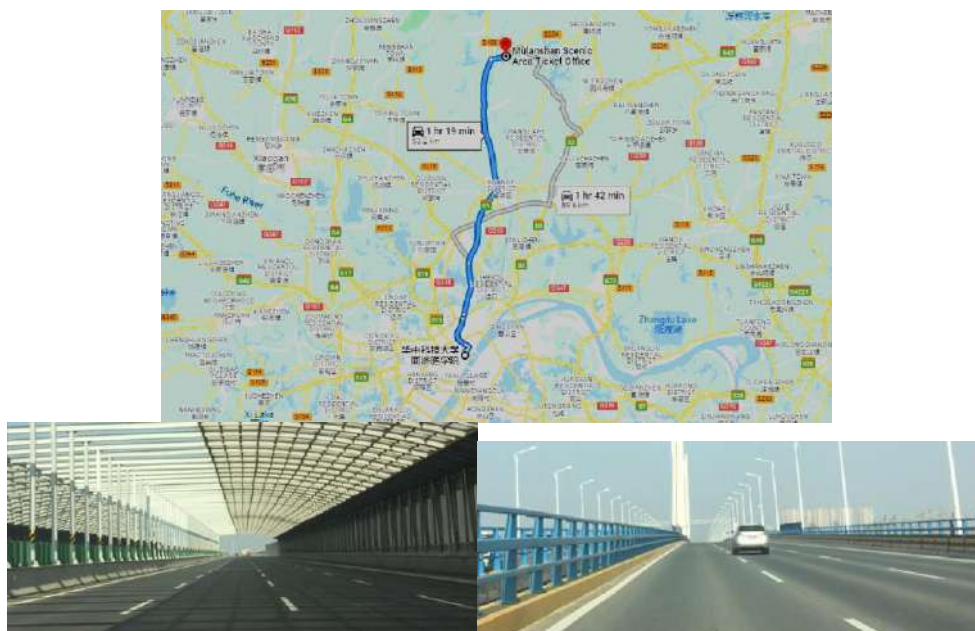


Figure 9: Location and condition of highway road

Experimental Field Test

In order to ensure the consistency of the test, the same person will drive the same car, Toyota C-HR EV, to collect the data of charge level, speed, duration, mileage, road conditions, altitude and surrounding driving conditions. The vehicle is serviced and checked priorly to ensure all systems are operating well. For road safety, the data collection is in the mode of automatic recording or by means of automatic data logging. To enhance road safety, a companion passenger is required to assist in the data collection process and alert the driver if there is any emergency.

The test is only carried out when the weather is clear and there is no strong wind to ensure road safety as well as avoiding added aerodynamic effects on the car. It has been assumed that ambient temperature of the test environment is relatively constant. Due to limited funds and time, under the same type of test conditions, the test was performed twice for the conditions of opening and closing of the air conditioner. In addition, the test was carried out at 2 battery charged conditions, in which when the battery condition is of high level of starting battery charge status ($>70\%$) and low level of starting battery charge status ($<40\%$). This is to note that due to soon exhaustion of the low level of starting battery test, the battery needs to be maintained until the next test session, thus the entire test session needs to be charged multiple times.

Due to the manufacturer's data confidentiality and restriction, the field test data was recorded via the on-screen vehicle data. To obtain the experimental data accurately and manageably, the test time was controlled at 30 minutes. 2 high-definition cameras were used to record the real time energy consumption and the running conditions of vehicles during driving.

Figure 10 shows the set up of cameras and navigators in vehicle.



Figure 10: Set up of cameras and navigator in vehicle

As the charge level reading on-screen is indicated in analog signal with 34 grids, an average prorated calculation has been performed to determine the actual remaining charge level, in which 1 grid is equal to 2.94%. For the data of charging cost and energy, it can be retrieved through the handphone standard charging app, in which the total charging cost, the total power charged, the charging time, and the starting and ending of charging power can be recorded. Refer to Figure 3.11 as an example, the charging bill shows that it has taken 29 minutes to charge from the start of 18% to the end of 81%, using the night electricity price costing RMB 14.25 and charged 17.83 kWh. From the total amount and the amount of charging, the electricity price per kWh of electricity at night can be calculated which is BMB 0.80/kWh.



Figure 11: Charging bill

3. RESULTS AND DISCUSSION

Figure 12 shows the battery charge level under the different road conditions with high level of starting battery charge status ($>70\%$), whereas Figure 13 shows the one with low level of starting battery charge status ($<40\%$). Figure 14 demonstrated the comparison of the amount of change in power charge reduction by between the effect of air conditioner under the different road conditions.

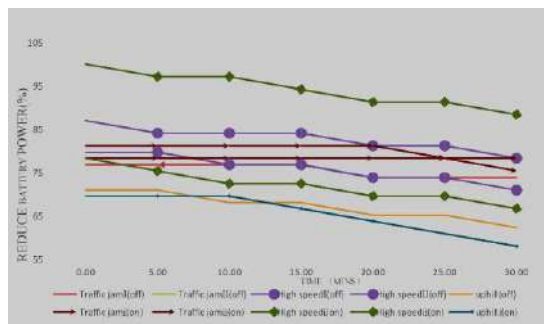


Figure 12: Battery power change under different road conditions (starting battery status of $>70\%$)

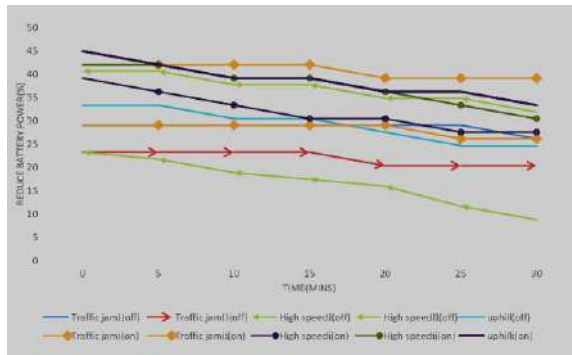


Table 13: Battery power change under different road conditions (starting battery status of <40%)

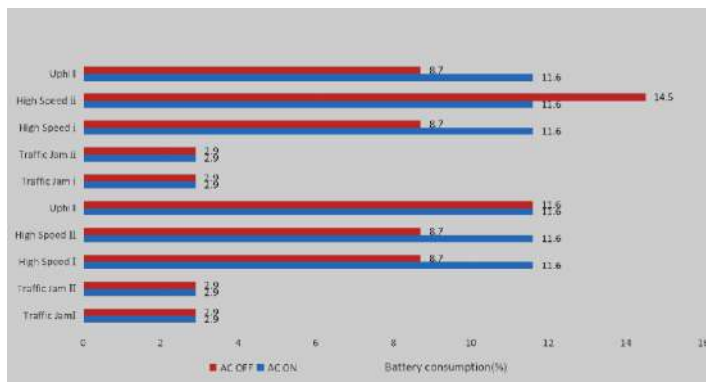


Figure 14: Amount of change in power reduction by AC on and off under different road conditions

By comparing the power consumption of different road conditions at the same time, one can see that the traffic jam road condition consumes the least power, and the power consumption of the highway and uphill sections is almost the same. The low level of starting battery charge status on the highway section consumes the most power. Even when the air conditioner is turned off, the power consumption in 30 minutes reaches 14.5%, which is reduced from 23.2% to 8.7%. The power consumption of the traffic jam section is the same 2.9%, whether the air conditioner is turned on or not, but turning on the air conditioner will reduce the power in advance. As expected, both high-speed and uphill sections with air conditioner turned on have increased the power consumption. Turning on the air conditioner on the highway and the mountain road sections will significantly increase the power consumption, indicating that the air conditioner, as a high-power electrical appliance, has a significant change in the power consumption. Considering that the power consumption and time of the uphill section and the high-speed section are the same, according to the short distance of the uphill section during the test, it can be concluded that the uphill section will consume more power than the high-speed section, even if the speed is not as fast as the high-speed section.

When people use vehicles, it is a norm to consider the daily driving cost. It is

particularly apparent in China as the fuel price is getting more and more expensive. The rise of electric vehicles has driven the growth of the electric energy industry, and the price of national electric tariff is relatively cheaper and stable. In China, the tariff is divided into daytime price and nighttime price.

Tables 1, 2 and 3 tabulated the difference of distance travelled and its corresponding energy consumption and cost under different road conditions of traffic jam, highway and uphill, respectively. Table 4 shows the charging cost per charging energy under the daytime and nighttime tariffs. It can be seen clearly from the table that the cost of charging for electric vehicles is much lower (about RMB 0.11 to RMB 0.44 per kilometer) than the fuel cost for traditional gasoline cars (about RMB 0.70 to 1.00 per kilometer). It denoted that EV has obvious advantages under the China pricing system.

The results indicated the cost per distance at highway is the lowest, whereas at the mountain road with air conditioner on is the highest. Typically, air conditioning resulted in a higher cost. However, the present data indicated that the air conditioner did not affect the energy consumption under the traffic jam condition. It could be caused by the regenerative braking energy mechanism that has compensated for part of the energy consumed by the air conditioner. In the actual test, electric vehicles typically use the public charging piles, and the average unit price can be ranging RMB 0.63 to RMB 1.33 per kWh.

Table 1: Difference of distance travelled and its corresponding energy consumption and cost on traffic road condition.

Mode	Distance Travelled (km)							Power Consumption (kWh)	Cost per km	
	0	0.8	1.6	2.4	3.6	4.2	5.0		Day Price (RMB)	Night Price (RMB)
AC OFF	76.8	76.8	76.8	76.8	73.9	73.9	73.9	1.57	0.371	0.223
	29	29	29	29	29	29	26.1	1.57	0.371	0.223
AC ON	81.2	81.2	81.2	81.2	78.3	78.3	78.3	1.57	0.371	0.223
	42	42	42	42	39.1	39.1	39.1	1.57	0.371	0.223

Table 2: Difference of distance travelled and its corresponding energy consumption and cost on highway road condition.

Mode	Distance Travelled (km)							Power Consumption (kWh)	Cost per km	
	0	5	10	15	20	25	30		Day Price (RMB)	Night Price (RMB)
AC OFF	79.7	79.7	76.8	76.8	73.9	73.9	71	4.71	0.185	0.111
	23.2	21.7	18.8	17.4	15.9	11.6	8.7	7.85	0.308	0.185
AC	78.	75.	72.	72.	69.	69.	66.	6.28	0.247	0.148

ON	3	4	5	5	6	6	7			
	39.1	36.2	33.3	30.4	30.4	27.5	27.5	6.28	0.247	0.148

Table 3: Difference of distance travelled and its corresponding energy consumption and cost on uphill road condition.

Mode	Distance Travelled (km)							Power Consumption (kWh)	Cost per km	
	0	5	10	15	20	25	30		Day Price (RMB)	Night Price (RMB)
AC OFF	33.3	33.3	30.4	30.4	27.5	24.6	24.6	4.71	0.327	0.197
AC ON	44.9	42.0	39.1	39.1	36.2	36.2	33.3	6.28	0.436	0.262

Table 4: Charging Cost

Sample	Charging energy (kWh)	Charging Times	Cost (RMB)	Cost/ Charging Energy (RMB/kWh)	Remarks
1	10.08	54' 48''	13.37	1.326	Daytime price
2	15.95	25' 12''	18.02	1.130	Daytime price
3	7.69	17' 32''	9.69	1.260	Daytime price
4	6.71	17' 00''	7.91	1.179	Daytime price
5	5.15	14' 25''	5.19	1.008	Daytime price
6	15.14	53' 4''	9.51	0.628	Night Price
7	17.83	29' 40''	14.25	0.799	Night Price
Total	78.55	211' 41''	77.94		

4. CONCLUSION

The experimental field test of the discharge rate of the battery and the economic aspect of the EV under the different on-the-road driving modes have been demonstrated and assessed. The findings showed that when the air conditioner is turned on, the discharge rate of battery under the highway and uphill road conditions is almost the same. Turning on the air conditioner on the highway and the mountain road conditions will significantly increase the power consumption. The present data indicated that the air conditioner did not affect the discharge rate under the traffic jam condition, which could be due to the regenerative braking energy mechanism that has compensated part of the energy consumed by the air conditioner. Besides, it has been discovered that driving in the mountains is unfavourable for EV as there are typically less charging stations in the mountain area. Under the China pricing system for EV, it is obvious that the “fuel cost” for EV is much lower than the traditional petrol vehicles, promoting the popularity of EV in China.

REFERENCES

- IEA analysis based on country submissions, complemented by ACEA (2021); CAAM (2021); EAFO (2021); EV Volumes (2021) and Marklines (2021).
- Traveset-Baro O, Rosas-Casals M, Jover E. Transport energy consumption in mountainous roads. A comparative case study for internal combustion engines and electric vehicles in Andorra. *Transportation Research Part D: Transport and Environment*, 2015;34:16-26.
- He Z, Gao M, Wang C, Wang L, Liu Y. Adaptive state of charge estimation for li-ion batteries based on an unscented kalman filter with an enhanced battery model. *Energies*. 2013;6:4134-4151.
- Kambly KR, Bradley TH. Estimating the HVAC energy consumption of plug-in electric vehicles. *J. Power Sources*. 2014;259:117 –124.
- Liu K, Wang JB, Yamamoto T, Morikawa T. Modeling the Multilevel Structure and Mixed Effects of Influence Factors on Energy Consumption of Electric Vehicles. *Applied Energy*, 2016; 183(1):1351-1360.
- Smith, W.J., 2010a. Plug-in hybrid electric vehicles—a low-carbon solution for Ireland. *Energy Policy* 38, 1485 –1499.
- Tzirakis, E., Pitsas, K., Zannikos, F., Stournas, S., 2006. Vehicle emissions and driving cycles: comparison of the Athens driving cycle (ADC) with ECE- 15 and European driving cycle (EDC). *Glob. Nest J.* 8, 282 –290.
- Wu XK, Freese D, Cabrera A, Kitch WA. Electric vehicles' energy consumption measurement and estimation. *Transp Res D Transp Environ.* 2015;34:52 –67.
- Cuma MU, Koroglu T. A comprehensive review on estimation strategies used in hybrid and battery electric vehicles. *Renew Sustain Energy Rev.* 2015;42:517 –31.

LINEAR STATIC ANALYSIS AND PERFORMANCE OF LOWER SUSPENSION ARM USING FINITE ELEMENT METHOD

**Muhammad Fahmi Md Isa, Araoye Ibrahim Oyeyemi, Ida Rasyada Daud
& Norhaslina Abdul Aziz**

Infrastructure University of Kuala Lumpur

1. INTRODUCTION

The function of the suspension system is to reduce the vibrations that transmit to occupant due to rough terrains or road disturbances and to provide stability during accelerating, cornering and braking. The suspension arm is responsible for the up and down movement of wheels when hitting bumps. It is also designed to maximize the friction between tire contacts, patch the road surface to provide vehicle stability under any circumstances. It can be seen in many types of the suspensions like wishbone or double wishbone suspensions. It is also called an A-type control arm. In this chapter, the control arm was reverse-engineered. This refers to the process of obtaining the Computational Aided Design (CAD) model from an existing article. The CAD model is developed using SolidWorks software and the linear static analysis is conducted using same software. The model is subjected to loading and boundary conditions and then analysed using the Finite Element Analysis (FEA) techniques. The static structural analysis was done to find out the stress, deformation, and safety factor of the component. The model was meshed using 10-noded tetrahedral elements. The result obtained from the analysis were studied to check whether the design is safe or not. In some cases, the stresses become more than the safe limit. In that case optimization approach is carried out to increase the structural strength of the component concerning weight with three different materials (AISI 1040, AISI 1018, AISI 4130).

According to Jagwinder Singh & Siddhartha Saha (2018), the lower suspension arm is connected to the vehicle frame with bushing and permits the wheel to go up and down in response to the road surface. The control arm is the most crucial part of the suspension system. It is made from materials like steel, iron, or aluminium. The suspension arm is very important for all vehicles on the road, if there is no suspension arm in the suspension system, then it is expected that it can result in annoying vibrations and unwanted driving irregularities that could sometimes lead to road accidents like collisions with another car or obstruction on the road. The suspension arm is one of the most important components of the suspension system. It is fitted in various types of the suspensions like Macpherson, wishbone, or double wishbone suspensions. During actual working conditions, the maximum load is transferred from the tire to the ball joint in the Macpherson strut system and the double-wishbone maximum load is transferred from the upper arm to the lower arm which is responsible for the failure and twisting of the lower suspension arm at the ball joint locations as well as control arm because of more impact load. Hence it essential to focus on the stress and deformation study of the lower suspension arm to develop and the changes in the existing design. The Finite Element Analysis (FEA) approach is

used for the analysis of a suspension link for static and Von-Mises stress analysis of the lower suspension arm. An analysis is to be done considering the Gross vehicle weight. As stress is higher than the safe limit or yield strength some geometric changes are adopted in design to make it safe.

According to D. Kothawale (2013), the main function of the lower control arm is to manage the motion of the wheels & keep it relatively to the body of the vehicle. The control arms hold the wheels to go up and down when hitting bumps. Chassis parts are a critical part of a vehicle, leaving no room for error. As a vehicle goes through speed breaker, bumps, etc., and many other kinds of forces transmitted from the car wheels which are transmitted to the control arm via ball joint assembly to the wheel. Force values are mentioned in the load case. So, in this case, the key concern is to discover the maximum stress section and stress value in the control arm and relate these values with the tensile yield strength of the material. The aim of this study are to develop a 3D suspension arm model by using Solidwork software and to predict de behaviour of conventional suspension arm on linear static analysis using finite elements method. The result will be analysed and compare the effect of materials on Von-Misses stresses and performance of the suspension arm using Finite Element Method.

2. LITERATURE REVIEW

The suspension system is always derived in some mechanical way. Generally speaking, the designs of the suspension systems are classified into two main groups such as dependent suspension system (solid axle) and independent suspension system. The dependent suspension system is the system in which two wheels (front or rear) are connected by one continuous rod called a trailing rod. In this system, if any bump or potholes disturb one wheel automatically pair wheel also affected because of the trailing rod. The trailing rod is shown by the arrow in Figure 1.



Figure 1: Early Suspension system [Online image] (1912). Retrieved from <https://www.precisioncarrestoration.com>.

An independent suspension allows wheels to rise and fall on their own without affecting the opposite wheel. In this case, the wheels are connected through universal joints with a swing axle. Suspensions with other devices, such as sway bars that link the wheels in some way are still classed as independent. The independent suspension system (front view) is shown in Figure 2.

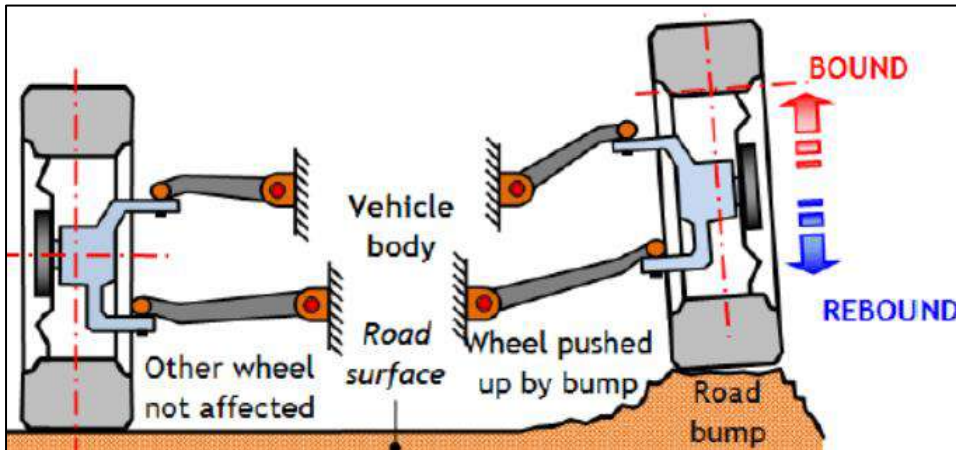


Figure 2 The independent suspension system (front view). (Živković, V., Nedić, B., & Đurić, S. (2020).

There are two important types of independent systems such as Macpherson Strut and Double Wishbone system. The double-wishbone suspension can also be referred to as double 'A' arms, and short-long arm (SLA) suspension if the upper and lower arms are of unequal length. A single wishbone or A-arm can also be used in various other suspension types, such as the McPherson strut and Chapman strut. The upper arm is usually shorter to induce negative camber as the suspension jounces (rises). When the vehicle is in a turn, body roll results in positive camber gain on the inside wheel. The outside wheel also jounces and gains negative camber due to the shorter upper arm. This is especially important for the outer tire because of the weight transfer to this tire during a turn. The double-wishbone is shown in Figure 3.

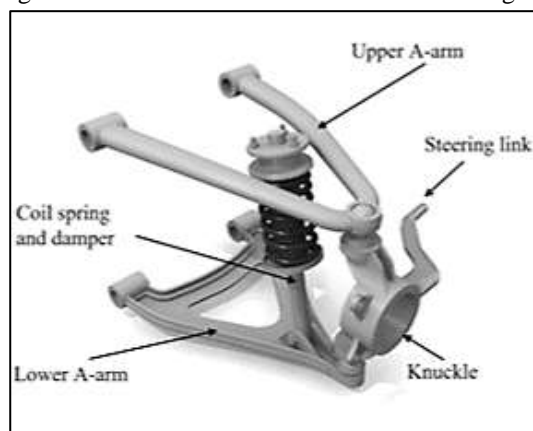


Figure 3. The double-wishbone suspension system (Arikere, A., Saravana Kumar, G., & Bandyopadhyay, S. (2010)).

For a rear suspension, a pair of joints can be used at both ends of the arm, making them more H-shaped in plain view. Alternatively, a fixed-length driveshaft can perform the function of a wishbone as long as the shape of the other wishbone provides control of the upright. The suspension is a 4-bar link, and it is easy to work out the camber gain see camber angle and other parameters for a given set of bushing or ball joint locations. The trailing arm system is literally that a shaped suspension arm is joined at the front to the chassis, allowing the rear to swing up and down Sridharan, M., & Balamurugan, S. (2016). Pairs of these become twin-trailing arm systems and work on the same principle as the double wishbones in the systems described above. Trailing arm suspension is shown in Figure 4.

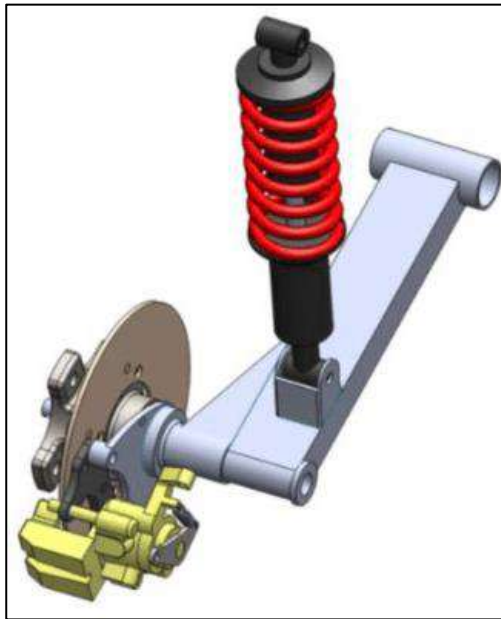


Figure 4: The trailing arm suspension system. (Huang, H. H., & Chen, S. L. 2019).

The difference is that instead of the arms sticking out from the side of the chassis, they travel back parallel to it Kothawale, D., Kharde, Y. R., & Rahata, T. (2013). This is an older system not used so much anymore because of the space it takes up, but it doesn't suffer from the side-to-side scrubbing problem of double wishbone systems. If you want to know what I mean, find a VW beetle and stick your head in the front wheel arch - that's a double-trailing- arm suspension setup. The McPherson strut is a type of car suspension system which uses the axis of a telescopic damper as the upper steering pivot, widely used in modern vehicles and named after Earle S. McPherson who developed the design. Macpherson struts suspension is shown in Figure 5.

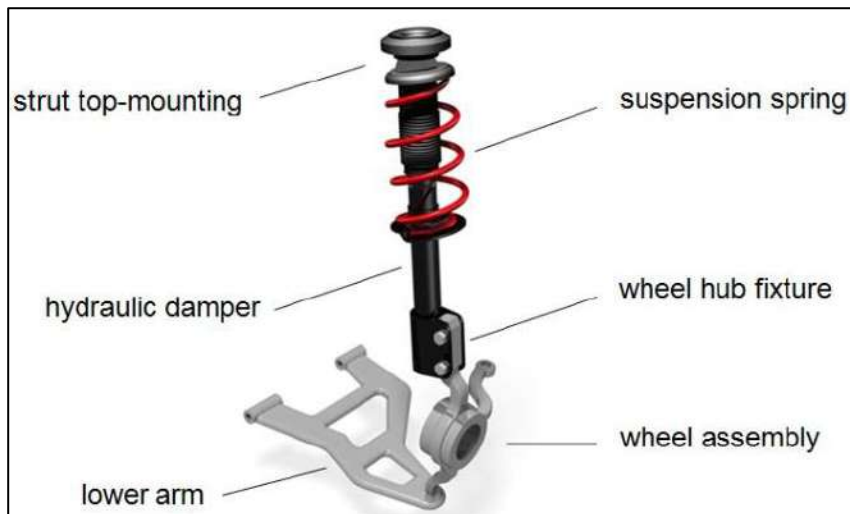


Figure 5: Schematic view of a McPherson front strut suspension system Czop, P. (2011)

The McPherson strut required the unibody construction because it needs a substantial vertical space and a strong top mount, which unibodies can provide while benefiting them by distributing stresses. The strut will usually carry both the coil spring on which the body is suspended and the shock absorber, which is usually in the form of a cartridge mounted within the strut. The strut also usually has a steering arm built into the lower inner portion. The whole assembly is very simple and can be preassembled into a unit; also, by eliminating the upper control arm, it allows for more width in the engine bay, which is useful for smaller cars, particularly with transverse-mounted engines such as most front wheel drive vehicles have. It can be further simplified, if needed, by substituting an anti-roll bar (torsion bar) for the radius arm. For those reasons, it has become almost ubiquitous with low-cost manufacturers. Furthermore, it offers an easy method to set suspension geometry.

3. METHODOLOGY

The methodology initiates with a detailed theoretical study of A-Type lower suspension arm utilized in cars followed by modelling of the lower suspension arm in SolidWorks software from the particular component. Then a validation of simulation results from the SolidWorks model and the results are compared, if the results are satisfied then the problem is solved and if not then editing of the model is done.

Preliminary research was conducted to determine the most suitable component for this project. To identify the design requirements for the sake of modelling the 3D component on the software. A 2D model was revised, selecting the material and boundary conditions for analysis which consist of AISI 1040 AISI 1018 and AISI 4130. The boundary condition such as the loads and constraints are applied to run the linear static analysis.

Figure 6 show a 3D structure of the lower control arm is developed using CAD modelling software supported measurements from the particular component. The particular model was manufacture as per Design by using AISI 1040 material. The finite element modelling and analysis are performed by using SOLID WORKS software. Mesh was created with a 10-node tetrahedral element. Tetra elements give improved results as compared to other types of elements; therefore, tetrahedral elements were used. Analysis of the A-type lower suspension arm is required to find out the maximum stress (weaker section) and maximum deflection in the arm. Maximum stress and deflection in the LSA can be found by using the software.

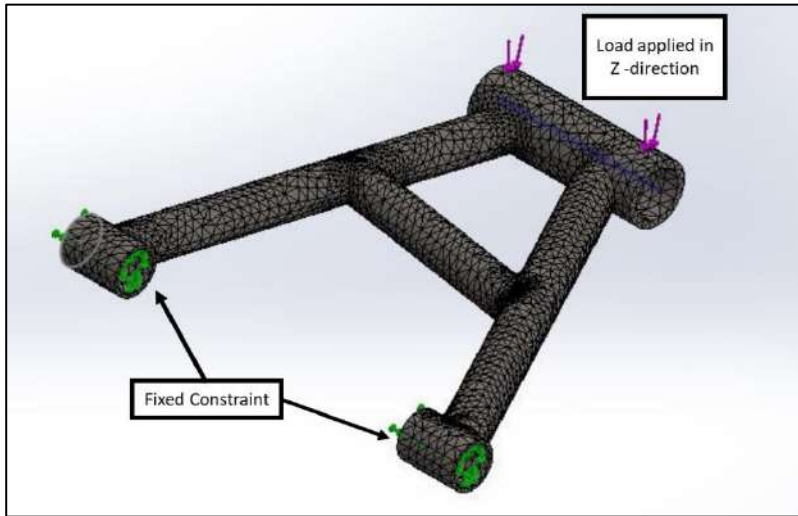


Figure 6: Boundary condition for numerical study.

The vehicle of total mass 2300 kg and at a constant speed of 30 km/hr., we can calculate the load on one wheel of the vehicle which will be the weight on the lower suspension arm of the front wheel. The static load on the front axle can be calculated using Eq. 1

$$G_{RAW} = G_{RA} / 2 \quad (\text{Eq.1})$$

where G_{RAW} is static load on rear wheel and G_{RA} represent load on the rear axle.

From theoretical analysis, the load at the front wheel suspension can be determined. The bush connected to the chassis is considered as the constraint and the total load is applied on the wheel hub bush in the downward direction.

A stress calculation For AISI 1040 material, allowable stress is obtained by using Eq.2 Assume factor of safety equal to 1.2 as is a ductile material.

$$\sigma = S_{yt}/FS \quad (\text{Eq. 2})$$

where S_{yt} represent the yield strength for material and FS is factor of safety.

The value of allowable stress value 345.83 MPa. The designed wishbone is safe when the induced stress is lesser than the allowable stress value. The allowable stress is determined using

SOLIDWORKS software. From theoretical analysis, the load at the front wheel suspension can be determined. The bush connected to the chassis is considered as the constraint and the total load is applied on the wheel hub bush in the downward direction.

4. DISCUSSION

The results and discussion of some criteria for design and finite element analysis of lower suspension arm which was modelled using Solid works software. By conducting theoretical calculations, the load on one wheel of the vehicle which will be the weight on the lower suspension arm of the front wheel can be determined. Further analysis will be considered to determine the load on the lower suspension arm. Theoretically, the result shows the load on the front wheel is 4997.8715 N and for the rear wheel it's 282.6284 N. Our interest is within the front wheel, for further analysis, we consider the load on lower suspension arm as 4997.8715 N. Thus, the load of exert on the lower suspension arm is assume as 5000 N.

The meshed model is analysed within the component under the load of 5000 N and considering all the boundary conditions and every one parameter. The Von-Misses Stress for AISI model is shown Figure 7. The design stress-induced in the arm should be less than the yield strength of the material. The stress found using this alloy is 283 MPa considering AISI 1018 alloy. The stress found using this alloy is 325MPa. And the stress found using AISI 4130 alloy is 460MPa.

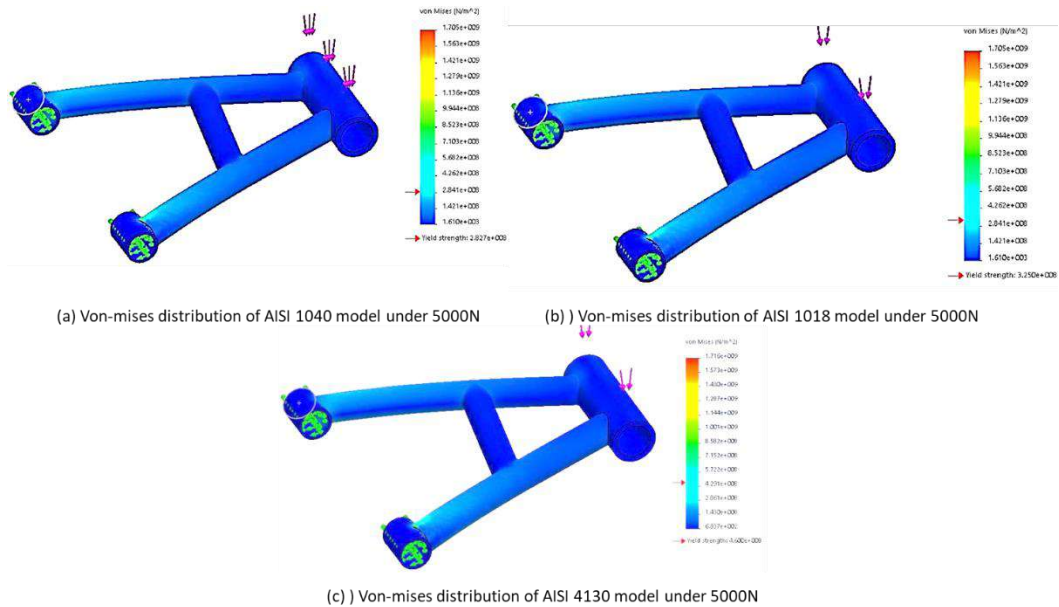


Figure 7: Von mises distribution of AISI 1040, AISI 1018 and AISI4130 model under 5000N.

Figures 8 below show the deflection of the lower control arm using AISI 1040, AISI 1018, and AISI 4130 alloy. The total deformation shows at what stage the component will deflect from its original position. The total deformation of the LSA should be within the limits and the total deformation found in the analysis are 4.12mm, 4.117mm, and 4.117mm

respectively for AISI 1040, AISI 1018, & AISI 4130 alloys.

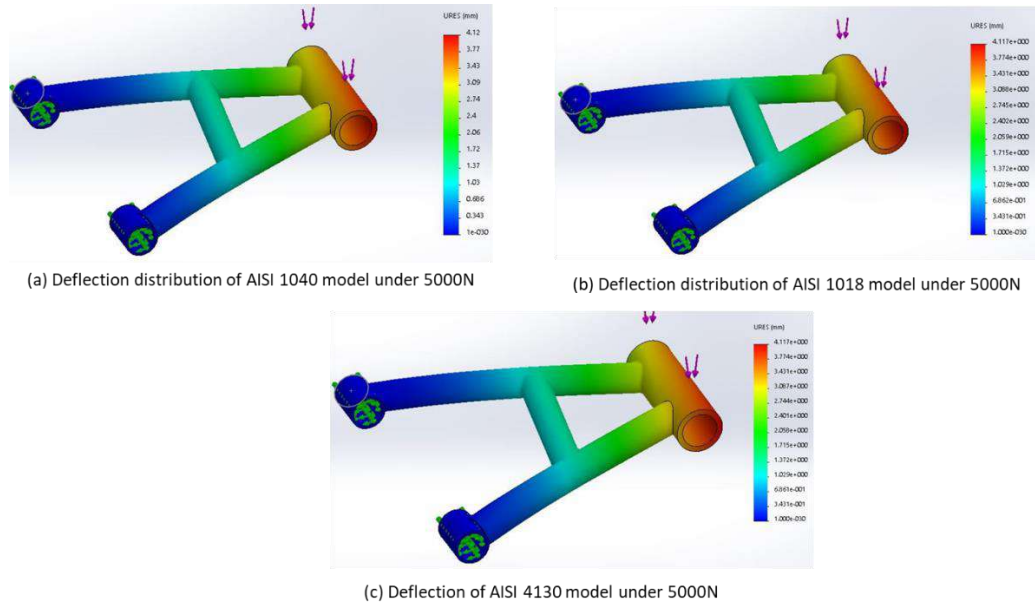


Figure 8: Deflection distribution of AISI 1040, AISI 1018 and AISI4130 model under 5000N.

The result summary from Table 1, gives details of the stress and deflection of the control arm. The analysis is conducted with the necessary load and boundary conditions that occur during the turning of the vehicle. The stresses in these cases i.e load case1 considering the AISI 1040 steel material, load case 2 considering AISI 1018 material, and load case3 considering AISI 4130 material. Deflection wise they are almost the same but the maximum stresses are different. The design is safe only if the maximum stress of the model falls under the allowable stress load. Here it is seen that AISI 1018 & AISI 1040 fall under this category and as our benchmark material AISI 1040 is safer because the maximum stress is less than the yield strength of the material.

Table 1: Results of the analysis of A-type LSA in FEA

Parameters	AISI 1040	AISI 1018	AISI 4130
Maximum Stress (MPa)	283	325	460
Maximum Deflection (mm)	4.117	4.117	4.117
Yield Strength (MPa)	415	370	460
Allowable stress (MPa)	345.83	308.33	383.33

The results and discussion of some criteria for design and finite element analysis of lower suspension arm which was modelled using Solidworks software. Selected the 10 nodes meshing as it gives better results for cylindrical and curved shaped faces. After meshing, a load of 5000N was applied on hub bush, and the weaker section in the model was found. The maximum stress in model 1 which is AISI 1040 was 283 MPa and the deflection is 4.117mm. As the allowable stress for this material is 345.83MPa, it means that the design is safe under such loading. To

verified the FEA results, a typical A-type suspension arm of materials AISI 1018 & AISI 4130 was considered. The results from the comparison test indicated that all three materials had the same deflection but different stress values. It was also observed that AISI 4130 could not meet the design specifications because its maximum stress was higher than the allowable stress. And in the case of AISI 1018, its allowable stress is very small hence, AISI 1040 is the most suitable.

5. CONCLUSION

In conclusion, the stresses of the material for the given loading and boundary conditions fall within the yield strength 283 MPa for AISI 1040. The total deformation due to the force applied on the suspension arm was 4.117mm which is maximum at the ball bearing of the suspension arm. Strength wise the chosen material is good but the design is also based on the cost of fabrication, safety, and low weight then AISI 1040 is the better choice. Thus, the model of the A-type lower suspension arm is safe under working conditions.

The control arm parameter has a great influence for vehicles on the road. It provides comfort and stability. Without the control arm, the vehicle is expected to cause significant vibrations and may lead to the noise. This also experiences maximum load which is transferred from the upper arm to the lower. To generate stress evaluation, simulation is conducted to determine stress concentration and maximum stress value. In this project, it is found that the stress analysis for considering lower arm deformation, von-mises stress and maximum shear stress and also using different lower arm materials were tested and it was observed that AISI 1040 material was much better than AISI 1018 and AISI 4130 material. Further research on the proposed material can be done using experimental approach or to optimize the shape of the control arm.

REFERENCES

- Dattatray Kothawale, Dr. Y.R. Kharde, (2013) "Analysis of Lower Control Arm in Front Suspension System Using FEA Approach" Internationals Journals of Engineering Research and Development 2013.
- Noname. Early Suspension system [Online image] (1912). Retrieved January 10, 2020, from <https://www.precisioncarrestoration.com/automobile front suspension> .
- Živković, V., Nedić, B., & Đurić, S. (2020). Manufacturing Specificity of Vehicle's Independent Suspension System Parts. *Mobility & Vehicle Mechanics*, 46(1), 31-41.
- Arikere, A., Saravana Kumar, G., & Bandyopadhyay, S. (2010, December). Optimisation of double wishbone suspension system using multi-objective genetic algorithm. In *Asia-Pacific Conference on Simulated Evolution and Learning* (pp. 445-454). Springer, Berlin, Heidelberg.
- Sridharan, M., & Balamurugan, S. (2016). Design and analysis of lower control ARM. *International Journal of Innovative Research in Science, Engineering and Technology*, 5(4), 6510-6528.
- Huang, H. H., & Chen, S. L. (2019). Effect of compliant linkages on suspension under load. *Mechanical Sciences*, 10(2), 505-516.

Analysis of lower control arm in front suspension system using FEA approach. Internationals Journals of Engineering Research and Development.

Czop, P. (2011). Application of an inverse data-driven model for reconstructing wheel movement signals. Metrology and Measurement Systems, (3).

RUNNER SIZING ON CAVITY FILLING IN PLASTIC INJECTION MOULDING

**Abdulrahman Adil Elhag Eltahir, Yap Ai Kin, Ida Rasyada Daud &
Mohd Shahrudin Mohd Alias**

Infrastructure University Kuala Lumpur

1. INTRODUCTION

Plastic injection moulding is a process of melting plastic pellets become malleable adequately, are injected at pressure into a mould cavity, which fills and solidifies to produce the final product. Typically, it is used as a mass production tool to manufacture high-volume of identical parts and is known for being low cost, high precision, high productivity and the ability to produce complex products (Lan, 2015). Due to plastic injection moulding's manufacturability and high versatility, it has many applications across different industries. Particularly, custom plastic molds present significant advantage to numerous types of businesses by being designable to match the client specifications and design requirements exactly. Experienced and qualified plastic injection moulding manufacturers can exploit this method of customizing moulds to produce products of a variety of shapes and sizes. Plastic injection moulding is applied not only in industries such as consumer electronics, pharmaceutical and medical industry, automotive industry and also is extended to other industries such as aerospace, building and construction, and household articles.

The controls of the quality of the plastic parts produced in injection moulding generally can be distinguished to part design, mould design, operation process parameters and material characterises. Additionally, the four basic operations of the injection moulding process are complex and require numerous distinct techniques to reduce the scrap and improve the quality of parts. Runner system is one of the important sections in mould design in order to produce high quality of part. Ideally, the runner system should drive the plastic melt into the cavity of a mould with the shortest way possible and with the least amount of heat loss and pressure loss feasible. Additionally, molten plastics must enter a cavity (or cavities) at all gates at the same time with an equal pressure and temperature. This chapter is to investigate the correlation between the runner sizing design on the part's quality through the simulation analysis on the filling of cavity in injection moulding.

2. CAVITY FILLING IN INJECTION MOULDING

Typically, an injection moulding procedure covers four basic operations: (1) the heating of the plastic in the injection moulding machine which allow it to flow under pressure; (2) the injection of the molten plastic into a mould cavity or cavities that of which are defined by two mould halves that have been closed; (3) the cooling and hardening of the plastic in the cavity or cavities while under pressure; and (4) the ejection of the part by opening the two mould halves.

According to Zhou, 2013, there are three successive stages in injection moulding that involve the filling of the cavity: filling, packing/holding and cooling. The filling stage is the molten plastic resin injected into the mould cavity and the plastic melt is forcibly pushed through the cavity by the injection moulding machine so that the plastic resin can reach the location in the cavity that is furthest away from the gate. The injected molten plastic is then followed with the packing/holding stage under pressure in the mould cavity, to be hardened and cooled. Additional amount of polymer is forced into the cavity to compensate for the injected molten plastic shrinkage during the cooling stage which solidifies the part enough to make it be able to be ejected that effectively duplicates the cavity shape of the mould. The ensuing length and wall thickness of the final part is a resemblance of the shape of the mould cavity.

The required injection pressure to complete the filling stage is connected to various factors such as material, mould design, and operation process parameters. As illustrated in Figure 1, the injection pressure decreases along the feed system until the end of cavity filling stage.

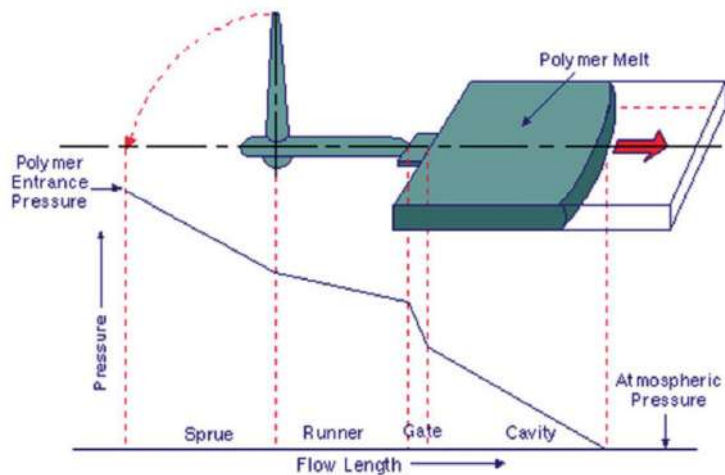


Figure 1: Pressure decrease along the feed system, (Zhou, 2013)

Viscosity becomes higher when the polymer becomes colder, making cavity filling harder. It is easier for molten plastic with higher temperature to fill the cavity; however, it requires more time to cool down. Consequently, it may be more efficient to inject the material into the cavity with the lowest feasible temperature. After the filling of the cavity, packing and holding stages take place, during of which the pressure increases and reaches its peak as shown in Figure. 2.

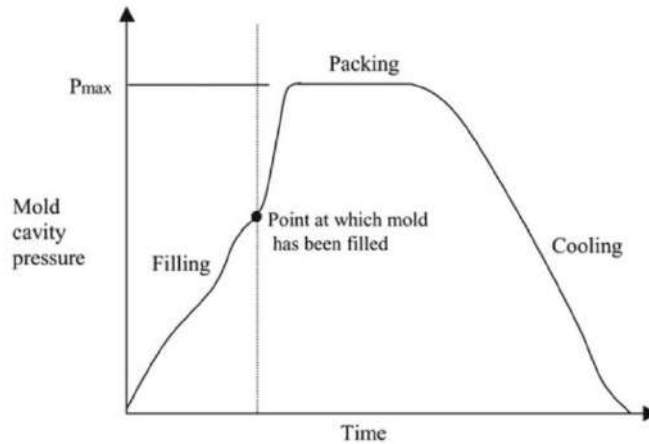


Figure 2: Pressure along the processes (Zhou, 2013)

It consists of the starting or switchover point and the end point (the end of the holding pressure employed by the machine). The necessary needed time at this stage can be varied by the selected material and the cooling rate. Throughout the course of this stage, the material’s temperature goes down and hardens. However, the material flow is still going on at a slower rate due to partial solidification, material shrinkage and any material loss in that specific volume. Lastly, for the duration of the cooling stage, cooling initiates starting from the first stage of the injection, i.e., filling, and continues until the ejection. Thus, according to Zhou 2013, the release of residual stresses can have an effect on the shrinkage and warpage of the injected parts.

3. RUNNER SYSTEM

Figure 3 shows a schematic of the sprue, runner and gate. The sprue, the primary path through by the molten plastics flow into the mould, followed with the runner and finally goes through the gate to fill up the cavity which is the part shape. The sprue, the runner, and the gate will be discarded after a part is complete. However, the runner and the gate are important items that affect the quality or the cost of parts.

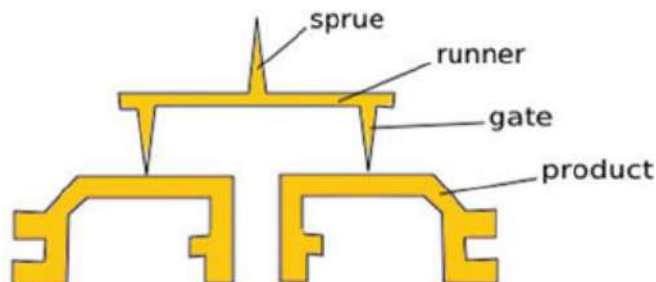
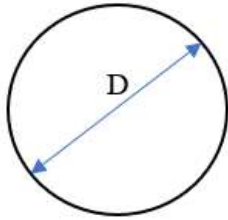
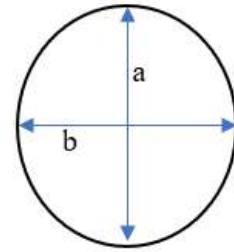


Figure 3: Sprue, runner and gate diagram. (Mehdi, 2019)



Round cross section



Elliptical cross section $b = 0.8a$

There are 3 main factors to be considered in the design of runner system which are cross-sectional shape, diameter and cavity layout. According to the rules set by Jones, 2008, runners should be designed to fill the cavity as fast as possible. Smaller runners are favoured over larger ones because they can reduce scrap and increase the frictional heating which helps in raising the melt temperature. The cross-sectional area of runner cannot be smaller than cross sectional area of sprue and the runner diameter is recommended to be no less than 1.5mm.

4. METHODOLOGY

In order to investigate the correlation between the runner sizing in the cavity filling, two different runner cross-sections were tested, that are circular/round and ellipse shape. The sizes chosen were adopted from the mould design book which are based on the material selected which was Polypropylene. Three sizes were picked for each cross-section, resulting in six testing models in total. The testing models were named based on size from small to big as RS1, RS2 and RS3, while for the elliptical as ES1, ES2 and ES3. The sizes are 4.8mm, 7.2mm and 9.6mm for the round shape while the ellipse has the same sizes for the major axis but with a 0.8 ratio for the minor axis as illustrated in Figure 4 and the detailed of testing models in Table 1.

Figure 4: Runner cross-sections tested

Table 1: Six testing models of round and elliptical shape of runner

Model	Round Shape (RS)	Model	Elliptical Shape (ES)
RS1	D1= 4.8 mm	ES1	a = 4.8 mm b = 0.8(4.8) = 3.84 mm
RS2	D2 = 7.2 mm	ES2	a = 7.2 mm b = 0.8(7.2) = 5.76 mm
RS3	D3 = 9.6 mm	ES3	a = 9.6 mm b = 0.8(9.6) = 7.68 mm

The sprue length is adopted from the research carried out by Mehdi, 2019, in which the length of the sprue was determined to be 60 mm while the sprue diameter is based on the recommendations given by Jones, 2008 whereby the top diameter of the sprue as 2.7 mm, and

bottom diameter as 4 mm. The dimension of gate was referred to the size suggested by Mehdi, 2019, with the length of 1.25mm and diameter of 1.83mm. The feed schematic diagram is illustrated in Figure 5 and the geometry sizes are as detailed in Table 2. Figure 6 shows the CAD modelling of feed system designed in the project, which consists of sprue, runner and gate

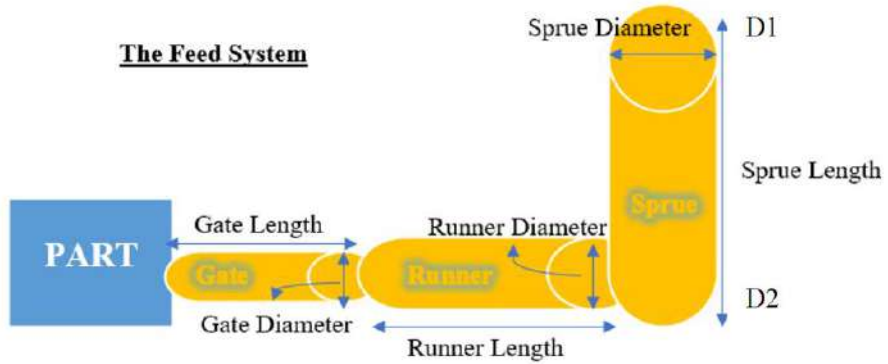


Figure 5: Schematic diagram of feed system

Table 2: The detailed dimensions of sprue and gate

Component	Length	Diameter
Sprue	60 mm	Top diameter = 2.7 mm Bottom diameter = 4 mm
Gate	1.25 mm	1.83 mm

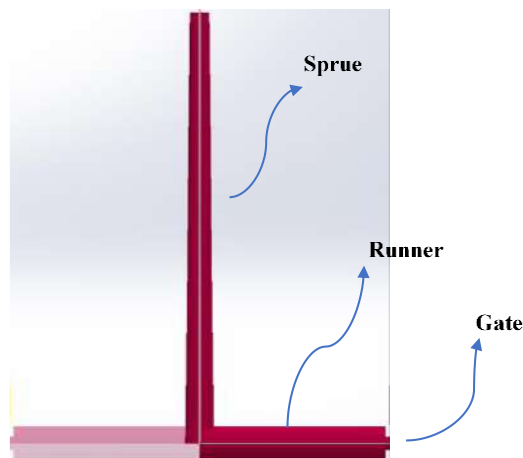


Figure 6: Feed system designed in CAD

A disposable spoon was used as a testing part modeling to investigate the effect of the size variability. The spoon was designed and modelled in SolidWorks Modeling, while the simulation was conducted using SolidWorks Plastics. Several parameters were investigated such as filling time, cooling time, injection pressure and sink mark. The disposable spoon was designed in two cavities with 2mm thickness and 154mm length as shown in Figure 7.

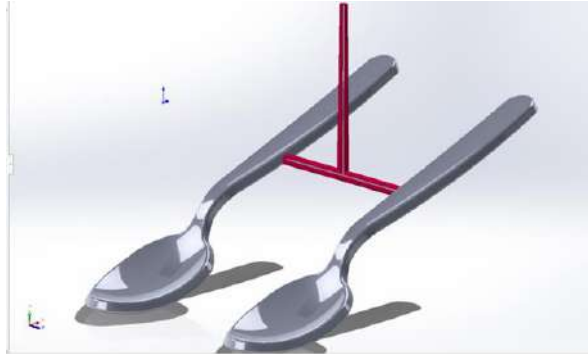


Figure 7: Two cavities of disposable spoon in the mould design

5. RESULTS & DICUSSION

Six modelling of two cavities disposable spoon attached with its feed system in different of runner sizes were simulated in Solidworks Plastic to analyze the flow of plastic melted in the mould cavity. The output parameter that was studies are the filling time (s), maximum injection pressure (MPa), maximum cooling time (s) and sink mark (mm) in related with the runner size and cross section. The simulation results for each model were recorded. Figure 8 shows one of the models' flow simulation results produced from the Solidworks Plastic. Table 3 summarizes all the data collected from the simulation results for six models.

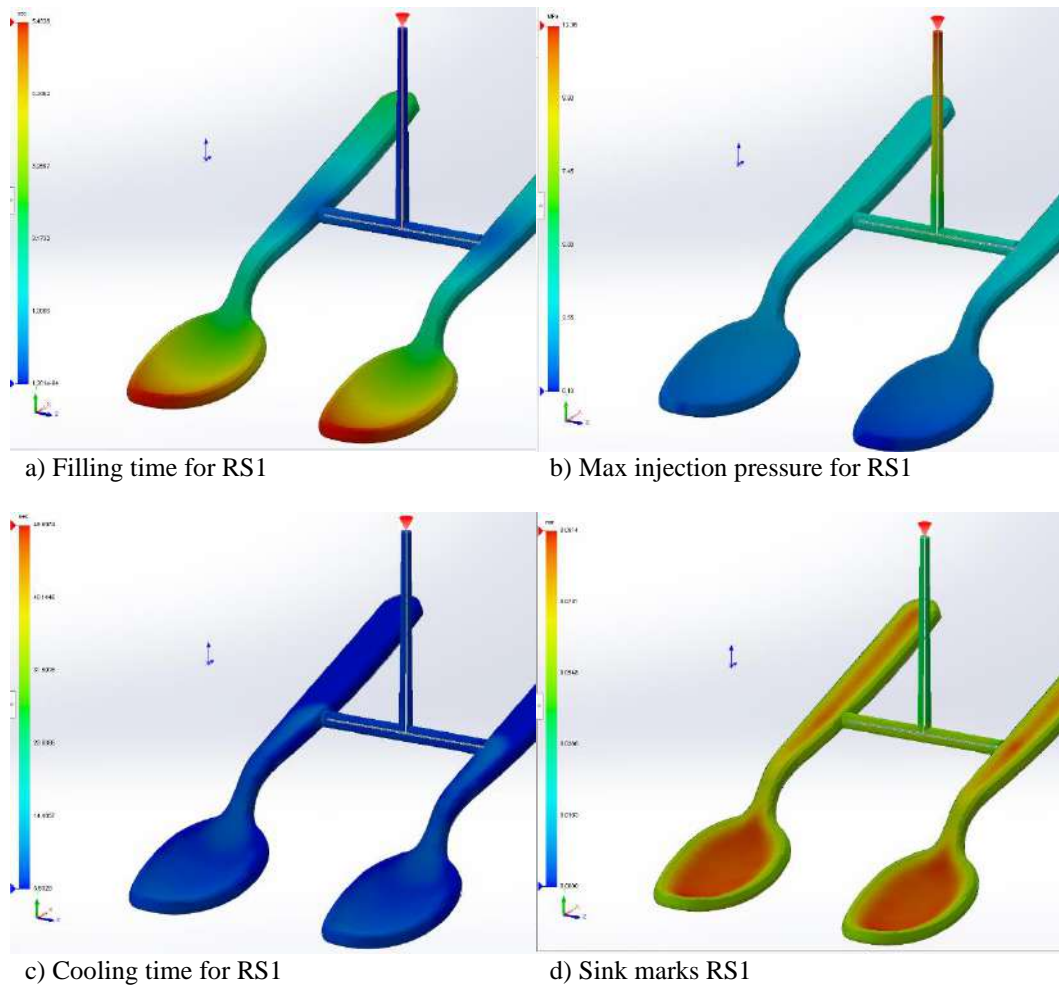


Figure 8: Simulation results for RS1 test model.

Table 3: Data Collection from the simulation results for all six models

PARAMETER	ROUND SHAPE			ELLIPTICAL SHAPE		
	RS1 ($\text{Ø}4.8$)	RS2 ($\text{Ø}7.2$)	RS3 ($\text{Ø}9.6$)	ES1	ES2	ES3
Filling Time (s)	5.4328	5.4187	5.4433	6.2215	6.2133	6.2271
Max Injection Pressure (MPa)	12.36	11.24	10.82	14.11	11.79	11.27
Max Cooling Time (s)	48.6974	50.4187	54.4433	48.493	50.2133	53.2271
Sink Marks (mm)	0.0914	0.1078	0.1877	0.0922	0.0915	0.1518

The chart in Figure 9 shows that the round shape of cross section runner only needs shorter filling time to fill up the plastic melted in cavities comparing to runner in elliptical shape with a reduced of 20% in size. Shorter filling time is important for high volume manufacturing.

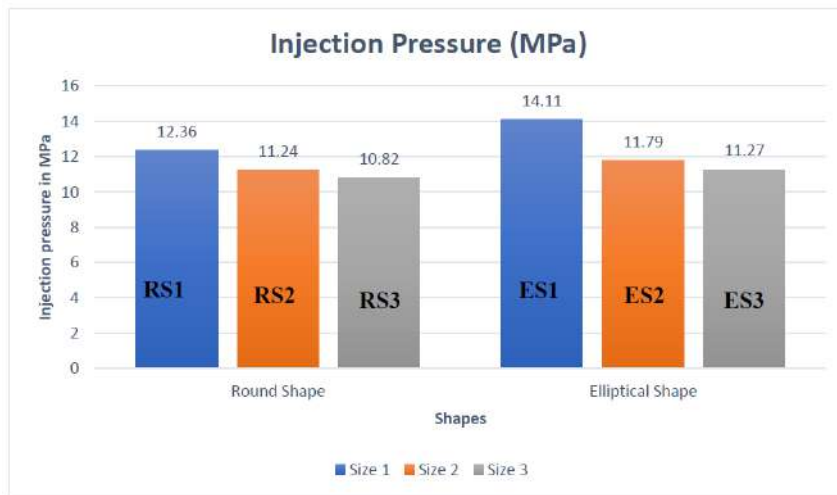


Figure 9: Filling time (s) in comparison with runner in round shape and elliptical shape.

The injection pressure can be observed as inverse proportion to runner size. This is naturally in related because pressure is a function of area. Therefore, when size increases, pressure value will decrease. This was proved in the graph shown in Figure 10, whereby RS1 and ES1, with the smallest size, both are showing the highest reading of injection pressure in comparing to others.



Figure 10: Injection pressure (MPa) in comparison with runner in round shape and elliptical shape

Figure 11 shows the cooling time ‘increasing’ when the runner size increases. RS1 and ES1 show the lowest reading of cooling time needed comparing to other models. A bigger part will result in more volume and more surface area to be cooled down which certainly will increase the cooling time. Overall, the smallest sizes (RS1 & ES1) seem to demonstrate the

better outcomes.

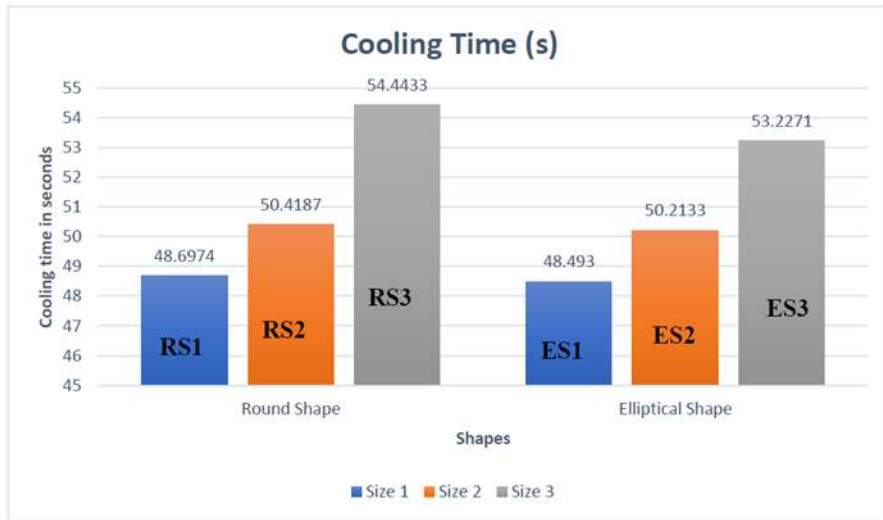


Figure 11: Cooling time (s) in comparison with runner in round shape and elliptical shape

The smallest sizes demonstrate the best outcome for having the lowest sink marks as seen in the Figure 12. Sink marks are vital for the quality of the produced part. Mehdi, 2019 states that sink marks are essentially a form of depression on the surface of the part. He also mentions that if the diameter of runner is too small, the cavities do not fill properly and this leads to internal stresses in the injected parts. When the runner is too small the pressure losses happen through the runner leading to sink marks due to sealing off the runner before the injected parts is packed out properly. (Mehdi, 2019).

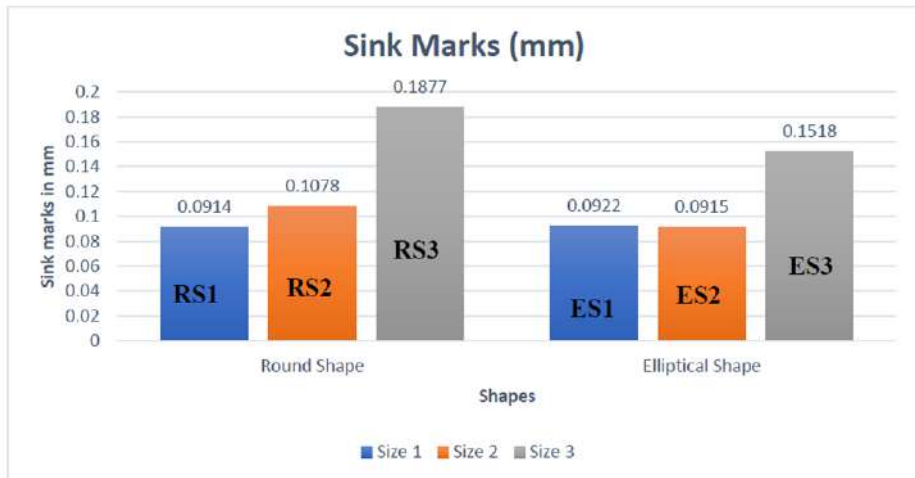


Figure 12: Sink marks (mm) in comparison with runner in round shape and elliptical shape

After comparing all the above parameters sizes, the subsequent comparison is about the different cross sections. RS1 and ES1 were selected as the preferable model evaluation because they demonstrated the best results.

From the above table, it can be deduced that the round cross section yields improved outcomes over the elliptical cross section. While sink marks and cooling time are very similar, the filling time is significantly less in favour of the round cross section, about 12.7% less time, which makes a huge difference in mass production environments.

6. CONCLUSION AND RECOMMENDATION

In conclusion, it was concluded that the smaller size generally has a better performance in the measurement of parameters studied in this chapter. Testing models with runner size RS1 and ES1, showing preferable results in shortest filling time, maximum injection pressure, shortest cooling time and lesser sink mark.

Overall, this chapter goes along with most of the researches related in feed system design, whereby a smaller runner size is more preferable to improve the part quality and produce less scrap which also leads to a lower cost.

REFERENCES

- A. Demirer, Y. S. (2006, May 6). *An experimental investigation of the effects of hot runner system on injection moulding process in comparison with conventional runner system.* , 28(5), 1467–1476. *ScienceDirect*. doi:10.1016/j.matdes.2006.03.015
- Andrew Hulme. (2016, March). *Injection moulding: Why understanding processing is vital for success.*
Retrieved from Smithers: <https://www.smithers.com/resources/2016/mar/injection-moulding-understanding-processing>
- D. Mathivanan, M. R. (2010). Minimization of sink mark defects in injection molding process – *International Journal of Engineering, Science and Technology.*
- DAYA Plastic Machinery. (2019, August 29). Retrieved from injection molding machine nozzle: <https://www.dayamachinery.com/injection-molding-machine-nozzle/>
- Fattori, J. (2020, May 27). *Tooling: How to Properly Size, Gates, Runners and Sprues, Part 3.* Retrieved from Plastics Technology: <https://www.ptonline.com/blog/post/tooling-how-to-properly-size-gates-runners-and-sprues-part-3>
- Gene Michael ALTONEN, V. S.-c. (2014). *US/Ohio Patent No. 086,356.*
- Jones, P. (2008). The Mould Design Guide. In P. Jones, *The Mould Design Guide* (pp. 347-350). Shawbury.
- Josue Obregon, J. H.-Y. (2021). Rule-based explanations based on ensemble machine learning for detecting sink mark defects in the injection moulding process. *Journal of Manufacturing Systems.*
- Lan, K.-M. T.-K. (2015). Correlation between runner pressure and cavity pressure. *Springer-Verlag London.*
- Liang, C.-H. W.-J. (2005). Effects of Geometry and Injection-Molding Parameters on Weld Line Strength. *Department of Mechanical and Automation Engineering, Da-Yeh University.*
- M. Zhai, Y. C. (2006). Runner sizing and weld line positioning for plastics injection. *Springer-Verlag London Limited.*

- Maddah, H. (2016). Polypropylene as a Promising Plastic: *American Journal of Polymer Science*.
- Mehdi, M. (2019). Intelligent Optimization of Mold Design and Process Parameters in Injection Molding. *Springer Theses*.
- Parthasarathy, D. M. (2009). Sink-mark minimization in injection molding through response surface regression modeling and genetic algorithm. *Springer-Verlag London Limited*.
- R. Sánchez, J. A. (2012). On the relationship between cooling setup and warpage in injection molding. *Elsevier Ltd*.
- S. Fathi, A. B. (2007). Visualization of In-Mold Shrinkage in Injection Molding Process. *Polymer Engineering and Science*.
- Sharon Olivera, H. B. (2016). Plating on acrylonitrile–butadiene–styrene (ABS) plastic: a review. *Springer*.
- Stevenson, C.-C. L. (1999). Optimized runner systems for multicavity injection molds. Part I: Runner sizing. *Journal of reinforced plastics and composites*, 375–384.
- Vannessa Goodship, B. M. (2015). *Design and Manufacture of Plastic Components for Multifunctionality*. Norwich: William Andrew Publishing.
- Zhou, H. (2013). *Computer Modeling for Injection Molding*. Wuahn, Hubei, China: Wiley.

PERFORMANCE ANALYSIS OF DC-DC CONVERTERS FOR STAND-ALONE HYBRID ENERGY SYSTEM

N. Sulaiman, Y.K. Lim, L.C. Kuan, K. Thana Pakkiam
Infrastructure University Kuala Lumpur

1. INTRODUCTION

The energy consumption from commercial and domestic consumer demands is drastically increasing i(Akikur, 2013). Since energy generation using conventional methods such as fossil fuel leads to global warming, engineers and scientists find out the means to harvest the alternative energy sources. Production of clean energy with renewable energy sources is the best environmental friendly solution, such as solar PV, wind, biomass, biogas, and small hydro. Solar power are extensively used nowadays to generate electricity all over the globe to reduce pressure on fossil fuel and to reduce environmental impact ii(Das, 2021).

Renewable energy sources also have their disadvantages such as PV systems depend on the environmental irradiance and temperature, while wind system may face irregular wind speed. Meanwhile, fuel cells are expensive and less efficient. Therefore, to deal with these issues, power electronic devices are used, such as DC-DC converters which are highly effective for DC voltage regulation and also to improve the efficiency of renewable energy systems. Apart from that, a suitable DC-DC converter selection is important because it has impact on the overall performance of power systems.

2. LITERATURE REVIEW

Renewable energy having their limit application such as stand-alone hybrid energy systems are more economically reliable compared with a single energy system (Das, 2021). Whereas, the renewable energy system having limit application mostly with low output voltage. Due to those issues the solution is combining two or more renewable energies to design a reliable system with constant output performance iii(Razmjoo, 2019). Hybrid energy system with multiple input DC-DC converter is needed to satisfy the requirement. Some DC-DC converters are discussed in the next section.

2.1 Buck Converter

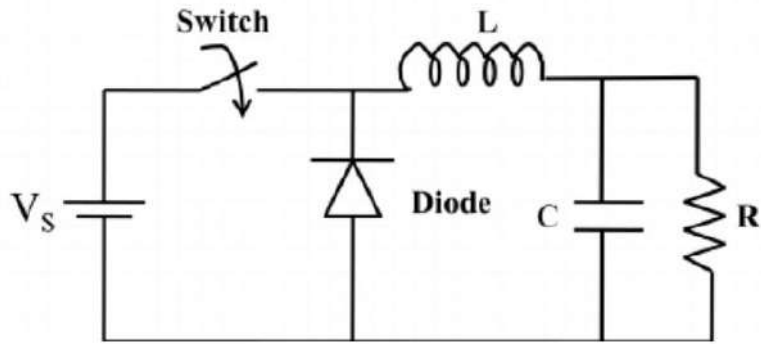


Figure 1: Schematic diagram for buck converter.

Buck converter is one of the DC-DC power converter involved for renewable energy system conversion, by tracking maximum power point of system and controlling their duty cycle. The duty cycle is controlled by switching ON and OFF the circuit at high frequency which step down the voltage level to charge the lower battery voltage of the system iv(Dileep, 2017). Circuit of Buck converter is shown in Figure 1.

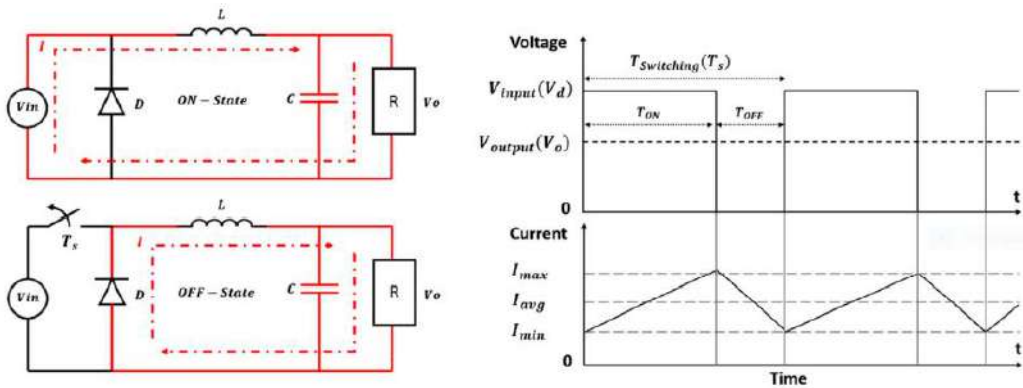


Figure 2: Buck converter circuit and characteristic.

The current commutation and waveforms of Buck converter is shown in Figure 2. Switching ON and OFF, the output voltage can be reduced to desired level by controlling the switching frequency ν (Namazi, 2021). The capacitor is to smoothen the output voltage and to eliminate the ripples caused by the switching frequency of buck converter. The general formula for buck converter as:

$$V_o = D \cdot V_d \quad (2.1)$$

V_o is the average output for the buck converter, while V_d is the diode voltage or direct current voltage source V_s . Moreover, D as the duty ratio is represented by percentage of period where circuit ON time.

2.2 Boost Converter

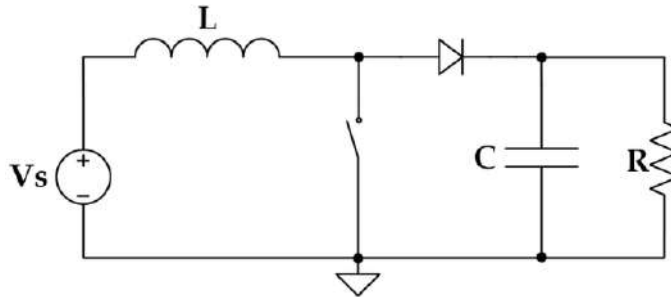


Figure 3: Schematic diagram for boost converter.

Boost converter is one of the DC-DC power converter that involved for renewable energy system conversion to step up the voltage level due to the renewable energy's intermittency vi(Adnan, 2017)vii(Bahmor, 2020). Therefore, when voltage is lower than the system require the boost converter which would increase the voltage level of the system. Boost converter circuit is shown in Figure 3.

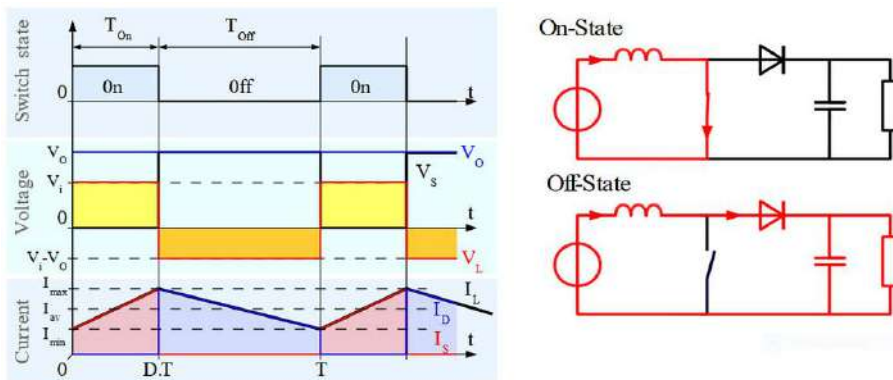


Figure 4: Boost converter characteristic and state of circuit.

The duty cycle waveform and commutation of boost converter circuit is shown in Figure 4 viii(Kumar, 2022). By switching ON and OFF, the output voltage can be increased to desired level. The general formula for boost converter as:

$$V_o = \frac{1}{1-D} V_s \quad (2.2)$$

V_o is the average output for the boost converter, while V_s as direct current voltage source. Moreover, D as the duty ratio is represented by percentage of period where circuit ON time.

2.3 Buck-Boost Converter

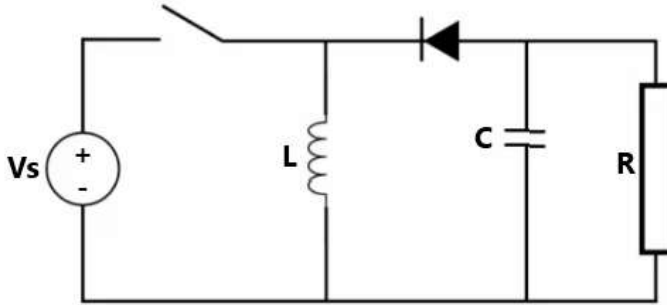


Figure 5: Schematic diagram for buck-boost converter.

Buck-boost converter is a converter that combining principle of buck converter and boost converter features in a single circuit shown in Figure 5. Buck-boost converter can produce output voltage by controlling their duty cycle which will step up or step down the voltage level. Therefore, buck-boost converter is the most suitable DC-DC converter for renewable energy compared to buck or boost converter alone due to renewable energy drawback with intermittency i_x (Shetty, 2017). When renewable energy voltage is lower than the system then buck-boost converter step-ups the voltage and vice-versa to maintain the performance of the system.

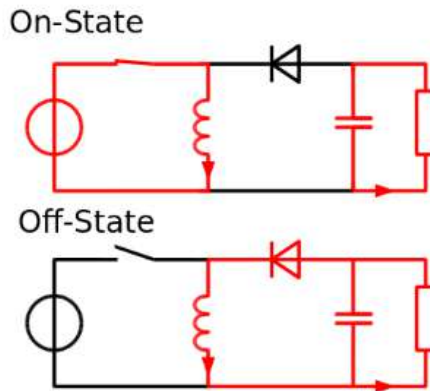


Figure 6: Buck-boost converter state of circuit.

Figure 6 shows the circuit commutation of a buck-boost converter. During ON and OFF stage the output voltage is either raised or dropped to the desired level. Switching frequency acts as ON and OFF to determine the duty ratio and increasing average output voltage or vice-versa x (Sivakumar, 2015). Therefore, the general formula for buck-boost converter as:

$$V_o = -V_s \cdot \frac{D}{1-D} \quad (2.3)$$

V_o is the average output for the buck-boost converter, while V_s as direct current voltage source. Moreover, D as the duty ratio is represented by percentage of period where circuit ON time.

2.4 Zeta Converter

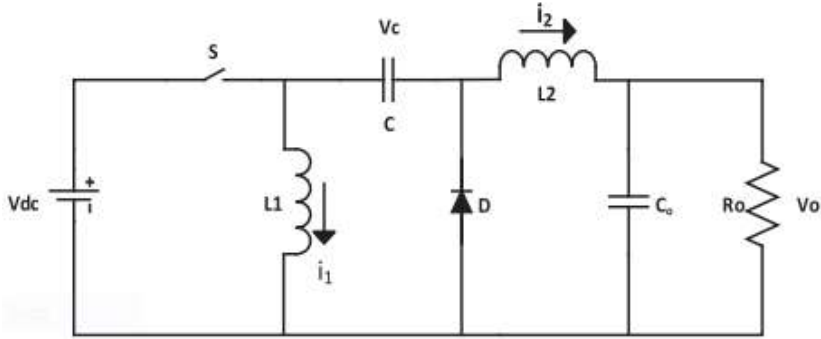


Figure 7: Schematic diagram for zeta converter.

Zeta converter, as shown in Figure 7, is a converter similar as buck-boost converter which can produce output voltage to step up or step down voltage level. However, zeta converter has features of non-inverting output, regulated output voltage and continuous output current. Besides that, it also has advantage of lower output ripple and easier compensation ξ (Admane, 2017). Therefore, zeta converter is suitable for renewable energy system.

The duty cycle concept is similar as buck-boost converter, with difference of the extra capacitor and the non-inversed output voltage (Admane, 2017). Therefore, the general formula for zeta converter as:

$$V_o = V_s \cdot \frac{D}{1-D} \quad (2.4)$$

V_o is the average output for the zeta converter, while V_s as direct current voltage source. Moreover, D as the duty ratio is represented by percentage of period where circuit ON time.

2.5 Cuk Converter

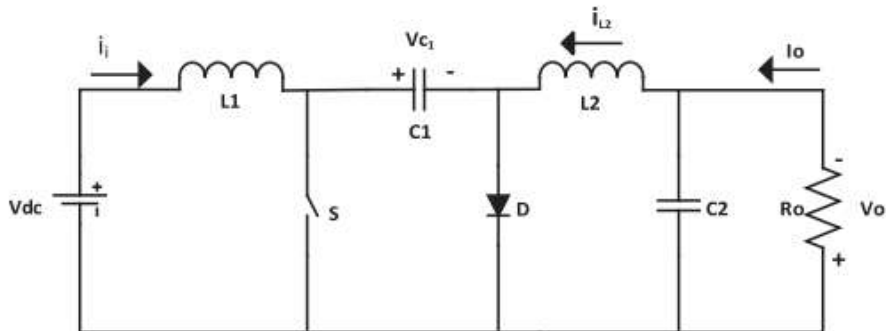


Figure 8: Schematic diagram for Cuk converter.

Cuk converter, as shown in Figure 8, is similar to buck-boost converter with the

inverted output polarity but with less switching losses and better efficiency ^{xii}(Mao, 2020). The output voltage is in negative value due to the inductor characteristic in the circuit during OFF state which produces a back emf having opposite polarity. The Cuk converter steps up or steps down the voltage level. The general formula for Cuk converter is same as buck-boost converter as:

$$V_o = -V_s \cdot \frac{D}{1-D} \quad (2.5)$$

V_o is the average output for the Cuk converter, while V_s as direct current voltage source. Moreover, D as the duty ratio is represented by percentage of period where circuit ON time.

2.6 SEPIC Converter

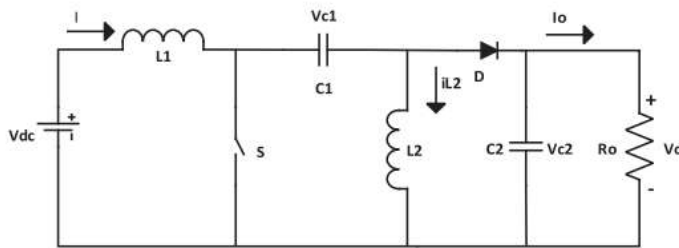


Figure 9: Schematic diagram for SEPIC converter.

SEPIC converter as single ended primary inductor converter that similar as zeta converter as shown in Figure 9. It can produce higher or lower output voltage by controlling their duty cycle. Moreover, SEPIC converter has features of continuous input current and non-inverting output gives high power efficiency, which is preferred for high power application ^{xiii}(Hussain & Mishra, 2019).

The general formula for SEPIC converter as:

$$V_o = V_s \cdot \frac{D}{1-D} \quad (2.6)$$

V_o is the average output for the zeta converter, while V_s as direct current voltage source. Moreover, D as the duty ratio is represented by percentage of period where circuit ON time.

2.7 Cuk-SEPIC Converter

DC-DC converter act as a switched regulator used to convert a variable input dc to a certain dc output, which for Cuk and SEPIC converter can perform buck and boost operations. While, Cuk and SEPIC converter has negative polarity and positive polarity output respectively. Fused converter minimise the number of component used in the circuit, which reducing the cost of the converter and filtering high frequency harmonics. Thus, Cuk and SEPIC converter are fused together to form a fused Cuk-SEPIC converter. The equivalent circuit of Cuk-SEPIC converter is shown in Figure 10. V_1 and V_2 represent the DC input voltage for the Cuk-Sepic converter ^{xiv}(Kumar, 2017) ^{xv}(Suresh, 2015) ^{xvi}(Mutharasu, 2016). MOSFET M_1 and M_2 act as

the switch to connect the input resources.

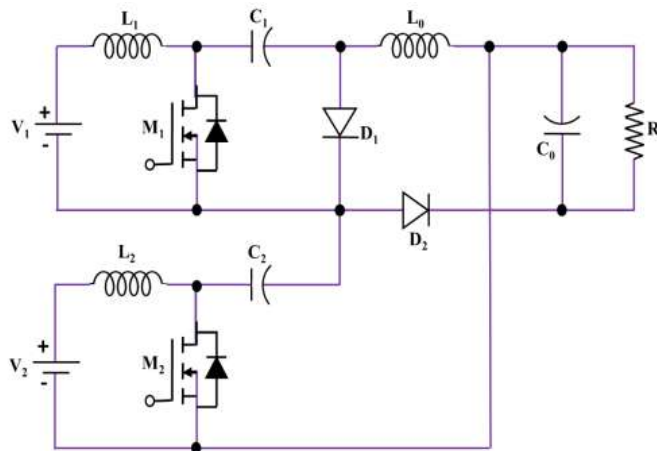


Figure 10: Fused Cuk-SEPIC converter equivalent circuit.

3. METHODOLOGY

In this chapter, the DC-DC converter circuit and simulation are performed by model-based design in the MATLAB Simulink. The design value for the converter are determined by calculation through the desired constant value such as the input voltage, output voltage and etc. Thus, multiple input for the DC-DC converter will resulting different value for the passive component due to the input voltage are not the same. Therefore, need to identify and determine the suitable value to construct the DC-DC converter circuit in the MATLAB Simulink.

3.1 Multiple input Buck-Boost Converter

The output voltage of buck-boost converter can be higher or lower than the input voltage. From the Figure 11 is the multiple input buck-boost converter circuit generate by MATLAB software. Simulation parameters for multiple input buck-boost converter is shown in Table 1.

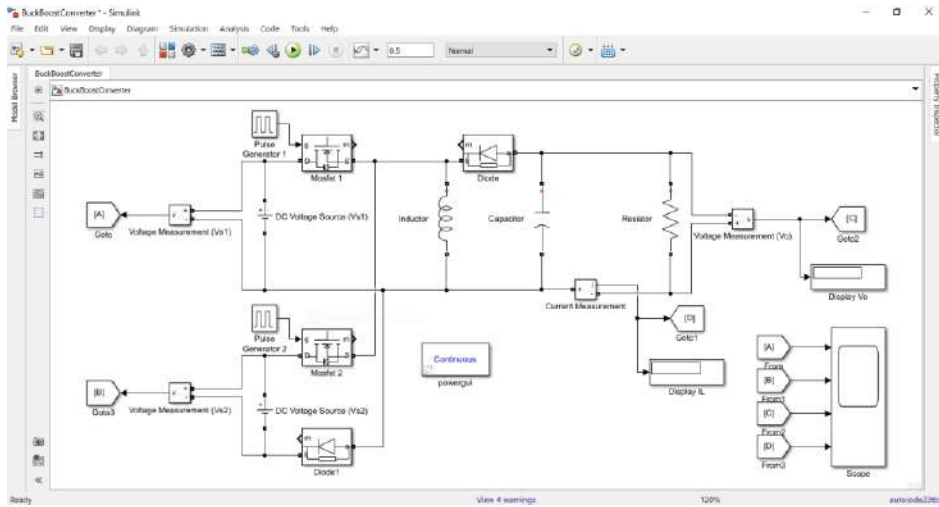


Figure 11: Multiple input buck-boost converter circuit using MATLAB

Table 1: Parameter for Buck-Boost converter

Parameter	Value
V_{S1}	36V
V_{S2}	24V
Resistor	3.24Ω
Capacitor	$265\mu\text{F}$
Inductor	$424\mu\text{H}$
change of inductor current (ΔI_L)	10%
Output ripple voltage ($\Delta V_o/v_o$)	1%
f_s (switching frequency)	50kHz
Duty ratio D1, D2	0.33, 0.43

3.2 Multiple input Cuk-SEPIC Converter

The output voltage of Cuk-SEPIC converter also same as buck-boost converter, it can be higher or lower than the input voltage. From the Figure 12 is the multiple input Cuk-SEPIC converter circuit are generated by MATLAB software. As multiple input, which more than one voltage sources as V_{s1} and V_{s2} are assume generated by solar panel and wind turbine source. Simulation parameters for multiple input Cuk-SEPIC converter is shown in Table 2.

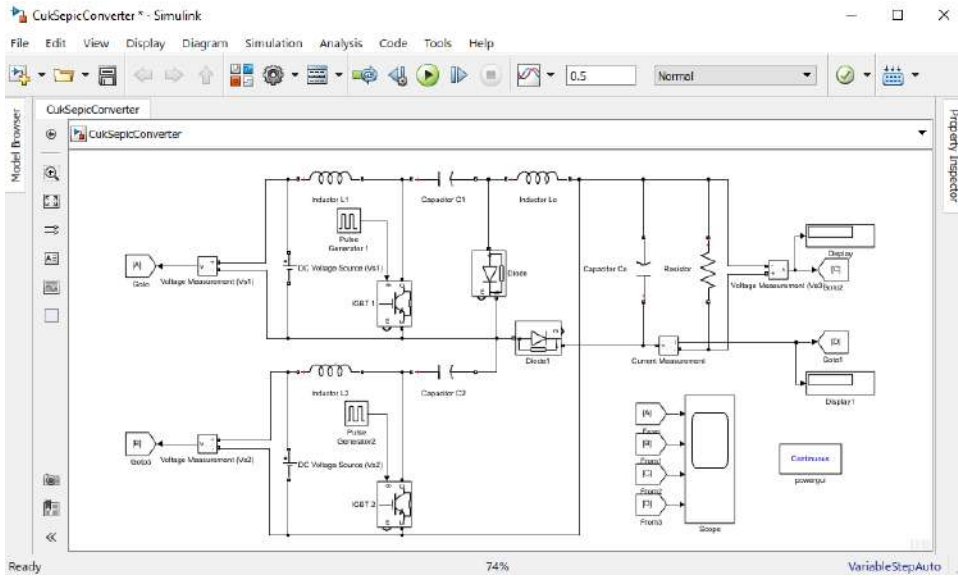


Figure 12: Multiple input Cuk-SEPIC converter circuit using MATLAB

Table 2: Parameter for Cuk-SEPIC converter

Parameter	Value
V_{S1}	36V
V_{S2}	24V
Resistor	3.24 Ω
Capacitor	265 μ F
Inductor	424 μ H
change of inductor current (Δi_{L})	10%
Output ripple voltage ($\Delta v_o/v_o$)	1%
ripple voltage across capacitor (ΔV_c)	5%
f_s (switching frequency)	50kHz
Duty ratio D1, D2	0.33, 0.43

4. RESULTS AND DISCUSSION

During the simulation, both sources will be operating in different simulation conditions such as when one voltage source active another voltage source will be deactivated. Which, the deactivate voltage sources transistor will not function and act as open switch. The reason because of the simulation have more than one switching device but without the controller, so than only can be activated one voltage sources at one time.

4.1.1 Buck-Boost converter with 36 V input

In Figure 13 is the result for Buck-Boost converter when input voltage set at 36 V. While, in the Figure 13 the graph show that from top to bottom line as input voltage 36 V, output voltage 18.18 V and output current 5.612 A respectively. Moreover, for Buck-Boost converter the graph is underdamped. Thus the rise time calculate from 10 percent to 90 percent of the steady state value which is from 236.7 microseconds to 927.1 microseconds of the output voltage value, since steady state value same as output voltage value and the rise time between both 10 percent and 90 percent of the output voltage value time is 690 microseconds. Moreover, the delay time is 50 percent from the output value time which is 607 microseconds and settling time is additional 5 percent of the output value time which is 2.56 milliseconds as shown in Figure 13. Lastly, the maximum overshoot value is the difference between maximum peak value and steady state value which is between 24.64 and 18.18, then the maximum overshoot value is 6.46 for Buck-Boost converter when input voltage set at 36 V.

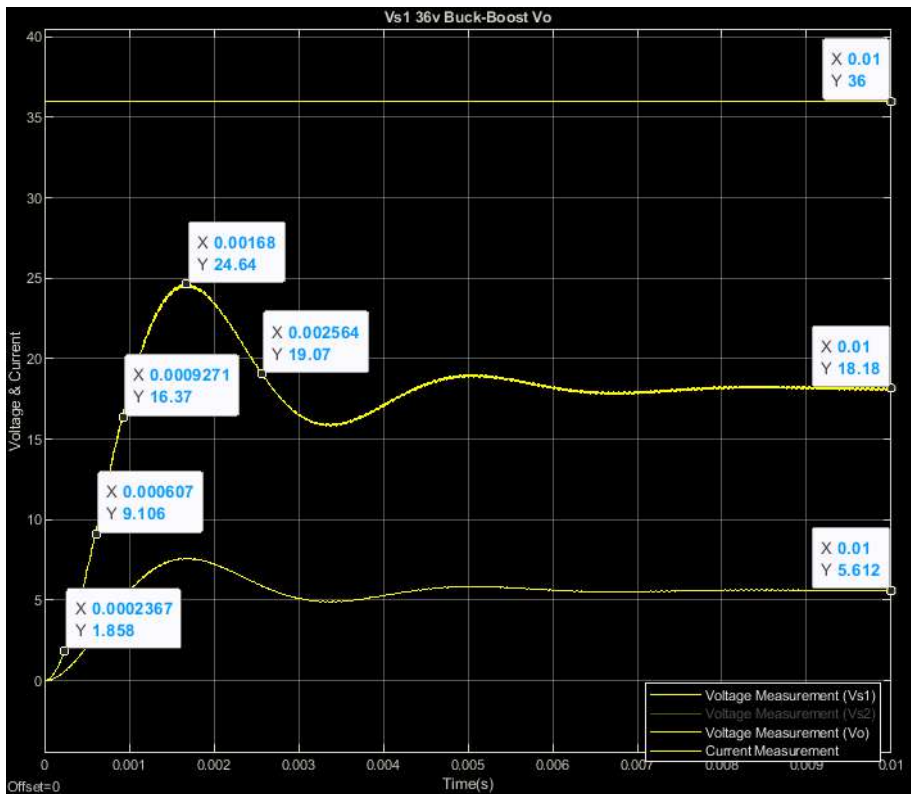


Figure 13: Buck-boost output voltage when voltage source 1 active only.

4.1.2 Cuk converter with 36 V input

In Figure 14 is the result for Cuk converter when input voltage set at 36 V. While, in the Figure 14 graph shows that from top to bottom line as input voltage 36 V, output voltage 18.18 V and output current 5.611 A respectively. Thus, this input and output result value are

similar to Buck-Boost converter result value. Moreover, for Cuk converter the graph is underdamped. Therefore, the rise time calculate from 10 percent to 90 percent of the steady state value which is from 187.2 microseconds to 789.2 microseconds of the output voltage value, since steady state value same as output voltage value then the rise time between both 10 percent and 90 percent of the output voltage value time is 602 microseconds. Moreover, the delay time is 50 percent from the output value time which is 527 microseconds and settling time is additional 5 percent of the output value time which is 4.92 milliseconds as showing in Figure 14. Lastly, the maximum overshoot value is the difference between maximum peak value and steady state value which is between 24.64 and 18.18, then the maximum overshoot value is 8.31 for Cuk converter when input voltage is 36 V.

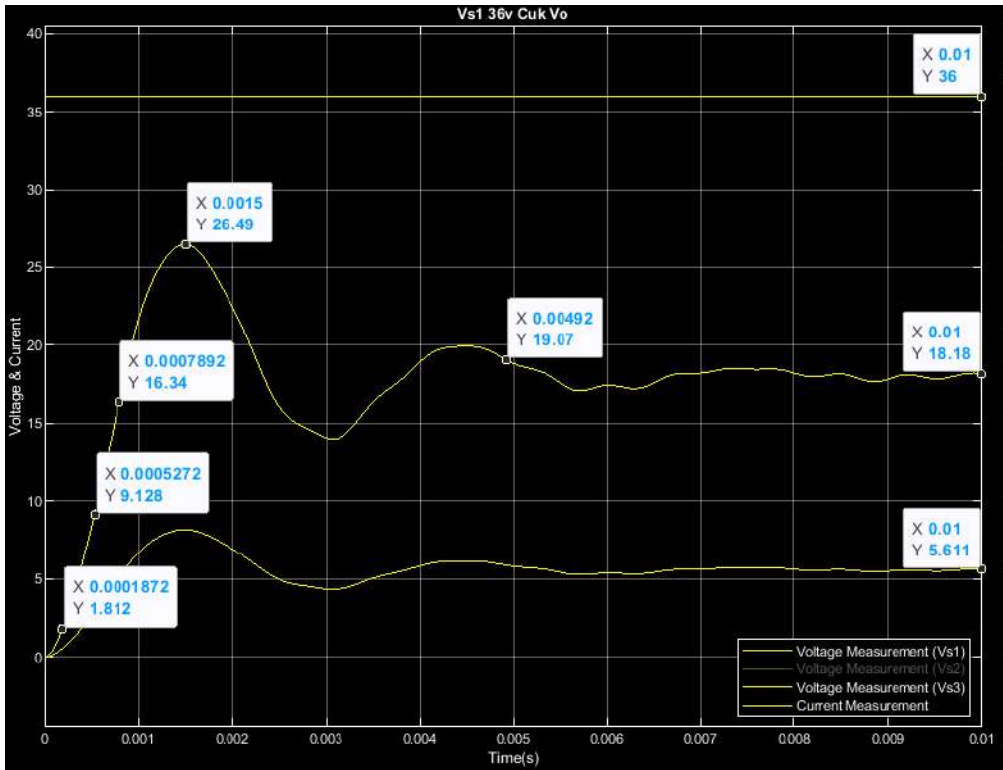


Figure 14: Cuk output voltage when voltage source 1 active only.

4.1.3 SEPIC converter with 36 V input

In Figure 15 is the result for SEPIC converter when input voltage set at 36 V. While, in the Figure 15 graph show that from top to bottom line as input voltage 36 V, output voltage 18.25 V and output current 5.634 A respectively. Thus, this input and output result value are similar to Buck-Boost converter and Cuk converter result value. The different are the output waveform graph pattern, Buck-Boost converter output waveform is smoother than Cuk converter and SEPIC converter output waveform, while Cuk converter and SEPIC converter output waveform are similar. Moreover, for SEPIC converter the graph also is underdamped. Thus the rise time calculate from 10 percent to 90 percent of the steady state value which is output voltage value

time as 507 microseconds. Moreover, the delay time is 50 percent from the output value time which is 432 microseconds and settling time is additional 5 percent of the output value time which is 4.15 milliseconds as showing in Figure 15. Lastly, the maximum overshoot value is the difference between maximum peak value of 27.06 and steady state value of 18.25 which is 8.81 for SEPIC converter when input voltage is 36 V.

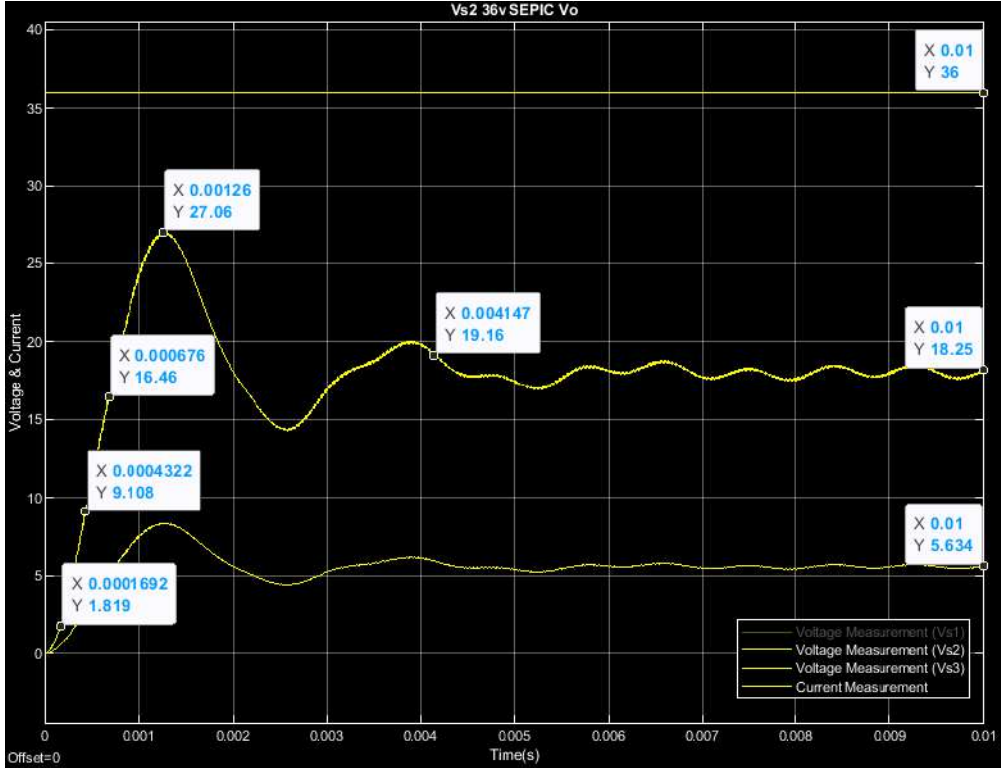


Figure 15: SEPIC output voltage when voltage source 2 active only.

4.1.4 Summary result for different types converter when 36 V input

In the Table 3 is the different types of converter result namely Buck-Boost converter, Cuk converter and SEPIC converter. From the table it shows all of the different types of converter output voltage and output current are approximated to desired output value that is 18 V and 5.6 ampere respectively. Thus, the best result for different types converter with 36 V input is Buck-Boost converter. Due to the Buck-Boost converter have lesser maximum overshoot and less settling time compare to Cuk converter and SEPIC converter, which Buck-Boost converter is more stable than other two converters.

Besides that, due to observation from the Table 3 the most stable converter is Buck-Boost converter and it can be verifying in Figure 16 that is a single graph figure representation for different types of converter result when input voltage set as 36 V. From the Figure 16 starting from the cyan colour straight line represented by the supply source DC voltage that is 36 V, then following by red, yellow and blue colour waveform line represented as Buck-Boost

converter, Cuk converter and SEPIC converter respectively. While, the red colour waveform is the most stable waveform compare to yellow and blue colour waveform by red colour waveform with minimum overshoot value and lesser settling time. Thus, it also is the smoother waveform to reach the steady state compare to other two waveforms. Therefore, through the result from Table 3 and Figure 16, the Buck-Boost converter is the most stable and efficiency converter.

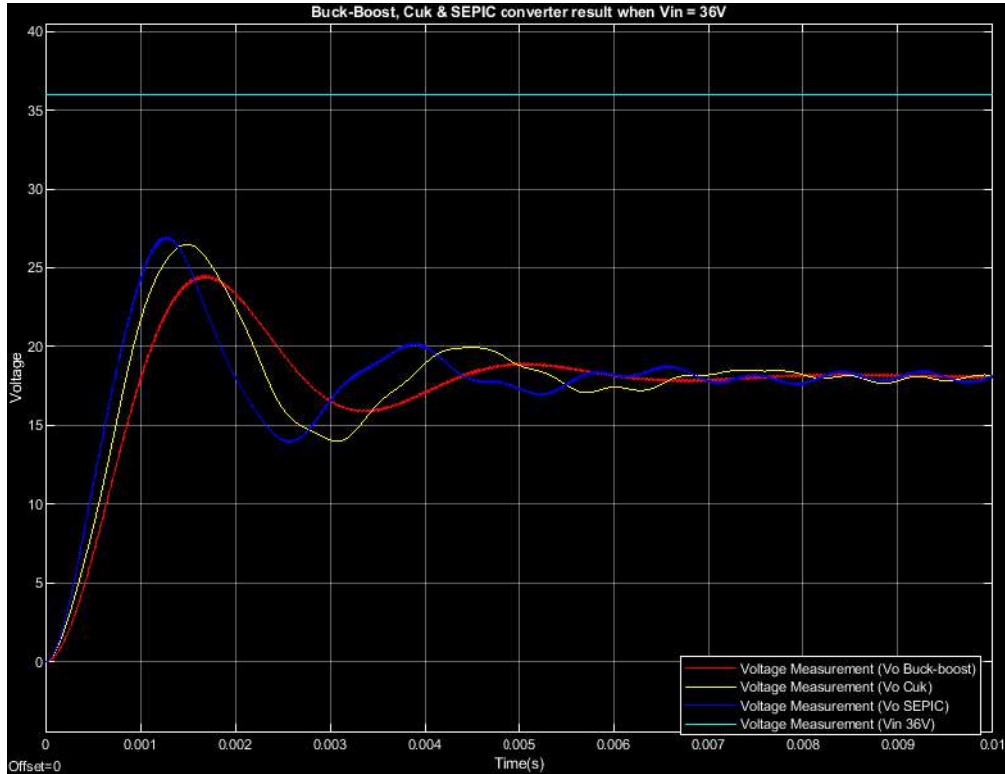


Figure 16: Different types of converter result when input is 36 V.

Table 3 :Types of converter result with 36 V input.

Types of converter	Maximum overshoot	Rise time (Tr)	Delay Time (Td)	Settling Time (Ts)	Steady-state error	Output voltage	Output current
Buck-Boost	6.46	690 μ s	607 μ s	2.56ms	-0.18	18.18V	5.612A
Cuk	8.31	602 μ s	527 μ s	4.92ms	-0.18	18.18V	5.611A
SEPIC	8.81	507 μ s	432 μ s	4.15ms	-0.25	18.25V	5.634A

4.2.1 Buck-Boost converter with 24 V input

In Figure 17 is the result for Buck-Boost converter when input voltage set at 24 V. The graph shows that from top to bottom line as input voltage 24 V, output voltage 18.18 V and output current 5.61 A respectively. Moreover, for Buck-Boost converter the graph is underdamped. Thus the rise time calculate from 10 percent to 90 percent of the steady state value which is from

289.2 microseconds to 1.16 milliseconds of the output voltage value, since steady state value same as output voltage value and the rise time between both 10 percent and 90 percent of the output voltage value time is 871 microseconds. Moreover, the delay time is 50 percent from the output value time which is 749 microseconds and settling time is additional 5 percent of the output value time which is 3.087 milliseconds as shown in Figure 17. Lastly, the maximum overshoot value is the difference between maximum peak value and steady state value which is between 23.02 and 18.18, then the maximum overshoot value is 4.84 for Buck-Boost converter when input voltage set at 24 V.

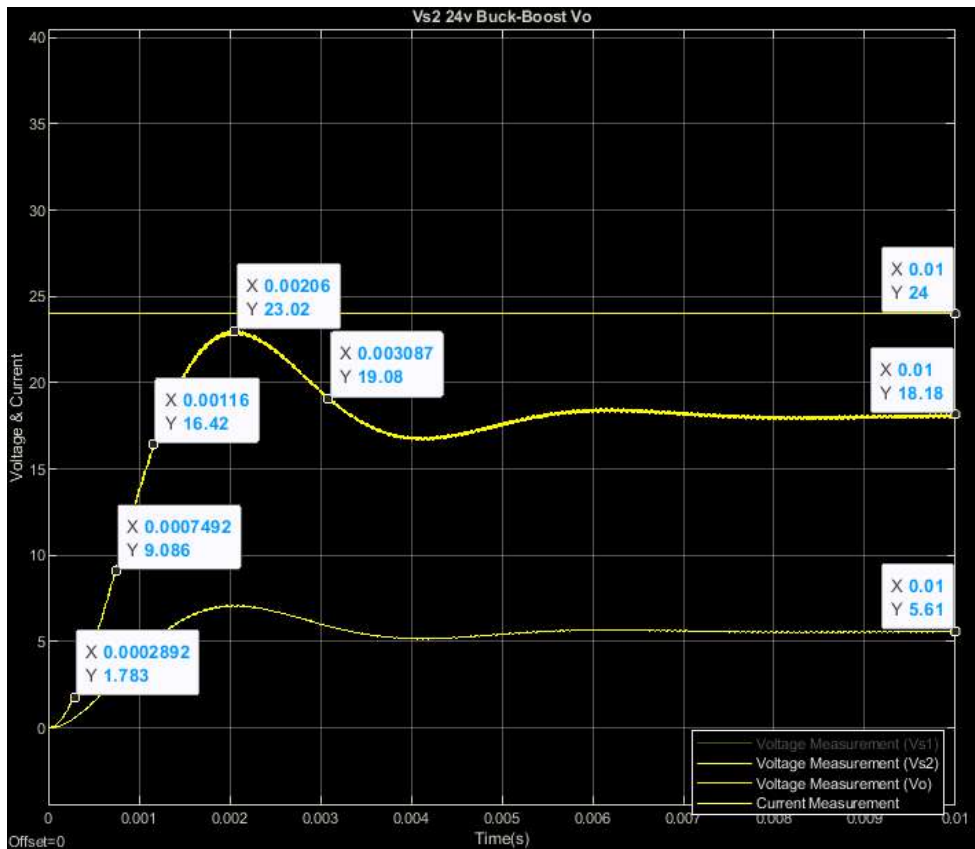


Figure 17: Buck-boost output voltage when voltage source 2 active only.

4.2.2 Cuk converter with 24 V input

In Figure 18 is the result for Cuk converter when input voltage set at 24 V. The graph shows that from top to bottom line as input voltage 24 V, output voltage 17.45 V and output current 5.386 A respectively. Thus, this input and output result value are similar to Buck-Boost converter result value. Moreover, for Cuk converter the graph is underdamped. Therefore, the rise time calculate from 10 percent to 90 percent of the steady state value which is from 127.2 microseconds to 938.4 microseconds of the output voltage value, since steady state value same as output voltage value, then the rise time between both values as 10 percent to 90 percent of the output voltage value time is 811 microseconds. Moreover, the delay time is 50 percent from the

output value time which is 709 microseconds and settling time is additional 5 percent of the output value time which is 6.75 milliseconds as showing in Figure 18. Lastly, the maximum overshoot value is the difference between maximum peak value and steady state value which is between 24.7 and 17.45, then the maximum overshoot value is 7.25 for Cuk converter when input voltage is 24 V.

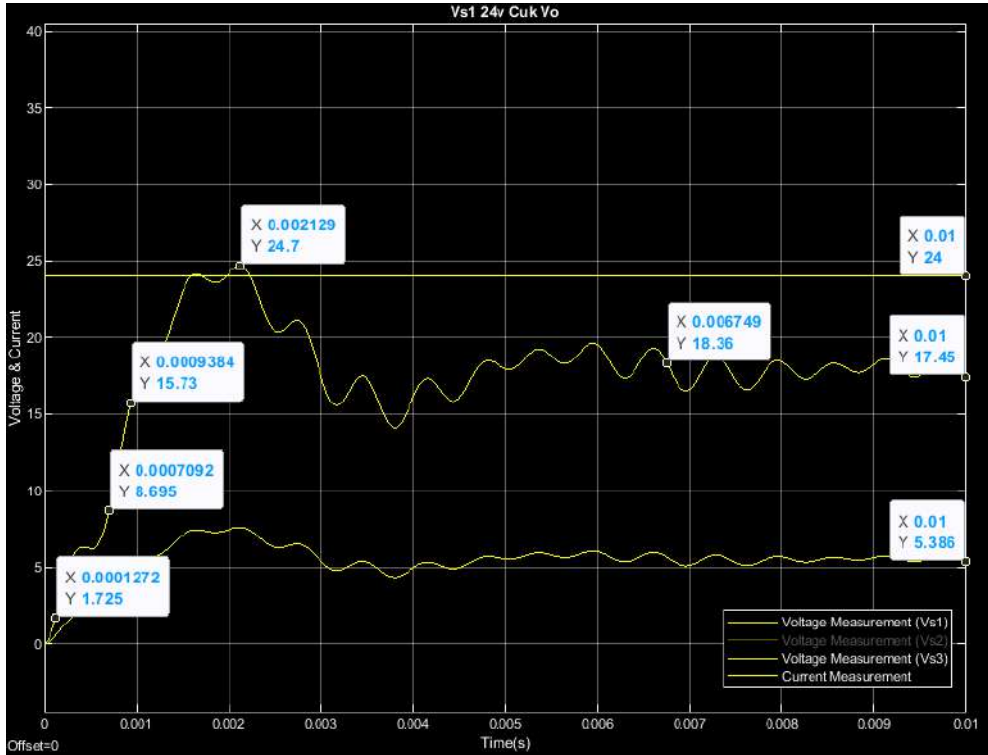


Figure 18: Cuk output voltage when voltage source 1 active only.

4.2.3 SEPIC converter with 24 V input

In Figure 19 is the result for SEPIC converter when input voltage set at 24 V showing that from top to bottom line as input voltage 24 V, output voltage 18.09 V and output current 5.583 A respectively. Thus, this input and output result value are similar to Buck-Boost converter and Cuk converter result value. The different are the output waveform graph pattern, SEPIC converter output waveform is similar as Buck-Boost converter output waveform and both of them output waveform is smoother than Cuk converter output waveform. Besides that, for SEPIC converter the graph also is underdamped. Thus the rise time calculate from 10 percent to 90 percent of the steady state value which is output voltage value time as 571 microseconds. Moreover, the delay time is 50 percent from the output value time which is 529 microseconds and settling time is additional 5 percent of the output value time which is 4.8 milliseconds as showing in Figure 19. Lastly, the maximum overshoot value is the difference between maximum peak value of 25.64 and steady state value of 18.09 which is 7.55 for SEPIC converter when input voltage is 24 V.

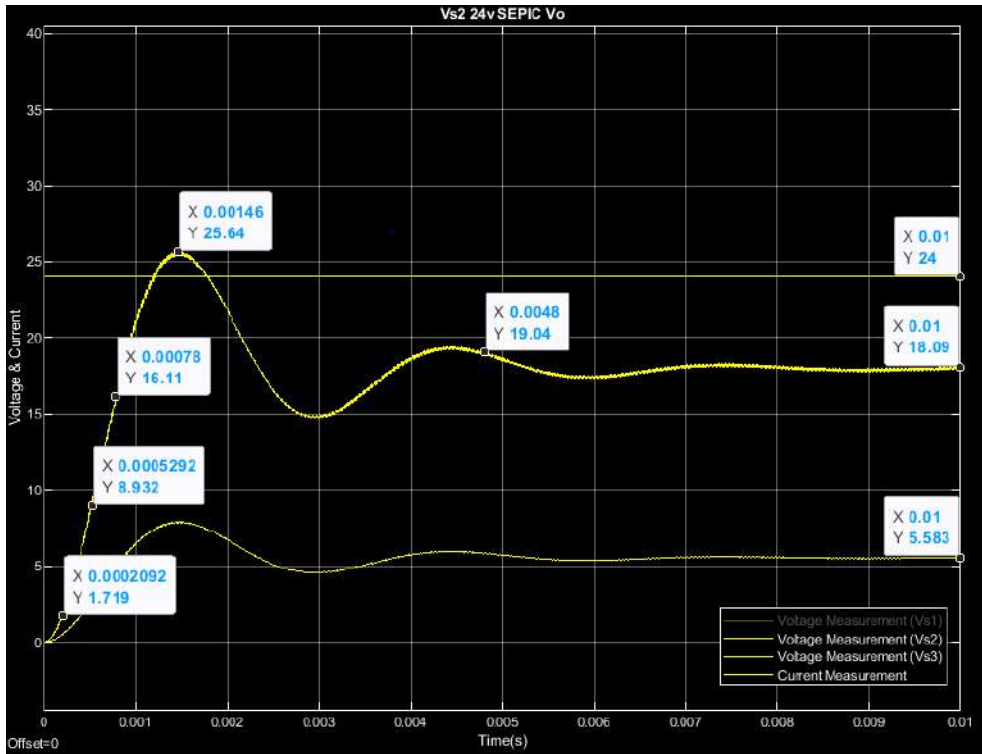


Figure 19: SEPIC output voltage when voltage source 2 active only.

4.2.4 Summary result for different type converter with 24 V input

In the Table 4 is the different types of converter result that are Buck-Boost converter, Cuk converter and SEPIC converter. From the table we can know that all of the different types of converter output voltage and output current are approximated to desired output value that is 18 V and 5.6 ampere respectively. Thus, the best result for different types converter with 24 V input is same as 36 V input that is Buck-Boost converter. Due to the Buck-Boost converter have lesser maximum overshoot and less settling time compare to Cuk converter and SEPIC converter, which Buck-Boost converter is more stable than other two converters.

Besides that, due to observation from the Table 4 the most stable converter is Buck-Boost converter and it can be verified in Figure 20 as a single graph figure representation for different types of converter result when input voltage set as 24 V. From the Figure 20 starting from the cyan colour straight line represented by the supply source DC voltage that is 24 V, then following by red, yellow and blue colour waveform line represented as Buck-Boost converter, Cuk converter and SEPIC converter respectively. While, the red colour waveform is the most stable waveform compare to yellow and blue colour waveform by red colour waveform with minimum overshoot value and lesser settling time. Thus, it also is the smoother waveform to reach the steady state compare to other two waveforms. Therefore, through the result from Table 4 and Figure 20, the Buck-Boost converter is the most stable and efficiency converter.

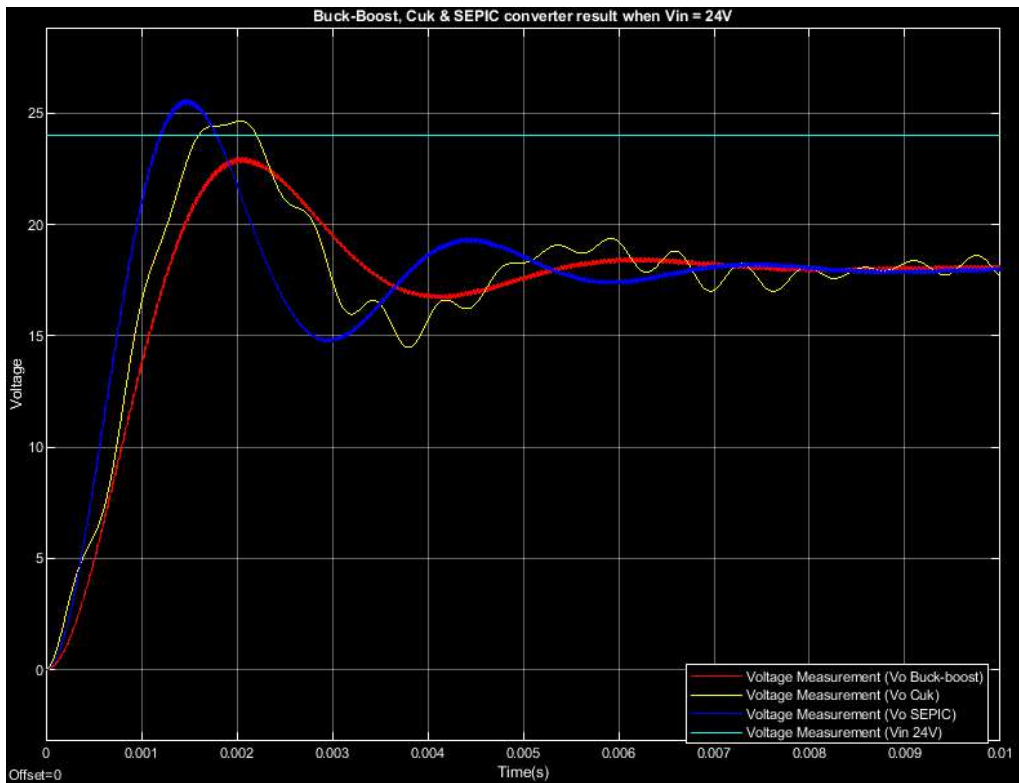


Figure 20: Different types of converter result when input is 36 V.

Table 4: Types of converter result with 24 V input.

Types of converter	Maximum overshoot	Rise time (Tr)	Delay Time (Td)	Settling Time (Ts)	Steady-state error	Output voltage	Output current
Buck-Boost	4.84	871 μ s	749 μ s	3.087ms	-0.18	18.18V	5.61A
Cuk	7.25	811 μ s	709 μ s	6.75ms	0.55	17.45V	5.386A
SEPIC	7.55	571 μ s	529 μ s	4.8ms	-0.09	18.09V	5.583A

4.4 Summary

During the simulation, having two resources will be operating in different simulation, which one voltage source active then another voltage source will be deactivating. This is because the circuit without the controller but have more than one switching device. Besides that, even only have two circuit that is Buck-Boost converter circuit and Cuk-SEPIC converter circuit but due to without controller. Therefore, Cuk-SEPIC will be separated as Cuk converter and SEPIC converter to simulate the result. Thus, the simulation result has different result by two different resources and each resources have simulated three different converters as the simulation result comparison in Figure 21. By multiple input as two resources with different types of converter as Buck-Boost, Cuk and SEPIC converter comparison result, through observation in Figure 21 the Buck-Boost converter is the most stable converter, determine by having lesser settling time and lower maximum overshoot value in both different resources compare to.

Moreover, for steady state error the lesser error value is SEPIC converter when input voltage at 24 V but when input voltage at 36 V the error value is almost 3 times higher than input voltage at 24 V. Thus, during this problem SEPIC converter will not be the better steady state error converter even having lesser steady state error but will be varying the error when higher input voltage. So that, the better steady state error converter will be Buck-Boost converter due to even the voltage varying from high to low or low to high, the steady state error still maintains the same value that is 0.18 as showing in Figure 21.

Furthermore, the delay time and rise time SEPIC converter is getting the better time in both different resources, which is lesser time taken compare to Cuk converter and Buck-Boost converter. While, follow by Cuk converter then the longer time taken for both delay time and rise time is Buck-Boost converter. In additional, for both resources the different types of converter as Buck-Boost, Cuk and SEPIC also getting closer to desired setting value that is output voltage 18 V and output current 5.6 A. Hence, for resources wind turbine that is when input voltage at 24 V, Cuk converter is slightly run out the desired setting value that is 5.386 A and 17.45 V but still in the acceptable range within 5 percent of the desired value.

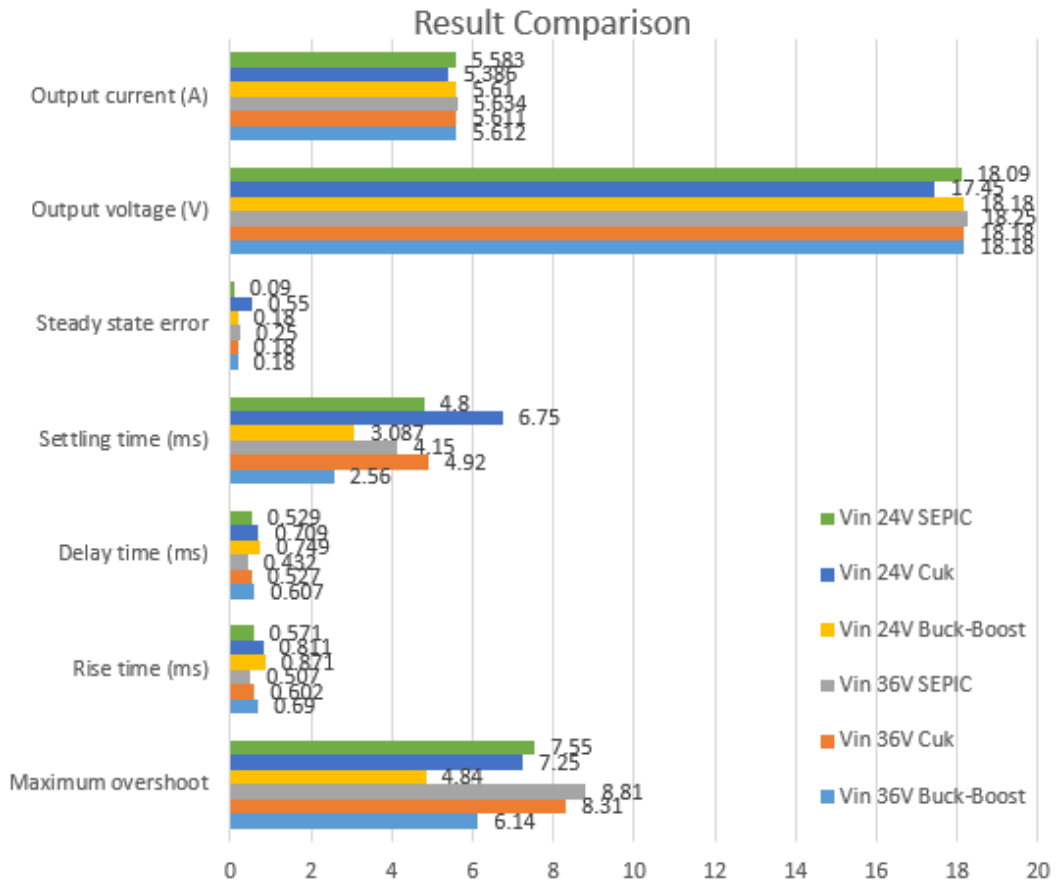


Figure 21: Multiple input with different types of converter comparison result.

5. CONCLUSION

In this chapter two resources as 36 V and 24 V is represented by solar renewable energy source and wind turbine renewable energy source respectively. Different types of DC-DC converter are simulated to identify which one has the higher efficiency. In this project, the simulation result is simulated by MATLAB Simulink. For the simulation, both sources as solar energy resource with 36 V and wind turbine energy resource with 24 V were replaced in direct current voltage resources in MATLAB Simulink. Thus, the multiple input voltage resources will be operating in different simulation such when one voltage source active another voltage source will be deactivated and act as open switch at the transistor side.

Through analysis performance between different types of DC-DC converter result, Buck-Boost converter is the most stable converter. However, Buck-Boost converter with lesser settling time and lower maximum overshoot value, which mean it can be reach desired output value in low latency compare to another both converter. Thus, in this project all the different types of converter also can be achieving the desired output value which is less than the acceptable range and maximum run out is only slightly closer to 3 percent of the desired value.

REFERENCE

- R. K. Akikur, R. Saidur, H. W. Ping, K. R. Ullah, "Comparative study of stand-alone and hybrid solar energy systems suitable for off-grid rural electrification", *A review. Renewable and Sustainable Energy Reviews*. Elsevier Ltd. 2013.
- B. K. Das, M. A. Alotaibi, P. Das, M. S. Islam, S. K. Das, M. A. Hossain, "Feasibility and techno-economic analysis of stand-alone and grid-connected PV/Wind/Diesel/Batt hybrid energy system", *A case study. Energy Strategy Reviews*. Elsevier Ltd. 2021.
- A. Razmjoo, R. Shirmohammadi, A. Davarpanah, F. Pourfayaz, A. Aslani, "Stand-alone hybrid energy systems for remote area power generation", *Research paper. Energy Reports*. Elsevier Ltd. 2019.
- G.Dileep, S. N. Singh, "Selection of non-isolated DC-DC converters for solar photovoltaic system", Research scholar. *Renewable and Sustainable Energy Reviews*. Elsevier Ltd. 2017.
- M. M. Namazi, H. R. Koofgar, M. A. Amirian, J. M. Guerrero, "Voltage regulation of buck converter with constant power load: An adaptive power shaping control". *Control Engineering Practice*. Elsevier Ltd. 2021.
- Mirza Fuad Adnan, Mohammad Abdul Moin Oninda, Mirza Muntasir Nishat, Nafiul Islam, "Design and Simulation of a DC - DC Boost Converter with PID Controller for Enhanced Performance", Department of Electrical and Electronic Engineering, Islamic University of Technology (IUT). *International Journal of Engineering Research & Technology*. IJERT 2017.
- N. B.Mahmor, N. B. M. Posdzi, R. B. A. Rani, "Design and develop a boost converter by using matlab simulink simulation", Department of Electrical Engineering, Ungku Omar Polytechnic, Negeri Perak, Malaysia. *Southeast Asian Journal of technology and Science*.

2020.

- C. H. Kumar, G. Malleshham, "A new hybrid boost converter with P & O MPPT for high gain enhancement of solar PV system", Department of Electrical and Electronics Engineering, University College of Engineering, OU, Hyderabad, TS 500007, India. *Materialstoday Proceedings Volume, Part 5, January 2022, Pages 2262-2269.*
- S. N. Shetty, M. A. Raheman, "Modelling of Dual Input DC/DC Converter for Hybrid Energy System", In *Electronics Information & Communication Technology (RTEICT)*. IEEE. 2017.
- S. Sivakumar a,n , M. Jagabar Sathik b,2 , P.S. Manoj c,1 , G. Sundararajan, "An assessment on performance of DC–DC converters for renewable energy applications", Department of Electrical and Electronics Engineering, J.J. College of Engineering and Technology. *Renewable and Sustainable Energy Reviews*. Elsevier Ltd. 2015.
- A. Admane, Dr.H. Naidu, "Analysis and Design of Zeta Converter", Department of Electrical Engineering Tulsiramji Gaikwad-Patil College of Engineering & Technology, Nagpur. *International Journal for Innovative in Multidisciplinary Field. IJIRMF*. 2018.
- M. Mao, Li Zhang, Lei Yang, B. Chong, Han Huang, Lin Zhou, "MPPT using modified salp swarm algorithm for multiple bidirectional PV-Ćuk converter system under partial shading and module mismatching", Electric Power Research Institute of Yunnan Power Grid Co. Ltd., Kunming 650217, China. *Solar Energy*. **Volume 209**, October 2020, Pages 334-349.
- J. Hussain and M. K. Mishra, "Design of current mode controlled sepic dc-dc converter for mppt control of wind energy conversion systems", 2015 International Conference on Computation of Power, Energy, Information and Communication (ICCPEIC), pp. 0177–0182, April 2015.
- K. Kumar, R. Babu, K.R. Prabhu, "Design and Analysis of an Integrated Cuk-SEPIC Converter with MPPT for Standalone Wind/PV Hybrid System", School of Electrical Engineering, VIT University, Vellore, India. *International Journal of Renewable Energy Research*. 2017.
- Suresh K V, Vinayaka K U, Rajesh U, "A Cuk-SEPIC fused conveter topology for wind-solar hybrid systems for stand-alone systems", Asst. Prof., Department of EEE, SIT, Tumkur, India. *International Journal of Emerging Technology in Computer Science & Electronics (IJETCSE)*. 2015.
- S. Mutharasu, R. Meena, "Modelling of hybrid wind and photovoltaic energy system using cuk and sepic converter", Department of EEE, Vivekanandha College of engineering for women, Tiruchengode. *International Journal of Emerging Technology in Computer Science & Electronics (IJETCSE)*. 2016

Multi Band Micro Strip Patch Antenna Design for WLAN Applications

K. Thana, Aiman, R.Sanjay, N. Ajlaa & N. Sulaiman
Infrastructure University Kuala Lumpur

1. INTRODUCTION

An antenna is a conventional device which is used in the conversion of multi and Omnidirectional EM Waves into electrical signals as well as the other way around. Frequency is one of the main factors which affects the antennas working performance. Consumer demand of Microstrip patch antennas in everyday technology has been exponentially increasing over the years. The reason for this exponential increase in the demand for wireless micro strip patch antenna technology is due to the reliability, ease of integration, mass production at low costs, shapes, sizes and relatively light in weight characteristics [1]. In Layman's terms, transducers and band pass filters can also be used to describe the operations of an antenna. Understanding the core workings of an antenna as well as the basic structure is important to understand the role of antennas in wireless communicationsystems [2].

2. LITERATURE REVIEW

An immense increase in the need of wireless communication technology has been seen and this has driven up the demand for versatile and small antennas exponentially. Antenna technology is being rapidly minimized, made more lightweight, reliable and versatile to keep up with demands from consumers for more compact electronic devices for everyday use. The main markets for applications of antennas is the consumer market and secondly academic sector for work on communications technology which focus mainly on further improvements and research on new generations of antenna technology. Due the miniature size and thin profile of the new and advanced antennas they can be molded into various shaped and designs suitable for the task at hand [3].

Microstrip patch antennas were first conceptualized by Deschamps in the year of 1953[4]. A patent in France following this was filed in 1955 when Gutton and Baissinot improved on Deschamp's idea [5]. In the 1970's, upon further improvements and enhancements based on the previous findings and research the antenna design was finally pioneered and made reality by Munson and Howell [6][7].

3. METHODOLOGY

3.1 Proposed Antenna Design

The proposed design consist of a microstrip-line fed with a rectangular radiators on top and bottom. A scrapped circle slot is placed inside the rectangular radiators. It is printed on one side of the substrate and the other side of the material is pasted with ground plane. The size of the designed antenna is 60 x 60 x 1.6 mm³. Satisfactory performance was obtained by using FR4 substrate. The proposed structure predicted its result using a Microwave studio CST software.

The predicted results and experimented results of the operating bandwidth closely matched. The results cover the wide frequency range of 2.4 GHz and 5.2 GHz for WLAN applications. Table 1 and 2 shows parameters of the designed antenna.

Table 1: Designed Parameter of Micro strip patch antenna.

Operation Frequency in (GHz)	2.4 GHz and 5.2 GHz
Dielectric Constant of The Substrate,	4.3
Height of Substrate, (mm)	1.6
Return Loss in (dB)	16.344 and 22.165

Table 2: Dimensions of the Antenna (mm)

Symbol	Value (mm)	Comments
WS	60	Substrate width
LS	60	Substrate length
Wg	30	Ground Width
Lg	60	Ground length
WP	28	Patch width
LP	28	Patch length
H	1.6	height of substrate
Y	4	Y Axis of the slot
R	5	Radius of the slot

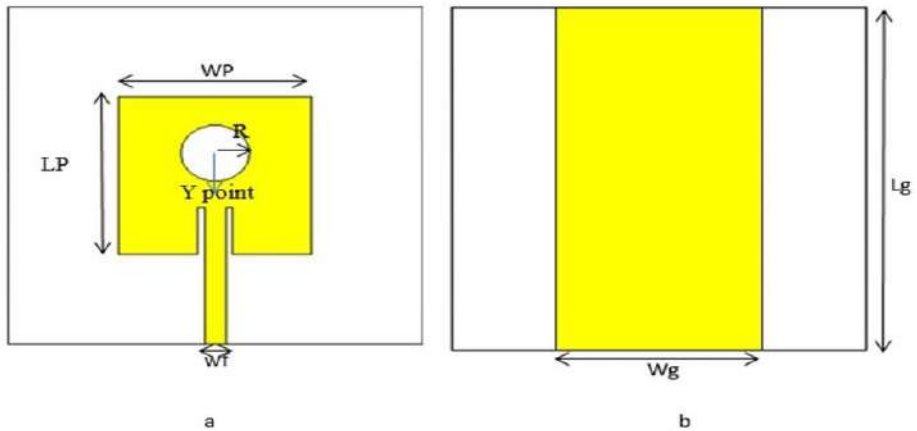


Figure 1: Geometric design of the proposed antenna

Figure 1, shows the geometric design of the proposed antenna. The patch of the antenna is shaped in a rectangular form with the measurements of (28 mm x 28 mm) which has a circle shaped slot scraped with radius of 5 mm in the middle. A thickness of 1.6 mm, was deemed sufficient for the purposes of construction and proper working of the antenna. (30 mm x 60 mm) was chosen as the measurements of the ground plane at which the operability of the antenna is to specifications. The antenna is finally joined to an SMA connector to ensure power can be introduced to the antenna and it can be used for testing and evaluation purposes. This type of antenna if compared to a plain antenna performs much better due to the suppression of unwanted and extra waves produced which can result in decreased efficiency.

3.2 Fabricated Antenna

The patch of the antenna is shaped in a rectangular form with the measurements of (28mmx28mm) which has a circle shaped slot cutout in the middle. A thickness of 1.6 mm was deemed sufficient for the purposes of construction and proper working of the antenna. (30mmx60mm) was chosen as the measurements of the ground plane. In the Figure 2 below, the fabricated antenna joined with the SMA connector is visible.

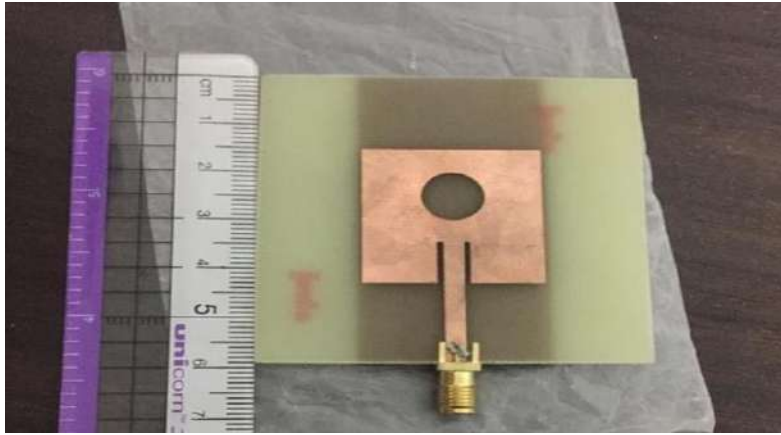


Figure 2: Manufactured antenna.

4. RESULTS AND DISCUSSIONS

A 3D representation modeled through software is shown in Figure 3 which will further help in the antenna manufacturing process. The preferred manufacturing process is commonly referred to as PCB etching and it was used for the production of this antenna:

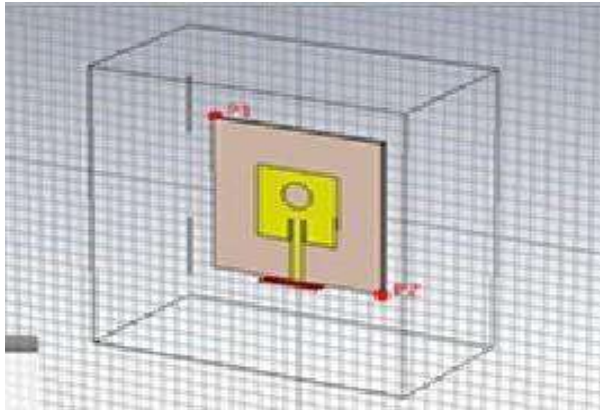


Figure 3: 3D Model of the proposed Antenna design.

4.1 Return Loss

Figure 4 shows the simulated return loss. Resonant frequency is 16.344 dB at 2.4 GHz and 22.165 dB at 5.2 GHz. This shows the amount of power reflected from the radiation being produced in the antenna in laymen's terms.

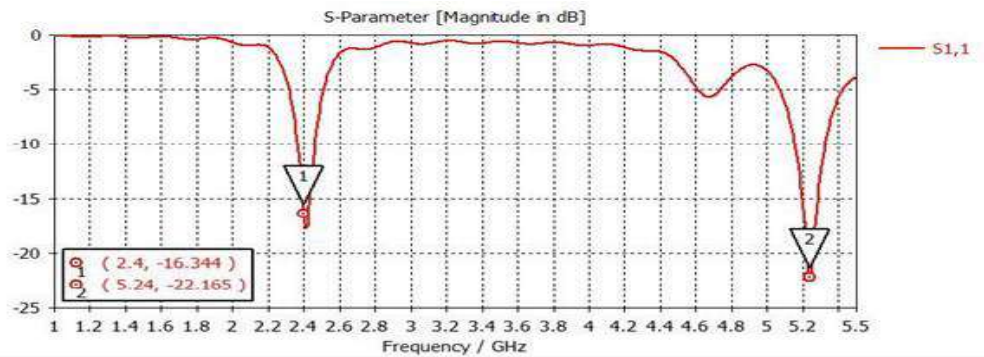


Figure 4: Bandwidth at 2.4 GHz and 5.2 GHz

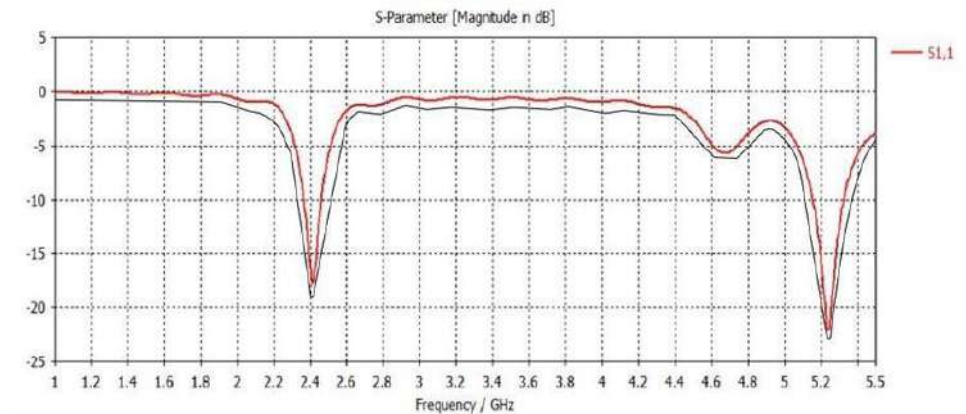


Figure 5: Difference between simulated and measured Return loss

The measured and simulated return loss for the proposed antenna against the resonant frequency are plotted in Figure 5. From the results, it can be established that both resonant modes is to achieve a -10 dB for simulations at 2.4 GHz and 5.23 GHz. Likewise, the measurements of the resonant modes of 2.43 GHz and 5.22 GHz are also successfully reported. The return loss for both the simulation and measurements at 2.4 GHz and 5.2 GHz are 16.344 dB, 22.165 dB and, 19.31 dB and 23.54 dB respectively. These meets the specifications of the Wireless LAN applications.

5. CONCLUSION

Properties of a good antenna include versatility and multiple use case scenarios. This design, for Wireless Local Area Network (WLAN) applications is proposed, design, fabricated and measured successfully. The antenna consideration will be based on the abilities to work with two bands i.e. 2.4 GHz and 5.2 GHz that are also suitable in accordance to the IEEE 802 standards. Due to the versatility and ease of use the software of choice is the widely used CST Microwave Studio (2015 Edition). In accordance to the concept design an inset feed is required on the surface of the antenna and the suitable substrate for this antenna design is the substrate known as FR-4. The proposed antenna is extremely compact, and can easily be fabricated. It is

also fed with a 50Ω microstrip line; which marks it to be an attractive choice to be used for current and future WLAN applications.

REFERENCE

- Liao, T. Y., Chen, I. F., Peng, C. M., & Cheng, H. (2016, July). Dual-band patch antenna for WLAN applications. In *Antennas and Propagation (APCAP), 2016 IEEE 5th Asia-Pacific Conference on* (pp. 31-32). IEEE.
- Chen, I. F., & Peng, C. M. (2018, May). Dual-band patch antenna array for WLAN applications. In *2018 IEEE International Symposium on Electromagnetic Compatibility and 2018 IEEE Asia-Pacific Symposium on Electromagnetic Compatibility (EMC/APEMC)* (pp. 387-389). IEEE.
- Pawar, S. J., & Joshi, M. P. (2016, September). Design of dual band circular Microstrip patch antenna for ISM and WLAN. In *Automatic Control and Dynamic Optimization Techniques (ICACDOT), International Conference on* (pp. 608-611). IEEE.
- K. R. Carver, J. W. Mink, "Microstrip Antenna Technology". *IEEE Transactions on Antennas and Propagation*, vol. 29, pp. 2-24, January 1981.
- R. E. Munson, "Conformal Microstrip Antennas and Microstrip Phased Arrays," *IEEE Trans. Antenna Propagation*, vol. 22, no. 1, pp. 74-78, January 1974.
- J. Q. Howell, "Microstrip Antennas," *IEEE Transactions on Antennas and Propagation*, vol. 23, no.1 pp.90-93 January 1975.
- Ramesh Garg, Prakash Bhartia, Inder Bahl, Apisak Ittipiboon, "Microstrip Antenna Design Handbook", ISBN 0-89006-513-6, Artech House Inc. Norwood, MA, pp 168,253-316, 2001.
- G. Devakirubai D et al., "Design and comparative study of pin feed and line feed microstrip patch antenna for x-band applications," *International Journal of Applied Information Systems*, vol. 1, pp. 21–25, 2001.

MONITORING AND CONTROLLING FOR PRECISION HYDROPONICS

LC Kuan, K.W. Hon, N. Sulaiman & M. Ramesh
Infrastructure University Kuala Lumpur

Keywords: *Hydroponics Agriculture System, IoT monitoring system, Arduino UNO, pH value, temperature, humidity, water level, LED light, DC fan.*

1. INTRODUCTION

Hydroponics Farming (HF) is a food production method that uses a vertical dimension to hydroponically grow crops with indoor-controlled agriculture technologies such as artificial lighting ¹[1]. In the last decades, vertical farming has seen an increase in demand and is seen by many as a method of combating a wide range of global challenges facing food production, such as growing populations, resource depletion and food safety. Hydroponics farming can be adjusted to be fit in any space. Hydroponics can also feed more people than regular farming can as they grow 75 times more food per square foot than traditional farms. Hydroponics also do not use pesticides or fungicides to make food healthier and safer ²[2]. Hydroponics farming is a proactive thinking approach that aims to ensure the sustainability of cities by dealing with the issue of food security. When compared to traditional farming, the hydroponics farm may reduce the need for fossil fuel required for tractors, plough, or shipping.

Life in soil and growing media is a huge contributor to nutrient availability, good structure, plant, soil and growing media health. Biological farms can use technology or practices that help increase this biology, and ideal conditions are reached, for biology to thrive. Bacteria prefer mildly acidic or low pH conditions. Fungi prefer conditions that are slightly more basic or have a higher pH. A neutral pH is ideal for earthworms. None of the species that aid the crops will survive if the pH is too far toward either extreme. Since there is no effect from heavy rain that could leach elements like Ca and Mg and create acidic conditions in a greenhouse, pH regulation can be done very precisely. Apart from that's table temperature of soil is also an important key factor. It is recommended to keep soil covered with growing plants or plant residues and avoid bare ground in order for roots and soil life to survive. Temperatures of media and water can be precisely managed in container growing using technology (heating and cooling systems) that maintains ideal greenhouse temperatures. The temperature of the water can also be regulated to best suit the needs of biology.

Hydroponics farming is often done in a controlled environment to maximize plant yield

¹ K. Al-Kodmany, *The Vertical Farm: A Review of Developments and Implications for the Vertical City*, vol. 8, no. 2, 24, 2018

² Despommier, D., *The Vertical Farm: Feeding the World in the 21 st Century*, Thomas Dunne Books: New York, NY, USA, 2010.

with maintaining the quality of the production. In a controlled environment, the surrounding temperature, light intensity, irrigation and air circulation is closely monitored and controlled for the best optimum factors for the vegetables to grow healthily. By having an option to control the Books: New York, NY, USA, 2010.environment, a farmer has the capability to make some adjustments depending on the type of crops grown since different types of crops need different optimum environment to grow healthily. Weather condition does not affect the growth of the crops in a vertical farm as environment is controlled indoors by the user. Other benefits include reduction of water consumption up to 70 percent compared to conventional farming.

Reducing water consumption enables the world to cope up with water shortage where a majority of water is supplied to traditional farming. Moreover, there is no pesticide use in vertical farming and therefore eliminates chemical traces found in vegetables that we consume daily ³[3].

This chapter focuses on the implementation of an IoT monitoring system that is able to monitor water level, air temperature and humidity level, pH value, water temperature and the air quality level for hydroponic farm by using of sensors and Arduino UNO microcontroller. In addition, a mobile application with the BLUETOOTH smart switch is used to control and monitor the proposed design and therefore minimize human intervention besides provide the plants with adequate nutrients.

2. LITERATURE STUDY

The automatic indoor hydroponic farming system by Muhammad E. H. Chowdhury et. al ⁴[4] uses ultrasonic sensor to check the water level in the water tank. A GSM Module is added, when the water is getting lesser, the sensor will notify the user. Arduino is used in this system to manipulate the water level.

Maintaining of the basic water level of the tank and providing water to the vegetables are the main aim of this system. It used software that can automate and build a control command to make the functions work perfectly. This system is able to send a SMS of the remaining amount of water level to the end-user if the water is getting lesser. In addition, it provides water for the vegetables in the Hydroponic farming. However, the system does not notify about the watering system and the end-user must be on the spot to on the water pump to increase the water level. To minimize the supervision, a mobile application would have been better.

Meanwhile Muhammad E. H. Chowdhury et. al ⁵[5] proposed IoT Based Hydroponic

³ M. Mehra, S. Saxena, S. Sankaranarayanan and R. J. T. a. M. Veeramanikandan, IoT based hydroponics system using Deep Neural Networks, Computers and Electronics in Agriculture, no. 155, pp. 473-486, 2018.

⁴ Muhammad E. H. Chowdhury, Amith Khandakar , Saba Ahmed, Fatima Al-Khuzaei, Jalaah Hamdalla, Fahmida Haque, Mamun Bin Ibne Reaz, Ahmed Al Shafei and Nasser Al-Emadi, Design, Construction and Testing of IoT Based Automated Indoor Vertical Hydroponics

⁵ Lata S. Handigolkar, M.L. Kavya and P.D. Veena, Iot Based Smart Poultry Farming using Commodity Hardware and Software, Bonfring International Journal of Software Engineering and Soft Computing,

Farming Using Commodity Hardware and Software as shown in Figure 1.1. Arduino UNO and Raspberry Pi Model B are used in this automatic farming system. A real-time alarming system is added to notify the owner via a smartphone. The information such as lowest/highest temperature of the farm, humidity of the farm, and weather quality inside the farm will be reported to the arm owners. The end users can also customize the notification system to the smart phone and control the filter fan switches.

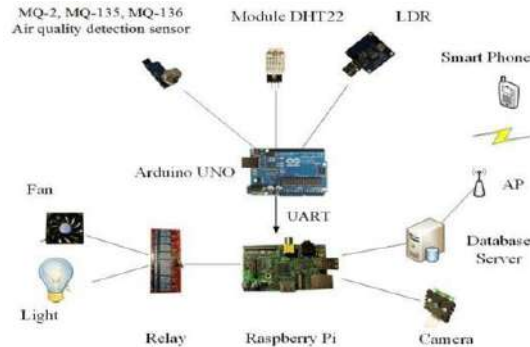


Figure 1: Block Diagram of the System [5]

This system is all about using opensource software and low-cost commodity hardware. A framework was developed using raspberry pi, which was utilized as an embedded device board for Linux and an Arduino Uno to communicate with various sensor. These frameworks have been extensively investigated for many physical boundaries incorporated along with successful monitoring management of Hydroponics farming which contains temperature moisture content of the air and the quality of air, and humidity. Other than monitoring these parameters, these systems also effectively regulate these parameters. These is a useful system for the farmers because they can access and monitor the framework remotely by using their mobile phone. Moreover, the system lowers the human interaction, saves time, enhances the use of resources, and increases the yield of the poultry.

For this system, the farm owner will be notified with the real-time alarm if the temperature goes higher or lower than the required temperature. The moisture content of the air and the quality of air is tested which is not very common in other system. The farm owner will be notified with the real-time alarm if the humidity level is less that the required humidity. Besides, light sensors are used to improve the quality of the vegetables.

3. METHODOLOGY

Overall Block Diagram of the Proposed Design

Figure 1 shows the overall block diagram of the proposed design. The system that was proposed is the Study and Implementation of Internet of Things (IoT) based on Monitoring and Controlling System for Precision Hydroponics Agriculture system interface with Android

Technology. In this system, an (IoT) monitoring system that will allow the end-user to monitor the precision hydroponic vegetables from anywhere with the mobile application. The pH sensor will be used to measure the amount of alkalinity and acidity in the water for the vegetables. The ultrasonic sensor will measure the water level in the water tank, when the water is getting lesser, the sensor will notify the user. Arduino is used in this system to manipulate the water level. Other than that, this system will allow the end user to monitor the temperature, humidity and also the light in the farm. Finally, in this Hydroponics system, there will be UV light added additionally to sterilize against bacteria and viruses.

This proposed design is able to send notification to the end user about the pH value, temperature, humidity, and water level. The farm owner will be notified with the real-time alarm if the water level is less that the required level. In addition, UV light is used to sterilize against bacteria and viruses.

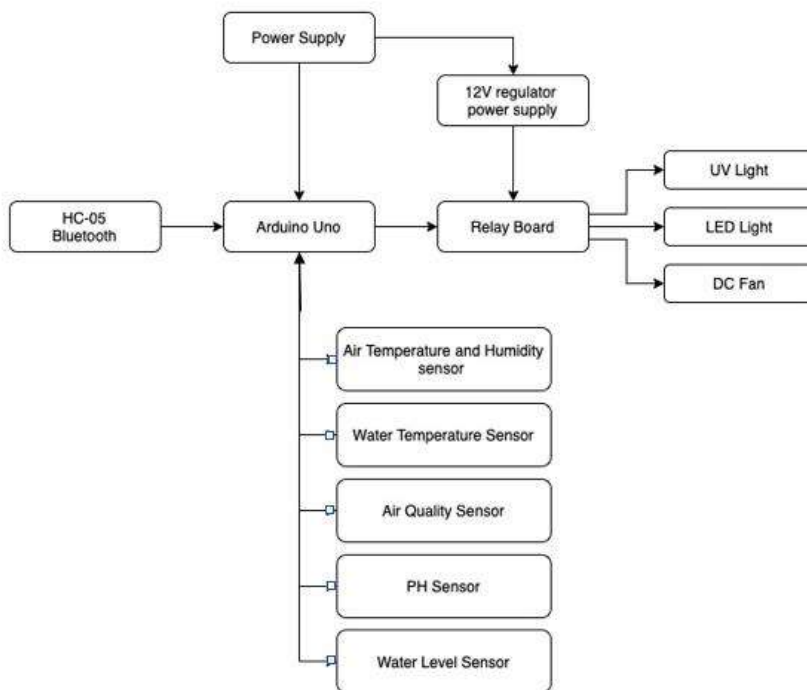


Figure 2: Overall Block Diagram of the Proposed Design

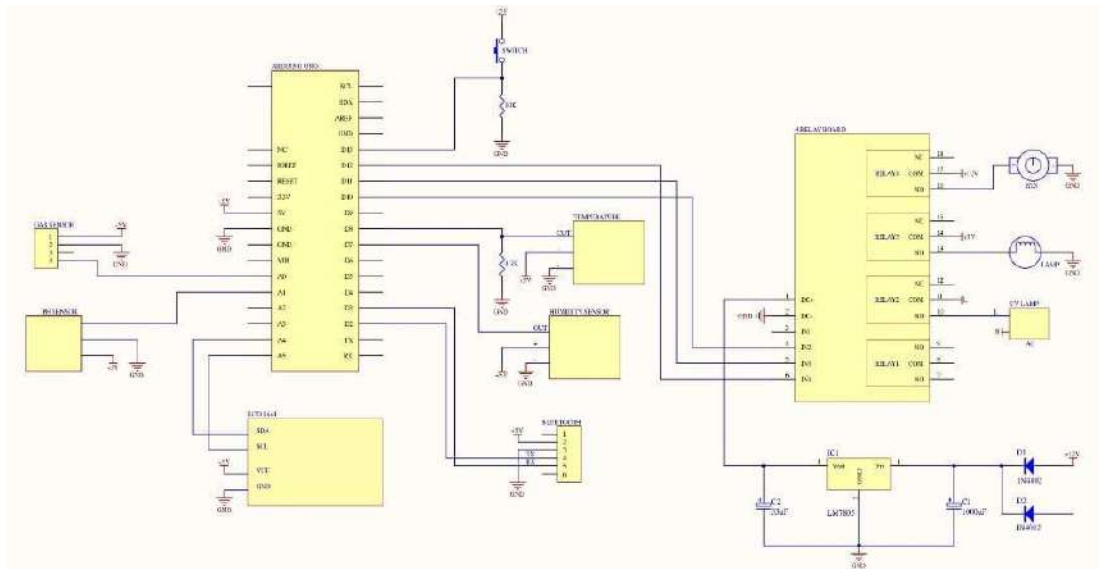


Figure 3: Schematic Diagram of the Proposed Design

Figure 3. shows the schematic diagram of the Proposed Design developed using EasyEDA Software. This schematic shows the connection that have designed manually in hardware.

Firstly, the 12V regulated power supply is connected to the Arduino Uno and to the main power supply. In this connection the regulator which adopt 12V input and decrease the high voltages from the main power supply to low current in electric power application, because the DC fan and LED light is 5V. The regulated power supply will stabilize the voltage to the circuit. The Bluetooth module device is connected to the Arduino as well in order to operate appliances using Smartphone. Then the main components were connected which are the pH sensor, Temperature and Humidity sensor, Water Temperature sensor, Air Quality sensor and Water Level sensor. These sensors are connected to monitor the Hydroponics Agriculture System to make sure the temperature and surrounding area are suitable for the vegetables. After the connection, Bluetooth application and Arduino Programming were done using MockFlow and Arduino IDE software respectively. After the sensor connections have done, the water level sensor is connected to the Arduino Uno to measure the level of the water in the storage tank, these probes send information bank to the control panel that is Arduino Uno. The last step is to connect the DC Fan, LED Light and UV Light to complete the system and ready to test. In the smartphone, using the Bluetooth application created the user has to select between three applications in mobile, Monitor sensor, Light and Fan and Water level. Once the user selects the application, the Bluetooth will send the commands to Arduino board, then the Arduino board will receive the input from the sensors which have been connected and the output will be displayed in the LCD Display and also in the app which have been created. The DC Fan, UV Light and LED Light can On/Off by using the app. The DC Fan will play the role of exhaust blower, so that the DC Fan will evacuate the gas or the toxic gas from the surrounding area of the Hydroponic farm. The DC Fan will automatically on if the air quality sensor detects the air

level more than 110ppm, than the DC Fan will off after the air quality level decrease below 110ppm.

App Software Coding

A program for App hardware is written using App Inventor software with compilers that produce binary machine code for the target processor. App Inventor lets you develop applications for Android phones using a web browser and either a connected phone or emulator. The App Inventor servers store your work and help you keep track of your projects. The app coding for the proposed design is stated as below:

```
initialize global AirTemp to 0
initialize global Humidity to 0
initialize global AirQuality to 0
initialize global PH to 0
initialize global WaterTemp to 0
initialize global WaterLevel to 0

when ListPickerBlueList .BeforePicking
do set ListPickerBlueList .Elements to BluetoothClient1 .AddressesAndNames

when ListPickerBlueList .AfterPicking
do set ListPickerBlueList .Selection to call BluetoothClient1 .Connect
address ListPickerBlueList .Selection
if BluetoothClient1 .IsConnected
then set LabelBlueStatus .Text to Status: Connected
else set LabelBlueStatus .Text to Status: Disconnected

when ButtonDisconnect .Click
do call BluetoothClient1 .Disconnect
set LabelBlueStatus .Text to Status: Disconnected

when ButtonExit .Click
do call BluetoothClient1 .Disconnect
close application
```

```

when ButonSensor1 . Click
do
  call BluetoothClient1 . SendText
  text "T"
  set TableOverall . Visible to false
  set TableMonitorSensor . Visible to true

when ButonLightFan . Click
do
  set TableOverall . Visible to false
  set TableLightFan . Visible to true

when ButonWaterLevel . Click
do
  call BluetoothClient1 . SendText
  text "W"
  set TableOverall . Visible to false
  set TableWaterLevel . Visible to true

when ButonBack . Click
do
  set TableOverall . Visible to true
  set TableMonitorSensor . Visible to false

when ButonBack2 . Click
do
  set TableOverall . Visible to true
  set TableLightFan . Visible to false

when ButonBack3 . Click
do
  set TableOverall . Visible to true
  set TableWaterLevel . Visible to false

when SwitchUV . Changed
do
  if SwitchUV . On
  then call BluetoothClient1 . SendText
  text "User change the state of the 'Switch' from On to Off or back."
  else call BluetoothClient1 . SendText
  text "0"

when SwitchLED . Changed
do
  if SwitchLED . On
  then call BluetoothClient1 . SendText
  text "3"
  else call BluetoothClient1 . SendText
  text "2"

when SwitchFan . Changed
do
  if SwitchFan . On
  then call BluetoothClient1 . SendText
  text "5"
  else call BluetoothClient1 . SendText
  text "4"

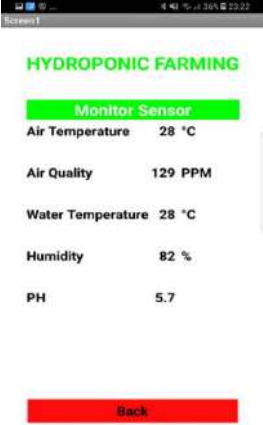
when Clock1 . Timer
do
  if TableMonitorSensor . Visible = true
  then
    if call BluetoothClient1 . BytesAvailableToReceive > 0
    then
      set global AirTemp to call BluetoothClient1 . ReceiveText
      numberOfBytes -1
      set global AirQuality to call BluetoothClient1 . ReceiveText
      numberOfBytes -1
      set global WaterTemp to call BluetoothClient1 . ReceiveText
      numberOfBytes -1
      set global Humidity to call BluetoothClient1 . ReceiveText
      numberOfBytes -1
      set global PH to call BluetoothClient1 . ReceiveText
      numberOfBytes -1
      set LabelAirTempVal . Text to get global AirTemp
      set LabelPHVal . Text to get global AirQuality
      set LabelWaterTemperatureVal . Text to get global WaterTemp
      set LabelHumidityVal . Text to get global Humidity
      set LabelPHVal . Text to get global PH

when Clock2 . Timer
do
  if TableWaterLevel . Visible = true
  then
    if call BluetoothClient1 . BytesAvailableToReceive > 0
    then
      set global WaterLevel to call BluetoothClient1 . ReceiveText
      numberOfBytes -1
      if get global WaterLevel = 1
      then
        set LabelLowFull . TextColor to green
        set LabelLowFull . Text to "Sufficient"
      else if get global WaterLevel = 0
      then
        set LabelLowFull . TextColor to red
        set LabelLowFull . Text to "Low"

```

Figure 4: App Software Coding

Procedure to operate Bluetooth Application

<p>Step 1: Select Bluetooth application</p> <p>The Bluetooth application is created using the software Mock Flow. The application has to be selected in order to control the appliances through smartphone. First, have to connect the android with the Bluetooth, then have to click the Hydroponic farming button to open the Main Application Screen.</p>	
<p>Step 2: Main Application Screen (Appliances Option)</p> <p>The screen will show two application, which is Monitor sensors, Lights and Fan and Water level. User are required to choose one of the selections.</p>	
<p>Step 3: Monitor sensors application</p> <p>The Monitor sensors application screen is designed to monitor the pH value, Air temperature, Water temperature, Humidity and Conductivity.</p>	

<p>Step 4: Lights and fan application</p> <p>In order to control the UV Light, LED Light and Fan, lights option and fan option has to be chosen from the main application screen where appliances option is. the lights and fan application screen which have design to control(on/off) the lights and fan.</p>	
<p>Step 5: Water level application</p> <p>The Water level application screen is designed to monitor the water level. Once the option water level is selected in the previous Home appliances option, the water level application will show the water level whether it is low or sufficient.</p>	

Hardware Design

After all the required parameters have been discussed, the design concept is based on a stacking hydroponic system. By using a stacking design, it can maximise space and can grow more crops in a small space. Other than that, the stacking design also very efficient and effective for the flow of the nutrient's solution. For the grow tray, a cuboid shape grow tray has been chosen because it can fit more crops than other shape designs.

For the electronics part, three sensors have been chosen for monitoring purpose. The sensors included in the design are the temperature and humidity sensor, pH sensor and air quality sensor. The temperature and humidity sensor aim to sense the temperature and humidity of the surrounding because different crops need different temperature for effective growth. For the pH and air quality sensors, the purpose is to check the nutrients solution quality and the air quality level. All the sensors are connected to the Arduino. So, the system can be monitored remotely and the LED light, UV light and DC fan can be turn on and off remotely by android. To neutralise and filter the nutrients solution, air filtration will be utilised.

Design specification

The specification of the final design is listed below:

Table 1: Specification of the final design

Dimension	6ft x 3ft
Materials	Structure frame: Steel Grow tray: PVC
Growing medium	Foam matrix
System design	Stacking design
Sensors	Temperature and humidity sensor, Air quality sensor, pH sensor
Light type	LED light and UV light strip
Light color	Purple light
Type of pumps	External water pump, air pump

3D Design

Figure 5 until Figure 11 show the design of the Single Side Hydroponic System was created using Solidwork version 2018 which is a 3D engineering drawing software.

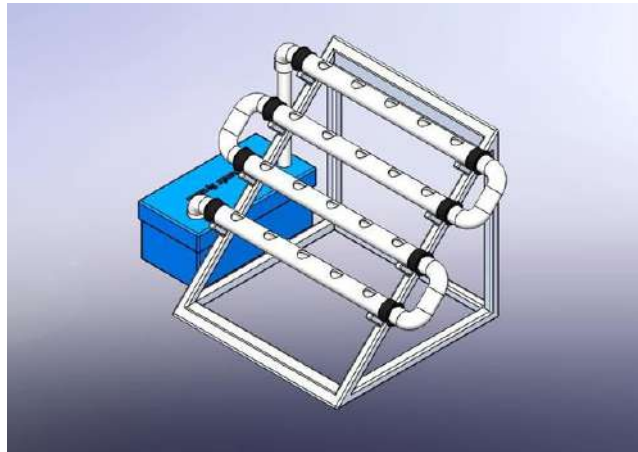


Figure 5: The standard orientation of the final design

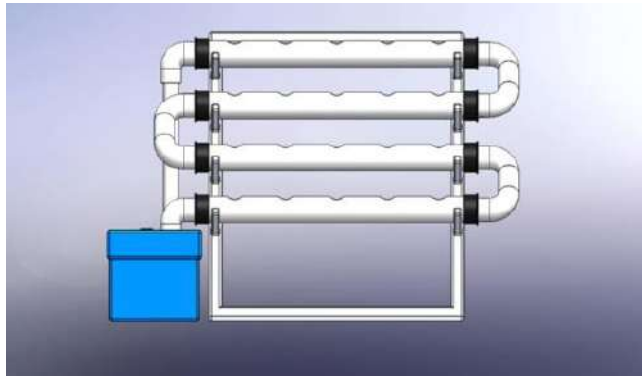


Figure 6: The front view of the final design

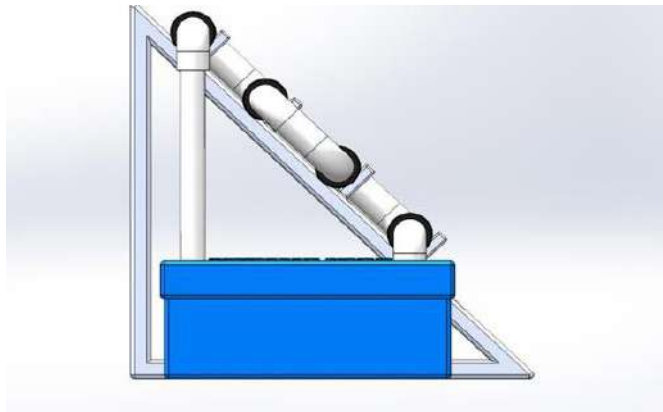


Figure 7: The left view of the final design

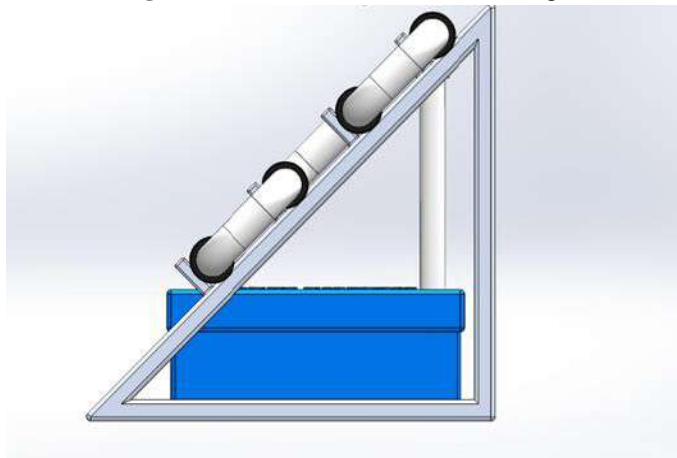


Figure 8: The right view of the final design

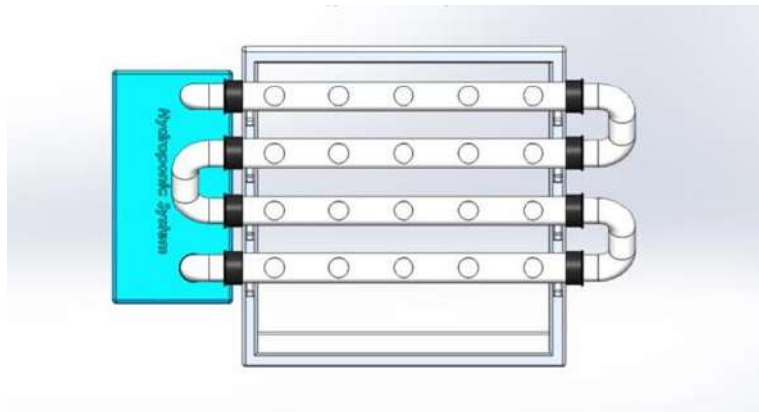


Figure 9: The top view of the final design

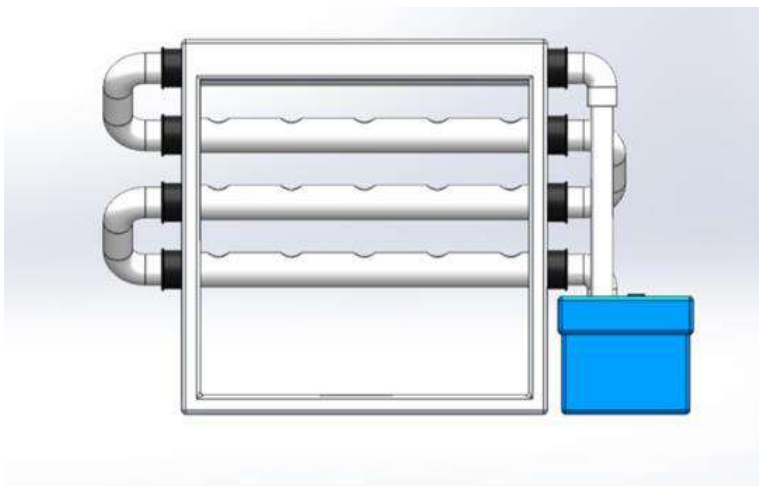


Figure 10: The back view of the final design

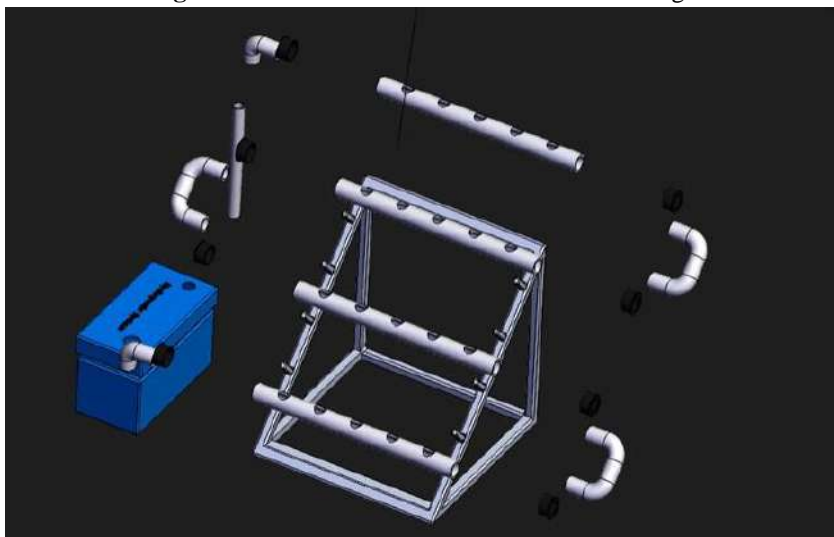


Figure 11: Exploded view

Mechanical drawing for the Proposed Design

The mechanical drawings for the proposed design as shown in Figure 12 and Figure 13 are drawn using Solidwork version 2018.

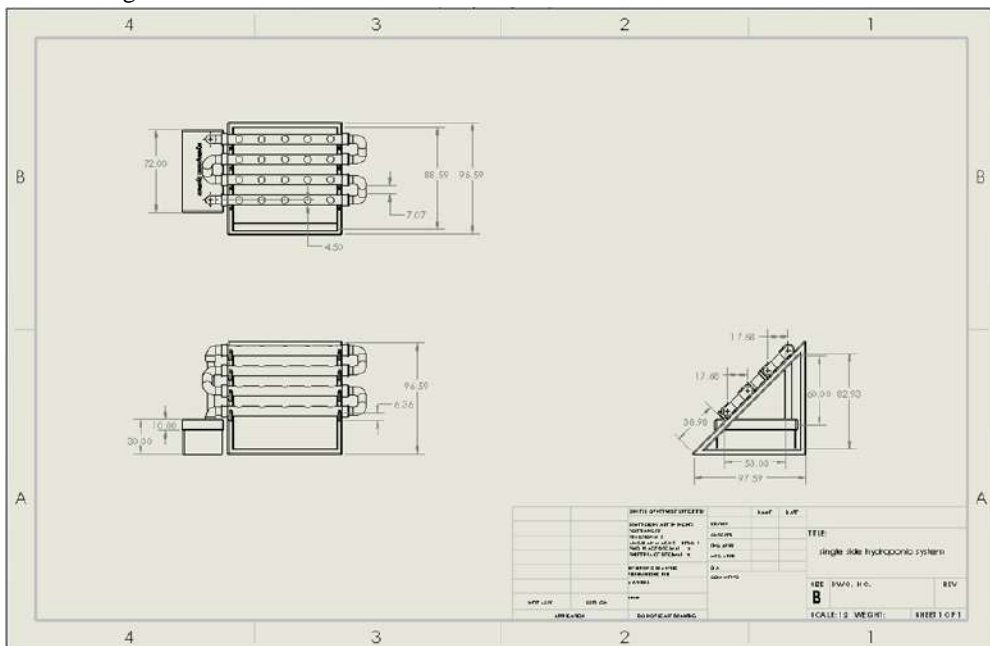


Figure 12: Single side hydroponic system

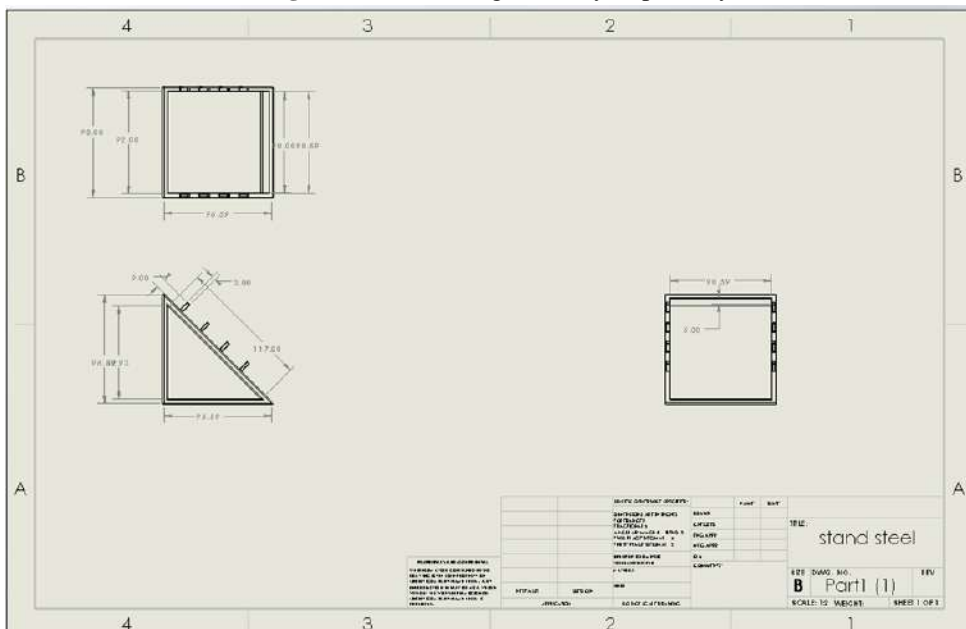


Figure 13: Stand Steel

Making of the Hydroponic tray

The hydroponic tray of the proposed design according to the specification as stated in Table 1 is

implemented as shown in Figure 14.



Figure 14: Hydroponic tray

4. RESULTS AND DISCUSSION

The hardware prototype of the control side is implemented as shown in Figure 15.





Figure 15: Hardware Connection



Figure 16: Monitoring of temperature, air quality, water temperature, humidity and pH value.

Figure 16 shows the display on LCD screen for different types of sensors, which monitor the temperature, air quality, water temperature, humidity and pH value of the hydroponic farming.



Figure 17: LED Light, UV Light and DC Fan

Figure 17 shows that users can turn on/ off the DC fan to control the humidity level. In addition, the mobile app also allows the users to turn on/ off LED light to enable the vegetables to do photosynthesis during cloudy and rainy days. Besides, users can turn on UV light in the rainy days by using the mobile app to reduce the growth of bacteria due to high humidity level during rainy days.

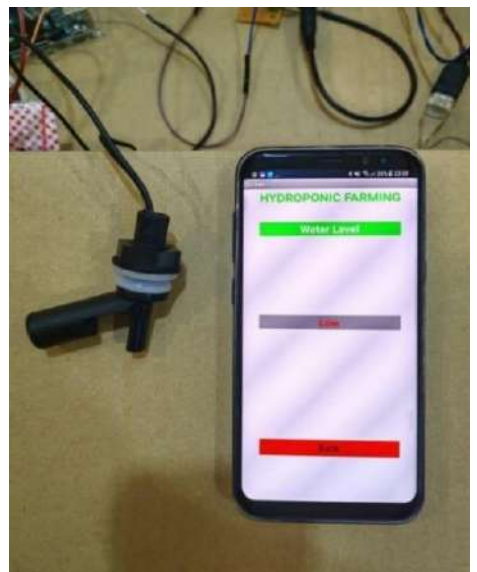


Figure 18: Water level

Figure 18 shows the results for water level. The level of the water is programmed to Low and Sufficient, it can be used to measure the water level, for that it has been connected to the +(Vcc) pin on the module to 5V on the Arduino and -(GND) pin to ground and the bluetooth sensor is connected to the Arduino to monitor the water level, if the water level in the tank decrease the water level sensor will detect it and will send the data to the app which have been created, then the application will show the output as Low.

After that LED Light, UV Light and DC Fan are connected to Arduino. The LED Light will help the plants to grow. It also last longer and uses less energy than alternative lighting system. In this proposed design, purple LED Light is used as it has a shorter wavelength and higher energy. Ultraviolet (UV) Light disinfectant is getting a lot of attention during the coronavirus pandemic. The main benefit is to kill pathogens like viruses and bacteria, so that it can help to kill the pathogens in the surrounding of the hydroponic farm. DC Fan has been connected to evacuate the toxic gas and or smoke from the farm.

Finally, there are some sensors have been connected to monitor the surrounding of the hydroponic farm. The sensors are pH sensor, temperatures and humidity sensor, water temperatures sensor and air quality sensor. These sensors will send the respective data to the Arduino and then display the output on the LCD. Besides that, it can also monitor by the app. The proposed system has faster transmission and it is very reliable as there will not be any connection problem. In addition, the wirings are very simple and there is no unwanted wiring where it might be dangerous as well.

5. CONCLUSION

This chapter proposes hydroponics agriculture system as a solution to combat climate change, to reduce environmental damage and species extinction caused by excessive exploitation and intensive agriculture. The proposed design incorporates with Internet of Things which is able to send notification to the end user about the pH value, temperature, humidity, and water level of the hydroponic. Upon receiving the notification from mobile app, users can turn on/ off the DC fan to control the humidity level. In addition, the mobile app also allows the users to turn on/ off LED light to enable the vegetables to do photosynthesis during cloudy and rainy days. Besides, users can turn on UV light in the rainy days by using the mobile app to reduce the growth of bacteria due to high humidity level during rainy days. It also allows for more rational use of water, an increasingly scarce source which satisfy the latest trends in smart farming to achieve higher crop yields. The implementation of the Bluetooth connection in the control board facilitates easy installation of the device. It allows the devices to be controlled faster and easier using smart phone comparing with other technologies. This system is designed in such way with minimal cost and maximum level of performance. An open source of Arduino UNO microcontroller board input output pin is used to connect the sensors while monitoring the collected data.

REFERENCES

- K. Al-Kodmany, The Vertical Farm: A Review of Developments and Implications for the Vertical City, vol. 8, no. 2, 24, 2018.
- Despommier, D., The Vertical Farm: Feeding the World in the 21st Century, Thomas Dunne Books: New York, NY, USA, 2010.
- M. Mehra, S. Saxena, S. Sankaranarayanan and R. J. T. a. M. Veeramanikandan, IoT based hydroponics system using Deep Neural Networks, Computers and Electronics in Agriculture, no. 155, pp. 473-486, 2018.
- Muhammad E. H. Chowdhury, Amith Khandakar , Saba Ahmed, Fatima Al-Khuzaei, Jalaa Hamdalla, Fahmida Haque, Mamun Bin Ibne Reaz, Ahmed Al Shafei and Nasser Al-Emadi, Design, Construction and Testing of IoT Based Automated Indoor Vertical Hydroponics Farming Test-Bed in Qatar, www.mdpi.com/journal/sensors, vol. 20, 5637, 2020.
- Lata S. Handigolkar, M.L. Kavya and P.D. Veena, Iot Based Smart Poultry Farming using Commodity Hardware and Software, Bonfring International Journal of Software Engineering and Soft Computing, Vol. 6, Special Issue, October 2016.

OPTIMIZATION OF TURNING PROCESS PARAMETERS USING TAGUCHI METHOD

Mohd Shahrudin Mohd Alias & Abueid Ammar Ahmed Mohammed
Infrastructure University Kuala Lumpur

1. INTRODUCTION

In manufacturing industries, priority is cost reduction and quality refinement during the machining phase as it is a competitive environment that requires machining focus parameters to attain optimum performance of the different parameters i.e. speed of cutting, the rate of feed and depth of the cut. The process parameters impact the product's responses, for example surface roughness (Ra), rate of material removal (MRR), precautionary cost and rate of output. According to Sapuan (2013), CNC-Computer Numerical Controls applied by current developed industries to circumvent traditional machining processes that focus only on Surface Roughness (Ra) and avoid other results such as machining time that results in higher costs and lower production rate. Goal of the modern industry is to improve manufacturing technology for high-level efficacy. According to Pinar (2013), quality in the latest machining industries could be achieved by the accuracy of workpiece measurements during the machining process, decreased wear, increased production rate, finished surface in cutting tools, the efficacy of the product and reduced environmental effect while processing, so for that purpose handbook for the manufacturing of the industries should be made for setting the criteria.

For cutting parameters, Taguchi method is used as an alternative approach for obtaining the proper strategy for enhancing efficiency and cost-effectiveness for a quality system. The Taguchi method can decrease the responsiveness in the performance of the device according to Kirby (2006). Professor Genichi Taguchi of Nippon Telephones and Telegraph Company of Japan developed the statistical method called Taguchi method for robust goods. According to this method, once the product is delivered, the loss can be calculated for the quality of the manufactured product.

The Taguchi method uses experimental design tools to decrease susceptibility to noise factors, make products more reliable, and improve the process and product design by identifying the factors and their setting. Its method is used for many fields such as marketing, engineering, biotechnology and advertising. Taguchi introduced orthogonal array experimental method for the observation with "variance" of control parameters which decreases the optimum setting. According to Jha (2016), the resultant of Design of Experiments application with control parameter optimization can help achieve the required results. Robust design uses two main instruments: the S/N ratio, which is the log function of the required output measurement quality that focuses on variance, and orthogonal collection which provides a collection of well-balanced experiments simultaneously to assure several design factors.

2. PROBLEM STATEMENT

In the manufacturing industries, one of the most significant machining processes is the turning operation and it is difficult to maintain the best quality of the output material. It faces many difficulties and to attain the best turning circumstances and the required results, certain complications should be considered. Noise influences the Ra during the process, one of the principal yields. Noise is an unmanageable factor like humidity, friction, temperature and vibration.

Failure of the product is caused by the variation in the roughness of the surface in the production unit, which is caused by poor execution of the machining process. Machining parameters were not set to their best levels due to higher prices and improper study of the parameters like rate of feeding, speed of cutting, and depth of cut that increases the manufacturing cost with good product quality, which is a difficult task in production units. Due to this reason, MRR is used, which is an efficient component that not only reduces the price of production but also enhances the quality of the product.

3. RESEARCH OBJECTIVES

The study is conducted to investigate the most significant factors of turning operation affecting the surface roughness (Ra) and material removal rate (MRR) experimentally by using the Taguchi Design of Experiment. It also determines the optimum combination of turning operation parameters to minimize the surface roughness (Ra) and maximize the material removal rate (MRR). A statistical prediction confirms the effect of the optimum parameters on Ra and MRR with the optimal parameters identified by the S/N ratio (larger-the-better).

4. LITERATURE REVIEW

According to Rusinel (2010) engineers and scientists have reported certain issues in manufacturing sector for achieving the desired quality such as cutting tool materials, work piece materials and cutting tool nomenclature which affect the quality characteristics such as Ra in any machined part. Attainment of the desired results is a difficult task. Benardos (2003) and Vosniakos (2002) reported that parameters of machining are convenient factors to be used for their importance for determination of Ra, machine condition, coolant, environmental condition, machine tool accuracy, etc. Taguchi method is used for the evaluation of cutting parameters to attain the optimal cutting parameters for the turning phase.

CNC is used for removal of the outer diameter by turning the process that provides the essential power for turning the work piece at a specified rotational speed; feed the cutting tool and cutting depth which aids to get the required shape of a metal. During the turning process, the cutting tool may have elevated temperatures and pressures concurrently, creating a harsh atmosphere for the cutting tool. According to Pinar (2013) it is essential to consider the life of the method due to the effect of Ra and MRR responses in this analysis.

For quality and efficiency, the performance of the machining process is crucial. High efficiency and quality can be achieved during the machining process by concentrating on the MRR (Lin & Chang, 2017). Furthermore, Ra has a vital role in determining the machining parameters in many fields. A very high mass output can be achieved to get the optimum MRR during the process, that is why CNC machine is used to increase the amount of productivity that results in the cost of machining along with the efficacy and quality of the manufacturing units.

4.1. Taguchi method and analysis of variance (ANOVA)

The Taguchi method aims to give great machining parameters which aid in attaining high quality and take into account the cost, which requires a robust design to minimize process variations (Somashekara, 2012). During the experiment, many possibilities get difficult as data inputs are enormous too, and there is a need to choose which ones are best for the experiment to attain the required objectives. Because of this, Taguchi developed an Orthogonal Array technique to explore and choose how critical parameters can influence the process mean and variance, decrease the choice, and use the least number of experiments, as mentioned by Abdulkareem et al. (2011). Thus, a system that runs on three parameters with three different levels is chosen and involves a collection of $3^3 = 27$ tests for the variety of possibilities for the parameters. However, OA decreases the number of tests to collect small quantities of data with the potential to convert the results into a brief and verifiable inference instead of performing 27 experiments (Hassan et al., 2012). The Taguchi Orthogonal Arrays selection table based on factors is also shown in Figure 1 and 2 for guidance in designing the experimental run.

The evaluation of data can be attained using ANOVA by gathering the procedures of the experiment along with mathematical models for describing the impact that occurs in several experiments from the input parameters using experiment design that can clarify the experiment data in the machining phase (Ranganath et al., 2013). In addition, ANOVA analyses all the input parameters, identifies the differences between the parameter sets and provides the means between all the parameters to make them equal.

The Taguchi method suggests that ANOVA can be used to test the machining process and the cutting efficiency that can affect Ra and MRR process parameters. In addition, ANOVA analyses and compares a collection of experiments that focus only on the effects of the variance. ANOVA is used to calculate the mean in the S/N to analyze the design variables and exclude any effects on the response that might occur significantly (Kumar et al., 2014).

Orthogonal Array	Number of Runs	Maximum Factors	Maximum of columns at these levels			
			2-level	3-level	4-level	5-level
L4	4	3	3			
L8	8	7	7			
L9	9	4		4		
L12	12	11	11			
L16	16	15	15			
L'16	16	5			5	
L18	18	8	1	7		
L25	25	6				6
L27	27	13		13		
L32	32	31	31			
L'32	32	10	1		9	
L36	36	23	11	12		
L'36	36	16	3	13		
L50	50	12	1			11
L54	54	26	1	25		
L64	64	63	63			
L'64	64	21			21	
L81	81	40		40		

Figure 1: Taguchi Orthogonal Arrays Selection Table Based on Factors (Balisnomo, 2008)

	A	B	C	D	E	F	G
1	1	1	1	1	1	1	1
2	1	1	1	2	2	2	2
3	1	2	2	1	1	2	2
4	1	2	2	2	2	1	1
5	2	1	2	1	2	1	2
6	2	1	2	2	1	2	1
7	2	2	1	1	2	2	1
8	2	2	1	2	1	1	2

Figure 2: Example of $L_8(2)^7$ Orthogonal Array

4.2. Parameters to Input

These are the basis of the turning process, which can be adjusted for the desired product's cutting speed, cutting depth and feed rate and cutting depth as these are key factors of the process due to the impact of both Ra and MRR responses (Khandey, 2009). The motion of the transfer operation is shown in figure 2.2.

4.3. Speed of Cut

The cutting tool is used in this theory to attain across the surface of the workpiece from the spindle speed, N. For this purpose, the expression used for the first parameter in the cutting velocity turning phase is V_c and its unit is m/min (Kumar, 2013).

$$V_c = \frac{\pi DN}{1000} \quad (1.0)$$

Where

V_c = workpiece cutting speed

N = workpiece spindle speed, rpm

D = cutter's diameter, mm

4.4 Rate of Feed

The feed rate is the tip tool's movement in each revolution along the path of the workpiece rotation. The feed rate symbol is (F) and its unit is (mm/rev), as mentioned by Kumar (2013).

$$Fm = f N \quad (2.0)$$

Where the symbols represent

N = workpiece spindle speed, rpm

f = feed rate, mm/rev

4.5. Depth of Cut

It is the required for cutting the work piece in order to remove the thickness of the work piece surface material by the deepness of infiltration into the work piece from the cutting tools which is determined previously from the rotation of the work piece as mentioned by Kumar (2013).

$$d = \frac{D_1 - D_2}{2} \quad (3.0)$$

Where symbol represent

D_1 = preliminary diameter of job

D_2 = final diameter of job

4.6. Surface Roughness (Ra)

Ra is affected by various factors because it is a complicated task to achieve and track compared to the physical dimension because of the various factors, some of which are controllable and some are not. Kadirgama et al. (2009) selected the feed rate, tool geometry, speed of cut, tool setup and depth of cut as their controllable variables in their experimental setup. On the other hand, the parameters which cannot be easily controlled are machine vibration, workpiece, tool wear and degradation and material. Kok (2011) observed that the influence of Ra and other parameters could be increased by cutting speed.

Various devices are used for the measurement of Ra known as Profilometer. This is similar to an inspection tool used to analyze the roughness, waviness, and other finish parameters. This task can be achieved either by stylus-based, which measures the texture of the surface by using a sharp pointed tool dragged across the surface, so the roughness or the waviness can be analyzed with surface profile data. Another way is to measure the surface by optical scan using light or laser (Mechlook, 2019).

4.7. Material Removal Rate (MRR)

One of the vital output parameters in manufacturing industries is MRR which alters the quality of the finished form and this is the material that is removed from the workpiece per time, which aids in the turning process by enhancing the quantity of the material removed from the workpiece and as a result we get greater production rate (Andhale, 2014). To improve the production rate, there should be a high cut speed. MRR in turning operation is considered that leads to less cost of the product with better quality, whereas; the reason for this research is to attain the maximum MRR along with high-performance turning operation (Singhvi, 2016).

$$MRR = \frac{W_i - W_f}{\rho \cdot t} \quad (4.0)$$

Where the symbols represent

W_i = initial weight before the machining, g

t = time of machining, sec

MRR = material removal rate, mm³/min

ρ = density of aluminium 6061, kg/m³

W_f = final weight after the machining, g

5. METHODOLOGY

5.1. Selection Criteria of the Cutting Parameters Along with their Levels

Parameters and the levels of this experiment are shown in Table 1 below in finding the optimal value of Ra and MRR.

Table 1: Cutting Parameters and Their Levels

Process parameters	Unit	Level 1	Level 2	Level 3
Cutting Speed	rpm	500	1000	1500
Feed Rate	mm /rev	0.10	0.40	0.70
Depth of the cut	mm	0.40	1.00	1.60

5.2. OA-Orthogonal Array Design

Design of Experiment aids the Taguchi technique in using Orthogonal Array in Minitab software for reducing the experiment numbers from twenty-seven (27) to nine (9) as implemented by Hassan (2012). Tables 2 and 3 show the analysis of Minitab programme.

Table 2: Orthogonal Array L₉(3)³

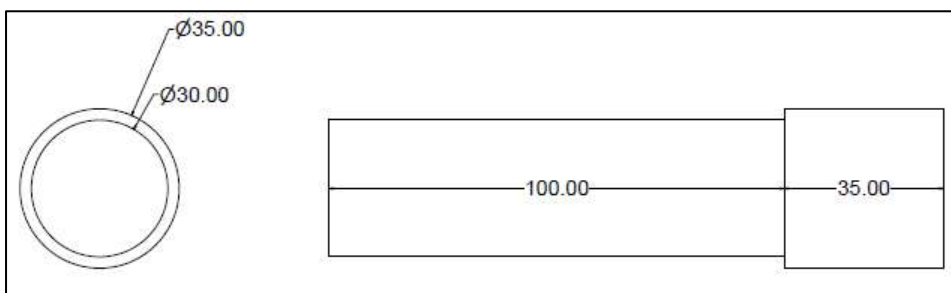
Trial No.	Cutting speed (rpm)	Rate of the feed (mm/rev)	Deepness of the cut (mm)
1	1	1	1
2	1	2	2
3	1	3	3
4	2	1	2
5	2	2	3
6	2	3	1
7	3	1	3
8	3	2	1
9	3	3	2

Table 3: The factors with the chosen level.

Test No.	Cutting speed (rpm)	Rate of the feed (mm/rev)	Deepness of the cut (mm)
1	500.0	0.10	0.40
2	500.0	0.40	1.00
3	500.0	0.70	1.60
4	1000.0	0.10	1.00
5	1000.0	0.40	1.60
6	1000.0	0.70	0.40
7	1500.0	0.10	1.60
8	1500.0	0.40	0.40
9	1500.0	0.70	1.00

5.3. Workpiece Dimensions

This experiment involves a turning operation. The sample to be cut is around 100mm from the total 135 mm long. The initial diameter is 35 mm before the operation and reduced to 30 mm (maximum) after the machining process, as shown in Figure 3. The selected material for this study is Aluminum 6061 under the aluminium alloy 6000 series.

**Figure 3: Workpiece sample dimension**

5.4. Cutting Condition

Water coolant dependent on synthetics is used for the cutting condition of this experiment. It is variable because of its support and is used during the machining process. It is an essential step for decreasing contact between the interfaces of the work piece and cutting tool that makes the instrument's performance better even at a high cutting temperature, as mentioned by Halim (2008).

5.5. Surface Roughness Measurement and Material Removal Rate Calculation

As shown in Figure 4 and 5, the Surfcom Nex is used to measure the surface roughness, Ra.



Figure 4: Surfcom Nex for Ra Measurement

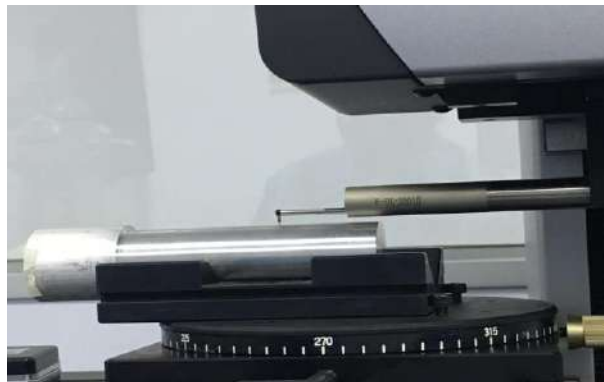


Figure 5: Setup of Surfcom Nex for Measurement of Ra

For MRR, it is calculated for each run before and after the machining process. The MRR difference in weight is calculated using equation 4 shown previously.

Results and Discussion

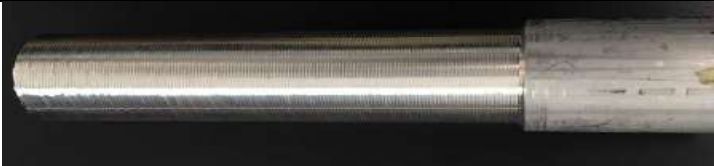
6.1. Data Collection and Main Effect Results for Surface Roughness (Ra)

To obtain the S/N ratio Taguchi method is used in Minitab software while performing the Ra. Experimental values are calculated using the Minitab software to find the average and S/N ratio in Table 4. For better control of the behaviour of noise parameters, greater numbers are suggested for the S/N ratio. The first round has more values of S/N ratio that indicates the lowest quantity of noise parameter in all runs. Table 5 shows the summary of the surface roughness profile measured for each of the experimental runs.

Table 4: Experimental Outcomes for Ra, S/N Ratio and Mean

Experiment No.	Cutting speed (rpm)	Feed rate (mm/rev)	Depth of cut (mm)	Ra (μm)	S/N ratio	MEAN
1	500.00	-0.10	0.40	1.1508	-1.2214	1.1505
2	500.00	0.40	1.00	6.4203	-16.1515	6.4207
3	500.00	0.70	1.60	18.7719	-25.4705	18.7719
4	1000.00	0.10	1.00	1.2995	-2.2783	1.2991
5	1000.00	0.40	1.60	9.6276	-19.6705	9.6274
6	1000.00	0.70	0.40	28.9904	-29.2456	28.9905
7	1500.00	0.10	1.60	1.6357	-4.2726	1.6356
8	1500.00	0.40	0.40	9.6246	-19.6689	9.6259
9	1500.00	0.70	1.00	18.6110	-25.3951	18.6101

Table 5: The Surface Roughness (Ra)

Trial Number	Workpiece after cutting
1	
2	
3	

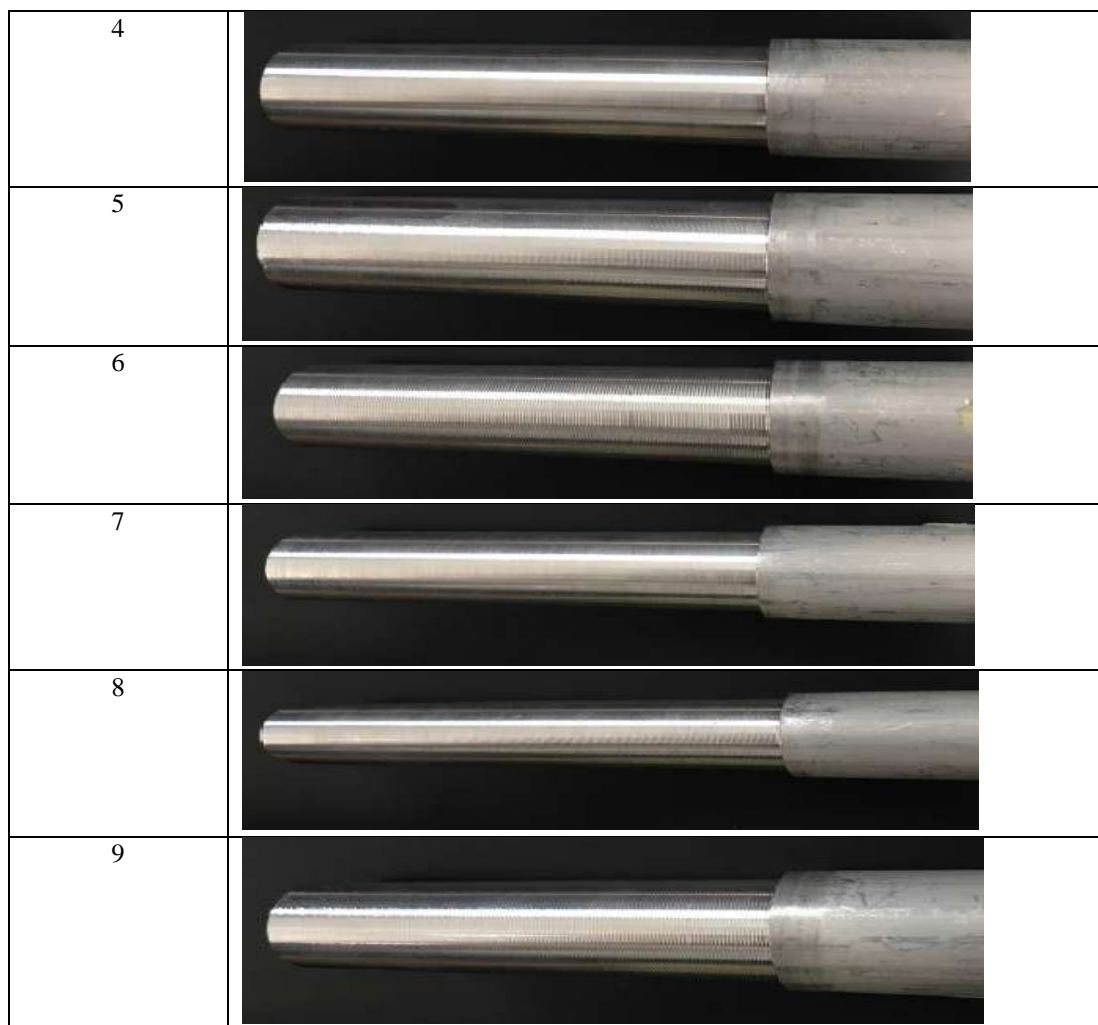


Table 6 shows the tabulation of the S/N ratio for Ra. Next, the optimal parameters are identified according to the nomi-the-Better setting. For this condition, further attention is given to the S/N ratio nearest to zero to select the optimal parameters for the next prediction. In this case, the selected level for optimal cutting speed and the feed rate are Level 1, and the depth of cut is Level 2. Figure 6 shows that the optimum combination is when the cutting speed is 500 rpm, the feed rate is 0.10 mm/rev and the depth of cut is 1.00 mm. These parameters are selected as the optimal parameters for Ra. In terms of rank, it is decided based on the difference in value (delta) between the factor of Levels 1, 2 and 3. The larger the difference (delta value), the higher the ranking.

Table 6: Result for S/ N Ratios (Smaller-the-Better)

Level	Cutting speed	Feed rate	Depth of cut
One	-14.2812	-2.5906	-16.7124
Two	-17.0653	-18.4977	-14.6083
Three	-16.4454	-26.7035	-16.4712

Delta	2.7846	24.1136	2.1031
Rank	2 nd	1 st	3 rd

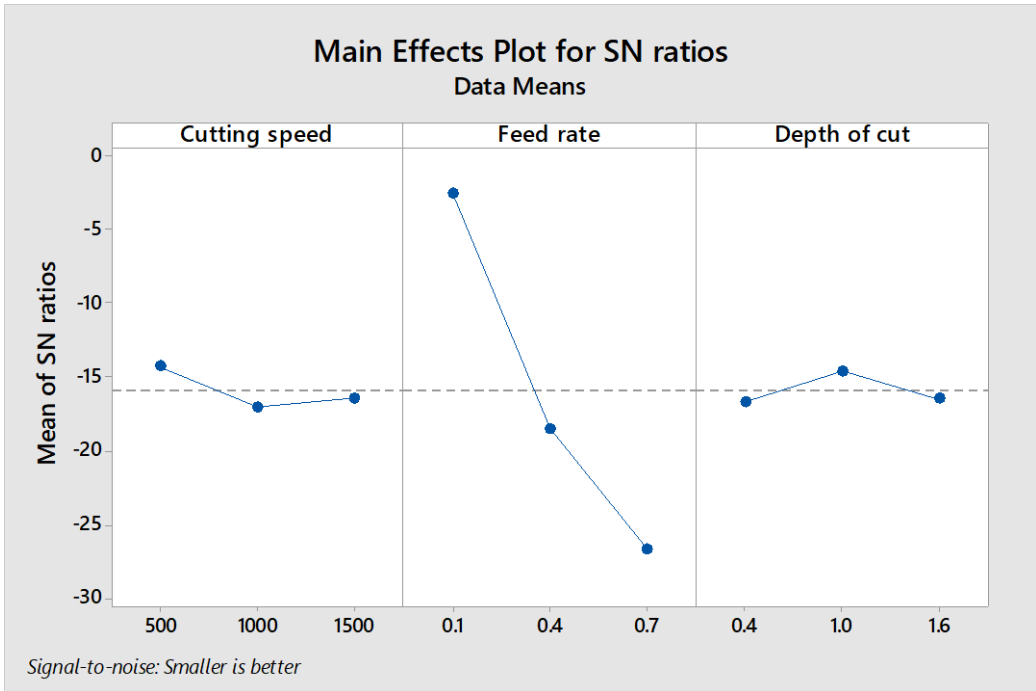


Figure 6: Major Effect graph for Signal to Noise Ratios for Ra (Smaller-the-Better)

Based on the response table for means (Table 7), delta results show that the feed rate has been ranked as the highest factor affecting response results, while the cutting speed has been ranked as the lowest factor affecting the response. The feed rate has the highest value. As shown in Figure 7, the plot shows the main effect of maximum to minimum parameters for three factors specified in the study. In overall, the feed rate factor has the greatest effect and largest change to the means response.

Table 7: The Response for Means - Ra

Level	Cutting speed	Feed rate	Depth of cut
One	8.7812	1.3621	13.25657
Two	13.3064	8.5589	8.7777
Three	9.9575	22.1245	10.0129
Delta	4.5252	20.7644	4.4792
Rank	2 nd	1 st	3 rd

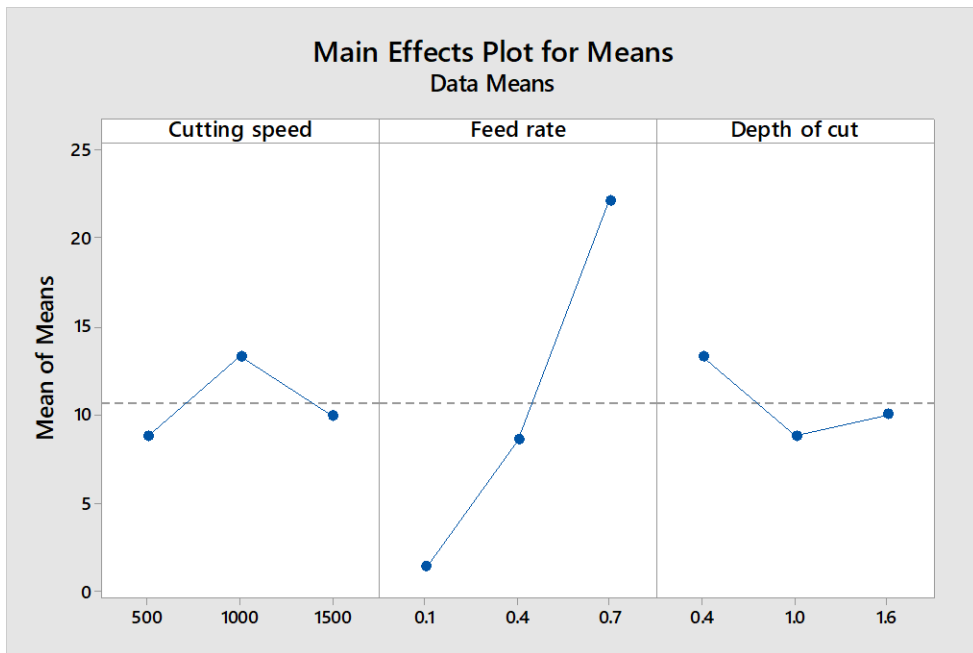


Figure 7: Major Effectiveness Plotting for Means for Ra

6.2. Analysis of the variance for the effects on Surface Roughness (Ra).

In order to identify the most significant factor that affects the response (Ra), ANOVA is used with the aid of Minitab software. This study implements the confidence level (95%) to identify the most significant factor based on the P-value.

As shown previously by the main effect plot (Figure 7), the feed rate has the greatest effect and largest change to the means response. Table 8 further specifies that the feed rate is the most significant factor, with a P-value of 0.019 based on the ANOVA model. It is followed by the Speed of Cut (P-value of 0.265) and Depth of Cut (0.282). In statistics, these factors have no significant effect on the response (Ra) since the P-values are larger than the 0.05 significant value.

Table 8: ANOVA of Ra

Sources	DFs	Adj SS	Adj MS	F-Values	P-Value
Feed rate	2.0	666.900	333.4489	53.24	0.019
Cutting speed	2.0	33.070	16.5368	2.644	0.265
Depth of cut	2.0	32.119	16.0537	2.567	0.282
Error	2.0	12.539	6.2631		
Total	8.0	744.607			

6.3. Prediction for Surface Roughness (Ra)

With the aid of Minitab software, the prediction function in the Taguchi analyzer is utilized to predict the mean of surface roughness, Ra value based on the optimal parameters identified previously using the S/N ratio value (Table 9). As shown in Table 10 the selected parameters are the optimal condition or even lower for ideal surface roughness, Ra level based on the statistical prediction with mean response is $-2.442 \mu\text{m}$ and S/N ratio is 0.382.

Table 9: Optimal Parameters for Ra

Factor	Levels	Optimal Values
Cutting speed	1	1000 rpm
Feed rate	1	0.10 mm/rev
Depth of cut	2	1.00 mm

Table 10: Surface Roughness (Ra) Prediction

Cutting speed	Feed rate	Depth of cut	S/N ratio	Mean (Ra)
500.00	-0.10	1.0	0.382228	-2.44269

6.4. Data Collection and Main Effect Results for Material Removal Rate (MRR)

The summary of the calculated Material Removal Rate, MRR is shown in Table 11 based on the experimental data results. With the aid of Minitab software, the Taguchi analysis function is used to find the S/N ratio and the average for the MRR data analysis.

Table 11: Experimental Data of the MRR

Trial No.	Cutting speed (rpm)	Feed rate (mm/rev)	Depth of cut (mm)	Initial weight (kg) (W_i)	Final weight (kg) (W_f)	Time (sec)	MRR (mm^3/min)
1	500.00	0.10	0.40	0.450	0.287	469	7723.2
2	500.00	0.40	1.00	0.450	0.287	409	8856.2
3	500.00	0.70	1.60	0.450	0.288	370	9729.7
4	1000.00	0.10	1.00	0.450	0.287	451	8031.5
5	1000.00	0.40	1.60	0.450	0.287	398	9101.0
6	1000.00	0.70	0.40	0.450	0.287	389	9311.6
7	1500.00	0.10	1.60	0.450	0.286	435	8378.0
8	1500.00	0.40	0.40	0.450	0.287	395	9170.1
9	1500.00	0.70	1.00	0.450	0.287	387	9359.7

The S/N ratio based on the experimental results summarized in Table 12 is calculated

using the Taguchi analysis function in the Minitab software. For the identification of optimal parameters with consideration of control and noise factors, the greater value of the S/N ratio is recommended. The 3rd trial in the table shows the highest value of the S/N ratio, which identifies the control factor parameters that minimize the effects of the noise factors.

Table 12: Experimental Results for MRR, S/N Ratio and Mean.

Trial No	Cutting speed (rpm)	Rate of feed (mm/rev)	Cut's deepness (mm)	MRR (mm³ per min)	S/N ratio	MEAN1
1.	500.0	0.10	0.40	7723.2	77.756	7723.2
2.	500.0	0.40	1.00	8856.2	78.945	8856.2
3.	500.0	0.70	1.60	9729.7	79.762	9729.7
4.	1000.0	0.10	1.00	8031.5	78.096	8031.5
5.	1000.0	0.40	1.60	9101.0	79.181	9101.0
6.	1000.0	0.70	0.40	9311.6	79.380	9311.6
7.	1500.0	0.10	1.60	8378.0	78.462	8378.0
8.	1500.0	0.40	0.40	9170.1	79.247	9170.1
9.	1500.0	0.70	1.00	9359.7	79.425	9359.7

Values in Table 13 shows the S/N ratio for MRR at each level, while Figure 8 visualizes the main effect plot for the S/N ratio values. It is observed that the optimum level based on the Larger-the-better condition is the depth of the cut at 1.6 mm, the speed of the cut at 1500 rpm, and the feed rate at 0.7 mm/rev. These parameters are then used as the optimal parameters for the confirmation stage run.

Table 13: Response for S/ N Ratios (Larger-the-Better)

Levels	Cutting speed	Rate of feed	Cut's deepness
1	78.821	78.101	78.791
2	78.893	79.122	78.82
3	79.052	79.523	79.148
Delta	0.223	1.426	0.348
Rank	3	1	2

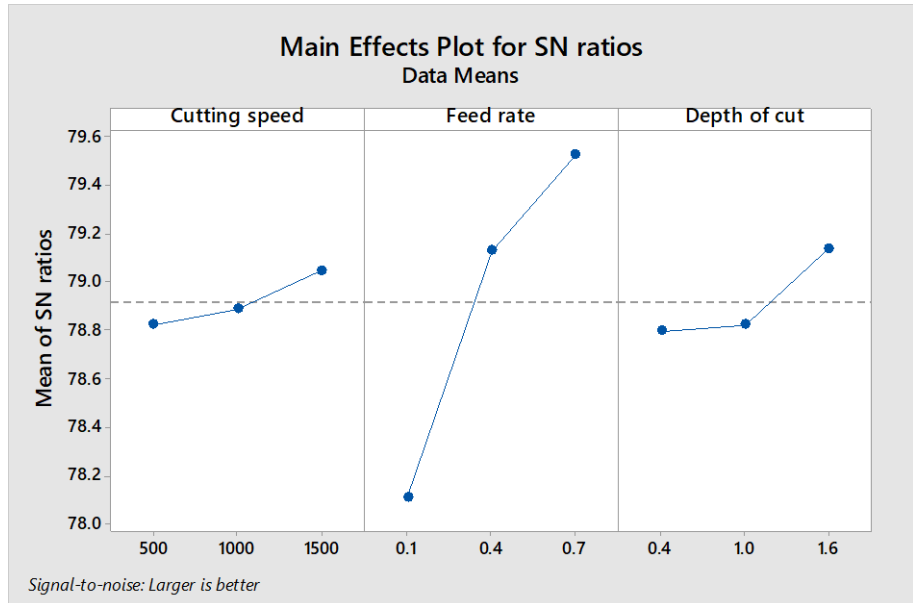


Figure 8: Main Effects Plot for S/N Ratios on MRR

Table 14 shows the delta value of each factor according to the mean result. The rank is given based on the magnitude of effects for each factor, where the largest difference in the mean from the factor level is ranked first. As shown in Figure 9, it is observed that the feed rate has the highest delta value at 1424 mm/rev, the depth of cut at 336 mm and the speed of the cut at 300 rpm.

Table 14: Response for Means for MRR

Levels	Cutting Speed	Feed Rate	Depth of cut
1	8771	8044	8736
2	8814	9049	8748
3	8968	9461	9071
Delta	200	1424	336
Rank	3 rd	1 st	2 nd

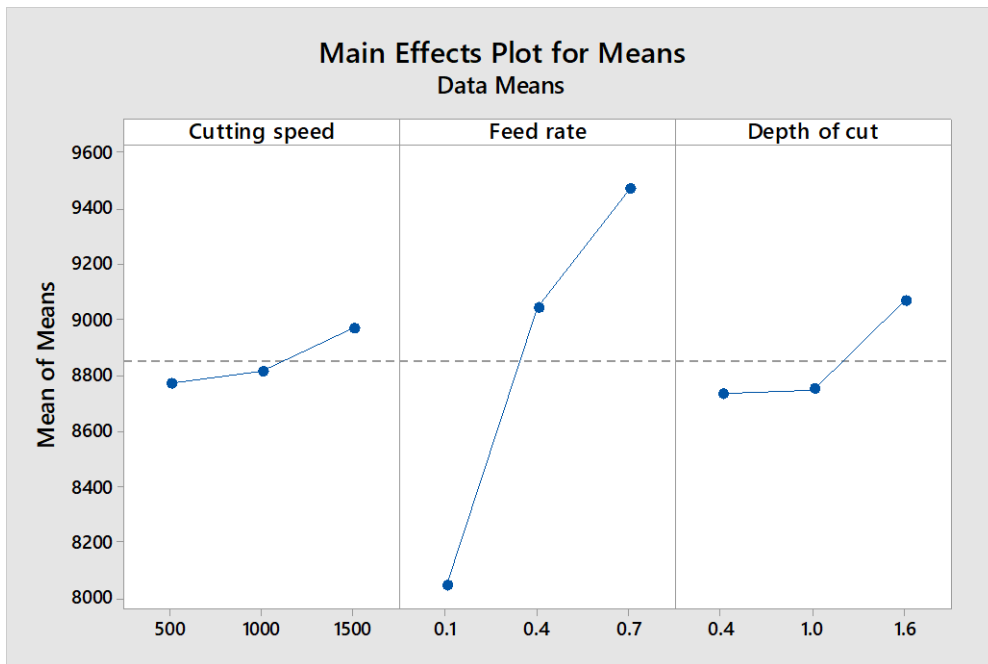


Figure 9: Main Effects Plot for Means for MRR

6.5. ANOVA for the Effects on the Material Removal Rate MRR.

For the purpose of investigating the importance of the parameters on the MRR response and to give some of the important results in this experiment the Minitab software is used by following the Taguchi method. The best part of this experiment is having the level of confidence which is 95%.

By careful evaluation of the values in Table 15, it is analyzed that feed rate is the most significant factor in this analysis, because of its important statistical influence ($P = 0.028$) in comparison to the depth of cut ($P = 0.302$) followed by speed of the cutting ($P = 0.586$). The P-value results explain the significance of the parameters after performing the experiment that is considered statistically significant when the model is less than 0.050 so the parameters have a significant influence on the MRR.

Table 15: ANOVA of MRR

Source	DF	Adj SS	Adj MS	F-Value	P-Value
Feeding rate	2	3200881	1600440	34.370	0.028
Depth of the cut	2	214805	107403	2.310	0.302
Cutting speed	2	65740	32870	0.71	0.586
Error	2	93118	46559		

Total	8	3573545			
--------------	---	---------	--	--	--

6.6. Prediction for Material Removal Rate (MRR)

With the aid of Minitab software, the prediction function in the Taguchi analyzer is utilized to predict the mean of material removal rate, MRR value based on the optimal parameters identified previously using the S/N ratio value (Table 16). As shown in Table 17 the selected parameters are the optimal condition or even higher than then ideal material removal rate, MRR level based on the statistical prediction with mean response is 9803.39 mm³/rev and S/N ratio is 79.869.

Table 16: Optimal Parameters for MRR

Factor	Levels	Optimal Values
Cutting speed	1	1500 rpm
Feed rate	1	0.7 mm/rev
Depth of cut	2	1.6 mm

Table 17: Material Removal Rate (MRR) Prediction

Cutting speed	Feed rate	Depth of cut	S/N ratio	Mean (MRR)
1500	-0.7	1.6	79.8685	9803.39

7. CONCLUSION

This study is conducted to analyse the machining parameters and turning process against two responses; Ra and MRR, while using the Aluminium 6061. Being less effective on machining parameters and for efficient results and methods, Taguchi method was applied effectively. To optimize the machine parameters and experimental results two important techniques were used such as S/N ratio and ANOVA.

The optimal combination process parameters for minimum Ra (Smaller-the-better) is obtained using the S/N ratio results which reflect that when cutting speed is 500 rpm, feed rate is 0.1 mm/rev and depth of cut is 1.0 mm. It is found that the most significant parameter in this experiment is the feed rate due to its significant statistical influence ($P = 0.019$) compared to the cutting speed ($P = 0.265$) followed by depth of cut ($P = 0.282$).

The optimal combination process parameters for maximum MRR (Larger-the-better) is obtained using S/N ratio results which reflect that when cutting speed is 1500 rpm, feed rate is 0.7 mm/rev and depth of cut is 1.6 mm. It is found that the most significant parameter in this experiment is the feed rate due to its significant statistical influence ($P = 0.028$) compared to the depth of cut ($P = 0.302$) followed by cutting speed ($P = 0.586$).

The prediction of the optimal parameters is conducted to both Ra and MRR, and according to the results, optimal responses are anticipated. This indicates that the study has successfully

identified the optimal parameters, which will significantly improve Ra and MRR results in turning operation.

REFERENCES

- Abdulkareem, S., Rumah, U. J., Adaokoma, A., 2011, Optimizing Machining Parameters during Turning Process,. *International Journal of Integrated Engineering, Vol. 3*, 23-27.
- Andhale S. R., Patokar P. T., Patil C. V., Bhambale S.S., 2014, Problems in Improving Production Rate in Turning Operation. *International Journal of Engineering Research & Technology*.
- Balisnomo, R. (2008). *Introduction to taguchi method*. Ingersoll Rand. <https://www.slideshare.net/rbalisnomo/Introduction-To-Taguchi-Method-05Sep08>
- Benardos, P. V. 2003, Predicting surface roughness in machining : a review. *Int. J. Mach. Tools Manuf.*, 833-844.
- C. Vosniakos. 2002, Predicting surface roughness in machining: a review. *International Journal of Machine Tools & Manufacture* 43.
- E, K. D. 2006, A parameter design study in a turning operation using the Taguchi method. *The Technology Interface Journal*.
- H.M.Somashekara. 2012, Optimizing Surface Roughness in Turning Operation Using Taguchi Technique And ANOVA,. *International Journal of Engineering Science and Technology.vol 4*, No.5.
- Halim, M.S.B., 2008, "Tool Wear Characterization of Carbide Cutting Tool Insert in a Single Point Turning Operation of AISI D2 Steel," B.Tech. thesis,. *Department of Manufacturing Engineering, Universiti Teknikal Malaysia Melaka*.
- Hassan, K., Kumar, A., Garg, M. P., 2012, Experimental investigation of Material removal rate in CNC turning using Taguchi method,. *International Journal of Engineering Research and Applications Vol2, issue 2*,, 1581-1590.
- Jha., Kumar, S., 2016, Parametric Optimization of Turning Process Using Taguchi Method and ANOVA Analysis . *International Journal of Advances in Engineering & Technology*,.
- Kadirgama, K., Noor, M. M., Rejab, M. R. M., Abou-El-Hossein, K. A., Bakar, R. A., Ismail, H., 2009, "Effect of Tool Holder Angles on Cutting Force When Machining Aerospace Material". *International Conference on Recent Advances in Materials, Minerals and Environment*, 2-10.
- Khandey, U. 2009, "*Optimization of Surface Roughness, Material Removal Rate and cutting Tool Flank Wear in Turning Using Extended Taguchi Approach*,". Rourkela: MTech thesis, National Institute of technology.
- Kok, M. 2011, "Modelling the effect of surface roughness factors in the machining of 2024 A/Al₂O₃ particle composites based on orthogonal arrays", *The international journal of advanced manufacturing technology*, 55, 911-920
- Kumar, G. 2013, "*Multi-Objective Optimization of Cutting and Geometric parameters in turning operation to Reduce Cutting forces and Surface*" B.Tech Thesis, National Institute of Technology, 1-24.

- Kumar, A., Chaudary, G., Kalra, M., Prabhakar, S. M., Jha, B. K., 2014, Optimization of Turning Parameters By Using Taguchi Method For Optimum Surface Roughness. *International Journal of Mechanical And Production Engineering*.
- Lin, C. S., Chang, M. F., 2017, A study on the effects of vibrations on the surface finish using a surface topography simulation model for turning. . *International Journal of Machine Tools & Manufacture*, , 763-788.
- Roughness,". Rourkela: B.Tech. thesis, Department of Mechanical Engineering, National Institute of Technology,.
- Mechlook, n. 2019, "*Surface Finish – Direct Measurements*,". Retrieved from Mechlook:<http://www.mechlook.com/surface-finish-direct-instrument-measurements/>
- Pinar, A. M. 2013, Optimization of Process Parameters with Minimum Surface Roughness in the Pocket Machining of AA5083 Aluminum Alloy via Taguchi Method. . *Arabian Journal for Science and Engineering*, , 705-714.
- Ranganath, M. S., Vipin, Mishra, R. S., 2013, Optimization of Process Parameters in Turning Operation of Aluminum (6061) with Cemented Carbide Inserts Using Taguchi Method and ANOVA. *International Journal of Advance Research and Innovation*.
- Rusinel, R. 2010, Cutting process of composite materials: An experimental study,. *International Journal of Non-linear Mechanics* 45, , 458-462.
- Sapuan, J. P. 2013, Taguchi design optimization of machining parameters on CNC end milling process of hallysite nanotube with aluminum rein forced epoxy matrix. *HBRC Journal*.
- Saurabh Singhvi, M. S. 2016, Investigation of Material Removal Rate in Turning Operation. *International Journal of Innovative Research in Science, Engineering and Technology*.
- Singhvi., S. 2016, Investigation of Material Removal Rate in Turning Operation. *International Journal of Innovation Research in Science, Engineering and Technology*.
- Sunil Kumar, Y. R. 2018, A Review Of Modelling And Optimization Techniques In Turning Processes. *International Journal of Mechanical Engineering and Technology (IJMET)*, pp 1146-1156.

PULSE OXIMETER WITH ALARMING NOTIFICATION FEATURE

A. H. Norazam, N. A. Omar, H. K. Wye, S. Kumar, T. Pakkiam & I. Sulaiman.

Infrastructure University Kuala Lumpur, Malaysia

ABSTRACT

A pulse oximeter that reads and measures blood oxygen level (SpO₂) in percentage is presented with an alarming notification feature that alerts an authority when the generally safe range of SpO₂ is violated. The device is aimed to read real time blood oxygen level of users with the aid of a sensor called MAX30100, whilst the Blynk application does the job of storing, monitoring and sending the notification when the situation calls for it. The oximeter uses ESP32 as the microcontroller to control and manage the components to work cohesively with each other to achieve its objectives i.e., send notifications when the oxygen level threshold is infringed. ESP32 is opted for the system as it provides seamless interfacing with other IoT devices and applications on grounds of its Wi-Fi and Bluetooth functionality.

1. INTRODUCTION

In the year 2020, a significant threat to public health has arisen. The novel severe acute respiratory syndrome coronavirus 2 epidemic outbreak has emerged from Wuhan City, China in December 2019. The disease or virus is called COVID-19 and it is still currently continuing to spread around the world, with more than four million deaths across nearly 200 countries. In Malaysia particularly, the cases of COVID-19 have increased worryingly despite the lockdown restricted by the government. The health authorities have raised concerns about a rising number of deaths happening due to the virus. Hospitals and quarantine centers have been overwhelmed by the number of COVID-19 patients coming in. This has led the authorities to urge some of the patients to undergo home quarantine or self-isolation for patients in the early stages i.e., patients with lower severe symptoms.

In a case of self-quarantining, oximeters would be a helpful tool to monitor their level of oxygen. Pulse oximetry is a method of measuring blood oxygen saturation by passing light through a translucent part of the human body. This is done in a safe manner, and the oxygen saturation level is calculated using the data. Ever since this tool was ideated and invented, it has helped saving countless of lives. Prior to the invention of the pulse oximeter, the oxygen saturation was determined by a painful arterial blood gas, which took at least 20-30 minutes to complete and obtain the result. This delay cannot be tolerated since severe damage can occur within mere minutes of low level of oxygenation. In the year 1971, Takuo Aoyagi, a bioengineer from Nihon Kohden, was the first to invent a pulse oximeter based on the ratio of red to infrared light absorption in blood. The possibility of using arterial pulsatile absorption waveforms to measure arterial oxygen saturation was a major milestone in the oximetry's history. Aoyagi was actually developing an earpiece densitometer for non-invasive cardiac output measurement by dye dilution and was troubled by an interference from pulsatile variations in the light signal. In attempting to eliminate the artefact, he noticed the possibility of measuring arterial oxygen saturation without the need for zero calibration in a bloodless sample. He then has chosen the

wavelengths of 630nm (red) and 900nm (infrared) for the oximeter. The 900nm wavelength was chosen because it was unresponsive to the dye used in his initial experiments, but it happened to be sensitive to haemoglobin, which has an oxygenation response that is the polar opposite of the 650nm wavelength. This has permitted the possibility to measure the level of blood oxygen saturation, in a non-invasive method using the different absorption spectrum of haemoglobin. The level of blood oxygen saturation indicates briefly and directly the amount of oxygen carried in the blood. It has been studied that oxygen level below 95% is considered concerning and oxygen level below 92% calls for immediate medical assistance. It is a must for them to be treated instantly and is in their best benefit for their condition to be notified to proper authorities when this situation comes forward.

Under the situation of patients practicing self-isolation, the country is seeing an exponential rise in brought-in-dead (BID) cases due to COVID-19 complications. BID refers to death that occurs outside of health facilities premises. Some COVID-19 patients that undergo home quarantine alone with no guardians have no other choice but to look after themselves on their own. An oximeter would help them in concerning their oxygen level. However, with COVID-19, one can never be sure of how fast or severe the virus can damage or get to their lungs. In consequence, it requires a fast action to be taken given that there is an alarming drop in a patient level of oxygen saturation. Thus, this proves the existence of a demand to implement a feature that is able to notify a guardian or a health authority in the oximeter system when such situations happen. This feature could make a vast difference to avert worse situations and the worst-case scenario i.e., death.

This project focuses on designing an oximeter that is able to measure real time oxygen level in human body. It is aimed to be equipped with a feature that can alarm a notification when the meter senses worrying readings of oxygen level. This project plans to utilize MAX30100 pulse sensor with ESP32 to display the blood oxygen level in human body on an LCD display. The blood oxygen concentration will be measured in percentage. The aid of ESP32 is used to ensure the system works as planned. ESP32 is a feature-rich microcontroller unit with integrated Wi-Fi and Bluetooth connectivity for a wide-range of application, namely in this case, to do most of the controlling works to ensure the components will work cohesively to achieve the goal of this project.

2. LITERATURE REVIEW

This pandemic has opened the eyes of the public that the health of human lungs is very closely related to our oxygen levels. Kimberly [1] has stated that the level of blood oxygen level is an indication of how much oxygen a person's red blood cells carry. The human body closely regulates the blood oxygen level, therefore sustaining the balance of oxygen-saturated blood is crucial to one's health. Collins [2] explained that the moment the virus has infected a person, it straight away moves down their respiratory tract. The respiratory tract is the airway that involves the lungs, throat, nose and mouth. As a result of being infected with COVID-19, the lungs may get inflamed, making it difficult and tough for the patient to breathe. This can result in pneumonia, which is an infection of the tiny air sacs inside the lungs where the blood exchanges carbon dioxide and oxygen. The symptoms typically end with a cough and a fever. But for more

unfortunate conditions, the infections can get worse. About a week after symptoms begin, the patient can start to have shortness of breath, or experience a condition called ARDS. Patients facing ARDS may experience rapid breathing, having abnormally faster heart rate, dizziness, and sweating. [1-2]

Collins [2] also mentioned that the virus damages the tissues and blood vessels in the alveoli, provoking debris to accumulate inside them. Alveoli is the endpoint in the respiratory system where the blood exchanges the carbon dioxide and oxygen during the process of breathing in and out. This makes it tough or sometimes impossible for a person infected with COVID-19 to breathe. As fluid collects in their lungs, they carry less oxygen to the blood.

Thus, the more the blood oxygen level drops, the more concerning a patient's condition is. It has been studied that an oxygen saturation or blood oxygen level of 95% and onwards are normal and patients with this percentage of oxygen saturation may continue to self-quarantine at home. An oxygen saturation from 93% to 94% are the threshold for health concerns but it is still within an acceptable range for the patient to continue self-quarantining at home. However, oxygen saturation of 92 percent or less, on the other hand, necessitates emergency medical attention. This indicates that their blood may not be supplying enough oxygen to their body's organs to keep them alive. This can possibly lead to the kidneys, lungs, and liver to stop working altogether.

Zatum et. al [3] suggested that oximeter systems are a system based on principles related to the characteristic of blood flow rate in the context of the oxygenated haemoglobin (oxy-haemoglobin) and deoxygenated haemoglobin (deoxy-haemoglobin) status. Oxy-haemoglobin and deoxy-haemoglobin are different in their absorption of red and infrared light. Therefore, the oximeter system uses the said physical property to measure the level of blood oxygen based on their difference in the absorption spectrum of haemoglobin. As both the haemoglobin, oxygenated and deoxygenated, have different absorbance and reflectance properties, the proposed oximeter system will utilise two different light sources namely, red and infrared LEDs for illumination of light at different wavelengths, in a non-invasive technique. [3] Anupama B. et. al [4] discussed that deoxy-haemoglobin absorbs more light at 660nm, while oxy-haemoglobin absorbs more light at 940nm, as seen elaborately in the graph in Figure 2.1 below,

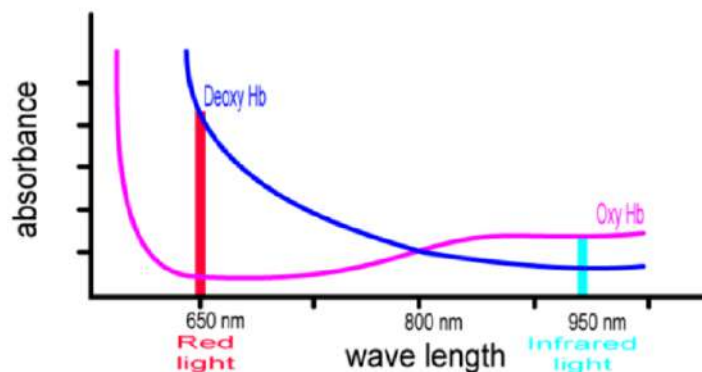


Figure 2.1: Wavelength of Red and Infrared Light [9]

Light illuminated from the red and infrared LEDs will pass through the fingertip, allowing the level of oxygen saturation to be measured using the method of observing the transmitted light, as the pulse oximeter calculates the level of blood oxygen saturation by comparing the amount of red and infrared light absorbed by the blood. The amount of light transmitted will pass through the photo detector and will be measured. Separate normalised signals are then produced for each wavelength. The ratio of the red light measurement to the infrared light measurement represents the ratio of oxygenated haemoglobin to deoxygenated haemoglobin which is converted to SpO₂ based on Beer-Lambert law . [4] For instance, at SpO₂ percentage of 100%, it indicates that all of the haemoglobin content in the body is carrying oxygen. The graph in Figure 2.2, depicts this situation. At percentage of 0%, this is an indication that there is only deoxygenated haemoglobin in the blood content. Figure 2.3 displays the graph of this ratio and Figure 2.4, depicts an SpO₂ percentage of 75%.

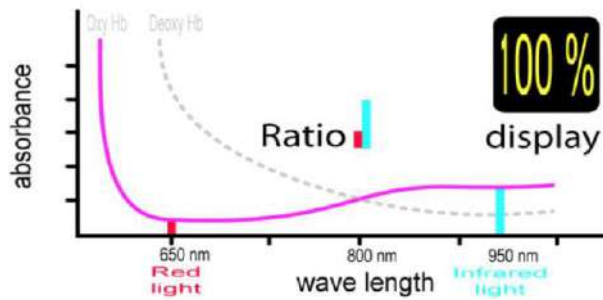


Figure 2.2: SpO₂ of 100% [9]

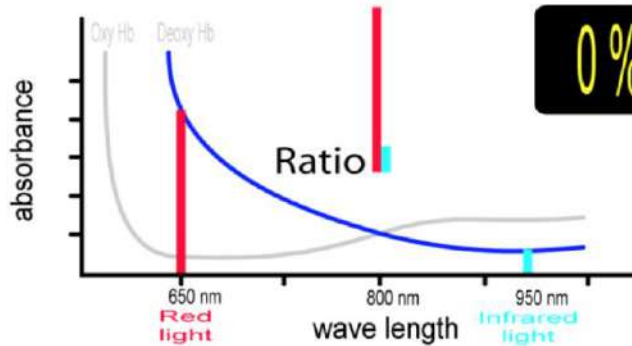


Figure 2.3: SpO₂ of 0% [9]

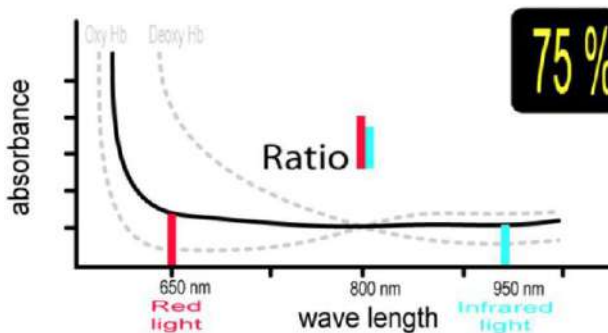


Figure 2.4: SpO₂ of 75% [9]

According to Bhuyan [5], there is a number of digital pulse measuring devices that are found reliable as a measuring device for pulse oximetry. Most of the designs he mentioned are based on microcontrollers. An Arduino microcontroller, a pulse oxygen sensor, a DC power supply unit and an LCD unit are all included in one of the system solutions he recommended. The Proteus software was used as a medium to design the circuit online and simulate it prior to event. In the software implementation, the MAX30100 Arduino library function is utilised to convert the ADC value to retrieve the oxygen saturation level in percentage. The MAX30100 is an IC (integrated circuit) that is utilised in the pulse oximeter system. This sensor is capable of sensing signals related to the user's blood oxygen saturation level and it is able to monitor the blood oxygen saturation level. The microprocessor, pulse oximeter sensor, and LCD unit all require current, which is supplied by the 5V DC power supply unit. Figure 2.5 below shows the block diagram of the digital oxygen saturation level measurement system Bhuyan [5] has suggested.

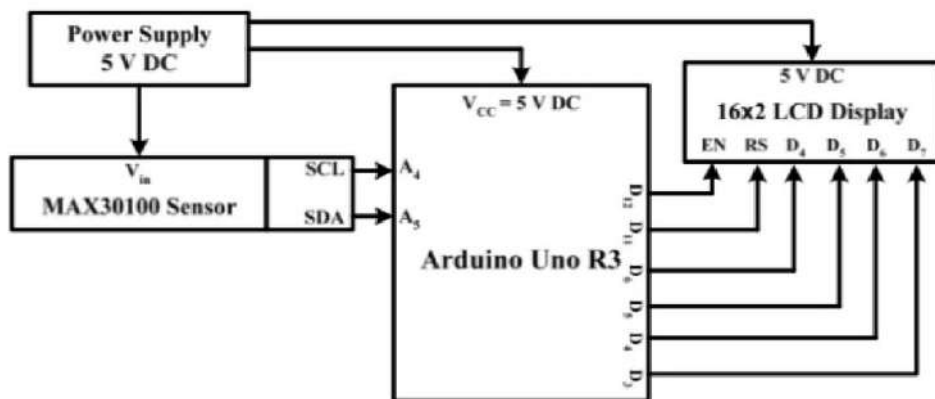


Figure 2.5: Block Diagram of Oxygen Saturation Measurement System [5]

Alsan [6] proposes a solution that supports the Internet of Things. It utilizes ESP32 development board as the microcontroller, and MAX30100 as the sensor. The oxygen level and pulse rate can be tracked via a web server, which means the parameters can be checked and monitored from any smartphone or PC with internet access and Wifi supported. The circuit assembly he suggested for MAX30100 Pulse Oximeter Webserver using ESP32 can be seen in Figure 2.6 below. The MAX30100 Oximeter Sensor works with an I2C bus. So, the sensor's SCL and SDA will be wired to ESP32 pins 21 and 22. The INT pin should be linked to pin 19 of the NodeMCU. [6]

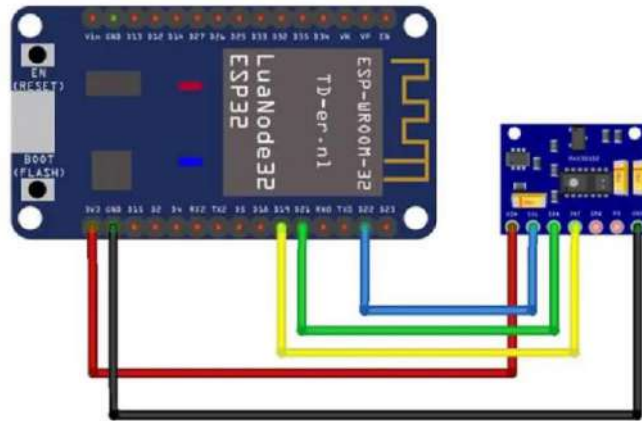


Figure 2.6: Interfacing MAX30100 with ESP32 [6]

3. METHODOLOGY

The overall design of the system is depicted in Figure 3.1 below, meaning the hardware construction will be constructed following and abiding by the design depicted in the mentioned figure.

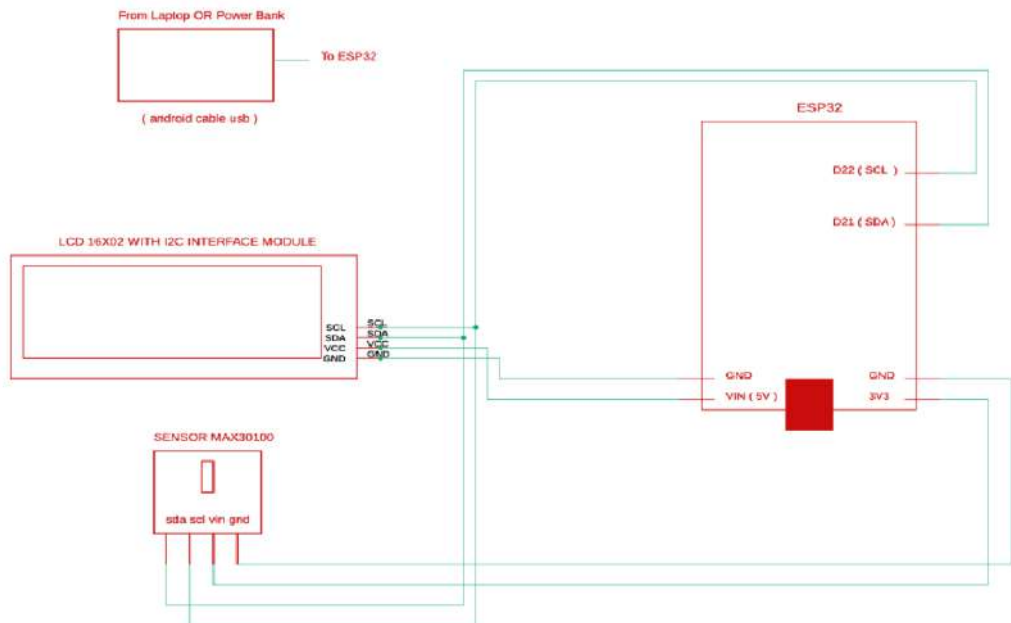


Figure 3.1: Circuit Schematic

The circuit construction will follow closely the schematic that was designed on Eagle Autodesk software, depicted in Figure 3.1. Once the procurement of materials has been made and the products have altogether arrived, the construction phase is to be executed. This procedure can be seen in Figure 3.2 below.

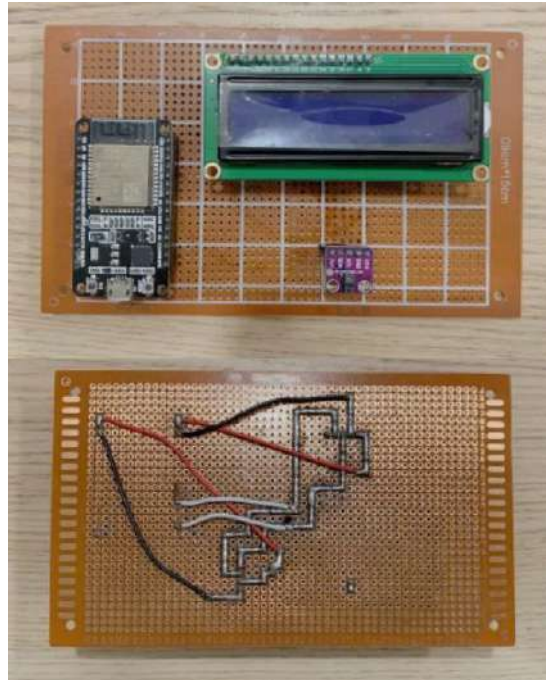


Figure 3.2: Hardware Construction

4. RESULTS AND DISCUSSION

Figures 4.1- 4.5 depicted in this section show the results of this project. Figure 4.1 below shows the LCD display of the system when the system is supplied with power but no reading is sensed and Figure 4.2 followed shows the LCD display when the system is switched on with a finger placed on the MAX30100 sensor. It can be observed that the LCD shows real time reading accordingly, indicating the system is delivering the supposed outcome. Following that, Figure 4.3 shows the notification that was received when the safe reading was violated. At the same time, notifications were also sent to the phones of the authorities that are set prior to the final test, which is shown on Figure 4.4. The screenshot of this notification was done by the authority set, located in Shah Alam, more than 20kms away from the prime user's location.

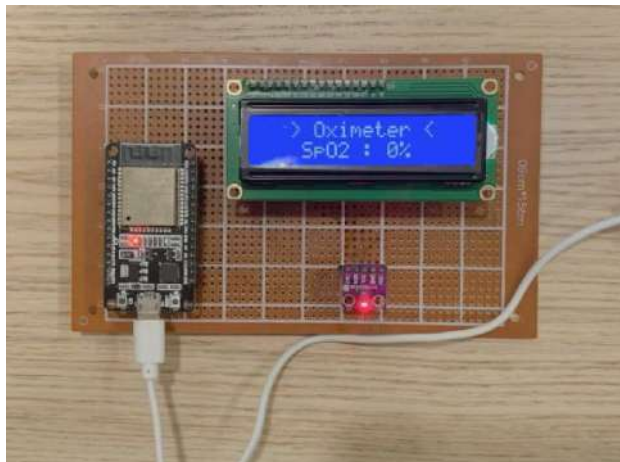


Figure 4.1: Oximeter Before User Places Finger



Figure 4.2: Oximeter When User Places Finger

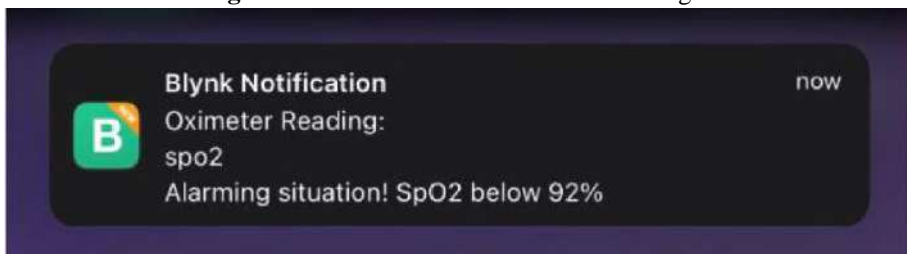


Figure 4.3: Notification Received when Safe Reading is Violated

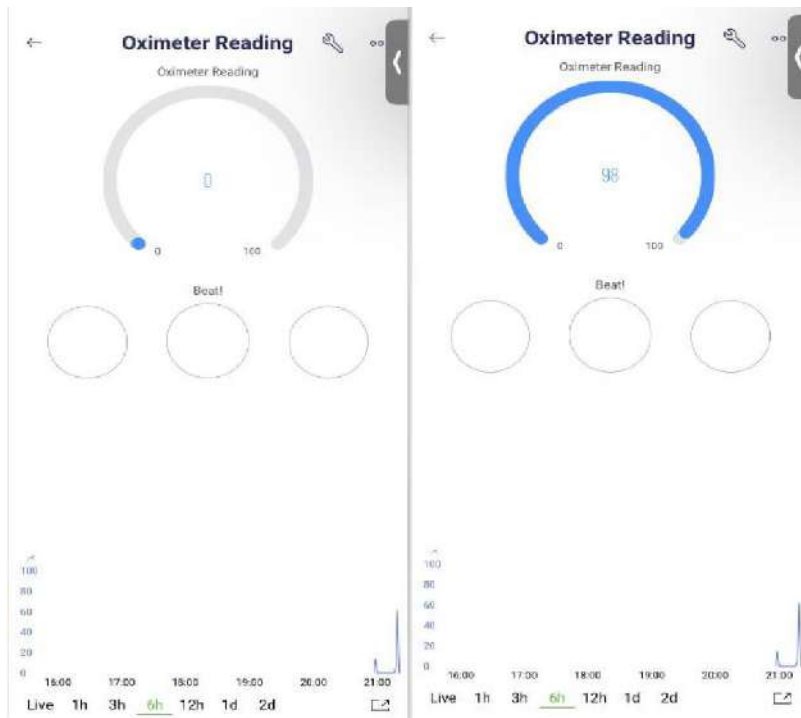


Figure 4.4: User and Set Authorities' Preview of the Application

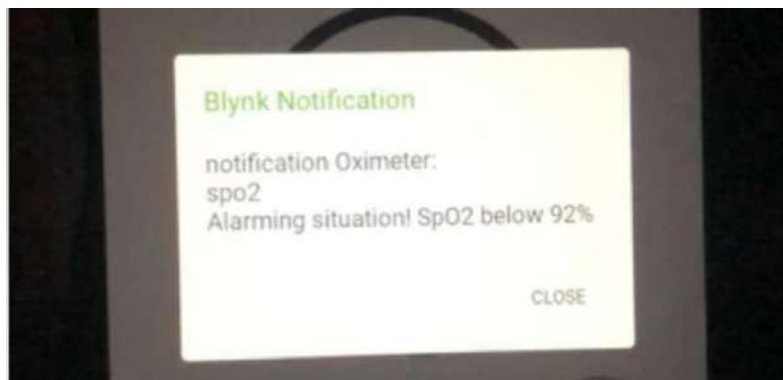


Figure 4.5: Notification Received in Shah Alam

For further promise the accuracy of the system, the output on the LCD display were compared to an actual commercialized oximeter. This comparison is elaborated Table 4.1 below,

Table 4.1: Output Comparison

Person	Commercial Oximeter		Oximeter Prototype	
	SpO2	Sensor Reading Time	SpO2	Sensor Reading Time
1	99%	4.30 s	98%	3.06s
2	99%	3.64s	97%	4.65s
3	99%	5.28s	98%	4.55s

It can be observed from the comparison in the table above that the SpO2 level between the prototype and a commercial oximeter are not significantly different or at variance. Thus, it can be analysed that the precision of the prototype assembled has only at most about 2% difference from an actual commercial oximeter. This is calculated using the formula below. As for the reading time, it can be observed that it varies time and time. As MAX30100 is highly sensitive, sometimes it can sense the blood oxygen level faster than the commercial oximeter but there are times that it detects the blood oxygen level later. However, the difference of the sensor reading between the two oximeters does not go beyond 1.5s. This can promise that the prototype assembled can deliver precise and decent outcome if compared to an actual oximeter that is available in the market, as the precision does not have significant and much difference.

5. CONCLUSION

The aim of this thesis was to design an oximeter that is able to measure blood oxygen level with a feature that enables notification via an application when worrying readings are sensed. A typical oximeter usually measures real time oxygen level with a bias of 1.85% and a precision error of 2.21%. [18] Hence the oximeter designed must be able to deliver as such a device with the said accuracy. To further enhance the practicality of the system, the prototype designed is integrated with a microcontroller unit that has WiFi connectivity which allows for notification feature through Blynk. The system obligates the users and the authorities to receive the notification to have internet connection to work the system. Although this could be an issue, however in Malaysia, statistics have shown a total of 88.48% population of Malaysians to own and utilise a smartphone. [19]

This automatically means they have the option of using their personal hotspot which is a viable connection to put this system to work. Apart from this foreseeable hiccup, this system promises to deliver sufficiently decent output with stable notification feature when the safe readings are violated. Because of this, it can be said that the objectives of this project are achieved as the prototype assembled is able to measure blood oxygen level in precision and send notification when supposed to.

REFERENCES

- [1] Holland, K. (2019, September 28). *Is My Blood Oxygen Level Normal?* Healthline. <https://www.healthline.com/health/normal-blood-oxygen-level#takeaway>
- [2] Collins, S. (2020, March 20). *Coronavirus: What Happens When You Get Infected?* WebMD. <https://www.webmd.com/lung/coronavirus-covid-19-affects-body#1>
- [3] Zaltum, M. A., Ahmad, M. S., Joret, A., & Abdul Jamil, M. M. (2010). Design and Development of a portable Pulse Oximetry system. *International Journal of Integrated Engineering*, 37-43. https://www.researchgate.net/publication/279495623_Design_and_Development_of_a_portable_Pulse_Oximetry_system/fulltext/57a5ce8a08aee07544bb7897/Design-and-Development-of-a-portable-Pulse-Oximetry-system.pdf?origin=publication_detail
- [4] B, A., & K, R. (2018). Working mechanism and utility of pulse oximeter. *International Journal of Sport, Exercise and Health Research*, 2(2), 111-113. <https://doi.org/10.31254/sportmed.2203>
- [5] Bhuyan, M. H. (2021). Design Simulation and Implementation of a Digital Pulse Oxygen Saturation Measurement System Using the Arduino Microcontroller. *International Scholarly and Scientific Research & Innovation*, 15(2), 105-111. https://www.researchgate.net/profile/Muhibul-Bhuyan/publication/349005931_Design_Simulation_and_Implementation_of_a_Digital_Pulse_Oxygen_Saturation_Measurement_System_Using_the_Arduino_Microcontroller/links/601ace8c299bf1cc269fe3bb/Design-Simulation-and-Implementation-of-a-Digital-Pulse-Oxygen-Saturation-Measurement-System-Using-the-Arduino-Microcontroller.pdf?origin=publication_detail
- [6] Parajuli, A. (2021, May 21). *IoT Based Pulse Oximeter Using ESP8266 & Blynk*. The IOT Projects. <https://theiotprojects.com/iot-based-pulse-oximeter-using-esp8266-blynk/>
- [7] Maxim Integrated. (2014). *Pulse Oximeter and Heart-Rate Sensor IC for Wearable Health*. <https://datasheets.maximintegrated.com/en/ds/MAX30100.pdf>
- [8] Minaie, D. A., Sanati-Mehrziy, D. R., Paredes, L. E., & Morris, J. (2019). *Design of a Bluetooth-Enabled Wireless Pulse Oximeter*. American Society for Engineering Education.
- [9] how equipment works .com. (2021, September 11). *How pulse oximeters work explained simply*. https://www.howequipmentworks.com/pulse_oximeter/
- [10] *IoT Devices - Sensors, Wireless, Hardware, Software Products*. (2020, May 29). Kickr Design®. <https://www.kickrdesign.com/iot-electronic-product-devices>
- [11] A. (2020, January 13). *What is Internet of Things (IoT)?* Electronics Hub. <https://www.electronicshub.org/internet-of-things/>
- [12] Grizhnevich, A. (2021, July 28). *IoT Architecture: Building Blocks and How They Work*. ScienceSoft. <https://www.scnsoft.com/blog/iot-architecture-in-a-nutshell-and-how-it-works>
- [13] X. (2021c, March 8). *Create a web interface to control your NodeMCU ESP32*. AranaCorp. <https://www.aranacorp.com/en/create-a-web-interface-to-control-your-nodemcu-esp32/>
- [14] Tech Explorations. (2021, December 14). *1. What is Blynk?* <https://techexplorations.com/guides/blynk/1-what-is-blynk/>
- [15] S., & Rif'an, M. (2019, March 25). *Internet of Things (IoT): BLYNK Framework for Smart Home | KnE Social Sciences*. Knowledge E. <https://knepublishing.com/index.php/Kne-Social/article/view/4128/8495>

- [16] Mazalan, N. (2019, September). *Application of Wireless Internet in Networking using NodeMCU and Blynk App*. 1-8. <https://www.researchgate.net/publication/346935386>
- [17] A. (2020b, May 10). *MAX30100 Pulse Oximeter with ESP8266 on Blynk IoT App*. How To Electronics. <https://how2electronics.com/max30100-pulse-oximeter-with-esp8266/>
- [18] da Costa, J. C., Faustino, P., Lima, R., Ladeira, I., & Guimarães, M. (2016). Research: Comparison of the Accuracy of a Pocket versus Standard Pulse Oximeter. *Biomedical instrumentation & technology*, 50(3), 190-193. <https://doi.org/10.2345/0899-8205-50.3.190>
- [19] Statista. (2021, August 17). *Smartphone penetration in Malaysia 2010–2025*. <https://www.statista.com/statistics/625418/smartphone-user-penetration-in-malaysia/>

TEMPERATURE COMPARISON ON THE EFFECTS OF AN AIR-COOLING SYSTEM INSTALLED ONTO A BRAKE ROTOR

Muhammad Fahmi Md Isa, Muhammad Eizlan Ezzat Abdul Shukor, Engku Amirul Rashidin Engku Ariff & Noorradiah Ismail
Infrastructure University of Kuala Lumpur, Malaysia

ABSTRACT

The modern car sector has difficulty increasing economy and efficiency. A vehicle's display is influenced by aerodynamics, fuel efficiency, engine cooling, gearbox, and other factors. As a result, it is crucial to make adjustments to a vehicle's design to improve engine performance. Vehicle safety is significantly influenced by the cooling architecture of the brake systems. Vehicle brake systems will experience brake fade as they get more powerful. The security of the driver and all passengers in the car will be unsafe. This leads to an increase in the temperature of the brake discs substantially. Brake fade is caused by a buildup of heat in the braking surfaces and the subsequent changes and reactions in the brake system components and can be experienced with both drum brakes and disc brakes. The aim of this chapter is proposed a cooling mechanism for vehicle braking system using an air cooled and to determine the heat reduction of the brake rotor before installing the cooling system and after installing the cooling system ventilation system.

1. INTRODUCTION

The modern car sector has difficulty increasing economy and efficiency. A vehicle's display is influenced by aerodynamics, fuel efficiency, engine cooling, gearbox, and other factors. As a result, it is crucial to make adjustments to a vehicle's design to improve engine performance. Vehicle safety is significantly influenced by the cooling architecture of the brake systems. Vehicle brake systems will experience brake fade as they get more powerful. The security of the driver and all passengers in the car will be unsafe. This leads to an increase in the temperature of the brake discs substantially. Brake fade is caused by a buildup of heat in the braking surfaces and the subsequent changes and reactions in the brake system components and can be experienced with both drum brakes and disc brakes. The aim of this chapter is proposed a cooling mechanism for vehicle braking system using an air cooled and to determine the heat reduction of the brake rotor before installing the cooling system and after installing the cooling system ventilation system.

2. LITERATURE REVIEW

Convection is the main mechanism by which heat is removed from a brake rotor. Convection will be enhanced by raising the rotor's surface area or heat transfer coefficient, respectively. It is necessary for a sufficient amount of cooling air to interact with the heated elements in order to maximized the cooling effect through convection process. It is obvious that cooling may be increased by dissipation of air toward surrounding; numerous examples of this can be found in motor racing. However, this may negatively impact the vehicle's drag. (Jerhamre, A. and

Bergström, C 2001).

This field of aerodynamics has received relatively little attention up to this point, and the majority of the research has focused on the effects of lift and drag created by both stationary and moving wheels. (Vdovin, A., & Le Gigan, G. 2020).

Additionally, experimental and computational fluid dynamic (CFD) studies on the link between the flow inside the wheel-well and lift and drag have been conducted by Bolzon, M. D. P. *et al.* 2019). According to Fabijanic (1996), the air flow within the wheel arch to be very unsteady, and alternated from entering the wheel arch to exiting at the same position with no obvious periodicity. The air flow is further complicated by the movement of the suspension creating an air pumping effect within the wheel arch. Most aerodynamic research in the area of brake cooling has focused on the airflow through internally ventilated rotors in isolation, and has not considered the effect on the flow under normal driving conditions.

The need for increased cooling of disc brakes led to the development of vented rotor discs, however the advantages of vented discs over solid discs is the subject of some conjecture. The primary advantage of vented rotors is increased heat dissipation from internal pumping of air, however under slow speeds the pumping action of the vanes is minimal and only becomes pronounced as rotor speed increases. At higher speeds the airflow flowing around the disc as a result of the forward movement of the vehicle, tends to prevent effective pumping of air through the vanes, (Limpert 1975).

Early work by Limpert (1975) indicated that the heat dissipation from internal ventilation amounted to about one third of the total heat dissipation from the rotor, but suggested it was the larger surface area and not the pumping action that made the major contribution to cooling. While vented rotors do provide a larger surface area for heat dissipation, and extra airflow from the pumping effects of the vanes, it must be remembered that they will usually have a reduced mass than their equivalent solid rotor and therefore have less capacity to store thermal energy.

Much of this work has involved attempts to increase the flow through internally ventilated rotors. One approach has been the use of curved vanes instead of straight vane ones. Curved vanes can create additional cooling in two ways; firstly an increase in surface area of up to 30% can be achieved, (Limpert 1975), and secondly optimization of the vanes can improve the pumping efficiency. Daudi (1999) used commercially available CFD software to compare the flow generated by straight and curve vane rotors, and found significant reductions in rotor temperatures using curved vane rotors when operating in still air. However curved vane rotors add to manufacturing complexity and introduce the need for different rotors for each side of the car, (Jerhamre, Anders & Bergström, Christer. (2001). Numerical Study of Brake Disc Cooling Accounting for Both Aerodynamic Drag Force and Cooling Efficiency. 10.4271/2001-01-0948.), potentially resulting in four different rotors for a given vehicle.

Many attempts have been made to improve the cooling ability of straight vane ventilated rotors. Zhang (1997) proposed a redesign of vented rotors to include an optimized

number of flow passages, improved rounding on inlet vanes, and a longshort alternative vane configuration. This design contains twice the number of outlet vanes as inlet vanes, in order to reduced inlet blockages and guide to flow though the exit more easily. The configuration was modelled on CFD software and a 42% increase in flow through the vanes is claimed, however no experimental verification is given. A similar technique was used by Daudi (1999) to develop a rotor with three times the number of outlet vanes as inlet vanes, providing 35% more flow through the vanes when tested on a model in still air.

Experimental on-vehicle testing of the modified rotor resulted in temperatures of between 3-6% lower than the production rotor at the end of a ten stop fade test. Daudi (1998) also concluded from CFD modelling that increased airflow through a vented rotor could be achieved by allowing air to enter the vents from both the inboard and outboard side of the rotor. Another development has been the cross-drilled or axial cooled rotor; this increases the surface area presented to the atmosphere and can potentially improve cooling, however the rotor mass and friction area are reduced. Analytical work by Limpert (1975) showed that the addition of axial cooling passages reduced cooling effectiveness; this is mainly attributed to the increased heat flux.

Visualization of the flow through ventilated rotors by Kubota, et al. (2000) using scale models submerged in water, indicated significant regions of separated flow within the vanes of the rotor, which would indicate that increased flow could be achieved with optimized designs. Measurement of the airflow through the vanes of a vented rotor is extremely difficult while on the vehicle, so it is usually done in isolation, (Hudson and Ruhl (1997); Jerhamre and Bergstrom (2001)).

3. METHODOLOGY

The chapter begins with fabrication of the brake cooling system that will redirect the flow of air from the front of the vehicle towards the brake rotor of the vehicle to provide cooling to the system as shown in Figure 1(a) and (b).



Figure 1 (a) Hose installation (b) Temperature sensor location

The data was obtained by conducting the project on a Perodua Kembara (Daihatsu Terios J100) 1.6L on a straight 2 km road. All the data collected was used to calculate the increase in temperature of the rotor before and after installing the cooling system. Then the result is use to predict the increase in the effect of cooling at speeds of 70, 80, 90, 100, 110, 120, 130 and 140 km/h. An Arduino Microprocessor was programmed and calibrated to get an accurate temperature reading and used it was used to measure the temperature of the brake rotor. The entire test will run eight times with the cooling system installed and another eight times without the cooling system installed. The project will be conduct on the road and the air that enters the ventilation system will be near to constant, as the vehicle will be travelling at 60 km/h at 3000 RPM by monitoring the gauge cluster while pressing the brake pedal and controlling the accelerator pedal simultaneously to replicate a controlled environment throughout the entire test. This method is slightly different from the method that was use in the previous studies by Eric Hazen (Versus Engineering), 2016. This is to adapt the method to suit this project.

The effect of cooling are recorded 2 kilometers after the brake is applied at a constant pressure. The initial temperature of the rotor will be at around the same range before the brake is apply throughout the entire test. The temperature of the rotor will be monitor with a temperature sensor to ensure the temperature remain at the same range during the start of every test. The system will be control by an Arduino. The sensor used is a LM35DZ type temperature sensor. The sensor will send data to the Arduino and the Arduino will display the temperature of the rotor. An Arduino Uno is a microcontroller board based on the ATmega328P (datasheet). It has 14 digital input/output pins (of which 6 can be used as PWM outputs), 6 analog inputs, a 16 MHz ceramic resonator (CSTCE16M0V53-R0), a USB connection, a power jack, an ICSP header and a reset button. It contains everything needed to support the microcontroller; simply connect it to a computer with a USB cable or power it with a AC-to-DC adapter or battery to get started. Figure 2 shows the schematics layout of the temperature measuring system. The component that was used is this schematics are, Arduino Microprocessor, LM35DZ temperature sensor, breadboard, LCD display and copper wires.

the system to cool down the brake rotor increases to 74.03% compared to the system without the brake cooling installed. Theoretically, this system would greatly affect the cooling ability of the brakes when the vehicle is traveling at higher speeds as shown in Table 1.

Table 1: Cooling ability increase in cooling at different speed after installing the cooling system.

Run	Vehicle Speed (km/h)	Ambient Air Temperature (°C)	Temperature increment (%) without cooling system	Temperature increment (%) with cooling system	Cooling Ability (%)
1	70	30	50.72	7.14	47.11
2	80	30	43.05	8.47	53.84
3	90	30	51.52	2.66	60.57
4	100	30	42.18	16.45	67.3
5	110	30	37.50	1.57	74.03
6	120	30	52.38	4.28	80.76
7	130	30	46.15	3.94	87.49
8	140	30	50.70	6.66	94.22
		Average	46.775	6.396	

The advantages of the proposed cooling system is being able to cool down the vehicle brake rotor to achieve an enhanced braking performance as cooler brake rotor equates to higher coefficient of friction. This is achieved by cooling the brake rotor with air. The air that is use for cooling comes from the frontal part of the vehicle and it is being route by a flexible hose straight to the brake rotor. While the disadvantages of this cooling system are the extra parts that needed to be mounted into the vehicle. Some original parts of the vehicle may need to be modified so the system can be installed properly.

5. CONCLUSION

The results indicates that the cooling ability of the system has quite an impact of temperature reduction on the brake rotors of the vehicle. The advantages of this project is being able to cool down the vehicle brake rotor to achieve an enhanced braking performance as cooler brake rotor equates to higher coefficient of friction. This is achieved by cooling the brake rotor with air. The air that is use for cooling comes from the frontal part of the vehicle and it is being route by a flexible hose straight to the brake rotor. The disadvantages of this project are the extra parts that needed to be mounted into the vehicle. Some original parts of the vehicle may need to be modified so the system can be installed properly.

The cooling system works as expected but the results shows that there are still more that can be improve. One of the ways to improve the system is to change the brake rotor to a vented rotor. This will help the system to dispel more heat effectively. With the vented rotor installed,

the vent system now can be placed at the center of the rotor so it can push out the hot air in the rotor faster.

REFERENCES

- Jerhamre, A., & Bergström, C. (2001). Numerical study of brake disc cooling accounting for both aerodynamic drag force and cooling efficiency. *SAE transactions*, 1156-1163.
- Vdovin, A., & Le Gigan, G. (2020). Aerodynamic and Thermal Modelling of Disc Brakes—challenges and limitations. *Energies*, 13(1), 203.
- Bolzon, M. D. P., Sebben, S., & Broniewicz, A. (2019). Effects of wheel configuration on the flow field and the drag coefficient of a passenger vehicle. *International Journal of Automotive Technology*, 20(4), 763-777.
- Limpert, R. (1975). Cooling analysis of disc brake rotors (No. 751014). SAE Technical Paper.
- Daudi, A. R. (1999). 72 Curved fin rotor design reduces maximum rotor temperature (No. 1999-01-3395). SAE Technical Paper.
- Jerhamre, A., & Bergström, C. (2001). Numerical study of brake disc cooling accounting for both aerodynamic drag force and cooling efficiency. *SAE transactions*, 1156-1163.
- Zhang, J. J. (1997). A high aerodynamic performance brake rotor design method for improved brake cooling (No. 973016). SAE Technical Paper.

UNIFIED GDI LIBRARY CREATION FOR THE STANDARD LOGIC CELL FOR SILTERRA 130NM PROCESS

Jebashini Ponnian, Ima Sulaiman, & Darshini Sankaran
Infrastructure University, Kuala Lumpur,

1. INTRODUCTION

Introduction In recent decades, power reduction has become increasingly crucial in semiconductor architecture, which has seen incredible, disruptive, and exciting growth in developing electronic communications devices such as cell phones, IPADS, and notebooks. This electronic gadget is implemented using a variety of technologies to optimize speed, area and energy. Several multi-faceted optimization methods, such as design technology, logic topologies, circuits, interfaces and algorithms, approach power reduction. The technology eliminates power consumption by scaling the threshold voltage, allowing the supply voltage to be lowered without impacting the circuit's speed. Self-reset logic and self-timed circuit features, for example, change the supply voltage selectively to decrease power consumption. Power conservation may also be accomplished at the circuit level through recycling signal energy using reversible or adiabatic logic rather than through dissipating signal energy as gas. Selecting the proper logic family and applying the specification using topology will also result in power savings (logic construction). Pipelining, retiming, encoding styles such as Gray text, one-hot, registry duplication, and registry balancing can all help with power efficiency at the architecture level. Static modules can be stored in sleep mode or turned off dynamically to preserve system-level power using power control mechanisms such as power gates, power-controlled grids, and Dynamic Power Management (DPM).

2. GDI Gate Diffusion Input

Major semiconductor companies such as Fujitsu and IBM, Intel, Texas Instruments, and TSMC debuted a semiconductor process technology (MOSFET CMOS) at the 130 nm (0.13 μ m) process level in 2001-2002. (Sudheer, R. V., et al., 2021). Based on historical data, 130 nm was chosen as the starting point since a two-thirds scaling tendency occurs every two to three years (Ponnian, et al., 2020). According to the Semiconductors International Technology Roadmap, this is a set deadline for the project (ITRS). The designers used the GDI approach to create a full subtractor utilising 130nm technology. Lower average power, a faster rise and fall duration, and a shorter peak-to-peak length were all required. Mentor Graphics EDA tools were used in the current work on 130nm technology (Ponnian, et al., 2020) A technique utilizing Gate Diffusion Input cells to minimize delay, i.e., speed improvement, power consumption reduction, and transistor count reduction, is described in Power reduction techniques involving measures such as scaling, architectural approaches, and transistor count reduction were proposed while meeting speed constraints (Sudheer, R. V., et al., 2021). A CMOS inverter power-delay model was developed to investigate power dissipation, propagation delays, and change over time.

The synthesis technique is based on a Boolean expression capable of rewriting the decomposing tool's algorithm. Several transistor-based VLSI technologies, such as 2 CMOS, PTL, TG, and GDI, and the main synthesis factors will be power dissipation, area usage, time delay, and pace. The Complementary Metal Oxide Semiconductor (CMOS) logic style has introduced the bulk of circuit designs. Because of its lowvoltage stability and tolerance for voltage scaling and transistor size, it has many fans (high noise margins). On the other hand, CMOS logic uses several massive PMOS transistors, resulting in heavy input loads and increased power dissipation as the operating frequency increases. The propagation delay is considerably longer than the other logical families due to higher node capacitances. Some studies argue substituting logic strategies for static design rather than dynamic logic types due to performance issues such as noise margin metastability, charging sharing, circuit design sophistication, and design. The PTL circuit outperforms the static CMOS circuit in terms of output. Most functions can be performed with fewer transistors, resulting in lower average capacitance, quicker switching times, and low power dissipation. The noise margin decreases due to the degraded voltage swing, resulting in more inadequate drive potential for large loads and unreliable circuit operation. Because of the difference in the threshold decline, the static dissipation of power in PTL is substantial.

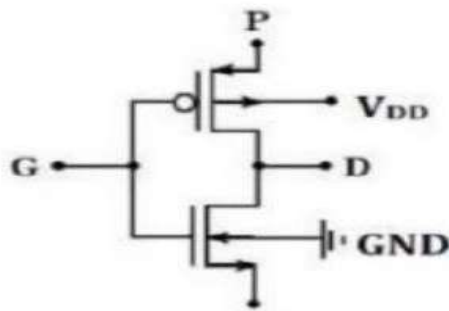


Figure 1.: Basic GDI cell

A cell that employs the Gate Diffusion Input method and is suitable for use in digital circuits. While a GDI cell is similar to a simple inverter, there are several significant differences (Mahendra, G. R., et al., 2019). It is equipped with three different inputs. A standard gate input G to two complementary P and N-type transistors, a P input to a P-type transistor's source/drain, and an N input to an N-type transistor's source/drain are among the distinctions (Mahendra, G. R., et al., 2019). The majority of each N and P-type device unit is associated with N or P. This technique connects each N and P-type transistor area unit to its diffusion, reducing the majority effect and the threshold's dependence on the source-bulk voltage (Mahendra, G. R., et al., 2019). GDI is a type of fuel injection system used in many modern vehicles. Before the development of multi-point fuel injection, low-pressure injection systems injected gasoline directly into the intake. Gasoline is injected into each cylinder's combustion chamber at high pressure using a fuel line in GDI engines (Mahendra, G. R., et al., 2019). This component enhances this GDI injection timing and fuel supply management. Compared to traditional fuel injection engines,

GDI engines provide several advantages, including reduced pumping and injection noise. Using gasoline direct injection technology, engines with lower displacement may extract more power (Mahendra, G. R., et al., 2019). Fuel efficiency and pollution are also improved in addition to that. Despite its outstanding abilities, the GDI engine's strengths are both positive and negative. While CNG-injected engines have several advantages, such as no carbon deposits, they all negate the advantages (Mahendra, G. R., et al., 2019). An inverter based on a CMOS inverter's basic design is the GDI primitive cell. Although it is more capable, it is not by much. The values of the three inputs greatly influence the circuit's performance: G, N, and P. G stands for gate width in NMOS and PMOS transistors. NMOS and PMOS are the two different types of source terminals, respectively. As a result, every one of them functions as a data receiver terminal (Bruun, E., 2018). A standard drain D is used to get the desired result. Primitive cells are shown schematically in Figure1. The primary GDI cell is capable of performing a wide range of tasks. There are inputs and outputs summarised in Figure2. Despite its versatility and capacity to execute a wide variety of activities independently, the GDI cell has a few drawback.

P	N	G	Output	Function
1	0	A	A'	NOT
0	B	A	AB	AND
B	1	A	A+B	OR
B	0	A	A'B	Function 1
1	B	A	A'+B	Function 2
A	B	S	AS+BS'	2:1 MUX
A	B'	B	A'B+AB'	XOR
A	B	B'	AB+A'B'	XNOR

Figure 2.: Functionalities of the primitive cell

Traditional CMOS manufacturing technologies have a severe drawback that makes fabrication difficult. Additionally, as previously indicated, swing degradation is a problem (Mahendra B. G. R., et al., 2019). The PMOS and NMOS balk terminals of the GDI or m-GDI cell are connected to VDD and ground. The ALU has a few GDI logical circuits that utilize m-GDI and many GDI logical circuits that utilize GDI (Mahendra B. G. R., et al., 2019). For instance, Figure 1 depicts the construction of an MGDI cell.

GDI (Gate diffusion input) is a paradigm shift in terms of designing energy efficient gadgets. With only two transistors, NMOS and PMOS, this method enabled the creation of digital logic circuits such as gates and adders. This approach uses fewer transistors in logic architecture, resulting in a smaller device. It enables digital devices to be smaller and more energy-efficient (Morgenshtein, A., et al., 2014). GDI methods improve the circuit's static power characteristics, and the circuit is developed from the ground up using a small cell library. The GDI primary cell is quite similar to CMOS logic (Saparov, Y., et al., 2015). Three terminals are available at GDI. The letter G represents the gate terminal, P represents the PMOS node, and N represents the NMOS node. Most PMOS and NMOS featured linked diffusions, which was a structural distinction between CMOS and GDI (Fu, J. S., 2015). In both NMOS and PMOS transistors, the gate serves as a common terminal. To reduce the impact of logic on the body, the

body terminal is linked to the diffusions (Murthy, G., et al., 2018). The GDI method significantly decreased sub-threshold and gate leakage currents. When it comes to creating p wells, GDI is not the best option (Eligar, S., et al., 2020). The twin tub or SOI procedures are utilised to manufacture GDI cells (silicon on insulator) (Murthy, G., et al., 2018). When the substrate is linked to the drain, the threshold voltage rises; however, when the substrate is connected to the source, the body effect disappears (Murthy, G., et al., 2018). The comparison results between CMOS and GDI is given in Table1.

FUNCTION	GDI	CMOS
INVERTER	2	2
OR	2	6
AND	2	6
MUX	2	12
XOR	4	16
XNOR	4	16
NAND	4	4
NOR	4	4

Table1 : Comparison of CMOS and GDI

3. METHODOLOGY

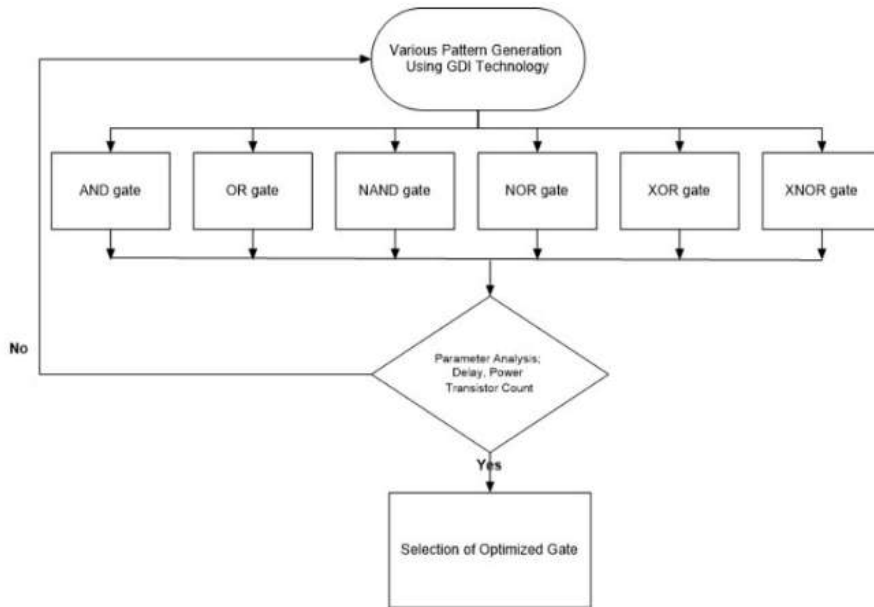
The MUX-based tactic is constructed this fieldwork focuses on the GDI Library's entire architecture, which consists of all the primitive regular logic gates. The process begins with the generation of different patterns using GDI Technology. The Small-Scale Integration (SSI) library components such as "AND, OR, NAND, NOR, XOR, and XNOR" components are used to produce patterns. In this pattern generation process, all possible outcomes such as "00,01,10,11" are observed, and specific parameters are also interpreted. Analyzing parameters are transistor count, power, delay and rise and fall time. On the other hand, other environmental adjustments, such as temperature, bias and architecture angles, have been retained during the simulation process. The Silterra Library is where all modules such as PMOS, NMOS, power sources, and active and passive components are chosen. Then multiple patterns are generated for each of the gates, and the truth table needs to be verified. Optimized primitive cells are selected based on the study of specific parameters, such as power, delay and speed. These trends are often compared with CMOS, PTL and TG in terms of transistor count, area and power and delay. 0 – 1.2V is given as input supply where the parameters taken into account are delay, transistor count, power dissipation, rise and fall time. Output comparison research will be conducted for CMOS Technology, PTL Technology, TG and GDI Technology. In order to perform GDI Technology to connect the input signal is mapping the 2-input logic gates using K-map. This is by having one of the variables as select terminal and another on act as a controlled signal. The complementary and true variables of the select terminal are kept along the row, and the PMOS and NMOS diffusion terminals are kept along the column, in the 2x2 Kmap. The values represented in the K map are used to determine the connection. When the column values of PMOS and NMOS diffusion inputs are (0,0), their terminals are linked to Ground, but when the column values are (1,1), they are connected to the source, VDD. Assume that the PMOS and NMOS diffusions have column values of (1,0) or (0,1), respectively, and that the appropriate

row value is linked to the PMOS and NMOS terminals.

The MUX-based GDI technology is constructed using a k-map implementation of the Boolean function. Any m-variable GDI logic can be constructed using (m-1) primitive GDI cells. The algorithm approach consists of constructing a 2x2 K-map having P-diffusion and N-diffusion along the column and the input variable as a complementary and true value along a row. An m-variable Boolean logic in GDI is converged as 2-input GDI primitive cells. Therefore, for a 2-input primitive gate one input is connected as a control input of MUX (connected across gate shorted input terminal of pMOS and nMOS), the other variable is linked based on the column entities of P-diffusion and N-diffusion. When the column literals of P-diffusion are (1,1) or (0,0) then the VDD or GND is tied to P-diffusion. Similarly, if column literals of N-diffusion are (1,1) or (0,0) then the VDD or GND is tied to N-diffusion. Presumes for the P and N-MOSFET diffusion region will have the column literals of (0, 1) or (1, 0) its adjacent equivalent row literal value is linked to P-diffusion or N-diffusion node.

This fieldwork focuses on the GDI Library's entire architecture, which consists of all the primitive regular logic gates. The process begins with the generation of different patterns using GDI Technology. The Small-Scale Integration (SSI) library components such as "AND, OR, NAND, NOR, XOR, and XNOR" components are used to produce patterns. In this pattern generation process, all possible outcomes such as "00,01,10,11" are observed, and specific parameters are also interpreted. Analyzing parameters are transistor count, power, delay and rise and fall time. On the other hand, other environmental adjustments, such as temperature, bias and architecture angles, have been retained during the simulation process. The Silterra Library is where all modules such as PMOS, NMOS, power sources, and active and passive components are chosen. Then multiple patterns are generated for each of the gates, and the truth table needs to be verified. Optimized primitive cells are selected based on the study of specific parameters, such as power, delay and speed. These trends are often compared with CMOS, PTL and TG in terms of transistor count, area and power and delay. 0 – 1.2V is given as input supply where the parameters taken into account are delay, transistor count, power dissipation, rise and fall time. Output comparison research will be conducted for CMOS Technology, PTL Technology, TG and GDI Technology.

Flow chart of the design



4. RESULTS AND DISCUSSION:

Comparison table shows the reading taken for CMOS, PTL, TG AND GDI and has been tabulate according to technologies. CMOS has high noise margins because of its low-voltage stability and high transistor size. CMOS logic, on the other hand, employs a large number of huge PMOS transistors, resulting in high input loads and higher power dissipation as the working frequency rises. Due to greater node capacitances, the propagation latency is significantly longer than for the other logical types. The PTL circuit outperforms the CMOS circuit in terms of output. Fast speed, minimal power dissipation, and low connection effects are all advantages of PTL. The GDI method eliminates some of the PTL's drawbacks. A wide range of complex logic functions may be achieved with only two transistors. It may also be utilised to build low-power, fast circuits with lesser transistors (than CMOS and traditional PTL techniques) and better power characteristics. In a digital CMOS circuit, a transmission gate (TG) is utilised to pass or not pass a signal. Using transmission gate logic, complicated logic functions may be realised with a minimal number of complementary transistors. The reason for adopting the apparent complexity of transmission gate, rather than using a simple n-switch or p-switch in most CMOS applications is to eliminate the undesirable threshold voltage effects which give rise to the loss of logic level in pass transistors. No such degradation occurs when the transmission gates, but more area is occupied and complementary signals are needed to drive it.

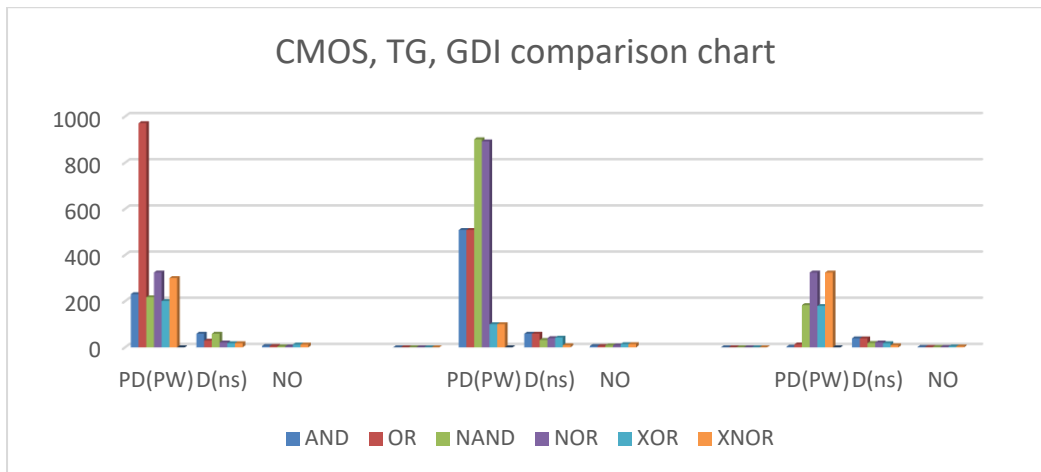
On the whole, GDI outperforms all these technologies by having low delay, power dissipation with a smaller number of transistors. These characteristics provide high performance gate. Yet, there is applicable of library for GDI and effort is taken in this research paper. Pattern creation is the crucial part of this research paper. Trial and error method is used in pattern

creation besides using Boolean implementation. Boolean implementation includes the De Morgan's Theorem, Boolean Rules, etc. Trial and error method is used in the software and checked the output waveform if it complements the truth table. Various pattern has been constructed using GDI basic gates such as NOR, NAND, AND, OR, XOR, XNOR, F1, F2, MUX and INV. This transistor-level circuit construction has been analysed depending on certain parameters like Rise time, Fall time, Power dissipation and delay with number of transistors that is used to create the optimized chip area.

Table 2: Experimental Results of GDI Basic Gates

GDI GATES	POWER DISSIPATION (WATTS)	RISING TIME (PS)	FALLING TIME (PS)	DELAY (NS)	NO OF TRANSISTORS
AND	2.8793p	1259.5	19035	39.771	2
OR	12.5554p	385.35	869.14	19.4511	2
NAND	183.6927p	180.43	135.98	30.905	4
NOR	324.0723p	189.38	148.84	21.064	4
EXOR	179.3707p	180.39	19.504	18.793	4
EXNOR	324.0723p	43.948	140.01	9.0157	4
F1	2.8793p	173.25	9230	28.886	2
F2	162.0933p	11337	173.20	41.018	2
MUX	1.7615n	73.887	403.64	9.4647	2

Above table shows the reading taken for CMOS, PTL, TG AND GDI and has been tabulate according to technologies. CMOS has high noise margins because of its low-voltage stability and high transistor size. CMOS logic, on the other hand, employs a large number of huge PMOS transistors, resulting in high input loads and higher power dissipation as the working frequency rises. Due to greater node capacitances, the propagation latency is significantly longer than for the other logical types. The PTL circuit outperforms the CMOS circuit in terms of output. Fast speed, minimal power dissipation, and low connection effects are all advantages of PTL. The GDI method eliminates some of the PTL's drawbacks. A wide range of complex logic functions may be achieved with only two transistors. It may also be utilised to build low-power, fast circuits with lesser transistors (than CMOS and traditional PTL techniques) and better power characteristics. In a digital CMOS circuit, a transmission gate (TG) is utilised to pass or not pass a signal. Using transmission gate logic, complicated logic functions may be realised with a minimal number of complementary transistors. The reason for adopting the apparent complexity of transmission gate, rather than using a simple n-switch or p-switch in most CMOS applications is to eliminate the undesirable threshold voltage effects which give rise to the loss of logic level in pass transistors. No such degradation occurs when the transmission gates, but more area is occupied and complementary signals are needed to drive it.



REFERENCES

- R.Uma and P. Dhavachelvan, “Modified Gate Diffusion Input Techniue: A New Technique for Enhancing Performance in Full Adder Circuits”, (ICCS2012) 6 (2012) September 2012, pp.74 – 81.
- G.R. Mahendra Babu and S. Bhavani “Primitive Cells using Gate Diffusion InputTechnique: a Low Power Approach”, International Journal of Recent Technology and Engineering (IJRTE) 8(2019). June 2019
- P.Jebashini, P.Senthil, R.Uma, Ooi Chee Pun, “A New Systematic GDI Circuit Synthesis Using MUX Based Decomposition Algorithm and Binary Decision Diagram for Low Power ASIC Circuit Design” Microelectronic Journal 108 (2021)
- Amrik Singh, & Dr. Sukhwinder Singh. “Evolution of CMOS Technology”. International Journal of Engineering Research And, V5(02), February 2016, pp. 304–307
- Khoirom Johnson Singh, Tripurari Sharan, Huiem Tarunkumar, “High Speed and Low Power Basic Digital Logic Gates, Half-Adder and Full-Adder Using Modified Gate Diffusion Input Technology” JoVDTT (2018) pp.34-42, V8 (01).
- Nishant, B., M., & Mehra, R.Efficient Layout Design using Transmission Gate in 45nm Technology. International Journal of Engineering and Technical Research (IJETR), 9(3), March 2019.11–14.
- Kunal & Nidhi Kedia, “GDI Technique: A Power-Efficient Method for Digital Circuits”, (IJAE) V1(03) (2019). [15] T.Sakurai and A.R.Newton, “Alpha power law MOSFET model and its applications to CMOS inverter delay and other formulas”, IEEE Journal. Solid State Circuits, vol 25, pg. 584-594, 1990.Input logic—Case-study of low-power CLA adder design“, INTEGRATION, the VLSI journal 47, pg 62–70, 2014.
- Bhaskar, K. (2019). Low-Power Digital VLSI Design. www.scribd.com. <https://www.scribd.com/document/421585492/Low-Power-Digital-VLSIDesign> [9]
- Blotnicki, Jan. (2020). Problem of floating debris. [10] Bruun, E. (2018). CMOS Analog IC Design: Fundamentals

IoT BASED REAL TIME MONITORING SYSTEM USING BLYNK APPLICATION

Sangeetha Valloo, Janagiammal Ramasamy, Jaya Malathy Poloha Nadan, Christopher Mark Mark Anthony, Norul Wahida Kamaruzaman, Nurazim Ibrahim & Naimah Yusoff
Infrastructure University Kuala Lumpur

1. INTRODUCTION

Wireless Sensor Networks (WSN) is known as a self-configured wireless network to witness physical or environmental conditions, example like temperature, pressure, motion, sound, vibration or pollutants and to straight pass their data of information through the network to descend which is also called the main locations where the information is often observed and processed (Pujara, Kukreja et al. (2020). According to Mosleh and Mahmood (2017), some wireless sensor networks are used to measure the range of a selected object by emitting ultrasonic sound waves, and transform the reflected sound into electrical signal, to detect the presence of water in a place where water should not present and to detect toxic gases, smoke and gas leaks in a closed environment (Prakoso, Bagas et al. (2018).

Prior to this, everything that human beings do requires manual attention to monitor or maintain a place or object. This makes their workload heavier, because of the need to appear physically in the required place to do the work. Moreover, humans can't be at the same place for monitoring and maintaining purpose all the time. According to Murugesh and Santhosha (2014), the physical data collection or report development of an incident will never be accurate in this case as humans can't be monitoring 24/7. Therefore, it is essential to develop a monitoring application with a network of cluster sensors integrating each other (Perumal, Sulaiman, & Leong, 2015). Thus, this will be a functional prototype of an IoT based monitoring system with data transmission wirelessly. Therefore, it is essential to develop a monitoring application with a network of cluster sensors integrating each other. Thus, this will be a functional prototype of an IoT based monitoring system with data transmission wirelessly (Ryu, Changsu, Chang-Wu, 2016).

The main objective of this chapter is to develop a network of cluster sensors using Arduino, to develop a monitoring application and integrate with a network of cluster sensors and last but not least to integrate Blynk application as a notification/output module.

The scope of this project is mainly on the transmission of data wirelessly. The development of this project is based on Arduino hardware and Blynk application. The sensors are scoped to 3 types which are ultrasonic sensor, gas sensor and water sensor. The ultrasonic sensor has been scoped to HC-SR04 ultrasonic sensor, which is to detect the movement such as opening or closing of an object. Following with the gas sensor which has been scoped MQ2 gas sensor, to detect gases such as methane, liquefied petroleum gas, butane and smoke. Water sensor has been scoped to Arduino water sensor, to detect water level, leakage and sensing

rainfall (Sidek, Othman et al. (2011).

2. HARDWARE

Arduino Uno

An open-source microcontroller board which is primarily based on Microchip ATmega328P microcontroller, developed by Arduino.cc. The Arduino Uno board is supplied with units of analog and digital input/output(I/O) pins that have been interfaced to different expansion boards and circuits (Deekshath, Dharanya et al. (2018). The following board incorporates 14 digital I/O pins and 6 analog I/O pins which is programmable with the Arduino Integrated Development Environment (IDE). Furthermore, the board may be powered by a USB cable or with an external 9-volt battery.

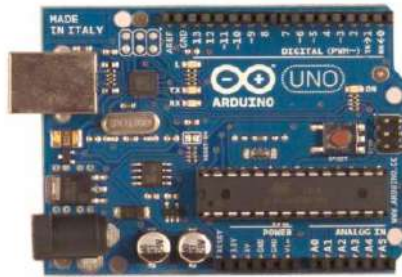


Figure 1.1: Arduino Uno R3

ESP Wi-Fi Shield

This ESP Wi-Fi shield grants Arduino boards to connect to the Internet using 802.11 wireless specification (Wi-Fi). This hardware comes with 5-volt operating voltage, ICSP headers, connection with Arduino on SPI port, FTDI connection for serial debugging, on board micro-SD slot and a mini-USB for firmware update of Wi-Fi shield.

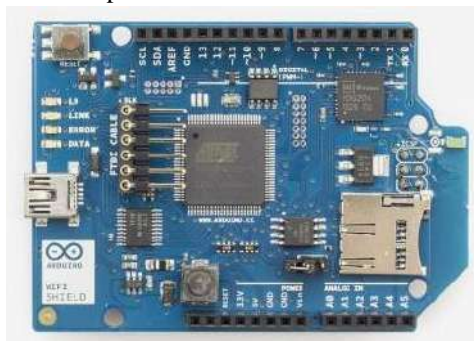


Figure 1.2: ESP Wi-Fi shield

Ultrasonic sensor

This HC-SR04 ultrasonic sensor is the best sensor for distance measurement and object detection. The sensor offers excellent range accuracy which is up to 1 millimeter and also with a stable reading at a very low price.



Figure 1.3: Ultrasonic sensor

Gas sensor (MQ2)

MQ2 gas sensor (also known as chemoreceptor), an electronic sensor that can be used for sensing the concentration of gases in the air such as methane, alcohol, LPG, hydrogen, propane, carbon monoxide and smoke. MQ2 sensor consists of a sensing material that makes its resistance changes when it is exposed with the specified gas.



Figure 1.4: Gas sensor

Arduino Water Sensor

This water sensor is designed to detect water presence, which can be used in sensing rainfall, liquid leakage and also water level. This sensor contains an array of exposed traces, which read “LOW” when water has been detected Pauzi, Hasan (2020).

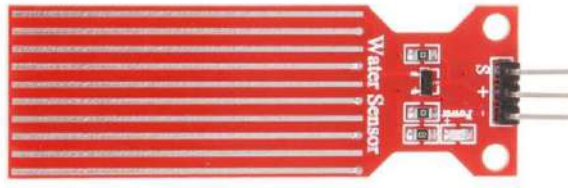


Figure 1.5: Arduino water sensor

Software

Blynk

A software developed mainly for the Internet of Things (IoT). Users can remotely control hardware such as Arduino using this Blynk, displaying and storing data, and many more. This Blynk contains 3 main components: -

- Blynk App – Allows to create different interfaces for projects using amazing widgets that Blynk provides.
- Blynk Server – Responsible for all the communications which take place between a smartphone and a hardware (Porkodi, Bhuvanewari 2014).
- Blynk libraries – Establish communications with servers and process the commands which is incoming or outgoing.

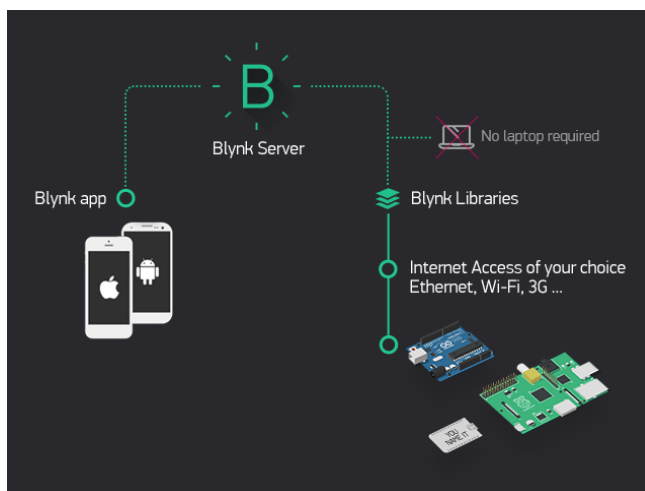


Figure 1.6 : Blynk Architecture

3. LITERATURE REVIEW

Wireless sensor networks (WSNs) contain multi nodes that are able to communicate with the environment by sensing or controlling the parameters (Mamalis, Basilis et al. (2009)). This is because the nodes are small in size and have limited power. The network often divides into a number of clusters in order to cooperate with themselves to deliver data to the specified station. Each cluster contains a number of nodes and one head which collects the data and sends it to the base station.

Network could be classified as single hop and multi hop clustering architecture as shown in Figure 1.7 and Figure 1.8 depending on the distance between cluster head and other members (Yu, Miao et al. 2006). Single hop defines that every node transmits directly to the cluster while in multi-hop, the far node sends packets through intermediate nodes which lead to saving power.

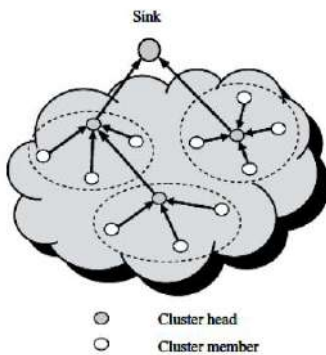


Figure 1.7: Single hop clustering

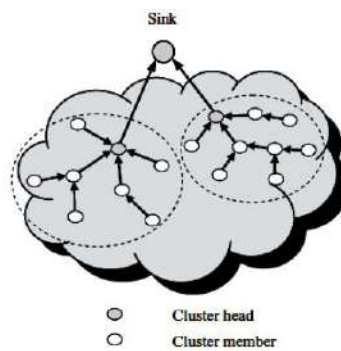


Figure 1.8: Multi hop clustering

Every sensor normally contains 4 main components which are communication, processing, sensing and power units (Pasha, 2016). All sensors are then connected to a processor for storage or any other applications. The following processing unit comprises a microprocessor or microcontroller with a memory. Power unit will consist of a battery to provide power for other components in the network. Communication unit consists of a short-range radio for data communication and reception over a radio channel (Al-Sarawi, Anbar, Alieyan, Alzubaidi, 2017). All those following units must be gathered into a small unit with low production cost and low power consumption

Comparison of Manual Monitoring vs. Real Time Monitoring of Manhole

Manual monitoring system adapts more difficulties in today's era compared to real-time monitoring system Muragesh, Santhosha (2014). It's because of the evolution of working the tasks by a human to a machine. Basically, machines do the task much faster and more reliably compared to humans. So, real-time monitoring will be perfect as it runs the monitoring part on its own, causing human effort less. Manual monitoring will be insufficient because humans

won't be able to monitor 24/7. It is just that the humans are able to do maintenance once the problem is detected (Raveena, Prasuna et al. (2020).

Moreover, real-time monitoring contains a lot more advantages compared to manual monitoring systems (Haswani, Naveen et al. (2018). Real-time monitoring can respond immediately, identify and classify the problem, proper justification of the problem, easy data sharing and more (Razali, Kassim et al (2020). The advantage of manual monitoring is that it doesn't need any paid system or software, simple to implement and use and resistant to power outages.

Table 1.1: Comparison of manual monitoring and real-time monitoring system

Manual Monitoring System	Real-time Monitoring System
Consume time to solve the problem	Responds to the problem immediately
Need to go through one by one to identify the problem	Helps in identifying and rectify the problem
Risk of human error	No risk of human error
Quick data sharing is not possible	Easy data sharing between users in real time
Low transparent performance tracking	More transparent performance tracking

4. METHODOLOGY

This chapter has discussed the advantages of using IoT based monitoring systems, in which the benefits of IoT based applications are valuable. Moreover, further details and implementations about the organized methodology for this system will be discussed. In other words, we will demonstrate how this monitoring system works phase by phase.

Agile Model

Agile is a combination of repetitive and gradual process models which process adaptability by fast delivery of a working project. Methods break into small-scale incremental builds which are provided in repetitions. Each repetition requires a cross functional group working simultaneously. Tasks are partitioned to time boxes such as small-time frames to deliver particular features for a release



Figure 1.9: Agile Model Diagram

Agile Development Model

This topic highlights that the development of this monitoring system is an added advantage to every human being. This is because of the ease which has been provided by the particular system. However, there are some difficulties such as costing, complexity and more which we have to overcome. Thus, this monitoring system decided to overcome those challenges by implementing an agile development model.

Agile development methodology is one of the easiest and effective to deliver a great product. Agile is flexible, error-proof, fast and has a better way in managing the developments. The main ideas of Agile is that:

- Change is unavoidable. The project wishes to adapt than ignore about it
- Delivering outcomes is greater essential than processes and tools.
- Real customer’s wishes take precedence over the necessities within the improvement plans.

Thus, the monitoring system will stick to an agile development model. It gives the flexibility and certainty for using the system. Furthermore, this methodology allows changeable adjustments and comfortability to the user’s needs. The nature of management in an agile model is not centralized, but is distributed among the co-workers.

Therefore, this IoT based monitoring system will provide confidence and validity when using the system which has been stated by the agile development model. This following methodology ensures convenience as well as modifications based on what the project needs. Moreover, this agile technique is adjustable in which the developer can adjust the process subsequent to Keep It Simple (KIS) principle.

Requirements

Gathering information is the main concern when developing a project. It is then we can identify and understand the requirements of the project. This will help in deciding the client’s needs. For

this monitoring system, the necessary requirements are as shown in Table 1.2.

Table 1.2: Requirements Table

Project Requirements	User Requirements
Detection of movement such as opening/closing	<ul style="list-style-type: none"> ● Receive the alert message via Blynk application ● Act based on the type of alert message
Detection of gases	
Detection of water presence	
Save the alert data to the database	<ul style="list-style-type: none"> ● Retrieve later for documentation and maintenance purpose

Design

It is to say that having a preliminary design of the system is the most important step to be a professional developer. So that it defines the work rules and regulations. Furthermore, it provides the developer a broad vision on how the monitoring system works and how data transmission is possible.

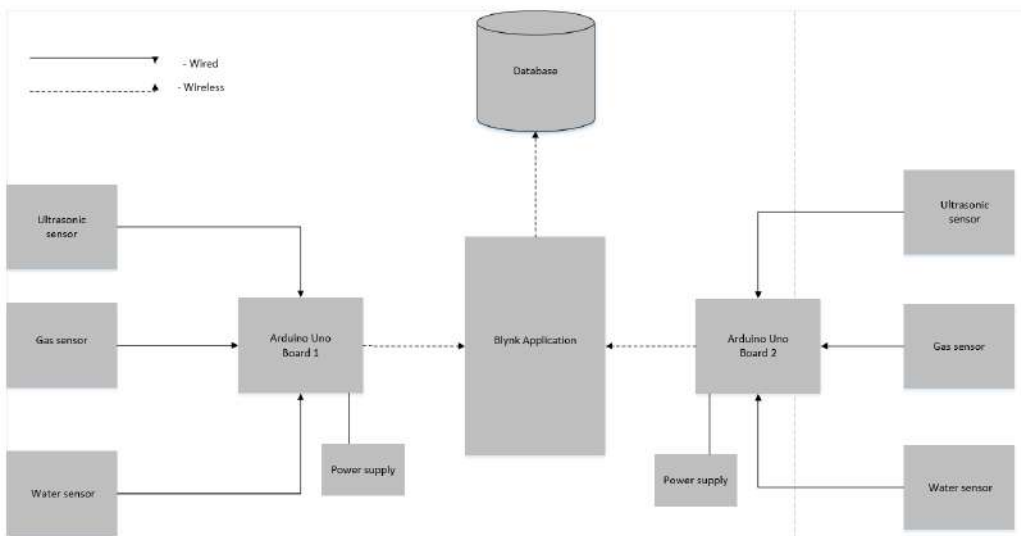


Figure 1.10 : Proposed system design

The proposed system design above shows the expected outcome of the system. The developed system is an IoT based monitoring system using Blynk application.

In this monitoring system, the management of sensors is done by an Arduino microcontroller. It is to say that the following types of sensors are connected to the microcontroller which helps in controlling the sensors. This Arduino is configured to

communicate with the Blynk application which sends data regarding sensors from the microcontroller to Blynk. This lets us monitor the condition of sensors in real-time. Moreover, Blynk receives alert detection messages from Arduino to alert the personnel on the change in situation. Later, the data about the detection will be saved in the database for record purpose.

UML Diagrams

UML diagram, also known as Unified Modelling Language is a diagram which is based on the UML with the intention of visually representing a system together with its actors, actions, roles and classes. Diagrams also can be used to communicate different aspects and characteristics of the system. Several types of UML diagrams are available such as communication diagram, use case diagram, sequence diagram and more. But in this project, I'm using 3 types of UML diagrams which are activity diagram use, case diagram and class diagram.

Use case Diagram

A use case diagram is the main form of a system requirements for a developing project. Use cases state the expected operation and not the required method of making it happen. Use case previously specified that it can denote both visual and textual representation. A central abstraction of use case modelling is that it guides on designing a system based on the user's opinion. It is a productive technique for communicating system behaviour based on the user's term by identifying every externally visible system behaviour.

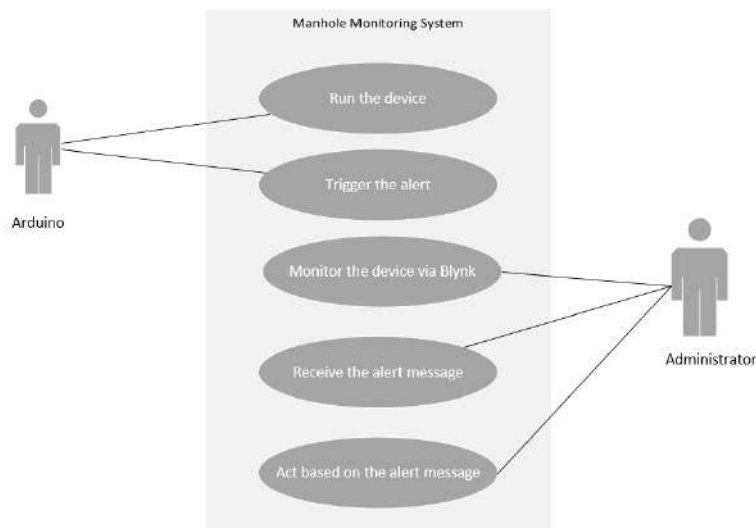


Figure 1.11: Use Case Diagram

As shown in the above Figure 1.11, this system consists of 2 types of actors with different roles. The first actor is the Arduino, because this project is based on the Internet of

Things (IoT) in which it doesn't require humans all the time. So, the Arduino plays the role of running the device via a power supply which later powers up the entire hardware together with sensors. Then, this Arduino will wait until it identifies any increase or decrease in sensor value. If any changes are possible, then the Arduino will trigger an alert to Blynk which converts to a message when receiving.

Following with the second actor of the system which is the administrator. The roles of the administrator are that he is able to monitor the device remotely via Blynk. In case an administrator receives any alert message saying that a problem has been detected, then this administrator must be responsible to act as soon as possible depending on the situation and type of alert. These are the roles of this administrator. Apart from that, the administrator is also responsible for maintaining the hardware implemented, which is because regular maintenance led to long-lasting conditions.

Conceptual Class Diagram

Class diagrams (Figure 1.12) explain the structure of the project by exposing the system classes, attributes and operations. This diagram also shows the relationship between the classes and their objects.

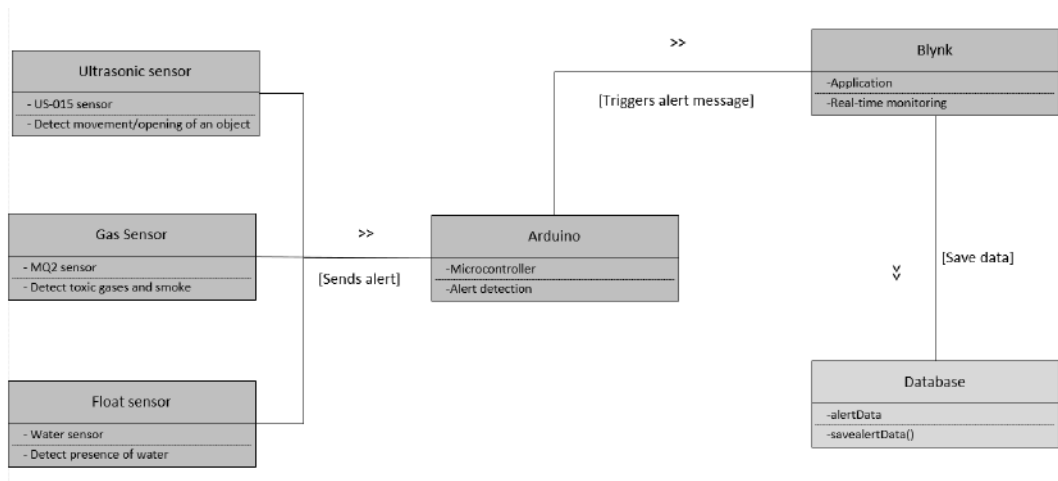


Figure 1.12: Conceptual Class Diagram

The Figure 1.12 explains on the class diagram of the proposed system. As shown above, this system has 3 subclasses and 2 main classes. The subclasses in this system are the types of sensors which consist of the main function in this project. Each sensor's function is to create an alert which sends alert information to the Arduino. The Arduino will then trigger it as an alert message to Blynk for monitoring. Furthermore, the main class is the system which consists of Arduino hardware, Blynk application and the database. The function of Arduino and Blynk has been stated previously whereas the database is where the alert data will be stored for record purpose.

Activity Diagram

Activity diagrams classify how activities are arranged to give a service which can be from different levels of concepts. For example, an event needs to be attained by some operations, precisely where the operation is intended to reach a number of different things that need coordination or how the events from one use case relate to each other, in detail, use cases where activities may intersect and require coordination. Activity diagram also suits for modelling on how a collection of use cases coordinate to represent workflows.

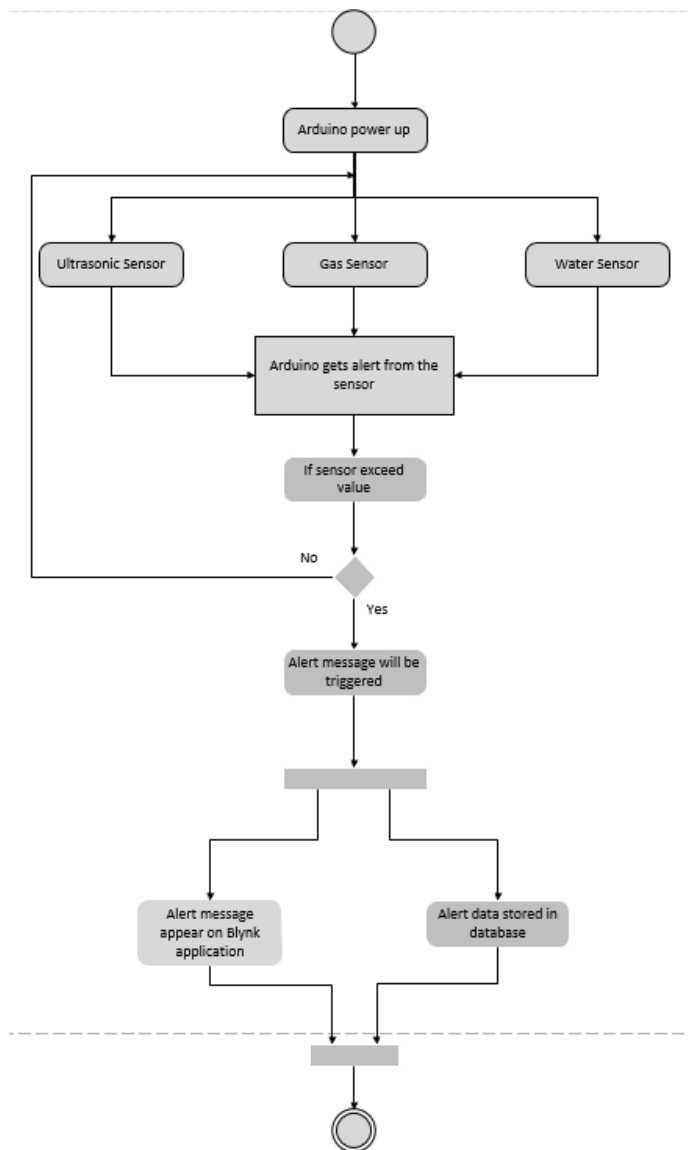


Figure 1.13 :Activity Diagram

As shown in the above Figure 1.13, this is the activity diagram for this proposed monitoring system. This diagram shows the flow on how this monitoring system works. It is to say that the system starts by powering up the Arduino which automatically powers the sensor that is embedded with the microcontroller. These sensors are scoped to a certain limit in which if the sensors exceed the limit, then the alert will be triggered from Arduino to Blynk in message form. The data of the alert that occurred also will be stored at the same time the message triggers. Therefore, this is how the monitoring system works based on this activity diagram.

5. CONCLUSION

In conclusion, this paper has shown the requirements to overcome the system on several standards. Developing this monitoring system based on the agile development methodology ensures the smooth flow of handling this system. Creating such an advanced system provides faster data transmission, good quality of service and time saving. Overall, developing this monitoring system will be a great advantage for those who are under a closed environment.

REFERENCES

- Mosleh, Mahmood F., and Duaa S. Talib. "Implementation of active wireless sensor network monitoring using ZigBee protocol." *Journal of Engineering Science and Technology* 12.11 (2017): 3082-3091.
- Ryu, Changsu, and Chang-Wu Hur. "A Monitoring System for Integrated Management of an IoT-based Home Network." *International Journal of Electrical and Computer Engineering* 6.1 (2016): 375.
- Mamalis, Basilis, et al. "Clustering in wireless sensor networks." *RFID and Sensor Networks: Architectures, Protocols, Security and Integrations*, Y. Zhang, LT Yang, J. Chen, eds (2009): 324-353.
- Yu, Miao, Jason H. Li, and Renato Levy. "Mobility Resistant Clustering in Multi-Hop Wireless Networks." *J. Networks* 1.1 (2006): 12-19.
- Prakoso, Bagas Mardiasyah, et al. "Performance Evaluation of Distribution Node in Case of LEACH Implementation on Wireless Sensor Network." *Jurnal Elektronika dan Telekomunikasi* 18.2 (2018): 67-74.
- Sidek, Othman, S. A. Quadri, and Shahid Kabir. "Multi agent system for an agile wireless sensor network to monitor structures." *Progress In Electromagnetics Research* 765 (2011).
- Raveena, C., K. Lakshmi Prasuna, and P. Likhitha. "Electronic NOSE-An IOT Based Smart Drainage Worker Safety System (2020)."
- Muragesh, S. K., and Santhosha Rao. "Automated internet of things for underground drainage and manhole monitoring systems for metropolitan cities." *International Journal of Information & Computation Technology* 4.12 (2014).
- Haswani, Navin G., and Pramod J. Deore. "Web-based realtime underground drainage or sewage monitoring system using Wireless Sensor Networks." *2018 Fourth International Conference on Computing Communication Control and Automation (ICCUBEA)*. IEEE, 2018.

- Lazarescu, M. T. (2013). Design of a WSN platform for long-term environmental monitoring for IoT applications. *IEEE Journal on emerging and selected topics in circuits and systems*, 3(1), 45-54.
- Deekshath, R., Dharanya, P., Kabadia, K. D., Dinakaran, G. D., & Shanthini, S. (2018). IoT based environmental monitoring system using arduino UNO and thingspeak. *Int. J. Sci. Technol. Eng*, 4, 68-75.
- Razali, M. A. A., Kassim, M., Sulaiman, N. A., & Saaidin, S. (2020, June). A ThingSpeak IoT on Real Time Room Condition Monitoring System. In *2020 IEEE International Conference on Automatic Control and Intelligent Systems (I2CACIS)* (pp. 206-211). IEEE.
- Pujara, D., Kukreja, P., & Gajjar, S. (2020, July). Design and Development of E-Sense: IoT based Environment Monitoring System. In *2020 IEEE Students Conference on Engineering & Systems (SCES)* (pp. 1-5). IEEE.
- Pauzi, A. F., & Hasan, M. Z. (2020, September). Development of IoT Based Weather Reporting System. In *IOP Conference Series: Materials Science and Engineering* (Vol. 917, No. 1, p. 012032). IOP Publishing.
- Al-Sarawi, S., Anbar, M., Alieyan, K., & Alzubaidi, M. (2017, May). Internet of Things (IoT) communication protocols. In *2017 8th International conference on information technology (ICIT)* (pp. 685-690). IEEE.
- Porkodi, R., & Bhuvaneswari, V. (2014, March). The internet of things (IOT) applications and communication enabling technology standards: An overview. In *2014 International conference on intelligent computing applications* (pp. 324-329). IEEE.
- Pasha, S. (2016). ThingSpeak based sensing and monitoring system for IoT with Matlab Analysis. *International Journal of New Technology and Research (IJNTR)*, 2(6), 19-23.
- Perumal, T., Sulaiman, M. N., & Leong, C. Y. (2015, October). Internet of Things (IoT) enabled water monitoring system. In *2015 IEEE 4th Global Conference on Consumer Electronics (GCCE)* (pp. 86-87). IEEE.

ZERO TRUST TAXONOMY FOR ACADEMIC DISHONESTY: A REVIEW PAPER

**Tadiwa Elisha Nyamasvisva, Atiff Abdalla Mahmoud Arabi, Noradibah Binti Adnan, &
Valeriano Dasalla Jr**

Infrastructure University Kuala Lumpur

1. INTRODUCTION

Academic dishonesty is one of the significant problems disturbing Institutions of Higher Learning (IHLs) across the globe for decades. [1]–[7]. Amzalag and others have defined academic dishonesty as a violation of professional behavior, widespread on college and university campuses. Academic dishonesty is a form of inappropriate behavior in which students get an unfair academic edge for themselves or their academic peers [8]. Recent empirical investigations have revealed that academic dishonesty by post-secondary students is widespread across a wide range of countries and educational levels [9]. According to [10], students commit academic dishonesty for assorted reasons. These reasons include but are not limited to avoiding failure, getting better grades, pleasing other people, etc. However, the main aim of committing academic dishonesty is to get a better outcome in an examination or other forms of learning assessment. In this sense, preventing failure is the primary cause of academic dishonesty.

Technology has tremendous advantages in various aspects of human life. Sometimes, it has some negative aspects. One of its disadvantages is that many college students worldwide use multiple ways to practice academic dishonesty. Thus, technology-oriented academic dishonesty has become one of the significant obstacles that encounter many universities and colleges around the globe. For instance, [11] realized in their study that among undergraduate students in Western Pennsylvania, 83% of the students had cheated during the last or current academic year, and 80% of them had upheld using crib notes or written materials on their shoes. Another important example that academic dishonesty is a universal problem is what has been reported by [12]: in the USA “more than 170 instructors and principals were found to have assisted cheating in exams in 2009”, or “fake candidates were sent into exams to get hold of the questions, the South China Morning Post reports,” or “Several hundred people have been arrested in connection with mass school exam cheating in the Indian State of Bihar”.

There are several ways to identify cheating among college students. For instance, [13] report that cheating may embody plagiarism, stealing a test, fabricating academic documents, purchasing term papers, or copying another person’s exam.

However, Academic dishonesty can be aggressive or inactive, and it can arise everywhere in the educational system. Academic dishonesty has been extensively investigated. Most studies concentrate on the prevalence, determinants, techniques, and ethical judgment [14]. Prior studies have not developed any classification model through which Institutions of Higher

Learning (IHLs) can classify the types of academic dishonesty. Therefore, this research reviews the literature on the prevention mechanisms of academic dishonesty in institutions of higher learning and proposes a classification model for academic dishonesty.

2. BACKGROUND

The effort by any learner to present as their work that which they have not generated is seen as a significant infraction by both the professor and the management [15]. The act of copying someone else's material during an examination, or the submission of a paper or assignment that has been prepared, in whole or part by someone else, is regarded as academic dishonesty and punishable by law [16]. Academic dishonesty is not a new problem; [17] discovered that 60% of students engaged in academically dishonest behavior, and [18] found that 66% of them confessed to academic misconduct in a related study more than 50 years later. Since ancient times, dishonesty has been a part of the human experience, both mentally and professionally. In ancient China, civil service job seekers were separated during interviews to prevent fraud, as the penalty for being detected was death. Employee theft is expected to cost employers anywhere from \$5 billion to \$50 billion each year [19]. We have been grappling with moral dishonesty for the same period. Academic dishonesty has been characterized in many forms. [17] described academic dishonesty as engaging in unethical activities that are not limited to plagiarizing, cheating, failing to cite a source, and changing someone else's words to make them sound like they were one's own in his meanings of academic dishonesty. Misuse or destruction of materials that prohibit students from accessing them should be applied to the list of academic dishonesty concepts [20]. Institutions of higher learning are notorious for academically dishonest conduct. It means attempting to take credit for anyone else's work, falsifying or forging documents, utilizing illegal or fake content, and bringing damage to other people's work.

According to [21], these styles of behaviors have been on the rise for decades; with references to many studies, intellectual dishonesty is more popular than ever. According to research by [22], [23], when students reveal themselves, the actual incidence of academic dishonesty is as high as 80%. When they confirm academic dishonesty that others have engaged in, the rate is as high as 99%. According to [23], [24], 88% of professors have seen their students engaging in academically dishonest conduct [24].

Nowadays, technology is rapidly changing the world around us, allowing professors to incorporate more technology into the classroom and educate more students remotely via hybrid and online classes [25]. Besides, the Covid-19 pandemic has ushered in a new era in the academic world characterized by remote teaching and learning. These opportunities have their advantages, but they also bring new challenges. When exams are given in un-proctored environments, the possibility of cheating on tests increases.

3. THE TRANSITION OF ACADEMIC DISHONESTY METHODS

Academic dishonesty is not a new phenomenon. It began long before technology entered our lives and included various behaviors [8]. Academic dishonesty has been controversial in academia for many years but has accelerated in recent years. One reason for this is the rise of distance learning and the technologies that enable these behaviors [8], [26]. In March 2020, institutions of higher learning and other educational institutions were forced to close for several months due to the ongoing Covid-19 pandemic. Educators worldwide moved from face-to-face teaching and learning to distance learning to continue teaching and learning activities during this challenging time [8], [27]. The integration of distance learning without integrating rules for ethical behavior suitable for the distance learning environment and special techniques to prevent academic dishonesty provides fertile ground for an increase in the frequency of inappropriate academic behavior [28]. Following the integration of technology in un-proctored learning environments, there are additional explanations for unethical behavior [29].

According to [30], high-tech devices took place at a top Thai medical college where three students used ‘spyglasses’ with wireless cameras to transmit the exam questions and received the answers through their smartwatches. During the covid 19 pandemic [31], students have cheated on online exams and several other forms of cheating on digital exams, including accessing exam-related websites, using mobile phones and social media platforms during exams, storing exam answers on their computers, and having non-exam Universal Serial Bus (USB) ports with them containing answers and solutions to exam questions. According to [32], hacking is one of the most prominent cyber issues within the higher education system. In addition, hackers use various methods to manipulate data and information, including hacking, malware, skimming hardware, and insider attacks [33], [34].

3.1. Traditional Methods

Academic dishonesty is described as a behavior or combination of practices that misrepresent scholarly work [35]. These conducts include but are not limited to:

Table 1.0: Types of Academic Dishonesty

No	Type of Academic Dishonesty	Description
1	Cheating	Defined as obtaining or providing data or material utilized to calculate academic credit [36].
2	Plagiarism	Defined as the unattributed use of a source in a case in which there is a legitimate assumption of authorship [35]
3	Fabrication	It is defined as the utilization of material that has been fabricated or misrepresented [37].
4	Impersonation	Other than the registered student sits the examination [38], [39].
5	Possession	Use of documents or tools that are not permitted during the examination, i.e., forbidden aids such as social media and

		phones [39], [40].
6	Information Tempering	It is defined as any act or error to deceive a teacher to get an educational advantage [41].
7	Unauthorized Access	Hacking the system to find the answers [39], [42].
8	Collusion	It is defined as the activity of two or more learners collaborating on a single project [39], [43].
9	Duplicate Submission	Unintentional duplication of work occurs when a learner submits the same work for two classes [37], [44].
10	Disruptive behavior	It is defined as any behavior that disrupts the procedure[37].
11	Conspiracy	It is defined as collaborating with one or more individuals to conduct or attempt to perpetrate academic dishonesty[37].
12	Bribery	Bribing somebody for an educational benefit, or receiving a bribe for an intellectual gain, "i.e., a student offers a professor money, goods, or services in exchange for a passing grade, or a professor accepts this bribe" [37].
13	Illegitimate Assistant	Illegitimate help from outsiders is received during the examination, i.e., outsider assistance or from a university employee during the examination[39], [40].
14	Forgery	described as theft or prohibited reproduction [44]

These acts can be done before, during, and after the actual assessment [45]. Recently, studies conducted in the United States revealed that certain types of academic dishonesty could arise [46]. According to [47], 1800 individuals at nine medium-to-large-sized State colleges in the United States, "all of which had participated in Bowers' 1964 study," were surveyed. They discovered that, while the total percentage of students who admitted to participating in at least one dishonest behavior had not risen significantly, the percentage of students who admitted to participating in significant exam cheating activities has grown [48]. The percentage of students who copied from some other students had enhanced from 26% to 52%, the rate of students who assisted another trainee in cheating rose from 23% to 37%, and the rate of students who used crib notes had increased from 16% to 27%. The researchers also discovered a significant rise (from 11% to 49%) in unlawful student collaboration (i.e., students working together when the lecturer specifically requested individual work). After doing their research, McCabe & Trevino reported that "despite only a minor rise in the number of students who cheat, the students who do cheat are engaging in a greater variety of test cheating activities today and are also cheating more frequently" [49]–[51]. [52], [53] found that 71% of students admitted to significant dishonesty on published material, which included "plagiarism, fabricating or falsifying a bibliography, turning in work done by someone else, or copying material without footnoting them in a paper, "or on exams" including copying on an exam with or without another student's knowledge, using crib notes, or assisting someone." Seventy-one percent of fraud is unavoidably prevalent in today's academic environment, which is clear. No educational institution is immune to the practice of cheating. As per a survey conducted by the Josephson Center of Ethics in 2012 with much more than 23,000 participating students from throughout the United States, 51% of high school students confess to cheating on a test at some point in their lives.

3.2. Modern Methods

Contractual fraud has lately become widespread in higher education [54]. During the COVID-19 pandemic, while educational institutions moved to digital training, the rate of contractual fraud among students soared to new heights. The absence of face-to-face engagement and proctoring in the educational institutions was advantageous for essay scammers, who utilized relentless marketing tactics to entice participants. According to [39], [42], students who cheated by using a network-based educational platform hacked academic networks to obtain examination questions and avoid the proctoring mechanisms implemented by virtual learning platforms. According to research conducted by [30], the utilization of social networking sites (SNS) such as Twitter, Facebook, and YouTube has helped improve teaching and learning in today's educational institutions. Regrettably, online social networks are many innovative technology artifacts that initiate new and significant dangers to learning settings. As a result, academic dishonesty, also known as cyber-cheating, has become more prevalent among students due to the enhanced preponderance of online social channels.

According to [30], the use of smartwatches with built-in cameras and glasses with embedded cameras may seem like standard spy equipment for the likes of James Bond. But, for three students enrolling in medical school in Thailand, they were high-tech cheating gadgets. Rangsit University in Bangkok has canceled its admissions exams for its medical and dental faculties on Saturday and Sunday due to three female students discovering the university's unorthodox mode of operation. Recently, three students at a prestigious Thai medical college were caught cheating by wearing 'spy glasses' with wireless webcams to broadcast exam questions and get answers through their smartwatches [30]. While cheating has long been an issue in Thai schools and colleges, the use of high-tech equipment such as cameras to take images of the test sheet and smartwatches to receive answers from someone outside the institution has elevated the activity to an entirely different level.

According to [55], college students frequently employ contemporary cheating tactics. According to [55], 38% of students plagiarized from traditional sources, with 40% admitting to plagiarizing using the Internet. [55], [56] investigated the attitudes and views of 291 science students and discovered that half of them were open to the possibility of using the Internet to cheat. The results of an investigation by [57] revealed that a total of 87 undergraduate nursing and health sciences students admitted to engaging in plagiarism. Eighty-seven percent of these students stated that the Internet was the only or primary method by which they could get plagiarized content [55]. Students confidentially report widespread use of electronic technology in dishonest ventures to circumvent test integrity, plagiarism, falsification of clinical records, attempting to alter grades, and sharing information that should be kept secure and confidential. According to [30], Algerian authorities stopped access to Facebook and Twitter throughout the entire country to avoid exam leaks through social media, particularly after a student was discovered cheating with an earpiece linked to a satellite system.

In his testimony [55], [58] stated that "cell phones have elevated the practice of duplicating assignments and sharing exam results to an entirely new level because they have made communication across classes so simple." The camera device on students' mobile phones is being used to take images of their tests, which they may save or email to their friends [55],

[58]–[62]. According to [55], [63], [64], students rely on their Web-connected cell telephones to find the answers during examinations and communicate with one another via instant messaging. As a result, some instructors have permanently banned electronic devices from their classrooms. Many other students have photographed their study guide and saved it on their phones, only to access it later during the exam.

3.2.1. Modern Attack Surfaces

Table 2.0 summarizes attack surfaces primarily used for academic dishonesty through modern methods. Most of the attack surfaces are prone to use during an attack, while some before an attack and after an attack. Remote access services such as LMS and live streaming services are mostly prone while they are in use only. This applies to FTP-based programs, which are more vulnerable during use. The rest of the attack vectors are deployed to be harmful and active before an application is used, while it is in use, and can still be active after the applications are not being used but previously launched.

Table 2.0: Attack Surfaces

No	Attack Surface	Attack Vectors	Attack Period		
			Before	During	After
1	Remote Access Services	TeamViewer, Zoom, Teams, AnyDesk, etc.		√	
		RDP Protocol (3389)	√	√	√
		Learning Management System (LMS)		√	
2	File Sharing	File transfer protocol programs (FTP)		√	
		TeamViewer, Zoom, Teams, AnyDesk, etc.	√	√	
		Learning Management System (LMS)	√	√	
3	End of Life exploits	Compromised credentials	√	√	√
		Weak Credentials	√	√	√
		Malicious Insiders	√	√	√
		Misconfigurations	√	√	√
4	Admin Portals	Learning Management System (LMS)	√	√	√
		Servers	√	√	√
5	Sensitive Business Applications	Learning Management System (LMS)	√	√	√
		Examination Management system (EMS)	√		√

6	Unencrypted Logins and text protocols	Telnet, SMTP, FTP	√	√	√
7	Directly Exposed IoT Devices	Smartphones, PCs, etc.	√	√	√
8	Weak and insecure crypto	Internet and network-based access	√	√	√
9	Exposed development infrastructure	Internet and network-based access	√	√	√
10	Insecure and abandoned marketing portals	Internet and network-based access	√	√	√

4. ACADEMIC DISHONESTY PREVENTION MECHANISMS

Educational institutes' methods of verifying and authenticating students' records at the examination hall or online exams can be falsified due to cheating "Impersonation" or ineffective measures of carrying out the verification processes. Therefore, biometric authentication has taken the place of traditional verification as the chances of false and tampered data are significantly reduced. [65] proposed an authentication platform for students appearing in an online examination system called Profile Based Authentication Framework (PBAF). It is based on an approach of multi-modal authentication to secure online examinations. This method comprises two layers of authentication, i.e., user ID and password and security question. Firstly, it includes user ID and password followed by security questions to refine and secure individual students' profiles. [66] formulated object-based authentication in which students possess identity objects for authentication purposes. The students are identified by presenting or smearing physical identities such as electronic chip cards, RFID tags, magnetic cards, and digital keys.

These physical identity objects, such as electronic and magnetic cards, help store individual physical features.[67] suggested an iris recognition method that recognizes the iris of each student. These iris patterns are unique identifiers of every student and are obtained through a video-based image acquisition system. Devices used for scanning iris have been used for several years; therefore, their prices have decreased. Its present framework can even be used in eyeglasses and contact lenses and does not require physical contact with a scanner. It can easily work with individuals of different ethnic groups and nationalities. [65], formulates another aspect of biometric verification by talking about facial recognition and its verification. Facial recognition biometric verification utilizes image recognition and pattern matching algorithms for user identification.

According to [68], their research entitled "Examining Online College Cyber Cheating Methods and Prevention Measures." The most prevalent technique to find plagiarism is to utilize similarity index software such as "Turnitin.com, WriteCheck.com, DupliChecker.com, and others," which also tests all signed documents and computes a similarity index for each one of the papers checked. In the similarity index, all instances of plagiarism are displayed. Once a similarity index has been calculated, the teacher should rationalize whether the student has plagiarized and whether to pursue further investigation [69]. Learners will be pushed to employ

original thought while authoring reports or responding to writing assignments if the teacher specifies a minimum concentration of resemblance between the two writing pieces—strict writing Standards. Once upon a time, paper hardening procedures were employed, which were effective as anti-plagiarism techniques. The approaches involved forcing learners to create printouts of the materials and writing assignments relevant to a classroom subject or book chapter rather than allowing students to choose their topic. [70] proposed an image processing toolbox in MATLAB to do facial authentication, and it was successful. Face recognition, like any other biometric authentication, necessitates the collection of specimens, their identification, extraction of relevant (features) information, and storage of the data to be recognized. When it comes to facial recognition, the Viola-Jones algorithm and SVM "Support Vector Machine" are the algorithms that are utilized. A student is presented with an assessment site constructed using PHP to write their assessment. After the face verification process is completed, every student's score reporting is issued as an electronic credential. XAMPP is a program that enables users to create a local webserver. Every student will receive an electronic certificate in the form of a pdf file. It is also available for purchase. The hash function of the pdf file is computed and saved in the blockchain database. The validation site generates the file's hash value once more and compares it to the hash value of the pdf stored in the blockchain. If the hash values match, the file is approved. Because we are utilizing blockchain technology, only those granted access to the files saved using their private keys can access them.[71] developed a way to reduce academic dishonesty by assigning personalized coursework criteria to students. For example, in a lab-based technical curriculum, students are often asked to design a piece of equipment or software that meets specific specifications such as usability and efficiency. So this approach can improve student productivity. In this situation, it is normal for learners to debate the issues at hand and trade opinions on achieving the requirements best. This type of engagement is strongly promoted in the engineering field since it improves cooperation, a critical ability for every practical engineer. Specific learners, nevertheless, may take full benefit of precisely an atmosphere and plagiarize answers from their colleagues, a practice known as complicity. To prohibit such behaviors, we propose in this part that each student be assigned a unique criterion so that every learner will be required to construct their concept and will no longer be permitted to replicate projects from their teammates. Suppose we raise the number of evaluations an instructor must do. In that case, this technique will become unworkable as it will if it increases the number of assessments a student must perform. [72] proposed that the Online proctor (e-proctor) approach is scheduled to be researched to oversee a student while participating in a D-exam. The e-responsibility proctors are to detect any instances of cheating during a D-exam session. E-Proctor is a comprehensive system that ensures the academic integrity of online training examinations and other assessments. The e-proctor requires a fingerprint scanner to identify a pupil's identification and an eye tracker with a camera to track the participant's facial movements during the course.

By collecting photos of the individual pupils and processing them via computer techniques, the webcam can follow even the slightest motions of their pupils. The algorithms read "On-screen gaze coordinates" and then assist the software in determining where the user is looking on the screen. As soon as the e-proctor is linked to the student's computer, it restricts access to only the exam program while simultaneously banning access to any other applications or previously stored information that could be used to cheat during an exam. The learner should

correctly complete the ID authentication procedure, which comprises placing the finger on a scanner and matching the fingerprints with the data acquired during the initial enrollment process before being admitted to the program.

The following policy was devised by [73] to prohibit learners from examining test questions: Implications of revealing examination questions to the public for all academic assignments, requesting a second, and the third or fourth chance will result in a 25 percent, 50 percent, or 75 percent reduction in your grade. A policy was devised to avoid the interchange of questions and the exposition of their answers in groups: There is a time limit. "An application for a second or third try must be submitted before the deadline." As an illustration, if a learner fails to finish a test within 24 hours of the scheduled start time, the individual will be required to repeat the examination within the specified period and not later. A policy was devised to avoid an exam break or to allow for an extended amount of time for each question: Controlling the passage of time "All questions have a time limit based on the time limit established for the exam in the instructions," says the professor.

Object-based verification is defined by [66], wherein learners have identification objects that can be utilized for authentication. Biometric identification like "electronic chip cards, RFID tags, magnetic cards, and digital keys" are used to identify the pupils. Physical identity devices like electrical and optoelectronic cards aid in the storing of personal physical characteristics. [67] introduced an iris identification approach that identifies each student's iris. These iris patterns, obtained via a video-based image acquisition technology, are critical differentiators for each learner. Because iris scanning equipment has been in operation for many years, their prices have significantly fallen. Its current architecture may be used even if eyeglasses or contact lenses are worn, and it does not necessitate physical contact with a scanner. It can effortlessly collaborate with people from many ethnicities and cultures.

Specifically, [74], in their investigation of plagiarism detection techniques for recognizing the unauthorized usage of textual material by students' curriculum assessments, explain that the software plagiarism instrument could be used to compute the similarity between a couple of initiatives using a token sequential and dependency chart characteristic, among other things. However, it is possible to get around these code plagiarism detection systems by altering the syntax. The authors developed a new language-independent way to combat plagiarism in programming classes that eliminates the need for code inspection or instructor participation. [75] conducted a study over a five-year period in which he studied the accomplishments and perspectives of learners about the computerized assessment process used in plagiarism detection in coding classes, which he published. Two hundred twenty-eight records were included in the data set, and the methodology was focused on tokenizing and aggregating different attributes from the source code. The report found a flaw in the method. Because plagiarism detection is entirely reliant on the adaptive threshold valuation, which is utilized to determine the degree of similarity in the material, adaptive threshold issues in this strategy can result in false positives for plagiarism detection and thus false positives for plagiarism prevention [76].

According to [77], authentication is a crucial aspect of digitized identity's integrity for academic dishonesty; as a result, authenticating a learner before and throughout an online test is

a significant part of online assessments. The authentication procedure is typically completed before administering the examination, providing an opportunity for the examinee to change their password after signing into the online examination or for someone to finish the test using another's login and password to avoid detection. Eliminating cheating throughout an exam is also a critical component of maintaining academic integrity in the classroom. Cheating during online examinations has increased significantly compared to traditional paper-based assessments, primarily due to the unavailability of a moderator during these examinations. For example, it is feasible that the student will utilize a forbidden item to assist them in finishing the exam, such as a mobile device.

To combat academic dishonesty,[78] used Physical Cameras to monitor students' behavior. The basic configuration is straightforward: position the needed range of cameras in the classroom where the E-A is conducted, ensuring that all students and their gadgets are always filmed from backstage. The essential advantage of this technique over direct video capture via program is that it is significantly less sensitive to technical issues or attacks, such as broadband connection dropouts or issues with the program installed on the students' devices, than the former.[79] outlines Measures for Preventing Cheating When Using Moodle Quizzes in her paper, Measures for Preventing Cheating When Using Moodle Quizzes. Comprehensive measures must be implemented to obtain a positive outcome in the battle against cheating. When constructing the evaluation system and creating the questions, it is essential to keep the likelihood of fraud in mind as you go along. When reviewing, it is critical to have a well-organized process. Meanwhile, the technological potential of LMSs, specifically Moodle, should be utilized to the greatest extent possible. [80] have proposed "An Ad Hoc Movement Monitoring Algorithm for Indoor Tracking During Examinations," which was published in 2021. Monitoring will be conducted regularly, and the time and length of monitoring at various levels will be determined during the planning process. The damage caused by the observed occurrences determines the scale and scope of monitoring (examinations). Examiners, the test division, proctors, and the examination board officials create the monitoring procedure. Each interested party's central individual will be recognized and participate in this monitoring activity.

According to [81], several methods can be used to avoid cheating during exams. Establishing solid administrative standards by academic institutions against misbehavior practices is one of the most effective strategies to prevent cheating during tests and student evaluations. Because many studies show that learners' ignorance of institutional policy concerning cheating remains a driving force for academic misconduct, clear standards about intellectual good moral values and unethical actions can help better manage this problem. According to [81], [82], practical academic ethics and competent faculty monitoring could provide best practices in academic misconduct. Punishments are perfect strategies for controlling cheating; nevertheless, other authors suggest that if the problem is evaluated for a long-term solution, repercussions may be less successful.

Li, Sikdar, Xia, and Wang are among those who have contributed to this work [83]. Using the Alg-Cyclic strategy, you can search for resources from the Cyclic Pool. As a result, they introduce Alg-Cyclic (Algorithm 2), which greedily searches for better tasks from a constrained set of cyclical series constructed via left circular shifting and SCS. When Algorithm

2 is used, the students are placed in descending order of their talents. The algorithm is divided into two phases or stages: as their chosen starting in Algorithm 1, the results A0 from war, Sikdar, Xia, and Wang employ the result A0 from Algorithm 1 in Phase 1, and together with other reasonable/random initializations, they will determine which is the best one out of the respective increased benefits. In Phase 2, a learner is picked following the established order. A sequence from SCS is selected to be allocated to the student to minimize the student's cumulative gain "the assignment is updated only if the update reduces current average cheating gain to ensure convergence." [73] experimented to see if usage of the Front-end method might stop academic dishonesty. The procedure is built on top of an exam policy, which typically includes the following components: It was decided that the following approach would be implemented to thwart end-users from asserting "that their computer had halted or/and there was a network connection disruption," as well as to provide students with the ability and time to view test queries as well as take snapshots or copies of them: Students make use of computers and networks; "it is your obligation to ensure that your computer and network connection are in good working order and are operating properly" [84]. To prohibit students from examining exam questions, the following policy was implemented: Consequences of revealing exam questions to the public for all exams and quizzes, requesting a second, third, or fourth attempt will result in a 25 percent, 50 percent, or 75 percent reduction in your grade for that exam or quiz.

The introduction of individualized Excel-based exams by [85] was intended to discourage pupils from cheating. Even though the learning takes place on digital sites, the evaluations should evaluate students' achievements accurately. Evaluations are also used as tools to check on students' progress, planned learning outcomes, feedback, and monitoring tools for instructors to keep track of their classes. Online exams can be configured to optimize and expedite the impartiality of the educators' scoring. It is anticipated that online exams will reduce the likelihood of students engaging in dishonesty operations. Without good planning preparation, those exercises will motivate learners to engage in more cheating exercises such as making notes, utilizing devices to seek answers, or communicating with their classmates.

The primary objective of employing a database in a tool, according to [86], is to properly arrange and store knowledge on members, learners, programs, and so on, and it must also enable the program to communicate with this content using "Structured Query Language (SQL) queries." The system employs a database schema, which holds details in charts composed of rows (representing records) and columns (representing fields or characteristics). Administrators (admin and examiner), learners, and Programs are the key elements that will make up part of the MySQL database based on the network needs. These tables have the following apparent attributes: user login and password; a student's name, a registration number, email, phone number, and so on; "Courses course code, the course title, academic session, and so on." Each table has a primary key that uniquely identifies each record in the database. Relationships between tables are established using foreign keys. One-to-many, many-to-many, and one-to-one connections are all possible.

Table 3: Summary of The Academic Dishonesty Prevention Mechanisms

Name of the authors & title of their research paper	Summary in point format
[70] Detection of Impersonation in Online Examinations Using Blockchain.	<ul style="list-style-type: none"> • Proposed an image processing toolbox in MATLAB to do facial authentication, and they were successful • Face recognition, like any other biometric authentication, necessitates the collection of specimens, their identification, extraction of relevant (features) information, and storage of the data to be recognized • Every student will receive an electronic certificate in the form of a pdf file.
[71] Design and evaluation of plagiarism prevention and detection techniques in engineering education.	<ul style="list-style-type: none"> • Developed a way to reduce academic dishonesty by assigning personalized coursework criteria to students • This approach improves student productivity. • In this situation, it is normal for learners to debate the issues at hand and trade opinions on achieving the requirements best • Specific learners, nevertheless, may take full benefit of precisely an atmosphere and plagiarize answers from their colleagues, a practice known as complicity
[72] E-exam cheating detection system	<ul style="list-style-type: none"> • Proposed that the Online proctor (e-proctor) approach is scheduled to be researched to oversee a student while participating in a D-exam • The e-responsibility proctors are to detect any instances of cheating during a D-exam session • The e-proctor requires a fingerprint scanner
[73] Online Cheating: A Prevention Procedure	<ul style="list-style-type: none"> • A policy was devised to avoid the interchange of questions and the exposition of their answers in groups • A policy was devised to avoid an exam break or to allow for an extended amount of time for each question • All questions have a time limit based on the time limit established for the exam in the instructions • usage of the Front-end method might stop academic dishonesty • The procedure is built on top of an exam policy • Students make use of computers and networks
[66] A Framework of Secure Biometric-Based Online Exam Authentication	<ul style="list-style-type: none"> • Learners have identification objects that can be utilized for authentication • Biometric identification like "electronic chip cards, RFID tags, magnetic cards, and digital keys" are used to identify the pupils • Physical identity devices like electrical and optoelectronic cards aid in the storing of personal physical characteristics
(Fayyoubi & Zarrad, 2014) Novel Solution Based on Face Recognition to	<ul style="list-style-type: none"> • An iris identification approach that identifies each student's iris. • Iris patterns, obtained via a video-based image acquisition

Address Identity Theft and Cheating in Online Examination Systems.	<p>technology, are critical differentiators for each learner.</p> <ul style="list-style-type: none"> • It can effortlessly collaborate with people from many ethnicities and cultures.
[74] E-cheating Prevention Measures: Detection of Cheating at Online Examinations Using Deep Learning Approach--A Case Study	<ul style="list-style-type: none"> • Plagiarism detection techniques for recognizing the unauthorized usage of textual material • Software plagiarism instrument could be used to compute the similarity • The authors developed a new language-independent way to combat plagiarism in programming classes that eliminates the need for code inspection or instructor participation
[76] EFL teachers' use of plagiarism detection software	<ul style="list-style-type: none"> • computerized assessment process used in plagiarism detection in coding classes • Approximately 228 records were included in the data set, and the methodology was focused on tokenizing and aggregating different attributes from the source code • The report found a flaw in the method
[77] Continuous multi-biometric authentication for the online exam with machine learning	<ul style="list-style-type: none"> • Authentication is a crucial aspect of digitized identity's integrity for academic dishonesty. • The authentication procedure is typically completed before administering the examination. • Eliminating cheating throughout an exam is also a critical component of maintaining academic integrity in the classroom
[78] Best practices in e-assessments with a special focus on cheating prevention	<ul style="list-style-type: none"> • The invention of physical Cameras to monitor students' behavior • The basic configuration is straightforward • The essential advantage of this technique over direct video capture via program is that it is significantly less sensitive to technical issues or attacks
[79] Prevention of Cheating when Using Quizzes in Moodle	<ul style="list-style-type: none"> • Measures for Preventing Cheating When Using Moodle Quizzes in her paper. • When constructing the evaluation system and creating the questions, it is essential to keep the likelihood of fraud in mind as you go along. • Meanwhile, the technological potential of LMSs, specifically Moodle, should be utilized to the greatest extent possible.
[80] An Ad Hoc Movement Monitoring Algorithm for Indoor Tracking During Examinations	<ul style="list-style-type: none"> • An Ad Hoc Movement Monitoring Algorithm for Indoor Tracking During Examinations • Monitoring will be conducted regularly, and the time and length of monitoring at various levels will be determined during the planning process. • The damage caused by the observed occurrences determines the scale and scope of monitoring (examinations)
[81] Cheating during	<ul style="list-style-type: none"> • Establishing solid administrative standards by academic institutions against misbehavior practices is one of the most effective strategies

examinations: prevalence, consequences, contributing factors, and prevention	<p>to avoid cheating during tests and student evaluations.</p> <ul style="list-style-type: none"> • Clear standards about intellectual good moral values and unethical actions can help better manage this problem. • Punishments are perfect strategies for controlling cheating.
[83] Anti-cheating online exams by minimizing the cheating gain	<ul style="list-style-type: none"> • Alg-Cyclic strategy, you can search for resources from the Cyclic Pool. • As a result, they introduce Alg-Cyclic (Algorithm 2), which greedily searches for better tasks from a constrained set of cyclical series constructed via left circular shifting and SCS. • A sequence from SCS is selected to be allocated to the student to minimize the student's cumulative gain
[84] We use technologies to prevent cheating in remote assessments during the COVID-19 pandemic	<ul style="list-style-type: none"> • To prohibit students from examining exam questions • Consequences of revealing exam questions to the public for all exams and quizzes • Requesting a second, third, or fourth attempt will result in a 25 percent, 50 percent, or 75 percent reduction in your grade for that exam or quiz.
[85] Individualized Excel-Based Exams to Prevent Students from Cheating	<ul style="list-style-type: none"> • Intended to discourage pupils from cheating • Evaluations are also used as tools to check on students' progress, planned learning outcomes, feedback, and monitoring tools for instructors to keep track of their classes. • Without good planning preparation, those exercises will motivate learners to engage in more cheating exercises
[86] sVeriTool: A Verification Tool for Preventing Impersonation of Students in Examination Halls Using Fingerprints	<ul style="list-style-type: none"> • Properly arrange and store knowledge on members, learners, programs, and so on, and it must also enable the program to communicate with this content using "Structured Query Language (SQL) queries. • The system employs a database schema, which holds details in charts composed of rows (representing records) and columns (representing fields or characteristics). • These tables have the following apparent attributes: user login and password; students name, registration number, email, phone number, and so on; "Courses course code, the course title, academic session, and so on."
[88] Exam cheating and academic integrity breaches during the COVID-19 pandemic	<ul style="list-style-type: none"> • When tests shifted online in many universities, it opened the door for students to take advantage of possibilities to violate academic integrity that were formerly unavailable to them • This triggered a long-running discussion about whether this breakthrough made cheating easier for pupils • The existing preventative strategies, particularly in the distance learning context, are ineffective in deterring academic dishonesty (online learning).
[68] Examining online college	<ul style="list-style-type: none"> • The most prevalent technique to find plagiarism is to utilize similarity index software

cyber cheating methods and prevention measures.	<ul style="list-style-type: none"> • In the similarity index, all instances of plagiarism are displayed • The approaches involved forcing learners to create printouts of the materials and writing assignments relevant to a classroom subject or book chapter rather than allowing students to choose their topic
-------------------------------------------------	---------------------------------------------------------------------------------------------------------------------------------------------------------------------------------------------------------------------------------------------------------------------------------------------------------------------------------------------

5. PROPOSED CLASSIFICATION MODEL

Figure 1 below presents the proposed classification model “Atiff’s classification of academic dishonesty (ACAD).” The proposed classification model is presented in a Top-Down approach as in Figure 1. Table 4 shows the nomenclature for the proposed classification model.

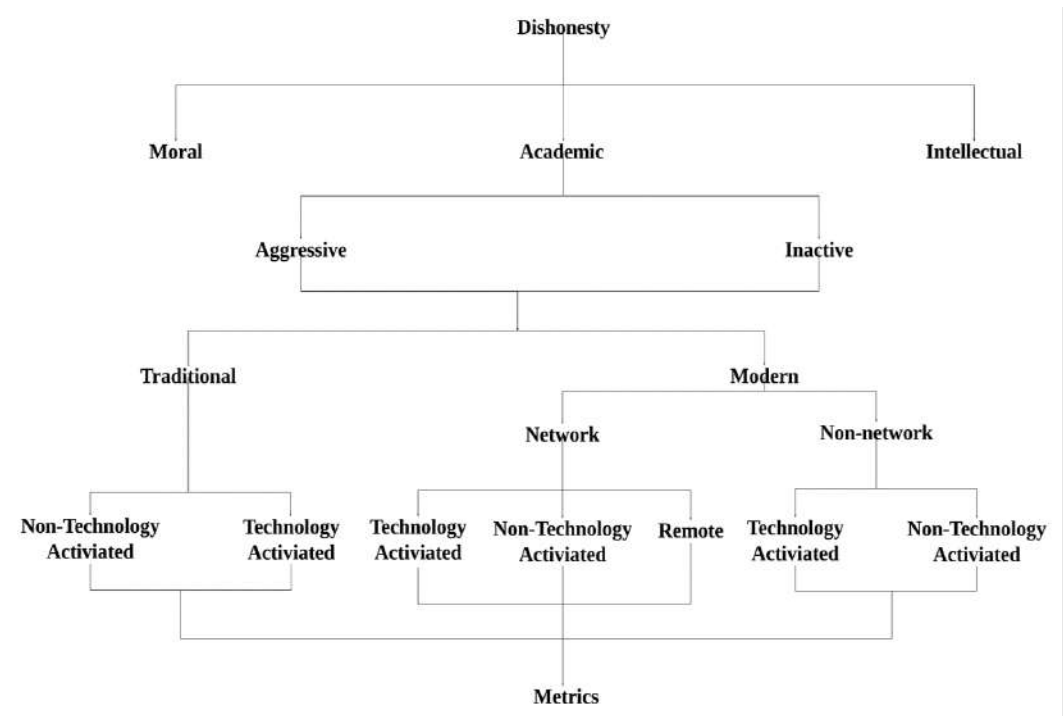


Figure 1: ACAD Classification of Academic dishonesty

Table 4: Nomenclature for classification model

No	Term	Contextual Meaning
1	Dishonesty	A fraudulent or deceitful act. It is used to describe a lack of probity, cheating, lying, or deliberately withholding information, or being deliberately deceptive, or a lack of integrity, deceitful, corruption or treacherousness. Dishonesty is the fundamental component of most offenses relating to the acquisition, conversion, and disposal of property (tangible or intangible) defined in criminal law, such as fraud.
2	Moral	Concerned with the principles of right and wrong behavior. Standards of behavior; principles of right and wrong. Concerned with or derived from the code of behavior that is considered right or acceptable in a particular society.
3	Academic	Things that relate to the work done in schools, colleges, and universities, especially work which involves studying and reasoning rather than practical or technical skills, associated with an academy or school, especially of higher learning
4	Intellectual	Relates to critical thinking, research, and reflection about the reality of society and solutions for the normative problems of society. possessing intellect and intelligence, especially when the intellectual's activities exerted positive consequences in the public sphere and so increased the intellectual understanding of the public, by means of moral responsibility, altruism, and solidarity, without resorting to the manipulations of demagoguery, paternalism, and incivility
5	Aggressive	Strong or emphatic in effect or intent. Growing, developing, or spreading rapidly behaving in a threatening way
6	Inactive	Activities such as wiretapping and idle scans are designed to intercept traffic traveling through the network without engaging in or involving any or much activity. Lacks the usual or anticipated action. Attempts to learn or make use of information from the system but does not affect system resources. This includes eavesdropping on or monitoring transmission. The goal is to obtain information that is being transmitted. Types may include the release of message content and traffic analysis
7	Traditional	A traditional IT framework involves purchasing, installing, and maintaining your IT devices on-site predominantly based on Deterrence, Defense, Balance of power, and Alliance building. Refer to perimeter network firewalls designed to protect corporate systems from malicious attacks by erecting security defenses that ward off threats from outside of the perimeters of the network.
8	Network	Network-based attacks are threats that are launched and controlled from a device or devices other than those under attack. An attack that uses one or more devices to overwhelm the target with so much network traffic or demands for services that the target cannot respond to legitimate requests.
9	Non-	Non-network-based attacks are threats that are NOT launched and

	Network	controlled from a device or devices other than those under attack. Attacks that DO NOT use one or more devices to overwhelm the target with so much network traffic or demands for services that the target cannot respond to legitimate requests. Direct attacks onto the device where the resources are residing and does not spread to other devices within the same network.
10	Technology Activated	That which is aided or enhanced or initiated by technology or technology-related mechanisms to either start, spread, or stay active.
11	Non-Technology Activated	That which is NOT aided or enhanced or initiated by technology or technology-related mechanisms to either start, spread, or stay active.
12	Remote	A malicious action that targets one or a network of computers and does not affect the computer or device the attacker is using; instead, the attacker will find vulnerable points in a computer or network's security software to access the machine or system.
13	Metrics	Units of measurement for prevalence, determinants, techniques, and ethical judgment

6. CONCLUSION

Academic dishonesty is and has been a threat to the integrity of the educational institutions and the entire system of education for as long as time can tell. The prevalence of this phenomenon is getting increasingly worse with the advent of modern technologies. As technology makes the dissemination of information and sharing of information accessible and more fluent, it also makes the avenues for carrying out dishonesty activities more complicated and easily accessible. This paper has analyzed academic dishonesty from the traditional and modern perspectives, where traditional methods were characterized by non-technology-based vectors and well described and boundary-based networks which span specified locations. Modern methods that are fueled by the use of network and networking technology to access distributed resources spanning several networks and those that cannot be defined by boundaries. The paper has proposed a classification model for academic dishonesty based on aggression, network type, and ad activation. This model will go a long way to classifying dishonesty.

REFERENCES

- [1] L. Fishbein, "Curbing cheating and restoring academic integrity.," *Chron. High. Educ.*, vol. 40, no. 15, pp. A52–A52, 1993.
- [2] V. J. Haines, G. M. Diekhoff, E. E. Labeff, and R. E. Clark, "College Cheating : Immaturity , Lack of Commitment , and the Neutralizing Attitude Author (s): Valerie J . Haines , George M . Diekhoff , Emily E . LaBeff and Robert E . Clark Published by : Springer Stable URL : <https://www.jstor.org/stable/40195757> CO," vol. 25, no. 4, pp.

- 342–354, 1986.
- [3] A. C. Singhal, “Factors in students’ dishonesty,” *Psychol. Rep.*, vol. 51, no. 3, pp. 775–780, 1982.
- [4] A. A. . Teixeira and M. de F. Rocha, “Academic cheating in Spain and Portugal: An empirical explanation,” *Int. J. Iber. Stud.*, vol. 21, no. 1, pp. 3–22, 2008.
- [5] E. Taderera, L. Nyikahadzoi, W. Matamande, and E. Mandimika, “Exploring management strategies to reduce cheating in written examinations: case study of Midlands State University,” *J. Case Stud. Educ.*, vol. 5, pp. 1–13, 2014.
- [6] A. Chirumamilla, G. Sindre, and A. Nguyen-duc, “Assessment & Evaluation in Higher Education Cheating in e-exams and paper exams: the perceptions of engineering students and teachers in Norway,” *Assess. Eval. High. Educ.*, vol. 0, no. 0, pp. 1–18, 2020.
- [7] A. Atiff, A. David, and T. Elisha, “A Zero-Trust Model-Based Framework For Managing Of Academic Dishonesty In Institutes Of Higher Learning,” vol. 12, no. 6, pp. 5381–5389, 2021.
- [8] M. Amzalag, N. Shapira, and N. Dolev, “Two Sides of the Coin: Lack of Academic Integrity in Exams During the Corona Pandemic, Students’ and Lecturers’ Perceptions,” *J. Acad. Ethics*, no. 0123456789, 2021.
- [9] S. A. Shariffuddin and R. J. Holmes, “Cheating in Examinations: A Study of Academic Dishonesty in a Malaysian College,” *Asian J. Univ. Educ.*, vol. 5, no. 2, pp. 99–124, 2009.
- [10] A. Musa and J. Ismail, “Academic Dishonesty: A Cause for Concern? Academic Dishonesty: A Cause for Concern?,” no. June, 2021.
- [11] T. Lord and D. Chiodo, “A look at student cheating in college science classes,” *J. Sci. Educ. Technol.*, vol. 4, no. 4, pp. 317–324, 1995.
- [12] E. Assoa, “A Study of Proctors’ Involvement in National Examination Cheating: the Case of ‘Collège Privé MBF d’Abobo’ Exam Center,” *J. Educ. e-Learning Res.*, vol. 5, no. 1, pp. 22–27, 2017.
- [13] H. S. Pincus and L. P. Schmelkin, “Faculty Perceptions of Academic Dishonesty,” *J. Higher Educ.*, vol. 74, no. 2, pp. 196–209, 2003.
- [14] D. Heriyati and W. F. Ekasari, “A Study on Academic Dishonesty and Moral Reasoning,” *Int. J. Educ.*, vol. 12, no. 2, pp. 56–62, 2020.
- [15] C. L. Jocoy, D. Dibiase, and C. Jocoy, “International Review of Research in Open and Distributed Learning Plagiarism by Adult Learners Online: A case study in detection and remediation detection and remediation Abstract Detecting and combating plagiarism from Web-based sources is a concern for,” 2021.
- [16] Z. Ercegovac and J. V. Richardson, “Academic Dishonesty, Plagiarism Included, in the Digital Age: A Literature Review,” *Coll. Res. Libr.*, vol. 65, no. 4, pp. 301–318, 2004.
- [17] W. J. Bowers, *Student dishonesty and its control in college*. Columbia University, 1966.
- [18] D. McCabe, K. Butterfield, and L. K. Treviño, “Cheating in college: Why students do it and what educators can do about it,” *Cheating Coll. Why Students do it what Educ. Can do About it*, pp. 1–225, Jan. 2012.
- [19] Á. Rocha, H. Adeli, L. P. Reis, S. Costanzo, and I. Orovic, *Trends and Innovations in Information Systems and Technologies*, vol. 3. 2020.
- [20] J. Clare, “How Prevalent is Contract Cheating and to What Extent are Students Repeat

- Offenders ? How Prevalent is Contract Cheating and to What Extent are Students Repeat Offenders ?,” no. June, 2017.
- [21] R. Mustapha, Z. Hussin, S. Siraj, and G. Darusalam, “Academic Dishonesty Among Higher Education Students: The Malaysian Evidence (2014 To 2016),” *J. KATHA*, vol. 13, no. 1, pp. 73–93, 2017.
- [22] K. A. Gillespie, “The frequency and perceptions of academic dishonesty among graduate students: a literature review and critical analysis [sic],” 2003.
- [23] K. A. Gillespie, “THE FREQUENCY AND PERCEPTIONS OF ACADEMIC DISHONESTY AMONG GRADUATE STUDENTS: A LITERATURE REVIEW AND CRITICAL ANALYSIS,” 2003.
- [24] D. Faucher and S. C. Rn, “Academic dishonesty : Innovative cheating techniques and the detection and prevention of them,” *Teach. Learn. Nurs.*, vol. 4, no. 2, pp. 37–41, 2020.
- [25] J. M. Dyer, “Academic dishonesty and testing: How student beliefs and test settings impact decisions to cheat,” *J. Natl. Coll. Test. Assoc. 2020*, vol. 4, no. 1, pp. 1–31, 2020.
- [26] S. Etgar, I. Blau, and Y. Eshet-Alkalai, “White-collar crime in academia: Trends in digital academic dishonesty over time and their effect on penalty severity,” *Comput. Educ.*, vol. 141, no. September 2018, p. 103621, 2019.
- [27] E. Bilen and A. Matros, “Munich Personal RePEc Archive Online Cheating Amid COVID-19 Online Cheating Amid COVID-19 *,” no. 103185, 2020.
- [28] L. L. Marshall, C. Girardeau, and A. W. Varnon, “Attack on Academic Dishonesty : What ‘ Lies ’ Ahead ?,” 2017.
- [29] R. Peytcheva-Forsyth, L. Aleksieva, and B. Yovkova, “The impact of technology on cheating and plagiarism in the assessment - The teachers’ and students’ perspectives,” *AIP Conf. Proc.*, vol. 2048, no. December, 2018.
- [30] R. F. Parks, P. B. Lowry, R. T. Wigand, N. Agarwal, and T. L. Williams, “Why students engage in cyber-cheating through a collective movement: A case of deviance and collusion,” *Comput. Educ.*, vol. 125, no. April, pp. 308–326, 2018.
- [31] Y. Abdelrahim, “HOW COVID-19 QUARANTINE INFLUENCED ONLINE EXAM CHEATING : A CASE OF BANGLADESH UNIVERSITY STUDENTS 新冠肺炎 检 疫如何影响在 线 考 试 作 弊 : 以孟加拉国大学学生 为 例,” *J. SOUTHWEST JIAOTONG Univ.*, 2021.
- [32] I. Bandara, F. Ioras, and K. Maher, “Cyber Security Concerns in E-Learning Education,” *Proc. ICERI2014 Conf.*, no. November, pp. 728–734, 2014.
- [33] N. Rahim, Z. Othman, and F. Z. Hamid, “Cyber security and the higher education literature: A bibliometric analysis,” *Int. J. Innov. Creat. Chang.*, vol. 12, no. 12, pp. 852–870, 2020.
- [34] L. Coleman and B. M. Purcell, “Data breaches in higher education,” *J. Bus. Cases Appl.*, vol. 15, no. 15, pp. 1–7, 2015.
- [35] International Center for Academic Integrity, “The fundamental values project: Clemson, SC: Clemson University Press.,” *Edition, Third*, 2015. [Online]. Available: www.academicintegrity.org.
- [36] I. Chirikov, E. Shmeleva, and P. Loyalka, “The role of faculty in reducing academic dishonesty among engineering students,” *Stud. High. Educ.*, vol. 45, no. 12, pp. 2464–2480, 2020.

- [37] L. Baran and P. K. Jonason, "Academic dishonesty among university students: The roles of the psychopathy, motivation, and self-efficacy," *PLoS One*, vol. 15, no. 8, p. e0238141, 2020.
- [38] K. M. Apampa, G. Wills, and D. Argles, "User Security Issues in Summative E-Assessment Security," *Int. J. Digit. Soc.*, vol. 1, no. 2, pp. 135–147, 2010.
- [39] F. Crime, "Lessons learned during Covid-19 concerning cheating in e-examinations by university students," *J. Financ. Crime*, 2021.
- [40] T. Lancaster and R. Clarke, "Rethinking Assessment By Examination in the Age of Contract Cheating," *Plagiarism Across Europe and Beyond 2017*, pp. 215–228, 2017.
- [41] M. R. Krou, C. J. Fong, and M. A. Hoff, "Achievement motivation and academic dishonesty: A meta-analytic investigation," *Educational Psychology Review*, vol. 33, no. 2. Springer, pp. 427–458, 2021.
- [42] L. PECULEA and A. PECULEA, "Ethical Perceptions of Engineering Students About Cheating and Plagiarism.," *J. Plus Educ. / Educ. Plus*, vol. 27, no. 2, pp. 30–49, 2020.
- [43] K. Trost, "Psst, have you ever cheated? a study of academic dishonesty in Sweden," *Assess. Eval. High. Educ.*, vol. 34, no. 4, pp. 367–376, 2009.
- [44] A. Pennycook, "Borrowing Others' Words: Text, Ownership, Memory, and Plagiarism," *TESOL Q.*, vol. 30, no. 2, p. 201, 1996.
- [45] S. H. M. S. Et.al, "An Ad Hoc Movement Monitoring Algorithm for Indoor Tracking During Examinations," *Turkish J. Comput. Math. Educ.*, vol. 12, no. 3, pp. 3840–3846, 2021.
- [46] Y. C. Cheng, F. C. Hung, and H. M. Hsu, "The relationship between academic dishonesty, ethical attitude and ethical climate: The evidence from Taiwan," *Sustain.*, vol. 13, no. 21, pp. 1–16, 2021.
- [47] D. E. Allmon, D. Page, and R. Rpberts, "Determinants of perceptions of cheating: Ethical orientation, personality and demographics," *J. Bus. Ethics*, vol. 23, no. 4, pp. 411–422, 2000.
- [48] R. Arnold, B. N. Martin, and L. Bigby, "Is There a Relationship Between Honor Codes and Academic Dishonesty?," *J. Coll. Character*, vol. 8, no. 2, 2007.
- [49] D. L. McCabe and L. K. Trevino, "Individual and contextual influences on academic dishonesty: A multicampus investigation," *Res. High. Educ.*, vol. 38, no. 3, pp. 379–396, 1997.
- [50] D. L. McCabe, L. K. Treviño, and K. D. Butterfield, "Cheating in academic institutions: A decade of research," *Ethics & Behavior*, vol. 11, no. 3, pp. 219–232, 2001.
- [51] D. L. McCabe and L. K. Trevino, "Academic dishonesty: Honor codes and other contextual influences," *J. Higher Educ.*, vol. 64, no. 5, pp. 522–538, 1993.
- [52] N. J. Auer and E. M. Krupar, "Mouse click plagiarism: The role of technology in plagiarism and the librarian's role in combating it," *Libr. Trends*, vol. 49, no. 3, pp. 415–432, 2001.
- [53] S. Endris, "Gene Conserve - Articles - Articles - - Articles - - Articles - Gene Conserve - Articles - Articles - Volume 7 - Issue 30 - October / December , 2008 .," *Production*, vol. 7, no. 27, pp. 2008–2010, 2008.
- [54] R. Ramos, J. Gonçalves, and S. P. Gonçalves, "The unbearable lightness of academic fraud: Portuguese higher education students' perceptions," *Educ. Sci.*, vol. 10, no. 12, pp. 1–16, 2020.

- [55] M. Witherspoon, N. Maldonado, and C. H. Lacey, "Academic Dishonesty of Undergraduates: Methods of Cheating," no. May, p. 210, 2010.
- [56] A. Szabo and J. Underwood, "Cybercheats: Is Information and Communication Technology Fuelling Academic Dishonesty?," *Act. Learn. High. Educ.*, vol. 5, no. 2, pp. 180–199, 2004.
- [57] D. McCabe, "Academic Dishonesty in Nursing Schools: An Empirical Investigation," *J. Nurs. Educ.*, vol. 48, pp. 614–623, Aug. 2009.
- [58] D. S. Gomez, "Putting the shame back in student cheating," *Educ. Dig.*, vol. 67, no. 4, p. 15, 2001.
- [59] P. J. Boehm, M. Justice, and S. Weeks, "Promoting academic integrity in higher education," *Community Coll. Enterp.*, vol. 15, no. 1, pp. 45–61, 2009.
- [60] C. Moran, "Cellphones, Handy Tools for Emergency Alerts, Could Be Used for Cheating during Tests.," *Chron. High. Educ.*, vol. 55, no. 7, 2008.
- [61] C. Q. Choi, "The pull of integrity," *ASEE Prism*, vol. 18, no. 7, p. 29, 2009.
- [62] R. I. Maitland, "Disturbing trends in education," *Am. Dent. Assoc. News*, vol. 38, no. 7, p. 4, 2007.
- [63] A. Richardson, "High-tech cheating: Where there's a will, there's a gadget," *Divers. Issues High. Educ.*, vol. 19, no. 11, p. 32, 2002.
- [64] J. D. Heyman *et al.*, "Pssst... what's the answer," *People*, vol. 63, no. 3, pp. 1–4, 2005.
- [65] A. Ullah, H. Xiao, M. Lilley, and T. Barker, "Using Challenge Questions for Student Authentication in Online Examination," vol. 5, no. 3, pp. 631–639, 2012.
- [66] T. Ramu and T. Arivoli, "A Framework of Secure Biometric Based Online Exam Authentication: an Alternative To Traditional Exam," *Int. J. Sci. Eng. Res.*, vol. 4, no. 11, pp. 52–60, 2013.
- [67] A. Fayyumi and A. Zarrad, "Novel Solution Based on Face Recognition to Address Identity Theft and Cheating in Online Examination Systems," no. April, 2014.
- [68] J. Moten, A. Fitterer, E. Brazier, J. Leonard, and A. Brown, "Examining online college cyber cheating methods and prevention measures," *Electron. J. e-Learning*, vol. 11, no. 2, pp. 139–146, 2013.
- [69] M. Badiger, J. B. Limited, K. G. Badiger, and D.- Bangalore, "PLAGIARISM : DETECTION AND," vol. 2, no. VII, pp. 297–305, 2017.
- [70] S. Aishwarya, S. Ramya, S. Subhiksha, and S. Samundeswari, "Detection of Impersonation in Online Examinations Using Blockchain," *ICPECTS 2020 - IEEE 2nd Int. Conf. Power, Energy, Control Transm. Syst. Proc.*, pp. 1–5, 2020.
- [71] B. Halak and M. El-Hajjar, "Design and evaluation of plagiarism prevention and detection techniques in engineering education," *High. Educ. Pedagog.*, vol. 4, no. 1, pp. 197–208, 2019.
- [72] R. Bawarith, B. Abdullah, F. Anas, and S. Gamalel-Din, "E-exam Cheating Detection System," *Int. J. Adv. Comput. Sci. Appl.*, vol. 8, no. 4, pp. 176–181, 2017.
- [73] W. AlHamdani, "Online Cheating: A Prevention Procedure," *Proc. 2018 Int. Conf. Found. Comput. Sci.*, no. March, pp. 21–25, 2020.
- [74] L. C. O. Tiong and H. J. Lee, "E-cheating Prevention Measures: Detection of Cheating at Online Examinations Using Deep Learning Approach -- A Case Study," vol. XX, no. Xx, pp. 1–9, 2021.
- [75] D. Pawelczak, "Benefits and drawbacks of source code plagiarism detection in

- engineering education,” *IEEE Glob. Eng. Educ. Conf. EDUCON*, vol. 2018-April, no. UniBw M, pp. 1048–1056, 2018.
- [76] A. Syahid, “EFL teachers’ use of plagiarism detection software: A usability study,” *Int. (International Conf. English Lang. Teaching)*, vol. 4432, no. November, pp. 14–16, 2019.
- [77] R. Ryu, “Continuous multibiometric authentication for online exam with machine learning,” pp. 1–7, 2020.
- [78] D. Von Grünigen, B. Pradarelli, and M. Cieliebak, “Best Practices in E-Assessments with a Special Focus on Cheating Prevention,” *2018 IEEE Glob. Eng. Educ. Conf.*, pp. 899–905, 2018.
- [79] P. Tanya, “Prevention of Cheating when Using Quizzes in Moodle,” *Proc. 14th Int. Conf. Virtual Learn.*, no. October, 2019.
- [80] S. Sibghatullah H M, N. Elisha Tadiwa, A. Atiff Abdalla Mahmoud, B. Abudhahir, and H. Fares Anwar Salem, “An Ad Hoc Movement Monitoring Algorithm for Indoor Tracking During Examinations,” *Turkish J. Comput. Math. Educ.*, vol. 12, no. 3, pp. 3840–3846, 2021.
- [81] Z. Iqbal *et al.*, “Cheating during examinations: Prevalence, consequences, contributing factors and prevention,” *Int. J. Innov. Creat. Chang.*, vol. 15, no. 6, pp. 601–609, 2021.
- [82] C. A. Simon, J. R. Carr, S. M. McCullough, S. J. Morgan, T. Oleson, and M. Ressel, “The other side of Academic Dishonesty: The relationship between faculty scepticism, gender and strategies for managing student academic dishonesty cases,” *Assess. Eval. High. Educ.*, vol. 28, no. 2, pp. 193–207, 2003.
- [83] M. Li, S. Sikdar, L. Xia, and G. Wang, “Anti-cheating Online Exams by Minimizing the Cheating Gain,” *preprint*, no. May, pp. 1–14, 2020.
- [84] L. Jihyun, K. R. Jinyoung, S.-Y. Park, and M. A. Henning, “Using technologies to prevent cheating in remote assessments during the COVID-19 pandemic,” *J. Dent. Educ.*, vol. 85, no. S1, pp. 1015–1017, 2021.
- [85] A. W. Suryani, “Individualized Excel-Based Exams to Prevent Students from Cheating,” *Jabe (Journal Account. Bus. Educ.)*, vol. 5, no. 1, p. 14, 2020.
- [86] U. S. Haruna, “sVeriTool: A Verification Tool for Preventing Impersonation of Students in Examination Halls using Fingerprints,” *sVeriTool African J. Comput. ICT Ref. Format U. S. Haruna*, vol. 11, no. 2, pp. 37–52, 2018.
- [87] A. Fayyumi and A. Zarrad, “Novel solution based on face recognition to address identity theft and cheating in online examination systems,” *Adv. Internet Things*, vol. 2014, 2014.
- [88] R. Comas-Forgas, T. Lancaster, A. Calvo-Sastre, and J. Sureda-Negre, “Exam cheating and academic integrity breaches during the COVID-19 pandemic: An analysis of internet search activity in Spain,” *Heliyon*, vol. 7, no. 10, 2021.

ANTIMICROBIAL ACTIVITY OF GUM ARABIC (*Acacia senegal* & *Acacia seyal*) AGAINST PYOGENIC BACTERIA_PROBIOTIC PROVEN

Noura Karam M. Salih, Fazlen S. M. Khan, Ahmed A. Bagi
Infrastructure University Kuala Lumpur

1. INTRODUCTION

For centuries, plants have been a profitable wellspring and still a considerable lot of the present medications and drugs are based on plants (Kingston, 2011). Around 60 to 90% of nation in the developing countries utilize plant-based medicine (Alviano & Alviano, 2009; Malini et al., 2013). Gum Arabic is one of the medicinal plants which belong in the family of Leguminosae and is a branched heteropolysaccharide. The dried sap of Gum Arabic is in light orange or white in color. It is mainly distributed in Sudan, Chad, Nigeria, Senegal, and Ethiopia. Gum Arabic is a dried sap from *Acacia senegal* and *Acacia seyal* which has commercial potential as a worldwide item by and large gathered in Africa and Western Asia. 70% of the world Gum Arabic is created in Sudan (Bnuyan, 2015).

Gum Arabic is also considered as generally recognized as safe (GRAS) status that leads to its celebrity in the food industry (Patel & Goyal, 2015). Edible gums are tears or flakes of dried sap (exudates) of many (mostly thorny) trees and shrubs either after natural or manmade injuries to wooden stem and branches. They are ionic, natural, complex polymers of glycopeptides containing several other compounds and mineral salts. Many of the gums are edible specifically those obtained from trees/ shrubs of *Fabaceae* family including *Acacia*, *Sterculia*, *Astragalus*, *Balanites*, *Buchnania* and *Anogeissus* species.

Infectious diseases are a vital medical issue and are one of the causes of mortality around the world because of the excessive utilization of antibiotics and occurrence of numerous antibiotic resistances among human pathogens (Bnuyan, 2015). Thus, it is important to find an alternative which is better particularly in developing countries (Cowan, 1999; Perveen et al., 2012). A wide assortment of plant/natural items has been utilized as a part of the treatment of various diseases. In conventional medication, assorted uncontrollable ailments have been treated with homegrown items (Mehrotra et al., 2010).

Infections which occur in soft tissue will lead to the creation of discharge or pus is known as pyogenic infection. Infection happens when the pyogenic bacteria escape from the body defense and multiplies into a massive amount of numbers and thus fight against the host tissues (Fatema et al., 2016). Pyogenic bacteria will mostly invade the tonsils, periapical dental, impetigo on the face and pimples where *S. aureus* is often appearing in these cases (Brook, 2007).

Microorganisms are the hidden adversaries to the humankind and cause an extremely significant harm in the human body and other living life forms. Antimicrobial agents have the

ability to eliminate bacteria or to arrest the multiplication (Sharma et al., 2015). The aimless utilization of antimicrobial has prompted the rise of antimicrobial resistance. Resistant microorganism affects public health and causes failures in the treatment and builds medicinal services costs as more current and more costly drugs are expected to treat diseases (Srinu et al., 2012). Thus the main purpose of this study is to determine the antimicrobial activity of Gum Arabic (*A. senegal* and *A. seyal*) against some pyogenic bacteria.

The objectives of this study are to isolate and identify pyogenic bacteria from abscesses and sputum, to investigate the antibacterial activity of Gum Arabic (*A. senegal* and *A. seyal*) in aqueous and ethanol extraction and to compare the antibacterial activity of Gum Arabic (*A. senegal* and *A. seyal*) in aqueous and ethanol extraction.

Gum Arabic (*A. senegal* and *A. seyal*)

The Gum Arabic (characteristic gum; Gum acacia) is identified with two sub-Saharan types of the acacia tree, *A. senegal* and *A. seyal*. *Acacia senegal* or Arabic gum tree is a notable therapeutic plant in Arabian Peninsula and in districts of Africa, specifically in Sudan (Al Alawi et al., 2018). Gum Arabic is a natural exudate which is polysaccharide (Maslin, 2003). This plants are utilized as culinary and therapeutics for ages (Singh et al., 2015). It also contains numerous secondary compounds for examples, flavone, catechin, polyphenols, tannins, chalcones, alkaloids and flavonoids (Marwah et al., 2006). Gum Arabic consists of highly branched chain either partial acidity or neutral and have calcium, magnesium and potassium (Ali et al., 2008; Hadi et al., 2010). Gum Arabic also consists of hydroxyproline, aspartic acid, serin and proline, (Ali et al., 2008). Gum from *A. senegal* is also known as "hashab gum" whereas gum from *A. seyal* is known as "talha gum". In Zimbabwe, the gum exchanged locally as gum Arabic originates from *Acacia karoo* (Dauqan & Abdullah, 2013).

Morphology of *A. senegal* and *A. seyal*

The shade of leaves of *A. senegal* is dim green and has flower in cream color and also greenish colored seed (Duke, 2012). *Acacia seyal* trees are up to 17 m tall in Sudan. It has a particular smooth fine bark, from white to greenish yellow or orange red, with a green layer underneath. In some populace, barks with red and yellow can be found (Awad et al., 2017). Gum Arabic from *A. senegal* is a pale to darker orange shaded and in glass structure. Gum from *A. seyal* (gum talha) is more friable than the hard tears created by *A. senegal* and is once in a while found as entire bumps (Coppen, 1995).

Distribution of *A. senegal* and *A. seyal*

Acacia senegal is the best quality of Gum Arabic. It is the mainly found in Sudan. It is a small sized prickly tree, with irregular stem and excessively branched. In leaf, in the same way as other different Acacias, it has a thick, spreading crown. A tree common of Sahel atmospheres, *A. senegal* is across the board in the dry districts of tropical Africa, from Senegal and Mauritania, Eritrea, Ethiopia and South Africa. It is additionally found in Oman, Pakistan, India and has likewise been presented in Egypt, Australia, Puerto Rico and the Virgin Islands (Eisa et al.,

2008). A tree normal of semi-dry African locales, the *A. seyal* assortment is the most across the board extending all through the Sahel from Senegal, through Sudan, Egypt, Ethiopia, East Africa and Tanzania (Eisa et al., 2008; Mohamed & Röhle, 2011).

Uses of *A. senegal* and *A. seyal*

Dried saps of Gum Arabic are utilized in a mind-boggling number of utilizations. Gum Arabic is as a rule broadly utilized for industrial purposes, for example, a stabilizer, a thickener, an emulsifier, textiles, ceramics and pharmaceutical industry. In the food business, Gum Arabic is basically utilized in sweet shop, pastry kitchen, dairy, beverages and as a microencapsulation (Montenegro et al., 2012).

Active compound of *A. senegal* and *A. seyal*

The pharmacological and therapeutic properties of plants are due to secondary metabolites (Heinrich et al., 2012). Certain plants do have these properties (Kayani et al., 2015). Active compound of the plant will protect itself from the harm and diminishes the growth of other plant in terms of competition and takes up the unfavourable radiation of ultraviolet (Ahmed et al., 2015). Abdllha et al., 2016 have stated that there are presence of alkaloids, flavonoids, steroids and terpenoids in stem extract of *A. seyal* in ethanol that leads to the antimicrobial property of the plant.

Pharmacological property of *A. senegal* and *A. seyal*

Antimicrobial property

In a study by Okoro et al., (2012), the stem bark of *A. senegal* in ethanol and methanol were able to inhibit the *Klebsiella pneumoniae*, *Pseudomonas aeruginosa*, *Proteus vulgaris*, *Salmonella typhi*, *Shigella dysenteriae* and *Escherichia coli* except on *Staphylococcus aureus*, *Streptococcus pneumoniae* and *Streptococcus pyogenes*. The antimicrobial activity of Gum Arabic was reported effectively as other antimicrobial herbals treatment (garlic concentrate or cinnamon) to frame an antimicrobial covering on nourishments (Rakshit & Ramalingam, 2013). Abdllha et al., 2016, have conducted research on the stem extract of *A. seyal* in ethanol and found out that the extracts were able to prevent the growth of *Staphylococcus aureus* and *Candida albicans*.

Enhances renal function

The utilization of Gum Arabic through drinking water (15%, w/v) lessens the plasma urea and creatinine in adenine-induced chronic renal failure (CRF) in rats. It likewise diminished the creatinine clearance. Further, the treatment with Gum Arabic altogether enhanced all unfavourable impact that prompted by adenine (Ali et al., 2003).

Antidiabetic

In India, Gum Arabic is one of the native medicines, and it has numerous medicinal employments. In Tunisia, the utilization of Gum Arabic as hypoglycemic therapeutic plants to

treat diabetic patients was found to achieve over 70% contrasted with other restorative plants (Othman et al., 2013). A clinical preliminary utilized 40 members with a day by day supplement of powdered Gum Arabic (10 g/day) for about four months in solid people, prediabetes patients, type 2 diabetic mellitus patients, and diabetic nephropathy patients. The outcomes demonstrated that supplementation of Gum Arabic essentially diminished fasting blood glucose levels and glycosylated haemoglobin together with critical decrease of blood uric acid and total concentration of protein (Nasir et al., 2010).

Enhanced lipid metabolism

Gum Arabic is considered as a dietary supplement that diminishes the body fat. Ingestion of Gum Arabic will lead to diminishment of body mass index (BMI) and among the adult female human, Gum Arabic is able to reduce the percentage of body fat (Babiker et al., 2012). Administration of Gum Arabic diminished cholesterol, triglyceride, and low density lipoprotein (LDL) focuses in human (Mohamed et al., 2015) and mice (Ahmed et al., 2015). In concurrence with these discoveries, Gum Arabic supplementation diminished plasma, low density lipoprotein and total cholesterol concentration, though expanded HDL.

Pyogenic infection

Pyogenic infection is termed as infection that occurs in soft part of tissue which then leads to the generation of pus (Fatema et al., 2016). There are different routes by which pyogenic disease may cause by various sorts of microorganisms. Pyogenic or pus discharge is portrayed by extreme nearby irritation which happens after the injuring tissue gets infected by pyogenic bacteria (Rijal et al., 2017). The most well-known pyogenic bacteria are *Staphylococcus aureus*, *Streptococcus pyogenes*, *Escherichia coli*, *Proteus sp.* and *Pseudomonas aeruginosa*. Other Gram positive bacteria, that also leads to pyogenic infection is *Streptococcus pyogenes*. It also causes mild superficial skin infection and mainly starts from throat or even skin (Ryan & Ray, 2003).

Staphylococcus aureus

The most imperative injury pathogen is thought to be *Staphylococcus aureus*. It is Gram positive cocci, non-motile, non-capsular, and non-sporulation. *Staphylococcus aureus* causes strong, discharge of pus poisons in human. It can deliver skin sicknesses like shallow skin sores, for example, boils, carbuncles, furunculosis and wound infection. *S. aureus* is main source gastroenteritis due to the utilization of infected food. Sir Alexander Ogston in 1880 have come out that *Staphylococci* is the one that frequently appeared on skin surface (Murugesan et al., 2017). *Staphylococcus aureus* is known to be positive to catalase test and methyl red test and gives negative result to indole test and oxidase test (Holt et al., 1994).

Staphylococcus epidermidis

Staphylococcus epidermidis is a coagulase-negative *Staphylococcus* that is present in both mucosa and skin people (Otto, 2008). The skin, as a physical obstruction and interface with the

outside condition, is physiologically colonized by a large number of assorted microorganisms (Grice & Segre, 2011). In complexity, *S. epidermidis* was present among healthy people (Widerström et al., 2011). In like manner, *S. epidermidis* keeps up a generally kind association with its host and dodges colonization from different people, some of the time possibly more dangerous (Otto, 2009). *Staphylococcus epidermidis* is gram positive coccus which gives positive to catalase test and methyl red test and negative result to oxidase test and indole test (Johansson, 2014).

Staphylococcus sciuri

Coagulase-negative staphylococci (CoNS) are methodically recognized from *S. aureus* by the absence of coagulase. CoNS contain a large number of animal varieties, a considerable lot of which are shrewd pathogens (Otto, 2004). *Staphylococcus sciuri* is which is present in human clinical materials, food as well as from the environment (Švec et al., 2016). *Staphylococcus sciuri* gram positive cocci and gives positive result to catalase and oxidase and give negative to methyl red test and indole (Kloos et al., 1997). *Staphylococcus sciuri* has a specific pathogenic potential and can lead to infection towards, animals (Frey et al., 2013; dos Santos et al., 2016) and people (Stepanovic et al., 2003). In a study by Stepanovic et al., (2001), the virulence property of *Staphylococcus sciuri* shows a wide range and some of it are alike to the pathogenic nature of the *Staphylococci*. Indeed, Stepanovic et al., (2001) have also stated that *Staphylococcus sciuri* is indistinct whether it has the virulence features or it is regular highlights of the bacterium.

Skin abscess

Abscess is a skin disease that is expanding with the rise of methicillin-resistant *Staphylococcus aureus* (MRSA). Apart from that, *S. aureus* also leads to pneumonia, toxic shock syndrome, skin disease and enteritis. Abscess comes about because of the aggregation of discharge or pus in the dermis or tissue (Singer & Talan, 2014). The symptoms of abscess are the skin will be appeared as swollen, red, skin becomes tendered, fluctuant mass, regularly with encompassing cellulitis. Kobayashi et al., 2015, have studied on the pathogenic nature *Staphylococcus aureus* in abscess. It is stated that, *Staphylococcus aureus* has the ability to secrete molecules that has the capability to cause abscess. When *Staphylococcus aureus* in contact with the skin, the keratinocytes of the skin will send signal to proinflammatory responses with the help of its recognition receptor (Krishna & Miller 2012). Thus, neutrophil will acts as defence system to combat *Staphylococcus aureus* and causes abscess or formation of pus. Pus contains dead cells, fibrin and bacteria (Kobayashi et al., 2015)

Respiratory tract infection

According to Anjum et al., (2013), the pyogenic bacteria that leads to respiratory tract infection are *Klebsiella pneumoniae*, *Pseudomonas Aeruginosa*, *Escherichia Coli*, *Staphylococcus Aureus* and Coagulase negative staphylococci where sputum samples were used. Respiratory infections includes common cold, fever and occasional cough (Heinrich et al., 2012). These pyogenic organisms are often causes fever, cough, body pains and ordinary cold indications. Treatments

given for common cold are Echinacea, vitamin C, zinc, humidified air and increased fluid consumption (Simasek & Blandino, 2007). Apart from that, acetaminophen and ibuprofen will be given to patient with common cold which is accompanied with body pain and cough syrup; expectorant will be given to patients with cough (Holzinger et al., 2001).

Treatment

Antibiotic treatment will be performed under a few conditions such as when the disease gets worse or have a fast progression due to cellulitis, presence of systemic illness, over aged, presence of abscess in completed areas such as face and hands. Antibiotics that will be prescribed for outpatient with soft skin tissue infection are clindamycin, trimethoprim-sulfamethoxazole (TMP-SMX), tetracycline (doxycycline or minocycline) and linezolid (Singer & Talan, 2014). Hence, Gum Arabic is also utilized as medicine in curing skin infections such as wounds, burns, dry fingers and lips (Upadhyay, 2017).

2. MATERIALS AND METHODOLOGY

Nutrient agar, glucose phosphate broth, bacteriological peptone, oxidase strip, 3% hydrogen peroxide, indole reagent, methyl red reagent, absolute ethanol, crystal violet, safranin, Gram's iodine, oxidase strip test, nutrient broth, antibiotic discs dried sap of *Acacia Senegal* and dried sap of *Acacia seyal*.

Methodology

Sample collection

Ten samples of sputum and pus from abscesses and any pyogenic infections were collected among publics. The samples were kept in sterilized falcon tubes and kept in an ice box containing ice and were brought to the lab for isolation. The identities of publics are remained anonymous but the age, gender and condition of the publics were noted. Samples were inoculated on nutrient agar plates and incubated for 24 hours at 37 °C. Subculture was performed on nutrient agar every 24 hours at 37 °C (Singh et al., 2017).

Identification pyogenic bacteria

Gram staining

Unknown bacteria smear was performed on slide. Heat fixation was performed. Crystal violet was added and kept for 2 to 3 minutes. The slide was washed with tap water. Gram's iodine was added and kept for 1 minute. The slide was washed with tap water. 70% ethanol was added on the slide and kept for 5-15 seconds. The slide was then washed with tap water. Safranin was added and kept for 40 seconds. The slide was then washed with tap water and analyzed under oil immersion lens of the microscopic at 100x. Red is Gram negative whereas, purple is Gram positive.

Catalase test

The inoculation loop was sterilized under flame and let cool. A few drops of hydrogen peroxide were added on the centre of clean microscopic slide. A small portion of the pure colony was taken using the loop and placed on the hydrogen peroxide solution. Formation of bubbles was observed. The bacteria that have catalase enzyme will gives bubbles that shows positive result and negative if no bubbles (Vasanthakumari, 2009).

Oxidase test

Oxidase strip test was used. The inoculation loop was sterilized under flame and let cool. Pure colony was taken and smeared on the strip. Positive if purple color present within 5-10 seconds and negative if there is no color change. Positive result is due the presence of cytochrome oxidase (Vasanthakumari, 2009).

Methyl red test

Unknown bacteria was inoculated in glucose phosphate broth and incubated at 37 °C for 24-48 hours. After 24-48 hours, a few drops of methyl red were added. Positive if red colored solution formed which is due to the ability of the bacteria to ferment the glucose and negative if yellow colored solution formed (Nagoba, 2008; Vasanthakumari, 2009)

Indole

Unknown bacteria was inoculated in bacteriological peptone and incubated at 37 °C for 24-48 hours. After 24-48 hours, a few drops of indole reagent were added. The occurrence of pink ring formed on the surface indicates positive which is due to the degradation of the tryptophan into indole and negative if a yellow ring formed (Nagoba, 2008; Vasanthakumari, 2009).

Preparation of plant sap extracts

Dried sap of *Acacia senegal* and *Acacia seyal* were purchased from local store. *Acacia senegal* will have glossy surface while *Acacia seyal* have wrinkled surface. Dried sap of both of the plants were crushed separately near to the flame using sterilized pestle and mortar into smaller pieces and kept in sterilized plastic bags.

Aqueous extract

4 g, 6 g, 8 g and 10 g of *Acacia senegal* were added separately into sterilized falcon tubes containing 10 mL sterilized distilled water and mixed. The concentrations were kept in an incubator shaker at room temperature for 24 hours at 150 rpm. After 24 hours, the extracts kept in the cabinet at room temperature. These methods were repeated for dried sap of *Acacia seyal*.

Ethanol Extract

4 g, 6 g, 8 g and 10 g of *Acacia senegal* were added separately into sterilized falcon tubes containing 10 mL of absolute ethanol and mixed. The concentrations were kept in an incubator shaker at room temperature for 24 hours at 150 rpm. After 24 hours, the extracts kept in the cabinet at room temperature. These methods were repeated for dried sap of *Acacia seyal*.

Antimicrobial activity of plant extracts

Disk diffusion assay

Filter papers by Double rings filter papers No.202 were punched into 6 mm diameter using paper puncher and were autoclaved. The presumptive identification bacteria were grown in 10 mL of nutrient broth at 37 °C for 24 hours. 200 µl were pipetted from the bacteria culture and dispersed onto the nutrient agar. The hockey stick was flamed and used to spread the bacterial lawn. The plates were let to dry. The sterilized filter paper discs were aseptically taken using sterilized forceps and dipped into the respective concentration of the of *Acacia senegal* extracts. The impregnated paper discs were allowed to semi dry. Again by using sterilized forceps, the filter paper discs were placed onto the bacterial lawn. Negative control which was the sterilized distilled water and absolute ethanol was used and standard antibiotic disc chloramphenicol (30 µg) as positive control was used. The whole steps were repeated for *Acacia seyal*. This experiment was repeated in triplicates. The average of the zone of inhibition was calculated.

3. RESULTS AND DISCUSSION

Results

Bacterial Samples isolates

Samples of pus and sputum were obtained from 10 publics. Based on table 4.1, the age of publics ranged from 10 years old to 50 years old. There were seven sputum and three pus samples. The samples were obtained by swabbing with sterilized cotton buds for pus samples then were kept in sterilized falcon tubes. The sputum samples were collected by spitting in sterilized bijou bottles. The samples were then placed in an icebox containing ice. There were seven sputum and three pus samples. The condition of the publics were with occasional cough, cold and facial pimple and abscesses.

Table 4.1 Demographic of public

Name	Gender	Age	Sample type	Condition
S1	Female	23	Sputum	Occasional cough
S2	Male	19	Sputum	Cold
S3	Female	50	Sputum	Cold
S4	Female	14	Sputum	Cold
S5	Female	28	Pus	Abscess
S6	Male	14	Sputum	Cold
S7	Male	10	Pus	Facial pimple
S8	Female	42	Sputum	Occasional cough
S9	Male	14	Sputum	Cold
S10	Male	19	Pus	Abscess

Table 4.2 biochemical tests for 11 bacterial isolates

Sample name	Gram stain	Shape	Catalase test	Oxidase test	Indole Test	Methyl red test	Identified bacteria*
S1	+	Cocci	+	+	-	+	<i>Staphylococcus sciuri</i>
S2	+	Cocci	+	+	-	+	<i>Staphylococcus sciuri</i>
S3A1	+	Cocci	+	-	-	+	<i>Staphylococcus aureus</i>
S3A2	+	Cocci	+	+	-	+	<i>Staphylococcus sciuri</i>
S4	+	Cocci	+	-	-	-	<i>Staphylococcus epidermidis</i>
S5	+	Cocci	+	+	-	+	<i>Staphylococcus sciuri</i>
S6	+	Cocci	+	-	-	+	<i>Staphylococcus aureus</i>
S7	+	Cocci	+	-	-	+	<i>Staphylococcus aureus</i>
S8	+	Cocci	+	-	-	+	<i>Staphylococcus aureus</i>
S9	+	Cocci	+	+	-	+	<i>Staphylococcus sciuri</i>
S10	+	Cocci	+	-	-	+	<i>Staphylococcus aureus</i>

Legends

+: positive

-: negative

*presumptive identification

Howard, (1994) states that *Staphylococcus aureus* formed yellow pigmented colonies in nutrient agar medium. Mahon et al., (2014) *Staphylococci* is catalase positive and in Gram positive cocci and present in human such as from skin and mucous. *Staphylococcus epidermidis* forms colonies of white to gray. The bacteria that gives positive result toward catalase and methyl red test and negative result towards oxidase and indole is *Staphylococcus aureus* Kloos et al., (1997) states that *Staphylococcus sciuri* will give positive result towards catalase and oxidase. *Staphylococcus epidermidis* present in mouth and skin as stated by Zhou & Li (2015). There is little information available regarding to the pathogenicity of *Staphylococcus sciuri* among animals (Chen et al., 2007). However, *Staphylococci* are commonly responsible for pus causing infections (Mahon et al., 2014).

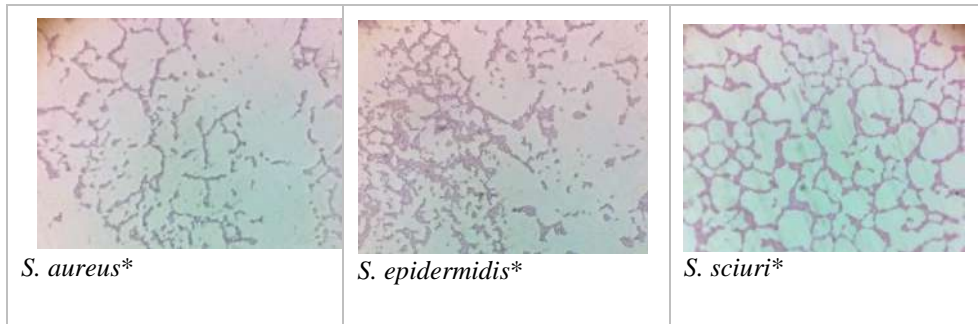


Figure 4.1 Gram stain of the three presumptive bacteria



Figure 4.2 Presumptive *S. aureus* growth in nutrient agar plate

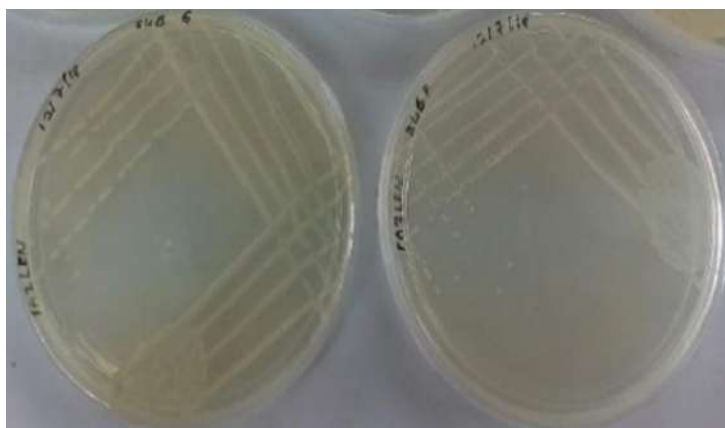


Figure 4.3 presumptive bacterial plate of *Staphylococcus sciuri* (Left) and *Staphylococcus epidermidis* (Right)

Table 4.3 Frequency and percentage of occurrence of three presumptive identified bacteria

Bacteria isolates	Frequency	Percentage (%)
<i>Staphylococcus aureus</i> *	5	45
<i>Staphylococcus sciuri</i> *	5	45
<i>Staphylococcus epidermidis</i> *	1	10

Ten samples were cultured and subculture in freshly prepared nutrient agar plates. Then, there were eleven isolates. All the eleven isolates were then subjected to Gram staining, colony morphology and biochemical tests. Biochemical tests comprises of oxidase test, catalase test, Indole test and Methyl Red test. Table 4.2 shows the result of the presumptive identification of the eleven isolates. The identification was made based on Holt et al., 1994. Oxidase positive bacteria were identified based on (Kloos et al., 1997; Webster et al., 1994). Figure 4.1 shows the three presumptive identified bacteria were Gram positive which were in purple color and in cocci shapes. These reveals all the isolates were *Staphylococcus spp.* Figure 4.2 shows colony of yellow pigment which resembles *Staphylococcus aureus*. Figure 4.3 shows the *Staphylococcus sciuri** and *Staphylococcus epidermidis** based on biochemical tests made on Table 4.2. Based on table 4.3, there are 5 (45%) which identified as *Staphylococcus aureus** and 5 (45%) as *Staphylococcus sciuri**. There is only one (10%) isolates which is *Staphylococcus epidermidis** (Table 4.5).

Disc diffusion assay

Disc diffusion assay was conducted to determine whether dried sap of *Acacia senegal* and *Acacia seyal* in aqueous and ethanol extraction in varying concentration can inhibit the growth of the *Staphylococcus aureus** and *Staphylococcus sciuri**. *Staphylococcus epidermidis** could not be proceeded in this test because it was died during storage. Based on table 4.4, aqueous extracts of *Acacia senegal* in 4 g, 6 g, 8 g and 10 g in sterile distilled water were not able to inhibit the growth of *Staphylococcus aureus** and *Staphylococcus sciuri**. This results also same

to *Acacia seyal* in aqueous extracts. Thus, there was no zone of inhibition for aqueous extraction of the both plants. In comparison with positive control, chloramphenicol (30 µg) was able to inhibit the growth of *Staphylococcus aureus* and *Staphylococcus sciuri* by producing a clear zone. In ethanol extraction of *Acacia senegal* and *Acacia seyal* in 4 g, 6 g, 8 g and 10 g in the solvent were not able to produce zone of inhibition for *Staphylococcus sciuri**. For *Staphylococcus aureus**, there is presence of zone of inhibition in 8 g and 10 g of *Acacia seyal* in ethanol extraction which were 4 mm and 6 mm. 8 g of *Acacia senegal* in ethanol extraction also shows zone of inhibition which was 5 mm. However, positive control, chloramphenicol (30 µg) shows the largest zone of inhibition compared to the extracts.

Table 4. 4 Average of zone of inhibition in aqueous and ethanol extractions.

Extracts	Conc. (g in 10 mL)	Zone of Inhibition (mm)			
		<i>Staphylococcus aureus</i> *		<i>Staphylococcus sciuri</i> *	
Aqueous		<i>A. senegal</i>	<i>A. seyal</i>	<i>A. senegal</i>	<i>A. seyal</i>
	4	Absent	Absent	Absent	Absent
	6	Absent	Absent	Absent	Absent
	8	Absent	Absent	Absent	Absent
	10	Absent	Absent	Absent	Absent
	Sterile distilled water	Absent	Absent	Absent	Absent
	Chloramphenicol (30µg)	24	23	24	24
Ethanol	4	Absent	Absent	Absent	Absent
	6	Absent	Absent	Absent	Absent
	8	5	4	Absent	Absent
	10	Absent	6	Absent	Absent

Disc diffusion assay in aqueous extraction

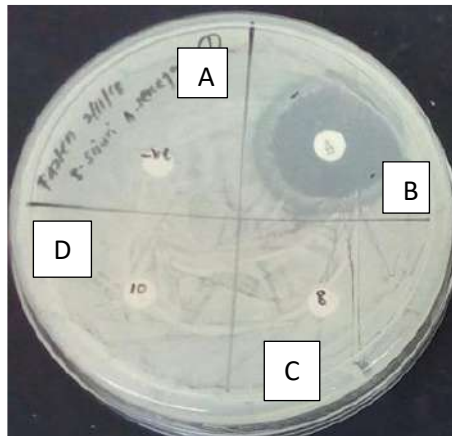


Figure 4.4 Susceptibility test of *S. aureus** against *Acacia senegal*

Legends: A: negative control (sterile distilled water), B: positive control (chloramphenicol), C: 8 g of *Acacia senegal* in 10 mL of sterile distilled water, D: 10 g of *Acacia senegal* in 10 mL of sterile distilled water



Figure 4.5 Susceptibility test of *S. aureus** against *Acacia seyal*



Figure 4.6 Susceptibility test of *S. sciuri** against *Acacia Senegal*



Figure 4.7 Susceptibility test of *S. sciuri** against *Acacia seyal*

Disc diffusion assay in ethanol extraction

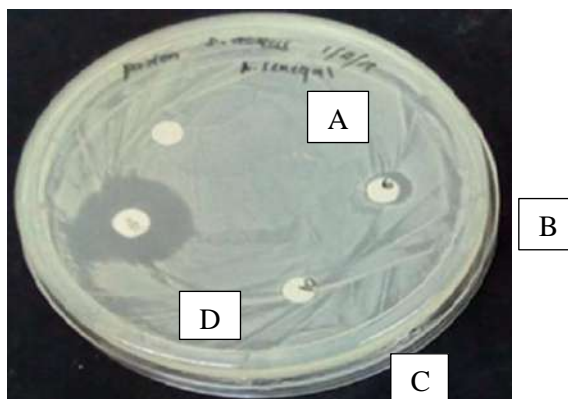


Figure 4.8 Susceptibility test of *S. aureus** against *Acacia Senegal*

Legends: A: negative control (absolute ethanol), B: positive control (chloramphenicol), C: 8 g of *Acacia senegal* in 10 mL of absolute ethanol, D: 10 g of *Acacia senegal* in 10 mL of absolute ethanol.



Figure 4.9 Susceptibility test of *S. aureus** against *Acacia seyal*



Figure 5.1 Susceptibility test of *S. sciuri** against *Acacia Senegal*



Figure 5.2 Susceptibility test of *S. sciuri** against *Acacia seyal*

4. DISCUSSION

Based on the study in this chapter, *Staphylococcus aureus*, *Staphylococcus sciuri*, *Staphylococcus epidermidis* were isolated from pyogenic infection. *Staphylococci* are present in all of the pus and sputum samples. In fact, Gram positive bacteria are well known causative agents in pyogenic infection as stated in research by Acharya et al., (2008), Rai et al., (2017) and Yakha et al., (2014). According to Heikkinen et al., (2003) cold often associated with rainy or winter season. Thus, the sampling in this is associated with the rainy time.

There are no studies being conducted particularly on the dried sap of *Acacia senegal* and *Acacia seyal*. However, there is some studies that have been conducted on the stem, stem bark, and the leaves of *Acacia senegal* and *Acacia seyal*. Disc diffusion assay in this study shows the dried sap of *Acacia seyal* and *Acacia senegal* in ethanol extraction are effective towards *Staphylococcus aureus* may be due to the ethanol as an antiseptic and ineffective towards *Staphylococcus sciuri*. Aqueous extraction of *Acacia senegal* and *Acacia seyal* were not effective to both of the presumptive bacteria. Yet, positive control which was the standard antibiotic, chloramphenicol (30 µg) gives larger zone of inhibition compared to the ethanol extracts of the dried sap of *Acacia seyal* and *Acacia senegal*. This indicates that the Arabic gum sap is a strong probiotic that feeds the good bacteria in the digestive tract and the stem, stem bark, and the leaves of *Acacia senegal* and *Acacia seyal* can be used as an antimicrobial.

5. CONCLUSION

In this chapter, the effect of antimicrobial activity of *Acacia senegal* and *Acacia seyal* in aqueous and ethanol extracts towards some pyogenic bacteria were studied. The three pyogenic bacteria (*Staphylococcus aureus*, *Staphylococcus sciuri* and *Staphylococcus epidermidis*) were identified and tested against the sap extract of *Acacia senegal* and *Acacia seyal* that indicated no bactericidal effect. Yet, the standard antibiotic showed the largest zone of inhibition.

Throughout history, plant gums Known as a strong probiotic and have been used for their medicinal, gastronomic, and nutritional benefits. Gums have a variety of medicinal uses as a tonic, anti-diarrheic, laxative, immune-stimulant, strength givers, many industrial uses as a thickeners, refining agents, and pharmaceutical uses as an excipient, adhesives, binders purposes, with a few notable exceptions. Gums have recently been used to create green nanoparticles from metals including silver, copper, and palladium, which have opened the door to their usage in the creation of antimicrobial nanomaterials and casings.

REFERENCES

- Abdllha, H. B., Mohamed, A. I., Almoniem, K. A., Adam, N. I., Alhaadi, W., Elshikh, A. A., Ali, A. J., Makuar, I. G., Elnazeer, A. M., Elrofaei, N. A., Abdoeltah, S. F., & Hemidan, M. N. (2016). Evolution of Antimicrobial, Antioxidant Potentials and Phytochemical Studies of Three Solvent Extracts of Five Species from *Acacia* Used in Sudanese Ethnomedicine. *Advances in Microbiology*, 6, 691-698. <http://dx.doi.org/10.4236/aim.2016.69068>

- Acharya, J., Mishra, S. K., Kattel, H. P., Rijal, B., & Pokhrel, B. M. (2008). Bacteriology of Wound Infections Among Patients attending Tribhuvan University Teaching hospital, Kathmandu, Nepal. *Journal of Nepal Association for Medical Laboratory Sciences P*, 9(1), 76-80.
- Ahmed, A. A., Fedail, J. S., Musa, H. H., Kamboh, A. A., Sifaldin, A. Z., & Musa, T. H. (2015). Gum Arabic extracts protect against hepatic oxidative stress in alloxan induced diabetes in rats. *Pathophysiology*, 22(4), 189-194.
- Ahmed, I. M., Nadira, U. A., Bibi, N., Cao, F., He, X., Zhang, G., & Wu, F. (2015). Secondary metabolism and antioxidants are involved in the tolerance to drought and salinity, separately and combined, in Tibetan wild barley. *Environmental and Experimental Botany*, 111, 1-12.
- Al Alawi, S. M., Hossain, M. A., & Abusham, A. A. (2018). Antimicrobial and cytotoxic comparative study of different extracts of Omani and Sudanese *Gum acacia*. *Beni-Suef University Journal of Basic and Applied Sciences*, 7(1), 22-26.
- Ali, B. H., Al-Qarawi, A. A., Haroun, E. M., & Mousa, H. M. (2003). The effect of treatment with Gum Arabic on Gentamicin Nephrotoxicity in Rats: A Preliminary Study. *Renal failure*, 25(1), 15-20.
- Ali, B. H., Ziada, A., & Blunden, G. (2008). Biological effects of gum Arabic: A review of some recent research. *Food Chem. Toxicol*, 47(1), 1-8.
- Alviano, D. S., & Alviano, C. S. (2009). Plant extracts: search for new alternatives to treat microbial diseases. *Current Pharmaceutical Biotechnology*, 10(1), 106–121.
- Anjum, P., Rajkumari, V. A., Pavani, N., Yamini, K., & Sabarinathan, T. (2013). Antibiotic Susceptibility Pattern of Pyogenic Bacterial Isolates in Sputum. *IOSR Journal of Pharmacy and Biological Sciences*, 13-17.
- Awad, S. S., Rabah, A. A., Ali, H. I., & Mahmoud, T. E. (2017). *Acacia Seyal* Gums in Sudan: A review. *University Of Khartoum Engineering Journal.*, 94-98.
- Babiker, R., Merghani, T. H., Elmusharaf, K., Badi, R. M., Lang, F., & Saeed, A. M. (2012). Effects of gum Arabic ingestion on body mass index and body fat percentage in healthy adult females: two arm randomized, placebo controlled, double-blind trial. *Nutrition journal*, 1-7.
- Bnuyan, I., Hindi, N. K., Jebur, M., & Mahdi, M. A. (2015). In Vitro Antimicrobial Activity of Gum Arabic (Al Manna and Tayebat) Prebiotics against Infectious Pathogens. *Human Journals*, 77-85.
- Brook, I. (2007). *Anaerobic Infections: Diagnosis and Management*. Boca Raton, Florida: CRC Press.
- Chen, S., Wang, Y., Chen, F., Yang, H., Gan, M., & Zheng, S. J. (2007). A highly pathogenic strain of *Staphylococcus sciuri* caused fatal exudative epidermitis in piglets. *PLoS One*, 2(1). doi:https://doi.org/10.1371/journal.pone.0000147
- Coppen, J. J. (1995). *Gums, Resins and Latexes of Plant Origin Issue 6 of Non-wood forest products*, ISSN 1020-3370. Rome: Food and Agriculture Organization of the United Nations.
- Cowan, M. M. (1999). Plant Products as Antimicrobial Agents. *Clinical Microbiology Reviews*, 564-582.
- Dauqan, E., & Abdullah, A. (2013). Utilization Of Gum Arabic For Industries And Human Health. *American Journal of Applied Sciences*, 10(10), 1270-1279.

- dos Santos, F. F., Mendonça, L. C., de Lima Reis, D. R., de Sá Guimarães, A., Lange, C. C., Ribeiro, J. B., Machado, M. A., & Brito, M. A. V.P (2016). Presence of mecA-positive multidrug-resistant *Staphylococcus epidermidis* in bovine milk samples in Brazil. *Journal of dairy science*, 99(2), 1374-1382.
- Duke, J. (2012). *Handbook of legumes of world economic importance*. Springer Science & Business Media.
- Eisa, M. A., Roth, M., & Sama, G. (2008). *Acacia senegal* (Gum Arabic Tree): Present Role and Need for Future Conservation/ Sudan. *In Deutscher Tropentag*, 1-5.
- Fatema, K., Mondol, K., Akter, T., & Datta, S. (2016). Detection of Pus Sample of Various Pyogenic Infections from Diabetic and Non Diabetic Patient and Compare their Socioeconomic Status in Bangladesh. *American Scientific Research Journal for Engineering, Technology, and Sciences (ASRJETS)*, 26(1), 159-165.
- Frey, Y., Rodriguez, J. P., Thomann, A., Schwendener, S., & Perreten, V. (2013). Genetic characterization of antimicrobial resistance in coagulase-negative *staphylococci* from bovine mastitis milk. *Journal of dairy science*, 96(4), 2247-2257.
- Grice, E. A., & Segre, J. A. (2011). The skin microbiome. *Nat Rev Microbiol*, 9(4), 244–253.
- Hadi, A. H., Elderbi, M. A., & Mohamed, A. W. (2010). Effect of Gum Arabic on Coagulation System of Albino Rats. *International Journal of PharmTech Research*, 2(3), 1762-1766.
- Heikkinen, T., & Järvinen A. (2003). The common cold. *The Lancet*, 361, 51-59.
- Heinrich, M., Barnes, J., Gibbons, S., & Williamson, E. M. (2012). *Fundamentals of Pharmacognosy and Phytotherapy*. Elsevier Health Sciences.
- Holt, J., Krieg, N., Sneath, P., Safety, J., & Williams, S. (1994). *Bergey's Manual of Determinative Bacteriology*. Baltimore, USA,: Lippincott Williams & Wilkins.
- Holzinger, F., Beck, S., Dini, L., Stöter, C., & Heintze, C. (2001). The diagnosis and treatment of acute cough in adults. *Deutsches Arzteblatt international*, 111(20), 356-63.
- Howard, B. J. (1994). *Clinical and Pathogenic Microbiology*. Mosby.
- Johansson, KE. (2014). VetBact - culturing bacteriological knowledge for veterinarians. *Vet Rec* 174:162– <http://dx.doi.org/10.1136/vr.g162>.
- Kayani, S., Ahmad, M., Sultana, S., Shinwari, Z. K., Zafar, M., Yaseen, G., Hussain, M., & Bibi, T. (2015). Ethnobotany of medicinal plants among the communities of Alpine and Sub-alpine regions of Pakistan. *Journal of ethnopharmacology*, 164, 186-202.
- Kingston, D. G. (2011). Modern Natural Products Drug Discovery and its Relevance to Biodiversity Conservation. *J Nat Prod*, 74(3), 496–511.
- Kloos, W. E., Ballard, D. N., Webster, J. A., Hubner, R. J., Tomasz, A., Couto, I., Sloan, G. L., Dehart, H. P., Fiedler, F., Schubert, K., & De Lencastre, H. (1997). Ribotype delineation and description of *Staphylococcus sciuri* subspecies and their potential as reservoirs of methicillin resistance and *staphylolytic* enzyme genes. *International Journal of Systematic and Evolutionary Microbiology*, 47(2), 313-323.
- Kloos, W. E., Ballard, D. N., Webster, J. A., Hubner, R. J., Tomasz, A., Couto, I., Sloan, G. L., Dehart, H. P., Fiedler, F., Schubert, K., & De Lencastre, H. (1997). Ribotype delineation and description of *Staphylococcus sciuri* subspecies and their potential as reservoirs of methicillin resistance and *staphylolytic* enzyme genes. *International Journal of Systematic and Evolutionary Microbiology*, 47(2), 313-323.
- Kobayashi, S. D., Malachowa, N., & DeLeo, F. R. (2015). Pathogenesis of *Staphylococcus aureus* abscesses. *The American journal of pathology*, 185(6), 1518-1527.

- Krishna, S., & Miller, L. S. (2012). Innate and adaptive immune responses against *Staphylococcus aureus* skin infections. *Semin Immunopathol*, 34(2): 261–280.
- Mahon, C. R., Lehman, D. C., & Manuselis, G. (2014). *Textbook of Diagnostic Microbiology*. USA: Elsevier Health Sciences.
- Malini, M., Abirami, G., Hemalatha, V., & Annadurai, G. (2013). Original Article Antimicrobial activity of Ethanolic and Aqueous Extracts of medicinal plants against waste water pathogens. *International Journal of Research in Pure and Applied Microbiology*, 3(2), 40-42.
- Marwah, R. G., Fatope, M. O., Al Mahrooqi, R., Varma, G. B., Al Abadi, H., & Al-Burtamani, S. K. (2006). Antioxidant capacity of some edible and wound healing plants in Oman. *Food chemistry*, 101(2), 465-470.
- Maslin, B. R., Miller, J. T., & Seigler, D. S. (2003). Overview of the generic status of *Acacia* (Leguminosae: Mimosoideae). *Australian Systematic Botany*, 16(1), 1-18.
- Mehrotra, S., Srivastava, A. K., & Nandi, S. P. (2010). Comparative antimicrobial activities of Neem, Amla, Aloe, Assam Tea and Clove extracts against *Vibrio cholerae*, *Staphylococcus aureus* and *Pseudomonas aeruginosa*. *Journal of Medicinal Plants Research*, 4(18), 2473-2478.
- Mohamed, M. H., & Röhle, H. (2011). Evaluation of Height Functions for *Acacia seyal* Del. Variety *Seyal* in Natural Stands, South Kordofan Sudan. *International Journal of Sustainable Agriculture*, 3(3), 88-96.
- Mohamed, R. E., Gadour, M. O., & Adam, I. (2015). The lowering effect of Gum Arabic on hyperlipidemia in Sudanese patients. *Frontiers in physiology*, 1-4.
- Montenegro, M. A., Boiero, M. L., & Borsarelli, C. D. (2012). Gum Arabic: More Than an Edible Emulsifier. In D. J. Verbeek, *Products and Applications of Biopolymers* (pp. 3-26). Croatia: InTech.
- Murugesan, K., Vijayan, H., Ezhilarasi, M. R., Maheshwaran, P., & Radha, R. S. (2017). Antibacterial Activity of Honey against Selected Pyogenic Bacteria. *International Journal of Pharmaceutical Sciences Review and Research*, 45(2), 142-145.
- Nagoba, B. S. (2008). *Microbiology for Physiotherapy Students*. New Delhi: BI Publications Pvt Ltd.
- Nasir, O., Artunc, F., Wang, K., Rexhepaj, R., Föller, M., Ebrahim, A., Kempe, D. S., Biswas, R., Bhandaru, M., Walter, M., Mohebbi, N., Wagner, C. A., Saeed, A.M., & Lang, F. (2010). Downregulation of mouse intestinal Na⁺-coupled glucose transporter SGLT1 by Gum Arabic (*Acacia senegal*). *Cellular Physiology and Biochemistry*, 25(2-3), 203-210.
- Okoro, S., Kawo, A., & Arzai, A. (2012). Phytochemical Screening, Antibacterial And Toxicological Activities Of *Acacia Senegal* Extracts. *Bayero Journal of Pure and Applied Sciences*, 163-170.
- Othman, R. B., Ibrahim, H., Mankai, A., Abid, N., Othmani, N., Jenhani, N., Tertek, H., Trabelsi, N., Trimesh, A., & Mami, F. B. (2013). Use of hypoglycemic plants by Tunisian diabetic patients. *Alexandria Journal of Medicine*, 49(1), 261-264.
- Otto, M. (2004). Virulence factors of the coagulase-negative *staphylococci*. *Front Biosci*, 9(1), 841-863.
- Otto, M. (2008). *Staphylococcal Biofilms*. *Curr Top Microbiol Immunol*, 322, 207–228.
- Otto, M. (2009). *Staphylococcus epidermidis*—the 'accidental' pathogen. *Nature Reviews Microbiology*, 7(8), 555–567.

- Patel, S., & Goyal, A. (2015). Applications of Natural Polymer Gum Arabic: A Review. *International Journal of Food Properties*, 18(5), 986-998. doi:doi:10.1080/10942912.2013.809541
- Perveen, K., Bokhari, N. A., & Soliman, D. A. (2012). Antibacterial activity of *Phoenix dactylifera* L. leaf and pit extracts against selected Gram negative and Gram positive pathogenic bacteria. *Journal of Medicinal Plants Research*, 296-300.
- Rai, S., Yadav, U. N., Pant, N. D., Yakha, J. K., Tripathi, P. P., Poudel, A., & Lekhak, B. (2017). Bacteriological profile and antimicrobial susceptibility patterns of bacteria isolated from pus/wound swab samples from children attending a tertiary care hospital in Kathmandu, Nepal. *International journal of microbiology*, 2017, 1-5.
- Rakshit, M., & Ramalingam, C. (2013). *Gum acacia* coating with garlic and cinnamon as an alternate, natural preservative for meat and fish. *African J Biotechnol*, 406-413.
- Rijal, B. P., Satyal, D., & Parajuli, N. P. (2017). High Burden of Antimicrobial Resistance among Bacteria Causing Pyogenic Wound Infections at a Tertiary Care Hospital in Kathmandu, Nepal. *Hindawi*, 1-7.
- Ryan, K. J., & Ray, C. G. (2003). *Sherris Medical Microbiology Lange Basic Science McGraw Hill professional*. New York: McGraw Hill Medical.
- Sharma, V., Parihar, G., Sharma, V., & Sharma, H. (2015). A Study of Various Isolates from Pus Sample with Their Antibiogram from Jln Hospital, Ajmer. *IOSR Journal of Dental and Medical Sciences*, 14(10), 64-68.
- Simasek, M., & Blandino, D. A. (2007). Treatment of the Common Cold. *American Family Physician*, 75(4).
- Singer, A. J., & Talan, D. A. (2014). Management of Skin Abscesses in the Era of Methicillin-Resistant *Staphylococcus aureus*. *New England Journal of Medicine*, 1039-1047.
- Singh, B. R., Dubey, S., & Zakira, M. S. (2015). Antimicrobial Activity of Natural Edible Gums. *World Journal of Pharmaceutical Sciences*, 2217-2221.
- Srinu, B., Vijaya, K. A., Kumar, E., & Madhava, R. (2012). Antimicrobial resistance pattern of bacterial foodborne pathogens. *Journal of Chemical and Pharmaceutical Research*, 4(7), 3734-3736.
- Stepanovic, S., Jezek, P., Vukovic, D., Dakic, I., & Petra's, P. (2003). Isolation of Members of the *Staphylococcus sciuri* Group from Urine and Their Relationship to Urinary Tract Infections. *Journal Of Clinical Microbiology*, 41(11), 5262-5264.
- Stepanović, S., Vuković, D., Trajković, V., Samardžić, T., Čupić, M., & Švabić-Vlahović, M. (2001). Possible virulence factors of *Staphylococcus sciuri*. *FEMS microbiology letters*, 199(1), 47-53.
- Švec, P., Petráš, P., Pantůček, R., Doškař, J., & Sedláček, I. (2016). High intraspecies heterogeneity within *Staphylococcus sciuri* and rejection of its classification into *S. sciuri* subsp. *sciuri*, *S. sciuri* subsp. *carnaticus* and *S. sciuri* subsp. *rodentium*. *International journal of systematic and evolutionary microbiology*, 66(12), 5181-5186.
- Upadhyay, R. K. (2017). Nutritional, therapeutic, and pharmaceutical potential of plant gums: A review. *International Journal of Green Pharmacy*, 11(1).
- Vasanthakumari. (2009). *Practical Microbiology*. New Delhi: BI Publications Pvt Ltd.
- Webster, J. A., Bannerman, T. L., Hubner, R. J., Ballard, D. N., Cole, E. M., Bruce, J. L., Fiedler, F., Schubert, K., & Kloos, W. E. (1994). Identification of the *Staphylococcus sciuri* Species Group with *Eco* RI Fragments Containing rRNA Sequences and

Description of *Staphylococcus vitulus* sp. nov. *International Journal of Systematic and Evolutionary Microbiology*, 44(3), 454-460.

- Widerström, M., Wiström, J., Ek, E., Edebro, H., & Monsen, T. (2011). Near absence of methicillin-resistance and pronounced genetic diversity among *Staphylococcus epidermidis* isolated from healthy persons in northern Sweden. *Apmis*, 119(8), 505-512.
- Yakha, J. K., Sharma, A. R., Dahal, N., Lekhak, B., & Banjara, M. R. (2014). Antibiotic susceptibility pattern of bacterial isolates causing wound infection among the patients visiting B & B hospital. *Nepal Journal of Science and Technology*, 15(2), 91-96.
- Zhou, X., & Li, Y. (2015). *Atlas of Oral Microbiology: From Healthy Microflora to Disease*. Elsevier Science.

ASSESSMENT OF BACTERIAL CONTAMINATION IN PUBLIC SWIMMING POOLS

Noura Karam M. Salih & Ibrahim M. Oumar
Infrastructure University Kuala Lumpur

1. INTRODUCTION

Many people attend swimming pools for sport, entertaining, or healthy lifestyle. In these environments, the elderly, pregnant women, babies, people with handicaps or movement disabilities, and sports persons can be predisposed to contracting infections (Guida et al., 2009). Swimming pool water contamination with microorganism can result from the environment as well as pool users. Swimming pools remain a transmission vehicle for infectious diseases by several microorganisms causing acute gastrointestinal, cutaneous and respiratory illnesses (Hlavsa et al., 2011). Swimming pools is usually opened for public usage where it can accommodate more than hundreds people used a pool for water based-recreational activities. Therefore, water in the pool is a good transmission tool for infectious diseases among human population throughout the world (WHO, 2006).

Most states require pool operators to maintain chlorine levels at a minimum of 1.0 ppm in swimming pools and wading pools (Hooker, et al., 2010). A small number of states require higher levels (Vermont, 2.0; Nebraska, 2.0; Georgia, 1.5; and Maryland, 1.5), and ten states have lower minimum levels. The National Swimming Pool Foundation (NSPF) recommends that free chlorine levels should optimally be maintained between 2.0 and 4.0 ppm for swimming pools (3.0–5.0 ppm for spas) and should never fall below 1.0 ppm (Rabi et al 2008). Minimum required chlorine levels spas are extremely variable across the United States. Required levels range from 0.4 ppm to 10 ppm (Hooker, 2010).

The release of faeces by bathers may be inadvertent, in the case of diarrheic stool. Aside from contaminations through the release of faecal materials, non-faecal human shedding (vomit, mucus, skin or saliva) in the pool is potential sources of disease-causing microorganisms (Ezeet, 2015). Isolated bacteria such as, *Enterococcus faecalis*, *Clostridium perfringens*, *B.cereus*, *Escherichia coli*, *P.aeruginosa*, *S.aureus*, *S.epidermidis* and *Proteus vulgaris* (Bello, 2012). It was reported that the presence of high level of coliform, faecal coliform bacteria and *E.coli* showing that the swimming pools had not met the World Health Organization (WHO) hence, the need for urgent and effective intervention. Swimming pool also may directly or indirectly contaminated by air, soil, dust, rain water, sewage, human or animal excrement and individual bather which may cause diseases that include diarrhea, typhoid fever, hepatitis and cholera as reported from drinking of contaminated water by the swimmers (Bello et al., 2012). For this reason periodic evaluations of bacteriological quality of water as well antimicrobial susceptibility patterns of possible isolated organisms, are necessary. Researches had been described the bacterial contamination of swimming pools and to study their antimicrobial

susceptibility to common clinical antimicrobial drugs used in clinical practice, it was found that poor-quality water in swimming pools is associated with a substantial risk of otitis externa due to *Pseudomonas aeruginosa* (Castor ML, Beach MJ.200, Craun GF, et al., 2005).

The objectives of this research are to identify dominant bacterial species from sampled swimming pools water around three locations in Kajang- Malaysia, to determine the Chlorine levels, temperature and pH performers of sampled swimming pools water and to detect the antibiotics sensitivity of isolated bacterial species.

2. MATERIALS AND METHODS

Sample collection, pH, temperature and chorine determination

Water samples were collected from three different swimming pools for three times over three weeks. Three samples were collected from each location. Samples were collected and transported to the laboratory in sterile plastic bottles. Sampling was undertaken on a weekly basis before changes the water pools.

pH of the swimming pool water was determined in location using the pH paper. According to Judd, S.J., Bullock, G., 2003 Temperature of the swimming pool water was determined in location using the thermometer. Thermometer was taken inside the pools.

The swimming pools water samples were tested using poolside technology for chlorine, Testing for chlorine was performed using ferrous ammonium sulfate—n,n-diethylp-phenylenediamine (FAS DPD) method according to Hooker et al,2010 and Judd, S.J., Bullock, G., 2003.

Three samples were collected from each location. The first sample was collected the first day of changing the swimming pool water, 7 days and 14 days of changing the swimming pool water for second and third samples from each location, each sample were performed to determine chlorine and bacterial contamination to measure the effectiveness of chlorine as disinfectant agent in swimming pool.

Bacteria isolation and identification

0.8 g of nutrient agar powder was suspended in 100ml of distilled water and autoclaved at 121° C for 15 minutes. Nutrient agar was pour into each plate and leave plates on the sterile surface until the agar has solidified. Petri dishes were replaced and stored in a refrigerator (Fawole and Oso, 2004). In order to identify the bacterial contaminations, Gram Stain Indole, Methyl Red Voges–Proskauer, Citrate, Oxidase, and Catalase were performed (Cheesbrough, 2006,Olutiola et al., 2000, Fawole and Oso, 2004).

Antibiotics sensitivity test

Antibiotic sensitivity test was performed for all the isolates using the Kirby Bauer disk diffusion method with five different antibiotic disks are Penicillin G, ampicillin, streptomycin, tetracycline and kanamycin (Clinical and Laboratory Standard Institute 2006).

The method was Kirby-Bauer. In this test, small filter paper disks was used to impregnated with a standard amount of antibiotic were placed onto an agar plate to which bacteria had been swabbed. The plates are incubated overnight, and the zone of inhibition of bacterial growth is used as a measure of sensitivity. Large zones of inhibition indicate that the organism was sensitive, while small or no zone of inhibition indicates resistance. An interpretation of intermediate was given for zones which fall between the accepted cutoffs for the other interpretations (Clinical and Laboratory Standard Institute 2006).

3. RESULTS

pH, temperature and chlorine determination of swimming pools samples

For pH, temperature and chlorine determination, it was found that the pH range was above 4-7 in all locations, pH for pool water should be maintained at 7, since this was the same as the pH in human eyes and mucous membranes (table 1a). A pH of 7 also gives good chlorine disinfection. In general, the temperatures were reading from swimming pools water was between (29°C and 30°C) (table 1b).

Higher free residual chlorine has been demonstrated to decrease likelihood of fecal contamination. Swimming pools with >1.0 (ppm) of chlorine (which is the same as milligrams per liter for chlorine) have very low levels of bacterial. Although the value of proper chlorination of swimming pools ranges were 0.8-2.25 ppm (table 1c & d). Immediately after changing the swimming pool water, chlorine concentrations were high (2.1-2.3) ppm which is considered as disinfectant agent and prevent bacterial contamination only 6 % of the samples were positive for bacterial contamination, while swimming pool water after 7 days of changing was ranged (1.6-1.9) ppm with 12-15 % of the samples were contaminated of bacteria. Chlorine concentration was (0.7-0.9) ppm after 14 days from changing the water, with 82-92 % of bacterial contamination.

Bacteria isolation and identification

Biochemical tests were carried out for the identification of bacterial isolates. These includes gram staining, catalase test, citrate test, methyl red, Voges-Proskauer test, indole test and oxidation test, which were carried out according 18 to 24 h broth culture of each isolate. Colonial and cellular morphology dominant species bacterial isolates from three different swimming pools samples were identified as gram positive cocci, gram negative rod and gram positive rods for location 1,2,and 3 respectively (table 2). This study aimed to evaluate the bacteriological quality of some swimming pools investigated the presences of the dominant

species such as *Pseudomonas* sp, *Bacillus* sp and *Staphylococcus* sp in water samples. Therefore, in this research three different samples of swimming pools were selected to improve control of the evaluation of the microbial features of pool's water which showed high number of bacteria contaminated the water such as *Pseudomonas* sp, *Bacillus* sp and *Staphylococcus* sp. (Table 3).

Table 1a: The Hydrion Spectral pH Paper Dispenser (pH 1.0 to 14.0) of swimming pools water

Samples location	pH			
	Sample 1	Sample 2	Sample 3	Range
1	pH 4.0	pH 6.0	pH 6.0	pH 4-6
	yellow to blue	yellow to blue	yellow to blue	
2	pH 7.0	pH 6.0	pH 6.0	pH6-7
	yellow to blue	yellow to blue	yellow to blue	
3	pH 6.0	pH 6.0	pH 7.0	pH 6-7
	yellow to blue	yellow to blue	yellow to blue	

Table 1b: The temperature of swimming pools water

Samples location	Temperature			Range
	Sample 1	Sample 2	Sample 3	
1	29°C	29°C	31°C	29°C
2	30°C	31°C	29°C	30°C
3	30°C	32°C	29°C	30°C

Antibiotics sensitivity test

All three swimming pools samples from the confirmatory analysis serotype test were subjected to five different common antibiotics namely: Penicillin G, Ampicillin, Streptomycin, Tetracycline and Kanamycin antibiotics test. The antibiotic susceptibility test was performed using the disk diffusion method. The disk diffusion method was used, a qualitative technique, to test the sensitivity of bacteria isolated from swimming pools. Antibiotics sensitivity test as stated in tables 4 and 5.

Table 1c: Chlorine Concentration (ppm) of swimming pools water

Samples location	Chlorine ppm		
	Sample 1	Sample 2	Sample 3
1	2.3	1.9	0.9
2	2.1	1.7	0..8
3	2.3	1.6	0.7
Range	2.25	1.7	0.8

Table 1d: The percentage of bacterial contamination in swimming pool vs chlorine levels

Sample #	Chlorine ppm	% Bacterial Contamination		
		Sample Location		
		1	2	3
Sample 1	2.25	0%	6%	6.7%
Sample 2	1.7	15%	12.2%	13.55
Sample 3	0.8	88%	82%	92%

In *Pseudomonas* sp result showed that kanamycin and streptomycin was most effective for inhibiting bacterial growth, followed by tetracycline, ampicillin and penicillin did not inhibit bacterial growth and resistance as showed in (Figure 1b & table 4, 5). In *Staphylococcus* sp showed that kanamycin, tetracycline and streptomycin was most effective for inhibiting bacterial growth, followed by ampicillin and penicillin did not inhibit bacterial growth and resistance (Figure 1a & table 4, 5). In *Bacillus* sp showed that kanamycin, tetracycline and streptomycin was most effective for inhibiting bacterial growth, followed by ampicillin and penicillin did not inhibit bacterial growth and resistance (Figure 1c & table 4, 5). The high rate of resistance to kanamycin, tetracycline and streptomycin in *Pseudomonas* sp, *Staphylococcus* sp and *Bacillus* sp recorded in this study could be attributed to the fact that kanamycin, tetracycline and streptomycin is found naturally in ground and surface waters due to incomplete treatment of water using in swimming pools.

Table 2: Colonial and cellular morphology dominant species bacterial isolates from three different swimming pools samples.

Sample locations	Colony shape	Colony size	Elevation	Edge margin	Optical characteristics	Consistence	Colony surface	Gram stain	Colony morphology
1	irregular	0.1 - 05 μ m	Flat	Undulate	Opaque	Soft	Smooth	+ ve	Cocci
2	Round form	0.1 - 05 μ m	Flat	Entire	Greenish	Soft	Smooth	-ve	Rods
3	Round form	0.1 - 05 μ m	Flat	Undulate	Opaque	Soft	Smooth	+(ve)	Rod

The species of bacterial was isolated from three different swimming pools as shown in table 2 & 3. *Pseudomonas* sp *Bacillus* sp and *Staphylococcus* sp produces circular mucoid smooth colonies with emits sweat grape on Nutrient agar. Gram negative and Gram positive cocci and bacilli (*Bacillus* sp and *Staphylococcus* sp.), were isolated from three different swimming pools

after period of 14 days from the changing of water. The pH was taken immediately during collection of the samples from swimming pools an optimum range of pH was shown in table 1a, which are the average 5.3 to 6.3 and colour was from yellow to blue of all three samples of swimming pools. Accordingly when was detecting their bacteria by streaked the water samples on sterile nutrient agar plates and 24 hours incubation at 37°C. Bacterial colonies with light yellow color pigmentation were examined morphologically by gram's staining method and all Gram-negative and Gram-positive bacilli and cocci were detected. However, Table 1b, Shows the temperature that was determined at swimming pools water by using thermometer the average temperature was 29°C -30°C. In table 4.3 after the period of incubation, the bacteria was characterized and identified in all samples by observing the morphology, and carrying some primary and secondary biochemical tests. According to Fawole, et al., (2004) that were first described and characterized the bacteria by their morphological appearances (i.e. colony shape, edge or margin, pigmentation, elevation, colony surface, consistency and optical characteristics) on the plate. In addition to the colonial characterization, cellular morphologies and biochemical characteristics as described in the laboratory manual of microbiology and also used to characterize the bacteria.

Table 3: Results of the biochemical tests from different locations swimming pool sample

Sample locations	Gram stain	Catalase	Iodine	Oxidase	Methyl red	Voges-Proskauer	Citrate	Spices
1	+(ve)	+(ve)	-(ve)	+(ve)	+(ve)	-(ve)	-(ve)	<i>Staphylococcus</i>
	-(ve)	+(ve)	-(ve)	+(ve)	-(ve)	-(ve)	+(ve)	<i>Pseudomonas</i> sp
2	+(ve)	+(ve)	-(ve)	+(ve)	-(ve)	+(ve)	-(ve)	<i>Bacillus</i> sp
	+(ve)	+(ve)	-(ve)	+(ve)	+(ve)	-(ve)	-(ve)	<i>Staphylococcus</i>
	-(ve)	+(ve)	-(ve)	+(ve)	-(ve)	-(ve)	+(ve)	<i>Pseudomonas</i> sp
3	+(ve)	+(ve)	-(ve)	+(ve)	-(ve)	+(ve)	-(ve)	<i>Bacillus</i> sp
	+(ve)	+(ve)	-(ve)	+(ve)	+(ve)	-(ve)	-(ve)	<i>Staphylococcus</i>

* +ve = Positive reaction, -ve = negative.

The importance of insuring proper disinfection of pools and spas cannot be over emphasized. All states have recognized the importance through development of regulations for minimum levels of chlorine in pools and spas (Hooker, 2010). The results of research has demonstrated that maintaining levels of chlorine at a minimum of 1.0 ppm will minimize bacterial contamination in swimming pool and this was similar to the current data (table 1c).

The catalase test were positive in all samples, the methyl red tests were negative at *Bacillus* sp and *Pseudomonas* sp and were positive at *Staphylococcus* sp. The indole test was negative in all isolated bacteria which was carried out from each isolated bacteria (table 3).

The most serious one is the *Pseudomonas* sp which is reported to make many disease such as folliculitis that occurs within 8 hours to 5 days, otitis externa (swimmers ear), urinary and respiratory tracts infections, wounds and cornea infections, head and muscle aches and burning eyes and fever, (WHO 2006). According to some reports, *Staphylococcus* sp is

associated with the skin, eye, ear and gastrointestinal tract infection. (Ita, A.Y. & Ekpombok, M.U. 2004). *Bacillus* sp do not cause significant infections and are often considered to be a contaminant. In some cases it reported in food poisoning and gastrointestinal signs when ingested with the water during swimming (Drobniewski FA. and Gaur AH, et al., 2001).

The antibiotic susceptibility test was performed using the disk diffusion method as described by Jorgensen and Ferraro (2009). The disk diffusion method was used, a qualitative technique, to test the sensitivity of bacteria isolated from swimming pools. Antibiotics sensitivity test as stated in table 4.5 and 4.6 in this study, five common antibiotics (Penicillin G, Ampicillin, Kanamycin, Streptomycin and Tetracycline) were used for the susceptibility testing. As illnesses normally contracted in a swimming pool are mostly those of the skin rather than intestinal, it is suggested that the best indicators of the hygienic condition of water in a swimming pool are *staphylococci* because of their resistance to disinfection, high numbers in the environment, and ease of recovery. But also, poor-quality water in swimming pools is associated with a substantial risk of otitis externa due to *Pseudomonas aeruginosa* (Castor ML, Beach MJ.200, Craun GF, et al, 2005). The high rate of resistance to kanamycin, tetracycline and streptomycin in *Pseudomonas* sp, *Staphylococcus* sp and *Bacillus* sp recorded in this study could be attributed to the fact that kanamycin, tetracycline and streptomycin is found naturally in ground and surface waters due to incomplete treatment of wastewaters(Barber et al., 2009), which may find their way into this swimming pools. This may put selective pressure on organisms in the swimming pools hence may cause the higher rate of resistance to kanamycin, tetracycline and streptomycin.

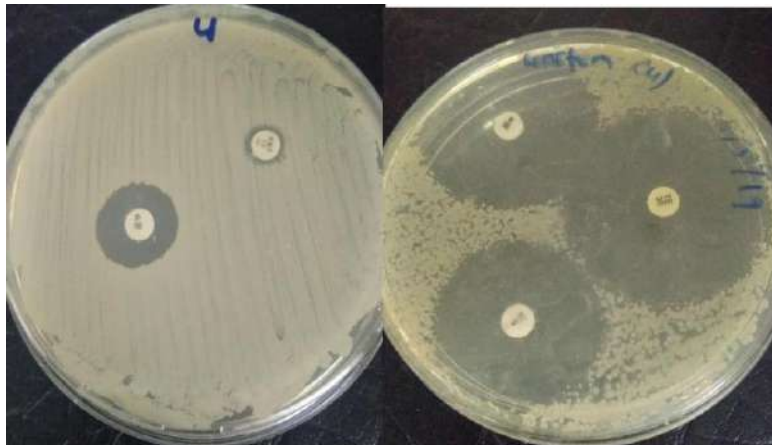


Figure 1a: Shows that Penicillin G, Ampicillin not inhibits. For Streptomycin, Tetracycline and Kanamycin sensitivity to the *Staphylococcus* sp, inhibition zone occur (location# 1)



Figure 1b: Shows that Penicillin G, Ampicillin, Streptomycin, Tetracycline and Kanamycin sensitivity *Pseudomonas* sp, no zone of inhibition (location#2)



Figure 1c: Shows that Penicillin G, Ampicillin not inhibits. For Streptomycin, Tetracycline and Kanamycin sensitivity to the *Bacillus* sp. (location#3)

Table 4: The inhibition zone size for *Staphylococcus* sp and *Bacillus* sp. test were subjected to five different common antibiotics namely: Penicillin G, Ampicillin, Streptomycin, Tetracycline and Kanamycin antibiotics test

Tests No:	Antimicrobial Agent	Diameter of Zone (cm)	
		<i>Staphylococcus</i> sp	<i>Bacillus</i> sp
1	penicillin G	1.7 mm	0.7 mm
2	Ampicillin	0.85 mm	0.0 mm
3	Kanamycin (K)	3.9 mm	2.7 mm
4	Streptomycin (S)	3.2 mm	2.6 mm
5	Tetracycline (Te)	4.4 mm	2.4 mm

Table 5: The inhibition zone size for *Pseudomonas* sp test were subjected to five different common antibiotics namely: Penicillin G, Ampicillin, Streptomycin, Tetracycline and Kanamycin antibiotics test

No	TEST	SAMPLE (mm)		
		First reading	Second reading	Average
1	Streptomycin(S)	16 mm	17 mm	16.5 mm
2	Tetracycline(Te)	No zone of inhibition	No zone of inhibition	No zone of inhibition
3	Kanamycin(K)	15 mm	16 mm	15.5 mm
4	Penicillin G (Pen G)	No zone of inhibition	No zone of inhibition	No zone of inhibition
5	Ampicillin (A)	No zone of inhibition	No zone of inhibition	No zone of inhibition
6	Rifampicin (R)	12 mm	12 mm	12 mm

Table 6: The inhibition zone size for *Pseudomonas* sp test were subjected to five different common antibiotics namely: Penicillin G, Ampicillin, Streptomycin, Tetracycline and Kanamycin antibiotics test.

No	TEST	SAMPLE (mm)		
		First reading	Second reading	Average
1	Streptomycin(S)	16 mm	17 mm	16.5 mm
2	Tetracycline(Te)	No zone of inhibition	No zone of inhibition	No zone of inhibition
3	Kanamycin(K)	15 mm	16 mm	15.5 mm
4	Penicillin G(Pen G)	No zone of inhibition	No zone of inhibition	No zone of inhibition
5	Ampicillin (A)	No zone of inhibition	No zone of inhibition	No zone of inhibition
6	Rifampicin (R)	12 mm	12 mm	12 mm

Statistical Analysis

Multiple logistic regression analysis was performed to identify any associations between poolside testing results and laboratory evidence of fecal contamination. Data were analyzed using SPSS for Windows, version 17.0 (SPSS, Inc., Chicago, IL). All statistical tests were performed using two-tailed analysis, and the alpha was set at 0.05.

4. DISCUSSION

Swimming pools have been identified as affectation some public health risks to users due to either bacterial fungi or chemical contamination. As a result, maintaining good swimming pools water quality is an important issue in preventing health risks for bathers.

Hence, this data discusses the identification of the three species that were isolated from different swimming pools water. Bacterial contamination was affected by chlorine levels. This has shown the bacterial presence of morphology dominant species. However, A recent study from Ireland

reported a very high prevalence of *Pseudomonas* sp which almost similar to our overall prevalence of 44% (1/3 pools), (J.E. Moore, et al., 2002). This study aimed to evaluate the bacteriological quality of some swimming pools investigated the presences of the dominant species such as *Pseudomonas* sp, *Bacillus* sp and *Staphylococcus* sp in water samples. Therefore, in this research three different samples of swimming pools were selected to improve control of the evaluation of the microbial features of pool's water which showed high number of bacteria contaminated the water such as *Pseudomonas* sp, *Bacillus* sp and *Staphylococcus* sp.

5. CONCLUSION

Based on the results in this chapter, it can be concluded that the some of the swimming pools can be contaminated by dominant hazardous bacteria such as *Pseudomonas* sp. and *Staphylococcus* sp. at the tested locations due the poor hygiene and improper chlorination. The sanitary condition of swimming pools water should be examined periodically according to the number of people that use it to ensure safety. The pH pool should be monitored and adjusted frequently to reduce the risk of waterborne-illness due to *Pseudomonas* sp., *Bacillus* sp. and *Staphylococcus* sp. These data may recommend that future swimming pool water guidance should include raising awareness among swimmers, pool operators and managers about hygienic behavior and better hygiene measures. We believe that, current recommendations to avoid public indoor and outdoor swimming pools are inappropriate, as long as the water is well maintained according to local hygiene guidelines.

REFERENCES

- Barber, L.B., S.H. Keefe, D.R. LeBlanc, P.M. Bradley & F.H. Chapelle. (2009). Fate of sulfamethoxazole, 4-nonylphenol and 17 β -estradiol in groundwater contaminated by wastewater treatment plant effluent, 43, 4843-4850.
- Bello, O. O., Mabekoje, O.O., Egberongbe, H .O., & Bello, T.K. (2012). Microbial qualities of Swimming Pools in Lagos, Nigeria. *International Journal of Applied Science and Technology*, 2(8), 89-96.
- Castor ML, Beach MJ. Reducing illness transmission from disinfected recreational water venues: swimming, diarrhea and the emergence of a new public health concern. *Pediatr Infect Dis J* 2004; 23 (9): 866-870.
- Cheesbrough, M. (2006). *District laboratory practice in tropical countries* (eds Cambridge University Press Cambridge, UK.), ISBN-13: 9781139449298.
- Clinical and Laboratory Standard Institute. Performance standards for antimicrobial susceptibility: Sixteenth informational supplement. Wayne, PA: CLSI; 2006, p. M100-S16.
- Craun GF, Calderon RL, Craun MF. Outbreaks associated with recreational water in the United States. *Int J Environ Health Res*. 2005; 15(4):243-62.
- Drobniewski, FA. (1993). *Bacillus cereus* and related species. *Microbiol Rev*, 6, 38–324.
- Ezeet, V.C., Onwuakor, C.E., & Ikwuegbu, A.L. (2015). Microbiological and physicochemical characteristics of swimming pool water in Owerri State, Nigeria. *Journal of Applied and Environmental Microbiology*, 3, 6-10.

- Fawole, M.O., & B.A., Oso. (2004). Characterization of bacteria laboratory manual of microbiology. *Spectrum Book Ltd., Ibadan, Nigeria*, 24-33.
- Guida. (2009). Microbiological quality of the water of recreational and rehabilitation pools A 2 year survey in Naples, Italy public health, 123, 448–451..
- Hlavsa, M. C., Roberts, V. A., Anderson, A. R., Hill, V. R., Kahler, A. M., Orr, M., Wade, T. J. (2011). Surveillance for waterborne disease outbreaks and other health events associated with recreational water United States, 60(12), 1–32.
- Hooker et al.: Determinants of Bacterial Contamination in Pools, Spas, and Wadin *International Journal of Aquatic Research and Education*, 2010, 4, 33-38 © 2010 Human Kinetics, Inc.
- J.E., Moore, N., Heaney, B.C., Millar, M., & Crowe, J.S. (2002). Elborn incidence of *Pseudomonas aeruginosa* in recreational and hydrotherapy pools. *Commune public health*, 23-26.
- Jorgensen, J.H., & Ferraro, M.J. (2009). Antimicrobial susceptibility testing review of general principles and contemporary practices, 49, 1749–1755.
- Judd, S.J., Bullock, G., 2003. The fate of chlorine and organic materials in swimming pools. *Chemosphere*, 51 (9), 869-879
- Olutiola, P.O., Famurewa, & H.G., Sonntag. (2000). Introduction to general microbiology practical approach. Bolabay Publications, Ikeja, Nigeria.
- Rabi, A., Khader, Y., Alkafajei, A., & Aqoulah, A.A. (2008). Sanitary conditions of public swimming pools in Amman, Jordan. *International Journal of Environmental Research and Public Health*, 5(3), 152–157
- World Health Organization. (2006). Guidelines for safe recreational water environments swimming pools and similar environments, ISBN: 9789241546805, 118.

IDENTIFICATION OF MARINE SPONGE USING DNA-BARCODING APPROACH.

Aizat Mohd Razali, Dr. Samson Soon & Teffanie Arputheraj
Infrastructure University Kuala Lumpur

1. INTRODUCTION

Marine sponges live in a wide range of ocean habitats, from the polar regions to the tropics. Having the great weather on her side, Malaysia is blessed with colours on the ocean floor by the huge varieties of marine organism and marine sponges is one of the contributor. The vibrant colour and shape creates beautiful attraction to human tourism activity and attract marine organism for their prey-predatory relationship. Marine sponges' unique characteristics correspondingly play huge role in balancing the ecosystem and the food chain on the oceans floor. The filtration capacity of sponges in an instance, convert suspended particles or dissolved matter into food for other animals and play a role for the recirculation of carbon, silicon, and nitrogen.

Sponges are also known as the largest members of bioactive compound producer – mostly reported on pharmaceutical potency[1,2]. Even more interesting is that up to 40% volume of sponges may consist of bacteria [3] and the presence of these bacteria aid in removing waste and producing chemical defences [4]. These bacteria also contribute to the bioactive metabolites [5] that may include anticancer, antibacterial, antifungal, antiviral, antiprotozoal and antifouling agents [6,7]. Despite the contribution to the ecosystem, pharmaceutical, tourism and even entertainment (our beloved SpongeBob), the community in general is lack of understanding on sponges. As a starter, marine sponge is an animal!. Yes, it is a benthic, bottom dwelling, minimal movement organism [8], but marine sponge was historically concluded to be the earliest form of animal life (recent finding state Comb Jelly being the world's first).



Figure 1: Marine sponge sampling work in progress. The photos and the environmental details (depth and temperature) were documented prior to the sampling of approximately 3cm² of each sponges.

In Malaysia, no official directory of sponge species has been created so far - hence be deficient of information on the species that we may have in our seas. A matter of fact is that the accurate identification of marine sponges from the Phylum Porifera has always been a daunting task due to its inherent taxonomic complexities and error-prone morphology-based identification process. Misidentification of this organism has occurred in several studies [9] and may lead to failure in the prediction of chemical compositions [10], hence affecting the results of studies. Spicules identification, the conventional method for sponge identification is found to be time and cost consuming [11]. Even more, it is not able to explain the relationship among species or its evolution.

2. METHODOLOGY

The utilization of DNA barcodes and taxonomic system with a DNA sequence provides an opportunity to understanding the evolutionary factors that shape species distributions in space and time. Furthermore, the tiny amount of sample needed for DNA barcode identification approach is perceived as a more environmental friendly method as it may support the sustainability of the sponge colony.

This Chapter utilizes a rapid and simple molecular approach to circumvent this problem and tested the method to investigate the species of marine sponges found in Pulau Bidong fore reef zone (latitude: 5°61'49.33", longitude: 103°07'11.36") based on the COI DNA barcode of marine sponges. Approximately 0.3 g DNA of the marine sponge were extracted and amplified using polymerase chain reaction (PCR). Amplification of the DNA barcode from the marine sponge samples was based on the standard COI barcoding fragment using degenerate primers in a PCR followed by gel electrophoresis. Identification of sponge was conducted based on molecular technique following the method introduced by Meyer *et al* (2005) [12]. The DNA sequencing were conducted by 1st Base Laboratory Malaysia and analyzed using BioEdit Sequence Alignment Editor 7.2.3 program for homology of sequencing results and Basic Local Alignment Search Tool (BLAST) program at <http://blast.ncbi.nlm.nih.gov/> for the detection with the most similar species in NCBI data base.

3. RESULTS

The results of our research found out that the marine sponge DNA identification is not an easy mission indeed - sponge itself is known to contain several meta-genomic DNA [13, 14]. However, the study on DNA barcode for marine sponge identification is compulsory as it is the only way to determine the exact species and the evolution of marine sponge can be understood. In this study, the marine sponge DNA successfully extracted using spin column method followed by successful establishment of degenerate forward/reverse primer set for DNA barcoding work. A COI DNA barcode fragment was successfully amplified from all specimens using PCR using the standard three step PCR method [15, 16]. Despite good quality of DNA obtained from the extraction process, re-amplification of the DNA is required to obtain decipherable sequence of DNA. Molecular analysis based on the gene sequence was confirmed

that the sponge belongs to *Hemiasterella sp.* UCMPWC1021 - a marine sponge that held several possibilities of the production of anticancer compound [6, 17, 18, 19, 20, 21, 22].



Figure 2: *In-situ* photograph of the specimens colony. All samples were morphologically similar (yellow and firm). The sponge appear to be orange color when photographed with the flash on. Colony A was found at the depth of 7.9 meter while B and C were found at the average depth of 15.8 meter.

Bidong Archipelago as one of the marine spots with active numbers of marine research in Malaysia. Several studies have been conducted on marine sponges in Bidong Archipelago, ranging from acid degrading bacterium from *Gelliodes sp.* [23], antibacterial activity of *Aaptos aaptos* [24], antiinflammatory activity of *Theonella sp.* [25], fatty acids of *Xetospongia* [26], and anti-ameobic of *Aaptos sp.* [27]. However, there is no research reported for *Hemiasterella sp.* in Bidong Archipelago and Malaysia. The successful identification of this sponge marks the first report on *Hemiasterella sp.* in Malaysian waters.

These successful identifications of *Hemiasterella sp.* marks as the first report on this particular species found in Bidong Archipelago and Malaysian waters. The water parameters may suggest the optimum condition for the growth of this marine sponge, further studies on the environmental factors may confirm the details. The profile data generated can be transformed into a reliable depository platform for species confirmation and distribution. This depository could contribute to future novel biocompound discoveries and efficient marine sponge conservation efforts.

4. CONCLUSION

The marine sponge DNA identification is not an easy mission to fulfil as sponge itself is known to contain several meta-genomic DNA. However, the study on DNA barcode for marine sponge identification is compulsory as it is the only way to determine the exact species and the evolution of marine sponge can be understood. In this study, the marine sponge DNA successfully extracted using spin column method followed by the successful establishment of degenerate forward/reverse primer set for DNA barcoding work. A COI DNA barcode fragment was successfully amplified from all specimens using PCR using the standard three steps PCR method. Despite the good quality of DNA obtained from the extraction process, re-amplification of the DNA is required to obtain decipherable sequence of DNA. Molecular analysis based on the gene sequence confirmed that the sponge belongs to *Hemiasterella sp.* UCMPWC1021 - a

marine sponge that held several strong possibilities for the production of anticancer compound. The successful identification of *Hemiasterella sp.* marks the first report on this particular species found in Bidong Archipelago and Malaysian waters. The water parameters may suggest the optimum condition for the growth of this marine sponge, further studies on the environmental factors may confirm the details. The profile data generated can be transformed into a reliable depository platform for species confirmation and distribution. This depository could contribute to future novel biocompound discoveries and efficient marine sponge conservation efforts.

REFERENCES

- [1] Kijjoa, A. and Sawangwong, P. 2004. Drugs and cosmetics from the Sea. *Mar. Drugs*. 2: 7382.
- [2] Thakur, N.L. and Muller, W.E.G. 2004. Biotechnological potential of marine sponges. *Current Science*. 86 (11): 1506–1512.
- [3] Thiel, V., Neulinger, S.C., Staufenberger, T., Schmaljohann, R. and Imhoff, J.F. 2006. Spatial distribution of sponge-associated bacteria in the Mediterranean sponge *Tethya aurantium*. *FEMS Microbiol. Ecol.* 59(1): 4763. xx : 1–11.
- [4] Taylor, M.W., Radax, R., Steger, D., and Wagner, M. 2007. Sponge associated microorganisms: evolution, ecology, and biotechnological potential. *Microbiol. Mol. Biol. Rev.* 71: 295.
- [5] Haygood, M.G., Schmidt, E.W., Davidson, S.K., and Faulkner, D.J. 1999. Microbial symbionts of marine invertebrates: opportunities for microbial biotechnology. *Mol. Microbiol. and Biotechnology*. 1(1):3343.
- [6] Ruiz-Torres, V., Encinar, J.A., Herranz-López, M., Pérez-Sánchez, A., Galiano, V., Barrajón-Catalán, E., and Micol, V. (2017). An Updated Review on Marine Anticancer Compounds: The Use of Virtual Screening for the Discovery of Small-Molecule Cancer Drugs
- [7] Tran, T.D., Pham, N. B., Fechner, G. A., Hooper, J.N.A and Quinn, R.J. (2014). Potent Cytotoxic Peptides from the Australian Marine Sponge *Pipestela candelabra*. *Mar. Drugs* 2014, 12, 3399-3415; doi: 10.3390/md12063399
- [8] Vargas, S., Schuster, A. Sacher, K., Buttner, G., Schatzle, S., Lauchli, B., Hall, K., Hooper, J. N. A., Erpenbeck, D., Worheide, G. (2012) Barcoding Sponges: An Overview Based on Comprehensive Sampling. *PLoS ONE* 7(7): e39345. doi:10.1371/journal.pone.0039345
- [9] Cardenas, P., Xavier, J.R., Reveillaud, J., Schander, C., and Rapp, H. T. (2011). Molecular Phylogeny of the Astrophorida (Porifera, Demospongiae) Reveals an Unexpected High Level of Spicule Homoplasy. *PLoS ONE* April 2011: Vol 6: Issue 4 / e18318
- [10] Worheide, G., Erpenbeck, D., and Menke, C. 2007. The Sponge barcoding project: aiding in the identification and description of poriferan taxa. *Porifera research: Biodiversity, innovation and sustainability*: 123128.
- [11] Trivedi, S., Aloufi, A. A., Ansari, A. A., Ghosh S. K. (2015). Role of DNA barcoding in marine biodiversity assessment and conservation: An update. *Saudi Journal of Biological Sciences* (2016) 23, 161–171.
- [12] Meyer, C.P., Geller, J.B., and Paulay, G. 2005. Fine scale endemism on coral reefs: Archipelagic differentiation in turbinid gastropods. *Evolution*. 59: 113125.

- [13] Webster NS, Taylor MW (2011) Marine sponges and their microbial symbionts: love and other relationships. *Environmental Microbiology* 14: 335–346.
- [14] Erpenbeck D, Breeuwer J, van der Velde H, van Soest R (2002) Unravelling host and symbiont phylogenies of halichondrid sponges (Demospongiae, Porifera) using a mitochondrial marker. *Marine Biology* 141: 377–386.
- [15] Erpenbeck D, Van Soest RWM (2007) Status and perspective of sponge chemosystematics. *Mar Biotechnol* 9: 2–19.
- [16] Chelossi E, Milanese M, Milano A, Pronzato R, Riccardi G (2004). Characterisation and antimicrobial activity of epibiotic bacteria from *Petrosia ficiformis* (Porifera, Demospongiae). *Journal of experimental marine biology and ecology* 309: 21–33.
- [17] Talpir, R.; Benayahu, Y.; Kasman, Y.; Pannell, L.; Schleyer, M. Hemiasterlin and Geodiamolide TA; Two new cytotoxic peptides from the marine sponge *Hemiasterella minor* (Kirkpatrick). *Tetrahedron Lett.* 1994, 35, 4453–4456.
- [18] Nieman, J.A.; Coleman, J.E.; Wallace, D.J.; Piers, E.; Lim, L.Y.; Roberge, M.; Andersen, R.J. Synthesis and antimitotic/cytotoxic activity of hemiasterlin analogues. *J. Nat. Prod.* 2003, 66, 183–199.
- [19] Kowalczyk, J.J.; Kuznetsov, G.; Schiller, S.; Seletsky, B.M.; Spyvee, M.; Yang, H. Hemiasterlin Derivatives and Uses Thereof. US Patent US7,192,972B2, 20 March 2007.
- [20] Campagna, S.A.; Fang, F.G.; Kowalczyk, J.J.; Schiller, S.; Seletsky, B.M.; Spyvee, M.; Yang, H. Hemiasterlin Derivatives and Uses Thereof. US Patent US7, 585,976B2, 8 September 2009.
- [21] Newman, D.J.; Cragg, G.M. Marine Natural Products and Related Compounds in Clinical and Advanced Preclinical Trials. *J. Nat. Prod.* 2004, 67, 1216–1238.
- [22] Zheng, L. H., Wang, Y. J., Sheng, J., Wang, F., Zheng, Y., Lin, X. K. and Sun M. (2011). Antitumor Peptides from Marine Organisms. *Mar. Drugs* 2011, 9, 1840-1859; doi: 10.3390/md9101840
- [23] Nurul Hanani, M.S., Mohd Azrul, N., Tengku Haziyaamin, T. A. H., Fahrul, H., Azzmer Azzar, A. H. (2015). Isolation and identification of 3-chloropropionic acid degrading bacterium from marine sponge. *Jurnal Teknologi (Sciences & Engineering)* 77:25 (2015) 71–75
- [24] Habsah M, Zalilawati M. R., Khozirah S., Jalifah L., Md. Nordin H. L. and Abd. Manaf A. (2009). Antibacterial and DPPH Free Radical-Scavenging Activities of Methanolic Extracts of *Aaptos* sp. (Marine Sponges). *Pertanika J. Trop. Agric. Sci.* 32(1): 43 - 50 (2009).
- [25] Jasnizat Saidin, Siti Aisha, M. R., Yosie, A., Habsah, M., and Tengku Siffizul, T. M., (2015). In-vitro anti inflammatory activities of extracts from bacteria associated with marine sponge: *Theonella* sp. *Jurnal Teknologi (Sciences & Engineering)* 77:25 (2015) 165–169.
- [26] Habsah M., Wan Ainur N. W. A. J., Faridah A., Khamsah Suryati M. and Abdul Manaf A. Octacosanoic Acid, Long Chains Saturated Fatty Acid from the Marine Sponges *Xestospongia* sp.
- [27] Nukes, M. A., Ida Muryany, M. Y., Fatimah, H., Nor Fadilah, R., Zalilawati, M. R., Khamsah, S., and Habsah, M. (2011). Anti-amoebic properties of a Malaysian marine sponge *Aaptos* sp. on *Acanthamoeba castellanii*.

MEDICAL CANNABINOIDS AS PROMISING THERAPEUTICS IN MAINSTREAM MEDICINE

Samson Soon; Lenny Chong; Noor Inayah Ya'akub; Sai-Keong Chan; Chee Fai Tan & Khai Mun Ng².

Infrastructure University Kuala Lumpur³.

1. INTRODUCTION

Cannabis or marijuana is one of the earliest cultivated plants in human history. It is a multi-purpose crop with many industrial applications ranging from paper production, wood, fibre, food and more importantly therapeutics and medicines. *Cannabis sativa* L. is currently one of the world's most important medicinal plant. Traditionally, the cannabis plant has been used to treat diseases such as asthma, epilepsy, fatigue, glaucoma, pain, and rheumatism (Chandra *et al.*, 2020). Today, cannabis is in great demand for its medicinal properties that stem from the various secondary metabolites such as terpenoids, flavonoids, sterols and abundant phytochemicals or cannabinoids. Despite these potentials, the cannabis plant has been subjected to strict regulations globally due to its narcotic effects which are due to the psychoactive agent Δ^9 -tetrahydrocannabinol (THC). This compound is produced as an acid (Δ^9 -tetrahydrocannabinolic acid) in the cannabis plant and undergoes decarboxylation with age or when heated to form THC. The other important medicinal compound in cannabis is the non- psychoactive cannabidiol (CBD). CBD is currently the subject of intense research for broad therapeutic and medical use.

Non-psychoactive cannabis or hemp in general plays an important role as the variant contains very low THC but high cannabidiol (CBD) content. The high demand for CBD has made it an extremely high-value crop. The global cannabidiol market size was valued at USD 5.18 billion in 2021 and is expected to expand at a compound annual growth rate (CAGR) of about 16.8% from 2022 to 2030 (Grand View Research, 2022). The CBD market growth is expected to be driven by the increasing demand for cannabidiol (CBD) in the medical and wellness segment. Numerous industries ranging from pharmaceuticals, personal care and cosmetics, nutraceuticals, and even food and beverages are developing CBD-derived products for health and wellness purposes.

The global medicinal cannabis market was estimated at USD 25.7 billion in 2021 and is expected to reach USD 176 billion by 2030 at a CAGR of 23.9%, 2021-2030 (Business Wire, 2022). In 2021, North America dominated the global market with a revenue share of over 85% and will continue to retain its leading position in the market. The growing acceptance of CBD-based products, the presence of major manufacturers, and approval of the U.S. Farm Bill in 2020 will continue to drive the global market. However, regions like Europe and the Asia Pacific are projected to witness significant growth as cannabis propagation increases in countries like China. Currently, China is the largest cannabis cultivator in Asia, producing nearly half of the world's supply. It exports around 90% of its products to the U.S., Germany, the United

Kingdom, the Netherlands, and Japan (Grand View Research, 2022).

Cannabis has been used medicinally for millennia. Cannabis extract was used to treat a variety of conditions such as malaria, gout, rheumatic pain and muscle spasms since 5,000 years ago by the ancient Chinese (Russo, 2017). The cannabis plant was also used as an analgesic, hypnotic, tranquilliser and anti-inflammatory compound in India 3,000 years ago (Touw, 1981). Since the 17th century, physicians have recommended the use of cannabis extracts to ally inflammation (Ryz et al., 2017). Research in the therapeutic use of medicinal cannabis however was largely ignored due to its narcotic properties and strict legislation as an illicit drug. Once the psychoactive THC component in cannabis was identified and the medicinal CBD compound elucidated, a rapid change of policies was observed globally, paving the way for increased access to medicinal cannabis supply and treatments.

The demand for cannabis-derived CBD products has increased substantially as scientific data continues to demonstrate many health benefits such as anti-inflammatory, anti-ageing, and antioxidant properties. And CBD therapeutic potential has been investigated for cardiovascular, cancer, neurodegenerative, and metabolic diseases. An important therapeutic target for CBD is to treat chronic inflammation. Unresolved inflammation from acute, chronic, or auto-inflammatory conditions can lead to serious complications such as organ function failure. CBD anti-inflammatory properties have been extensively studied and has demonstrated efficacy in modulating the molecular inflammation processes in numerous pre-clinical and clinical trials. Despite these strong scientific evidences, the use of CBD in modern medicine for chronic inflammation therapeutics is still lacking and largely unnoticed.

2. CANNABIS PLANT BIOLOGY AND GENETICS

Cannabis sativa L. has a diploid genome ($2n = 20$) with an estimated size of 818 MB for female plants and 843 MB for males. The plant has an upright stem and can grow between 1–6 m high, according to its phenotype and chemical type. The plant roots can reach 2.5 m deep with a well-developed lateral root. The leaves are palmate with a varying number of leaflets. The surface of the leaf has white to yellowish resinous glands. Cannabis flowers are divided into staminate (male) or pistillate (female) (Figure 1). The plants are hermaphroditic or dioecious following their genetic factors or the environment they are grown in.



Figure 1 : The anatomy of a cannabis plant (Scholl, 2019)

The genome is composed of nine pairs of autosomes and a pair of sex chromosomes (X and Y) (Romanova *et al.* 2016). Sex determination mechanics in cannabis plants are still poorly understood because other than genetic elements, they are affected by environmental conditions such as stress and chemical treatments (Lynch *et al.*, 2016). However, pollination from the male plant has been reported to lower cannabinoid yield by 50% (Meier and Mediavilla, 1998). This has led growers to use only feminised seeds or clones of female plants for propagation works. The use of seeds in the commercial production of cannabis plants is still popular due to their lower costs.

The complete growth cycle of the cannabis plant can be divided into four distinct stages. The first stage is seed germination which will normally take 1- 2 weeks. The second stage involves the seedling stage which will take another 2 - 3 weeks. Stage 3 is where the plant's vegetative growth takes place. The plant will continue to grow rapidly through its stems and leaves and will take about 2 – 8 weeks to complete. The growth cycle will enter the final stage of the cycle called flowering whereby a total of 6 – 8 weeks are required for completion before it can be harvested and processed. The cannabis flowers will be covered by tiny crystal-like structures or frost that are called trichomes. The trichomes function as tiny resin glands that hold all the powerful phytochemicals responsible for their medicinal values (Figures 2 & 3).

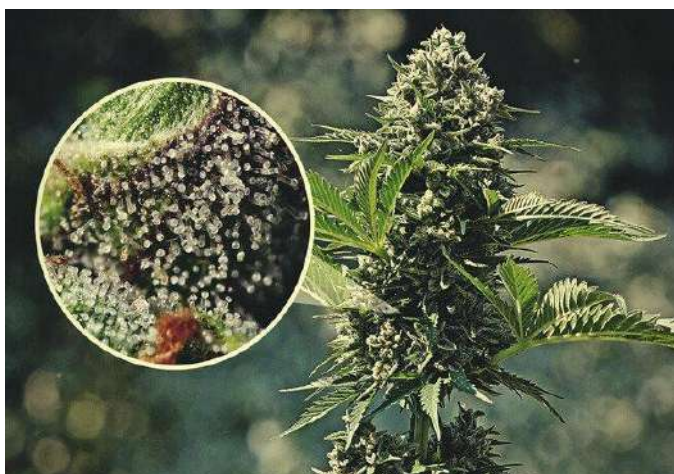


Figure 2 : Crystal-like structures called trichomes on a cannabis plant (Royal Seeds, 2022).



Figure 3 : A close-up image of a cannabis plant's trichomes (Philosopher Seeds, 2022).

3. CANNABIS CANNABINOIDS

The cannabis plant contains an abundant source of phytochemical compounds. More than one thousand compounds, i.e., 278 cannabinoids, 174 terpenes, 221 terpenoids, 19 flavonoids, 63 flavonoid glycosides, 46 polygons, 92 steroids have so far been identified (Radwan *et al.*, 2017). The major cannabinoids in cannabis include THC, CBD, and CBC (cannabichromene), their precursor CBG (cannabigerol) and cannabinol (CBN). To date, 10 CBN-type, 17 CBG-type, 8 CBD-type, and 18 THC-type cannabinoids have been isolated. The central precursor for the biosynthesis of psychoactive THC and non-psychoactive CBD is cannabigoleic acid (CBGA) (Hussain *et al.*, 2021).

THC, CBD, cannabinol (CBN), cannabigerol (CBG) and cannabichromene (CBC) are cannabis phytocannabinoids that have been well characterised. These cannabinoids are present as precursors generally referred to as tetrahydrocannabinolic acid (THCA), cannabidiolic acid

(CBDA), cannabigerolic acid (CBGA), and cannabichromenic acid (CBCA), respectively. A conversion of THCA, CBDA, CBGA, and CBCA to THC, CBD, CBN, CBG, and CBG, respectively through decarboxylation is required for before the compounds are biologically active. Decarboxylation of these carboxylic acids can be achieved using heat above 105 °C, when cannabis is smoked or baked (Maayah et al., 2020).

Delta-9-tetrahydrocannabinol (THC), is a major psychotropic cannabinoid, which causes transient psychotic, and anxiety symptoms. The biological activity of THC is mediated primarily through the activation of CB1 and CB2 receptors with preferential binding to CB1 receptors (Parcher et al., 2006). The major unwanted physiological effect of THC is cognitive impairment dysfunction, in particular short-term memory loss (Misner & Sullivan, 1999).

Whereas cannabidiol (CBD), which is not psychotropic is linked to many health benefits such as treatment for inflammation, pain, emesis, appetite, obesity, gastro-intestine, anxiety, schizophrenia and psychosis, depression post-traumatic stress, multiple sclerosis, epilepsy, hepatic, neurological and neurodegenerative disorders as well as Alzheimer's disease; further, cannabinoids possess antispastic, antineoplastic, anticancer and antiemetic activity (Kiskova *et al.*, 2019, Bonini *et al.*, 2018, Ligresti *et al.*, 2009, Romero *et al.*, 2020). CBD also promotes neuronal inhibition and anti-epileptic effects through adenosine A1 receptors and gamma-aminobutyric acid A (GABA-A) dependent mechanisms (Ibeas Bih et al, 2015). The potential benefits of CBD are extensive and are independent of the endocannabinoid receptors effected by THC.

Cannabinol (CBN) is closely related to CBD in terms of the chemical structure. It also shares similar effects with CBD such as anti-inflammatory activities. The major difference however is that CBN physiological effect is modulated through the CB2 receptor (Maayah et al., 2020). Cannabichromene (CBC) is a major phytocannabinoid that does not bind to CB1 and CB2 endocannabinoid receptors (De Long et al., 2010). However similar to CBD, it possesses anti-inflammatory properties viz. the inhibition of the cyclooxygenase enzyme and associated prostaglandins. Cannabigerol (CBG) is particularly interesting as it only exist in trace amounts but is a precursor compound of THC, CBD and CFC. Although it does not follow the usual CB receptor binding, it can still reduce pain, erythema and inflammation through the inhibition of peripheral lipoxygenase enzyme and the activation of central α 2-adrenergic receptor (Evans, 1991).

These breakthroughs in cannabis cannabinoid research have led to the development of new drugs such as Nabiximols (trade name Sativex®) (multiple sclerosis), Epidiolex® (epilepsy), Dronabinol (MARINOL®) and Nabilone (CESAMET™) (nausea and vomiting). More CBD-based drugs are being developed as the positive effects of cannabinoids are unraveled (Figure 4).

Cannabis phytochemicals have also exhibited tremendous therapeutic benefits against COVID-19 infection. Phytocannabinoids especially CBD have demonstrated a remarkable anti-inflammatory effect that would limit the overproduction of pro-inflammatory cytokines called cytokine storms during severe COVID-19 that leads to high cases of mortality among COVID-

19 patients (Esposito *et al.*, 2020). Pre-clinical studies using full-spectrum cannabis extract have shown several convincing and beneficial anti-inflammatory and analgesic effects by modulating the binding of endogenous endocannabinoids. Thus, full-spectrum cannabis extract represents a promising therapeutic agent against a variety of medical disorders associated with pain and inflammation.

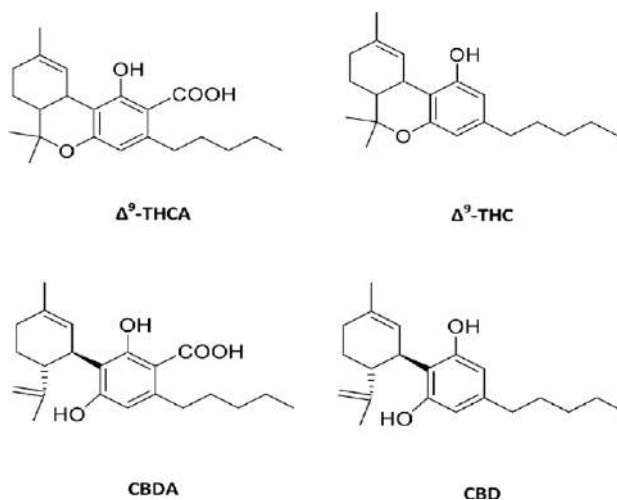


Figure 4 : Chemical structures of the major cannabinoids.

4. THE ENDOCANNABINOID SYSTEM

The endocannabinoid system (ECS) is a modulator of many physiological and pathological activities such as pain, immune response, appetite, thermoregulation, energy metabolism, depression, memory and fertility (Di Marzo *et al.*, 1998). Regulation impairment of ECS will lead to various pathological conditions such as inflammation. However, the ECS can be managed therapeutically against various medical conditions such as chronic inflammation. This is achieved by modulating various receptors in the ECS system that includes cannabinoid receptors types 1 and 2 (CB1 and CB2, respectively) and other non-cannabinoid receptors such as the peroxisome proliferator-activated receptors (PPARs) and ion channels (e.g., the transient receptor potential ankyrin [TRPA] family and the transient receptor potential vanilloid [TRPV] family) (Biringner, 2021). The endogenous cannabinoids or ligands to these receptors are anandamide and 2-arachidonoylglycerol (Devane *et al.*, 1992).

The cannabinoid CB1 and CB2 receptors are expressed in immune cells. CB1 receptors are widely expressed throughout the central nervous system for which they are responsible for the psychoactive and analgesic effects of THC. The CB2 receptors however are expressed mainly in peripheral tissues. CB2 receptors are also expressed 10–100 times higher than CB1 in these cells in which they directly control anti-inflammatory responses (Rahaman and Ganguly, 2021). The activation of CB2 receptors by its agonist directly inhibits the release of the pro-inflammatory cytokine IL-12 and IL-23 and enhanced the release of the anti-inflammatory cytokine IL-10

from cultured activated macrophages. This study suggested that the inhibitory effect of CB2 on IL-12 production was mediated by ERK1/2- MAPK (Correa et al., 2009). The activation of peripheral CB2 receptors also blocks pain transduction signal to the central nervous system (Valenzano et al., 2005).

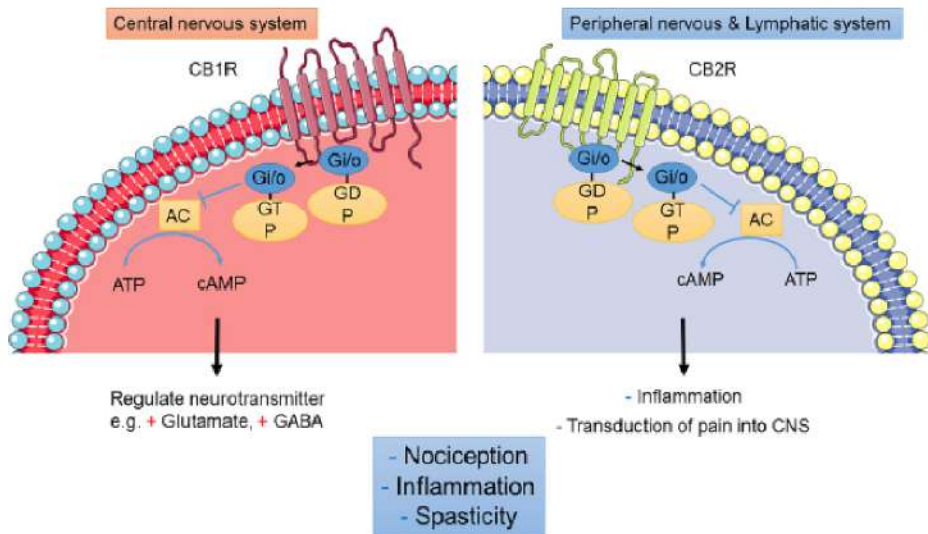


Figure 2. Proposed anti-nociceptive and anti-inflammatory mechanism of cannabinoid receptors (Maayah et al., 2020).

5. CONCLUSION

CBD is the most studied cannabinoid and has led to the approval as medicines for the treatment of epilepsy in Lennox-Gastaut and Dravet syndromes in young children and seizures caused by rare tumors in the brain. CBD has a huge potential to treat other diseases as evident from the many clinical trials and investigation presently underway. Similarly, other cannabinoids i.e, cannabichromene (CBC), cannabidivarin (CBDV), tetrahydrocannabivarin (THCV), and cannabigerol (CBG) have also been found to have potentials in treating a wide range of clinical conditions where clinical trials are currently in progress (Khalsa et al., 2022).

Cannabinoids have the capacity to be integrated into mainstream medicine as preliminary and clinical research have shown efficacy in treating a wide range of clinical conditions. Medical cannabinoids can be used to treat neuroinflammation, inflammatory cytokines, psychosis, fibrosis, and immunomodulation, seizures/epilepsy in adults, schizophrenia, obesity, nausea, neuropathy, retinopathy nephropathy, pain, and dermal conditions like dermatitis and acne. The complex cannabinoid properties from the cannabis plant are amazing and warrants its legalization globally for its huge medicinal benefits.

REFERENCES

- Biringer, R. G. (2021). Endocannabinoid signaling pathways: Beyond CB1R and CB2R. *Journal of cell communication and signaling*, 15(3), 335-360.
- Bonini, S. A., Premoli, M., Tambaro, S., Kumar, A., Maccarinelli, G., Memo, M., & Mastinu, A. (2018). Cannabis sativa: A comprehensive ethnopharmacological review of a medicinal plant with a long history. *Journal of ethnopharmacology*, 227, 300-315.
- Business Wire (2022, February). Global Cannabis Market Size & Forecast Report 2021: A \$176 Billion by 2030 - Growing Legalization of Medical Cannabis in Various Countries Driving Growth. www.businesswire.com/news/home/20220203005879/en/Global-Cannabis-Market-Size-Forecast-Report-2021-A-176-Billion-by-2030---Growing-Legalization-of-Medical-Cannabis-in-Various-Countries-Driving-Growth-ResearchAndMarkets.com
- Chandra, S., Lata, H., & ElSohly, M.A. (2020). Propagation of Cannabis for Clinical Research: An Approach Towards a Modern Herbal Medicinal Products. *Frontiers in Plant Science*, 11, 958.
- Chesney, E., Oliver, D., Green, A., Sovi, S., Wilson, J., Englund, A., ... & McGuire, P. (2020). Adverse effects of cannabidiol: a systematic review and meta-analysis of randomized clinical trials. *Neuropsychopharmacology*, 45(11), 1799-1806.
- Correa, F., Docagne, F., Mestre, L., Clemente, D., Hernangómez, M., Loría, F., & Guaza, C. (2009). A role for CB2 receptors in anandamide signalling pathways involved in the regulation of IL-12 and IL-23 in microglial cells. *Biochemical pharmacology*, 77(1), 86-100
- DeLong, G. T., Wolf, C. E., Poklis, A., & Lichtman, A. H. (2010). Pharmacological evaluation of the natural constituent of Cannabis sativa, cannabichromene and its modulation by Δ^9 -tetrahydrocannabinol. *Drug and alcohol dependence*, 112(1-2), 126-133.
- Devane, W. A., Hanuš, L., Breuer, A., Pertwee, R. G., Stevenson, L. A., Griffin, G., ... & Mechoulam, R. (1992). Isolation and structure of a brain constituent that binds to the cannabinoid receptor. *Science*, 258(5090), 1946-1949.
- Di Marzo, V., Melck, D., Bisogno, T., & De Petrocellis, L. (1998). Endocannabinoids: endogenous cannabinoid receptor ligands with neuromodulatory action. *Trends in neurosciences*, 21(12), 521-528.
- Evans, F. J. (1991). Cannabinoids: the separation of central from peripheral effects on a structural basis. *Planta medica*, 57(S 1), S60-S67.
- Esposito, G., Pesce, M., Seguella, L., Sanseverino, W., Lu, J., Corpetti, C., & Sarnelli, G. (2020). The potential of cannabidiol in the COVID-19 pandemic. *British journal of pharmacology*, 177(21), 4967-4970.
- Grand View Research (2022). Cannabidiol Market Size, Share & Trends Analysis Report By Source Type (Hemp, Marijuana), By Distribution Channel (B2B, B2C), By End-use (Medical, Personal Use), By Region, And Segment Forecasts, 2022 – 2030. GVR-3-68038-122-. 132 pp.
- Hackel, A., Aksamit, A., Bruderek, K., Lang, S., & Brandau, S. (2021). TNF- α and IL-1 β sensitize human MSC for IFN- γ signaling and enhance neutrophil recruitment. *European Journal of Immunology*, 51(2), 319-330.

- Harirforoosh, S., Asghar, W., & Jamali, F. (2013). Adverse effects of nonsteroidal antiinflammatory drugs: an update of gastrointestinal, cardiovascular and renal complications. *Journal of Pharmacy & Pharmaceutical Sciences*, 16(5), 821-847.
- Hesami, M., Pepe, M., Alizadeh, M., Rakei, A., Baiton, A., & Jones, A. M. P. (2020). Recent advances in cannabis biotechnology. *Industrial Crops and Products*, 158, 113026.
- Hussain, T., Jeena, G., Pitakbut, T., Vasilev, N., & Kayser, O. (2021). Cannabis sativa research trends, challenges, and new-age perspectives. *Iscience*, 24(12), 103391.
- Ibeas Bih, C., Chen, T., Nunn, A. V., Bazelot, M., Dallas, M., & Whalley, B. J. (2015). Molecular targets of cannabidiol in neurological disorders. *Neurotherapeutics*, 12(4), 699-730.
- Khalsa, J. H., Bunt, G., Blum, K., Maggirwar, S. B., Galanter, M., & Potenza, M. N. (2022). Cannabinoids as Medicinals. *Current addiction reports*, 1-17.
- Kisková, T., Mungenast, F., Suváková, M., Jäger, W., & Thalhammer, T. (2019). Future aspects for cannabinoids in breast cancer therapy. *International journal of molecular sciences*, 20(7), 1673.
- Ligresti, A., Petrosino, S., & Di Marzo, V. (2009). From endocannabinoid profiling to 'endocannabinoid therapeutics'. *Current opinion in chemical biology*, 13(3), 321-331.
- Lynch, R.C., Vergara, D., Tisttes, S., White, K., Schwartz, C.J., Gibbs, M.J., Ruthenburg, T.C., deCesare, K., Land, D.P., & Kane, N.C. (2016). Genomic and Chemical Diversity in *Cannabis*, *Critical Reviews in Plant Sciences*, 35:5-6, 349-363, DOI: 10.1080/07352689.2016.1265363
- Market watch (2022. September). Anti-inflammatory Therapeutics Market Size 2022: New Business Prospects by Identifying Trends and Driving Forces and Forecast up to up to 2028. <https://www.marketwatch.com/press-release/anti-inflammatory-therapeutics-market-size-2022-new-business-prospects-by-identifying-trends-and-driving-forces-and-forecast-up-to-2028-104-report-pages-2022-09-18>
- Maayah, Z. H., Takahara, S., Ferdaoussi, M., & Dyck, J. R. (2020). The molecular mechanisms that underpin the biological benefits of full-spectrum cannabis extract in the treatment of neuropathic pain and inflammation. *Biochimica et Biophysica Acta (BBA)-Molecular Basis of Disease*, 1866(7), 165771.
- Meier, C. & Mediavilla, C. (1998). Factors influencing the yield and the quality of hemp (*Cannabis sativa* L.) essential oil. *J. Int. Hemp Assoc*, 5(1), 16-20.
- Misner, D. L., & Sullivan, J. M. (1999). Mechanism of cannabinoid effects on long-term potentiation and depression in hippocampal CA1 neurons. *Journal of Neuroscience*, 19(16), 6795-6805.
- Pacher, P., Bátkai, S., & Kunos, G. (2006). The endocannabinoid system as an emerging target of pharmacotherapy. *Pharmacological reviews*, 58(3), 389-462.
- Parisien, M., Lima, L. V., Dagostino, C., El-Hachem, N., Drury, G. L., Grant, A. V., ... & Diatchenko, L. (2022). Acute inflammatory response via neutrophil activation protects against the development of chronic pain. *Science Translational Medicine*, 14(644), eabj9954.
- Perez, E., Fernandez, J. R., Fitzgerald, C., Rouzard, K., Tamura, M., & Savile, C. (2022). In Vitro and Clinical Evaluation of Cannabigerol (CBG) Produced via Yeast Biosynthesis: A Cannabinoid with a Broad Range of Anti-Inflammatory and Skin Health-Boosting Properties. *Molecules*, 27(2), 491.

- Philosopher Seeds. (N.D). The Cannabis Trichomes.
<https://www.philosopherseeds.com/blog/en/cannabis-trichomes/>
- Radwan, M. M., Wanas, A. S., Chandra, S., & ElSohly, M. A. (2017). Natural cannabinoids of cannabis and methods of analysis. In *Cannabis sativa L.-botany and biotechnology* (pp. 161-182). Springer, Cham.
- Rahaman, O., & Ganguly, D. (2021). Endocannabinoids in immune regulation and immunopathologies. *Immunology*, *164*(2), 242-252.
- Romanova, O.V., Alexandrov, O.S., Divashuk, M.G., Sukhorada, I.S., & Karlov, G.I. (2016). Molecular cytogenetic analysis of monoecious hemp (*Cannabis sativa* L.) cultivars reveals its karyotype variations and sex chromosomes constitution. *Protoplasma*, *253*, 895-901.
- Romero-Zerbo, S. Y., García-Fernández, M., Espinosa-Jiménez, V., Pozo-Morales, M., Escamilla-Sánchez, A., Sánchez-Salido, L., ... & Bermúdez-Silva, F. J. (2020). The atypical cannabinoid Abn-CBD reduces inflammation and protects liver, pancreas, and adipose tissue in a mouse model of prediabetes and non-alcoholic fatty liver disease. *Frontiers in Endocrinology*, *11*, 103.
- Royal Queen Seeds. (N.D.) Complete Guide To The Cannabis Flowering Phase.
<https://www.royalqueenseeds.com/content/46-the-blooming-phase>.
- Russo, E. B. (2017). Cannabis and epilepsy: An ancient treatment returns to the fore. *Epilepsy & Behavior*, *70*, 292-297.
- Ryu, B. R., Kim, C. H., Kwon, T. H., Han, J. H., Gim, G. J., Jahirul Islam, M., ... & Lim, Y. S. (2022). Industrial Hemp Clone Selection Method under LED Smart Farm Condition Based on CBD Production per Cubic Meter. *Agronomy*, *12*(8), 1809.
- Ryz, N. R., Remillard, D. J., & Russo, E. B. (2017). Cannabis roots: a traditional therapy with future potential for treating inflammation and pain. *Cannabis and cannabinoid research*, *2*(1), 210-216.
- Scholl, L. (2019). Cannabis Anatomy: Getting To Know The Cannabis Plant. Zamnesia.
<https://www.zamnesia.com/grow-weed/446-cannabis-plant-anatomy>.
- Touw, M. (1981). The religious and medicinal uses of Cannabis in China, India and Tibet. *Journal of psychoactive drugs*, *13*(1), 23-34.
- Valenzano, K. J., Tafesse, L., Lee, G., Harrison, J. E., Boulet, J. M., Gottshall, S. L., ... & Whiteside, G. T. (2005). Pharmacological and pharmacokinetic characterization of the cannabinoid receptor 2 agonist, GW405833, utilizing rodent models of acute and chronic pain, anxiety, ataxia and catalepsy. *Neuropharmacology*, *48*(5), 658-672.

GLUCAGON-LIKE PEPTIDE-1 (GLP-1) EFFECTS ON TYPE 2 DIABETES MELLITUS (T2DM)-INDUCED 3T3-L1 ADIPOCYTES

Noor Mazuin Abu Bakar¹, Shatrah Othman² & Kavitha Rajagopal³

¹Infrastructure University Kuala Lumpur (IUKL), Kajang, Selangor

²University of Malaya

³Universiti Teknologi MARA

1. INTRODUCTION

Glucagon-like peptide 1 (GLP-1) is a member of the incretin group hormone. It is produced by the L-cells of the intestines, serving as a postprandial communication messenger between the gut and other organs. It has numerous physiological roles, such as improving glucose-stimulated insulin secretion, enhancement of pancreatic β -cell proliferation, inhibition of glucagon release, and promotion of satiety. GLP-1 has attracted immense interest in research due to its potential anti-diabetic effects for the treatment of patients with Type-2 Diabetes Mellitus (T2DM). However, the direct effects of GLP-1 on adipocytes are poorly characterized. In this study, an *in vitro* model of a dexamethasone-induced T2DM 3T3-L1 mouse adipose cells was chosen to demonstrate the metabolic effects of GLP-1 treatment, and its actions on the cell's glucose uptake are reported.

2. METHODOLOGY

Cell line preparation

The 3T3-L1 adipose cell line of mouse origin was selected for the entire work of this study. Pre-adipocytes cell of 3T3-L1 cells was cultured in Pre-Adipocyte Expansion Medium (PM) consisting of Dulbecco's Modified Eagle Medium (DMEM) supplemented with 10% (v/v) bovine calf serum (BCS) and 1% (v/v) Penicillium-Streptomycin in T25 flask (surface area of 25 cm²) (Woon *et al.*, 2014; Yang & Xiong, 2012), incubated at 37 °C incubator supplemented with 5% CO₂ and 95% humidity. Medium changing was done every other day until cells reached confluency. Observation of the changes in morphology, size, number, and confluency of the cells was carried out every other day, and the image was captured by using an Inverted Microscope Nikon ECLIPSE TI-S.

T2DM induction

After 3T3-L1 cells have undergone differentiation and 90% of the cells stained with oil red O showed the presence of lipid droplets, cells were ready to be induced with T2DM. Induction of T2DM was carried out by exposing the differentiated adipocytes to a T2DM Induction Medium (TIM) consisting of 1.0 μ mol/L dexamethasone, 10 μ g/mL insulin, and 1% (v/v) Penicillin–streptomycin in DMEM for 48 hours. The medium was changed every 24 to 48 hours (Adam *et*

al., 2017; Sakoda *et al.*, 2000).

Treatment of Cells with GLP-1

Mature and T2DM-induced 3T3-L1 cells were used for treatment with GLP-1. Glibenclamide, an antidiabetic medicine called sulfonylurea is known for its effect in the reduction of glycemia, was used at a concentration of 2 nM as the positive control (Adam *et al.*, 2017; Hussein *et al.*, 2015; Kahn *et al.*, 2014), while normal and T2DM cells were used to compare the effect of GLP-1 at different concentrations. Untreated (UT) normal 3T3-L1 and T2DM 3T3-L1 cells were used as negative controls, maintained in Post-Differentiation Medium (PDM) and T2DM Induction Medium (TIM) respectively. For GLP-1 effects analysis, the cells were treated with the concentration of GLP-1 at 10 nM and 50 nM (Egan *et al.*, 1994). Treatment with GLP-1 was carried out by exposing the T2DM cells with GLP-1 in DMEM for 10 minutes for three times with medium change and washing with PBS at every interval (Baggio & Drucker, 2007).

Glucose Uptake Assay

Differentiated 3T3-L1 in a 96 well plate was induced to have T2DM condition and treated with GLP-1 Treatment Medium. In the last medium change, 100 μ L of 2-NBDG solution was added to the cell culture and incubated for 10 minutes. Then, the cell medium was aspirated and 200 μ L of cell-based assay buffer solution was added to each well. An amount of 100 μ L of Propidium iodide was also added at this step. Another 100 μ L of the cell-based assay was added again into each well and analysis was carried out immediately. The 2-NBDG uptake by cells was detected using the microplate reader to detect fluorescein excitation/emission = 485/535 nm. Propidium iodide fluoresces in dead cells only, with excitation/emission = 488/650 nm, so gating from the dead cells excluded them from the analysis. The effects of GLP-1 on glucose uptake in T2DM differentiated 3T3-L1 adipocytes were calculated as a relative comparison to T2DM 3T3-L1 cells (100%) (Adam *et al.*, 2017; Yang *et al.*, 2012).

Fluorescence Microscopy

To observe the glucose uptake and the nuclear region of the 3T3-L1 cells, two stainings were used; DAPI (4',6-diamidino-2-phenylindole) Nucleic Acid Stain (Invitrogen) and 2-NBDG (Cayman). After the Glucose Uptake Assay was carried out, the 2-NBDG stain was left attached to the cells. Then, the solution in the plate was drained. DAPI stock solution was diluted to 300 nM in PBS. Approximately 2 mL of the diluted DAPI staining solution was added to the plate until the cells were completely covered with the dye. Then the plate was incubated for 1-5 minutes. After incubation, the sample was then rinsed several times in PBS and excessive buffer from the plate was drained. The sample was viewed using a fluorescence microscope with appropriate filters. The intracellular fluorescence signals in the cells were observed at excitation/emission = 358 nm/461 nm for DAPI and excitation/emission = 475 nm/550 nm for 2-NBDG (Adam *et al.*, 2016). All images were viewed under Nikon Eclipse 80i microscope.

3. RESULT AND DISCUSSION

Cultivation of 3T3-L1 cells and T2DM induction

Observation on the cultivation of the 3T3-L1 cells was carried out to record changes in the size, growth, and confluency of the cells. On day 1, less than 10% of confluency was recorded. The cells appeared to attach to the surface of the T25 flask individually with a large distance between them. The spindle-like morphology was observed, with a less branched shape of the cells.

On day 3, the number of cells increased. The cells appeared to undergo elongation and the spindle-like structure was more obvious. The number of cells increased and some cells appeared to have a rounded center appearance. The increase in the number and size of the cells was made possible with the adequate amount of nutrients supplied and the elimination of waste during each medium changing as well as the suitable environment including provision of space for cell attachment, suitable humidity, temperature, and gaseous exchange.

Continuous observation from day 5 to day 7 showed a further increase in cell number, branches in the spindle-like morphology, and cell size. The morphology of the cells remained the same and new cells were seen to form and fill up the space between the existing cells. The 3T3-L1 pre-adipocytes reached confluency on day 9, where less space was seen between the cells. After allowing the cells to grow for 2 more days, the cells were ready for differentiation.

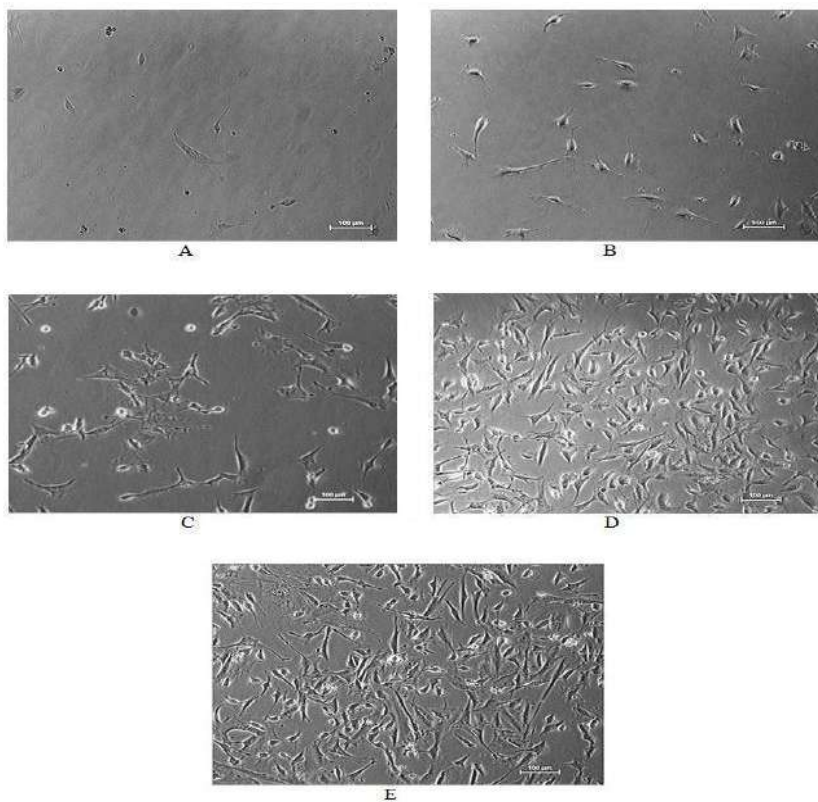


Figure 1: Images of 3T3-L1 Cells

(A) Day 1; 24 Hours, (B) Day 3, (C) Day 5, (D) Day 7, and (E) Day 9 after cell seeding. Magnification 40X.

Two days after the 3T3-L1 cells reached confluency, they were induced to differentiate using the differentiation mixture, or MDI mix, to produce mature 3T3-L1 adipocytes which were used in treatments and assays.

The addition of the MDI mix that contained methylisobutylxanthine, dexamethasone, and insulin has helped the cells to transform from their original fibroblastic pre-adipocyte to mature adipocytes. Figure 2 shows the lipid droplets in the mature adipocytes on day 6 post-differentiation. The lipid droplets were seen to fill the space in the center of the cells around the nuclear region. Some lipid droplets were also found in the branches of the spindle-like adipocytes. This observation confirmed that the cells have undergone differentiation into mature adipocytes and are ready to be used in assays and analysis.

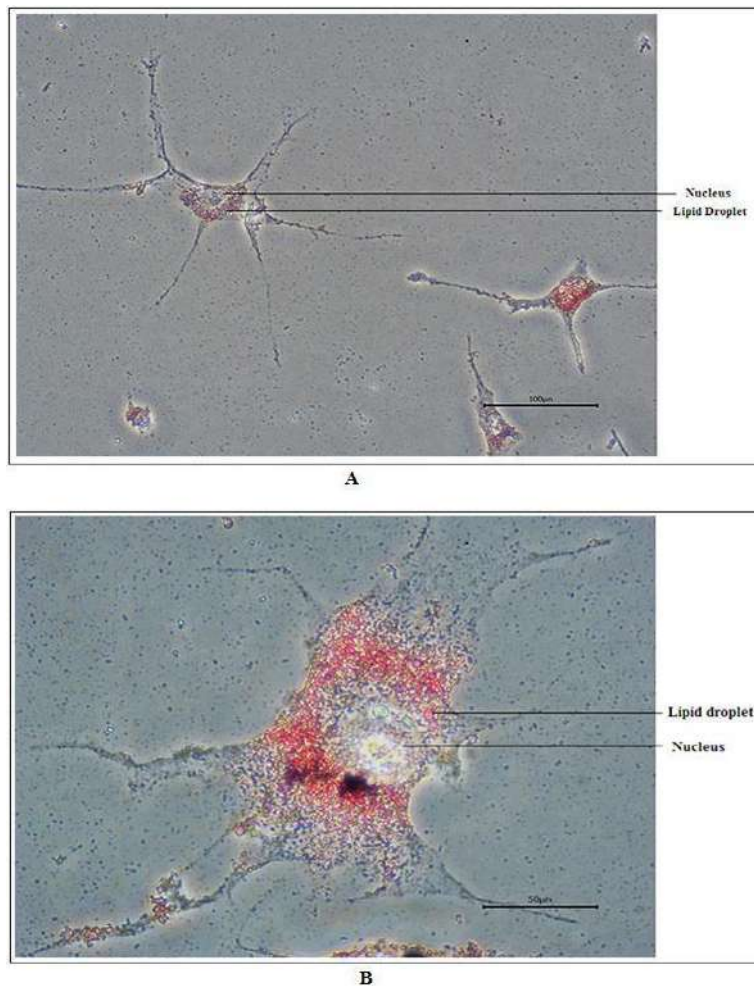


Figure 2: Post-differentiation Day 6. Magnification: 100X (A) and 200X (B).

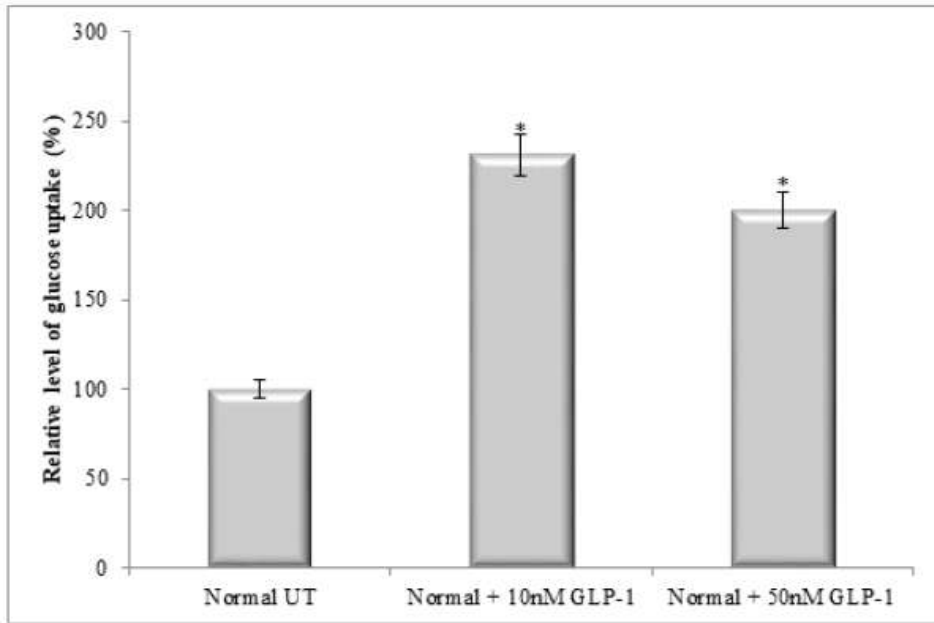
Glucose Uptake Assay

In glucose metabolism for T2DM, studying the cellular uptake of glucose is fundamental. Cells require glucose as their primary source of energy and biomaterials to maintain cellular homeostasis. Glucose uptake in cells is dynamic and it is tightly regulated by several factors such as hormones and growth factors. In this work, Glucose Uptake Cell-Based Assay Kit (Item No. 600470) from Cayman Chemical provides a convenient tool to study the modulators of cellular glucose uptake. The kit uses a direct detection of glucose taken up by cells with the employment of the fluorescently-labeled deoxyglucose analog 2-NBDG which acted as a probe for the detection of glucose taken up by cultured cells. The 2-NBDG uptake by cells was detected using the microplate reader to detect fluorescein at excitation/emission = 485/535 nm.

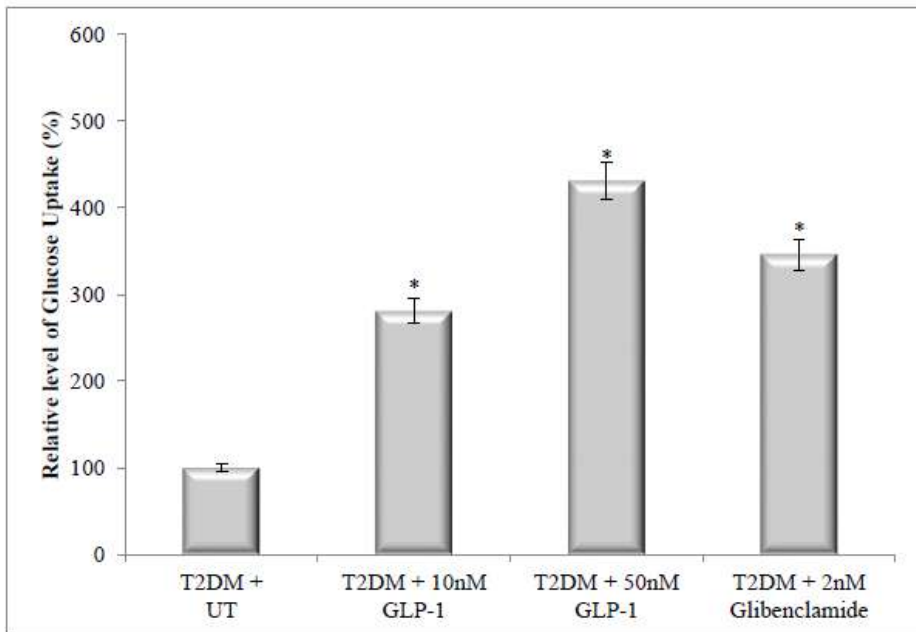
Figure 3 (A) shows the glucose uptake of normal 3T3-L1 cells; untreated and treated with two different concentrations of GLP-1. Untreated normal cells were assigned as 100%, as a reference, and any changes in the glucose uptake in the treated cells were recorded as relative to the reference. Significant values were observed in the 3T3-L1 normal cells treated with 10 nM and 50 nM GLP-1 as compared to the untreated normal cells (* $P < 0.05$).

On the other hand, Figure 3 (B) exhibited the glucose uptake of T2DM-induced 3T3-L1 cells; untreated and treated with two different concentrations of GLP-1 and 2 nM of glibenclamide. Glibenclamide-treated cells were used as a positive control in the assay. Untreated T2DM cells were assigned as 100%, as a reference, and any changes in the glucose uptake in the treated cells were recorded as relative to the reference.

In the T2DM-induced cells, T2DM cells treated with 10 nM and 50 nM GLP-1 as well as the 2 nM glibenclamide showed significant values as compared to the Untreated T2DM cells (* $P < 0.05$). The increments of glucose uptake in T2DM cells treated with GLP-1 are concentration-dependent.



(A) Normal Differentiated 3T3-L1 Adipocytes



(B) T2DM-induced Differentiated 3T3-L1 Adipocytes

Figure 3 : The Effects of GLP-1 on Glucose Uptake of 3T3-L1 Adipocytes. (A) Normal Differentiated 3T3-L1 Adipocytes and (B) T2DM-induced Differentiated 3T3-L1 Adipocytes.

Glucose Uptake Fluorescent Staining in 3T3-L1 Cells

To verify the glucose uptake by cells, cellular staining was carried out by using different dyes to stain the nuclei and glucose molecules in cells. DAPI Nucleic Acid Stain (Invitrogen) and 2-NBDG (Cayman) were used on the cells. DAPI staining dyed the nucleus region blue and 2-NBDG appeared green under THE fluorescent microscope to reflect the appearance of cellular glucose molecules. These dyes provided qualitative results on cell proliferation and its glucose uptake.

Figure 4 shows normal differentiated 3T3-L1 cells, untreated and treated with GLP-1, and they were stained with DAPI and 2-NBDG. Untreated normal cells were regarded as the negative control. Upon treatments with GLP-1, the regions stained blue had increased reflecting better proliferation of cells with an increased number of cells. With GLP-1 treatment too, the green glucose molecules also increased with more glucose uptake in 50 nM GLP-1 treated cells, indicating an amelioration of cellular glucose uptake in cells. The merged images compared cell proliferation with glucose uptake, where; as the number of nuclei increased, so does glucose uptake in the cells.

Figure 5 shows T2DM-induced differentiated 3T3-L1 cells, untreated and treated with GLP-1 as well as the positive control cells treated with 2 nM glibenclamide, and they were stained with DAPI and 2-NBDG. Untreated T2DM cells were regarded as the negative control. Upon treatments with GLP-1 and glibenclamide, the density of blue and green regions has increased reflecting better cell proliferation and glucose uptake. The increase was more obvious in the cells treated with 50 nM GLP-1 and 2 nM glibenclamide. The merged images confirmed the amelioration of cell proliferation and glucose uptake in the T2DM-induced 3T3-L1 cells.

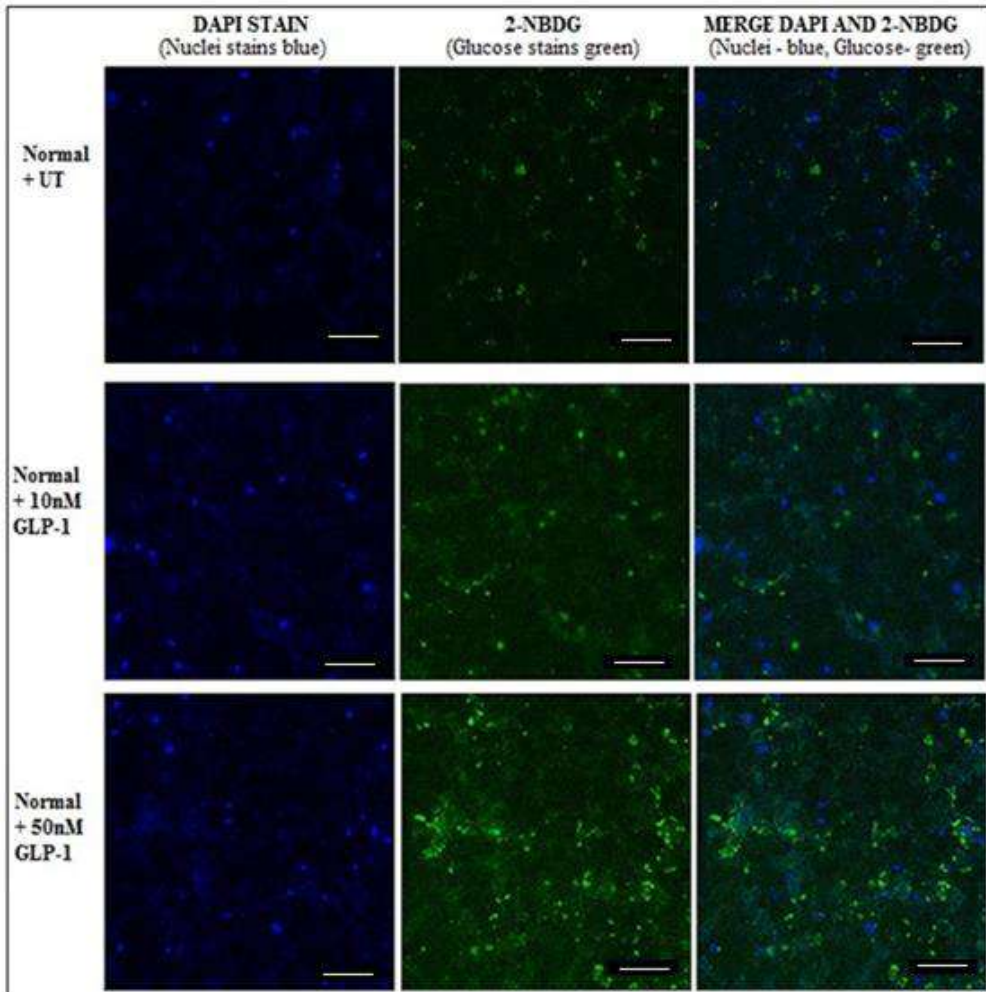


Figure 4: Glucose Uptake Fluorescent Staining in Normal Differentiated 3T3-L1 Cells. Scale bar: 20 μ m.

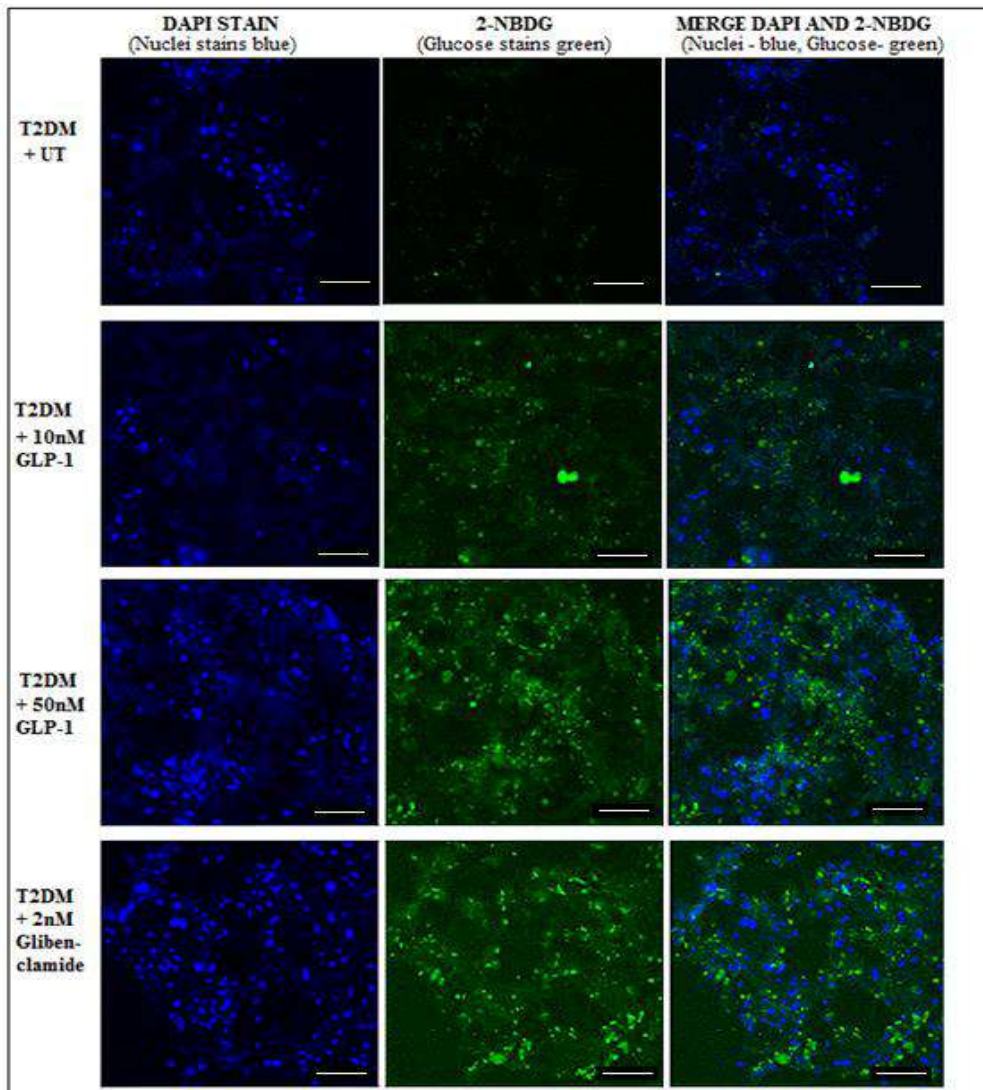


Figure 5: Glucose Uptake Fluorescent Staining in T2DM-Induced Differentiated 3T3-L1 Cells.
Scale bar: 20 μ m

4. CONCLUSION

5.

From the findings, GLP-1 has demonstrated ameliorative effects on the glucose metabolic process in 3T3-L1 cells. Thus, GLP-1 may have a potential role as an antidiabetic therapy in the treatment of T2DM, and other key markers in glucose metabolism studies are worthy of future investigation subjects.

6. ACKNOWLEDGEMENT

We thank the Ministry of Higher Education for funding this project through the Research Acculturation Collaborative Effort (RACE) grant, and the Department of Molecular Medicine, University of Malaya for their outstanding support.

REFERENCES

- Adam, S. H., Giribabu, N., Abu Bakar, N. M., & Salleh, N. (2017). *Marantodes pumilum* (Kacip fatimah) enhances in-vitro glucose uptake in 3T3-L1 adipocyte cells and reduces pancreatic complications in streptozotocin-nicotinamide induced male diabetic rats. *Biomedicine & Pharmacotherapy*, 96, 716–726. <https://doi.org/10.1016/j.biopha.2017.10.042>
- Adam, S. H., Giribabu, N., Rao, P. V., Sayem, A. S. M., Arya, A., Panichayupakaranant, P., & Salleh, N. (2016). Rhinacanthin C ameliorates hyperglycaemia, hyperlipidemia and pancreatic destruction in streptozotocin-nicotinamide induced adult male diabetic rats. *European Journal of Pharmacology*, 771, 173–190. <https://doi.org/10.1016/j.ejphar.2015.12.028>
- Baggio, L. L., & Drucker, D. J. (2007). Biology of Incretins: GLP-1 and GIP. *Gastroenterology*, 132(6), 2131–2157. <https://doi.org/10.1053/j.gastro.2007.03.054>
- Egan, J. M., Montrose-Rafizadeh, C., Wang, Y., Bernier, M., & Roth, J. (1994). Glucagon-Like Peptide- 1(7-36) Amide (GLP- 1) Enhances Insulin-Stimulated Glucose Metabolism in 3T3-L1 Adipocytes: One of Several Potential Extrapancreatic Sites of GLP- 1 Action. *Endocrinology*, 135(5), 2070–2075.
- Hussein, Z., Taher, S. W., Gilcharan Singh, H. K., & Chee Siew Swee, W. (2015). Diabetes Care in Malaysia: Problems, New Models, and Solutions. *Annals of Global Health*, 81(6), 851–862. <https://doi.org/10.1016/j.aogh.2015.12.016>
- Kahn, S. E., Cooper, M. E., & Del Prato, S. (2014). Pathophysiology and treatment of type 2 diabetes: Perspectives on the past, present, and future. *The Lancet*. Elsevier Ltd. [https://doi.org/10.1016/S0140-6736\(13\)62154-6](https://doi.org/10.1016/S0140-6736(13)62154-6)
- Sakoda, H., Ogihara, T., Anai, M., Funaki, M., Inukai, K., Katagiri, H., & Asano, T. (2000). Dexamethasone-induced insulin resistance in 3T3-L1 adipocytes is due to inhibition of glucose transport rather than insulin signal transduction. *Diabetes*, 49(10), 1700–1708. <https://doi.org/10.2337/diabetes.49.10.1700>
- Woon, S. M., Seng, Y. W., Ling, A. P. K., Chye, S. M., & Koh, R. Y. (2014). Anti-adipogenic effects of extracts of *Ficus deltoidea* var. *deltoidea* and var. *angustifolia* on 3T3-L1 adipocytes. *Journal of Zhejiang University SCIENCE B*, 15(3), 295–302. <https://doi.org/10.1631/jzus.B1300123>
- Yang, Y., Wolfram, J., Boom, K., Fang, X., Shen, H., & Ferrari, M. (2012). Hesperetin impairs glucose uptake and inhibits proliferation of breast cancer cells. *Cell Biochem Funct*, (July), 1–6. <https://doi.org/10.1002/cbf.2905>
- Yang, Z., & Xiong, H. (2012). Culture Conditions and Types of Growth Media for Mammalian Cells. In *Biomedical Tissue Culture* (pp. 3–18). <https://doi.org/10.5772/52301>

Gene Expression Profile of Psychrophilic Yeast *Glaciozyma antarctica* PI12 under Stationary Growth Phase

Tay Lih Jinq^{1,2}, Farah Diba Abu Bakar², Nor Muhammad Mahadi¹ & Abdul Munir Abdul Murad²

¹ Infrastructure University Kuala Lumpur

² Malaysia Genome Institute

³ Universiti Kebangsaan Malaysia

1. INTRODUCTION

Nearly 70% of the Earth's biosphere are permanently below 5°C and yet we just gain so little understanding over these cold-adapted organisms (or we generally named it as psychrophiles). Psychrophiles have been studied primarily to understand the adaptation strategies towards the prolonged cold environment. Several adaptative strategies discovered including alteration of membrane fluidity and expression of anti-freeze protein to overcome freezing problems [1-2], expression of cold-shock or cold-acclimation proteins [3] and the production of solutes, exopolysaccharides and cold-adapted enzymes for nutrient transportations and enzyme activities for low temperature [2,4-5]. In reaching for an understanding of the biological mechanism in cold adaptation, much of the focus have been on the properties of the psychrophilic enzymes. No much study have been detailed on the gene expression during each microbial growth phase or stage of psychrophilic organism. To date, no report is found on the genes that characterise growth phase of psychrophiles, as we just rely on the data from mesophilic organism to predict the happening during the cell growth.

Among the growth phase, stationary phase is particularly of interest. Stationary phase is the steady-state equilibrium where the rate of cell growth is exactly balanced by the rate of cell death. The cell struggles to survive and stressed by the lack of nutrients and accumulation of toxic metabolites, primarily those generated by oxidative metabolism. Thus, the cell tend to utilize alternative carbon sources and secrete protein to combat with the accumulated reactive oxygen species. Besides that, the cell in stationary phase also known to produce secondary metabolite in order to protect the cell against the competitor [6]. In the previous studies on *Saccharomyces cerevisiae*, the gene expression and key enzymes affects the entry and exit of stationary phase have been focused [7-11]. However, the gene expression characterized stationary phase of psychrophile still remain unclear. Several gene expression studies tend to use cold-induced mesophilic organism to study both the stationary phase and low temperature related genes. To date, there are no reports on the stationary phase related genes of psychrophile.

G. antarctica PI12 is a basidio-yeast isolated from sea ice nearby Casey Research Station. Since its first discovery in 1969 [12], it had been widely exploited for various enzymes, such as subtilisine-like proteinase [13], serine proteinase [14], invertase and α -glucosidase [15], α -amylase [16], antifreeze protein [17] and chitinase [18-19]. Notwithstanding its high biotechnological interest, molecular studies on *G. antarctica* PI12 still remain scarce. The latest

information from Genomes OnLine Database [20] indicates that, among 70 whole genome sequencing projects for psychrophiles that have been carried out, only four of them are eukaryotic organism (assessed 28 February 2014). So far, only a marine algae eukaryotic psychrophile, *Fragilariopsis cylindrus* CCMP 1102, fish parasite *Spironucleus salmonicida* NOR-1, ATCC 50377, Chrysophyceae sp. CCMP 2298, and an unknown organism CCMP 2058 have been sequenced. Thus, any further molecular studies in *G. antarctica* PI12 will be greatly useful towards the general understanding of cold-adaptation mechanism of eukaryotic psychrophile.

Expressed sequence tags (ESTs) are simply segment of sequences being sequenced from random selected cDNA clones that correspond to an mRNA expressed under certain conditions [21]. Analysis of ESTs has been preferentially used for gene discovery and estimating gene expression levels, particularly when study on the organisms with little or no genetic article history [22-23]. At the time the present study was initiated, there were no reports on the cDNA library construction as well as the generation and submission of ESTs in public databases for psychrophile *G. antarctica* PI12 (Genbank, 17 November 2011). Therefore, in this study, we reported on the generation of total 3139 ESTs from cDNA library *G. antarctica* PI12 under stationary growth phase. With the EST approach, we contribute to a better understanding on the stationary phase related genes of psychrophile. Besides gene discovery, this study also reported on the secondary metabolite related transcripts expressed during the stationary growth phase of the psychrophile yeast *G. antarctica* PI12.

2. MATERIALS AND METHODS

Culture condition

G. antarctica PI12 was isolated from Casey Research Station, Antarctic and provided by Prof Dr Nazalan Najimudin from University Science Malaysia. Stock culture *G. antarctica* PI12 was grown on Yeast Peptone Dextrose (YPD; 1% yeast extract, 2% peptone, 2% dextrose) agar, with ampicillin (50 µg/mL) and kanamycin (50 µg/mL) at 4°C for 14 days until the formation of single colony on the agar plate. Starter culture was prepared by inoculated the single colony in 10 ml YPD broth with same antibiotic concentration in YPD agar. After 7 days growth in 4°C with 150 rpm shaking, yeast cells were transferred to 50 mL YPD broth, with the final concentration of 1×10^6 cell/mL. Cell count was performed every 24 hours and the measurement was obtained by using haemocytometer slide and OD₆₀₀ reading. According to the generated growth curve, cells from lag growth phase, log growth phase and stationary growth phase were determined and harvested. The harvested cells were frozen in liquid nitrogen and stored at -80°C for further RNA isolation process.

Total RNA and mRNA isolation

About 0.1 g of frozen cells was quickly ground into fine powder by the cell breaking machine Dismembrator (B.Braun, Germany). Total RNA was extracted using TRIzol[®] reagent, with following manufacturer's instructions, while the mRNA isolation was further proceeded by

using PolyAtract® mRNA Isolation Systems (Promega Corporation, USA). The quality of RNA and mRNA were verified by Agilent 2100 Bioanalyzer (Agilent Technologies, Inc, USA) while amount measured by Nanodrop® ND-1000 Spectrophotometer (NanoDrop Technologies, Inc, USA).

cDNA library construction and sequencing

cDNA library was constructed by using the CloneMiner™ cDNA Library Construction (Invitrogen, USA) following the manufacturer's instructions. The generated double stranded cDNAs from the good quality mRNA, were cloned into the pDONR™ 222 by recombination reaction. The recombinant plasmids were subsequently transformed into *Escherichia coli* ElectroMAX™ DH10B™ competent cell (Invitrogen, USA) by electroporation. Successful transformed recombinants were screened by growing on the Luria-Bertani (LB) medium supplemented with kanamycin (50 µg/mL). About 3,552 white colonies were randomly selected from each library and incubated at 37°C, 18 hours with 320 rpm orbital agitation in 96 well plates containing LB medium with kanamycin (50 µg/mL). Large-scale plasmid extractions were performed by using Montage™ Plasmid Miniprep₉₆ kit (Miliipore, USA), according to the manufacturer's instructions. Sequencing reactions were performed on the ABI PRISM® 3100 Genetic Analyzer (Applied Biosystem Inc., USA) using the ABI®BigDye™Terminator v3.1 Cycle Sequencing kit (Applied Biosystem Inc., USA) and M13 forward primer.

Sequence analysis and annotation

Generated ESTs were subjected to Phred analysis [24-25] with cut-off value (QV) 20. Vector sequences were trimmed with Cross_match and stackPACK™ v2.2 [26] were used to cluster the ESTs data. The unique transcripts were compared against the nonredundant (nr) Genbank protein databases of National Center for Biotechnology Information (NCBI) through the BLASTX algorithm [27] in Blast2GO tool [28]. Homologies with expected-values (E-value) $\leq 1E-6$ were defined as significant. For those unique transcripts that presented 'no database matches' (no hits) were further analyzed by the ESTScan program [29-30], employing the Arabidopsis thaliana model for coding regions prediction.

From the BLASTX hits obtained, the annotations were performed by assigning the Gene Ontology (GO) terms [31] to the unique transcripts. The GO terms obtained were categorized into biological process, molecular function, and cellular component. Besides that, annotation against Kyoto Encyclopedia of Genes and Genomes (KEGG) database in generating KEGG pathways also had performed through KAAS (KEGG Automatic Annotation Server) (www.genome.ad.jp/tools/kaas/) [32].

Quantitative Real-time PCR

Total RNA extracted from lag growth phase, log growth phase and stationary growth phase of *G. antarctica* PI12 as described were treated with DNase I (Invitrogen, USA) and purified by using the QIAGEN RNeasy Mini Kit (Qiagen, Germany) to free from genomic DNA contamination. Oligonucleotide primers used for reverse transcription were designed using the Primer Premier

3.0 software (PREMIER Biosoft International, USA) and synthesized by First Base, Malaysia. Quantitative real-time PCR (qRT-PCR) were performed according to the manual of QuantiFast SYBR Green RT-PCR (Qiagen, Germany) on the Mastercycler® ep *realplex* (Eppendorf, Germany). The cycling conditions were: 10 min/50°C, 5 min/95°C and 40 cycles of 10s/95°C and 30s/60°C. For identification of the PCR products, a melting curve was performed from 60°C to 95°C with read every 0.4°C. The β -actin and glyceraldehyde 3-phosphate dehydrogenase were selected as internal reference genes and the expression level were used to normalize the qRT-PCR results for each gene. The standard curve testing was performed using a series of five-fold diluted samples, respectively, for different genes. The PCR efficiency and R^2 for these genes were calculated to confirm if the qRT-PCR data were precise and trustworthy. Melting curves were analyzed to make sure that a single PCR product was amplified for each pair of primers. Expression levels of these genes were verified from three technical replicates and two biological replicates along with the internal reference gene. Data generated were analyzed using GenEx Standard version 5.4.3 (MultiD Analyses AB, Sweden) using the $2^{-\Delta\Delta C_t}$ method [33].

3. RESULTS

Sequence analysis and functional annotation

A cDNA library from stationary growth phase *G. antarctica* PI12 was successfully constructed with the library titer of 1.25×10^5 cfu/mL and cDNA insert size ranged from 550 bp to 1600 bp (Table 1). A total of 3552 clones were randomly selected for sequencing. Using the Phred [25,24] and Cross_match program, the vector sequences were trimmed and clones with no insert or sequences shorter than 100 bp were excluded. The sequence filtering results in 3139 high quality ESTs, with average sequence length of 574 bp. All ESTs were deposited in the dbEST division of GenBank under accession numbers from JZ555921 to JZ559059. By using the stackPACK™ v2.2 [26], ESTs obtained were clustered into 1710 unique transcripts, consist of 516 consensus and 1194 singletons. About 82.1% of the unique transcripts (490 consensus, 913 singletons) have sequence length equal or more than 500 bp. The redundancy of the library is 63.0% and that the gene discovery rate was 37.0%.

All the unique transcripts were aligned against the NCBI non-redundant (nr) protein database using BLASTX under the Blast2GO analysis tool [34] to identify the putative function of every sequence (accessed 23 October 2013). Of 1710 unique transcripts, about 83.4% (1426 unique transcripts) showed significant hits (E value $< 10^{-6}$) to the nr protein database. This includes 82 unique transcripts hit to hypothetical protein, 3 unique transcripts hit to unknown function protein and 2 unique transcripts hit to predicted protein. Among the 1426 unique transcripts with known function, 98.6% of unique transcripts (1406 unique transcripts) with known or putative function hits to fungal sequences.

Gene ontology assignments

Following the BLAST, Gene Ontology (GO) terms were further assigned to the unique transcripts through the Blast2GO program. Three main categories of GO terms include

biological process, molecular function and cellular component with the terms in different levels. About 1149 unique transcripts (67.2% of total unique transcripts) were assigned with at least one GO term regardless of categories. Figure 1

Table 1 Summary of EST analysis from stationary growth phase

Description	Number
Library titer (cfu/mL)	1.25×10^5
Total CFU	1.00×10^6
cDNA insert size range (bp)	550-1600
Average insert size (bp)	1188
Total number of clones sequenced	3552
High quality ESTs	3139 (88.4% ¹)
Number of consensus	516
Number of ESTs in consensus	2033 (63.0% ²)
Number of singletons	1194 (37.0% ³)
Total unique transcripts (UT)	1710
Number of UT with known/putative function	1426
Number of UT with unknown function	283 (16.5% ⁴)

¹Percentage of high quality sequences (after sequence filtering with Phred analysis) from number of clones sequenced;

²percentage of transcript redundancy (number of clustered ESTs / total ESTs);

³percentage of gene discovery (number of singletons / total ESTs);

⁴percentage of unique transcripts with unknown function

shows the percentage of unique transcripts that hit to the level 3 GO terms within the molecular function, biological process and cellular component categories. Functional classification of *G. antarctica* unique transcripts in biological process category (Fig 1) showed that organic substance metabolic process (GO:0071704), cellular metabolic process (GO:0044237) and primary metabolic process (GO:0044238) were among the highly represented groups. Metabolic process is the key activity during under stationary growth phase. Besides primary metabolic process, cells under stationary growth phase also tend to produce energy from other organic substance. For molecular function, heterocyclic compound binding (GO:1901363), organic cyclic compound binding (GO:0097159), ion binding (GO:0043167) and small molecule binding (GO:0036094) were among the most representative of GO term (Fig 1). Regarding cellular component, most of the unique transcripts involved in cell part (GO:0044464), followed by membrane-bounded organelle (GO:0043227) (Fig 1).

Pathway analysis

As an alternative method for categorizing unique transcripts by biochemical functions, transcripts were assigned to metabolic pathways via KEGG using the web-based server KAAS (accessed 20 March 2014) [32]. Of the 1710 unique transcripts, 509 of them were hit to 471

in stationary growth phase. Three main GO categories are: molecular function, biological process and cellular component.

Table 2: The mostly abundantly expressed genes in the stationary growth phase library of *G. antarctica*.

Seq. Name	No. of ESTs	Accession No.	Annotation [organism]	E value
La07f_cn380	44	JZ556870	Unknown	N/A
La07f_cn549	35	JZ558947	fysh domain-containing protein [<i>Dactylellina haptotyla</i>]	4E-29
La07f_cn374	29	JZ558877	fructose-bisphosphate aldolase [<i>Rhodospiridium torulooides NP11</i>]	3E-176
La07f_cn126	26	JZ556890	acetyl-CoA synthetase [<i>Rhodospiridium torulooides NP11</i>]	0
La07f_cn378	24	JZ556895	glutathione s-transferase c-terminal-like protein [<i>Dacryopinax</i> sp. DJM-731 SS1]	9E-28
La07f_cn34	22	JZ558624	alternative oxidase [<i>Rhodospiridium torulooides NP11</i>]	1E-129
La07f_cn200	20	JZ558577	hypothetical protein MELLADRAFT_90060 [<i>Melampsora larici-populina</i> 98AG31]	5E-23
La07f_cn534	19	JZ556917	hypothetical protein RHTO_06340 [<i>Rhodospiridium torulooides NP11</i>]	2E-45
La07f_cn212	18	JZ556914	malic enzyme [<i>Rhodospiridium torulooides NP11</i>]	0
La07f_cn448	17	JZ556830	hypothetical protein RHTO_06341 [<i>Rhodospiridium torulooides NP11</i>]	1E-09
La07f_cn191	17	JZ558608	ubiquitin activating enzyme [<i>Rhodospiridium torulooides NP11</i>]	4E-176
La07f_cn168	16	JZ556750	adenylosuccinate synthetase [<i>Rhodospiridium torulooides NP11</i>]	0
La07f_cn464	15	JZ556590	amino-acid permease indal [<i>Coprinopsis cinerea okayama7#130</i>]	0
La07f_cn371	15	JZ556991	iron-sulfur cluster assembly-related protein [<i>Cryptococcus gattii</i> WM276]	3E-73
La07f_cn483	15	JZ557191	mitochondrial phosphate carrier protein 2 [<i>Rhodospiridium torulooides NP11</i>]	0
La07f_cn554	14	JZ556919	elongation factor 1-alpha [<i>Puccinia graminis</i> f. sp. tritici CRL 75-36-700-3]	0
La07f_cn565	13	JZ556868	40s ribosomal protein s4 [<i>Coprinopsis cinerea okayama7#130</i>]	2E-150
La07f_cn499	13	JZ557578	copper amine oxidase [<i>Trichophyton rubrum</i> CBS 118892]	0
La07f_cn553	13	JZ556806	hypothetical protein E5Q_00852 [<i>Mixia osmundae</i> IAM 14324]	4E-74
La07f_cn314	13	JZ557589	mfs general substrate transporter [<i>Trametes versicolor</i> FP-101664 SS1]	4E-177
La07f_cn529	13	JZ557023	probable fun34-transmembrane protein involved in ammonia production [<i>Ustilago hordei</i>]	2E-80
La07f_cn370	12	JZ556934	60s ribosomal protein 119 [<i>Rhodospiridium</i>]	1.57E-81

			<i>toruloides NP11</i>	
La07f_cn369	12	JZ556772	arylamine n-acetyltransferase 1 [<i>Rhodotorula glutinis</i> ATCC 204091]	7.03E-109
La07f_cn558	12	JZ556838	hypothetical protein PDE_04474 [<i>Penicillium oxalicum</i> 114-2]	1.39E-85
La07f_cn366	12	JZ556961	hypothetical protein ASPNIDRAFT_143688 [<i>Aspergillus niger</i> ATCC 1015]	8E-80
La07f_cn526	11	JZ558552	40s ribosomal protein s1 [<i>Gloeophyllum trabeum</i> ATCC 11539]	1.72E-144
La07f_cn160	10	JZ557595	2-oxoglutarate dehydrogenase complex E1 component mitochondrial precursor [<i>Gloeophyllum trabeum</i> ATCC 11539]	0
La07f_cn432	10	JZ558581	oligopeptide transporter [<i>Trametes versicolor</i> FP-101664 SS1]	6E-167
La07f_cn475	9	JZ558847	atp12-domain-containing protein [<i>Fomitiporia mediterranea</i> MF3/22]	2E-88
La07f_cn437	9	JZ558640	fructose-1,6-bisphosphatase [<i>Rhodospiridium toruloides NP11</i>]	0
La07f_cn363	9	JZ557630	hypothetical protein AGABI1DRAFT_123657 [<i>Agaricus bisporus</i> var. <i>burnettii</i> JB137-S8]	2.84E-50
La07f_cn476	9	JZ557587	NAD-aldehyde dehydrogenase [<i>Trametes versicolor</i> FP-101664 SS1]	0
La07f_cn147	9	JZ557081	transcription factor [<i>Rhodospiridium toruloides NP11</i>]	1.10E-17
La07f_cn507	9	JZ556995	transcription initiation factor TFIIB [<i>Rhodospiridium toruloides NP11</i>]	1.44E-141
La07f_cn568	9	JZ556948	voltage-dependent ion-selective channel [<i>Rhodospiridium toruloides NP11</i>]	3.19E-161
La07f_cn555	8	JZ556921	atp synthase f1 alpha subunit [<i>Puccinia graminis</i> f. sp. <i>tritici</i> CRL 75-36-700-3]	0
La07f_cn137	8	JZ558884	atp synthase f1 beta subunit [<i>Puccinia graminis</i> f. sp. <i>tritici</i> CRL 75-36-700-3]	0
La07f_cn562	8	JZ559027	guanine nucleotide binding protein beta subunit [<i>Rhizoctonia solani</i> AG-1 IB]	4E-172
La07f_cn68	8	JZ557194	long-chain-fatty-acid-CoA-ligase [<i>Trametes versicolor</i> FP-101664 SS1]	3E-174
La07f_cn248	8	JZ557657	nad-aldehyde dehydrogenase [<i>Gloeophyllum trabeum</i> ATCC 11539]	0
La07f_cn106	8	JZ556829	nadp-specific glutamate dehydrogenase [<i>Claviceps purpurea</i> 20.1]	0
La07f_cn361	8	JZ558247	phenol 2-monooxygenase [<i>Rhodospiridium toruloides NP11</i>]	1.88E-159
La07f_cn225	7	JZ557600	2-nitropropane dioxygenase [<i>Punctularia strigosozonata</i> HHB-11173 SS5]	5E-111
La07f_cn286	7	JZ557220	40s ribosomal protein s8 [<i>Trametes versicolor</i> FP-101664 SS1]	6.51E-116
La07f_cn513	7	JZ556774	40s ribosomal protein s9 [<i>Schizophyllum commune</i> H4-8]	3E-113
La07f_cn155	7	JZ557581	DAHP synthetase [<i>Coniophora puteana</i> RWD-64-598 SS2]	1E-162

La07f_cn401	7	JZ558276	E3 ubiquitin-protein ligase [Rhodosporidium toruloides NP11]	HUWE1	0
La07f_cn543	7	JZ556790	glutamine synthetase [Rhodosporidium toruloides NP11]		0
La07f_cn442	7	JZ556957	Transporter [Cryptococcus gattii WM276]		3E-132
La07f_cn489	7	JZ558868	Unknown		N/A
La07f_cn360	7	JZ558738	hypothetical protein [Puccinia graminis f. sp. tritici CRL 75-36-700-3]	PGTG_04016	1E-12

N/A - non available

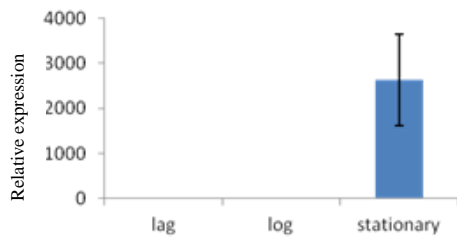
from stationary growth phase, cells from lag growth phase and log growth phase were also used to validate the gene expression by performing qRT-PCR.

Overall, 19 over 21 genes shows higher expression during in stationary growth phase (Figure 2). Among of them, 8 unique transcripts showed high expression over 50 folds during in stationary growth phase, compare to lag and log growth phase (La07f_cn380, La07f_cn212, La07f_cn499, La07f_cn200, La07f_cn369, La07f_cn314, La07f_cn371 and La07f_cn529). These unique transcripts were found to be involved in ion binding function (metal ion binding and iron ion binding), transferase activity and transmembrane transport process. About 11 other unique transcripts also showed higher expression in stationary growth phase culture but less than 50 folds compare to lag and log growth phase culture (La07f_cn366, La07f_cn191, La07f_cn464, La07f_cn168, La07f_cn549, La07f_cn448, La07f_cn534, La07f_cn378, La07f_cn126, La07f_cn483 and La07f_cn374). These unique transcripts comprises mainly the ATP binding function, glycolysis process and transporter activity. Among the highly expressed unique transcripts during stationary growth phase, three of them hit to hypothetical proteins while one with no hit to NCBI protein database. This indicates that these unique transcripts might play an important role in the stationary phase of psychrophilic organisms whose functions have not yet been discovered.

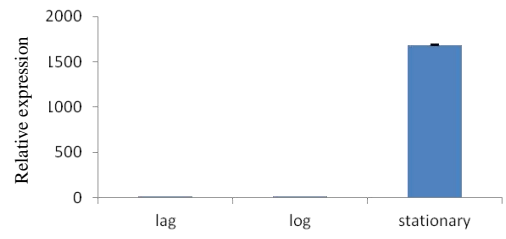
4. DISCUSSION

In the absence of fully sequenced genome, the analysis of ESTs data inevitability provided a deeper insight of genome view on this cold-adapted *G. antarctica*. Although stationary growth phase had been well studied in mesophile organism, the gene expression profile of psychrophilic organism under stationary growth phase still remain unclear. Thus, our EST analysis comes as useful preliminary indication for the gene expression of psychrophilic organism under stationary growth phase.

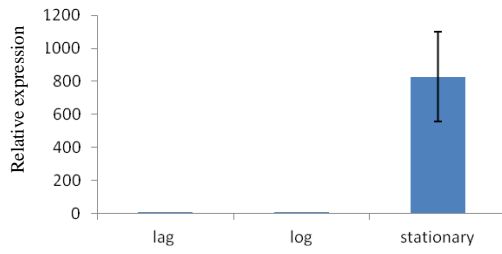
In this study, we produced a total of 3,139 ESTs, representing 1,710 unique transcripts. About 16.5% of them (283 unique transcripts) still remain unknown, which none of significant hits (E value $\leq 1E-5$) to non-redundant (nr) NCBI protein database (Table 1). Of those with significant hits to nr NCBI protein database, 82



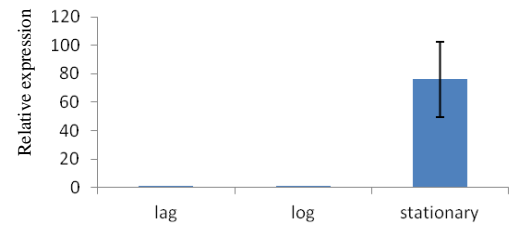
(a)



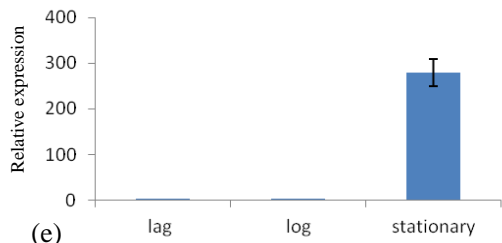
(b)



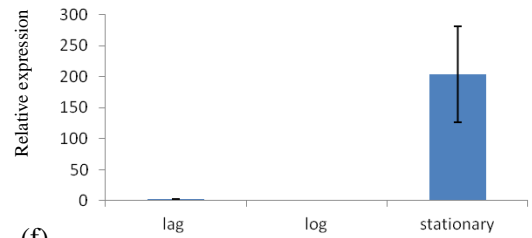
(c)



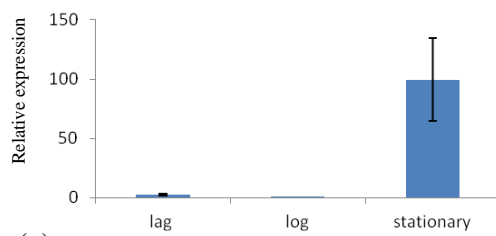
(d)



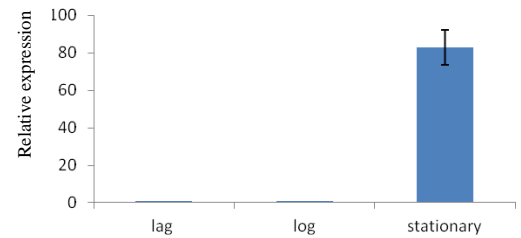
(e)



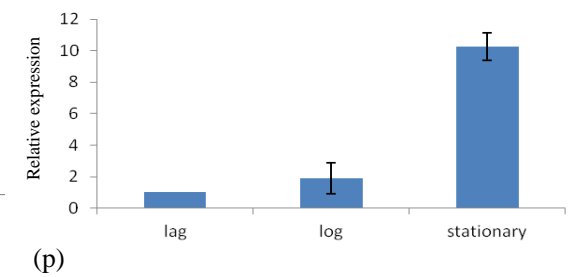
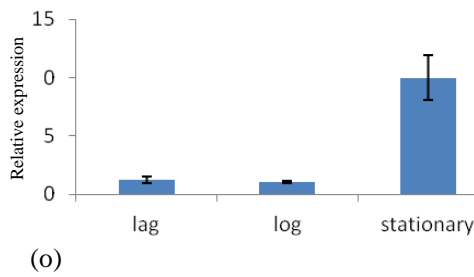
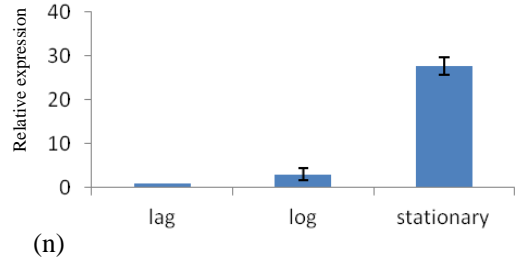
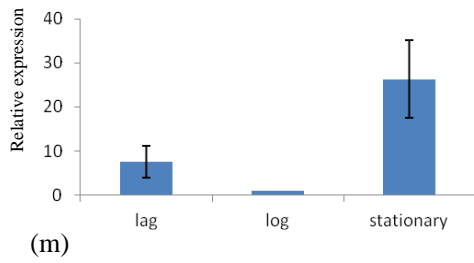
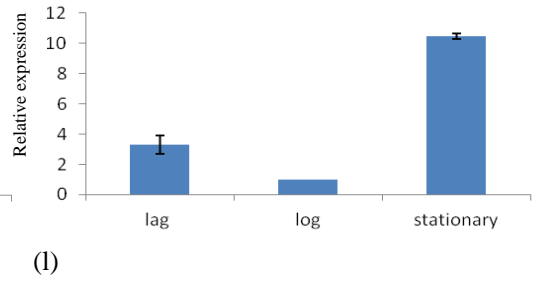
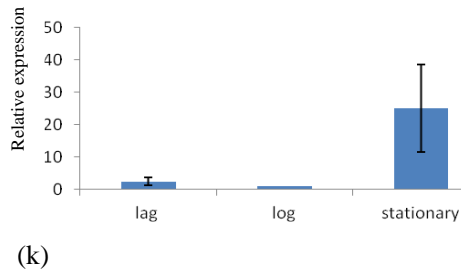
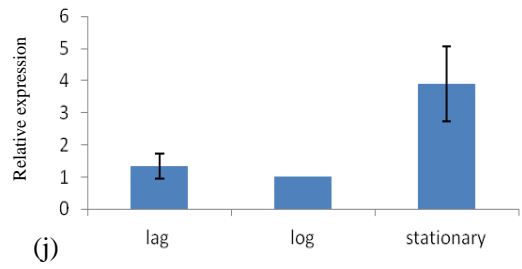
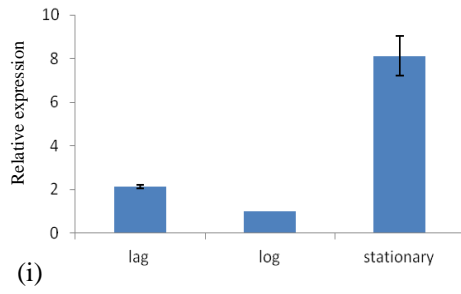
(f)



(g)



(h)



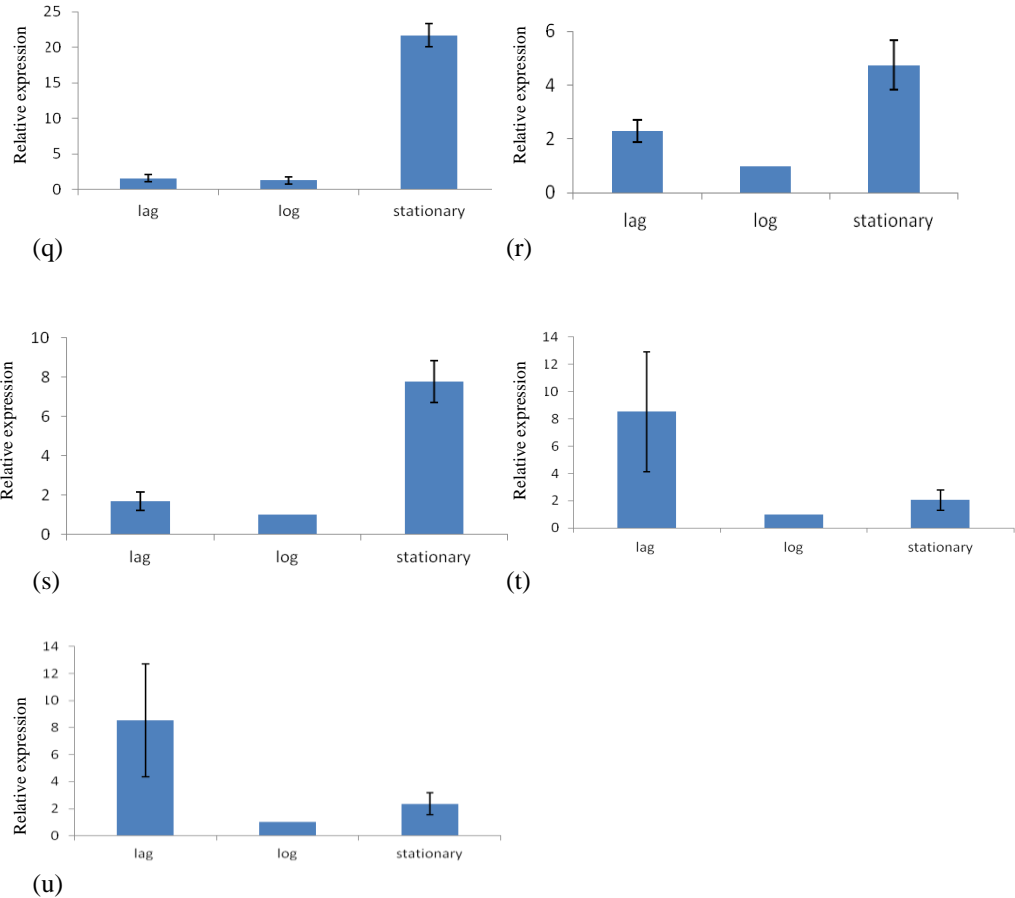


Figure. 2 : qRT-PCR analysis of differentially expressed transcripts during stationary growth phase in comparing to lag and log growth phases. 19 over 21 genes shows higher expression in stationary growth phase, 8 of them with high expression over 50 folds [(a) La07f_cn380 (b) La07f_cn212 (c) La07f_cn499 (d) La07f_cn200 (e) La07f_cn369 (f) La07f_cn314 (g) La07f_cn371 and (h) La07f_cn529] while some with expression below 50 folds [(i) La07f_cn366 (j) La07f_cn191 (k) La07f_cn464 (l) La07f_cn168 (m) La07f_cn549 (n) La07f_cn448 (o) La07f_cn534 (p) La07f_cn378 (q) La07f_cn126 (r) La07f_cn483 (s) La07f_cn374]. Among the 21 genes, two of them [(t) La07f_cn370 (u) La07f_cn565] shows higher expression in lag growth phase instead of stationary growth phase.

unique transcripts hit to hypothetical proteins, 2 unique transcripts hit to predicted protein while 3 unique transcripts hit to unknown function protein. Thus, this make up around 21.6% of total unique transcripts (370 unique transcripts) are remain without known function. In addition, 11 unique transcripts among those without known function (hits to hypothetical proteins or no matches to nr NCBI protein database) are listed as abundantly expressed unique transcripts. Through the qRT-PCR, several unique transcripts (La07f_cn380, La07f_cn200,

La07f_cn534) were proven to have high expression level uniquely in stationary growth phase (Figure 2). With the high gene expression, this indicates that some of unknown unique transcripts might play pivotal role during stationary growth phase or maybe unique only for psychrophilic organism.

The rapid growth of cells will eventually encounter with nutrient exhausted and cessation of reproduction and growth. During in the stationary phase, this severity is added as mitochondrial respiration tends to produce a large amount of harmful reactive oxygen species (ROS). In the list of abundantly expressed unique transcripts, several of them encoded the ability to confront with ROS production (La07f_cn378, La07f_cn34, La07f_cn212) and carbohydrate metabolism (La07f_cn126, La07f_cn374, La07f_cn212). The function of La07f_cn126 as acetyl Co-A synthetase (ACS) exhibit the uniqueness of stationary phase cells. In order to maintain its viability under nutrient depletion, cells tend to utilize acetate as alternative carbon sources. ACS served its importance in converting the acetate to acetyl Co-A, to complete the tricarboxylic acid cycle. This finding agrees with previous studies on *Saccharomyces cerevisiae* [35-36] and *Escherichia coli* [37-38] as high transcriptional level of ACS is detected during in the stationary phase culture.

Mitochondrial respiration is the major energy production of the stationary phase cells. However, this energy generated factory also tend to produce large amount of ROS which posed a threat to the living cells [39-40]. The situation gets worse as nutrient deprivation accelerates the accumulation of ROS [41]. To encounter this problem, several genes were expressed during stationary growth phase, such as alternative oxidase (La07f_cn33, La07f_cn34, La07f_cn439), glutathione reductase (La07f016C11.b1.ab1), glutathione s-transferase (La07f_cn378, La07f004D08.b1.ab1, La07f030C04.b1.ab1), manganese superoxide dismutase (La07f019C06.b1.ab1), catalase (La07f_cn204) and cytochrome c peroxidase (La07f034D10.b1.ab1). In the mitochondrial respiratory chain, alternative oxidase play a crucial role in preventing the ROS production and increasing the metabolic plasticity of the cell. This had been well-studied in *Saccharomyces cerevisiae*, *Ustilago maydis* and several plant respiratory mechanism [42-45]. Besides served its importance in antioxidant defense system, Watanabe et al. [45] reported that the high ability of alternative oxidase for low temperature acclimation. This findings correlated with our study on the stationary phase of psychrophile, as high transcriptional level for alternative oxidase also detected while combat with the high ROS production. As an antioxidant molecule, glutathione reacts with a series of ROS through the formation of thiyl radicals. The superoxide radicals generated by the thiyl radicals can be further eliminated by superoxide dismutase, catalase and peroxidase [41]. This is therefore several related enzyme in glutathione metabolism were co-expressed during stationary growth phase. Glutathione S-transferase (GST) is one of the highly expressed transcripts during in the stationary phase. This result is consistent with a previous finding that high mRNA amount of GST genes were detected in a response to oxidative stress [46]. In addition, previous findings also suggested that GST might participate in detoxification of phase accumulated xenobiotics [47-48,41]. Thus, this explained the uniquely high expression level of GST during in stationary phase.

One striking characteristic of basidiomycetes is their ability to synthesize secondary metabolites. Numerous compounds with antiviral, anti-inflammatory, antimicrobial or anticancer activities, as well as antioxidants, aromas and flavors had been identified in *Ganoderma lucidum*, *Laetiporus sulphureus*, *Trametes versicolor*, *Grifola umbellata*, *Inonotus obliquus*, and *Wolfiporia cocos* [49]. In psychrophilic yeast *G. antarctica*, several genes were found involved in isoquinoline alkaloid biosynthesis, tropane, piperidine and pyridine alkaloid biosynthesis, streptomycin biosynthesis and novobiocin biosynthesis. For the tropane, piperidine and pyridine alkaloid biosynthesis, primary-amine oxidase [EC 1.4.3.21], histidinol-phosphate aminotransferase [EC 2.6.1.9], aromatic amino acid aminotransferase [EC 2.6.1.57] and esterase/lipase [EC 3.1.1.-] were expressed during stationary growth phase. Through qRT-PCR, expression of La07f_cn499 which encode primary-amide oxidase function was proven nearly 800 fold higher only in stationary growth phase, compare to lag and log growth phase culture (Fig. 2). The high expression of primary-amine oxidase is not a common characteristic of stationary growth phase or psychrophilic organism. Thus, this suggests that when the yeast *G. antarctica* was under during stationary growth phase, the expression of primary-amide oxidase might be induced and further influence the biosynthesis of tropane, piperide and pyridine alkaloid.

5. CONCLUSION

In conclusion, a total of 3,139 ESTs representing 1,710 unique transcripts obtained in stationary growth phase cDNA library served as pivotal preliminary insight into the genomic of psychrophile eukaryotes. About 21.6% of total unique transcripts (370 unique transcripts) still had no known homologue to non-redundant protein database NCBI. These unique transcripts are particularly interesting as they may represent genes that are uniquely to stationary growth phase or psychrophilic yeast. For the rest 78.3% of total unique transcripts, genes related to nutrient depletion, oxidative stress and secondary metabolite synthesis were found to highly expressed. For several abundantly expressed unique transcripts, results from qRT-PCR again confirmed the gene expression, in comparison to the lag and log growth phase culture.

REFERENCES

- Muryoi N, Sato M, Kaneko S, Kawahara H, Obata H, Yaish MWF, Griffith M, Glick BR (2004) Cloning and expression of *afpA*, a gene encoding an antifreeze protein from the arctic plant growth-promoting Rhizobacterium *Pseudomonas putida* GR12-2. *The Journal of Bacteriology* 186 (17):5661-5671.
- D'Amico S, Collins T, Marx JC, Feller G, Gerday C (2006) Psychrophilic microorganisms: challenges for life. *EMBO Reports* 7 (4):385-389.
- Phadtare S, Alsina J, Inouye M (1999) Cold-shock response and cold-shock proteins. *Current Opinion in Microbiology* 2 (2):175-180
- Georlette D, Blaise V, Collins T, D'Amico S, Gratia E, Hoyoux A, Marx JC, Sonan G, Feller G, Gerday C (2004) Some like it cold: biocatalysis at low temperatures. *FEMS Microbiology Reviews* 28 (1):25-42

- Pavlova K, Panchev I, Krachanova M, Gocheva M (2009) Production of an exopolysaccharide by Antarctic yeast. *Folia Microbiologica* 54 (4):343-348.
- Price-Whelan A, Dietrich LEP, Newman DK (2006) Rethinking 'secondary' metabolism: physiological roles for phenazine antibiotics. *Nature Chemical Biology* 2 (2):71-78
- Werner-Washburne M, Braun E, Johnston GC, Singer RA (1993) Stationary phase in the yeast *Saccharomyces cerevisiae*. *Microbiology Reviews* 57 (2):383-401
- Gasch AP, Werner-Washburne M (2002) The genomics of yeast responses to environmental stress and starvation. *Functional and Integrative Genomics* 2 (4-5):181-192.
- Herman PK (2002) Stationary phase in yeast. *Current Opinion in Microbiology* 5 (6):602-607
10. Martinez MJ, Roy S, Archuletta AB, Wentzell PD, Anna-Arriola SS, Rodriguez AL, Aragon AD, Quinones GA, Allen C, Werner-Washburne M (2004) Genomic analysis of stationary-phase and exit in *Saccharomyces cerevisiae*: gene expression and identification of novel essential genes. *Molecular Biology of the Cell* 15 (12):5295-5305.
- Galdieri L, Mehrotra S, Yu S, Vancura A (2010) Transcriptional Regulation in Yeast during Diauxic Shift and Stationary Phase. OMICS. doi:10.1089/omi.2010.0069
- Fell JW, Statzell AC, Hunter IL, Phaff HJ (1969) *Leucosporidium* gen. n., the heterobasidiomycetous stage of several yeasts of the genus *Candida*. *Antonie Van Leeuwenhoek* 35 (4):433-462
- Turkiewicz M, Pazgier M, Kalinowska H, Bielecki S (2001) Properties of cold-adapted subtilisine-like proteinase of endemic yeast *Leucosporidium antarcticum*. *Meded Rijksuniv Gent Fak Landbouwk Toegep Biol Wet* 66 (3a):329-332
- Turkiewicz M, Pazgier M, Kalinowska H, Bielecki S (2003) A cold-adapted extracellular serine proteinase of the yeast *Leucosporidium antarcticum*. *Extremophiles* 7 (6):435-442.
- Turkiewicz M., Pazgier M., Donachie S.P., H K (2005) Invertase and alpha-glucosidase production by the endemic Antarctic marine yeast *Leucosporidium antarcticum*. *Polish Polar Research* 26 (2):125-136
- Ramli AN, Azhar MA, Shamsir MS, Rabu A, Murad AM, Mahadi NM, Illias RM (2013) Sequence and structural investigation of a novel psychrophilic alpha-amylase from *Glaciozyma antarctica* PI12 for cold-adaptation analysis. *J Mol Model* 19 (8):3369-3383.
- Hashim NH, Bharudin I, Nguong DL, Higa S, Bakar FD, Nathan S, Rabu A, Kawahara H, Illias RM, Najimudin N, Mahadi NM, Murad AM (2013) Characterization of Afp1, an antifreeze protein from the psychrophilic yeast *Glaciozyma antarctica* PI12. *Extremophiles* 17 (1):63-73.
- Ramli AN, Mahadi NM, Rabu A, Murad AM, Bakar FD, Illias RM (2011) Molecular cloning, expression and biochemical characterisation of a cold-adapted novel recombinant chitinase from *Glaciozyma antarctica* PI12. *Microb Cell Fact* 10:94.
- Ramli AN, Mahadi NM, Shamsir MS, Rabu A, Joyce-Tan KH, Murad AM, Illias RM (2012) Structural prediction of a novel chitinase from the psychrophilic *Glaciozyma antarctica* PI12 and an analysis of its structural properties and function. *J Comput Aided Mol Des* 26 (8):947-961. doi:10.1007/s10822-012-9585-7
- Bernal A, Ear U, Kyrpides N (2001) Genomes OnLine Database (GOLD): a monitor of genome projects world-wide. *Nucleic Acids Research* 29 (1):126-127
- Adams MD, Kelley JM, Gocayne JD, Dubnick M, Polymeropoulos MH, Xiao H, Merril CR, Wu A, Olde B, Moreno RF, Kerlavage AR, McCombie WR, Venter JC (1991) Complementary DNA sequencing: expressed sequence tags and human genome project.

Science 252 (5013):1651-1656.

- Johjima T, Taprab Y, Noparatnaraporn N, Kudo T, Ohkuma M (2006) Large-scale identification of transcripts expressed in a symbiotic fungus (*Termitomyces*) during plant biomass degradation. *Applied Microbiology and Biotechnology* 73 (1):195-203.
- Ewing RM, Kahla AB, Poirot O, Lopez F, Audic S, Claverie J-M (1999) Large-Scale Statistical Analyses of Rice ESTs Reveal Correlated Patterns of Gene Expression. *Genome Research* 9 (10):950-959. doi:10.1101/gr.9.10.950
- Ewing B, Green P (1998) Base-Calling of Automated Sequencer Traces Using Phred. II. Error Probabilities. *Genome Research* 8 (3):186-194.
- Ewing B, Hillier L, Wendl MC, Green P (1998) Base-Calling of Automated Sequencer Traces Using Phred. I. Accuracy Assessment. *Genome Research* 8 (3):175-185.
- George RA (2001) StackPACK clustering system. *Briefings in Bioinformatics* 2 (4):394-397.
- Altschul SF, Gish W, Miller W, Myers EW, Lipman DJ (1990) Basic local alignment search tool. *Journal of Molecular Biology* 215 (3):403-410.
- Aparicio G, Gotz S, Conesa A, Segrelles D, Blanquer I, Garcia JM, Hernandez V, Robles M, Talon M (2006) Blast2GO goes grid: developing a grid-enabled prototype for functional genomics analysis. *Studies in Health Technology and Informatics* 120:194-204
- Iseli C, Jongeneel CV, Bucher P (1999) ESTScan: a program for detecting, evaluating, and reconstructing potential coding regions in EST sequences. *Proceedings of International Conference on Intelligent Systems for Molecular Biology*:138-148
- Lottaz C, Iseli C, Jongeneel CV, Bucher P (2003) Modeling sequencing errors by combining Hidden Markov models. *Bioinformatics* 19 Suppl 2:ii103-112
- Ashburner M, Ball CA, Blake JA, Botstein D, Butler H, Cherry JM, Davis AP, Dolinski K, Dwight SS, Eppig JT, Harris MA, Hill DP, Issel-Tarver L, Kasarskis A, Lewis S, Matese JC, Richardson JE, Ringwald M, Rubin GM, Sherlock G (2000) Gene ontology: tool for the unification of biology. The Gene Ontology Consortium. *Nature Genetics* 25 (1):25-29.
- Moriya Y, Itoh M, Okuda S, Yoshizawa AC, Kanehisa M (2007) KAAS: an automatic genome annotation and pathway reconstruction server. *Nucleic Acids Res* 35 (Web Server issue):W182-185.
- Livak KJ, Schmittgen TD (2001) Analysis of relative gene expression data using real-time quantitative PCR and the $2^{-\Delta\Delta C(T)}$ Method. *Methods* 25 (4):402-408.
- Conesa A, Gotz S, Garcia-Gomez JM, Terol J, Talon M, Robles M (2005) Blast2GO: a universal tool for annotation, visualization and analysis in functional genomics research. *Bioinformatics* 21 (18):3674-3676.
- De Virgilio C, Bürckert N, Barth G, Neuhaus J-M, Boller T, Wiemken A (1992) Cloning and disruption of a gene required for growth on acetate but not on ethanol: The acetyl-coenzyme A synthetase gene of *Saccharomyces cerevisiae*. *Yeast* 8 (12):1043-1051.
- van den Berg MA, de Jong-Gubbels P, Kortland CJ, van Dijken JP, Pronk JT, Steensma HY (1996) The Two Acetyl-coenzyme A Synthetases of *Saccharomyces cerevisiae* Differ with Respect to Kinetic Properties and Transcriptional Regulation. *Journal of Biological Chemistry* 271 (46):28953-28959.
- Kumari S, Beatty CM, Browning DF, Busby SJW, Simel EJ, Hovel-Miner G, Wolfe AJ (2000) Regulation of Acetyl Coenzyme A Synthetase in *Escherichia coli*. *The Journal of Bacteriology* 182 (15):4173-4179.

- Wolfe AJ (2005) The Acetate Switch. *Microbiology and Molecular Biology Reviews* 69 (1):12-50.
- Laun P, Pichova A, Madeo F, Fuchs J, Ellinger A, Kohlwein S, Dawes I, Fröhlich K-U, Breitenbach M (2001) Aged mother cells of *Saccharomyces cerevisiae* show markers of oxidative stress and apoptosis. *Molecular Microbiology* 39 (5):1166-1173.
- Zuin A, Castellano-Esteve D, Ayte J, Hidalgo E (2010) Living on the edge: stress and activation of stress responses promote lifespan extension. *Aging (Albany NY)* 2 (4):231-237.
- Pocsi I, Prade RA, Penninckx MJ (2004) Glutathione, altruistic metabolite in fungi. *Advances in Microbial Physiology* 49:1-76.
- Hanqing F, Kun S, Mingquan L, Hongyu L, Xin L, Yan L, Yifeng W (2010) The expression, function and regulation of mitochondrial alternative oxidase under biotic stresses. *Molecular Plant Pathology* 11 (3):429-440.
- Juarez O, Guerra G, Velazquez I, Flores-Herrera O, Rivera-Perez RE, Pardo JP (2006) The physiologic role of alternative oxidase in *Ustilago maydis*. *FEBS Journal* 273 (20):4603-4615.
- Osiewacz HD, Scheckhuber CQ (2006) Impact of ROS on ageing of two fungal model systems: *Saccharomyces cerevisiae* and *Podospora anserina*. *Free Radical Research* 40 (12):1350-1358.
- Watanabe CK, Hachiya T, Terashima I, Noguchi KO (2008) The lack of alternative oxidase at low temperature leads to a disruption of the balance in carbon and nitrogen metabolism, and to an up-regulation of antioxidant defence systems in *Arabidopsis thaliana* leaves. *Plant, Cell & Environment* 31 (8):1190-1202.
- Michan C, Pueyo C (2009) Growth phase-dependent variations in transcript profiles for thioredoxin- and glutathione-dependent redox systems followed by budding and hyphal *Candida albicans* cultures. *FEMS Yeast Research* 9 (7):1078-1090.
- Castro FAV, Herdeiro RS, Panek AD, Eleutherio ECA, Pereira MD (2007) Menadione stress in *Saccharomyces cerevisiae* strains deficient in the glutathione transferases. *Biochimica et Biophysica Acta (BBA) - General Subjects* 1770 (2):213-220
- Emri T, Oláh B, Sámi L, Pócsi I (2003) Does the detoxification of penicillin side-chain precursors depend on microsomal monooxygenase and glutathione S-transferase in *Penicillium chrysogenum*? *Journal of Basic Microbiology* 43 (4):287-300.
- Zjawiony JK (2004) Biologically active compounds from Aphylophorales (polypore) fungi. *J Nat Prod* 67 (2):300-310.



Infrastructure University Kuala Lumpur
Block 11,
Infrastructure University Kuala Lumpur,
De Centrum City,
Jalan Ikram-Uniten,
43000 Kajang, Selangor

